Characterization of Metabolic Dysfunction in the BACHD Rat Model of Huntington Disease and Therapeutic Targeting with Olesoxime

Dissertation

der Mathematisch-Naturwissenschaftlichen Fakultät
der Eberhard Karls Universität Tübingen
zur Erlangung des Grades eines
Doktors der Naturwissenschaften
(Dr. rer. nat.)

vorgelegt von
Laura Emily Clemensson, geb. Clemens
aus Zweibrücken

Tübingen
2015

Tag der mündlichen Qualifikation:	13.07.2017
Dekan:	Prof. Dr. Wolfgang Rosenstiel
1. Berichterstatter:	Prof. Dr. Olaf Rieß
2. Berichterstatter:	Prof. Dr. Bernd Wissinger
3. Berichterstatter:	Prof. Dr. Susann Schweiger

"…, although there was a borderline significant trend towards BACHD rats needing more time…"

E.K.H. Jansson
Publication VI

Table of contents

Table of contents

Abbreviations

ALS	amyotrophic lateral sclerosis
ATP	adenosine triphosphate
BAC	bacterial artificial chromosome
BACHD	bacterial artificial chromosome containing full-length huntingtin
Ca^{2+}	calcium ions
CNS	central nervous system
DIV	day(s) *in vitro*
Drp 1	dynamin-related protein 1
E	embryonic day
Fis 1	fission protein 1
GABA	γ-aminobutyric acid
HD	Huntington disease
Hdh	mouse huntingtin gene
HTT	human huntingtin gene, also *IT15*
HTT	human huntingtin protein
Htt	rat or mouse huntingtin protein
H^+	proton(s)
IGF-1	insulin-like growth factor 1
IT15	interesting transcript 15, Huntington disease gene, also *HTT*
Mfn	mitofusin
Miro 1	mitochondrial Rho-GTPase 1
MSNs	medium-sized spiny neurons
mPT	mitochondrial permeability transition
NAA	N-acetylaspartic acid
NMDA	N-methyl-D-aspartate
OD	optical density
Opa 1	optic atrophy 1
PGC-1α	peroxisome proliferator-activated receptor γ coactivator 1α
PR	progressive ratio
polyQ	polyglutamine

RQ	respiratory quotient
SEM	standard error of the mean
SMA	spinal muscular atrophy
ST*Hdh*	immortalized striatal mouse neurons with human exon 1
TCA	tricarboxylic acid, in *TCA cycle*
TSPO	translocator protein/tryptophan-rich sensory protein
VCO_2	volume of oxygen consumed
VDAC	voltage-dependent anion channel
VO_2	volume of carbon dioxide released
WT	wild type
8OHdG	8-hydroxy-2'-deoxy guanosine
^{1}H NMRS	^{1}H nuclear magnetic resonance spectroscopy

Summary

Summary (English)

The current work addresses the characterization of metabolic abnormalities in the BACHD rat and the therapeutic effects of olesoxime treatment.

The BACHD rat is a recently established transgenic model of Huntington disease (HD), which expresses full-length human mutant huntingtin (mHTT) with 97 CAG repeats. It is shown here that metabolic dysfunction is a prominent, early feature of the HD-related pathological phenotype in these rats. BACHD rats suffer from growth impairment and obesity due to deficits in energy metabolism. These deficits are traceable during growth and senescence based on altered physiological parameters. It can be concluded that metabolic abnormalities underlie temporal changes, which when considered a general feature of HD, could explain discrepancies in the outcomes of earlier studies on metabolic dysfunction in HD patients and animal models.

In order to therapeutically address metabolic dysfunction in the BACHD rat, a long-term treatment study with the mitochondria-targeting, neuroprotective compound olesoxime was conducted. Although olesoxime did not influence the growth deficit and development of obesity in the BACHD rat, it revealed a positive influence on mitochondrial function and specific behavioral and neuropathological phenotypes. It is suggested that these benefits resulted from improved mitochondrial function and a stabilizing effect on intracellular calcium homeostasis, leading to decreased calcium-dependent activation of the protease calpain-1 and reduced calpain-mediated proteolysis of mutant huntingtin. Further studies with earlier start of olesoxime treatment could help to understand why the compound only exerted selective beneficial effects in the BACHD rat, and to provide further insight into the mechanism of action.

Zusammenfassung (Deutsch)

Die vorliegende Arbeit befasst sich mit der Charakterisierung stoffwechselphysiologischer Auffälligkeiten in der BACHD-Ratte, sowie den therapeutischen Auswirkungen einer Behandlung mit Olesoxime.

Die BACHD-Ratte ist ein aktuelles Tiermodell der Huntington Erkrankung (HD), welches das vollständige mutierte Huntingtin-Gen mit 97 CAG-Wiederholungen exprimiert. Wie hier gezeigt wird, stellen Stoffwechselauffälligkeiten prominente Krankheitsmerkmale der BACHD-Ratte dar. BACHD-Ratten zeigen beeinträchtigtes Wachstum und ausgeprägte Fettleibigkeit infolge von Defiziten im Energiestoffwechsel, welche während des Wachstums und der Seneszenz anhand veränderter physiologischer Parameter nachweisbar sind. Die Befunde lassen darauf schließen, dass Defizite im Energiestoffwechsel zeitlichen Änderungen unterliegen, was unter der Annahme der Allgemeingültigkeit für HD, widersprüchliche Ergebnisse früherer Studien zur Stoffwechseldysfunktion in HD-Patienten und Tiermodellen erklären könnte.

Zur Therapie der Stoffwechselstörungen wurde eine Behandlung mit der auf Mitochondrien wirkenden Substanz Olesoxime durchgeführt. Obwohl kein Einfluss auf die zuvor beschriebene Wachstumsstörung und Fettleibigkeit festgestellt werden konnte, zeigte sich ein positiver Effekt auf die Funktion der Mitochondrien sowie auf bestimmte Verhaltens- und neuropathologische Merkmale der BACHD-Ratte. Es wird angenommen, dass Olesoxime durch Verbesserung der mitochondrialen Funktion den Kalziumhaushalt stabilisiert, und dadurch der Kalzium-abhängigen Prozessierung von mutiertem Huntingtin durch die Protease Calpain-1 entgegenwirkt hat. Zukünftige Studien mit frühem Behandlungsbeginn könnten Aufschluss darüber geben, warum der Wirkstoff nur selektive Verbesserungen in der BACHD-Ratte gezeigt hat, und darüber hinaus helfen den genauen Wirkmechanismus zu entschlüsseln.

Publications

List of publications

Journal articles are listed in chronological order according to publication date. Equal contribution of two authors is indicated by an '&' sign linking the authors' names.

I. Verwaest KA, Vu TN, Laukens K, Clemens LE, Nguyen HP, Van Gasse B, Martins JC, Van Der Linden A, Dommisse R. (1)H NMR based metabolomics of CSF and blood serum: a metabolic profile for a transgenic rat model of Huntington disease. *Biochimica et Biophysica Acta* 2011; 1812:1371-1379.

II. Yu-Taeger L, Petrasch-Parwez E, Osmand AP, Redensek A, Metzger S, Clemens LE, Park L, Howland D, Calaminus C, Gu X, Pichler B, Yang XW, Riess O, Nguyen HP. A novel BACHD transgenic rat exhibits characteristic neuropathological features of Huntington disease. *Journal of Neuroscience* 2012; 32(44):15426–15438.

III. Gouarné C, Tardif G, Tracz J, Latyszenok V, Michaud M, Clemens LE, Yu-Taeger L, Nguyen HP, Bordet T, Pruss RM. Early deficits in glycolysis are specific to striatal neurons from a rat model of huntington disease. *PLoS One* 2013; 8(11):e81528.

IV. Clemens LE, Jansson EK, Portal E, Riess O, Nguyen HP. A behavioral comparison of the common laboratory rat strains Lister Hooded, Lewis, Fischer 344 and Wistar in an automated homecage system. *Genes, Brain & Behavior* 2013; 13(3):305-21.

V. Eckmann J & Clemens LE, Eckert SH, Hagl S, Yu-Taeger L, Bordet T, Pruss RM, Muller WE, Leuner K, Nguyen HP & Eckert GP. Mitochondrial Membrane Fluidity is Consistently Increased in Different Models of Huntington Disease: Restorative Effects of Olesoxime. *Molecular Neurobiology* 2014; 50(1):107-18.

VI. Jansson EKH & Clemens LE, Riess O, Nguyen HP. Reduced motivation in the BACHD rat model of Huntington disease is dependent on the choice of food deprivation strategy. *PLoS One* 2014; 9(8):e105662.

VII. Clemens LE & Weber JJ, Wlodkowski TT, Yu-Taeger L, Michaud M, Calaminus C, Eckert SH, Gaca J, Magg JCD, Weiss A, Jansson EKH, Eckert GP, Pichler BJ, Bordet T, Pruss RM, Riess O and Nguyen HP. Olesoxime suppresses calpain activation and mHTT fragmentation in the BACHD rat. *Brain* 2015; 138(12):3632-53.

Statement of personal contribution

Statements are given according to the order, in which the publications were listed above.

I. Involved in breeding and maintenance of animals, dissection, blood sampling and serum preparation.

II. Involved in maintenance of animals, automated homecage assessment of metabolic parameters, dissection of animals and preparation of the manuscript.

III. Assessment of mHTT accumulation in primary neurons. Involved in data interpretation and manuscript preparation.

IV. Main investigator. Performed the experiments. Main role in data analysis and interpretation as well as preparation of the manuscript.

V. Main investigator (together with J. Eckmann). Breeding and maintenance of animals, dissection and sample collection. Involved in data analysis. Main role in data interpretation and manuscript preparation.

VI. Main investigator (together with E. Jansson). Shared main role in study design, breeding, maintenance of animals, metabolic measurements and dissection, data analysis, interpretation, manuscript preparation.

VII. Main investigator (together with J. Weber). Breeding and maintenance of animals. Main role in performance of behavioral experiments and animal dissection. Assisting role in immunohistochemical staining, main role in microscopy. Assisting role in isolation of mitochondria and western blotting. Main role in data analysis and interpretation as well as in manuscript preparation.

Introduction

Huntington disease (HD)

Natural history of the disease

Huntington disease (HD) is an autosomal-dominantly inherited, fatal, neurodegenerative disorder. Its prevalence is estimated highest in Europe and populations of European descent[1]. The average frequency of affected persons in Europe, North America and Australia amounts to a minimum of 6 per 100,000[2,3].

The behavioral symptoms of HD are historically classified as a triad of motor dysfunction, psychiatric disturbances and cognitive impairments. Symptoms are multifaceted and vary considerably among patients[4]. Motor symptoms present as involuntary movements (chorea) and hindered voluntary motor function through bradykinesia, rigidity and dystonia[5]. Psychiatric abnormalities include apathy, depression, irritability and obsessive compulsive behavior[5]. Finally, cognitive impairment comprises difficulties in information processing, memorization as well as executive function[6].

Behavioral changes are directly associated with central nervous system (CNS) dysfunction[7] and degeneration[8]. Brain atrophy is characterized by a loss of both gray and white matter, as well as gliosis[8–10]. The earliest and most severe decay occurs in the striatum, although cortical thinning and loss of white matter can also be observed before manifestation of the clinical disease[8,11]. Degeneration of extra-striatal, subcortical areas follows during early disease stages and includes hippocampus, amygdala, thalamus as well as hypothalamus[8–10,12,13]. The magnitude of brain atrophy differs among patients and is likely connected to the large variability in behavioral symptoms[14].

Clinical onset of HD typically refers to the appearance of gross motor abnormalities. However, more subtle behavioral changes as well as neurodegenerative processes are already detectable in mutation carriers many years before motor symptom onset[15,16].

The sole cause of developing HD is the expansion of an unstable repeat of CAG base triplets in the coding region of the *IT15* gene (consequently later termed *Huntingtin* gene, *HTT*) on chromosome 4p16.3[17]. CAG repeat lengths up to 34 are considered to lie in the normal range,

while more than 35 CAG repeats likely lead to the development of HD[18,19]. Full penetrance is assumed for repeat lengths of 42 CAGs and more[18].

Transmission of the disease typically results from inheritance of one mutated allele from an affected parent. The incidence of *de novo* mutation was estimated to lie around 0.1 % for transmission from a father with a high, but normal CAG repeat[20], but to account for up to 10 % of diagnosed cases[21]. An anticipatory effect has been described, based on the finding that intergenerational changes in CAG repeat lengths more often concern expansions than contractions, particularly when transmitted paternally[22,23].

The age of disease onset correlates inversely with CAG repeat length[24–26]. An average patient with a repeat length of 40 CAGs has a 50 % probability to develop the disease around the age of 60 years, while this decreases to around 40 years in case of 45 CAGs, and 30 years in case of 50 CAGs[18]. Patients with more than 60 CAG repeats, which typically arise from large intergenerational expansions transmitted by the father[27], can develop juvenile HD, defined by disease onset before the age of 20 years[28].

CAG repeat length has further been reported to correlate with progression and duration of disease, with higher CAG repeats (and early disease onset) leading to faster progression and thus shorter disease duration[29]. However, despite these correlations, CAG repeat length explains only about 50 % of the variation in onset and course of disease[24,26]. Other genetic as well as environmental factors constitute significant modifiers of HD[30,31].

Wild type huntingtin protein

HTT mRNA is expressed throughout the body with highest expression levels in neurons[32–34]. It is translated into the ~350 kDa (3144 amino acid) HTT protein with similar expression pattern[35–37]. Within cells, HTT is localized predominantly in the cytoplasm, where it seems to be concentrated along microtubules and attached to many membranous structures within cell somata, neurites and synapses[38–41].

Based in particular on its co-localization with microtubules, HTT has been considered to function as a scaffold protein involved in intracellular trafficking. This idea received support

from subsequent studies performed on cell and animal models of HD. HTT was found to interact directly with proteins involved in transport processes[42–45] and to promote vesicular transport[46] as well as endo-[45,47] and exocytosis[48]. Further studies identified a multitude of other interaction partners of HTT, linking it to cellular pathways such as autophagy[49–51], Ca^{2+} homeostasis[52,53], cell metabolism[54,55], cell signaling[56,57], synaptic transmission[58,59] and apoptosis[60]. Moreover, HTT has been found to bind to a variety of transcription factors[61–64] and proteins involved in translation[60,65], which strongly implicates a role in gene expression. Interestingly, HTT is able to translocate from the cytoplasm to the nucleus in response to cellular stress signaling[66].

Due to its various functions within the cell, HTT is crucial for embryonic and postembryonic development, as demonstrated in mouse models of HD[67–76]. Its absence leads to early embryonic lethality[67–69], while severely reduced expression results in a significant growth impairment[75] and downregulation in adolescence causes neurodegeneration[74]. HTT's vital function during adulthood is ascribed to anti-apoptotic properties[77–80].

Mutant huntingtin protein

In HD patients, the *mHTT* allele is translated into a mutated protein (mutant huntingtin, mHTT), which carries an abnormally long glutamine (polyQ) stretch after amino acid 17 close to the N-terminus[81]. Similar to HTT, mHTT is abundant throughout the body[82–84], even though degenerative processes are restricted to selective, neuronal tissues. In contrast to HTT, mHTT shows an abnormally high concentration in cell nuclei[82,85]. In addition, mHTT-expressing cells develop mHTT-containing protein aggregates in both nucleus and neurites[85,86].

The presence of the elongated polyQ stretch leads to a disruption of normal HTT function[87] as well as a toxic gain of function[88]. The pathogenic events in HD concern a multitude of different cellular pathways related to normal HTT function and beyond. These are affecting intracellular transport, gene as well as protein expression, protein degradation pathways, cellular energy metabolism, ion homeostasis, cell signaling and apoptosis[88].

It was initially believed that the mHTT aggregates found in HD patients[85,86] and disease models[89,90] were the primary source of disease pathogenesis. Characteristics of the

aggregation process seemed to explain the late age of onset of HD[91] as well as the dependency of disease onset and progression on the polyQ repeat length[90,92,93]. However, a series of follow-up studies dissected the process of aggregate formation in relation to cytotoxicity[94–98], leading to the overall conclusion that cell death is primarily induced by toxic aggregation precursors and that earlier results had been misinterpreted due to the causal relationship of precursors to aggregate formation[99].

N-terminal fragments of mHTT have been proposed to constitute such toxic aggregation precursors. This assumption is in part based on the findings that N-terminal mHTT fragments are more prone to form aggregates than full-length mHTT[93,100,101]. Fragments of mHTT are further found in the brains of HD patients *post mortem*[89,92], and their abundance increases with longer CAG repeats and positively correlates with cell death *in vitro*[77,95,100,102]. Most importantly, it has been demonstrated that N-terminal mHTT fragments are more cytotoxic than full-length mHTT[77,100,103]. N-terminal fragments of mHTT derive from the cleavage by proteolytic enzymes. The two most prominent protease families implicated in proteolytic cleavage are calpains[104,105] and caspases[106]. Inhibition of either protease has been shown to reduce aggregate formation and mHTT toxicity both *in vitro*[105,107] and *in vivo*[108,109]. The particular toxicity of mHTT fragments is thought to be conveyed via a conformational change[110–112], which affects protein interactions[60,98,113] and disrupts signaling pathways. In addition, truncation of mHTT impairs its ability to shuttle between cytoplasm and nucleus in response to cellular stress signaling[66]. As a result, mHTT fragments accumulate in the nucleus[85,89,105,114], which has been shown to enhance their detrimental effects[94,100,115,116].

Models of human HD

As molecular pathways underlying the mHTT-mediated pathogenesis cannot easily be investigated in HD patients, a multitude of disease models have been established to imitate the human pathological condition.

Cell and animal models of HD

Molecular aspects of HD have been studied intensely in mammalian cells including lymphoblasts[35], fibroblasts[117], embryonic stem cells[118,119] and inducible pluripotent stem cells[120] from HD patients and control subjects. In addition, cell lines[93,106,121–123] and primary cell cultures[94] expressing mHTT with various lengths of the protein and polyQ tract have been used. In order to further understand the disease on organismic level, animal models of HD have been established. Small invertebrates such as worms[124] and flies[125] can be used to study the order and progression of molecular HD-related phenotypes, while larger, mammalian species such as mouse[126–140], rat[141,142], sheep[143], pig[144] and monkey[145] enable the analysis of systemic abnormalities and the interplay between cell populations in the body. Of these, rodent models certainly had the most impact on the evaluation of disease mechanisms as well as preclinical testing.

As HD does not naturally occur in animals, it needed to be induced. In the first rodent models of HD, this was achieved by lesioning the striatum with injections of toxins such as kainate[146,147], ibotenate[148], quinolinate [149] or 3-nitroproprionate[150]. After the identification of the disease-causing gene, a range of genetic animal models were generated[88]. The models are typically classified according to the specific nature of their transgenic constructs. Some carry classic transgenic constructs that are inserted at random positions in the genome, and express either full-length or truncated mHTT under endogenous or exogenous promotors (transgenic models). In contrast, there are models where the CAG repeat of the endogenous *HTT* locus has been extended (knock-in models). Although knock-in and full-length transgenic models offer a better opportunity to study the mechanism behind mHTT pathogenicity, they are limited by having more discrete and slowly developing phenotypes compared to the transgenic fragment models, which express the more toxic species of mHTT[88]. The exact phenotypes associated with mHTT expression in these various models differ[151–153].

Figure 1. Cell and animal models of HD

The most widely used model organisms of HD are mammalian cell lines, such as the immortalized striatal precursor cell line ST*Hdh* (left), and genetic mouse models of HD, like the *Hdh*^{Q111} knock-in mouse, the donor organism for the ST*Hdh* cell line. A common background strain for transgenic mouse models is the C57BL/6 mouse (middle). Sprague Dawley rats (right) were used as a background strain to create the two existing transgenic rat models. The latest of them, the BACHD rat, was characterized in this work. Photographs were taken in our laboratory and animal facilities. Scale bar: 10 µM.

The BACHD rat model of HD

The BACHD rat is the latest rat model of HD and has been generated in our laboratory[142]. BACHD rats overexpress full-length human m*HTT* with 97 alternating CAA/CAG repeats on a bacterial artificial chromosome (BAC). This construct has also been used to generate the BACHD mouse[130].

Two lines of mHTT-overexpressing BACHD rats have been established[142]. Line TG9 expresses mHTT at 2.5 fold of the expression level of the endogenous rat huntingtin (Htt), which is comparable to the expression level of mHTT in the BACHD mouse. Line TG5 expresses mHTT at 4.5 fold of the expression level of Htt, the highest expression level among the available founders. In both lines, the transgene is inserted at a single site. The position within the genome as well as the copy number of inserts likely define the differential expression between the two lines. In this work, primarily TG5 rats (Crl:CD(SD)-Tg(HTT*97Q)21.2Hpn/Hpn) hemizygous for mHTT have been used, and will in the following simply be referred to as BACHD rat.

In the original publication of the BACHD rat model, behavioral and neuropathological abnormalities reminiscent of HD in humans have been reported[142]. Similar phenotypes have

been detected in both lines, although they were stronger in line TG5 compared to line TG9. The behavioral abnormalities consist of motor dysfunction and psychiatric disturbances. With regard to neuropathology, BACHD rats display mHTT aggregates and nuclear accumulation of mHTT throughout the brain, detectable from early on and increasing with age. At advanced ages, the presence of dark neurons and reduced dopamine uptake in the striatum point to neurodegenerative processes. Later studies confirmed these initial findings and added to our current knowledge on the behavioral phenotype of the BACHD rat by providing indications for cognitive impairments[154,155].

A prominent pathological feature of the BACHD rat, which became apparent shortly after the generation of the rats, is the development of obesity. Metabolic abnormalities are part of the human HD pathology, and other mouse and rat models display various forms of metabolic disturbances, as detailed below. Thus, it was of interest to further investigate their characteristics, and to address them in a therapeutic approach, which was realized in this work.

Metabolic dysfunction in HD

Systemic metabolic abnormalities in HD patients

Besides the classical triad of symptoms, a variety of other abnormalities contribute to the burden of HD, which can be broadly classified as metabolic disturbances. Similar to the classical HD symptoms, metabolic disturbances vary largely in frequency and severity of manifestation among HD patients, suggesting a modulatory role of other genetic or environmental factors and making it difficult to assess their general role in HD.

Symptomatic patients can present with endocrine abnormalities of the major hypothalamus-pituitary axes, such as hypercorticotropism, hypersomatotropism and hypogonadotropism[156]. They often suffer from signs of autonomous nervous system dysfunction, like gastrointestinal, urinary, cardiovascular and, in men, sexual problems[157]. HD patients become progressively cachectic at late stages[158–160], which has been attributed to the exhausting choreatic movements[161–163] as well as dysphagia[164], and the most common cause of death is aspiration pneumonia[165].

Preceding these severe manifestations during the end stage of HD, earlier signs of abnormal energy metabolism have been recognized, which are detectable before clinical symptom onset. There are indications for growth deficits, as significantly lower measures of head circumference, weight and BMI have been detected in children carrying the mHTT allele compared to healthy children[166]. Furthermore, intracranial volume has been found to be already reduced at the prodromal stage in HD mutation carriers[167]. In some studies, reduced body mass[168–173] and increased metabolic rate[161,162,174] have been detected before motor symptom onset. In addition, increased brain glucose consumption has been found in some areas of presymptomatic HD patients[175,176], preceding overall reduced consumption rates at late stages of disease[177–183]. Remarkably, some mutation carriers have been shown to fail countervailing increased energy expenditure, despite increased caloric intake[168,170,184]. Some patients further show impaired glucose tolerance[185–187] and insulin response[174,188,189] as well as a higher risk to develop diabetes[190], despite the waste of both lean[170,172,184] and fat mass[168,170]. This suggests that the regulation of energy metabolism is highly disturbed.

It is still unclear, how this condition develops. As for the classical symptoms, the progressive degeneration of cell populations in the CNS, particularly the loss of hypothalamic neurons[13], is held responsible.

Systemic metabolic abnormalities in HD animal models

Metabolic abnormalities, as well as causes and consequences, have been studied more intensely in rodent models of HD[191]. HD mice and rats develop metabolic abnormalities, although with variable characteristics (Table 1).

Transgenic mouse models expressing N-terminal fragments of mHTT, are reported to have similar body weights as WT mice at young ages, but eventually show indications of impaired growth followed by progressive weight loss. These mice die prematurely during early adulthood. Knock-in mouse models in general show similar phenotypes, although they appear much later in life compared to the fragment mice, and are not always detected. On the contrary, the full-length mHTT-expressing mouse models are found to have increased body weights compared to their WT littermates. Reports on the tgHD fragment rat model of HD are inconsistent, with the initial characterization showing reduced growth and body weights, while later studies reported increased body weights compared to WT rats, particularly in females.

Differences in body weight among animal models of HD are the result of changes in body size and body composition. Several models show an initial accumulation of fat mass and wasting of both fat and lean mass at older ages. Onset and severity of this catabolic condition seem to depend on the HD-related genetic context[74–76] as well as on other genetic and environmental factors such as background strain[192], gender[152,193,194] and housing conditions[195]. Impaired growth and enhanced fat accumulation have been attributed to the decreased availability of insulin-like growth factor 1 (IGF-1)[196,197], as well as dysfunctional adipocyte metabolism with impaired lipolysis and increased secretion of the hormone leptin[198,199]. Similar to HD patients, it could be demonstrated that cerebral hypometabolism is preceded by a hypermetabolic state with increased glucose consumption in the forebrain of HD mice[153], supporting the idea of early hypermetabolism as a general feature of HD[200].

Table 1: Abnormalities with regard to energy balance in rodent models of HD

	rat	mouse			
	tgHD	**R6/2**	**N171-82Q**	**YAC128**	**BACHD**	***Hdh*Q80–200**
Body weights	Reduced weight originally reported for males from about 4 m onwards[222]. Follow-up studies report unchanged for males[193,223], but increased for females[193]	Frequent reports of similar weight until the age of 4–6 w, followed by halted growth and progressive weight loss from 10–12 w onwards[89,152,195,211,217–221]. This appears to apply for both genders[211,219]	Similar weight as WT mice for males at 1 m of age, followed by halted growth around 2 m, and progressive weight loss from 4 m onwards[128,214,215]	Generally increased weight, although onset varies between 8 and 48 w depending on gender and background strain[76,152,192]. Phenotype is not present on some backgrounds[192]	Generally increased weight from 8 to 16 w[130,152,194,212,213]. Present for both genders, although more pronounced[152,194,212,213] and reported to appear earlier in females[152]	Generally halted growth at different ages, depending on gender and CAG repeat length[134,152,201,202]. Only a trend to reduced weight after 19 w in Q111 mice[203]. Progressive weight loss in Q150 and Q200 males at around 40 w[204–207]
Body size	No report found	Reduced size at 8 w for males[199]. No reports on females or age progression	Smaller size due to growth impairment after 1 m[128,+]	No report found	No report found	Smaller size of Q80 and Q150 mice at 34 and 52 w respectively[134,+]
Organ sizes	No report found	Progressive brain atrophy after 4 w[89,+]	Internal organs including brain initially develop normally[128,+], but atrophy has been found in 16 w-old mice[214,+]	Similar brain size at 6 m, but smaller brains in 12 m-old male mice[130]. Several internal organs are larger at 12 m on certain genetic backgrounds[76,192,#]	Similar brain size at 6 m, but selectively reduced forebrain volume at 12 m[130,+]	Brain seems to develop normally, but shows atrophy in Q119, Q140 and Q175 mice at 4–12 m[201,208,209,#]. Several internal organs are smaller in Q150 mice at 22 m[210,#]
Body composition	No report found	Increased fat mass until at least 8 w, and progressive loss of lean mass from around 8 w onwards in both genders[219]	Increased fat mass and reduced lean mass at 10 w in males[216]. No reports on females or age progression	Increased fat mass but unchanged lean mass at 3 m[76#]	Increased fat mass from 2 m onwards in females, largely similar body composition as WT in male mice[194,212,213]	No difference in Q111 mice[203]. Trend to increased fat mass in Q140 mice at 7 m, no difference at 13 m[#], and reduced at 22 m due WT rats gaining more fat[211]

	rat **tgHD**	**R6/2**	**N171-82Q**	mouse **YAC128**	**BACHD**	***Hdh*Q80–200**
Food intake	No differences in feeding reported for males, but generally increased for females from 5 m onwards[193]	Increased feeding in males between 6 and 7 w[195], unchanged between 7 and 11 w[195,219], and decreased from 11 w onwards[195]	Moderately decreased feeding in 10 w-old males, and reduced during refeeding after fasting[216]. No reports on females or age progression	No difference in feeding at 3–4 m[76,#]	Increased feeding reported for both genders at 2 and 4 m[194]	Not extensively studied, although Q111 mice show no phenotypes at 13 w[203,#]
Locomotor activity	Generally increased dark phase activity after 6 m in both genders, although apparently more pronounced among females[193,223]	Frequent reports of normal activity in both genders until 10–13 w, and progressive decline thereafter[152,221,230–232]. Some, however, report a lack of difference even at 18 w[195,219].	Generally reduced from 7–12 w onwards without clear progression[214,216,229]	Both genders appear generally hypoactive without clear age progression [152,192,228]	No difference before 4 m[152,194], but reduced activity in both genders at older ages[152,227]. Controversially, the phenotype has been reported to either remain stable[227], or to progress with age[152]	Increased activity in some young mice[133]. No difference at 13 w in Q111 mice[203]. Frequent reports of reduced activity with varying onset from 8–100 w[201,203,206,224–226,]. No difference in old mice[152]
Metabolic rate	Trend towards increased metabolism during the dark phase after 6 m in both genders[193,223]	Generally increased metabolism in males[195,218,219], although the onset has been reported to be before 4 w[219] and at 14 w[218]. No reports on females	No significant difference in VO_2 relative to lean mass in 10 w-old male mice[216]	No difference in weight loss, or weight gain during 24 h of fasting and refeeding at 3 m[76,#]	4 m-old female mice have been shown to have similar VO_2, but increased VCO_2 and thus increased RQ[194].	Not extensively studied. Q111 mice show no phenotypes at 13 w[203,#]

*The results displayed, reflect the combined interpretation of all studies rather than conclusions drawn in the individual studies

+ Authors did not describe, which gender was investigated

Mixed genders were investigated

w = weeks; m = months

Studies on insulin metabolism have demonstrated that insulin insensitivity is unlikely to be the cause for impaired glucose utilization in HD. Although it seems to be clear that insulin secretion is hampered due to impaired gene expression[189] and exocytosis[233,234], the deficits likely occur only in the presence of mHTT with very long CAG stretches, which are rarely found in adult onset HD patients[235].

Several studies suggest that not only central dysregulation, but also individual tissue defects seem to add to the metabolic phenotype in HD, as abnormalities in intrinsic pathways in muscle[219,236], adipose[199,211] and bone[237] tissues (among many others[238]) have been demonstrated in HD animal models. However, by switching off mHTT expression only in the hypothalamus of the BACHD mouse, the metabolic phenotype has been completely abolished[194], arguing against an important role of these individual pathways in shaping systemic metabolic abnormalities.

Cellular energy metabolism in HD

Similar to the classical signs of HD, metabolic abnormalities appear like a part of the HD symptomology that stems from neuronal dysfunction and degeneration. However, disturbed energy metabolism at the cellular level might play a much more important etiological role by triggering neuronal dysfunction in the first place[153].

Compromises in cellular energy metabolism in HD

A large body of evidence has been collected to support the idea of disturbed cellular energy metabolism in HD based on findings in patients and animal models. Early glycolytic deficits are indicated by impaired glucose consumption despite unchanged oxidative phosphorylation in presymptomatic HD mutation carriers[239]. Reduced activity of several tricarboxylic acid (TCA) cycle enzymes further points to decreased TCA cycle turnover[240–243], which can be a result of defective substrate supply via upstream oxidation processes (i.e. glycolysis, proteolysis and lipolysis), or reduced downstream flux (i.e. respiratory chain activity). Impaired respiratory chain activity mainly due to the decreased activity of complexes II, III and IV has also been found. However, the deficit has specifically been detected at symptomatic[243–246] but

not presymptomatic[247] stages, suggesting that these defects are secondary to other energetic restraints[200].

Metabolic disturbances can also be traced in tissues and body fluids from HD patients as well as HD animal models, with the most consistent findings being a decline in amino acid levels[248–250] and creatine[251–253], as well as an accumulation of lactate[253–256].

Mitochondrial dysfunction in HD

Irrespective of their probable secondary role in dysfunctional cellular energy metabolism[200], mitochondria are considered to be key players in translating energetic deficits into cytotoxicity[257–262]. Mitochondria host major metabolic pathways and orchestrate energy supply, Ca^{2+} homeostasis as well as cell death in response to cellular demands[263]. The presence of mHTT seems to interfere with all of these processes. Toxic effects have been suggested to result from direct binding of the N-terminal region of mHTT to the outer mitochondrial membrane[264–268] or by disturbing the transcription of nuclear-encoded mitochondrial genes[269,270]. In HD patients and disease models, mitochondria have a reduced production rate of adenosine triphosphate (ATP)[271–273], show impaired Ca^{2+} handling[264–266,274–277] and release more reactive oxygen species resulting in oxidative damage[242,243,278–280]. More recent reports further highlight the importance of altered properties for morphological adaptations of mitochondria that are required for mitochondrial function and maintenance of mitochondrial integrity upon cellular stress[281]. In this regard, mHTT alters the activity of proteins of the fission and fusion machinery resulting in the fragmentation of the mitochondrial network[267,282–287] and disrupts HTT-mediated transport processes leading to impaired mitochondrial trafficking[285,287–289].

Cellular energetic deficits and neurodegeneration in HD

A causal relationship between energetic deficits and the neurodegenerative processes underlying the HD pathogenesis has been assumed after noting that inherited mitochondriopathies as well as disruption of mitochondrial function with the respiratory chain complex II inhibitors 3-nitropropionate[150] and malonate[290] were accompanied by selective

neurodegeneration and associated symptoms highly reminiscent of HD[291]. It was concluded that striatal neurons would probably demise through an excitotoxic mechanism, as excitotoxin application revealed similar selective lesions[291].

Excitotoxicity[292] refers to the excessive activation of glutamate receptors, prominently the ionotropic N-methyl-D-aspartate (NMDA) receptor, leading to intracellular Ca^{2+} overload and ultimately the death of the postsynaptic neuron[293]. Mitochondria are crucially involved in this cascade. When mitochondrial Ca^{2+} buffering is insufficient, elevated cytosolic Ca^{2+} levels lead to the activation of numerous signaling pathways that act back on the organelles and trigger the initiation of cell death[294]. This is mediated by mitochondrial permeability transition (mPT), a process characterized by the formation of a pore complex in the inner mitochondrial membrane. Pore formation results in the dissipation of the proton gradient, disruption of ion homeostasis as well as ATP production, and subsequent organelle swelling and outer membrane rupture, although the details of this process are still under debate[295,296].

Energetic deficits enhance the vulnerability for excitotoxicity[297,298], particularly in striatal medium-sized spiny neurons (MSNs)[299]. MSNs show a generally reduced Ca^{2+} buffering capacity[277,300,301] and preferentially express the NR2B subtype of the NMDA receptor[302], which has been linked to excitotoxicity[303]. The selective vulnerability to excitotoxicity is further enhanced in the presence of mHTT. Studies have identified several pathological effects of mHTT expression that can trigger excitotoxicity in HD striatum, including impaired glutamate reuptake, increased postsynaptic glutamate receptor activity as well as intracellular sensitization of Ca^{2+} release by the endoplasmic reticulum (ER)[304]. It remains elusive though, where the cascade of events that ultimately terminates in the selective death of vulnerable neurons starts. The detrimental processes might not be triggered by one event alone, but rather be the result of a multitude of concurrent insults overcharging the cell.

Therapeutic strategies for HD

To date, there is no medication available that can slow down or prevent the onset or progression of HD in humans. Current therapies are restricted to alleviating disease symptoms and thereby improving the patients' quality of life. However, several promising treatment strategies are under investigation, which raise hope for the future.

Present and future treatment of HD

A variety of symptomatic treatments are indicated for HD. Exercise and a balanced nutrition are recommended to support health in general. Physiotherapy can be useful to strengthen muscles or loosen rigidities, and speech language therapy can ameliorate speech and swallowing problems. In addition, psycho-social support can help patients and their family members to cope with the burden of HD. Symptomatic medical treatment further targets motor as well as cognitive and psychiatric pathologies, but as the drugs often evoke side effects and interfere with each other, their usefulness has to be outweighed according to the symptoms of the individual patient. Commonly prescribed drugs to reduce involuntary movements are dopamine antagonists (e.g. haloperidol) or presynaptic dopamine depleters (e.g. tetrabenazine). Psychiatric symptoms are treated with antidepressants (e.g. carbamazepine), antipsychotics (e.g. clozapine), anxiolytics (e.g. benzodiazepine) or tranquilizers (e.g. chlorpromazine).[305]

Therapeutic strategies for HD have been developed for basically every aspect discovered to be involved in the disease pathogenesis, and at least minor benefits have been demonstrated for a multitude of compounds and approaches in preclinical studies[88]. Unfortunately, promising candidates have so far failed to exert disease-modifying effects in clinical trials in HD patients[306]. Due to the increasing understanding of the disease though, the research community awaits a breakthrough in the coming years[307]. Among strategies such as enhancing mHTT degradation, improving neurotrophic support and reducing inflammation, the most promising therapeutic approach is the reduction of mHTT expression[308]. The single mutation and sole genetic cause responsible for HD enables the direct targeting of the inflicted protein on the transcriptional or translational level. RNA interference[309,310], translational repression with antisense oligonucleotides[311] and transcriptional repression using zinc finger

proteins[312] have proven to be successful and beneficial in animal models. Delivery and distribution issues as well as allele-selectivity and -specificity constitute the major areas of research in this area[308].

The therapeutic compound olesoxime

Olesoxime is a cholesterol derivative, which was discovered in a small-molecule screen for neuroprotective compounds at Trophos SA, Marseille (www.trophos.com). In the initial screening, primary motor neurons were deprived of serum, incubated in the presence or absence of olesoxime, and survival was monitored[313]. The screen revealed highly beneficial effects of the compound. Further assays on neurons subjected to other pathological stimuli, including striatal neurons transfected with mHTT, all showed increased survival[314].

Binding and localization analysis revealed that the compound concentrates at the site of mitochondria[314] and interacts with the voltage-dependent anion channel (VDAC)[315] as well as the translocator protein (TSPO)[316] on the outer mitochondrial membrane[313]. As these proteins are considered to play a role in mPT[317], it was proposed that olesoxime's mechanism of neuroprotection was the inhibition of mPT and subsequent cell death[313]. In accordance with this idea, olesoxime was found to prevent cell death induced by various toxins[313,314,318] to a similar magnitude as cyclosporine A, a potent mPT inhibitor. Further studies discovered a variety of interesting aspects around olesoxime's molecular effects, but the exact mechanism of cytoprotection remained elusive. Olesoxime was reported to prevent cytochrome *c* release from mitochondria and the subsequent activation of caspases in the cytosol[319]. These effects did not seem to derive from improved mitochondrial Ca^{2+} handling or inhibition of Ca^{2+} release[314]. Olesoxime further did not directly inhibit caspases, activate prosurvival kinases or modulate the transcription of proapoptotic genes via the transcriptional regulator p53[319]. Besides the direct effect on the initiation of mitochondria-mediated apoptosis, olesoxime was found to promote microtubule-based neurite outgrowth and microtubule-dependent mitochondrial transport, specifically in differentiated neuronal cells[320], and to improve oligodendrocyte-mediated remyelination[321].

In vivo studies demonstrated consistently beneficial outcomes regarding neuroprotection and regeneration in animal models of motor neuron diseases[313,314,322] as well as neurodegenerative disorders[314,321,323], and neuroprotective and antinociceptive effects in models of peripheral neuropathies[320,324–326].

The therapeutic potential of olesoxime was further investigated in clinical trials on motor neuron diseases. Olesoxime showed excellent safety and tolerability in the patients[314]. Moreover, the treatment was easy to apply, as olesoxime reaches the brain in sufficient amount upon oral administration of one daily dose[327], and therefore medication does not involve invasive or time-consuming procedures. Two trials, one on survival in end-stage amyotrophic lateral sclerosis (ALS) patients[327] and one on motor symptom onset in early stage spinal muscular atrophy (SMA) patients[328] were conducted. The ALS trial revealed a negative outcome, while the trial on SMA patients showed striking beneficial effects on the clinical end point, suggesting better efficacy of olesoxime in early phases of disease.

As no further studies were performed to investigate the effects of olesoxime treatment in an animal model of HD despite the positive *in vitro* results[329] and the implication of mitochondrial dysfunction in HD[200], it would be of significant interest to investigate a potential therapeutic effect of olesoxime on the HD pathology *in vivo*, as performed in this work.

Objectives of the current work

The primary aims of this work were to identify and characterize abnormalities in energy metabolism in the BACHD rat model of HD, as well as to therapeutically target metabolic defects with the compound olesoxime. These aims were pursued in several independent studies:

I. Validation of a system for automated metabolic phenotyping of rats

The reliability of automated behavioral phenotyping in general and the assessment of metabolic parameters in particular were investigated in four commonly used wild type rat strains.

II. Characterization of metabolic abnormalities in the BACHD rat

Three studies were designed to assess the body constitution, systemic energy homeostasis and blood metabolite profile of the BACHD rat. Moreover, mitochondrial function was analyzed in primary neuronal cultures and in brain tissue from adult BACHD rats.

III. Evaluation of olesoxime treatment effects

A treatment study was carried out in order to evaluate a potential therapeutic effect of olesoxime in the BACHD rat. This study included phenotypes evaluated before, but also extended the characterization of the BACHD rat. Thus, it should be noted that the 2nd and 3rd part are not completely separate, and some findings on metabolic abnormalities, represent data obtained during the treatment study.

Ethical statement

All experiments described herein involving animals were carried out by persons with appropriate training and expertise. Operating procedures were approved by the local ethics committees and carried out in accordance with the guidelines of the Federation of European Laboratory Animal Science Associations and the German Animal Welfare Act, based on European Union legislation (Directive 2010/63/EU).

Results and discussion

I. Automated metabolic phenotyping in rats

Detailed behavioral characterization is an important part of establishing novel animal models in a variety of research fields, and automated behavioral observation has been promoted to provide in several ways better behavioral measurements than classical tests[330,331]. First, these systems offer a standardized testing environment to reduce variability, while also allowing for customization of the setup to run specific protocols. Second, as measurements are highly computerized, behavioral data are gathered objectively. Third, the systems are able to measure a broad spectrum of parameters simultaneously, providing amounts of data which an experimenter could not obtain manually. Last, the systems offer the opportunity to assess behavioral parameters over longer periods of time, so that – theoretically - novelty-induced and baseline behavior can be separated. Due to these extended possibilities, we aimed at utilizing an automated test system for the behavioral and metabolic characterization of the BACHD rat.

Validity of automated phenotyping in rats

(Publication IV and Appendix A)

For the characterization of the BACHD rat, the PhenoMaster automated behavioral phenotyping system for rats, produced by TSE Systems Germany, was purchased. As the system had not been validated before, the reliability of its test results was addressed by analysis of behavioral data from four commonly used wild type (WT) rat strains known to differ in their behavioral characteristics (Publication IV[332]). WT rats of the strains Lister Hooded, Lewis, Fischer 344 and Wistar (Figure 3) were observed at three different ages over 70 hours in individual home cage-like testing cages, measuring locomotor activity, fine movements, food and water intake, the volume of oxygen (VO_2) consumed and the volume of carbon dioxide (VCO_2) released.

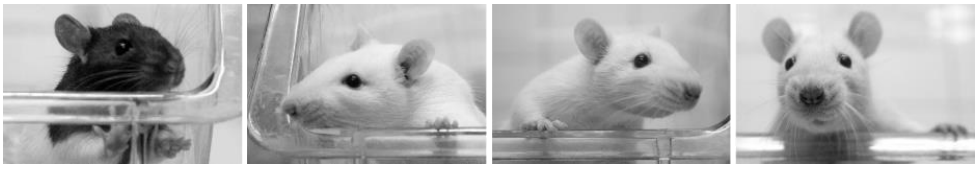

Figure 2. The rat strains used for the validation of automated phenotyping
In order to validate the automated behavioral phenotyping system, PhenoMaster, the behavior of rats from the four rat strains Lister Hooded, Lewis, Fischer 344 and Wistar (from left to right), was assessed. The rats differ in morphological appearance, physiological parameters and behavioral characteristics. Photographs display 6 weeks old rats in our animal facility.

The measurements were found to be sensitive enough to reveal phenotypic differences between the strains, and reliable enough to recapitulate general behavioral characteristics that were in accordance with previous results from classical tests[333,334]. In addition, the automated phenotyping generated new data on the rat strains such as the dissection of novelty-induced and baseline behavior as well as differences in the circadian activity pattern. However, when rats from the same four strains were reinvestigated in another automated phenotyping system (PhenoTyper, Noldus Information Technology, The Netherlands), specifically the differences in circadian activity were not reproduced, questioning their actual validity (Appendix A and Reference[335]). Moreover, detailed analysis of the metabolic data revealed the presence of some form of stressor, as two of the four rat strains showed a drop

in body weight gain during the experiments compared to the week before and after the measurement (Publication IV[332] and Reference[336]). This stress effect was also found in Sprague Dawley rats, which form the background of the BACHD rat model[336].

It can be assumed that the stress response had been induced by the social and environmental changes during the test, specifically the individual housing in cages differing from the home cage in acoustic and olfactory environment as well as micro-climate. In this regard, it is known that the transfer of animals to a novel environment and the separation from their social group can induce stress in rats[337–341]. Also, the stress response was less pronounced for rat strains known to be less anxious[342,343].

Importantly, as the negative effect differed in magnitude for all rats, it can be considered to be a confounding factor. This is illustrated by the finding that values for food intake and VO_2 from strongly affected rats were lower than expected from their respective body sizes. Thus, the automated phenotyping did not seem to give a fair picture of the differences between the rat strains, and metabolic data in particular was likely biased by inter-strain differences in stress resistance.

Summary and outlook

The data suggest that automated behavioral phenotyping offers the possibility of gathering large data sets, which would likely be impossible to obtain in similar amount and detail in a manually manner. However, the studies also point out that the outcomes from such tests need to be analyzed carefully, as their validity is unclear and results might be confounded by potential stress-inducing factors. Systems with the opportunity of measuring groups of animals might provide more reliable outcomes, but this needs further evaluation.

To resolve the role of isolation and novelty in inducing stress during automated behavioral phenotyping, three groups of rats will be studied, either socially housed throughout the study, individually housed directly upon transfer to the test cages or individually housed after acclimatization to the test cages in a social environment. With this setup it should be possible to determine, if stress is induced by changes in the social environmental conditions, by changes in the environment alone, or by an interaction of social and non-social factors.

II. Metabolic abnormalities in the BACHD rat

Soon after the generation of the BACHD rat, it became clear that the animals display some form of metabolic dysfunction, as they appeared obese. Knowing of metabolic abnormalities in other HD disease models including the BACHD mouse (Table 1), and the occurrence of metabolic problems in HD patients, this observation led to evaluate abnormalities in metabolic function as HD-related pathology in the BACHD rat.

The chapter is divided into the three major parts:

- Systemic metabolic disturbances
- Mitochondrial dysfunction
- Conclusion

Systemic metabolic disturbances

Longitudinal analysis of body constitution

(Publication VI[344] and Appendix B)

In order to confirm the impression of altered body constitution, the body weight, size and composition of BACHD and WT rats were assessed.

Body weight

The body weight development of numerous cohorts of BACHD rats from line TG5 has been followed by now (Publication II[142], VI[344], Reference[154] as well as Jansson and Clemens *et al.*, unpublished) up to an age of 18 months (Publication II[142]). In most cases, BACHD rats have been found to show identical body weights to WT rats. Occasionally though, significantly reduced body weights have been found in some cohorts, particularly when the thorough analysis of litter pairs was conducted (Clemens and Jansson *et al.*, unpublished). These results stand in contrast to what was expected given the rats' obese appearance. The assumed increase in fat mass despite similar or even reduced body weight further suggests that BACHD rats have a lower lean mass compared to WT rats.

Body size and composition

In order to test the hypothesis of reduced lean mass, the rats' body composition was investigated by detailed dissection (Publication VI[344] and Appendix B). As proposed, BACHD rats were found to carry excess amounts of adipose tissue and to have lower lean masses. The difference in lean mass was the result of reduced bone and muscle as well as organ mass and came along with an overall reduced body size. Differences were already detectable at 1 month of age, and did not show any progression from 3 months onwards. Thus, BACHD rats show growth impairment and obesity.

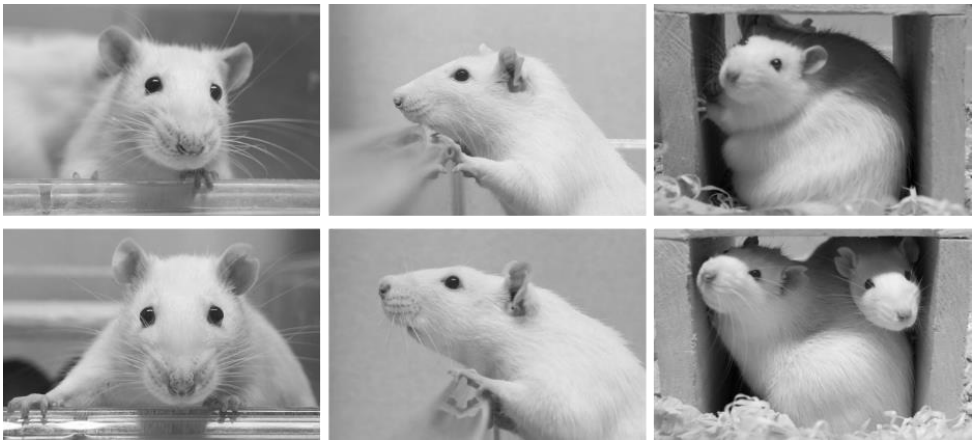

Figure 3. The BACHD rat

BACHD rats (upper row) have a distinct morphological phenotype. Most prominent are an adolescent face, small head and obese appearance compared to WT littermates (lower row). The pictures show adult rats at the age of 6 months.

Interestingly, male rats of line TG9 show consistently lower body weights compared to their WT littermates (Publication II[142] and Yu-Taeger *et al.*, unpublished). Thus, it is possible that the lean mass phenotype is similar for rats of line TG9 and TG5, while the obesity phenotype is more pronounced in TG5 rats. Preliminary results from the dissection of female BACHD rats further indicate that females do not show similar differences in body size and body composition, with the brain being the only detectable dystrophic organ (Yu-Taeger and Clemens *et al.*, unpublished). Similar gender differences were found in HD patients[168], suggesting that gender is an important modifier of the metabolic phenotype in HD.

It has been assumed in the past that developmental deficits do not play a role in HD, as mHTT expression was found to rescue embryonic lethality caused by loss of HTT[69,130,131], and homozygous HD mutation carriers appeared to develop normally before the onset of HD symptoms[345]. However, subtle differences might have been overlooked, as morphometric measurements had not specifically been undertaken in those study groups, while there are indications for reduced body size in children at risk for HD[166]. It is likely that the magnitude of

this phenotype might be enhanced in rats not only due to the long CAG repeat and the overexpression of mHTT, but also due to species-specific effects of large litter sizes and nursing effects, which are not present in humans. Thus, further investigations on HD patients are required to better understand the disease and to evaluate the role of body size and body composition phenotypes in HD.

Effects of altered body constitution on other phenotypes

(Publication VI[344])

Differences in body size and body composition in an animal model might obscure results obtained from behavioral analyses. For instance, it has been shown that Rotarod performance, a commonly used indicator for striatum-based motor dysfunction[346], depends on body weight with lighter animals performing better than heavier ones[347]. It was further found that motivational aspects play an important role in modulating motor test outcomes[348]. This again relates to differences in body constitution, as it has been shown that leptin, which is positively associated with the amount of white adipose tissue stored in the body[198], is a negative regulator of neuronal circuits of motivation[349].

In the light of these findings, and considering the abnormal body constitution observed in the BACHD rat, it was reasoned that the altered body constitution of BACHD rats likely modulates the outcome of tests based on the motivation to work for food rewards, a common strategy used for the positive reinforcement in conditioning experiments (Publication VI[344]). A variety of operant conditioning tests working with food reward are currently used in our laboratory for the cognitive characterization of the BACHD rat (Publication VI[344] and Jansson *et al.*, unpublished). Thus, it was of interest to investigate, if BACHD rats displayed altered motivation to work for food rewards. For this reason, the rats' performance was assessed in the progressive ratio (PR) test, a common motivational test, as well as in a free-feeding experiment measuring the rats' general hunger levels. When WT and BACHD rats were food-restricted to reach the same percentage of their free-feeding body weight, BACHD rats were less motivated in the PR test. However, the free-feeding test revealed that BACHD rats were *per se* less hungry under this food restriction regimen. Adjusting the level of food restriction

by feeding WT rats more than BACHD rats eliminated the difference in free food intake as well as in PR performance. This suggests that BACHD rats do not have a general lack of motivation, but need to be food-restricted differently from WT rats to be equally hungry due to their obscured body constitution. The idea is supported by the finding that food restriction to equal free-feeding and PR results, concomitantly led to a discrete difference in body weight between BACHD and WT rats, which reflected the difference in lean mass.

Measurement of energy homeostasis

(Publication I[350], II[142], VI[344], Appendix B, C and D)

Impaired growth and the development of obesity can be indicators of disrupted energy balance, which is characterized by a dysequilibrium in the relation of energy intake to energy expenditure. In order to investigate why BACHD rats display a distorted body constitution, aspects of the rats' energy balance were therefore assessed in several longitudinal studies.

Activity

Locomotor activity, a considerable contributor to energy expenditure, was measured in individually-housed rats kept for 70 hours in the PhenoMaster system (Publication II[142]). BACHD rats displayed reduced horizontal (ambulation) and vertical (rearing) activity compared to WT rats at 3 and 6 months of age, when a metal grid cage top (similar to the rats' home cage lid) was used. The difference in both parameters disappeared after changing to flat, solid, plastic lids in order to implement respirometric measurements at the age of 9 months, as described below. Although it is possible that the vanishing of this phenotype was due to age-related changes, this is rather unlikely as a second cohort of rats subsequently tested in the metabolic cage setup from 2 months onwards, did not show hypoactivity at any age (Appendix C). Thus, it is probable that the metabolic cage setup itself had influenced the behavior of the rats, possibly by leading to reduced activity of WT rats under these conditions.

In a separate study performed by collaboration partners[155], the activity of BACHD rats was reinvestigated during a 1 hour exposure to an empty arena. Interestingly, the rats exhibited initial hyperactivity at 1 month of age and a gradual decline in locomotor activity with age,

becoming significantly reduced compared to WT rats at 4 months. It is likely that the measurement of locomotor activity in such short trials reflects differences in exploratory behavior, anxiety or habituation rather than baseline activity. In this regard, BACHD rats have been found to be more explorative[155] as well as less anxious (Publication II[142] and VII) than WT rats using different tests. However, such differences might still be important, as they might translate into altered activity levels and affect daily energy expenditure under normal housing conditions.

Altogether, it remains uncertain, if the rats differ in their baseline locomotor activity. A separate analysis of locomotor activity starting before the age of 1 month and conducted in the rats' home cages might reveal a final conclusion. This should also preferably be performed with social groups rather than isolated animals, as the studies on the establishment of the PhenoMaster system have indicated potential stressful effects of the temporary isolation (Publication IV[332] and Appendix A).

Food intake

Data on food intake as a measure of energy intake were gathered in the PhenoMaster system in the course of study II[142] and VII (Appendix C). The overall amount of food consumed was significantly lower in the BACHD rat. However, considering that BACHD rats were found to be smaller than WT rats, this reduced food intake in absolute measures might simply reflect the rats' smaller body size. Relating food intake to body weight is unlikely to reveal a better measurement, as the rats also differ in body composition. Thus, the rats' food intake was normalized to their approximate lean mass to account for their smaller body size (Appendix C). After lean mass adjustment, BACHD rats showed significantly higher food intake at 2 months, and similar food intake compared to WT rats at older ages (Appendix C).

As the studies on establishing the PhenoMaster system had indicated that animals might not feed properly during the observation period (Publication IV[332] and Appendix A), the results were validated in a manual, longitudinal assessment of *ad libitum* food intake in a cohort of pair-housed BACHD and WT rats in their home cages (Publication VI[344]). Despite the initial doubts, the results from the second study replicated the earlier findings. The study confirmed

the increased food intake at early ages (here detected between the age of 6 and 9 weeks), and revealed stable, but moderately lower, food intake from approximately 19 weeks onward.

Interestingly, an additional difference in food spillage was detected between BACHD and WT rats, with BACHD rats leaving significantly less food spillage behind than WT rats (Publication VI[344]). It is unknown, if this reflects a lower amount of food spilled by the rats, or if BACHD rats eat more of the food dust they produced, since the food dust might be easier to access compared to the food in the food grid. This behavioral difference represents an interesting aspect for further evaluation and has to be taken into account in future studies involving food intake measurements in BACHD rats.

Water intake

During studies II[142], VI[344] (Appendix B) and VII (Appendix C), the rats' water intake was measured. BACHD rats showed dramatically reduced water intake in all studies. When the water intake measured in the PhenoMaster was normalized to lean mass, the phenotype vanished (Appendix C). However, the difference in absolute water intake was much more pronounced when measured in the rats' home cages, still suggesting a true difference.

Considering the results from the dissection study (Publication VI[344]), reduced water intake might be linked to the particularly low weights of organs involved in water balance, such as pancreas, salivary glands and kidneys (Appendix B). The results further imply that even though BACHD rats were obese, they did not develop diabetes at least until the age of 12 months, as this would typically be accompanied by increased water intake[351].

In an earlier study on water balance, which is commonly referred to, the assumption has been made that increased thirst and drinking reflect general features of HD[352]. However, the data presented in this study does not support the authors' conclusion. First, they had observed that R6/2 mice have a higher absolute water intake, but this was only found at older ages, when these mice tend to be diabetic[353]. Considering that R6/2 mice (like BACHD rats) have been described to have increased food intake at young ages[195], this suggests a reduced water to food ratio and thus reduced water consumption of R6/2 mice at young ages, similar to our findings. Second, HD patients had been asked to fill a questionnaire on dry mouth experiences, where they reported the frequent incidence of such situations. That the patients did frequently experience a feeling of dry mouth, however, rather points to inadequate fluid

intake or disturbed water balance, which would again indicate decreased and not increased water intake in relation to their demands.

Oxygen consumption rate and respiratory quotient

The PhenoMaster system was equipped to measure the rates of VO_2 and VCO_2 (Appendix C), which provide information on energy expenditure and substrate oxidation[354]. BACHD rats were found to have decreased absolute values of VO_2, but again the difference disappeared when related to lean mass.

Interestingly, a progressive increase in VO_2 was detected with age during the light phase, reaching statistical significance at 12 months. This finding was accompanied by a trend towards increased fine movements during the light phase at 12 months of age, and is reminiscent of higher sedentary energy expenditure found in early symptomatic patients due to chorea[162]. Thus, this might indicate that BACHD rats develop involuntary movements at older ages.

The presence of increased food intake despite similar levels of activity and VO_2 suggests that the rats were in a positive energy balance and might thus give an explanation for the development of obesity in the BACHD rat. On the other hand, increased food intake does not necessarily correlate with increased calorie intake. Gastrointestinal malabsorption has been described for HD mice[355] and might also be present in BACHD rats.

In line with the difference in relative food intake, an increase in the respiratory quotient (RQ, the ratio of VCO_2 to VO_2) was detected in the BACHD rat at 2 months of age, and a trend towards reduced RQ was found from 6 months onwards (Appendix C). Viewed together with the results on food intake and VO_2, this indicates a high energy demand at young ages, which is covered specifically by carbohydrate metabolism. A low RQ is typically found under starvation, when carbohydrate sources are unavailable. This latter result might be related to suppressed feeding in older animals in response to PhenoMaster exposure as shown earlier (Appendix A and Reference[336]). Since it is unclear, if BACHD and WT rats were similarly affected by the stress-inducing effect, the results should be interpreted with caution.

Defects in the regulation of metabolic functions have been implicated in HD[174]. Although, explicit studies on this issue were not performed, several observations suggest that regulatory function *per se* is not impaired in the BACHD rat. As BACHD rats have been found to grow

improperly, the increased food intake observed at young ages might be considered as a regulatory response to provide better nutritional supply and enhance growth. As BACHD rats further become obese, the subsequent reduction in food intake might be regarded as a regulatory response to counteract further fat accumulation. Another important regulatory function that concerns energy metabolism is the regulation of body temperature. N171-82 Q mice have been reported to have difficulties maintaining their body temperature, particularly upon cold exposure[216]. Cold stress response was not evaluated here, however body temperature was measured at baseline (Yu-Taeger *et al.*, unpublished) and during stress-induced hyperthermia experiments (Clemens *et al.*, unpublished). No difference between BACHD and WT rats were detected up to 12 months of age, further suggesting functional regulatory circuits at these ages.

Blood parameters as surrogate markers of HD

(Appendix D)

As blood parameters can be useful surrogate markers of disease, specific parameters related to the growth defect and obesity found in BACHD rats were investigated, and a serum metabolite profile was generated.

IGF-1 and leptin levels

In line with the body size and body composition phenotype of BACHD rats (Publication V[344] and Appendix B), plasma levels of IGF-1 were found to be decreased and leptin levels to be increased in BACHD compared to WT rats (Appendix D). Reduced IGF-1 levels were also detected in primary striatal neurons from BACHD rat embryos (Appendix E), underlining the contribution of this pathology to the BACHD rat phenotype, and pointing to an early deficit. Seemingly controversial results have been obtained for IGF-1 and leptin levels in patients and mouse models of HD. However, when taking a closer look, the results indicate that alterations in these two factors are quite certainly linked to mHTT expression, and that temporal changes in IGF-1 and leptin levels in the course of disease are responsible for the differential outcomes. Moreover, a masking effect of background strain differences, as well as a modulating effect of the specific characteristics of the mHTT protein introduced, likely contribute, as discussed in Appendix D.

Blood metabolite profile

Based on CSF and serum metabolites, a dysregulation of energy metabolism was found in the tgHD fragment rat model of HD[222], as analyzed by ^{1}H nuclear magnetic resonance spectroscopy (^{1}H NMRS) performed by a collaboration partner (Publication I[350]). An additional longitudinal analysis of serum samples from BACHD rats produced valuable data on the time course of metabolic alterations (Reference[356] and Appendix D). In this study, significant abnormalities in serum metabolites related to energy metabolism were detected in the BACHD rat. Reduced serum levels of glucose, lactate, and amino acids, as well as increased lipid levels were found at young ages, while an accumulation of glucose and lactate as well as the depletion of lipids was detected at old ages. These results are interpreted as a triphasic course of metabolic dysfunction, with an early phase of energetic restraint during the major growth phase due to impaired utilization of lipids for energy supply, a phase of normal metabolic function during adulthood, and a phase of energetic restraint due to impaired glucose utilization based on mitochondrial dysfunction during senescence.

The early deficit in lipid utilization cannot only explain the accumulation of fat mass, but also the growth deficit in the BACHD rats, as it suggests that the rats had to use amino acids to cover their energy demands, leading to a lack of building units for protein synthesis, and to reduced secretion of IGF-1[357].

Moreover, the results support the idea of temporal changes in the appearance of metabolic abnormalities. Early alterations seem to be triggered by the high energy demand of growth processes, while alterations at the late age of 18 months are likely associated with ageing, and mirror changes found in symptomatic HD patients. It is possible that similar, early changes are present in HD mutation carriers during development, but this has not been investigated so far. Furthermore, the temporal variability of metabolic alterations might possibly explain why metabolic abnormalities are not always detected in HD mutation carriers.

Summary and outlook

The studies demonstrate that BACHD rats show systemic metabolic abnormalities, which lead to growth impairment and obesity. The alterations underlie a specific temporal pattern related to growth and ageing, and are likely triggered by sustained compromise in mitochondrial function. Moreover, metabolic phenotypes can confound other test results.

The confounding effect of differences in body constitution on motivational aspects might underlie differences in leptin levels. Measurement of the rats' leptin levels at different food restriction regimes could reveal conclusions on this. A thorough reanalysis of behavioral parameters assessed in the rats so far on possible bias due to the obscured body constitution, should further be considered.

Concerning the temporal pattern of metabolic alterations, it would be particularly interesting to evaluate, if HD patients show similar early changes. In order to address this question, the analysis of metabolic dysfunction in HD patients would need to be extended to very early, presymptomatic ages, preferably to the growth phase. However, involving children at risk is difficult because of ethical concerns. Thus, another approach to evaluate the generality of these early alterations in HD would be to assess early metabolic dysfunction in other HD animal models.

For future studies on the BACHD rat, it would be important to implement younger as well as older ages into the screening. Concerning the young ages, malnourishment of pups during their early postnatal development might be a possible enhancing factor in the development of growth deficits, and could be causal for the variability observed in body weight among different cohorts. A study of the phenotypes of BACHD rats from large and small litters might shed light on this issue. Older ages would be interesting to assess, as it is possible that BACHD rats reach an age, where they ultimately start losing weight and show neurodegeneration similar to the late appearance of such phenotypes in the tgHD rat[141].

Finally, it would be of utmost interest to know what the initial events leading to fat accumulation and impaired glucose metabolism are. Still, only little is known about the exact cellular pathologies leading to these deficits[199,211]. Also, it is unclear to which proportion CNS and peripheral tissue dysfunction contribute to the initiation of systemic metabolic dysfunction. In this regard, the BACHD rat constitutes an excellent model to study the contribution of different organs to disease pathogenesis, as the transgene contains LoxP sites, which enable the directed inactivation of the gene through Cre-mediated excision. Studies on this have been made in the BACHD mouse, and the results suggest that the development of obesity depends largely on the expression of mHTT in the hypothalamus[194]. However, the cellular mechanisms behind this finding could not be identified so far[212,213].

Mitochondrial dysfunction

As mitochondrial dysfunction is a prominent feature of HD[257–262], and the investigations on systemic metabolic abnormalities of BACHD rats revealed indications for mitochondrial deficits, markers of mitochondrial function were analyzed e*x vivo*. Mitochondrial oxidative phosphorylation via the enzymes of the respiratory chain represents the major pathway of cellular energy production and hence an important target. Furthermore, compromised respiratory function might cause, or result from, other deficits such as reduced glycolytic flux or impaired mitochondrial network dynamics, which were also addressed in the following studies.

Mitochondrial respiration

(Publication III[358] and VII)

A collaboration partner investigated mitochondrial respiration in the presence of different substrates in primary cortical and striatal neurons from BACHD rat embryos (Publication III[358]). Interestingly, mitochondrial respiratory capacity rather than the activity of individual complexes was found to be compromised. This deficit was only observed in striatal neurons when relying on physiological levels of glucose for energy production. In the presence of supraphysiological glucose levels, or when supplemented with pyruvate or lactate, striatal neurons showed no deficits, suggesting hampered glycolytic flux as underlying cause. Anaerobic glycolysis was also found to be impaired in these cells. The findings suggest a defect in glycolysis rather than mitochondrial respiratory chain deficiency at early ages in the BACHD rat. Mitochondrial respiratory chain deficits are also not found in HD patients before reaching late stages[200], while decreased glycolytic capacity is detectable at prodromal stages[239].

However, it is important to note that the reactions of the glycolytic pathway are not disconnected from mitochondria. In particular, the initial step of glycolysis and crucial pacemaker for glucose import into cells, the phosphorylation of glucose by the enzyme hexokinase, depends on hexokinase binding to mitochondria[359].

In contrast to the results from primary embryonal cultures, a mild respiratory deficit was detected in live brain mitochondria from 13 months old BACHD compared to WT rats, with significantly lower complex II and IV activities (Publication VII). This deficit was accompanied by a distinct decrease in the protein levels of ATP synthase (Publication VII), suggesting reduced mitochondrial energy production in these rats. Reduced complexes II–IV activities have been found particularly in striata from HD patients[246,360]. The findings add support to the conclusion made from serum metabolite analysis, which is that dysfunctional mitochondrial respiration plays a role in the BACHD rat, but at older ages.

Ca^{2+} homeostasis

(Publication VII)

Changes in respiratory activity might in several ways be linked to altered Ca^{2+} homeostasis. Reduced mitochondrial respiratory activity might evoke increases in intracellular Ca^{2+}, as this would lead to impaired energy availability for maintenance of ion homeostasis and to reduced mitochondrial Ca^{2+} buffering capacity due to reduced mitochondrial membrane potential. On the other hand, increased intracellular Ca^{2+} levels might be causative for mitochondrial respiratory defects due to mitochondrial Ca^{2+} overload. Although there was no opportunity to directly measure Ca^{2+} levels, indications for disrupted Ca^{2+} homeostasis were found specifically in the cerebral cortex of 13 months old BACHD rats, as discussed below.

IP3R 1

BACHD rats showed increased cortical levels of the ER Ca^{2+}-exporter inositol-1,4,5-trisphosphate receptor 1 (IP3R 1), which is upregulated in response to elevated cytosolic Ca^{2+} levels[361] (Publication VII). Interaction with mHTT has been shown to facilitate IP3R 1 activity upon stimulation, and render neurons more vulnerable to excitotoxic stimuli[53,362]. Excessive IP3R 1-mediated Ca^{2+}-release into the cytosol can further prime apoptosis[363]. Thus, the finding suggests a selective dysregulation of Ca^{2+} balance in cortex of 13 months old BACHD rats, which might give rise to apoptotic cell death.

The calpain proteolytic system

Furthermore, an overactivation of the Ca^{2+}-dependent protease calpain-1 was detected in cortical but not striatal samples from BACHD rats (Publication VII). The enhanced calpain-1 activity was accompanied by reduced levels of the endogenous calpain inhibitor calpastatin, which is known to be degraded in the presence of high Ca^{2+} levels[364], further supporting the idea of cortical Ca^{2+} derangements in the BACHD rat at 13 months of age. Ca^{2+}-mediated calpain activation has been recognized as a major executer of degradation processes in neurodegenerative diseases[365–368] and plays a particular role in HD due to proteolytic cleavage of mHTT into the more toxic fragments[104,105]. Accordingly, enhanced cortical calpain-1 activation in the BACHD rat resulted in increased proteolytic cleavage of mHTT in this tissue (Publication VII). Furthermore, cortex hosted a higher amount of mHTT aggregates and showed stronger mHTT nuclear accumulation compared to striatum (Publication VII), in line with the idea that mHTT fragments are particularly prone to aggregate formation[93,100,101] and nuclear accumulation[85,89].

Interaction of mHTT with mitochondria

(Publication VII)

Accumulation of mHTT fragments on mitochondria is thought to be directly connected to mitochondrial dysfunction in HD[369]. In order to assess the possibility of a direct influence of mHTT on mitochondria, levels of mitochondria-associated mHTT were measured in isolated mitochondria from 13 months old rats. Both, HTT and mHTT, as well as full-length and fragmented forms of the proteins, were detected in these samples. Prominently, fragments were present in higher amounts in the mitochondrial fractions from BACHD rats, than in those from WT rats. It has previously been argued that binding of mHTT to mitochondria might disrupt the communication of the organelles with their surroundings, leading to a loss of mitochondrial sensory function and regulatory capacity[266,370]. Thus, the interaction of mHTT with mitochondria might ultimately be responsible for mitochondrial pathologies observed in the BACHD rat, and in HD in general.

Oxidative stress

(Appendix E)

Signs of oxidative stress have been detected in symptomatic HD patients[242,243,278–280], and can be cause for or consequence of mitochondrial deficits[371].

8OHdG

As a marker for oxidative stress that might arise from dysfunctional mitochondria[372], the amount of 8-hydroxy-2'-deoxy-guanosine (8OHdG) was measured in culture media from primary BACHD rat neurons (Appendix E). No differences between BACHD and WT rat primary neuronal cultures were found in the amount of 8OHdG produced. These results are in accordance with the general idea of oxidative damage being a rather late event in HD[200].

PGC-1α

The presence of mHTT fragments in cell nuclei is considered to cause transcriptional dysregulation. One important protein that has been shown to be affected is the peroxisome proliferator-activated receptor γ coactivator 1-α (PGC-1α), which mediates the transcriptional response to oxidative stress[373] and is believed to play a major role in the mitochondria-related pathology of HD[374,375]. To assess a possible role of PGC-1α for metabolic abnormalities in the BACHD rat, mRNA and protein levels were assessed. No differences in PGC-1α expression were detected between BACHD and WT rats at 13 months of age (Clemens *et al.*, unpublished), suggesting that oxidative stress might not be prominent at that age either. It is possible though that the expression levels of different splice variants of PGC-1α[376] or levels of downstream targets[211] are altered in BACHD rats instead, as such alterations have previously been described for HD. However, based on the results discussed so far, which point to a late onset of mitochondrial respiratory deficits in the BACHD rat, a prominent role of oxidative damage up to the age of 13 months is rather not expected.

Mitochondrial membrane fluidity

(Publication V[377])

The viscosity or fluidity of cellular membranes determines the properties of membrane-associated enzymes, receptors and ion channels[378–381] and might thus be connected to altered mitochondrial function in HD.

Mitochondrial membrane fluidity

Significantly increased mitochondrial but not plasma membrane fluidity was detected in 13 months old BACHD rats as well as two other HD models (the *Hdh*^{Q111} knock-in mouse as well as ST*Hdh*^{Q111} cells), suggesting that mitochondrial membrane fluidity changes represent a general pathological feature of HD (Publication V[377]). The role of mitochondrial membrane fluidity changes remains unclear though. Increased membrane fluidity in general is thought of as a coping strategy under conditions of reduced nutrient supply or increased energy demand[382–385], for which several indications were found in the BACHD rat. The changes might therefore reflect a mechanism to overcome energy shortage. However, it might at the same time leave the cells more vulnerable towards stressors, as increased mitochondrial membrane fluidity has been specifically linked to mPT[386–388].

Mitochondrial membrane cholesterol

Cholesterol is the major determinant of membrane fluidity[389]. As disturbances in cholesterol metabolism and associated cholesterol deficits have been described in HD[329,390,391], levels of mitochondrial membrane cholesterol were determined. However, out of the three HD models investigated, a reduction of membrane cholesterol, concomitant with increased membrane fluidity, was only detected in the BACHD rat (Publication V[377]). This implies that either the increased membrane fluidity was not caused by a cholesterol deficit, or that the detection of cholesterol deficits in the other models had failed. The latter has to be considered, since methodological shortcomings of measuring cholesterol levels have been pointed out recently and held responsible for contradictive findings on cholesterol levels in HD[392]. As changes in membrane fluidity were found to be restricted to mitochondrial membranes, it is possible that specifically the import of cholesterol into mitochondria might be responsible for this phenotype.

In this regard, mHTT has been reported to bind to the outer mitochondrial membrane transporter VDAC[393], which regulates cholesterol import into mitochondria[394]. Thus, VDAC constitutes a potential target for further studies on the connection between membrane fluidity changes, mitochondrial cholesterol import and mitochondrial mHTT accumulation.

Mitochondrial dynamics

(Publication VII and Appendix E)

In order to investigate, if other mitochondrial deficits are present, which might account for the respiration deficit observed in the BACHD rat, or otherwise contribute to impaired intracellular energy supply, mitochondrial network dynamics were analyzed. Dynamic functions are crucial for mitochondrial network integrity[281] and disturbances are highly implicated in HD[260].

Fusion and fission

The levels of the mitochondrial fusion-promoting factors mitofusin (Mfn) 1 and 2, as well as optic atrophy (Opa) 1, and the fission-promoting factors fission (Fis) 1 and dynamin-related protein (Drp) 1, which are crucial for mitochondrial morphological adaptations[395], were measured in cortical and striatal brain lysates from 13 months old rats (Publication VII). A tendency to reduced levels of fusion factors and increased levels of fission factors was detected on mRNA (Clemens *et al*., unpublished) and protein level (Publication VII).

As changes in the levels of fusion and fission factors have only been reported for late stage HD patients[284], this finding is again in line with the idea that 13 months old BACHD rats do not suffer from profound mitochondrial impairments and are not in a condition reminiscent of end-stage HD. However, mitochondrial deficits might start to develop in BACHD rats around the age of 13 months, as indicated by the respiratory deficit and the cortex-restricted Ca^{2+} derangements. Specifically, increased cytosolic Ca^{2+} levels have been linked to disrupted mitochondrial dynamics. Ca^{2+} activates the phosphatase calcineurin, leading to the dephosphorylation of Drp 1 and its translocation to mitochondria[282]. Moreover, Ca^{2+} activates calpains (which was detected in the cortex of 13 months old BACHD rats in Publication VII), resulting in the degradation of Mfns[396]. In addition, calpain-derived mHTT fragments

accumulate on mitochondria, where mHTT has been shown to bind to Mfn 2[267] and Drp 1[285,287] and to enhance Drp 1's fission-promoting activity[285,287]. That these processes are important for the pathogenesis of HD has been demonstrated by the finding that both overexpression of Mfn 2 and Opa 1, as well as functional silencing of Drp 1, can rescue mHTT-expressing cells from mitochondrial dysfunction and improve cell survival[267,282].

Axonal mitochondrial transport

A second important aspect of mitochondrial dynamics is the organelles' intracellular transport in response to local demands[397]. To assess possible transport defects, the transport of mitochondria along axonal processes was recorded in primary cortical and striatal neurons from BACHD rat embryos (Appendix E). Significantly reduced relative motility of mitochondria was observed in both cortical and striatal cultures from BACHD rats. As such transport defects have been found in embryonal cultures from other HD disease models[287], this phenotype seems to constitute a general and very early HD-related pathology.

It is debated[398], whether axonal transport defects occur due to physical hindering by mHTT aggregates[399] or the loss of a promoting effect of HTT on axonal trafficking[288]. The latter might to some degree also be influenced by the presence of aggregates, as HTT is sequestered into these structures. The results from the present study suggests a rather minor role of aggregate load in promoting axonal transport defects, as impaired mitochondrial motility was found to be of similar magnitude in striatal and cortical neuronal cultures, although aggregates are found in much higher concentration in cortex (demonstrated for BACHD rats in Publication II[142], for BACHD rat primary neurons in Publication III[358] and Appendix E, and for HD patients in Reference[86]).

Several other mechanisms have been described, which might be responsible for axonal transport defects in the BACHD rat. It has been shown that decreased phosphorylation of HTT due to disrupted IGF-1/Akt signaling halts axonal transport processes[400]. As decreased levels of IGF-1 were also observed in the BACHD rat primary neuronal cultures (see Appendix E), this might provide a reasonable explanation for the reduced motility. Two further mechanisms have recently been highlighted: The first one concerns reduced translocation of GAPDH to vesicles, a process mediated by HTT, and disrupted in the presence of mHTT[401]. The other one regards the blockage of the mitochondrial Rho-GTPase Miro 1, which links the transport

machinery to mitochondria via connection with Mfn 2[402,403]. A direct link to HD has not been established yet, but Ca^{2+}-mediated disruption of Miro 1 binding to mitochondria[404] has been described for a model of ALS. This mechanism might contribute to HD-related transport defects, given that Ca^{2+} derangements are early features of HD[264] and the enhanced binding of mHTT to Mfn 2 might disturb the interaction of Mfn 2 with Miro 1.

Summary and outlook

Our data suggest that mitochondrial disturbances can be detected at earliest ages, although mitochondrial respiratory chain dysfunction is likely a late event. Moreover, mitochondrial dysfunction might results from abnormal binding of mHTT to the organelles.

In order to add evidence to the hypothesis of profound mitochondrial damage as a late event in the pathogenesis of HD, further studies should investigate both glycolytic and mitochondrial respiratory chain function longitudinally from birth to senescence. This would enable to evaluate when the deficits appear, how they progress with age and how they might be interrelated.

Many of the findings are potentially linked to a direct pathological effect of mHTT binding to mitochondria. Further studies should address the physiological role of HTT binding to mitochondria and the pathological consequences of mitochondria-associated mHTT in order to reveal better insight into the molecular mechanisms of mitochondrial dysfunction in HD. Such studies should further evaluate possible links between the mitochondrial pathologies, as some proteins such as VDAC and Mfn 2 seem to be ubiquitously involved. The identification of common pathways might offer better targets for future therapeutic approaches.

Conclusion

Metabolic dysfunction has emerged as a prominent feature of HD. However, many questions around the development, characteristics and importance of metabolic abnormalities are still awaiting an answer. Major reasons for this are the lack of detailed longitudinal data from HD patients, particularly including early prodromal stages, as well as seemingly contradicting results from rodent models of HD. The present work implies that discrepancies in study outcomes might be due to temporal changes in surrogate markers in the course of disease.

In case of the BACHD rat, this manifests in a triphasic pattern of metabolic abnormalities with early changes during growth, normal values during adulthood, and late alterations during senescence. Mitochondria-associated deficits are present at early ages, but the burden of mitochondrial dysfunction with respiratory chain impairment most likely forms a later event (Figure 4).

The individual phenotypes detected in the BACHD rat might be regarded as a network of interconnected pathologies, evoking and enhancing each other (Figure 5). The presence of mHTT leads to deficits in mitochondria-associated cellular pathways of energy metabolism. Prominently, a deficit in lipid oxidation likely triggers fat accumulation and the development of obesity, and further contributes to energetic deficits. Energetic deficits in turn are probably responsible for the improper growth and the smaller body size of the BACHD rats. Finally, it is reasonable to assume that mitochondrial function becomes increasingly impaired as the rats age, eventually triggering the degeneration of tissues vulnerable to energetic deficits.

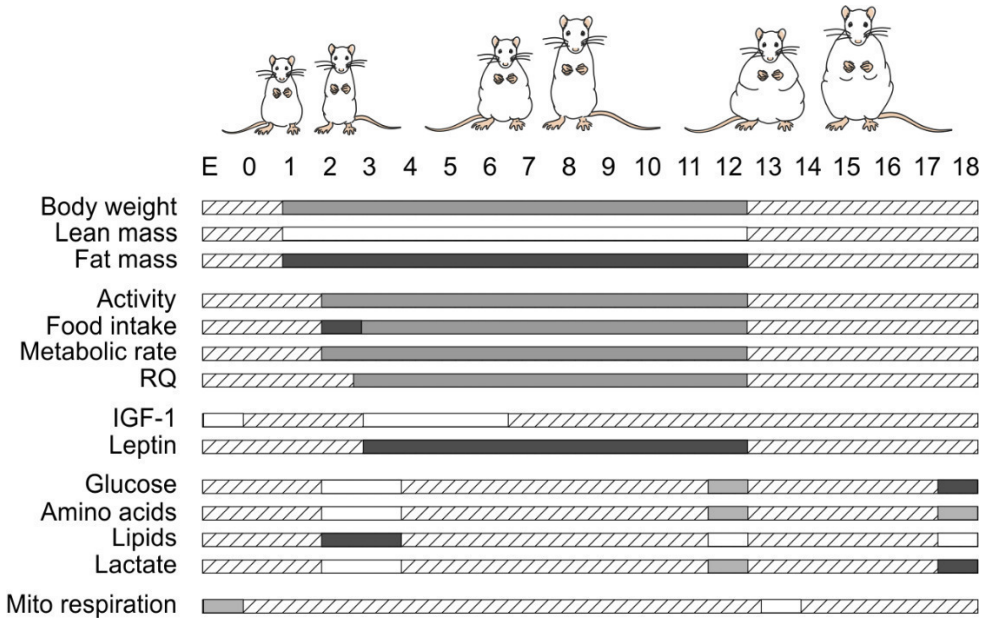

Figure 4. Summary of metabolic abnormalities in the BACHD rat

The scheme shows the metabolic abnormalities detected in BACHD rats at different ages, with white squares meaning reduced compared to WT rats, light gray squares meaning similar to WT rats and dark gray squares meaning increased compared to WT rats. The age at observation is indicated in the top line in monthly steps from prenatal (E) to 18 months of age. The gross morphological appearance of young, middle-aged and old rats is illustrated on top of the scheme.

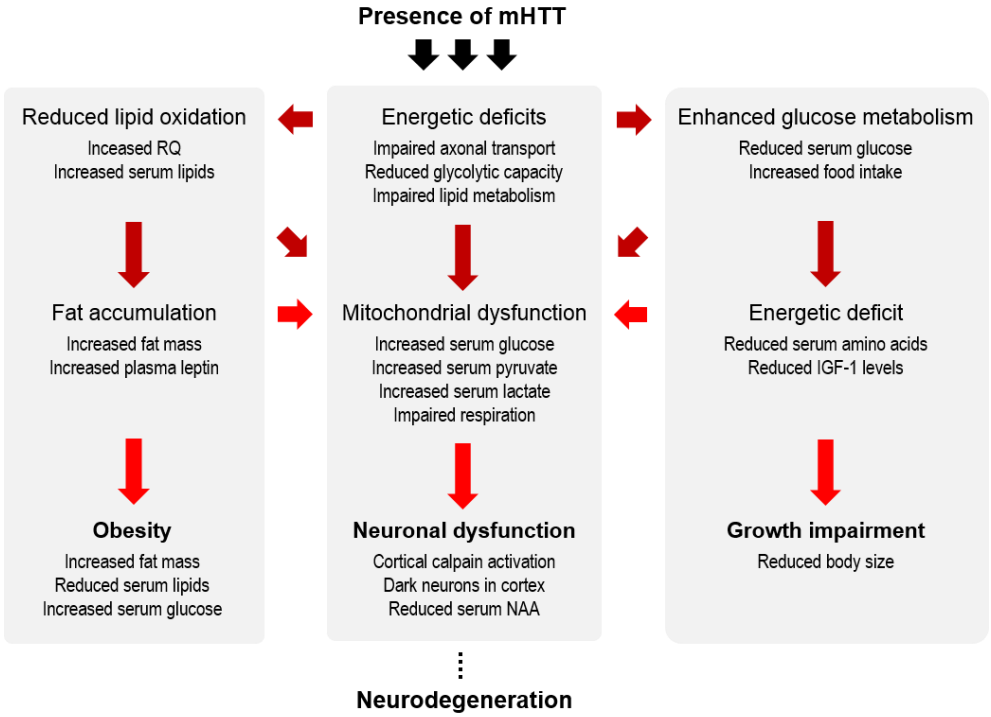

Figure 5. Possible interconnectivity of metabolic phenotypes in the BACHD rat

The presence of mHTT leads to discrete deficits in mitochondria-associated cellular pathways of energy metabolism, which are likely to be the cause for growth impairment and obesity. Furthermore, mitochondrial function becomes increasingly compromised with age, and might finally culminate in neuronal demise. The arrows represent the hypothetical connections between the phenotypes investigated.

III. Olesoxime treatment study

In a longitudinal therapeutic study, BACHD rats were treated with olesoxime supplied via the food from the age of 5 weeks until the age of 13 months, their behavior and metabolic function was assessed, and neuropathological phenotypes were investigated.

The chapter is divided into four major parts:

- Main effects of olesoxime
- Mechanism of action of olesoxime
- Outlook
- Conclusion

Main effects of olesoxime

Olesoxime-treated BACHD rats showed specific improvements in behavior and neuropathology compared to placebo-treated BACHD rats (Publication VII, Appendix B and C). These concerned the selective amelioration of cognitive and psychiatric abnormalities, increased cortical thickness and a significant reduction in mHTT aggregation and nuclear accumulation throughout the brain. The drug effect appeared to be the result of reduced calpain-mediated proteolysis, which seemed to be the main source of mHTT fragments in the BACHD rat (Publication VII). Furthermore, olesoxime seemed to have influenced mitochondria in several ways (Publication V[377] and VII): Olesoxime treatment led to a restoration of mitochondrial membrane fluidity and respiratory function, and reduced the association of mHTT fragments with mitochondria. It further modulated the levels of several mitochondrial proteins involved in mitochondrial cholesterol import, metabolite exchange, respiratory chain function, Ca^{2+} homeostasis, calpain activation and mitochondrial dynamics, all of which could have contributed to improved mitochondrial function, enhanced Ca^{2+} handling capacity and reduced calpain activity.

Mechanism of action of olesoxime

The calpain proteolytic system

(Publication VII)

The most prominent effect of olesoxime was the reduction of calpain-1 overactivation and concomitant inhibition of mHTT fragmentation in BACHD rat cortex (Publication VII). A parallel decrease in calpain-1 activity and increase in calpastatin expression was detected (Publication VII), which represents a reversion of the initial pathological condition found in the BACHD rat (as discussed above). It is theoretically possible that the primary effect of olesoxime was a transcriptional upregulation of calpastatin, as calpastatin overexpression has been shown to abolish calpain activation and to have cytoprotective effects[405]. However, a more simple explanation is that calpastatin levels were restored as a downstream event of reduced calpain-1 activation, as calpastatin itself is a calpain target[364]. In addition, it is rather unlikely that olesoxime directly influenced transcription, as it has been found to be exclusively localized at mitochondria[314]. For the same reason, it is unlikely that olesoxime had acted as a direct inhibitor of calpains, but rather indirectly influenced their activation status via effecting mitochondria.

Ca^{2+} homeostasis

(Publication VII)

Given the mitochondrial localization of olesoxime[314], it was hypothesized that the compound had exerted its beneficial effects by improving mitochondrial function, thereby stabilizing Ca^{2+} homeostasis, decreasing Ca^{2+}-related calpain-1 activation and aborting the generation of toxic mHtt fragments, as well as their exaggerated negative influence on mitochondria. The finding of overactive calpain-1 and increased protein levels of IP3R 1 in untreated BACHD rats (Publication VII) support the idea of disturbed Ca^{2+} homeostasis, as discussed above. However, since there was no opportunity to measure Ca^{2+} levels, Ca^{2+} handling or the effects of olesoxime on Ca^{2+} balance in the BACHD rats directly in this study, the proposed mechanism remains hypothetical.

Mitochondrial permeability transition

(Publication VII)

Olesoxime has previously been suggested to inhibit mPT[313], but thus far a detailed mechanism could not be provided. On the contrary, there are indications that olesoxime (unlike the mPT inhibitor cyclosporine A) does not directly affect mitochondrial Ca^{2+} release and mitochondrial swelling in isolated organelles[314]. Instead, olesoxime inhibited the release of apoptosis-inducing factor (AIF)[319], which triggers cell death in an mPT-independent way[382]. Interestingly, calpains (which were found to be inhibited by olesoxime treatment in Publication VII) have been shown to mediate AIF release[406,407], which is executed in the presence of sufficiently high Ca^{2+} levels[408]. Thus, it is possible that olesoxime does not modulate mPT, but rather prevents AIF release through improved cellular Ca^{2+} handling and alleviation of calpain activation.

Interaction with VDAC and TSPO

(Publication VII)

Olesoxime has previously been shown to bind to VDAC and TSPO on the outer mitochondrial membrane[313]. VDAC seems to be particularly interesting, as also mHTT has been shown to interact with this protein[393], and VDAC is standing at the junction of glycolytic and mitochondrial respiratory function in the cell[359] (as explicated above). It has earlier been suggested that the interaction of mHTT with VDAC might impair the protein's transport function, and be responsible for deficits in mitochondrial energy metabolism[409]. Thus, reduction of mHTT fragment accumulation at mitochondria might improve the communication of the organelles with their surroundings, leading to a compensatory upregulation of VDAC protein expression (as observed in Publication VII), improved mitochondrial-cytoplasmic metabolite exchange and amelioration of cellular and mitochondrial deficits.

The study did not include the evaluation of olesoxime's influence on TSPO, which might also be involved in mediating its beneficial effects. Interestingly, TSPO ligands enhance γ-aminobutyric acid (GABA) signaling with similar effects on psychiatric disturbances as revealed by carbamazepine treatment[410]. Carbamazepine acts anticonvulsant, mood-stabilizing and reduces neuropathic pain. It is known to potentiate GABA signaling, and was found to reduce intracellular Ca^{2+} levels, calpain activation, mPT and cell death in

ischemia/reperfusion injury[411]. As this is highly reminiscent of the effects observed in this study (Publication VII), it seems likely that olesoxime's actions are, at least in part, mediated via enhanced TSPO function.

Both VDAC and TSPO are implicated in mitochondrial cholesterol import[412], and olesoxime restored mitochondrial cholesterol levels as well as membrane fluidity changes in the BACHD rat (Publication V[377]), further strengthening the idea of a crucial involvement of these two proteins in mediating olesoxime's beneficial effects.

Selective olesoxime effects in the BACHD rat

(Publication V[377], VII, Appendix C and D)

Olesoxime ameliorated deficits, which were selectively found in cortex but not striatum of BACHD rats (Publication VII). The absence of increased IP3R 1 levels, calpain-1 overactivation and extensive mHTT fragmentation in striatum suggests that Ca^{2+} derangements were not present in this tissue at 13 months of age. This could be due to an adaptive response of striatal neurons to Ca^{2+} insults, as a compensatory change in Ca^{2+} sensitivity has been reported for striatal but not cortical neurons from HD mouse models[301]. The results are further in accordance with our earlier findings, which show that signs of neurodegeneration can be found in cortex but not striatum of 13 months old BACHD rats (Publication II[142]).

Olesoxime also showed selective beneficial effects on systemic phenotypes. Although olesoxime restored the mitochondrial respiration deficit (Publication VII) and membrane fluidity changes (Publication V[377]), the drug failed to ameliorate systemic metabolic abnormalities in the BACHD rat, specifically the rats' obesity and growth defect as well as the associated changes in food intake, RQ, plasma IGF-1 and leptin levels (Appendix C and D). This implies that mitochondrial respiratory chain defects and altered membrane fluidity were not the primary cause for the systemic metabolic abnormalities in HD. In case of the respiration defect, this assumption would be in line with the idea that this pathology is a later event in HD.

Importantly, it is possible that olesoxime is not *per se* incapable of restoring systemic metabolic alterations. Considering the early appearance of metabolic abnormalities in the

BACHD rat, treatment might have simply started too late, and have only been ineffective in restoring phenotypes, which were already manifest. This is supported by the finding that olesoxime treatment in late stage ALS patients did not yield significant improvements[327], while the compound was highly effective in preclinical studies in ALS models where treatment had started early[322]. Moreover, treatment of children and young patients with SMA led to strong, beneficial outcomes[328].

Olesoxime in other HD animal models

(Publication V[377])

As mitochondrial dysfunction and Ca^{2+} dysregulation are consistent features of HD across different animal models, benefits from olesoxime treatment can be expect to be found beyond the BACHD rat. In this regard, olesoxime reversed alterations in mitochondrial membrane fluidity not only in the BACHD rat, but also in the *Hdh*^{Q111} knock-in mouse and ST*Hdh*^{Q111} cell model of HD (Publication V[377]). It is unclear though, how effective olesoxime treatment would be in a fragment model of HD, as the reduction in mHTT fragment generation might only be marginal due to constitutive expression of mHTT fragments through the transgene. In spite of this fact, investigation of olesoxime's effects in such a model would be of great interest for the dissection of direct effects of olesoxime on mitochondrial function, and indirect treatment effects via reduced fragment generation.

Outlook

Earlier start of treatment

In order to evaluate, if some selective effects of olesoxime were caused by its application after symptom onset, earlier start of treatment should be considered. In a first follow-up study, this was approached by starting olesoxime treatment in the *Hdh*^{Q111} knock-in mouse model of HD, already in the pregnant mother animal in order to exploit the full potential of the drug (Clemens *et al.*, unpublished). Thus far, only the molecular phenotypes of these mice were investigated to evaluate if the phenotypes found in the BACHD rat are recapitulated and to estimate sample sizes for main cohorts (Clemens and Weber *et al.*, unpublished). Future studies should investigate the effects of olesoxime on behavior and neuropathology upon earliest possible treatment. If olesoxime proves to be more efficient under these conditions, it might further be evaluated if drug application can be shifted towards postnatal ages. This might at the same time shed light on the time course of early HD-related phenotypes.

Mechanistic approach

To rule out the unlikely but still possible influence of olesoxime on gene expression, mRNA levels of proteins found to be altered upon olesoxime treatment should be assessed quantitatively.

To gain further insight into the mechanism behind olesoxime's actions, its exact role in Ca^{2+} homeostasis needs to be evaluated. In this regard, a study on Ca^{2+} handling in ST*Hdh*^{Q111} and other cells has been started. Preliminary results from fluorescence calcium imaging point to an increase in internal Ca^{2+} storage, suggesting improved Ca^{2+} handling capacity after olesoxime treatment (Klumpp, Weber and Clemens *et al.*, unpublished). Further studies should dissect the contribution of ER and mitochondria to the enhanced Ca^{2+} storage and favorably include *in vivo* calcium imaging[413].

In addition to Ca^{2+} homeostasis, it would be of importance to know if olesoxime affects glycolysis, as defects in glycolysis are implicated in early HD[239] and seem to be among the earliest signs of energetic defects in the BACHD rat (Publication III[358]). As explained above, hexokinase binding to VDAC provides a potential target, which should be further investigated.

Study validation

Validation of olesoxime's effects should be carried out in other full-length mHTT or fragment models of HD. This would further enable to investigate the contribution of reduced mHTT fragmentation to the beneficial effects of olesoxime, as discussed above. A pilot study to reproduce olesoxime's effects in *Hdh*^{Q111} knock-in mice has already been undertaken. Preliminary results revealed that similar pathological calpain activation and mHTT cleavage takes place in these mice, and that olesoxime counteracts this pathology (Clemens and Weber *et al.*, unpublished).

Summary and conclusion

Olesoxime constitutes an outstanding drug candidate for HD. The beneficial effects observed here, together with the positive outcomes of preclinical studies in several neurodegenerative disorders as well as the clinical trial on SMA suggest a high chance to achieve beneficial effects also in HD patients. Moreover, its high safety and tolerability as well as easy application pave the way to faster clinical use compared to a novel drug.

For further studies, it needs to be considered that olesoxime treatment might prove to be most effective when started early on. Due to the sole genetic mutation underlying the development of HD, HD patients have the opportunity to know about their disease before the onset of clinical symptoms. This enables to start treatment early and receive highest potential benefits from it.

Olesoxime's presumed mechanism of action is to improve mitochondrial function and through this regulate energy metabolism and Ca^{2+} balance as well as downstream pathologies. It was discovered that calpain activation is one of these downstream targets, and the calpain-calpastatin system has emerged as a key player in neurodegenerative diseases. Thus, not only the primary target of olesoxime, the mitochondrial network, but also its secondary one, the calpain system, might be responsible for its ubiquitous beneficial effects in neurodegeneration.

Although the details on how olesoxime stabilizes mitochondria are still elusive, the present studies suggest an important role for olesoxime in modulating the mitochondrial membrane environment. Deciphering olesoxime's mechanism of action might be of great value for the understanding of neurodegenerative processes and the development of effective treatments.

Funding

Research was funded by yearly funds allocated to the Institute of Medical Genetics and Applied Genomics by the Medical Faculty of the University of Tuebingen, to maintain animals, and the European Union 7th Framework Program for RTD, Project MitoTarget, Grant Agreement HEALTH-F2-2008-223388.

Acknowledgements

Author's comment

The random collection of information has been pressed into a form; probably not the best text I have ever written, but most certainly the longest. I want to apologize retrospectively for all the long and complicated sentences that might have remained even after rigorous red-marking and in-half-cutting by my proof-reading friends.

My work involved many animals, and as much as I know that I did my best to treat them with love, care and respect, I am uncertain if it can ever be justified to take a creature's life for the benefit of a human being. However, I truly hope that my work at least fulfilled its purpose by contributing to the understanding of HD and getting a tiny step closer to finding a treatment for this disease.

Many people contributed in different ways during the generation of this work, for which I would like to express my honest gratitude.

Contributors

First of all, I would like to thank my supervisors, Olaf Rieß and Hoa Nguyen, for their trust in and support of my work, as otherwise this thesis would not have happened. I hope you regard my work as a useful contribution to your scientific field.

I am grateful to all MitoTarget members for fruitful collaborations. In particular, many thanks to Rebecca Pruss, Thierry Bordet, Julien Veys and Caroline Gouarné from Trophos for continued support beyond project borders.

Thanks a lot to all other coauthors, who collaborated with me on the various projects included in my thesis.

I would like to thank the technicians Celina Tomczak, Therese Stanek, Patrycja Bambynek-Dziuk and Gregor Pahnke for support with animal caretaking, breeding, genotyping, blood sampling, body weight assessment, measurement of food and water intake as well as automated behavioral phenotyping.

Many thanks to all of my students (in chronological order): Alissa Mittnik, Borka Jojic, Tanja Wlodkowski, Jasmin Richlick, Damaris Franke, Tatiana Serr, Thomas Schlaich, Marco Seehawer, Lukas Klumpp and Elisabeth Singer. You contributed significantly to my work, and I had lots of fun working with you. I hope, I could teach you something valuable for your future research career.

I want to further thank all members of the Institute of Medical Genetics and Applied Genomics for an always friendly work atmosphere, and my direct colleagues for sharing good and bad lab times, for providing a research community without rivalry, and simply for being super nice people.

Some people provided their professional support during the preparation of this manuscript. Thanks, I owe you much, Erik Jansson, Janine Magg, Nicolas Casadei, Julian Clemens, Carolin Walter, Stefanie Flunkert, Meike Diepenbroek, Tobias Kittel, Tina Binder and Libo Yu-Taeger.

I am more than grateful that you were not only colleagues but also friends (this is roughly in the order I learned to know you): Jasmin Ehrismann, Libo Yu-Taeger, Janine Magg, Alexandra Kelp, Catherine Thömmes, Meike Diepenbroek, Nicolas Casadei, Esteban Portal, Karin Schäferhoff, Carolin Walter, Jonasz Weber, Tina Binder, Florian Harmuth, Anna Sowa, Sven Poths, Zinah Wassouf, Daniel Weishäupl, Arianna Novati and Giuseppe Manfré.

Many, many thanks to my family and my friends, who (I hope so) still love me, despite barely seeing me ever during my studies. Papa, Mama, Marie, Toni und Professor Knirpsi, Jule und Katha, Hanni und Robin, Oma Agnesi, Oma Nelly und Opa Kurt, Tante Anne, Onkel Patrick, Sébastien und Céline, Tati und Winni, Tati Tine, Onkel Heinz, Christian, Anna, Gregor und Max, Tante Monika, Tante Ilse, Tante Marianne, Tante Susanne, Onkel Jürgen, Markus und Thorsten, Tante Christel und Onkel Michael, Martin, Rebecca und Marc, Oli und Bernd, Sara, und Nin und Steff. My biggest wish is to spend more time with you in the future, and I know that only I can make this change happen. Love you all.

Finally. The most special thanks are due to my ‘colleague and good friend’ (so good that you will be my future husband) Erik Karl Håkan Jansson (the one and only), for your endless patience and support. This work would not be the same without you.

And many thanks to Frau Kerstin Ack.

References

1. Harper, P. S. The epidemiology of Huntington's disease. *Hum. Genet.* **89,** 365–76 (1992).
2. Pringsheim, T. *et al.* The incidence and prevalence of Huntington's disease: A systematic review and meta-analysis. *Mov. Disord.* **27,** 1083–1091 (2012).
3. Fisher, E. & Semaka, A. How Many People Have Huntington Disease? *HD Insights* **1,** 2 (2011).
4. Bates, G. P., Harper, P. S. & Jones, L. *Huntington's Disease*. (Oxford University Press, 2002).
5. Anderson, K. E. & Marder, K. S. An overview of psychiatric symptoms in Huntington's disease. *Curr. Psychiatry Rep.* **3,** 379–88 (2001).
6. Papoutsi, M., Labuschagne, I., Tabrizi, S. J. & Stout, J. C. The cognitive burden in Huntington's disease: pathology, phenotype, and mechanisms of compensation. *Mov. Disord.* **29,** 673–83 (2014).
7. Poudel, G. R. *et al.* Abnormal synchrony of resting state networks in premanifest and symptomatic Huntington disease: the IMAGE-HD study. *J. Psychiatry Neurosci.* **39,** 87–96 (2014).
8. Tabrizi, S. J. *et al.* Biological and clinical changes in premanifest and early stage Huntington's disease in the TRACK-HD study: the 12-month longitudinal analysis. *Lancet. Neurol.* **10,** 31–42 (2011).
9. Dogan, I. *et al.* Consistent neurodegeneration and its association with clinical progression in Huntington's disease: a coordinate-based meta-analysis. *Neurodegener. Dis.* **12,** 23–35 (2013).
10. Vonsattel, J. P. *et al.* Neuropathological classification of Huntington's disease. *J. Neuropathol. Exp. Neurol.* **44,** 559–77 (1985).
11. Tabrizi, S. J. *et al.* Biological and clinical manifestations of Huntington's disease in the longitudinal TRACK-HD study: cross-sectional analysis of baseline data. *Lancet. Neurol.* **8,** 791–801 (2009).
12. Vonsattel, J. P. & DiFiglia, M. Huntington disease. *J. Neuropathol. Exp. Neurol.* **57,** 369–84 (1998).
13. Kassubek, J., Gaus, W. & Landwehrmeyer, G. B. Evidence for more widespread cerebral pathology in early HD: an MRI-based morphometric analysis. *Neurology* **62,** 523–4; author reply 524 (2004).
14. Waldvogel, H. J., Kim, E. H., Thu, D. C. V, Tippett, L. J. & Faull, R. L. M. New Perspectives on the Neuropathology in Huntington's Disease in the Human Brain and its Relation to Symptom Variation. *J. Huntingtons. Dis.* **1,** 143–53 (2012).
15. Paulsen, J. S. *et al.* Detection of Huntington's disease decades before diagnosis: the Predict-HD study. *J. Neurol. Neurosurg. Psychiatry* **79,** 874–80 (2008).
16. Ross, C. A. *et al.* Huntington disease: natural history, biomarkers and prospects for therapeutics. *Nat. Rev. Neurol.* **10,** 204–16 (2014).
17. The Huntington's Disease Collaborative Research Group. A novel gene containing a trinucleotide repeat that is expanded and unstable on Huntington's disease chromosomes. The Huntington's Disease Collaborative Research Group. *Cell* **72,** 971–83 (1993).
18. Brinkman, R. R., Mezei, M. M., Theilmann, J., Almqvist, E. & Hayden, M. R. The likelihood of being affected with Huntington disease by a particular age, for a specific CAG size. *Am. J. Hum. Genet.* **60,** 1202–10 (1997).
19. Duyao, M. *et al.* Trinucleotide repeat length instability and age of onset in Huntington's disease. *Nat. Genet.* **4,** 387–92 (1993).
20. Hendricks, A. E. *et al.* Estimating the probability of de novo HD cases from transmissions of expanded penetrant CAG alleles in the Huntington disease gene from male carriers of high normal alleles (27-35 CAG). *Am. J. Med. Genet. A* **149A,** 1375–81 (2009).
21. Falush, D., Almqvist, E. W., Brinkmann, R. R., Iwasa, Y. & Hayden, M. R. Measurement of mutational flow implies both a high new-mutation rate for Huntington disease and substantial underascertainment of late-onset cases. *Am. J. Hum. Genet.* **68,** 373–85 (2001).
22. Kremer, B. *et al.* Sex-dependent mechanisms for expansions and contractions of the CAG repeat on affected Huntington disease chromosomes. *Am. J. Hum. Genet.* **57,** 343–50 (1995).
23. Trottier, Y., Biancalana, V. & Mandel, J. L. Instability of CAG repeats in Huntington's disease: relation to parental transmission and age of onset. *J. Med. Genet.* **31,** 377–82 (1994).
24. Stine, O. C. *et al.* Correlation between the onset age of Huntington's disease and length of the trinucleotide repeat in IT-15. *Hum. Mol. Genet.* **2,** 1547–9 (1993).

25. Lee, J.-M. *et al.* CAG repeat expansion in Huntington disease determines age at onset in a fully dominant fashion. *Neurology* **78,** 690–5 (2012).
26. Andrew, S. E. *et al.* The relationship between trinucleotide (CAG) repeat length and clinical features of Huntington's disease. *Nat. Genet.* **4,** 398–403 (1993).
27. Telenius, H. *et al.* Molecular analysis of juvenile Huntington disease: the major influence on (CAG)n repeat length is the sex of the affected parent. *Hum. Mol. Genet.* **2,** 1535–40 (1993).
28. Goebel, H. H., Heipertz, R., Scholz, W., Iqbal, K. & Tellez-Nagel, I. Juvenile Huntington chorea: clinical, ultrastructural, and biochemical studies. *Neurology* **28,** 23–31 (1978).
29. Foroud, T., Gray, J., Ivashina, J. & Conneally, P. M. Differences in duration of Huntington's disease based on age at onset. *J. Neurol. Neurosurg. Psychiatry* **66,** 52–6 (1999).
30. Gusella, J. F., MacDonald, M. E. & Lee, J.-M. Genetic modifiers of Huntington's disease. *Mov. Disord.* **29,** 1359–65 (2014).
31. Van Dellen, A., Grote, H. E. & Hannan, A. J. Gene-environment interactions, neuronal dysfunction and pathological plasticity in Huntington's disease. *Clin. Exp. Pharmacol. Physiol.* **32,** 1007–19 (2005).
32. Li, S. H. *et al.* Huntington's disease gene (IT15) is widely expressed in human and rat tissues. *Neuron* **11,** 985–93 (1993).
33. Strong, T. V *et al.* Widespread expression of the human and rat Huntington's disease gene in brain and nonneural tissues. *Nat. Genet.* **5,** 259–65 (1993).
34. Landwehrmeyer, G. B. *et al.* Huntington's disease gene: regional and cellular expression in brain of normal and affected individuals. *Ann. Neurol.* **37,** 218–30 (1995).
35. Trottier, Y. *et al.* Cellular localization of the Huntington's disease protein and discrimination of the normal and mutated form. *Nat. Genet.* **10,** 104–10 (1995).
36. Sharp, A. H. *et al.* Widespread expression of Huntington's disease gene (IT15) protein product. *Neuron* **14,** 1065–74 (1995).
37. Ferrante, R. J. *et al.* Heterogeneous topographic and cellular distribution of huntingtin expression in the normal human neostriatum. *J. Neurosci.* **17,** 3052–63 (1997).
38. DiFiglia, M. *et al.* Huntingtin is a cytoplasmic protein associated with vesicles in human and rat brain neurons. *Neuron* **14,** 1075–81 (1995).
39. Gutekunst, C. A. *et al.* Identification and localization of huntingtin in brain and human lymphoblastoid cell lines with anti-fusion protein antibodies. *Proc. Natl. Acad. Sci. U. S. A.* **92,** 8710–4 (1995).
40. De Rooij, K. E., Dorsman, J. C., Smoor, M. A., Den Dunnen, J. T. & Van Ommen, G. J. Subcellular localization of the Huntington's disease gene product in cell lines by immunofluorescence and biochemical subcellular fractionation. *Hum. Mol. Genet.* **5,** 1093–9 (1996).
41. Gutekunst, C. A. *et al.* The cellular and subcellular localization of huntingtin-associated protein 1 (HAP1): comparison with huntingtin in rat and human. *J. Neurosci.* **18,** 7674–86 (1998).
42. Li, X. J. *et al.* A huntingtin-associated protein enriched in brain with implications for pathology. *Nature* **378,** 398–402 (1995).
43. Wanker, E. E. *et al.* HIP-I: a huntingtin interacting protein isolated by the yeast two-hybrid system. *Hum. Mol. Genet.* **6,** 487–95 (1997).
44. Kalchman, M. A. *et al.* HIP1, a human homologue of S. cerevisiae Sla2p, interacts with membrane-associated huntingtin in the brain. *Nat. Genet.* **16,** 44–53 (1997).
45. Singaraja, R. R. *et al.* HIP14, a novel ankyrin domain-containing protein, links huntingtin to intracellular trafficking and endocytosis. *Hum. Mol. Genet.* **11,** 2815–28 (2002).
46. Gauthier, L. R. *et al.* Huntingtin controls neurotrophic support and survival of neurons by enhancing BDNF vesicular transport along microtubules. *Cell* **118,** 127–38 (2004).
47. Pal, A., Severin, F., Lommer, B., Shevchenko, A. & Zerial, M. Huntingtin-HAP40 complex is a novel Rab5 effector that regulates early endosome motility and is up-regulated in Huntington's disease. *J. Cell Biol.* **172,** 605–18 (2006).
48. Brandstaetter, H., Kruppa, A. J. & Buss, F. Huntingtin is required for ER-to-Golgi transport and for secretory vesicle fusion at the plasma membrane. *Dis. Model. Mech.* (2014). doi:10.1242/dmm.017368
49. Caviston, J. P., Ross, J. L., Antony, S. M., Tokito, M. & Holzbaur, E. L. F. Huntingtin facilitates dynein/dynactin-mediated vesicle transport. *Proc. Natl. Acad. Sci. U. S. A.* **104,** 10045–50 (2007).
50. Caviston, J. P., Zajac, A. L., Tokito, M. & Holzbaur, E. L. F. Huntingtin coordinates the dynein-mediated dynamic positioning of endosomes and lysosomes. *Mol. Biol. Cell* **22,** 478–92 (2011).

51. Ochaba, J. *et al.* Potential function for the Huntingtin protein as a scaffold for selective autophagy. *Proc. Natl. Acad. Sci. U. S. A.* **111,** 16889–94 (2014).
52. Bao, J. *et al.* Expansion of polyglutamine repeat in huntingtin leads to abnormal protein interactions involving calmodulin. *Proc. Natl. Acad. Sci. U. S. A.* **93,** 5037–42 (1996).
53. Tang, T.-S. *et al.* Huntingtin and huntingtin-associated protein 1 influence neuronal calcium signaling mediated by inositol-(1,4,5) triphosphate receptor type 1. *Neuron* **39,** 227–39 (2003).
54. Burke, J. R. *et al.* Huntingtin and DRPLA proteins selectively interact with the enzyme GAPDH. *Nat. Med.* **2,** 347–50 (1996).
55. Boutell, J. M., Wood, J. D., Harper, P. S. & Jones, A. L. Huntingtin interacts with cystathionine beta-synthase. *Hum. Mol. Genet.* **7,** 371–8 (1998).
56. Pryor, W. M. *et al.* Huntingtin promotes mTORC1 signaling in the pathogenesis of Huntington's disease. *Sci. Signal.* **7,** ra103 (2014).
57. Liu, Y. F., Deth, R. C. & Devys, D. SH3 domain-dependent association of huntingtin with epidermal growth factor receptor signaling complexes. *J. Biol. Chem.* **272,** 8121–4 (1997).
58. Sun, Y., Savanenin, A., Reddy, P. H. & Liu, Y. F. Polyglutamine-expanded huntingtin promotes sensitization of N-methyl-D-aspartate receptors via post-synaptic density 95. *J. Biol. Chem.* **276,** 24713–8 (2001).
59. Modregger, J., DiProspero, N. A., Charles, V., Tagle, D. A. & Plomann, M. PACSIN 1 interacts with huntingtin and is absent from synaptic varicosities in presymptomatic Huntington's disease brains. *Hum. Mol. Genet.* **11,** 2547–58 (2002).
60. Ratovitski, T. *et al.* Huntingtin protein interactions altered by polyglutamine expansion as determined by quantitative proteomic analysis. *Cell Cycle* **11,** 2006–21 (2012).
61. Faber, P. W. *et al.* Huntingtin interacts with a family of WW domain proteins. *Hum. Mol. Genet.* **7,** 1463–74 (1998).
62. Li, S.-H. *et al.* Interaction of Huntington disease protein with transcriptional activator Sp1. *Mol. Cell. Biol.* **22,** 1277–87 (2002).
63. Zuccato, C. *et al.* Huntingtin interacts with REST/NRSF to modulate the transcription of NRSE-controlled neuronal genes. *Nat. Genet.* **35,** 76–83 (2003).
64. Holbert, S. *et al.* The Gln-Ala repeat transcriptional activator CA150 interacts with huntingtin: neuropathologic and genetic evidence for a role in Huntington's disease pathogenesis. *Proc. Natl. Acad. Sci. U. S. A.* **98,** 1811–6 (2001).
65. Culver, B. P. *et al.* Proteomic analysis of wild-type and mutant huntingtin-associated proteins in mouse brains identifies unique interactions and involvement in protein synthesis. *J. Biol. Chem.* **287,** 21599–614 (2012).
66. Desmond, C. R., Maiuri, T. & Truant, R. A multifunctional, multi-pathway intracellular localization signal in Huntingtin. *Commun. Integr. Biol.* **6,** e23318 (2013).
67. Duyao, M. P. *et al.* Inactivation of the mouse Huntington's disease gene homolog Hdh. *Science* **269,** 407–10 (1995).
68. Zeitlin, S., Liu, J. P., Chapman, D. L., Papaioannou, V. E. & Efstratiadis, A. Increased apoptosis and early embryonic lethality in mice nullizygous for the Huntington's disease gene homologue. *Nat. Genet.* **11,** 155–63 (1995).
69. White, J. K. *et al.* Huntingtin is required for neurogenesis and is not impaired by the Huntington's disease CAG expansion. *Nat. Genet.* **17,** 404–10 (1997).
70. Dragatsis, I., Efstratiadis, A. & Zeitlin, S. Mouse mutant embryos lacking huntingtin are rescued from lethality by wild-type extraembryonic tissues. *Development* **125,** 1529–39 (1998).
71. Woda, J. M. *et al.* Inactivation of the Huntington's disease gene (Hdh) impairs anterior streak formation and early patterning of the mouse embryo. *BMC Dev. Biol.* **5,** 17 (2005).
72. Jeong, S.-J. *et al.* Huntingtin is localized in the nucleus during preimplanatation embryo development in mice. *Int. J. Dev. Neurosci.* **24,** 81–5 (2006).
73. Nguyen, G. D., Gokhan, S., Molero, A. E. & Mehler, M. F. Selective roles of normal and mutant huntingtin in neural induction and early neurogenesis. *PLoS One* **8,** e64368 (2013).
74. Dragatsis, I., Levine, M. S. & Zeitlin, S. Inactivation of Hdh in the brain and testis results in progressive neurodegeneration and sterility in mice. *Nat. Genet.* **26,** 300–6 (2000).
75. Auerbach, W. *et al.* The HD mutation causes progressive lethal neurological disease in mice expressing reduced levels of huntingtin. *Hum. Mol. Genet.* **10,** 2515–23 (2001).
76. Van Raamsdonk, J. M. *et al.* Body weight is modulated by levels of full-length huntingtin. *Hum. Mol. Genet.* **15,** 1513–23 (2006).
77. Rigamonti, D. *et al.* Wild-type huntingtin protects from apoptosis upstream of caspase-3. *J. Neurosci.* **20,** 3705–13 (2000).

78. Rigamonti, D. *et al.* Huntingtin's neuroprotective activity occurs via inhibition of procaspase-9 processing. *J. Biol. Chem.* **276,** 14545–8 (2001).
79. Leavitt, B. R. *et al.* Wild-type huntingtin reduces the cellular toxicity of mutant huntingtin in vivo. *Am. J. Hum. Genet.* **68,** 313–24 (2001).
80. Buren, C., Wang, L., Smith-Dijak, A. & Raymond, L. A. Region-specific Pro-survival Signaling and Global Neuronal Protection by Wild-type Huntingtin. *J. Huntingtons. Dis.* **3,** 365–76 (2014).
81. Persichetti, F. *et al.* Normal and expanded Huntington's disease gene alleles produce distinguishable proteins due to translation across the CAG repeat. *Mol. Med.* **1,** 374–83 (1995).
82. Sapp, E. *et al.* Huntingtin localization in brains of normal and Huntington's disease patients. *Ann. Neurol.* **42,** 604–12 (1997).
83. Aronin, N. *et al.* CAG expansion affects the expression of mutant Huntingtin in the Huntington's disease brain. *Neuron* **15,** 1193–201 (1995).
84. Gourfinkel-An, I. *et al.* Differential distribution of the normal and mutated forms of huntingtin in the human brain. *Ann. Neurol.* **42,** 712–9 (1997).
85. DiFiglia, M. *et al.* Aggregation of huntingtin in neuronal intranuclear inclusions and dystrophic neurites in brain. *Science* **277,** 1990–3 (1997).
86. Gutekunst, C. A. *et al.* Nuclear and neuropil aggregates in Huntington's disease: relationship to neuropathology. *J. Neurosci.* **19,** 2522–34 (1999).
87. Cattaneo, E., Zuccato, C. & Tartari, M. Normal huntingtin function: an alternative approach to Huntington's disease. *Nat. Rev. Neurosci.* **6,** 919–30 (2005).
88. Zuccato, C., Valenza, M. & Cattaneo, E. Molecular mechanisms and potential therapeutical targets in Huntington's disease. *Physiol. Rev.* **90,** 905–81 (2010).
89. Davies, S. W. *et al.* Formation of neuronal intranuclear inclusions underlies the neurological dysfunction in mice transgenic for the HD mutation. *Cell* **90,** 537–48 (1997).
90. Scherzinger, E. *et al.* Huntingtin-encoded polyglutamine expansions form amyloid-like protein aggregates in vitro and in vivo. *Cell* **90,** 549–58 (1997).
91. Chen, S., Ferrone, F. A. & Wetzel, R. Huntington's disease age-of-onset linked to polyglutamine aggregation nucleation. *Proc. Natl. Acad. Sci. U. S. A.* **99,** 11884–9 (2002).
92. Becher, M. W. *et al.* Intranuclear neuronal inclusions in Huntington's disease and dentatorubral and pallidoluysian atrophy: correlation between the density of inclusions and IT15 CAG triplet repeat length. *Neurobiol. Dis.* **4,** 387–97 (1998).
93. Li, S. H. & Li, X. J. Aggregation of N-terminal huntingtin is dependent on the length of its glutamine repeats. *Hum. Mol. Genet.* **7,** 777–82 (1998).
94. Saudou, F., Finkbeiner, S., Devys, D. & Greenberg, M. E. Huntingtin Acts in the Nucleus to Induce Apoptosis but Death Does Not Correlate with the Formation of Intranuclear Inclusions. *Cell* **95,** 55–66 (1998).
95. Arrasate, M., Mitra, S., Schweitzer, E. S., Segal, M. R. & Finkbeiner, S. Inclusion body formation reduces levels of mutant huntingtin and the risk of neuronal death. *Nature* **431,** 805–10 (2004).
96. Kuemmerle, S. *et al.* Huntington aggregates may not predict neuronal death in Huntington's disease. *Ann. Neurol.* **46,** 842–9 (1999).
97. Muchowski, P. J. *et al.* Hsp70 and hsp40 chaperones can inhibit self-assembly of polyglutamine proteins into amyloid-like fibrils. *Proc. Natl. Acad. Sci. U. S. A.* **97,** 7841–6 (2000).
98. Schaffar, G. *et al.* Cellular toxicity of polyglutamine expansion proteins: mechanism of transcription factor deactivation. *Mol. Cell* **15,** 95–105 (2004).
99. Arrasate, M. & Finkbeiner, S. Protein aggregates in Huntington's disease. *Exp. Neurol.* **238,** 1–11 (2012).
100. Martindale, D. *et al.* Length of huntingtin and its polyglutamine tract influences localization and frequency of intracellular aggregates. *Nat. Genet.* **18,** 150–4 (1998).
101. Cooper, J. K. *et al.* Truncated N-terminal fragments of huntingtin with expanded glutamine repeats form nuclear and cytoplasmic aggregates in cell culture. *Hum. Mol. Genet.* **7,** 783–90 (1998).
102. Sun, B. *et al.* Polyglutamine repeat length-dependent proteolysis of huntingtin. *Neurobiol. Dis.* **11,** 111–22 (2002).
103. Lunkes, A. & Mandel, J. L. A cellular model that recapitulates major pathogenic steps of Huntington's disease. *Hum. Mol. Genet.* **7,** 1355–61 (1998).

104. Gafni, J. & Ellerby, L. M. Calpain activation in Huntington's disease. *J. Neurosci.* **22,** 4842–9 (2002).
105. Gafni, J. *et al.* Inhibition of calpain cleavage of huntingtin reduces toxicity: accumulation of calpain/caspase fragments in the nucleus. *J. Biol. Chem.* **279,** 20211–20 (2004).
106. Goldberg, Y. P. *et al.* Cleavage of huntingtin by apopain, a proapoptotic cysteine protease, is modulated by the polyglutamine tract. *Nat. Genet.* **13,** 442–9 (1996).
107. Wellington, C. L. *et al.* Inhibiting caspase cleavage of huntingtin reduces toxicity and aggregate formation in neuronal and nonneuronal cells. *J. Biol. Chem.* **275,** 19831–8 (2000).
108. Ona, V. O. *et al.* Inhibition of caspase-1 slows disease progression in a mouse model of Huntington's disease. *Nature* **399,** 263–7 (1999).
109. Graham, R. K. *et al.* Cleavage at the caspase-6 site is required for neuronal dysfunction and degeneration due to mutant huntingtin. *Cell* **125,** 1179–91 (2006).
110. Poirier, M. A., Jiang, H. & Ross, C. A. A structure-based analysis of huntingtin mutant polyglutamine aggregation and toxicity: evidence for a compact beta-sheet structure. *Hum. Mol. Genet.* **14,** 765–74 (2005).
111. Nagai, Y. *et al.* A toxic monomeric conformer of the polyglutamine protein. *Nat. Struct. Mol. Biol.* **14,** 332–40 (2007).
112. Zhang, Q. C. *et al.* A compact beta model of huntingtin toxicity. *J. Biol. Chem.* **286,** 8188–96 (2011).
113. Li, S.-H. & Li, X.-J. Huntingtin-protein interactions and the pathogenesis of Huntington's disease. *Trends Genet.* **20,** 146–54 (2004).
114. Lunkes, A. *et al.* Proteases acting on mutant huntingtin generate cleaved products that differentially build up cytoplasmic and nuclear inclusions. *Mol. Cell* **10,** 259–69 (2002).
115. Hackam, A. S. *et al.* The influence of huntingtin protein size on nuclear localization and cellular toxicity. *J. Cell Biol.* **141,** 1097–105 (1998).
116. Truant, R., Atwal, R. S. & Burtnik, A. Nucleocytoplasmic trafficking and transcription effects of huntingtin in Huntington's disease. *Prog. Neurobiol.* **83,** 211–27 (2007).
117. Persichetti, F. *et al.* Differential expression of normal and mutant Huntington's disease gene alleles. *Neurobiol. Dis.* **3,** 183–90 (1996).
118. Metzler, M. *et al.* Life without huntingtin: normal differentiation into functional neurons. *J. Neurochem.* **72,** 1009–18 (1999).
119. Lu, B. & Palacino, J. A novel human embryonic stem cell-derived Huntington's disease neuronal model exhibits mutant huntingtin (mHTT) aggregates and soluble mHTT-dependent neurodegeneration. *FASEB J.* **27,** 1820–9 (2013).
120. HD iPSC Consortium. Induced pluripotent stem cells from patients with Huntington's disease show CAG-repeat-expansion-associated phenotypes. *Cell Stem Cell* **11,** 264–78 (2012).
121. Li, S. H., Cheng, A. L., Li, H. & Li, X. J. Cellular defects and altered gene expression in PC12 cells stably expressing mutant huntingtin. *J. Neurosci.* **19,** 5159–72 (1999).
122. Trettel, F. *et al.* Dominant phenotypes produced by the HD mutation in STHdh(Q111) striatal cells. *Hum. Mol. Genet.* **9,** 2799–809 (2000).
123. Ehrlich, M. E. *et al.* ST14A cells have properties of a medium-size spiny neuron. *Exp. Neurol.* **167,** 215–26 (2001).
124. Parker, J. A. *et al.* Expanded polyglutamines in Caenorhabditis elegans cause axonal abnormalities and severe dysfunction of PLM mechanosensory neurons without cell death. *Proc. Natl. Acad. Sci. U. S. A.* **98,** 13318–23 (2001).
125. Jackson, G. R. *et al.* Polyglutamine-expanded human huntingtin transgenes induce degeneration of Drosophila photoreceptor neurons. *Neuron* **21,** 633–42 (1998).
126. Mangiarini, L. *et al.* Exon 1 of the HD gene with an expanded CAG repeat is sufficient to cause a progressive neurological phenotype in transgenic mice. *Cell* **87,** 493–506 (1996).
127. Heng, M. Y. *et al.* Early autophagic response in a novel knock-in model of Huntington disease. *Hum. Mol. Genet.* **19,** 3702–20 (2010).
128. Schilling, G. *et al.* Intranuclear inclusions and neuritic aggregates in transgenic mice expressing a mutant N-terminal fragment of huntingtin. *Hum. Mol. Genet.* **8,** 397–407 (1999).
129. Slow, E. J. *et al.* Absence of behavioral abnormalities and neurodegeneration in vivo despite widespread neuronal huntingtin inclusions. *Proc. Natl. Acad. Sci. U. S. A.* **102,** 11402–7 (2005).
130. Gray, M. *et al.* Full-length human mutant huntingtin with a stable polyglutamine repeat can elicit progressive and selective neuropathogenesis in BACHD mice. *J. Neurosci.* **28,** 6182–95 (2008).

131. Hodgson, J. G. *et al.* A YAC mouse model for Huntington's disease with full-length mutant huntingtin, cytoplasmic toxicity, and selective striatal neurodegeneration. *Neuron* **23,** 181–92 (1999).
132. Wheeler, V. C. *et al.* Length-dependent gametic CAG repeat instability in the Huntington's disease knock-in mouse. *Hum. Mol. Genet.* **8,** 115–22 (1999).
133. Menalled, L. B., Sison, J. D., Dragatsis, I., Zeitlin, S. & Chesselet, M.-F. Time course of early motor and neuropathological anomalies in a knock-in mouse model of Huntington's disease with 140 CAG repeats. *J. Comp. Neurol.* **465,** 11–26 (2003).
134. Lin, C. H. *et al.* Neurological abnormalities in a knock-in mouse model of Huntington's disease. *Hum. Mol. Genet.* **10,** 137–44 (2001).
135. Kotliarova, S. *et al.* Decreased expression of hypothalamic neuropeptides in Huntington disease transgenic mice with expanded polyglutamine-EGFP fluorescent aggregates. *J. Neurochem.* **93,** 641–53 (2005).
136. Ishiguro, H. *et al.* Age-dependent and tissue-specific CAG repeat instability occurs in mouse knock-in for a mutant Huntington's disease gene. *J. Neurosci. Res.* **65,** 289–97 (2001).
137. Reddy, P. H. *et al.* Behavioural abnormalities and selective neuronal loss in HD transgenic mice expressing mutated full-length HD cDNA. *Nat. Genet.* **20,** 198–202 (1998).
138. Yamamoto, A., Lucas, J. J. & Hen, R. Reversal of neuropathology and motor dysfunction in a conditional model of Huntington's disease. *Cell* **101,** 57–66 (2000).
139. Tanaka, Y. *et al.* Progressive phenotype and nuclear accumulation of an amino-terminal cleavage fragment in a transgenic mouse model with inducible expression of full-length mutant huntingtin. *Neurobiol. Dis.* **21,** 381–91 (2006).
140. Usdin, M. T., Shelbourne, P. F., Myers, R. M. & Madison, D. V. Impaired synaptic plasticity in mice carrying the Huntington's disease mutation. *Hum. Mol. Genet.* **8,** 839–46 (1999).
141. Von Hörsten, S. *et al.* Transgenic rat model of Huntington's disease. *Hum. Mol. Genet.* **12,** 617–24 (2003).
142. Yu-Taeger, L. *et al.* A Novel BACHD Transgenic Rat Exhibits Characteristic Neuropathological Features of Huntington Disease. *J. Neurosci.* **32,** 15426–15438 (2012).
143. Jacobsen, J. C. *et al.* An ovine transgenic Huntington's disease model. *Hum. Mol. Genet.* **19,** 1873–82 (2010).
144. Baxa, M. *et al.* A transgenic minipig model of Huntington's Disease. *J. Huntingtons. Dis.* **2,** 47–68 (2013).
145. Yang, S.-H. *et al.* Towards a transgenic model of Huntington's disease in a non-human primate. *Nature* **453,** 921–4 (2008).
146. McGeer, E. G. & McGeer, P. L. Duplication of biochemical changes of Huntington's chorea by intrastriatal injections of glutamic and kainic acids. *Nature* **263,** 517–9 (1976).
147. Coyle, J. T. & Schwarcz, R. Lesion of striatal neurones with kainic acid provides a model for Huntington's chorea. *Nature* **263,** 244–6 (1976).
148. Isacson, O., Brundin, P., Kelly, P. A., Gage, F. H. & Björklund, A. Functional neuronal replacement by grafted striatal neurones in the ibotenic acid-lesioned rat striatum. *Nature* **311,** 458–60
149. Beal, M. F. *et al.* Replication of the neurochemical characteristics of Huntington's disease by quinolinic acid. *Nature* **321,** 168–71 (1986).
150. Beal, M. F. *et al.* Neurochemical and histologic characterization of striatal excitotoxic lesions produced by the mitochondrial toxin 3-nitropropionic acid. *J. Neurosci.* **13,** 4181–92 (1993).
151. Yu, Z.-X. *et al.* Mutant huntingtin causes context-dependent neurodegeneration in mice with Huntington's disease. *J. Neurosci.* **23,** 2193–202 (2003).
152. Menalled, L. *et al.* Systematic behavioral evaluation of Huntington's disease transgenic and knock-in mouse models. *Neurobiol. Dis.* **35,** 319–36 (2009).
153. Browne, S. E. & Beal, M. F. The energetics of Huntington's disease. *Neurochem. Res.* **29,** 531–46 (2004).
154. Abada, Y.-S. K., Nguyen, H. P., Ellenbroek, B. & Schreiber, R. Reversal learning and associative memory impairments in a BACHD rat model for Huntington disease. *PLoS One* **8,** e71633 (2013).
155. Abada, Y.-S. K., Nguyen, H. P., Schreiber, R. & Ellenbroek, B. Assessment of motor function, sensory motor gating and recognition memory in a novel BACHD transgenic rat model for huntington disease. *PLoS One* **8,** e68584 (2013).
156. Aziz, N. A., Swaab, D. F., Pijl, H. & Roos, R. A. C. Hypothalamic dysfunction and neuroendocrine and metabolic alterations in Huntington's disease: clinical consequences and therapeutic implications. *Rev. Neurosci.* **18,** 223–51 (2007).
157. Aziz, N. A., Anguelova, G. V, Marinus, J., van Dijk, J. G. & Roos, R. A. C. Autonomic symptoms in patients and pre-manifest mutation carriers of Huntington's disease. *Eur. J. Neurol.* **17,** 1068–74 (2010).

158. Kremer, H. P. & Roos, R. A. Weight loss in Huntington's disease. *Arch. Neurol.* **49,** 349 (1992).
159. Morales, L. M. *et al.* Nutritional evaluation of Huntington disease patients. *Am. J. Clin. Nutr.* **50,** 145–50 (1989).
160. Nance, M. A. & Sanders, G. Characteristics of individuals with Huntington disease in long-term care. *Mov. Disord.* **11,** 542–8 (1996).
161. Gaba, A. M. *et al.* Energy balance in early-stage Huntington disease. *Am. J. Clin. Nutr.* **81,** 1335–41 (2005).
162. Pratley, R. E., Salbe, A. D., Ravussin, E. & Caviness, J. N. Higher sedentary energy expenditure in patients with Huntington's disease. *Ann. Neurol.* **47,** 64–70 (2000).
163. Stoy, N. & McKay, E. Weight loss in Huntington's disease. *Ann. Neurol.* **48,** 130–130 (2000).
164. Kagel, M. C. & Leopold, N. A. Dysphagia in Huntington's disease: a 16-year retrospective. *Dysphagia* **7,** 106–14 (1992).
165. Heemskerk, A.-W. & Roos, R. A. C. Aspiration pneumonia and death in Huntington's disease. *PLoS Curr.* **4,** RRN1293 (2012).
166. Lee, J. K. *et al.* Measures of growth in children at risk for Huntington disease. *Neurology* **79,** 668–74 (2012).
167. Nopoulos, P. C. *et al.* Smaller intracranial volume in prodromal Huntington's disease: evidence for abnormal neurodevelopment. *Brain* **134,** 137–42 (2011).
168. Mochel, F. *et al.* Early energy deficit in Huntington disease: identification of a plasma biomarker traceable during disease progression. *PLoS One* **2,** e647 (2007).
169. Djoussé, L. *et al.* Weight loss in early stage of Huntington's disease. *Neurology* **59,** 1325–30 (2002).
170. Trejo, A. *et al.* Assessment of the nutrition status of patients with Huntington's disease. *Nutrition* **20,** 192–6 (2004).
171. Popovic, V. *et al.* Circulating and cerebrospinal fluid ghrelin and leptin: potential role in altered body weight in Huntington's disease. *Eur. J. Endocrinol.* **151,** 451–5 (2004).
172. Farrer, L. A. & Meaney, F. J. An anthropometric assessment of Huntington's disease patients and families. *Am. J. Phys. Anthropol.* **67,** 185–94 (1985).
173. Aziz, N. a. *et al.* Weight loss in neurodegenerative disorders. *J. Neurol.* **255,** 1872–1880 (2008).
174. Aziz, N. A. *et al.* Systemic energy homeostasis in Huntington's disease patients. *J. Neurol. Neurosurg. Psychiatry* **81,** 1233–1237 (2010).
175. Feigin, A. *et al.* Metabolic network abnormalities in early Huntington's disease: an [(18)F]FDG PET study. *J. Nucl. Med.* **42,** 1591–5 (2001).
176. Feigin, A. *et al.* Thalamic metabolism and symptom onset in preclinical Huntington's disease. *Brain* **130,** 2858–67 (2007).
177. Kuwert, T. *et al.* Cortical and subcortical glucose consumption measured by PET in patients with Huntington's disease. *Brain* **113 (Pt 5,** 1405–23 (1990).
178. Kuhl, D. E. *et al.* Local cerebral glucose utilization in symptomatic and presymptomatic Huntington's disease. *Res. Publ. Assoc. Res. Nerv. Ment. Dis.* **63,** 199–209 (1985).
179. Berent, S. *et al.* Positron emission tomographic scan investigations of Huntington's disease: cerebral metabolic correlates of cognitive function. *Ann. Neurol.* **23,** 541–6 (1988).
180. Grafton, S. T. *et al.* Serial changes of cerebral glucose metabolism and caudate size in persons at risk for Huntington's disease. *Arch. Neurol.* **49,** 1161–7 (1992).
181. Kuwert, T. *et al.* Striatal glucose consumption in chorea-free subjects at risk of Huntington's disease. *J. Neurol.* **241,** 31–6 (1993).
182. Antonini, A. *et al.* Striatal glucose metabolism and dopamine D2 receptor binding in asymptomatic gene carriers and patients with Huntington's disease. *Brain* **119 (Pt 6,** 2085–95 (1996).
183. Martin, W. R. *et al.* Cortical glucose metabolism in Huntington's disease. *Neurology* **42,** 223–9 (1992).
184. Farrer, L. A. & Yu, P. L. Anthropometric discrimination among affected, at-risk, and not-at-risk individuals in families with Huntington disease. *Am. J. Med. Genet.* **21,** 307–16 (1985).
185. Podolsky, S., Leopold, N. A. & Sax, D. S. Increased frequency of diabetes mellitus in patients with Huntington's chorea. *Lancet* **1,** 1356–8 (1972).
186. Podolsky, S. & Leopold, N. A. Abnormal glucose tolerance and arginine tolerance tests in Huntington's disease. *Gerontology* **23,** 55–63 (1977).
187. Schubotz, R., Hausmann, L., Kaffarnik, H., Zehner, J. & Oepen, H. [Fatty acid patterns and glucose tolerance in Huntington's chorea (author's transl)]. *Res. Exp. Med. (Berl).* **167,** 203–15 (1976).
188. Lalić, N. M. *et al.* Glucose homeostasis in Huntington disease: abnormalities in insulin sensitivity and early-phase insulin secretion. *Arch. Neurol.* **65,** 476–80 (2008).

189. Andreassen, O. A. *et al.* Huntington's disease of the endocrine pancreas: insulin deficiency and diabetes mellitus due to impaired insulin gene expression. *Neurobiol. Dis.* **11,** 410–24 (2002).
190. Farrer, L. A. Diabetes mellitus in Huntington disease. *Clin. Genet.* **27,** 62–7 (1985).
191. Petersén, A. & Björkqvist, M. Hypothalamic-endocrine aspects in Huntington's disease. *Eur. J. Neurosci.* **24,** 961–7 (2006).
192. Van Raamsdonk, J. M. *et al.* Phenotypic abnormalities in the YAC128 mouse model of Huntington disease are penetrant on multiple genetic backgrounds and modulated by strain. *Neurobiol. Dis.* **26,** 189–200 (2007).
193. Bode, F. J. *et al.* Sex differences in a transgenic rat model of Huntington's disease: decreased 17beta-estradiol levels correlate with reduced numbers of DARPP32+ neurons in males. *Hum. Mol. Genet.* **17,** 2595–609 (2008).
194. Hult, S. *et al.* Mutant huntingtin causes metabolic imbalance by disruption of hypothalamic neurocircuits. *Cell Metab.* **13,** 428–39 (2011).
195. Van der Burg, J. M. M. *et al.* Increased metabolism in the R6/2 mouse model of Huntington's disease. *Neurobiol. Dis.* **29,** 41–51 (2008).
196. Scicchitano, B. M., Rizzuto, E. & Musarò, A. Counteracting muscle wasting in aging and neuromuscular diseases: the critical role of IGF-1. *Aging (Albany. NY).* **1,** 451–7 (2009).
197. Pouladi, M. a. *et al.* Full-length huntingtin levels modulate body weight by influencing insulin-like growth factor 1 expression. *Hum. Mol. Genet.* **19,** 1528–1538 (2010).
198. Park, H.-K. & Ahima, R. S. Physiology of leptin: energy homeostasis, neuroendocrine function and metabolism. *Metabolism.* **64,** 24–34 (2015).
199. Fain, J. N., Del Mar, N. A., Meade, C. A., Reiner, A. & Goldowitz, D. Abnormalities in the functioning of adipocytes from R6/2 mice that are transgenic for the Huntington's disease mutation. *Hum. Mol. Genet.* **10,** 145–52 (2001).
200. Browne, S. E. Mitochondria and Huntington's disease pathogenesis: insight from genetic and chemical models. *Ann. N. Y. Acad. Sci.* **1147,** 358–82 (2008).
201. Heikkinen, T. *et al.* Characterization of neurophysiological and behavioral changes, MRI brain volumetry and 1H MRS in zQ175 knock-in mouse model of Huntington's disease. *PLoS One* **7,** e50717 (2012).
202. Trushina, E., Canaria, C. A., Lee, D.-Y. & McMurray, C. T. Loss of caveolin-1 expression in knock-in mouse model of Huntington's disease suppresses pathophysiology in vivo. *Hum. Mol. Genet.* **23,** 129–44 (2014).
203. Hölter, S. M. *et al.* A broad phenotypic screen identifies novel phenotypes driven by a single mutant allele in Huntington's disease CAG knock-in mice. *PLoS One* **8,** e80923 (2013).
204. Tallaksen-Greene, S. J. *et al.* Differential effects of delayed aging on phenotype and striatal pathology in a murine model of Huntington disease. *J. Neurosci.* **34,** 15658–68 (2014).
205. Zeng, L., Tallaksen-Greene, S. J., Wang, B., Albin, R. L. & Paulson, H. L. The de-ubiquitinating enzyme ataxin-3 does not modulate disease progression in a knock-in mouse model of Huntington disease. *J. Huntingtons. Dis.* **2,** 201–15 (2013).
206. Menalled, L. B. *et al.* Comprehensive behavioral and molecular characterization of a new knock-in mouse model of Huntington's disease: zQ175. *PLoS One* **7,** e49838 (2012).
207. Woodman, B. *et al.* The Hdh(Q150/Q150) knock-in mouse model of HD and the R6/2 exon 1 model develop comparable and widespread molecular phenotypes. *Brain Res. Bull.* **72,** 83–97 (2007).
208. Lerner, R. P., Trejo Martinez, L. D. C. G., Zhu, C., Chesselet, M.-F. & Hickey, M. A. Striatal atrophy and dendritic alterations in a knock-in mouse model of Huntington's disease. *Brain Res. Bull.* **87,** 571–8 (2012).
209. Rising, A. C. *et al.* Longitudinal behavioral, cross-sectional transcriptional and histopathological characterization of a knock-in mouse model of Huntington's disease with 140 CAG repeats. *Exp. Neurol.* **228,** 173–82 (2011).
210. Moffitt, H., McPhail, G. D., Woodman, B., Hobbs, C. & Bates, G. P. Formation of polyglutamine inclusions in a wide range of non-CNS tissues in the HdhQ150 knock-in mouse model of Huntington's disease. *PLoS One* **4,** e8025 (2009).
211. Phan, J., Hickey, M. a, Zhang, P., Chesselet, M.-F. & Reue, K. Adipose tissue dysfunction tracks disease progression in two Huntington's disease mouse models. *Hum. Mol. Genet.* **18,** 1006–16 (2009).
212. Lundh, S. H., Soylu, R., Petersén, A. & Petersén, Å. Expression of mutant huntingtin in leptin receptor-expressing neurons does not control the metabolic and psychiatric phenotype of the BACHD mouse. *PLoS One* **7,** e51168 (2012).
213. Baldo, B., Cheong, R. Y. & Petersén, Å. Effects of deletion of mutant huntingtin in steroidogenic factor 1 neurons on the psychiatric and metabolic phenotype in the BACHD mouse model of Huntington disease. *PLoS One* **9,** e107691 (2014).

214. Zádori, D. *et al.* Neuroprotective effects of a novel kynurenic acid analogue in a transgenic mouse model of Huntington's disease. *J. Neural Transm.* **118,** 865–875 (2011).
215. Dufour, B. D., Smith, C. a, Clark, R. L., Walker, T. R. & McBride, J. L. Intrajugular vein delivery of AAV9-RNAi prevents neuropathological changes and weight loss in Huntington's disease mice. *Mol. Ther.* **22,** 797–810 (2014).
216. Weydt, P. *et al.* Thermoregulatory and metabolic defects in Huntington's disease transgenic mice implicate PGC-1alpha in Huntington's disease neurodegeneration. *Cell Metab.* **4,** 349–62 (2006).
217. Mihm, M. J. *et al.* Cardiac dysfunction in the R6/2 mouse model of Huntington's disease. *Neurobiol. Dis.* **25,** 297–308 (2007).
218. Goodman, A. O. G. *et al.* The metabolic profile of early Huntington's disease--a combined human and transgenic mouse study. *Exp. Neurol.* **210,** 691–8 (2008).
219. She, P. *et al.* Molecular characterization of skeletal muscle atrophy in the R6 / 2 mouse model of Huntington ' s disease. *Am. J. Physiol. Endocrinol. Metab.* **301,** 49–61 (2011).
220. Ferrante, R. J. *et al.* Therapeutic effects of coenzyme Q10 and remacemide in transgenic mouse models of Huntington's disease. *J. Neurosci.* **22,** 1592–9 (2002).
221. Wacker, J. L. *et al.* Loss of Hsp70 exacerbates pathogenesis but not levels of fibrillar aggregates in a mouse model of Huntington's disease. *J. Neurosci.* **29,** 9104–14 (2009).
222. Von Horsten, S. *et al.* Transgenic rat model of Huntington's disease. *Hum. Mol. Genet.* **12,** 617–624 (2003).
223. Urbach, Y. K., Bode, F. J., Nguyen, H. P., Riess, O. & Hörsten, S. Von. in *Rat Genomics Methods Protoc. Methods Mol. Biol.* (Anegon, I.) **597,** 333–356 (Humana Press, 2010).
224. Heng, M. Y., Tallaksen-Greene, S. J., Detloff, P. J. & Albin, R. L. Longitudinal evaluation of the Hdh(CAG)150 knock-in murine model of Huntington's disease. *J. Neurosci.* **27,** 8989–98 (2007).
225. Hickey, M. A. *et al.* Evidence for behavioral benefits of early dietary supplementation with CoEnzymeQ10 in a slowly progressing mouse model of Huntington's disease. *Mol. Cell. Neurosci.* **49,** 149–57 (2012).
226. Loh, D. H., Kudo, T., Truong, D., Wu, Y. & Colwell, C. S. The Q175 mouse model of Huntington's disease shows gene dosage- and age-related decline in circadian rhythms of activity and sleep. *PLoS One* **8,** e69993 (2013).
227. Balci, F. *et al.* High-Throughput Automated Phenotyping of Two Genetic Mouse Models of Huntington's Disease. *PLoS Curr.* **5,** (2013).
228. Slow, E. J. *et al.* Selective striatal neuronal loss in a YAC128 mouse model of Huntington disease. *Hum. Mol. Genet.* **12,** 1555–67 (2003).
229. Klivenyi, P. *et al.* Behaviour changes in a transgenic model of Huntington's disease. *Behav. Brain Res.* **169,** 137–41 (2006).
230. Dunnett, S. B. *et al.* Striatal transplantation in a transgenic mouse model of Huntington's disease. *Exp. Neurol.* **154,** 31–40 (1998).
231. Zarringhalam, K. *et al.* An open system for automatic home-cage behavioral analysis and its application to male and female mouse models of Huntington's disease. *Behav. Brain Res.* **229,** 216–25 (2012).
232. Rudenko, O., Tkach, V., Berezin, V. & Bock, E. Detection of early behavioral markers of Huntington's disease in R6/2 mice employing an automated social home cage. *Behav. Brain Res.* **203,** 188–99 (2009).
233. Björkqvist, M. *et al.* The R6/2 transgenic mouse model of Huntington's disease develops diabetes due to deficient beta-cell mass and exocytosis. *Hum. Mol. Genet.* **14,** 565–74 (2005).
234. Smith, R. *et al.* Mutant huntingtin interacts with {beta}-tubulin and disrupts vesicular transport and insulin secretion. *Hum. Mol. Genet.* **18,** 3942–54 (2009).
235. Boesgaard, T. W. *et al.* Huntington's disease does not appear to increase the risk of diabetes mellitus. *J. Neuroendocrinol.* **21,** 770–6 (2009).
236. Lodi, R. *et al.* Abnormal in vivo skeletal muscle energy metabolism in Huntington's disease and dentatorubropallidoluysian atrophy. *Ann. Neurol.* **48,** 72–6 (2000).
237. Goodman, A. O. G. & Barker, R. a. Body composition in premanifest Huntington's disease reveals lower bone density compared to controls. *PLoS Curr.* **3,** RRN1214 (2011).
238. Van der Burg, J. M. M., Björkqvist, M. & Brundin, P. Beyond the brain: widespread pathology in Huntington's disease. *Lancet. Neurol.* **8,** 765–74 (2009).
239. Powers, W. J. *et al.* Selective defect of in vivo glycolysis in early Huntington's disease striatum. *Proc. Natl. Acad. Sci. U. S. A.* **104,** 2945–9 (2007).

240. Sorbi, S., Bird, E. D. & Blass, J. P. Decreased pyruvate dehydrogenase complex activity in Huntington and Alzheimer brain. *Ann. Neurol.* **13,** 72–8 (1983).
241. Butterworth, J., Yates, C. M. & Reynolds, G. P. Distribution of phosphate-activated glutaminase, succinic dehydrogenase, pyruvate dehydrogenase and gamma-glutamyl transpeptidase in post-mortem brain from Huntington's disease and agonal cases. *J. Neurol. Sci.* **67,** 161–71 (1985).
242. Perluigi, M. *et al.* Proteomic analysis of protein expression and oxidative modification in r6/2 transgenic mice: a model of Huntington disease. *Mol. Cell. Proteomics* **4,** 1849–61 (2005).
243. Tabrizi, S. J. *et al.* Biochemical abnormalities and excitotoxicity in Huntington's disease brain. *Ann. Neurol.* **45,** 25–32 (1999).
244. Brennan, W. A., Bird, E. D. & Aprille, J. R. Regional mitochondrial respiratory activity in Huntington's disease brain. *J. Neurochem.* **44,** 1948–50 (1985).
245. Damiano, M. *et al.* A role of mitochondrial complex II defects in genetic models of Huntington's disease expressing N-terminal fragments of mutant huntingtin. *Hum. Mol. Genet.* **22,** 3869–82 (2013).
246. Browne, S. E. *et al.* Oxidative damage and metabolic dysfunction in Huntington's disease: selective vulnerability of the basal ganglia. *Ann. Neurol.* **41,** 646–53 (1997).
247. Guidetti, P. *et al.* Early degenerative changes in transgenic mice expressing mutant huntingtin involve dendritic abnormalities but no impairment of mitochondrial energy production. *Exp. Neurol.* **169,** 340–50 (2001).
248. Nicoli, F. *et al.* CSF and serum metabolic profile of patients with Huntington's chorea: a study by high resolution proton NMR spectroscopy and HPLC. *Neurosci. Lett.* **154,** 47–51 (1993).
249. Phillipson, O. T. & Bird, E. D. Plasma glucose, non-esterified fatty acids and amino acids in Huntington's chorea. *Clin. Sci. Mol. Med.* **52,** 311–8 (1977).
250. Reilmann, R., Rolf, L. H. & Lange, H. W. Decreased plasma alanine and isoleucine in Huntington's disease. *Acta Neurol. Scand.* **91,** 222–4 (1995).
251. Sánchez-Pernaute, R., García-Segura, J. M., del Barrio Alba, A., Viaño, J. & de Yébenes, J. G. Clinical correlation of striatal 1H MRS changes in Huntington's disease. *Neurology* **53,** 806–12 (1999).
252. Ruocco, H. H., Lopes-Cendes, I., Li, L. M. & Cendes, F. Evidence of thalamic dysfunction in Huntington disease by proton magnetic resonance spectroscopy. *Mov. Disord.* **22,** 2052–6 (2007).
253. Reynolds, N. C., Prost, R. W. & Mark, L. P. Heterogeneity in 1H-MRS profiles of presymptomatic and early manifest Huntington's disease. *Brain Res.* **1031,** 82–9 (2005).
254. Jenkins, B. G., Koroshetz, W. J., Beal, M. F. & Rosen, B. R. Evidence for impairment of energy metabolism in vivo in Huntington's disease using localized 1H NMR spectroscopy. *Neurology* **43,** 2689–95 (1993).
255. Jenkins, B. G. *et al.* 1H NMR spectroscopy studies of Huntington's disease: correlations with CAG repeat numbers. *Neurology* **50,** 1357–65 (1998).
256. Koroshetz, W. J., Jenkins, B. G., Rosen, B. R. & Beal, M. F. Energy metabolism defects in Huntington's disease and effects of coenzyme Q10. *Ann. Neurol.* **41,** 160–5 (1997).
257. Oliveira, J. M. a. Nature and cause of mitochondrial dysfunction in Huntington's disease: focusing on huntingtin and the striatum. *J. Neurochem.* **114,** 1–12 (2010).
258. Reddy, P. H., Mao, P. & Manczak, M. Mitochondrial structural and functional dynamics in Huntington's disease. *Brain Res. Rev.* **61,** 33–48 (2009).
259. Rosenstock, T. R., Duarte, A. I. & Rego, A. C. Mitochondrial-associated metabolic changes and neurodegeneration in Huntington's disease - from clinical features to the bench. *Curr. Drug Targets* **11,** 1218–36 (2010).
260. Costa, V. & Scorrano, L. Shaping the role of mitochondria in the pathogenesis of Huntington's disease. *EMBO J.* **31,** 1853–64 (2012).
261. Quintanilla, R. A. & Johnson, G. V. W. Role of mitochondrial dysfunction in the pathogenesis of Huntington's disease. *Brain Res. Bull.* **80,** 242–7 (2009).
262. Pérez-De la Cruz, V., Carrillo-Mora, P. & Santamaría, A. Huntington's disease and mitochondrial alterations: emphasis on experimental models. *J. Bioenerg. Biomembr.* **42,** 207–15 (2010).
263. Scheffler, I. E. *Mitochondria.* (John Wiley & Sons, Inc., 2007).
264. Panov, A. V *et al.* Early mitochondrial calcium defects in Huntington's disease are a direct effect of polyglutamines. *Nat. Neurosci.* **5,** 731–6 (2002).

265. Choo, Y. S., Johnson, G. V. W., MacDonald, M., Detloff, P. J. & Lesort, M. Mutant huntingtin directly increases susceptibility of mitochondria to the calcium-induced permeability transition and cytochrome c release. *Hum. Mol. Genet.* **13,** 1407–20 (2004).
266. Gellerich, F. N. *et al.* Impaired regulation of brain mitochondria by extramitochondrial Ca2+ in transgenic Huntington disease rats. *J. Biol. Chem.* **283,** 30715–24 (2008).
267. Wang, H., Lim, P. J., Karbowski, M. & Monteiro, M. J. Effects of overexpression of huntingtin proteins on mitochondrial integrity. *Hum. Mol. Genet.* **18,** 737–52 (2009).
268. Rockabrand, E. *et al.* The first 17 amino acids of Huntingtin modulate its sub-cellular localization, aggregation and effects on calcium homeostasis. *Hum. Mol. Genet.* **16,** 61–77 (2007).
269. Cui, L. *et al.* Transcriptional repression of PGC-1alpha by mutant huntingtin leads to mitochondrial dysfunction and neurodegeneration. *Cell* **127,** 59–69 (2006).
270. Bae, B.-I. *et al.* p53 mediates cellular dysfunction and behavioral abnormalities in Huntington's disease. *Neuron* **47,** 29–41 (2005).
271. Milakovic, T. & Johnson, G. V. W. Mitochondrial respiration and ATP production are significantly impaired in striatal cells expressing mutant huntingtin. *J. Biol. Chem.* **280,** 30773–82 (2005).
272. Seong, I. S. *et al.* HD CAG repeat implicates a dominant property of huntingtin in mitochondrial energy metabolism. *Hum. Mol. Genet.* **14,** 2871–80 (2005).
273. Mochel, F. *et al.* Early alterations of brain cellular energy homeostasis in Huntington disease models. *J. Biol. Chem.* **287,** 1361–70 (2012).
274. Panov, A. V, Lund, S. & Greenamyre, J. T. Ca2+-induced permeability transition in human lymphoblastoid cell mitochondria from normal and Huntington's disease individuals. *Mol. Cell. Biochem.* **269,** 143–52 (2005).
275. Milakovic, T., Quintanilla, R. A. & Johnson, G. V. W. Mutant huntingtin expression induces mitochondrial calcium handling defects in clonal striatal cells: functional consequences. *J. Biol. Chem.* **281,** 34785–95 (2006).
276. Oliveira, J. M. A. *et al.* Mitochondrial-dependent Ca2+ handling in Huntington's disease striatal cells: effect of histone deacetylase inhibitors. *J. Neurosci.* **26,** 11174–86 (2006).
277. Brustovetsky, N. *et al.* Increased susceptibility of striatal mitochondria to calcium-induced permeability transition. *J. Neurosci.* **23,** 4858–67 (2003).
278. Chen, C.-M. *et al.* Increased oxidative damage and mitochondrial abnormalities in the peripheral blood of Huntington's disease patients. *Biochem. Biophys. Res. Commun.* **359,** 335–40 (2007).
279. Bogdanov, M. B., Andreassen, O. A., Dedeoglu, A., Ferrante, R. J. & Beal, M. F. Increased oxidative damage to DNA in a transgenic mouse model of Huntington's disease. *J. Neurochem.* **79,** 1246–9 (2001).
280. Tellez-Nagel, I., Johnson, A. B. & Terry, R. D. Studies on brain biopsies of patients with Huntington's chorea. *J. Neuropathol. Exp. Neurol.* **33,** 308–32 (1974).
281. Hoppins, S. The regulation of mitochondrial dynamics. *Curr. Opin. Cell Biol.* **29,** 46–52 (2014).
282. Costa, V. *et al.* Mitochondrial fission and cristae disruption increase the response of cell models of Huntington's disease to apoptotic stimuli. *EMBO Mol. Med.* **2,** 490–503 (2010).
283. Kim, J. *et al.* Mitochondrial loss, dysfunction and altered dynamics in Huntington's disease. *Hum. Mol. Genet.* **19,** 3919–35 (2010).
284. Shirendeb, U. *et al.* Abnormal mitochondrial dynamics, mitochondrial loss and mutant huntingtin oligomers in Huntington's disease: implications for selective neuronal damage. *Hum. Mol. Genet.* **20,** 1438–55 (2011).
285. Song, W. *et al.* Mutant huntingtin binds the mitochondrial fission GTPase dynamin-related protein-1 and increases its enzymatic activity. *Nat. Med.* **17,** 377–82 (2011).
286. Haun, F. *et al.* S-nitrosylation of dynamin-related protein 1 mediates mutant huntingtin-induced mitochondrial fragmentation and neuronal injury in Huntington's disease. *Antioxid. Redox Signal.* **19,** 1173–84 (2013).
287. Shirendeb, U. P. *et al.* Mutant huntingtin's interaction with mitochondrial protein Drp1 impairs mitochondrial biogenesis and causes defective axonal transport and synaptic degeneration in Huntington's disease. *Hum. Mol. Genet.* **21,** 406–20 (2012).
288. Trushina, E. *et al.* Mutant huntingtin impairs axonal trafficking in mammalian neurons in vivo and in vitro. *Mol. Cell. Biol.* **24,** 8195–209 (2004).
289. Orr, A. L. *et al.* N-terminal mutant huntingtin associates with mitochondria and impairs mitochondrial trafficking. *J. Neurosci.* **28,** 2783–92 (2008).

290. Beal, M. F. *et al.* Age-dependent striatal excitotoxic lesions produced by the endogenous mitochondrial inhibitor malonate. *J. Neurochem.* **61,** 1147–50 (1993).
291. Beal, M. F., Hyman, B. T. & Koroshetz, W. Do defects in mitochondrial energy metabolism underlie the pathology of neurodegenerative diseases? *Trends Neurosci.* **16,** 125–31 (1993).
292. Olney, J. W., Rhee, V. & Ho, O. L. Kainic acid: a powerful neurotoxic analogue of glutamate. *Brain Res.* **77,** 507–12 (1974).
293. Arundine, M. & Tymianski, M. Molecular mechanisms of calcium-dependent neurodegeneration in excitotoxicity. *Cell Calcium* **34,** 325–37
294. Calì, T., Ottolini, D. & Brini, M. Mitochondrial Ca(2+) and neurodegeneration. *Cell Calcium* **52,** 73–85 (2012).
295. Rasola, A. & Bernardi, P. The mitochondrial permeability transition pore and its involvement in cell death and in disease pathogenesis. *Apoptosis* **12,** 815–33 (2007).
296. Bonora, M. *et al.* Molecular mechanisms of cell death: central implication of ATP synthase in mitochondrial permeability transition. *Oncogene* (2014). doi:10.1038/onc.2014.96
297. Novelli, A., Reilly, J. A., Lysko, P. G. & Henneberry, R. C. Glutamate becomes neurotoxic via the N-methyl-D-aspartate receptor when intracellular energy levels are reduced. *Brain Res.* **451,** 205–12 (1988).
298. Hernández-Fonseca, K. & Massieu, L. Disruption of endoplasmic reticulum calcium stores is involved in neuronal death induced by glycolysis inhibition in cultured hippocampal neurons. *J. Neurosci. Res.* **82,** 196–205 (2005).
299. Pickrell, A. M., Fukui, H., Wang, X., Pinto, M. & Moraes, C. T. The striatum is highly susceptible to mitochondrial oxidative phosphorylation dysfunctions. *J. Neurosci.* **31,** 9895–904 (2011).
300. Oliveira, J. M. A. & Gonçalves, J. In situ mitochondrial Ca2+ buffering differences of intact neurons and astrocytes from cortex and striatum. *J. Biol. Chem.* **284,** 5010–20 (2009).
301. Brustovetsky, N. *et al.* Age-dependent changes in the calcium sensitivity of striatal mitochondria in mouse models of Huntington's Disease. *J. Neurochem.* **93,** 1361–70 (2005).
302. Landwehrmeyer, G. B., Standaert, D. G., Testa, C. M., Penney, J. B. & Young, A. B. NMDA receptor subunit mRNA expression by projection neurons and interneurons in rat striatum. *J. Neurosci.* **15,** 5297–307 (1995).
303. Zeron, M. M. *et al.* Increased sensitivity to N-methyl-D-aspartate receptor-mediated excitotoxicity in a mouse model of Huntington's disease. *Neuron* **33,** 849–60 (2002).
304. Miller, B. R. & Bezprozvanny, I. Corticostriatal circuit dysfunction in Huntington's disease: intersection of glutamate, dopamine and calcium. *Future Neurol.* **5,** 735–756 (2010).
305. Videnovic, A. Treatment of huntington disease. *Curr. Treat. Options Neurol.* **15,** 424–38 (2013).
306. Mrzljak, L. & Munoz-Sanjuan, I. Therapeutic Strategies for Huntington's Disease. *Curr. Top. Behav. Neurosci.* (2013). doi:10.1007/7854_2013_250
307. Clemens, L. E. & Jansson, E. K. H. Highlights from the 2014 EHDN Plenary Meeting. *HD Insights* **9,** 17 (2014).
308. Wild, E. J. & Tabrizi, S. J. Targets for future clinical trials in Huntington's disease: what's in the pipeline? *Mov. Disord.* **29,** 1434–45 (2014).
309. Harper, S. Q. *et al.* RNA interference improves motor and neuropathological abnormalities in a Huntington's disease mouse model. *Proc. Natl. Acad. Sci. U. S. A.* **102,** 5820–5825 (2005).
310. Stanek, L. M. *et al.* Silencing mutant huntingtin by adeno-associated virus-mediated RNA interference ameliorates disease manifestations in the YAC128 mouse model of Huntington's disease. *Hum. Gene Ther.* **25,** 461–74 (2014).
311. Carroll, J. B. *et al.* Potent and selective antisense oligonucleotides targeting single-nucleotide polymorphisms in the Huntington disease gene / allele-specific silencing of mutant huntingtin. *Mol. Ther.* **19,** 2178–85 (2011).
312. Garriga-Canut, M. *et al.* Synthetic zinc finger repressors reduce mutant huntingtin expression in the brain of R6/2 mice. *Proc. Natl. Acad. Sci. U. S. A.* **109,** E3136–45 (2012).
313. Bordet, T. *et al.* Identification and characterization of cholest-4-en-3-one, oxime (TRO19622), a novel drug candidate for amyotrophic lateral sclerosis. *J. Pharmacol. Exp. Ther.* **322,** 709–20 (2007).
314. Bordet, T., Berna, P., Abitbol, J.-L. & Pruss, R. M. Olesoxime (TRO19622): A Novel Mitochondrial-Targeted Neuroprotective Compound. *Pharmaceuticals* **3,** 345–368 (2010).
315. Colombini, M. VDAC: the channel at the interface between mitochondria and the cytosol. *Mol. Cell. Biochem.* **256-257,** 107–15
316. Gatliff, J. & Campanella, M. The 18 kDa translocator protein (TSPO): a new perspective in mitochondrial biology. *Curr. Mol. Med.* **12,** 356–68 (2012).

317. Veenman, L., Shandalov, Y. & Gavish, M. VDAC activation by the 18 kDa translocator protein (TSPO), implications for apoptosis. *J. Bioenerg. Biomembr.* **40,** 199–205 (2008).
318. Gouarné, C. *et al.* Protective role of olesoxime against wild-type α-synuclein-induced toxicity in human neuronally differentiated SHSY-5Y cells. *Br. J. Pharmacol.* **172,** 235–45 (2015).
319. Gouarné, C. *et al.* Olesoxime protects embryonic cortical neurons from camptothecin intoxication by a mechanism distinct from BDNF. *Br. J. Pharmacol.* **168,** 1975–88 (2013).
320. Rovini, A., Carré, M., Bordet, T., Pruss, R. M. & Braguer, D. Olesoxime prevents microtubule-targeting drug neurotoxicity: selective preservation of EB comets in differentiated neuronal cells. *Biochem. Pharmacol.* **80,** 884–94 (2010).
321. Magalon, K. *et al.* Olesoxime accelerates myelination and promotes repair in models of demyelination. *Ann. Neurol.* **71,** 213–26 (2012).
322. Sunyach, C. *et al.* Olesoxime delays muscle denervation, astrogliosis, microglial activation and motoneuron death in an ALS mouse model. *Neuropharmacology* **62,** 2346–52 (2012).
323. Richter, F. *et al.* Chronic administration of cholesterol oximes in mice increases transcription of cytoprotective genes and improves transcriptome alterations induced by alpha-synuclein overexpression in nigrostriatal dopaminergic neurons. *Neurobiol. Dis.* **69,** 263–75 (2014).
324. Bordet, T. *et al.* Specific antinociceptive activity of cholest-4-en-3-one, oxime (TRO19622) in experimental models of painful diabetic and chemotherapy-induced neuropathy. *J. Pharmacol. Exp. Ther.* **326,** 623–32 (2008).
325. Xiao, W. H., Zheng, F. Y., Bennett, G. J., Bordet, T. & Pruss, R. M. Olesoxime (cholest-4-en-3-one, oxime): analgesic and neuroprotective effects in a rat model of painful peripheral neuropathy produced by the chemotherapeutic agent, paclitaxel. *Pain* **147,** 202–9 (2009).
326. Xiao, W. H., Zheng, H. & Bennett, G. J. Characterization of oxaliplatin-induced chronic painful peripheral neuropathy in the rat and comparison with the neuropathy induced by paclitaxel. *Neuroscience* **203,** 194–206 (2012).
327. Lenglet, T. *et al.* A phase II-III trial of olesoxime in subjects with amyotrophic lateral sclerosis. *Eur. J. Neurol.* **21,** 529–36 (2014).
328. Dessaud, E. *et al.* A Phase II study to assess safety and efficacy of olesoxime (TRO19622) in 3-25 year-old Spinal Muscular Atrophy (SMA) patients. *Neurol. Emerg. Abstr.* **83,** e34–e40 (2014).
329. Valenza, M. *et al.* Dysfunction of the cholesterol biosynthetic pathway in Huntington's disease. *J. Neurosci.* **25,** 9932–9 (2005).
330. Kas, M. J. H. & Van Ree, J. M. Dissecting complex behaviours in the post-genomic era. *Trends Neurosci.* **27,** 366–9 (2004).
331. De Visser, L., van den Bos, R., Kuurman, W. W., Kas, M. J. H. & Spruijt, B. M. Novel approach to the behavioural characterization of inbred mice: automated home cage observations. *Genes. Brain. Behav.* **5,** 458–66 (2006).
332. Clemens, L. E., Jansson, E. K. H., Portal, E., Riess, O. & Nguyen, H. P. A behavioral comparison of the common laboratory rat strains Lister Hooded, Lewis, Fischer 344 and Wistar in an automated homecage system. *Genes, Brain Behav.* **13,** 305–321 (2014).
333. Van der Staay, F. J., Schuurman, T., van Reenen, C. G. & Korte, S. M. Emotional reactivity and cognitive performance in aversively motivated tasks: a comparison between four rat strains. *Behav. Brain Funct.* **5,** 50 (2009).
334. McDermott, C. & Kelly, J. P. Comparison of the behavioural pharmacology of the Lister-Hooded with 2 commonly utilised albino rat strains. *Prog. Neuropsychopharmacol. Biol. Psychiatry* **32,** 1816–23 (2008).
335. Franke, D. J. Verhaltensphysiologische Untersuchung von vier Rattenstämmen zur Detektion von Stammunterschieden mithilfe des automatisierten Verhaltenstestsystems PhenoTyper und den klassischen Verhaltenstests Open Field und Elevated Plus Maze. (2012).
336. Clemens, L. E., Franke, D. J., Magg, J. C. D., H, J. E. K. & Nguyen, H. P. Body weight gain is impaired in rats and mice during automated homecage system observations. in *Proc. Meas. Behav. 2014* (2014). doi:10.13140/2.1.1514.6244
337. Hall, F. S. Social deprivation of neonatal, adolescent, and adult rats has distinct neurochemical and behavioral consequences. *Crit. Rev. Neurobiol.* **12,** 129–162 (1998).
338. Lukkes, J. L., Watt, M. J., Lowry, C. A. & Forster, G. L. Consequences of post-weaning social isolation on anxiety behavior and related neural circuits in rodents. *Front. Behav. Neurosci.* **3,** 18 (2009).
339. Kalliokoski, O. *et al.* Mice do not habituate to metabolism cage housing--a three week study of male BALB/c mice. *PLoS One* **8,** e58460 (2013).
340. Gil, M. C. *et al.* Influence of age on stress responses to metabolic cage housing in rats. *Cell. Mol. Neurobiol.* **19,** 625–33 (1999).

341. Daskalakis, N. P. *et al.* Early experience of a novel-environment in isolation primes a fearful phenotype characterized by persistent amygdala activation. *Psychoneuroendocrinology* **39,** 39–57 (2014).
342. Chaouloff, F. *et al.* Male Fischer 344 and Lewis rats display differences in locomotor reactivity, but not in anxiety-related behaviours: relationship with the hippocampal serotonergic system. *Brain Res.* **693,** 169–78 (1995).
343. Dhabhar, F. S., McEwen, B. S. & Spencer, R. L. Stress response, adrenal steroid receptor levels and corticosteroid-binding globulin levels--a comparison between Sprague-Dawley, Fischer 344 and Lewis rats. *Brain Res.* **616,** 89–98 (1993).
344. Jansson, E. K. H., Clemens, L. E., Riess, O. & Nguyen, H. P. Reduced Motivation in the BACHD Rat Model of Huntington Disease Is Dependent on the Choice of Food Deprivation Strategy. *PLoS One* **9,** e105662 (2014).
345. Myers, R. H. *et al.* Homozygote for Huntington disease. *Am. J. Hum. Genet.* **45,** 615–8 (1989).
346. Soll, L. G., Grady, S. R., Salminen, O., Marks, M. J. & Tapper, A. R. A role for α4(non-α6)* nicotinic acetylcholine receptors in motor behavior. *Neuropharmacology* **73,** 19–30 (2013).
347. McFadyen, M. P., Kusek, G., Bolivar, V. J. & Flaherty, L. Differences among eight inbred strains of mice in motor ability and motor learning on a rotorod. *Genes. Brain. Behav.* **2,** 214–219 (2003).
348. Pallier, P. N., Drew, C. J. G. & Morton, A. J. The detection and measurement of locomotor deficits in a transgenic mouse model of Huntington's disease are task- and protocol-dependent: influence of non-motor factors on locomotor function. *Brain Res. Bull.* **78,** 347–55 (2009).
349. Kanoski, S. E., Alhadeff, A. L., Fortin, S. M., Gilbert, J. R. & Grill, H. J. Leptin signaling in the medial nucleus tractus solitarius reduces food seeking and willingness to work for food. *Neuropsychopharmacology* **39,** 605–13 (2014).
350. Verwaest, K. A. *et al.* (1)H NMR based metabolomics of CSF and blood serum: A metabolic profile for a transgenic rat model of Huntington disease. *Biochim. Biophys. Acta* **1812,** 1371–9 (2011).
351. Frayn, K. *Metabolic Regulation - A Human Perspective*. (Blackwell Science Ltd, 2003).
352. Wood, N. I. *et al.* Increased thirst and drinking in Huntington's disease and the R6/2 mouse. *Brain Res. Bull.* **76,** 70–9 (2008).
353. Hurlbert, M. S. *et al.* Mice transgenic for an expanded CAG repeat in the Huntington's disease gene develop diabetes. *Diabetes* **48,** 649–51 (1999).
354. Heldmaier, G. *Vergleichende Tierphysiologie Band 2 Vegetative Physiologie*. (Springer-Verlag, 2004).
355. Van der Burg, J. M. M. *et al.* Gastrointestinal dysfunction contributes to weight loss in Huntington's disease mice. *Neurobiol. Dis.* **44,** 1–8 (2011).
356. Verwaest, K. 1H NMR based metabolomics studies of biofluids and brain extracts from animal models for neurodegenerative diseases. (2011).
357. Harp, J. B., Goldstein, S. & Phillips, L. S. Nutrition and somatomedin. XXIII. Molecular regulation of IGF-I by amino acid availability in cultured hepatocytes. *Diabetes* **40,** 95–101 (1991).
358. Gouarné, C. *et al.* Early deficits in glycolysis are specific to striatal neurons from a rat model of huntington disease. *PLoS One* **8,** e81528 (2013).
359. Pastorino, J. G. & Hoek, J. B. Regulation of hexokinase binding to VDAC. *J. Bioenerg. Biomembr.* **40,** 171–82 (2008).
360. Gu, M. *et al.* Mitochondrial defect in Huntington's disease caudate nucleus. *Ann. Neurol.* **39,** 385–9 (1996).
361. Genazzani, A. A., Carafoli, E. & Guerini, D. Calcineurin controls inositol 1,4,5-trisphosphate type 1 receptor expression in neurons. *Proc. Natl. Acad. Sci. U. S. A.* **96,** 5797–801 (1999).
362. Kopil, C. M., Siebert, A. P., Foskett, J. K. & Neumar, R. W. Calpain-cleaved type 1 inositol 1,4,5-trisphosphate receptor impairs ER Ca(2+) buffering and causes neurodegeneration in primary cortical neurons. *J. Neurochem.* **123,** 147–58 (2012).
363. Stutzmann, G. E. & Mattson, M. P. Endoplasmic reticulum Ca(2+) handling in excitable cells in health and disease. *Pharmacol. Rev.* **63,** 700–27 (2011).
364. Goll, D. E., Thompson, V. F., Li, H., Wei, W. & Cong, J. The calpain system. *Physiol. Rev.* **83,** 731–801 (2003).
365. Getz, G. S. Calpain inhibition as a potential treatment of Alzheimer's disease. *Am. J. Pathol.* **181,** 388–91 (2012).
366. Samantaray, S., Ray, S. K. & Banik, N. L. Calpain as a potential therapeutic target in Parkinson's disease. *CNS Neurol. Disord. Drug Targets* **7,** 305–12 (2008).
367. Stifanese, R. *et al.* Role of calpain-1 in the early phase of experimental ALS. *Arch. Biochem. Biophys.* **562,** 1–8 (2014).
368. Haacke, A., Hartl, F. U. & Breuer, P. Calpain inhibition is sufficient to suppress aggregation of polyglutamine-expanded ataxin-3. *J. Biol. Chem.* **282,** 18851–6 (2007).

369. Bizat, N. *et al.* Calpain is a major cell death effector in selective striatal degeneration induced in vivo by 3-nitropropionate: implications for Huntington's disease. *J. Neurosci.* **23,** 5020–30 (2003).
370. Gellerich, F. N. *et al.* The regulation of OXPHOS by extramitochondrial calcium. *Biochim. Biophys. Acta* **1797,** 1018–27 (2010).
371. Browne, S. E., Ferrante, R. J. & Beal, M. F. Oxidative stress in Huntington's disease. *Brain Pathol.* **9,** 147–63 (1999).
372. Beckman, K. B. & Ames, B. N. Oxidative decay of DNA. *J. Biol. Chem.* **272,** 19633–6 (1997).
373. St-Pierre, J. *et al.* Suppression of reactive oxygen species and neurodegeneration by the PGC-1 transcriptional coactivators. *Cell* **127,** 397–408 (2006).
374. Johri, A., Chandra, A. & Beal, M. F. PGC-1α, mitochondrial dysfunction, and Huntington's disease. *Free Radic. Biol. Med.* **62,** 37–46 (2013).
375. McGill, J. K. & Beal, M. F. PGC-1alpha, a new therapeutic target in Huntington's disease? *Cell* **127,** 465–8 (2006).
376. Johri, A. *et al.* Truncated peroxisome proliferator-activated receptor-γ coactivator 1α splice variant is severely altered in Huntington's disease. *Neurodegener. Dis.* **8,** 496–503 (2011).
377. Eckmann, J. *et al.* Mitochondrial Membrane Fluidity is Consistently Increased in Different Models of Huntington Disease: Restorative Effects of Olesoxime. *Mol. Neurobiol.* (2014). doi:10.1007/s12035-014-8663-3
378. Helmreich, E. J. M. Environmental influences on signal transduction through membranes: a retrospective mini-review. *Biophys. Chem.* **100,** 519–34 (2003).
379. Los, D. A. & Murata, N. Membrane fluidity and its roles in the perception of environmental signals. *Biochim. Biophys. Acta* **1666,** 142–57 (2004).
380. Maxfield, F. R. & Tabas, I. Role of cholesterol and lipid organization in disease. *Nature* **438,** 612–21 (2005).
381. Ziegelhöffer, A. *et al.* Involvement of membrane fluidity in endogenous protective processes running on subcellular membrane systems of the rat heart. *Physiol. Res.* **61 Suppl 2,** S11–21 (2012).
382. Shi, C., Wu, F. & Xu, J. Incorporation of β-sitosterol into mitochondrial membrane enhances mitochondrial function by promoting inner mitochondrial membrane fluidity. *J. Bioenerg. Biomembr.* **45,** 301–5 (2013).
383. Pieri, C., Falasca, M., Moroni, F., Marcheselli, F. & Recchioni, R. Studies on cell membrane properties in food restricted rats. *Aging (Milano).* **3,** 401–3 (1991).
384. Levin, G., Cogan, U. & Mokady, S. Food restriction and membrane fluidity. *Mech. Ageing Dev.* **62,** 137–41 (1992).
385. Brady, L. J., Hoppel, C. L. & Brady, P. S. Hepatic mitochondrial inner-membrane properties, beta-oxidation and carnitine palmitoyltransferases A and B. Effects of genetic obesity and starvation. *Biochem. J.* **233,** 427–33 (1986).
386. Ricchelli, F., Gobbo, S., Moreno, G. & Salet, C. Changes of the fluidity of mitochondrial membranes induced by the permeability transition. *Biochemistry* **38,** 9295–300 (1999).
387. Rolo, A. P., Oliveira, P. J., Moreno, A. J. & Palmeira, C. M. Chenodeoxycholate induction of mitochondrial permeability transition pore is associated with increased membrane fluidity and cytochrome c release: protective role of carvedilol. *Mitochondrion* **2,** 305–11 (2003).
388. Colell, A. *et al.* Cholesterol impairs the adenine nucleotide translocator-mediated mitochondrial permeability transition through altered membrane fluidity. *J. Biol. Chem.* **278,** 33928–35 (2003).
389. Fajardo, V. A., McMeekin, L. & LeBlanc, P. J. Influence of phospholipid species on membrane fluidity: a meta-analysis for a novel phospholipid fluidity index. *J. Membr. Biol.* **244,** 97–103 (2011).
390. Valenza, M. *et al.* Cholesterol defect is marked across multiple rodent models of Huntington's disease and is manifest in astrocytes. *J. Neurosci.* **30,** 10844–50 (2010).
391. Leoni, V. & Caccia, C. Study of cholesterol metabolism in Huntington's disease. *Biochem. Biophys. Res. Commun.* **446,** 697–701 (2014).
392. Marullo, M. *et al.* Pitfalls in the detection of cholesterol in Huntington's disease models. *PLoS Curr.* **4,** e505886e9a1968 (2012).
393. Kaltenbach, L. S. *et al.* Huntingtin interacting proteins are genetic modifiers of neurodegeneration. *PLoS Genet.* **3,** e82 (2007).
394. Hu, J., Zhang, Z., Shen, W.-J. & Azhar, S. Cellular cholesterol delivery, intracellular processing and utilization for biosynthesis of steroid hormones. *Nutr. Metab. (Lond).* **7,** 47 (2010).
395. Chen, H. & Chan, D. C. Emerging functions of mammalian mitochondrial fusion and fission. *Hum. Mol. Genet.* **14 Spec No,** R283–9 (2005).
396. Wang, W. *et al.* Mfn2 Couples Glutamate Excitotoxicity and Mitochondrial Dysfunction in Motor Neurons. *J. Biol. Chem.* (2014). doi:10.1074/jbc.M114.617167

397. Hollenbeck, P. J. & Saxton, W. M. The axonal transport of mitochondria. *J. Cell Sci.* **118,** 5411–9 (2005).
398. Li, X.-J., Orr, A. L. & Li, S. Impaired mitochondrial trafficking in Huntington's disease. *Biochim. Biophys. Acta* **1802,** 62–5 (2010).
399. Chang, D. T. W., Rintoul, G. L., Pandipati, S. & Reynolds, I. J. Mutant huntingtin aggregates impair mitochondrial movement and trafficking in cortical neurons. *Neurobiol. Dis.* **22,** 388–400 (2006).
400. Zala, D. *et al.* Phosphorylation of mutant huntingtin at S421 restores anterograde and retrograde transport in neurons. *Hum. Mol. Genet.* **17,** 3837–46 (2008).
401. Zala, D. *et al.* Vesicular glycolysis provides on-board energy for fast axonal transport. *Cell* **152,** 479–91 (2013).
402. Chang, K. T., Niescier, R. F. & Min, K.-T. Mitochondrial matrix Ca2+ as an intrinsic signal regulating mitochondrial motility in axons. *Proc. Natl. Acad. Sci. U. S. A.* **108,** 15456–61 (2011).
403. Su, B., Ji, Y.-S., Sun, X., Liu, X.-H. & Chen, Z.-Y. Brain-derived neurotrophic factor (BDNF)-induced mitochondrial motility arrest and presynaptic docking contribute to BDNF-enhanced synaptic transmission. *J. Biol. Chem.* **289,** 1213–26 (2014).
404. Mórotz, G. M. *et al.* Amyotrophic lateral sclerosis-associated mutant VAPBP56S perturbs calcium homeostasis to disrupt axonal transport of mitochondria. *Hum. Mol. Genet.* **21,** 1979–88 (2012).
405. Schoch, K. M. *et al.* Calpastatin overexpression limits calpain-mediated proteolysis and behavioral deficits following traumatic brain injury. *Exp. Neurol.* **236,** 371–82 (2012).
406. Cao, G. *et al.* Critical role of calpain I in mitochondrial release of apoptosis-inducing factor in ischemic neuronal injury. *J. Neurosci.* **27,** 9278–93 (2007).
407. Ozaki, T., Yamashita, T. & Ishiguro, S.-I. Mitochondrial m-calpain plays a role in the release of truncated apoptosis-inducing factor from the mitochondria. *Biochim. Biophys. Acta* **1793,** 1848–59 (2009).
408. Norberg, E. *et al.* An increase in intracellular Ca2+ is required for the activation of mitochondrial calpain to release AIF during cell death. *Cell Death Differ.* **15,** 1857–64 (2008).
409. Giacomello, M., Hudec, R. & Lopreiato, R. Huntington's disease, calcium, and mitochondria. *Biofactors* **37,** 206–18 (2011).
410. Nothdurfter, C., Baghai, T. C., Schüle, C. & Rupprecht, R. Translocator protein (18 kDa) (TSPO) as a therapeutic target for anxiety and neurologic disorders. *Eur. Arch. Psychiatry Clin. Neurosci.* **262 Suppl ,** S107–12 (2012).
411. Kim, J.-S. *et al.* Carbamazepine suppresses calpain-mediated autophagy impairment after ischemia/reperfusion in mouse livers. *Toxicol. Appl. Pharmacol.* (2013). doi:10.1016/j.taap.2013.10.006
412. Rone, M. B., Fan, J. & Papadopoulos, V. Cholesterol transport in steroid biosynthesis: role of protein-protein interactions and implications in disease states. *Biochim. Biophys. Acta* **1791,** 646–58 (2009).
413. Grienberger, C. & Konnerth, A. Imaging calcium in neurons. *Neuron* **73,** 862–85 (2012).
414. Butler, A. A. & Kozak, L. P. A recurring problem with the analysis of energy expenditure in genetic models expressing lean and obese phenotypes. *Diabetes* **59,** 323–9 (2010).
415. Shlomi, T., Cabili, M. N., Herrgård, M. J., Palsson, B. Ø. & Ruppin, E. Network-based prediction of human tissue-specific metabolism. *Nat. Biotechnol.* **26,** 1003–10 (2008).
416. Cheng, C. M. *et al.* Insulin-like growth factor 1 regulates developing brain glucose metabolism. *Proc. Natl. Acad. Sci. U. S. A.* **97,** 10236–41 (2000).
417. Feng, Z. & Levine, A. J. The regulation of energy metabolism and the IGF-1/mTOR pathways by the p53 protein. *Trends Cell Biol.* **20,** 427–34 (2010).
418. Naia, L. *et al.* Activation of IGF-1 and Insulin Signaling Pathways Ameliorate Mitochondrial Function and Energy Metabolism in Huntington's Disease Human Lymphoblasts. *Mol. Neurobiol.* (2014). doi:10.1007/s12035-014-8735-4
419. Aziz, N. A. *et al.* Leptin secretion rate increases with higher CAG repeat number in Huntington's disease patients. *Clin. Endocrinol. (Oxf).* **73,** 206–11 (2010).
420. Wang, R. *et al.* Metabolic and hormonal signatures in pre-manifest and manifest Huntington's disease patients. *Front. Physiol.* **5,** 231 (2014).
421. Hubert, M. F., Laroque, P., Gillet, J. P. & Keenan, K. P. The effects of diet, ad Libitum feeding, and moderate and severe dietary restriction on body weight, survival, clinical pathology parameters, and cause of death in control Sprague-Dawley rats. *Toxicol. Sci.* **58,** 195–207 (2000).
422. Sáinz, N., Barrenetxe, J., Moreno-Aliaga, M. J. & Martínez, J. A. Leptin resistance and diet-induced obesity: central and peripheral actions of leptin. *Metabolism* **64,** 35–46 (2015).

423. Thissen, J. P., Ketelslegers, J. M. & Underwood, L. E. Nutritional regulation of the insulin-like growth factors. *Endocr. Rev.* **15,** 80–101 (1994).

424. Moffett, J. R., Ross, B., Arun, P., Madhavarao, C. N. & Namboodiri, A. M. A. N-Acetylaspartate in the CNS: from neurodiagnostics to neurobiology. *Prog. Neurobiol.* **81,** 89–131 (2007).

425. Van den Bogaard, S. J. A. *et al.* Longitudinal Metabolite Changes in Huntington's Disease During Disease Onset. *J. Huntingtons. Dis.* **3,** 377–86 (2014).

426. Van Oostrom, J. C. H., Sijens, P. E., Roos, R. A. C. & Leenders, K. L. 1H magnetic resonance spectroscopy in preclinical Huntington disease. *Brain Res.* **1168,** 67–71 (2007).

427. Wanker, E. E. *et al.* Membrane filter assay for detection of amyloid-like polyglutamine-containing protein aggregates. *Methods Enzymol.* **309,** 375–86 (1999).

428. De Vos, K. J. *et al.* Familial amyotrophic lateral sclerosis-linked SOD1 mutants perturb fast axonal transport to reduce axonal mitochondria content. *Hum. Mol. Genet.* **16,** 2720–8 (2007).

429. Abràmoff, M. D., Magalhães, P. J. & Sunanda, J. Image Processing with ImageJ. *Biophotonics Int.* **11,** 36–42 (2004).

430. De Vos, K. J. & Sheetz, M. P. Visualization and quantification of mitochondrial dynamics in living animal cells. *Methods Cell Biol.* **80,** 627–82 (2007).

431. Gunawardena, S. *et al.* Disruption of axonal transport by loss of huntingtin or expression of pathogenic polyQ proteins in Drosophila. *Neuron* **40,** 25–40 (2003).

432. Szebenyi, G. *et al.* Neuropathogenic forms of huntingtin and androgen receptor inhibit fast axonal transport. *Neuron* **40,** 41–52 (2003).

433. Tian, J. *et al.* Soluble N-terminal fragment of mutant Huntingtin protein impairs mitochondrial axonal transport in cultured hippocampal neurons. *Neurosci. Bull.* **30,** 74–80 (2014).

434. Cai, Q., Davis, M. L. & Sheng, Z.-H. Regulation of axonal mitochondrial transport and its impact on synaptic transmission. *Neurosci. Res.* **70,** 9–15 (2011).

435. Humbert, S. *et al.* The IGF-1/Akt pathway is neuroprotective in Huntington's disease and involves Huntingtin phosphorylation by Akt. *Dev. Cell* **2,** 831–7 (2002).

Appendix

The Appendix contains all data that has not been implemented in a manuscript for publication so far, but which is crucial for the understanding of the assumptions made in this work.

For each section, a brief summary, the contribution of each author, the description of the methods applied (if not available in one of the publications), the results and a discussion of the results is given.

The Appendix contains data sets of the following subjects:

A. Automated phenotyping in rats

B. BACHD rat body size and body composition

C. BACHD rat energy balance

D. BACHD rat blood parameters

E. BACHD rat primary neuronal cultures

A. Automated phenotyping in rats

Laura E. Clemens[1,2], Damaris J. Franke[1,2], Erik K. H. Jansson[1,2], Huu P. Nguyen[1,2]

[1] Institute for Medical Genetics and Applied Genomics, University of Tuebingen, Tuebingen, Germany.
[2] Centre for Rare Diseases, University of Tuebingen, Tuebingen, Germany.

Summary

Background: Automated behavioral phenotyping systems are promoted to produce robust outcomes, which relate better to natural animal behavior than results from classical tests that are run manually. In order to use automated phenotyping for the characterization of transgenic animal models of neurodegenerative diseases, we evaluated the validity of the commercially available automated phenotyping systems PhenoMaster and PhenoTyper.

Methods: We recorded and analyzed the behavior of five, commonly used, rat strains during 70-hour sessions in the automated phenotyping systems.

Results: Using the PhenoMaster system, we detected strain differences in novelty-induced behavior, activity-related behavior, metabolism, as well as the development of these parameters with age. Some but not all characteristics were replicated by the PhenoTyper. Importantly, we detected a significant drop in weight gain in two of the four investigated rat strains during the measurements in both automated systems.

Discussion: Automated phenotyping enabled the recording of large amounts of data and the detection of significant differences between the rat strains. However, the results differed between the two systems and the rats seemed to have experienced stress during the measurements. Thus, the validity of the outcomes is questionable and should be evaluated in further studies.

Author contributions

Conceived and designed the experiments: HPN, LEC
Performed the experiments: LEC (PhenoMaster), DJF (PhenoTyper)
Analyzed the data: LEC, DJF, EKHJ

Materials and Methods

Animals

Data presented here derive from rats of five different WT rat strains as part of three separate studies. WT rats from the strains Lister Hooded, Lewis, Fischer and Wistar were purchased from Charles River, Germany at the age of 3 weeks, as part of the studies described in Publication IV[332] (PhenoMaster), and Reference[335] (PhenoTyper). In addition, PhenoMaster data on Sprague Dawley rats derive from the study discussed in Publication VII and Appendix C. Housing conditions were similar for all rats and are described in Publication IV[332].

Body weight measurements

Body weight was measured on a weekly basis, as well as immediately before and after each test, enabling the comparison of body weight gain before, during and after behavioral testing. The measurements were made using a kitchen balance (accuracy was ± 1 g).

Automated phenotyping

Automated behavioral phenotyping was performed with two automated homecage systems for rats, the PhenoMaster (TSE Systems, Germany) and the PhenoTyper 4500 (Noldus Information Technology, The Netherlands), as displayed in Figure 1 and listed in Table 1.

The customized setup of the systems' test cages differed considerably from each other as well as from standard home cages. Both setups had smaller floor space compared to the standard housing cages, with the PhenoMaster cages being the smallest (Table 1). The PhenoMaster cages also used an air-tight lid, which resulted in a considerably lower cage height compared to the home cages. In contrast, the PhenoTyper cages were higher than the normal home cages (Table 1). The home cages used standard cage tops, where food and water was placed (Figure 1). The PhenoTyper cages had a large food hopper placed vertically on one of its walls, and a water bottle placed on either side of it. The PhenoMaster system used small, free-hanging water bottles and food baskets, which were connected to scales and placed on top of the setup. Additional differences were the availability of a small shelter as well as the use on non-standard bedding in the PhenoTyper cages. The PhenoMaster used

the regular bedding material, although in a much lower amount compared to the normal housing cages to avoid interference with activity measurements. Both systems were kept in the same experimental room, which was separate from the housing room the rats stayed in between experiments.

For the experiments, the animals were transferred to the experimental room and placed individually in the testing cages. The rats' behavior was investigated over a period of 2 days, during which they had *ad libitum* access to food and water and were left undisturbed except for a short daily visit. During visits, the animals were inspected for proper food and water intake. In between runs, the systems were cleaned thoroughly and new bedding as well as fresh water and food pellets were supplied. The exact procedures for each test system are given below.

Table 1. Dimensions of the phenotyping cages compared to the rats' home cages.
Cage length, width and height are given for the PhenoMaster for rats with metabolic cage setup, the PhenoTyper 4500 for rats with standard setup, and standard type IV rat home cages with high lids.

System	Provider	Species	Cage dimensions length - width - height
PhenoMaster	TSE	Rat	48 - 37.5 - 20 cm
PhenoTyper	Noldus	Rat	45 - 45 - 65 cm
Home cage		Rat	55 - 38 - 24.5 cm

PhenoMaster

A detailed description of setup and procedures are available in Publication IV[332]. Briefly, the PhenoMaster system (Figure 1) consisted of 12 home cage-like testing cages with metabolic setup, which were composed of a cage with 48 x 37.5 cm floor area and 20 cm high walls, a solid plastic lid with tubes connected for respirometric measurements, a free-hanging water bottle and small food basket equipped with sensors for the detection of food and water intake,

as well as a frame with infrared motion detectors for activity assessment surrounding the cage. The cage floor was covered with 200 g of wooden bedding. A total of 48 rats (12 rats per strain) were analyzed. The behavior of each animal was assessed during a 70-hour observation period. Thus, four runs were needed in order to measure all rats, resulting in a total duration of 12 days for the entire experiment. During a given run, the animals were assigned to one of the 12 test cages in a pseudo-randomized manner, so that each run included 3 animals from each of the 4 rat strains. Each measurement started 40 ± 5 minutes before the onset of the dark phase. Data were collected in 20-minute sample intervals. Measurements were carried out at the ages of 2, 4 and 6 months.

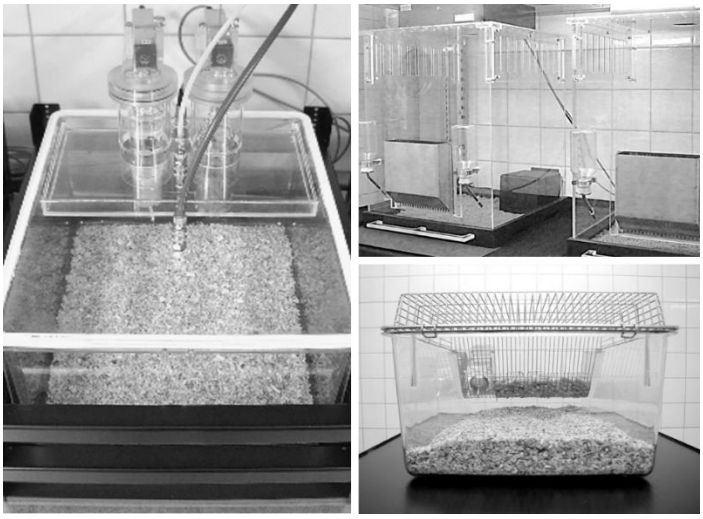

Figure 1. Setup of the phenotyping cages compared to the rats' home cages.
The PhenoMaster system for rats with metabolic cage setup (left), the PhenoTyper 4500 for rats with standard setup (upper right), and a standard type IV rat homecage with high lid (lower right) are shown.

PhenoTyper

A detailed description of setup and procedures are available in Reference[335]. Briefly, the PhenoTyper 4500 system (Figure 1) consisted of 4 test cages with a 45 x 45 cm large arena and 65 cm high transparent walls, as well as an infrared camera on top of the cage for continuous light and dark phase observation. Our setup included a black shelter located in one corner, and a large feeding area and two water bottles placed along one of the walls. The floor was covered with gray cellulose bedding (Cellu-Dri Soft®, Shepherd Speciality Papers, USA) for better detection of rats with white fur color. A total of 48 rats (12 rats per strain) were analyzed. The behavior of each animal was assessed during a 70-hour observation period. Thus, eight runs were needed in order to assess all rats, resulting in a total duration of 24 days for the entire experiment. A given cage was specifically assigned to measure the behavior of one of the rat strains. Pseudo-randomization could not be made, as camera settings needed to be individually adjusted to optimize the detection of the different fur colors and body sizes of the rats from the 4 strains. Each run included one animal from each of the 4 strains. Two types of measurements were taken at each age. The first measurement started 30 minutes before the onset of the dark phase and lasted for 1 hour. During the 1-hour observation time, a continuous video was recorded. After this, the rats were removed, the program settings changed, and the rats were put back into the cages for another 69 hours. During this second run, the rats' behavior was live-tracked, as the system was not capable of storing video files of such large size.

Data analysis

Raw data from the PhenoMaster were exported, pre-processed into hourly bins and sorted by genotype, treatment and age using a script for R statistics developed in our institute[332]. Video data from the PhenoMaster were tracked for activity-related parameters with the software EthoVision XT 7.1 (Noldus Information Technology) and additionally manually tracked for rearing behavior. All pre-processed data were then graphed and statistically analyzed with the software GraphPad Prism (GraphPad Prism version 6.00 for Windows, GraphPad Software, San Diego California USA, www.graphpad.com), and are presented in the following as mean and standard error of the mean (SEM).

Results

PhenoMaster compared to PhenoTyper

We detected significant differences between the strains in the PhenoMaster, which mainly derived from higher light phase and lower dark phase activity of Lister Hooded rats compared to the other three rat strains (as presented in detail in Publication IV[332]). During PhenoTyper observation, however, such a difference could not be detected (Figure 2). Moreover, all rat strains showed a more pronounced circadian rhythm in the PhenoTyper, with higher dark phase and lower light phase activity than during PhenoMaster observation (Figure 2).

Stress response during automated phenotyping

When analyzing data from the PhenoMaster experiment, we noticed that the body weight gain of the rats dropped during the test sessions (Publication IV[332]) and returned to normal when the rats were once again housed in their home cages. Therefore, we also investigated body weight gain before and after PhenoTyper tests (Figure 2), and found similar results. In both systems, the phenotype was most apparent in Wistar and Fischer rats.

The effect of automated homecage observation on body weight gain was more pronounced in older rats (Figure 2). It has to be noted that a body weight effect is more difficult to evaluate at younger ages due to a considerable decline in growth over the first 3 months. Due to this, the 2 months old rats, except for Lewis rats, did not return to their weekly weight gain baseline after the test sessions.

When comparing body weight development at two ages in old Sprague Dawley rats, which did not substantially grow anymore, the effect was significantly stronger at the oldest age (Figure 3). Furthermore, while younger rats showed a reduced body weight gain during automated homecage observation, older rats experienced explicit weight loss (Figure 2 and 3).

A. Automated phenotyping in rats

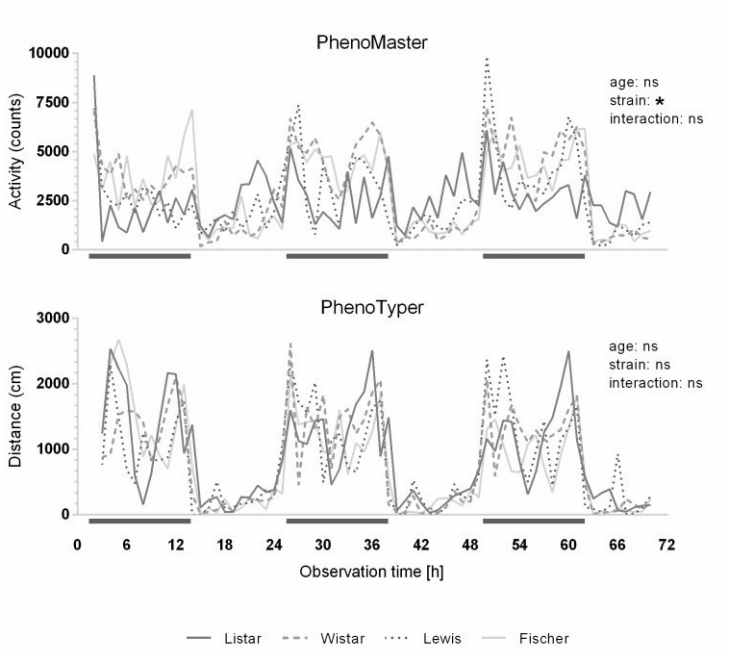

Figure 2. The circadian pattern of activity obtained during PhenoMaster and PhenoTyper observation.

Locomotor activity of Lister Hooded, Wistar, Lewis and Fischer 344 rats was measured during PhenoMaster and PhenoTyper observation at 2 months of age. The PhenoMaster activity measurement was based on motion detection with infrared light beams and is expressed as number of light beam activations (counts). The PhenoTyper activity measurements derive from video tracking and represents the distance moved (in cm). Group mean without SEM for better overview, two-way repeated measurements ANOVA, n = 12 per group, * $P < 0.05$, ** $P < 0.01$, *** $P < 0.001$.

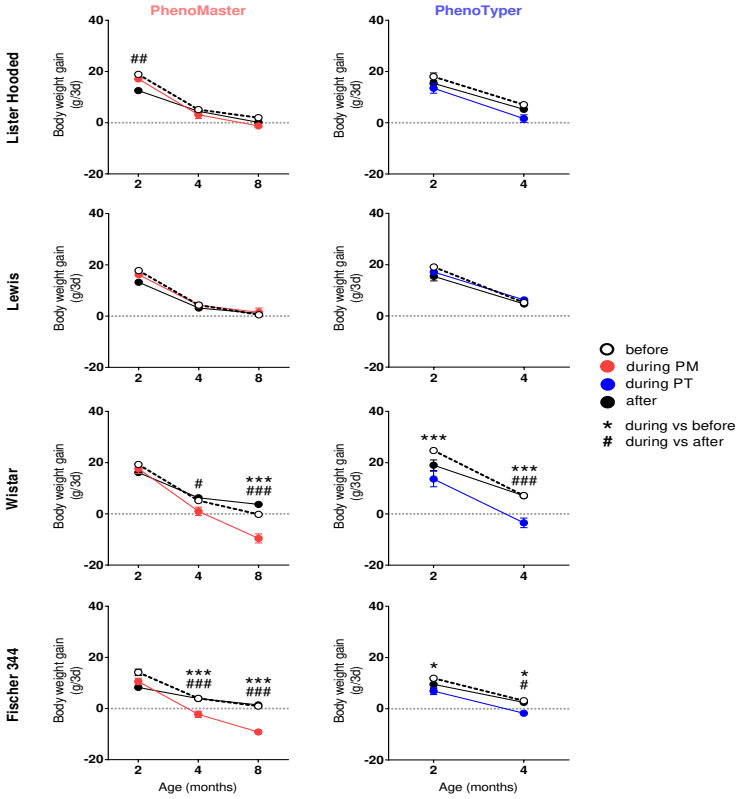

Figure 2. Effect of automated homecage observation on body weight gain in the different rat strains.

The behavior of Lister Hooded, Lewis, Wistar and Fischer 344 rats was recorded in the PhenoMaster at 2, 4 and 8 months of age, as well as in the PhenoTyper at 2 and 4 months of age. Body weight gain during the 3 days of observation was compared to the average body weight gain over 3 days during the week prior and post testing. Mean and SEM, two-way repeated measurements ANOVA, Fisher LSD post-test, n = 12 per group, */# $P < 0.05$, **/## $P < 0.01$, ***/### $P < 0.001$.

A. Automated phenotyping in rats

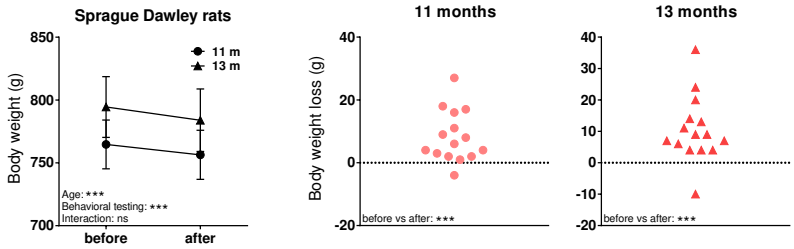

Figure 3. Body weight loss in aged rats during automated homecage observation.

Sprague Dawley rats were subjected to automated homecage observation in the rat PhenoMaster at 11 and 13 months of age. Body weight was measured before and after 3 days of observation. Statistical analysis of body weight before and after testing was performed using repeated measurements two-way ANOVA, and statistical analysis of body weight loss was evaluated using paired one-tailed *t*-tests, n = 12 per group, * $P < 0.05$, ** $P < 0.01$, *** $P < 0.001$.

Discussion

PhenoMaster compared to other tests

We initially reported significant inter-strain differences based on a particularly deviating behavior of Lister Hooded rats in the PhenoMaster system (Publication IV[332]). Lister rats showed significantly increased day-time activity, which might be ascribed to their pigmentation and thus better vision compared to the other rat strains investigated in our study. However, the difference in circadian activity could not be replicated in the PhenoTyper, implying that the first, peculiar results might not reflect the natural behavior of Lister Hooded rats. The deviant outcomes might derive from Lister Hooded rats behaving abnormally during PhenoMaster exposure based on the specific cage environment, or from differences in the detection method between the two systems. While the activity measurement in the PhenoMaster relies on motion detection via infrared light beams, the PhenoTyper system uses software-based tracking of the distance moved as obtained from video recordings. However, it remains unresolved why the systems gave different outcomes, and what the true behavioral characteristics of the rats are. Follow-up studies are needed to clarify this issue.

Stress response during automated phenotyping

Our data reveal a strain-dependent impairment in body weight gain during automated homecage observations. This drop in body weight gain was likely the effect of improper food intake, as susceptible rats had lower food intake than it would be expected from their respective body sizes. Furthermore, the rats showed a decline in RQ, which is reduced during starvation[354] (Publication IV[332]). Thus, as the effect had influenced the readouts of the measurements, outcomes of such studies need to be interpreted carefully.

Improper food intake and reduced body weight gain indicate that the animals experienced some form of stress, while being housed in the test cages. This idea is supported by the fact that Lister and Lewis rats, which showed little effect of automated homecage testing on body weight gain, are known as less anxious[342,343].

Interestingly, we further found that the drop in body weight gain during automated phenotyping was similar as when running classical behavioral tests[336], suggesting that the home cage-like

test setup does not improve animal welfare aspects compared to classical testing, although the systems are promoted to do so.

The stress effect of automated phenotyping seems to be of general importance, as it was observed in three out of the five rat strains investigated. In addition, we detected similar effects in mice[336].

B. BACHD rat body size and body composition

Laura E. Clemens[1,2], Erik K. H. Jansson[1,2], Huu P. Nguyen[1,2]

[1] Institute for Medical Genetics and Applied Genomics, University of Tuebingen, Tuebingen, Germany.
[2] Centre for Rare Diseases, University of Tuebingen, Tuebingen, Germany.

Summary

Background: Metabolic disturbances play a prominent role in HD. HD patients as well as disease models of HD display metabolic abnormalities including alterations in body weight, body size and body composition. The BACHD rat appears to be smaller and obese compared to WT littermates.

Methods: We investigated the body size and body composition of BACHD rats by detailed dissections at the ages of 1, 3, 6, 9 and 12 months. Body size measurements included head, trunk and tail length. Body composition was assessed by measuring body weight, fat mass, individual organ mass as well as bone/muscle mass.

Results: BACHD rats were found to have an overall shorter body length, increased fat mass, and reduced lean mass compared to WT rats. Consistent with their smaller size, organ weights were systematically reduced. Differences were present at 1 month, aggravated by 3 months, but did not progress from 3 to 12 months of age.

Discussion: In line with our qualitative observation, BACHD rats are smaller and obese. The data suggest a preadolescent growth impairment, and no signs of progressive degenerative processes were detected within the first 12 months of age.

Author contributions

Conceived and designed the experiments: LEC, EKHJ, HPN
Performed the experiments: LEC, EKHJ
Analyzed the data: LEC, EKHJ

B. BACHD rat body size and body composition

Animals, materials and methods

All procedures are described in detail in Publication VI[344].

Briefly, twelve BACHD rats and twelve WT littermates were dissected at 1, 3, 6, 9 and 12 months of age and the weights of the major adipose tissue deposits, skin and fur, visceral organs (heart, lungs, liver, kidneys, spleen, gastro-intestinal tract), testes, brain as well as remaining muscle and bone carcass, was measured.

The lean mass was calculated by taking total body weight minus gut and skin weight, as these two contained large amounts of adipose tissue.

At 12 months of age, the major glands (pancreas, thymus and salivary glands) were weighed, the length of the thigh bone was determined and the gastro-intestinal tract was dissected into its components (great omentum, gut content and gut wall) in addition to the other measurements.

Data were graphed and statistically analyzed with the software GraphPad Prism (GraphPad Prism version 6.00 for Windows, GraphPad Software, San Diego California USA, www.graphpad.com), and are presented as mean and standard error of the mean (SEM).

Results

Body size

BACHD rats are moderately but significantly smaller than WT rats (Figure 1). This is reflected by an overall shorter body length. The difference in head and tail length was larger than the difference in trunk length between BACHD and WT rats. Also the length of the thigh bone (femur) (Figure 4) showed a larger mean reduction at 12 months of age, suggesting a disproportionally large effect of mHTT on the growth of head and extremities. The body length difference was already apparent at 1 month of age and did not progress.

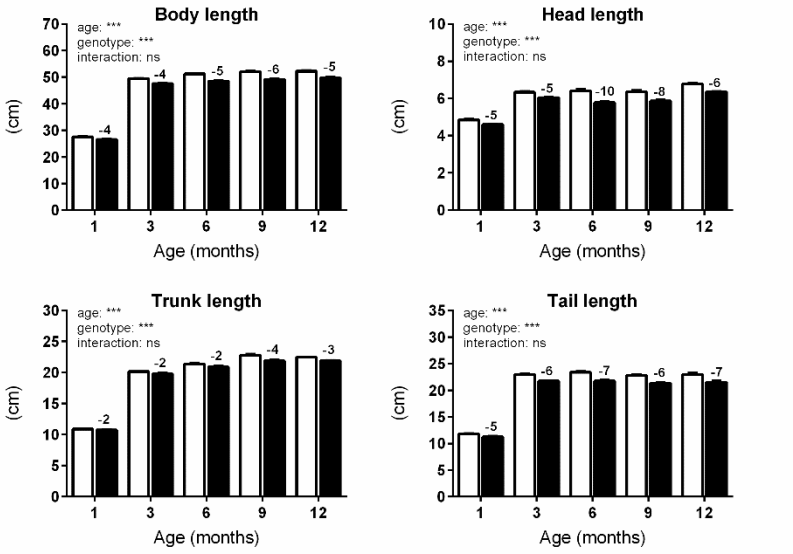

Figure 1. Body size is reduced in BACHD rats.

Total body length, as well as the separate lengths of head, trunk and tail, were measured in different cohorts of rats at 1, 3, 6, 9 and 12 months of age upon dissection. White bars = WT, black bars = BACHD rats. Numbers over the bars represent the mean percental difference between BACHD and WT rats. Mean and SEM, two-way ANOVA, Sidak's post-test, n = 12 per group, * $P < 0.05$, ** $P < 0.01$, *** $P < 0.001$.

Body composition

BACHD rats have an abnormal body composition (Figure 2). BACHD rats showed similar body (and skin/fur) weights as WT rats, but had increased fat and reduced lean mass, indicating a growth deficit and obesity. The difference in body composition was already present at 1 month of age, stronger at 3 months of age, but did not further progress at older ages.

The strongest difference between BACHD and WT rats was seen in bone and muscle mass. The difference in lean mass was less pronounced, as this included skin and fur mass, which was unchanged in BACHD rats. Also organ mass was not as strongly reduced as bone/muscle mass, as it varied considerably between individual organs (Figure 3).

All organs weighed less in BACHD compared to WT rats, except for the gastro-intestinal tract, which was increased in weight (Figure 3). A detailed dissection of the latter was performed at 12 months of age (Figure 4), revealing that the increase in total weight was the result of a significantly heavier great omentum, while gut content (chymus) and the actual gut tissue (gut wall) did not significantly differ from the respective parts in the WT rats. From the individual organs, heart, lungs, kidneys (Figure 3) as well as pancreas and salivary glands (Figure 4) differed strongest between BACHD and WT rats. The liver showed the least difference.

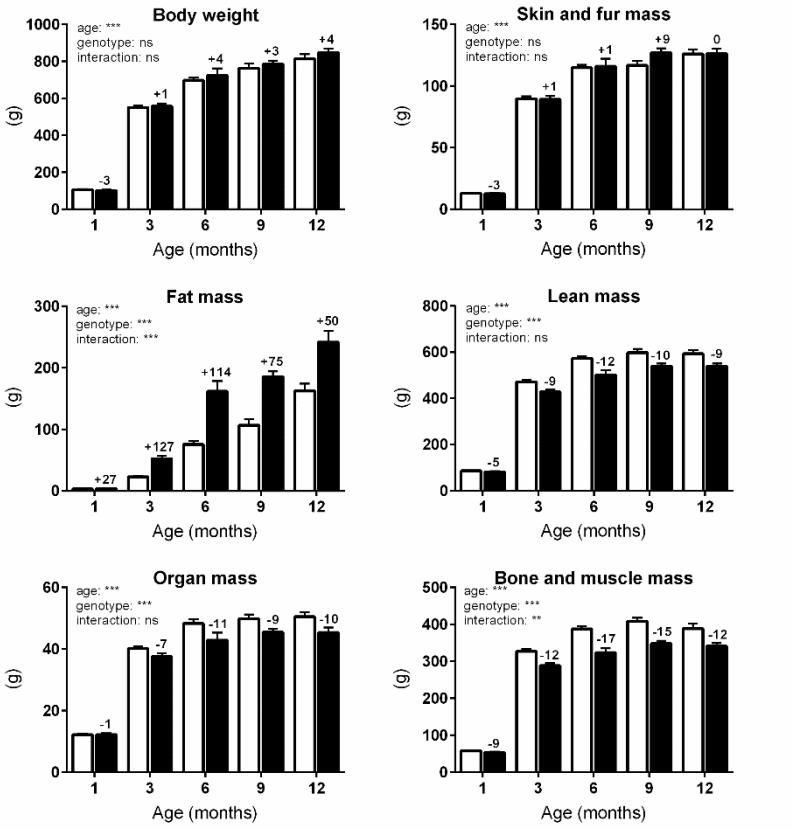

Figure 2. BACHD rats have a distorted body composition.

Body weight, as well as skin/fur, fat (weight of all large adipose tissue deposits), lean (body weight minus fat mass, gut and skin), organ, and bone/muscle mass are shown. White bars = WT, black bars = BACHD rats. Numbers over the bars represent the mean percental difference between BACHD and WT rats. Mean and SEM, two-way ANOVA, Sidak's post-test, n = 12 per group, * $P < 0.05$, ** $P < 0.01$, *** $P < 0.001$.

B. BACHD rat body size and body composition

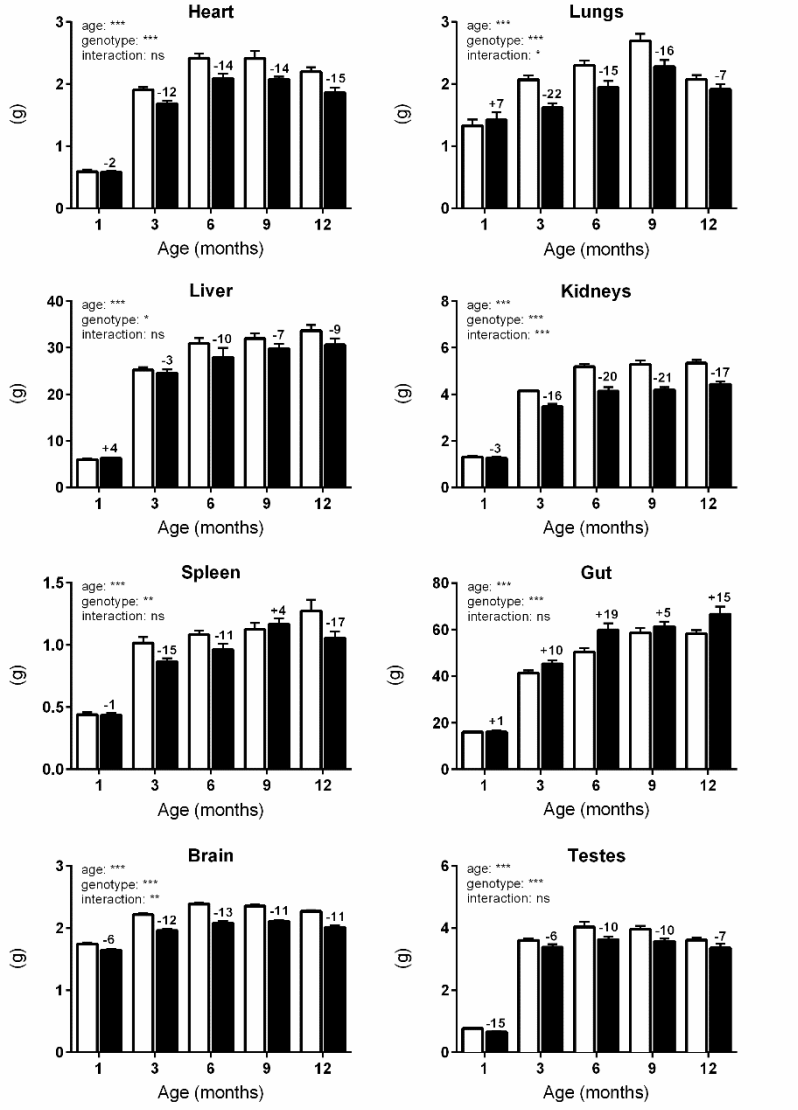

Figure 3. Organ weights are reduced in the BACHD rat.

The weight of all large visceral organs as well as brain and testicles are shown. White bars = WT, black bars = BACHD rats. Numbers over the bars represent the mean percental difference between BACHD and WT rats. Men and SEM, two-way ANOVA, Sidak's post-test, n = 12 per group, * $P < 0.05$, ** $P < 0.01$, *** $P < 0.001$.

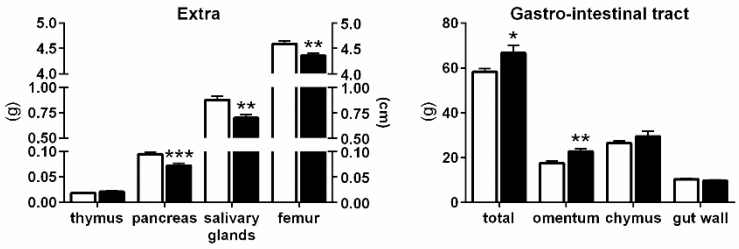

Figure 4. Extra measurements at 12 months of age.

Some smaller internal organs (thymus, pancreas and submaxillary salivary glands in g, as well as the thigh bone (femur) in cm), were dissected in addition to the other organs at 12 months of age (left figure). Furthermore, the gastro-intestinal tract was dissected into its components (right figure). White bars = WT, black bars = BACHD rats. Mean and SEM, unpaired *t*-test, or Mann-Whitney test, depending on data distribution, n = 12 per group, * $P < 0.05$, ** $P < 0.01$, *** $P < 0.001$.

Discussion

We performed a longitudinal dissection study in order to analyze the body size and body composition of the BACHD rat. We found BACHD rats to be smaller, but obese.

The reduced body size was reflected in all organs, although some organs seemed to be more affected than others. The strongest difference was observed in bone and muscle mass, which might relate to energetic demands of muscle tissue, or depend on muscle- and bone-specific intracellular signaling pathways disrupted in the presence of mHTT. Pancreas and salivary glands were further found to be particularly small. This might be attributed to compromised secretory functions, as exocytosis is impaired in HD[48,233,234]. The liver was among the few organs found to be increased at 1 month of age, and showed the least difference between BACHD and WT rats at later ages. As obesity typically accompanies hepatic steatosis, the reason for the relatively larger livers compared to the other organs might lie in an accumulation of fat in this organ, which is in line with an abnormal histological appearance of BACHD rat livers (Clemens *et al*., unpublished). Another interesting finding was that testicle weight was most severely reduced compared to that of WT rats at 1 month of age, which might suggest delayed sexual maturation, an indicator for delayed development.

The reduced body size was already present at 1 month of age and did not markedly progress, pointing to a preadolescent growth impairment. Little research has been done on anthropometric changes in HD. Several studies report normal body height of prodromal and early HD patients compared to control subjects[161,162,167,168,170]. The systematic investigation of 33 different measures of body size in middle-stage HD patients, persons at risk for HD, and normal subjects revealed similar results, and the study mainly concluded progressive emaciation through loss of muscle and fat mass[172]. However, body height in humans is highly variable and small differences are possibly hard to detect. Interestingly, a study investigating body size in children with expanded CAG and non-expanded CAG repeats from HD families found reduced height, lower BMI and smaller head sizes in the mutation carriers[166]. Smaller intracranial volumes were further found in prodromal HD[167], also indicating discrete growth impairment prior to any neurodegeneration. Given the important role of HTT for embryonic and postembryonic development[67–74], growth retardation seems to be a reasonable

consequence of disturbed HTT function, particularly in HD animal models with high CAG repeat numbers and mHTT protein expression levels.

We have previously reported that 13 months old BACHD rats show signs of HD-related neurodegenerative processes in the form of sporadic dark neurons in cortex and the limbic system[142]. The absence of a progressive reduction in brain weight up to the age of 12 months adds further support to the idea that BACHD rats do not experience a marked loss of neurons until that age.

The accumulation of fat mass on the other hand is a phenotype not observed in HD patients, although it is often found in rodent models of HD. It has been linked to abnormal adipocyte metabolism[199,211]. It is conceivable that the lack of fat accumulation in HD patients might derive from increased muscle activity due to chorea, as the severity of chorea correlates negatively with BMI and fat mass. Animal models of HD instead do not typically show chorea-like motor abnormalities, except for the fragment models of HD. The R6/2 mouse, which has increased fat mass at young ages[219], shows fat and muscle wasting along with chorea-like movements and tremor at symptomatic ages[126]. However, also species-specific differences as well the restricted housing conditions with little possibility for exercise that laboratory rodents are exposed to, probably contribute to the difference in fat accumulation in HD patients and animal models.

C. BACHD rat energy balance

Laura E. Clemens[1,2], Huu P. Nguyen[1,2]

[1] Institute for Medical Genetics and Applied Genomics, University of Tuebingen, Tuebingen, Germany.
[2] Centre for Rare Diseases, University of Tuebingen, Tuebingen, Germany.

Summary

Background: BACHD rats show altered growth and body composition, which might relate to differences in energy balance similar to HD patients.

Methods: In order to investigate the rats' energy balance, we conducted a longitudinal study of activity, food and water intake as well as VO_2 and VCO_2, using the PhenoMaster Systems. In addition, we measured the effects of the mitochondria-targeting compound olesoxime on these parameters.

Results: BACHD rats were found to weigh similar as WT rats, but to be smaller and obese. Activity levels did not seem to be decreased. In absolute measures, BACHD rats ate and drank less, and had a lower VO_2. When normalized to the rats' lean mass, BACHD rats turned out to have increased relative food intake at 2 months, while water intake and VO_2 ceased to be different at any age. The RQ was increased at 2 months of age. Olesoxime did not significantly influence any of the parameters analyzed.

Discussion: In line with the observation of a smaller body size and reduced lean mass, BACHD rats consumed less food and had a lower metabolic rate than WT rats in absolute terms. Due to the rats' abnormal body composition, lean mass and not body weight is considered a good parameter for normalization. Changes in food intake observed after normalization, as well as changes in RQ suggest that BACHD have an increased energy demand and high carbohydrate metabolism at young ages, during their major growth phase. As metabolic alterations occur very early in the BACHD rat, the lack of effect of olesoxime might be interpreted as its inability to reverse an already manifest phenotype.

Author contributions

Conceived and designed the experiments: HPN, LEC

Performed the experiments: LEC

Analyzed the data: LEC

Animals, materials and methods

Animals

All relevant information on the animals, such as study groups, housing conditions and olesoxime treatment are specified in Publication VII. Briefly, four groups of rats were investigated. BACHD rats and WT littermates received either placebo or olesoxime-loaded food pellets from the age of 5 weeks onwards (n = 15 per group), and metabolic analyses started thereafter.

Morphological measurement

Body weight was measured weekly, from the age of 5 weeks on, using a kitchen balance (accuracy was ± 1 g) in order to record body weight development and monitor the rats' general health status.

Obesity and body length scoring were conducted at 8 months of age by two individual observers blind to the animals' genotype. The rats were assigned to one out of three categories, i.e. normal, moderately fat and obese in order to estimate the degree of obesity, as well as small, medium and large in order to estimate the body length.

In addition, body length was measured at 13 months of age using a ruler (accuracy was ± 0.1 cm). The measurements were performed after the animals had been sacrificed.

Automated homecage observation

Activity-related and metabolic parameters were assessed using the PhenoMaster (TSE Systems, Germany). A detailed description of setup and procedures are available in Publication IV[332] and Appendix A. Briefly, the setup enabled the simultaneous assessment of 12 animals in individual homecage-like observation cages. All cages were equipped for the measurement of horizontal and vertical activity, food and water intake as well as VO_2 and VCO_2 (respirometry). Measurements were carried out in one cohort of rats longitudinally at the ages of 2, 4, 6 and 12 months. Each measurement started 40 ± 5 min before the onset of the dark phase. Data were collected in 20-minute sample intervals during a total of 70 hours of recording.

Lean mass correction

Food intake, water intake and VO_2 were normalized to lean mass in order to account for differences in body constitution. The lean mass of WT and BACHD rats was assessed in a dissection study, by subtracting the weight of adipose tissue and gastro-intestinal tract from total body weight (Publication VI[344] and Appendix B). For normalization of food intake, water intake and VO_2 at 2 months of age, the mean of the average lean mass of 1 and 3 months old rats was used, as the lean mass of 2 months old rats had not been assessed. For normalization at 4 and 6 months of age, the mean of the average lean mass of 3, 6 and 9 months old rats was used, as the lean mass did not significantly differ in rats of this age.

Data analysis and statistics

Raw data exported from the PhenoMaster software were pre-processed into hourly bins and sorted by genotype, treatment and age using a script for R statistics developed in our institute[332]. Graphs and statistics were created using GraphPad Prism 6.00 for Windows (GraphPad Software, San Diego California USA, http://www.graphpad.com).

Longitudinal data from two groups were analyzed using two-way repeated measurements ANOVA and Sidak's post-test. Longitudinal data from more than two groups were analyzed with two-way repeated measurements ANOVA and Tukey's post-test. Single measurements for more than two groups were analyzed with one-way ANOVA and Tukey's post- test, or a non-parametrical test. All data are presented as group mean and standard error of the mean. The α-level was set to 0.05.

Some data from the automated homecage observation had to be excluded from the analysis because of technical problems. In these cases, the complete data set for the respective animal was removed in order to enable the repeated measurements analysis. In total, we excluded 3 out of 48 animals for activity measurements, as these rats displayed extraordinarily high counts, likely because the rats had shifted around bedding inside of the test cage. We only excluded values that were more than three times higher than the group mean and did not occur repeated times for the same animal. From food and water intake data, we had to exclude a total of 6 out of 48 rats, as sometimes drinking bottles were leaking (leading to unreasonably

high values for water intake) and as sometimes food got stuck in the food basket, so that the animal was not able to reach it (leading to unreasonably low values for food intake). For these rats, we also excluded the calorimetric data, as this is likely to be confounded in this case. The values that had to be excluded were spread among groups and testing cages, suggesting that they were not the result of a systematic error or had any biological meaning.

Results

Body weight, body size and body composition

There was significant difference in body weight between BACHD and WT rats (Figure 1A). However, BACHD rats had an altered body constitution, characterized by reduced body size (Figure 1B and C) and obese appearance (Figure 1D).

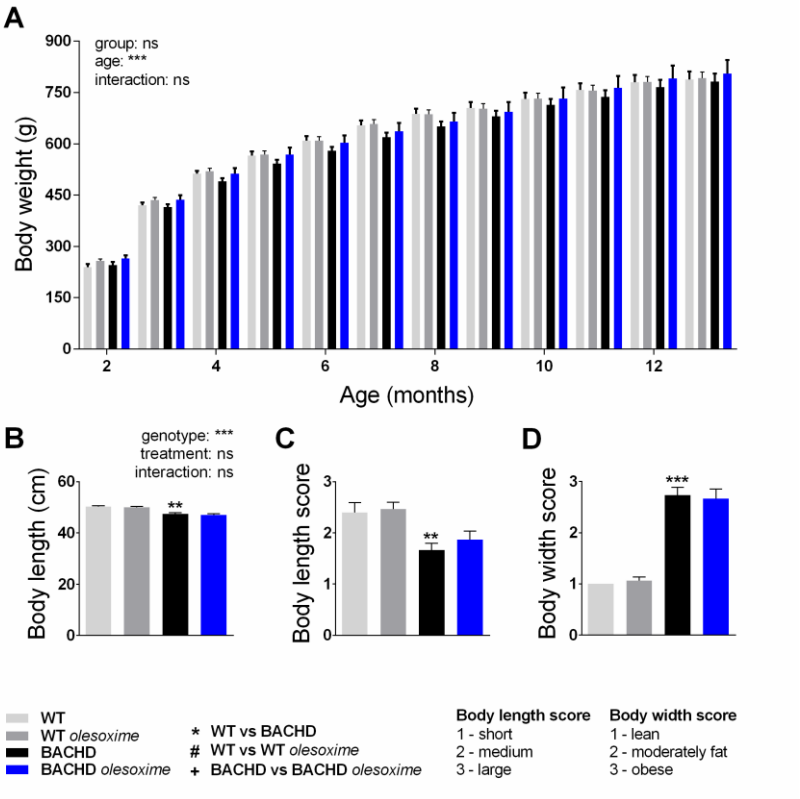

Figure 1. Similar body weight but abnormal body composition of BACHD rats.
BACHD rats weigh similar as WT rats (**A**), but are smaller (**B**, **C**) and appear obese (**D**). Olesoxime does not influence any of these parameters. Mean and SEM, two-way repeated measurements ANOVA and Tukey's post-test for body weight, two-way ANOVA and Sidak's post-test for body length measurement, and Kruskal-Wallis test and Dunn's post-test for scoring of body size and body width, n = 15 per group, * $P < 0.05$, ** $P < 0.01$, *** $P < 0.001$.

Energy balance

In order to assess if the increased fat mass found in BACHD rats had been the result of a positive energy balance, we assessed energy balance by measuring the rats' activity, food and water intake as well as VO_2 and VCO_2.

Activity

As expected for nocturnal animals, all rats were significantly more active during the dark phase compared to the light phase. No obvious genotype differences in circadian or ultradian rhythms were observed when looking at the pattern of activity over the 70-hour measurement (data not shown). No differences between WT and BACHD rats were further found in ambulatory activity or rearing behavior (Figure 2). However, BACHD rats showed a significant increase in fine movements during the dark phase at 6 months, and a trend during the light phase at 12 months of age (Figure 2).

Water and food intake

Absolute values for water and food intake differed significantly between BACHD and WT rats (Figure 3). Water intake was significantly reduced at 2, 4 and 6 months, but ceased to be different at 12 months of age due to a stronger decline in water intake with age in WT rats. Food intake was significantly reduced at 4, 6 and 12 months, while BACHD rats tended to have increased food intake compared to WT rats at 2 months of age.

Respirometry

Absolute values for VO_2 as well as VCO_2 were found to be reduced in BACHD compared to WT rats, indicating a lower basal metabolism (Figure 4). The RQ was also reduced, suggesting differences in nutrient metabolization (Figure 4).

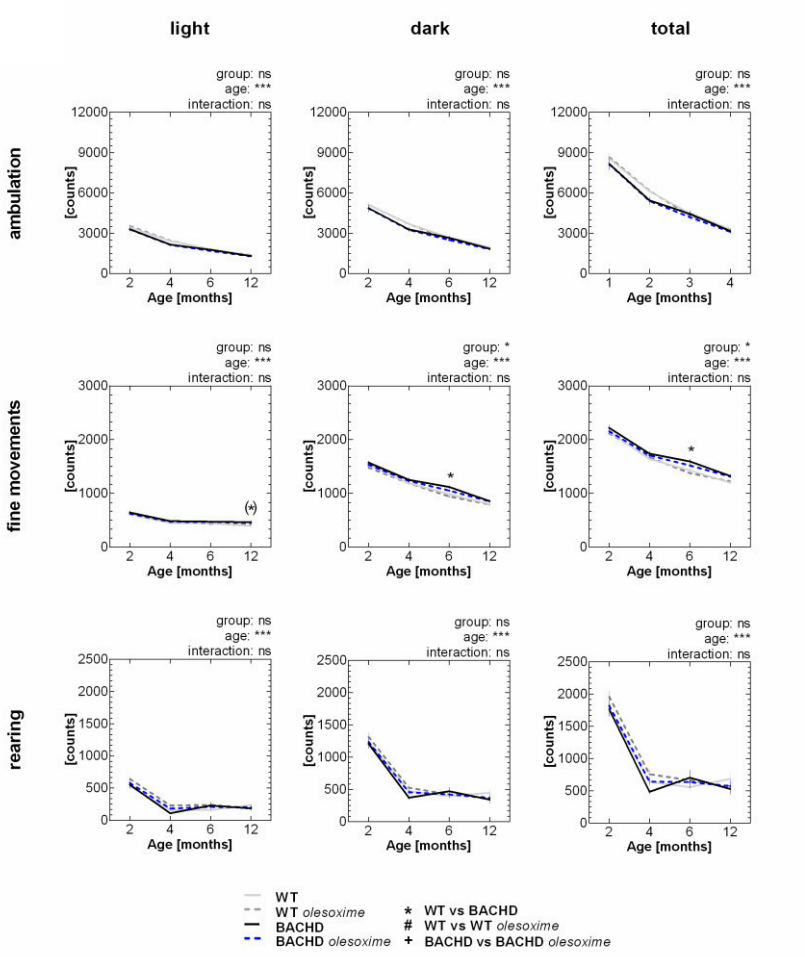

Figure 2. BACHD rats differ in absolute measures of energy balance.

BACHD and WT rats were subjected to automated behavioral observations for 70 hours at 2, 4, 6 and 12 months of age. The sum for light phase, dark phase and total observation period is given for activity-related parameters. Mean and SEM, two-way ANOVA, Tukey's post-test, * $P < 0.05$, ** $P < 0.01$, *** $P < 0.001$.

C. BACHD rat energy balance

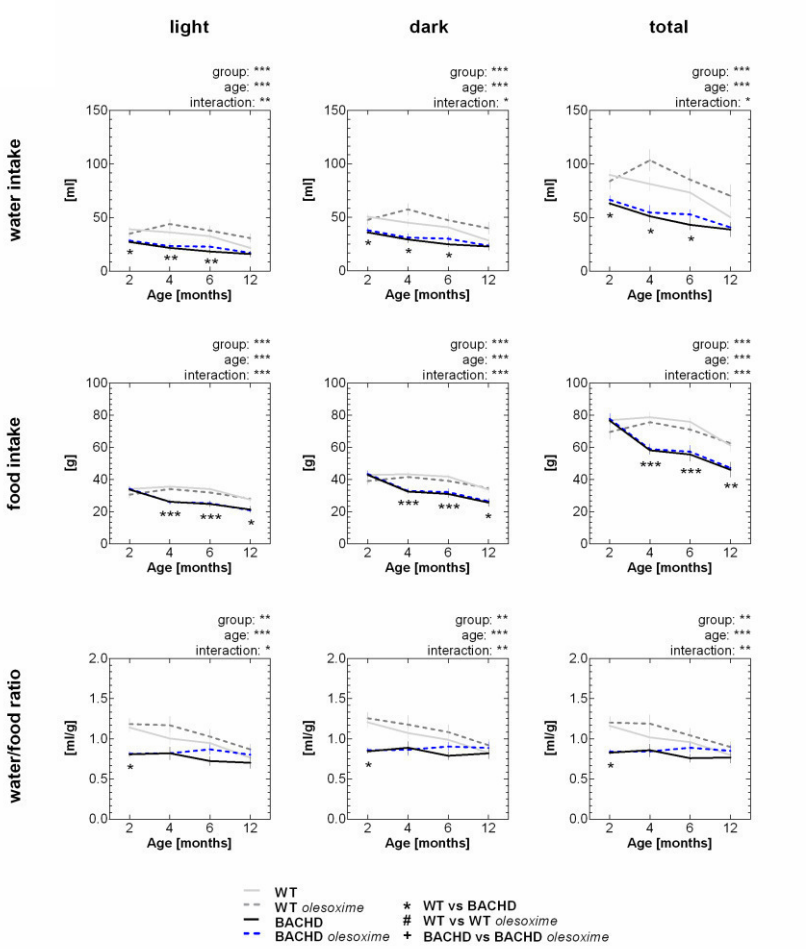

Figure 3. BACHD rats differ in absolute measures of energy balance.

BACHD and WT rats were subjected to automated behavioral observations for 70 hours at 2, 4, 6 and 12 months of age. The sum for light phase, dark phase and total observation period is given for water and food intake. Mean and SEM, two-way ANOVA, Tukey's post-test, * $P < 0.05$, ** $P < 0.01$, *** $P < 0.001$.

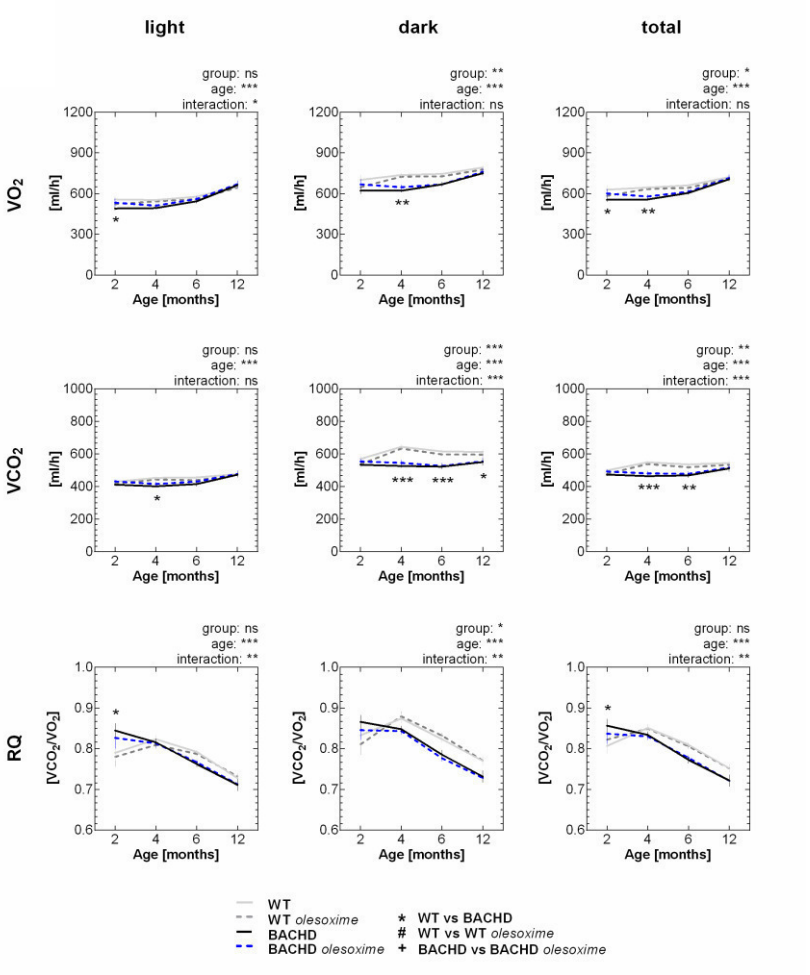

Figure 4. BACHD rats differ in absolute measures of energy balance.

BACHD and WT rats were subjected to automated behavioral observations for 70 hours at 2, 4, 6 and 12 months of age. The mean for light phase, dark phase and total observation period is given for respirometric data (**C**). Mean and SEM, two-way ANOVA, Tukey's post-test, * $P < 0.05$, ** $P < 0.01$, *** $P < 0.001$.

Lean mass-corrected values

Since BACHD rats were found to have a distorted body composition with higher fat and lower lean mass (Publication VI[344]), we normalized the total values for water intake, food intake and VO_2 from untreated WT and BACHD rats to the average lean mass calculated elsewhere (Appendix C). The results show that most of the differences that were found before, disappeared (Figure 5). Instead, BACHD rats presented with a significantly elevated food intake at 2 months of age (Figure 5).. Furthermore, a progressive increase in VO_2 from 4 to 12 months became apparent due to increased VO_2 during the light phase (Figure 5).

Olesoxime effect

We did not detect an influence of olesoxime on any of the metabolic parameters (Figure 2, 3 and 4). However, a lean mass-normalization could not be performed with olesoxime-treated rats, as their lean mass had not been assessed.

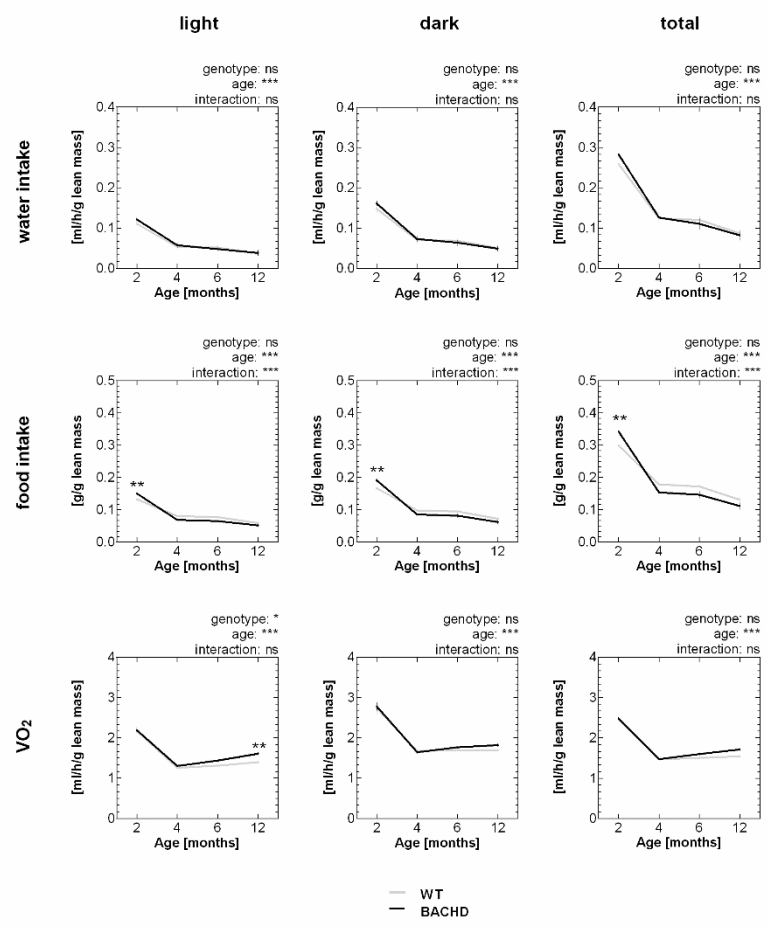

Figure 5. Relative values of energy metabolism show a different pattern.

Food intake and VO_2 measured at different ages, were normalized to lean mass to account for differences in body composition. The sum (food and water intake) or mean (VO_2) for light phase, dark phase and total observation period are shown. Mean and SEM. Two-way ANOVA, Sidak's post-test, n = 15 per group, * $P < 0.05$, ** $P < 0.01$, *** $P < 0.001$.

Discussion

We analyzed several metabolic parameters in the BACHD rat in order to evaluate possible alterations in energy balance, as the animals have a distorted body constitution (Publication VI[344] and Appendix B). Moreover, the therapeutic potential of olesoxime to interfere with metabolic abnormalities was investigated.

We manually rated the rats' body size and obesity phenotype at 8 months of age, receiving a gross similar outcome as obtained from detailed dissection (Publication V[344] and Appendix A). This suggests that the body size and composition phenotypes are strong enough to score them by eye at that age, which might be useful for future treatment studies. However, small differences due to treatment are unlikely to be detected by this method.

Due to the BACHD rats' apparent obesity, we expected to find either reduced exercise, increased caloric intake, or a combination of these two, which would point to a positive energy balance. In contrast, we detected reduced absolute caloric intake and a lower absolute metabolism. However, due to the difference in body constitution between BACHD and WT rats, their energy requirements are likely to be different. It is conceivable, that the lower values detected were simply attributed to the rats' smaller body size. Relating the absolute values to body weight to account for size differences, however, would have been confounding, as body weight is not a good denominator for energy expenditure when comparing animals with different body composition[414]. Different tissues are known to have different metabolic activities[415], and specifically fat mass contributes relatively little to the overall energy expenditure[414]. A more suitable determinant for metabolic rate is lean mass[414]. By normalizing to the average lean mass obtained from dissection (Publication VI[344] and Appendix B), we found that food and water intake, as well the rats energy expenditure (as indicated by VO_2), relate well to their smaller body size and thus lower lean mass, as most differences had vanished. Interestingly, what appeared after normalization was a significantly increased food consumption at 2 months of age. As VO_2 was not increased at that age, this could possibly explain the development of obesity in the rats.

Another interesting finding concerns the increasing VO_2 during the light phase with age. There were no indications for a parallel increase in ambulatory activity, but a trend towards increased fine movements was discernable specifically in the light phase at 12 months of age. Similar

results have been obtained from early symptomatic HD patients, who had a significantly higher sedentary energy expenditure due to spontaneous physical activity. Total free-living energy expenditure was unchanged in these patients, because they appeared to engage in less voluntary physical activity[162]. Thus, it would be informative to conduct a detailed ethological examination in addition to the quantitative assessment of activity levels in the BACHD rat.

We also calculated the RQ, which reflects the source of macronutrients utilized to fuel energy metabolism and maintain body functions. A value of 1.0 stands for the sole use of carbohydrates, a value of 0.7 would mean the use of only lipids, and a value of about 0.8 would be expected when only proteins were the substrate[351]. Thus, a high RQ points to high carbohydrate metabolism, while a low RQ indicates a large contribution of lipid oxidation, which occurs when carbohydrates cannot be utilized or are unavailable specifically under starvation. The finding of increased RQ in 2 months old BACHD rats is in line with their higher relative food intake and suggests high carbohydrate oxidation and increased energy demands. The decreasing RQ at older ages (after the major growth phase of the rats) on the other hand could point to a defect in glucose utilization or a higher glucose demand than the rats can cover by food intake. The trend towards higher VO_2 at older ages and rather reduced food intake further suggests a failure to respond to the energetic deficit, and implies that these moderate phenotypes do have biological significance. However, the results need to be interpreted with caution, as food intake seems to be impaired during PhenoMaster exposure in Sprague Dawley rats (Appendix A). Moreover, this stress effect seems to differ among rat strains depending on their emotionality, and might thus also differ between BACHD rats and their WT littermates. Indeed, when comparing the body weight gain of BACHD and WT rats before and during PhenoMaster exposure, BACHD rats seem to have a stronger decline in body weight gain (data not shown). Thus, the validity of the measurements (particularly those at old ages, when the rats lose weight during the exposure) is questionable.

We did not observe any significant influence of olesoxime treatment on body constitution or energy balance in the BACHD rat, although olesoxime targets mitochondria[313,314], and mitochondrial dysfunction is highly implicated in metabolic dysfunction in HD[257–262]. Thus, this negative result might imply that olesoxime's effects on mitochondria are not related to their role in energy metabolism. On the other hand, there is the possibility that olesoxime treatment

had started too late to restore metabolic abnormalities, as the difference in body constitution between BACHD and WT rats is already detectable at 1 months of age, which is prior to the start of olesoxime treatment. In this regard, it has been shown that switching off mHTT expression in the hypothalamus of the BACHD mouse abolished metabolic phenotypes when the procedure was performed at early ages[194]. Switching mHTT expression off when the phenotypes were fully developed, did not improve metabolic abnormalities anymore. Furthermore, a recent report points to a similar failure of olesoxime to rescue manifested phenotypes in a mouse model of Parkinson disease, despite other improvements[323]. Thus, it would be of interest to evaluate, if with earlier start of treatment, olesoxime also capable of ameliorating systemic metabolic abnormalities.

D. BACHD rat blood parameters

Laura E. Clemens[1,2], Libo Yu-Taeger[1,2], Kim Verwaest[3], Mahmoud A. Pouladi[4], Roger Dommisse, Michael R. Hayden[4], and Huu P. Nguyen[1,2]

[1] Institute for Medical Genetics and Applied Genomics, University of Tuebingen, Tuebingen, Germany.

[2] Centre for Rare Diseases, University of Tuebingen, Tuebingen, Germany.

[3] Department of Chemistry, University of Antwerp, Antwerp, Belgium

[4] Department of Medical Genetics, University of British Columbia, Vancouver, Canada

Summary

Background: Blood parameters can be useful surrogate markers for disease due to low invasive sample collection, time and cost effectiveness. Metabolic dysfunction can be traced in blood from HD patients. Thus, we aimed at characterizing metabolic markers in plasma and serum from BACHD rats.

Methods: We measured plasma IGF-1 and leptin levels by ELISA assays, as these factors are related to growth and obesity. We further prepared a longitudinal serum metabolite profile from ^{1}H NMR analysis to search for potential markers of metabolic dysfunction in the BACHD rat and to track disease progression.

Results: We found plasma levels of IGF-1 to be decreased, and plasma levels of leptin to be increased in BACHD rats at 3 months of age. IGF-1 levels remained stable from 3 to 12 months, while leptin levels further increased from 3 to 6 months of age. The serum metabolite profile further differed significantly in BACHD compared to WT rats. At 2–3 months, BACHD rats show reduced levels of glucose, lactate, amino acids and ketone bodies, but increased lipid levels. At 12 months of age, only lipid levels were found to be reduced. At 18 months, glucose, lactate and pyruvate levels were increased, while lipid levels were found to be reduced in BACHD compared to WT rats. In addition, BACHD rats showed reduced levels of N-acetylaspartic acid (NAA) at 18 months of age.

Discussion: Our results demonstrate that BACHD rats display profound changes in energy homeostasis, which can be traced in blood. Changes in IGF-1 and leptin levels are consistent with the earlier finding that BACHD rats suffer from growth impairment and obesity. The serum metabolite profile points to dysfunctional metabolic pathways, which are likely due to impaired

lipolysis in the first place, and deficits in mitochondrial respiration later on. Thus, the study strengthens the finding of metabolic dysfunction in the BACHD rat and confirms that blood analysis can be a useful tool for further treatment studies.

Author Contributions

Conceived and designed the study: HPN, RD, MAP
Performed the experiments: LY-T (serum sample collection) LEC (serum and plasma sample collection), KV (serum metabolite analysis), MAP (IGF-1 and leptin measurements)
Analyzed the data: LEC, KV, MAP

Animals, materials and methods

Animals

Detailed information on the animals are given in Publication VII. Briefly, for serum IGF-1 and leptin measurements, four groups of rats were investigated. WT as well as BACHD rats received either placebo or olesoxime-loaded food pellets from the age of 5 weeks onwards, and metabolic analyses started thereafter. For ^{1}H NMR spectroscopy on blood metabolite levels, different cohorts of untreated WT and BACHD rats were used.

Blood sampling

Blood was collected from the tail vein 2–3 hours before the onset of the light phase. Blood collected for plasma was kept on ice until centrifugation at 13,200 rpm for 15 minutes at 4 °C. Blood collected for serum samples was incubated for 30 minutes at 37 °C to allow for coagulation prior to centrifugation at 3,000 rpm for 30 minutes at 4 °C. After centrifugation, plasma and serum were transferred into cryotubes and stored at -80 °C until shipment to the University of Antwerp.

Blood metabolite analysis

IGF1 and leptin levels were measured at the University of Vancouver, using a commercial ELISA kit (Mouse Quantikine ELISA kit, R&D Systems), as applied previously[197]. Since the standards in this kit are mouse IGF-1, the concentration refers to the equivalent of mouse IGF-1.

Serum metabolites were assessed via ^{1}H NMR spectroscopy by our collaboration partner, as described in detail in Publication I[350] and Reference[356].

Results

IGF-1 and leptin

BACHD rats showed reduced IGF-1 and increased leptin levels at 3 and 6 months of age. IGF-1 levels decreased, while leptin levels increased with age in both genotypes. Leptin levels were also measured at 9 and 12 months of age, revealing a trend towards decreasing leptin levels with age in both genotypes (data not shown). Olesoxime treatment did not affect IGF-1 levels, but moderately increased leptin levels in WT and BACHD rats.

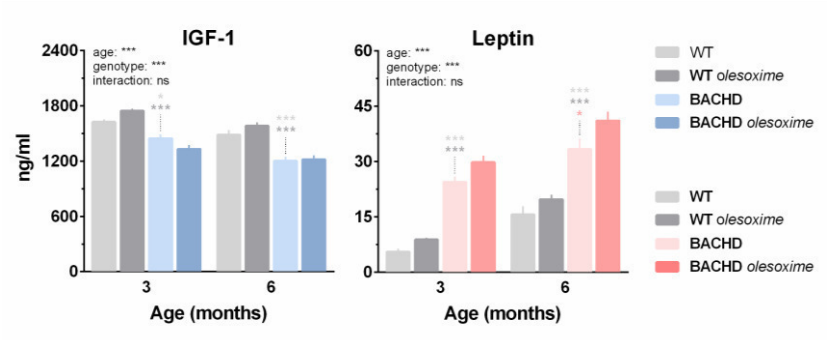

Figure 1. Reduced IGF-1 and increased leptin levels in BACHD rats.
IGF-1 and leptin were measured at 3 and 6 months of age in WT and BACHD rats receiving placebo or olesoxime treatment. Mean and SEM, two-way repeated measurements ANOVA, Sidak's post-test, n = 12 per group, * $P < 0.05$, ** $P < 0.01$, *** $P < 0.001$.

Serum metabolite profile

BACHD rats could be distinguished from their WT littermates based on their serum metabolite profile[356]. The difference was due to changes in several serum metabolites involved in energy metabolism, as summarized in Figure 2. At 2–3 months of age, BACHD rats showed reduced levels of glucose, lactate, amino acids and ketone bodies, but increased lipid levels compared to their WT littermates. At 12 months of age, no differences were detectable except for lipid levels, which were found to be reduced in BACHD compared to WT rats. At 18 months, serum glucose, lactate and pyruvate levels were higher, while lipid levels were still lower than those of WT rats.

Thus, serum energy metabolite concentrations showed age-dependent changes characterized by a triphasic course of metabolic dysregulation, with changes at young and old ages, and a normal phase at intermediate ages. A simplified, extrapolated model of BACHD rat metabolite changes over the course of 18 months is given in Figure 3.

Differences between WT and BACHD rats were most dramatic at 3 months of age. At that age, a variety of other metabolites appeared to be reduced in concentration in the BACHD rat. These concerned additional amino acids (i.e. valine, leucine and isoleucine, lysine, phenylalanine, tyrosine, glutamine, glycine and methionine) as well as molecules involved in the tricarboxylic acid (TCA) cycle (i.e. citrate, succinate and malonate), in neurotransmission (glutamate, glycine, phenylalanine, tyrosine, choline and myo-inositol), membrane constitution (choline and myo-inositol) and the phospagen system (creatine). At 18 months, we further detected a significant decrease in N-acetyl-aspartate (NAA), a marker for neuronal health.

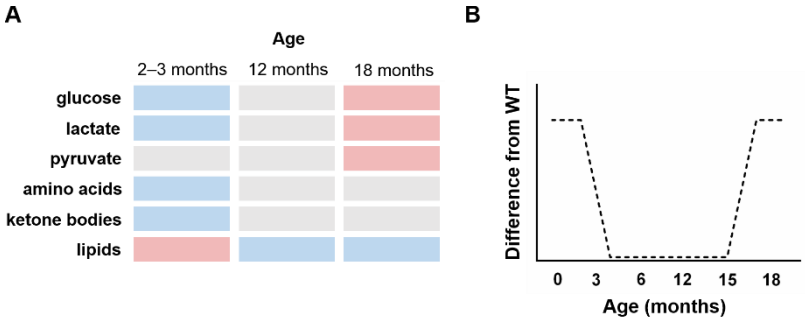

Figure 2. Changes in serum metabolites in the BACHD rat.
(**A**) The heat map shows the changes found in the main energy metabolism-related metabolites assessed via ^{1}H NMR spectroscopy in different cohorts of WT and BACHD rats at 2, 3, 12 and 18 months of age. The results from 2 and 3 months old rats were combined for better overview. Blue = reduced in BACHD rats, gray = similar between BACHD and WT rats, red = increased in BACHD rats. Number of samples from individual animals at the different ages were as follows: 2 months: WT = 12, BACHD = 6; 3 months: WT = 17, BACHD = 17; 12 months: WT = 17, BACHD = 13; 18 months: WT = 5, BACHD = 4. (**B**) Theoretical model of serum metabolite changes. BACHD rat serum metabolite levels reveal a triphasic pattern with early and late age dysregulation, and a normal intermediate phase.

Discussion

We investigated blood samples from BACHD rats in order to characterize metabolic dysfunction and identify potential disease markers. BACHD rats differed from WT rats in their overall metabolite profile, suggesting that blood markers are useful surrogate markers for further treatment studies in the BACHD rat.

IGF-1 and leptin

The targeted analysis of IGF-1 and leptin levels revealed that IGF-1 is reduced and leptin increased in the BACHD rat in accordance with the rats' smaller body size and obesity phenotype.

IGF-1 signaling is thought to be critical in HD, as it is associated with cellular and particularly brain energy deficits[416,417]. Moreover, increasing IGF-1 levels has been shown to restore the energetic deficits found in HD animal models[418]. IGF-1 levels have been reported to be moderately[171] or significantly[168,197] lower in HD patients, as well as in a variety of other HD disease models[197], in accordance with our findings. In contrast, the full-length mHTT expressing YAC128 and BACHD mice have increased levels of IGF-1[197]. However, while other models (including the BACHD rat) present with growth deficits, these mice do not show reduced body sizes[76,194]. Thus, although it is unclear why the levels of IGF-1 vary, they are obviously dysregulated in HD and seem to be responsible for the body size differences found in HD[197].

Leptin levels have been reported to be either unchanged[161,162,419,420] or reduced[168,171] in HD patients, while they were found to vary substantially between different HD mouse models. However, the thorough analysis of these data and the comparison with results from HD patients as well as the results from BACHD rats suggests that the variation derives from sampling at different stages of the disease, as the parameter underlies temporal changes. This can be illustrated with results from the following study: Leptin levels were measured in two mouse models of HD at different stages of disease[211]. The CAG140 knock-in mouse showed increased leptin levels at a presymptomatic stage, while the R6/2 mouse displayed similar leptin concentrations at an early symptomatic stage, compared to their respective WT counterparts. Leptin levels at a late symptomatic stage were reduced in both models. Thus,

leptin levels are likely to be increased early on (reflecting ages that have not been studied in HD patients), to reverse around symptom onset (leaving no changes detectable), and to decrease towards end stages (making it likely to detect reduced leptin levels in symptomatic HD patients).

Differences in the characteristics of mHTT expression across HD disease models likely further influence leptin levels, as it has been reported that leptin levels correlate positively with CAG repeat length in HD mutation carriers[419]. And also genetic differences between background strains probably have an additional influence, considering the obvious variation in the development of obesity among different WT strains. Sprague Dawley rats, which form the background for the BACHD rat, are known to be prone to develop obesity[421], a fact that likely adds to the strong obesity phenotype in this model.

The fact that BACHD rats developed obesity despite the dramatically increased leptin levels implies leptin resistance and might thus further indicate a deficit in leptin signaling in the brain[422]. Hypothalamic changes are well described as a part of HD[156]. Furthermore, it has been demonstrated that switching off the expression of mHTT in the hypothalamus restored the obesity phenotype in BACHD mice (interestingly without affecting IGF-1 levels)[194]. However, silencing mHTT specifically in leptin receptor-expressing cells, did not lead to marked improvements[212].

Serum metabolites

Serum metabolite analysis by ^{1}H NMR spectroscopy detected changes in the major metabolites involved in energy metabolism, as discussed previously[356]. The results indicate a triphasic pattern of metabolic changes with age.

BACHD rats display reduced levels of glucose, lactate, amino acids and ketone bodies, while the levels of lipids were found to be increased at 2-3 months of age, which is around the end of the rats' major growth phase (as can be obtained from the body weight curve in Appendix C). That glucose, lactate and amino acids were depleted from the rats' blood at that age suggests a temporary, high energy demand with higher carbohydrate-based energy metabolism in BACHD compared to WT rats. The reason for the high dependency on

carbohydrate metabolism is indicated by the increased lipid levels, which suggests impaired utilization of lipids for energy supply. Under such conditions, the tricarboxylic acid (TCA) cycle is likely to be unable to support amino acid synthesis, or amino acids participate in energy production, which is consistent the finding of reduced peripheral amino acid levels. The decrease in ketone bodies further supports this hypothesis, as under such circumstances, ketone bodies are utilized to provide additional energy, but cannot be replenished as this would require lipid oxidation. In fact, it has been shown that adipocytes isolated from mouse models of HD present a defect in lipolysis[199]. Furthermore, it is reasonable to assume that this deficit is responsible for the accumulation of fat mass as well as for the growth defect seen in BACHD rats. The latter is likely connected to the reduced IGF-1 levels observed, as IGF-1 levels depend on the availability of amino acids[357] and are lower during starvation[423].

After the major growth phase with its high energetic demands, BACHD rats do not seem to have metabolic deficits during a large part of adulthood, as we detected little differences in serum metabolites between the genotypes at 12 months of age. This is similar to HD patients, who live a relatively normal life before clinical symptom onset at midlife or older ages. Accordingly, at the old age of 18 months, energy metabolite levels are again found to be altered in the BACHD rat, showing a reversed pattern compared to the young ages. The accumulation of glucose, lactate and pyruvate suggests an impairment of carbohydrate metabolism at this age. Specifically, this points to impaired mitochondrial energy production, as respiratory chain activity is setting the pace for upstream oxidative pathways, meaning that a defect would lead to the accumulation of metabolites from glycolysis and TCA cycle. This at the same time explains why amino acid levels are restored, as with the increased availability of glucose, the demand for additional energy substrates would cease.

The late metabolic changes detected in the BACHD rat are consistent with abnormalities found in animal models and HD patients. Increased levels of lactate[253–256] and reduced glucose consumption[177–183] are found in presymptomatic and symptomatic HD patients. Furthermore, mitochondrial dysfunction is a prominent feature at symptomatic stages of HD[257–262]. Thus, alterations in the metabolite profile detected in 18 months old BACHD rats point to an advanced stage of the HD-related pathology at that age. In this regard, we further detected a reduction in the levels of NAA, a marker for neuronal health and degeneration[424]

in 18 months old BACHD rats. Reduced levels of NAA are commonly found in HD[251–255] with the most severe drop occurring around the age of disease onset[425], and changes hardly being detectable before[426]. Thus, it is likely that at 18 months of age, neurodegenerative processes become significant in the BACHD rat. We have previously reported the presence of dark neurons in BACHD rats at 13 months of age. For further studies, it would be interesting to analyze neurodegeneration and NAA levels in the BACHD rat in more detail at short intervals between the age of 12 months (where no changes were found) and at ages older than 18 months (after signs of neurodegeneration have occurred) to determine the start and progression of this phenotype. Unfortunately though, attempts to investigate the late phase of HD-related phenotypes in the BACHD rat are complicated by the fact that Sprague Dawley rats, the rat strains forming the background for the BACHD rat model, are generally known to develop obesity and a metabolic syndrome accompanied by high tumor incidence and mortality past the age of 12 months[421]. For this reason, end stage phenotypes or mortality have not been studied in the BACHD so far.

One of our results seems to be contradictory to findings in HD patients, which is that amino acid levels were only reduced at the very early ages and restored later on, while they are commonly found to be reduced in patients at symptomatic stages[248–250]. That we did not observe reduced levels of amino acids beyond the age of 3 months might be attributed to the increased fat mass in the BACHD rat, which is not found in HD patients. It is reasonable to assume that BACHD rats are not completely incapable of utilizing lipids to fuel their energy demands, which might be supported by the finding of reduced lipid levels and reduced RQ found at older ages (Appendix C). For this reason, the rats might not get into a severe energy deficit at older ages due to the availability of storage fat, while patients instead would experience progressive muscle wasting. For the same reason, it might be speculated that BACHD rats only show little signs of neurodegeneration up to an age of 18 months.

E. BACHD rat primary neuronal cultures

Laura E. Clemens[1,2], Jasmin Richlick[1,2], Mahmoud A. Pouladi[3], Michael R. Hayden[3] and Huu P. Nguyen[1,2]

[1] Institute for Medical Genetics and Applied Genomics, University of Tuebingen, Tuebingen, Germany.

[2] Centre for Rare Diseases, University of Tuebingen, Tuebingen, Germany.

[3] Department of Medical Genetics, University of British Columbia, Vancouver, Canada

Summary

Background: Primary neuronal cultures represent useful complementary tools for studying molecular aspects of neurological diseases, as they provide the original cell context with all neuron-specific features. However, these cultures are more complex to establish, longer to prepare and difficult to maintain compared to clonal cell lines. Here, we aimed at establishing a time-efficient, and reproducible protocol for the preparation of primary neurons from BACHD rats, to investigate molecular aspects in cells most vulnerable to HD. Our first analyses in these cells were addressed to investigate early mitochondrial pathologies, as mitochondrial dysfunction is a prominent feature of HD.

Methods: We prepared cultures of BACHD rat primary striatal and cortical neurons and determined their viability via MTT and LDH tests. HD disease phenotypes were then investigated, including the quantification of mHTT aggregates via a filter trap assay and immunoblotting, measurement of mitochondrial motility by time-lapse fluorescence microscopy, as well as assessment of IGF-1 and 8OHdG levels by ELISA.

Results: We established a time-efficient protocol for the extraction of primary striatal and cortical neurons from the same embryo in parallel. The neurons were maintained in culture for up to 12 days and recapitulated several specific, HD-related phenotypes. BACHD rat neurons contained aggregated forms of mHTT. Although neither cortical nor striatal cells from BACHD rats differed in viability or showed signs of oxidative stress compared to cells from WT rats, a distinct difference in mitochondrial motility along with reduced IGF-1 levels were detected.

Discussion: We describe a fast and reproducible protocol for the extraction of primary neuronal cultures from rats. This protocol could in principle be extended for the parallel culture of other brain regions and could be useful not only for studying molecular mechanisms of HD, but also of other neurological disorders. BACHD rat primary neurons display discrete HD-related phenotypes, which might aggravate with longer cultivation times. The results encourage the use of BACHD rat primary neurons for further studies on the molecular pathogenesis of HD, to identify therapeutic targets and to evaluate drug candidates for HD.

Author Contributions

Conceived and designed the study: HPN, RMP, MRH, LEC
Developed the new, combined protocol: LEC
Performed the experiments: LEC and JR (primary cultures, MTT assay, axonal transport), MAP (IGF-1 measurements)
Analyzed the data: LEC, MAP

E. BACHD rat primary neuronal cultures

Materials and methods

Buffers and reagents are listed in Table 1. Buffers, reagents and procedures used represent a combination of two previously established protocols for the isolation and cultivation of primary striatal (provided by Dr. Rebecca Pruss, Trophos SA, Marseille) and cortical (provided by Dr. Andrew Grierson, University of Sheffield) neurons from mice. These were combined to one conform protocol, yielding higher time-efficiency and practicability.

Table 1. Reagents.

Application	Reagent	Provider Catalogue Number	Volume Concentration
Buffers	HBSS (-) no Ca^{2+}, Mg^{2+}	Lifetechnologies, Gibco® 14175-095	500 ml
	HBSS (+) with Ca^{2+}, Mg^{2+}	Lifetechnologies, Gibco® 14025-050	500 ml
Digestion	Trypsin	Lifetechnologies, Gibco® 59427C	100 ml 2.5 %
Culture media	**Cortex**		
	Neurobasal	Lifetechnologies, Gibco® 21103	500 ml
	B-27 Supplement	Lifetechnologies, Gibco® 17504-044	10 ml
	L-Glutamine	Lifetechnologies, Gibco® 25030-032	5 ml 200 µM
	Penicillin/streptomycin	Lifetechnologies, Gibco® 15140-122	5 ml 10,000 U/ml
	Striatum		
	Neurobasal	Lifetechnologies, Gibco® 21103	500 ml
	B-27 Supplement	Lifetechnologies, Gibco® 17504-044	10 ml
	Sodium pyruvate	Lifetechnologies, Gibco® 11360-039	5 ml 100 mM
	BSA	Sigma Aldrich 9048-46-8 A4919-G	12.5 ml 4 %
Trituration	HBSS (+)	Lifetechnologies, Gibco® 14025-050	20 ml
	BSA	Sigma Aldrich A4919-G	2.5 ml 4 %
	Glucose	Sigma Aldrich G8270	2 g
	DNase I	Sigma Aldrich D5025	500 µl 5 mg/ml in H_2O
Coating	Poly-ornithine	Sigma Aldrich P4638	5 µg/ml in H_2O

Rat breedings for primary neuronal cultures

In order to obtain rat embryos from a specific developmental stage, terminated breedings were set up. Twelve weeks old female, WT Sprague Dawley rats (Crl:CD (SD)) were ordered from Charles River Germany and acclimatized to the new facility for 2 weeks prior to breeding. Housing conditions in our facility are detailed in Publication V[377] and VII. A total of 36 female rats were used in this study. For the breeding, two females were introduced into the home cage of one male rat. Breeding cages were prepared approximately 1 hour before the onset of the dark phase (this day refers to embryonic day (E) 0, prior to conception), and vaginal smears were made to detect mating activity, on the following morning (E 0.5, if the rat had conceived). The males were removed from the cages either after the first night, if clear indicators for mating activity had been seen, or after a total of two consecutive nights.

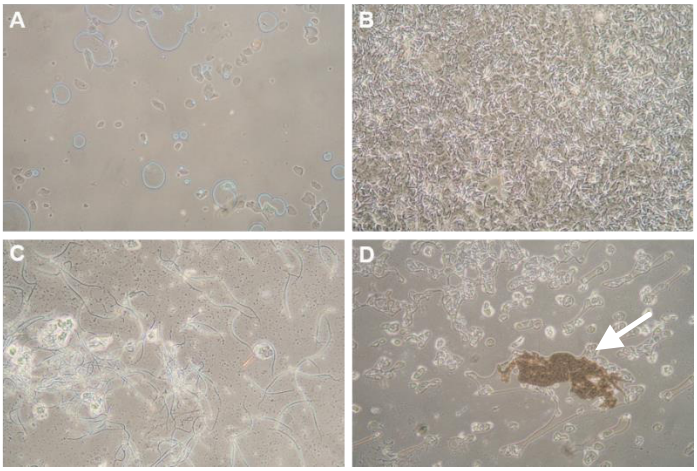

Figure 1. Vaginal smears to detect mating activity.
Vaginal smears were investigated light microscopically (magnification 100x). A: Negative smear; only few epithelial cells are visible. B–D: Positive smears; a high number of epithelial cells (B), hair (C) or sperm nests (as indicated by the arrow) (D) indicate mating activity.

For the vaginal smears, a swab with a sterile sodium chloride-soaked dabber, was gently obtained from the vagina of the female rat, smeared on a glass cover slide and covered with

a cover slip. The smears were investigated under the light microscope as displayed in Figure 1. In order to further check for mating success, the body weight of the females was measured after breeding.

Dissection of rat embryos

The dissection was conducted on embryonic day E 17.5 or E 18.5 post conception. Fifteen pregnant females were sacrificed by inhalation of CO_2. Caesarean sectioning was performed to extract the embryos, which were decapitated immediately. A piece of each body was collected for genotyping. The soft skull was incised using small eye scissors. Three cuts were made to open it, two placed along the sides, and one on top of the head from occipital to rostral until reaching the eyes. Afterwards, muscle and cartilage were folded away to reveal the brain, which was gently extracted with small, curved forceps, and collected in ice-cold HBSS (-) buffer.

Extraction and cultivation of primary neurons

Cortices and striata were extracted using a binocular microscope with a magnification of 5–10x. The stepwise extraction is illustrated in Figure 2.

Tissue from individual embryos (two samples per embryo and brain region) was collected in 1 ml ice-cold HBSS (-) buffer. Further procedures were carried out under sterile conditions. The tissue was washed once with HBSS (-) and incubated for 15 minutes at 37 °C and 5 % CO_2 with 0.5 ml HBSS (-) and 40 µl trypsin (2.5 %) for digestion. During digestion, tubes were inverted every 5 minutes. After digestion, the tissue was gently aspirated with a 1 ml pipette and transferred into a fresh tube containing 250 µl triturating solution (TS), which included Ca^{2+} to inactivate traces of trypsin left in the sample and DNase to avoid clumping through free DNA. The tissue was then disrupted by pipetting up and down 10 times using a 1 ml pipette. After the remaining tissue pieces had settled, supernatant was transferred into a fresh tube. Additional 250 µl of TS were added to the remaining tissue pieces and the tissue was triturated another 10 times. After this, either supernatant or whole samples (if no solid pieces

had remained) was transferred into the fresh tube. In case that parts of the tissue were still left, these were discarded. However, another trituration step can be added, if cell yield is crucial. Tubes containing the dissociated neuronal cells were then centrifuged for 5 minutes at 400xg, supernatant was discarded and pellets were resuspended in 1 ml of Neurobasal Medium with tissue-specific additives by pipetting up and down a few times with a 1 ml pipette. Striatal samples were filled up to a total volume of 2.5 ml (cortical samples to 5 ml) in order to achieve a concentration of approximately 1,000,000 cells per ml. Cells were seeded in 37 °C pre-warmed media on different precoated plates, depending on the assay performed afterwards. Media were changed after 24 hours in order to remove debris and dead cells. Half of the media per well were further removed on every 3rd day *in vitro* (DIV), and replaced by an equal amount of fresh media.

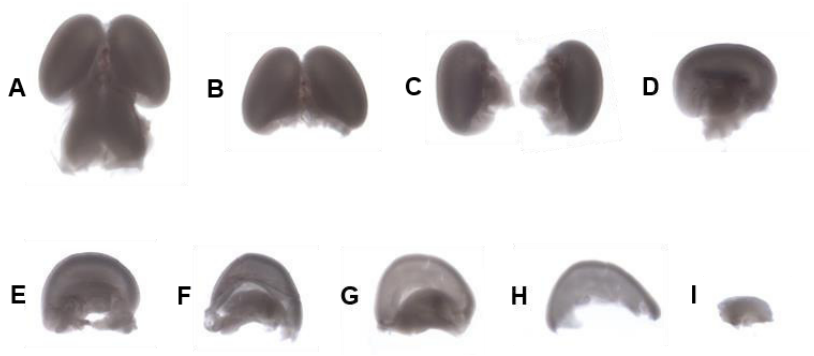

Figure 2. Tissue dissection steps for the extraction of striatum and cortex from intact embryonic brains.

Cortex and striatum were dissected from E17.5/18.5 embryos in a stepwise procedure. The brain was placed with its dorsal side facing upwards (**A**), the hindbrain was removed and discarded (**B**) and the forebrain hemispheres were separated (**C**). Hemispheres were then turned, placed with their medial side facing upwards (**D**), and protruding diencephalic tissue was removed and discarded (**E**). The cortex was spread open (**F**), the meninges were removed and discarded (**G**) and the dorsal part of the cortex (not attached to other tissues) was excised and collected (**H**). The striatum (loosely attached to the ventral part of the cortex) was gently separated and collected (**I**).

E. BACHD rat primary neuronal cultures

Genotyping

Embryonic tissue samples for genotyping were collected during the dissection procedure as mentioned above. A detailed description of primers and PCR protocol are given in Publication II[142].

Cell viability assays

We measured cell viability and cell death in primary striatal and cortical cultures. The assays were performed with commercially available kits (Cell Proliferation Kit I (MTT) and Cytotoxicity Detection Kit (LDH), Roche) following the provider's instructions. Both are based on the reduction of a tetrazolium salt to form formazan crystals. The MTT test depends on the presence of NADH + H^+ within the cells and is therefore considered to be a function of the activity of intracellular dehydrogenases and a measure of cell viability. The LDH test depends on the presence of dehydrogenases in the supernatant, which are released by dead cells and thus represent a measure of mortality.

Primary neurons were seeded at a density of 50,000 per well on 96 well plates (DIV 0). For the MTT test, tetrazolium salt was added at DIV6, and cells were incubated for 24 hours. After this, cells were lyzed by addition of lysis buffer, and the optical density (OD) was measured at 550 nm in a plate reader (BIO-TEK Synergy HT Microtiter Platereader) to measure the formazan concentration. For the LDH assay, cell culture media was collected at DIV 7, transferred to a fresh 96 well plate and incubated with tetrazolium salt. The OD was measured at 492 nm to measure the formazan concentration. For the analysis, OD measurements at an unspecific wavelength were subtracted to reduce background noise.

Mutant huntingtin in primary neuronal cultures

Procedures are as published in the supplemental information of Publication III[358].

The formation of insoluble (aggregated) forms of mHTT is a hallmark of HD[85,86]. Thus, we aimed at investigating, if aggregated forms of mHTT are present in the primary cultures. For this, striatal and cortical neurons prepared from individual BACHD and WT embryos were

cultured in 6-well plates at a density of 1,000,000 cells per well for cortex and 2,000,000 cells per well for striatum. On DIV 7, cells were harvested by trypsinization (1 ml of 0.25 % trypsin

with EDTA (Gibco) per well) and centrifugation (10 min at 400xg). Proteins were extracted from cell pellets by incubation in 100 µl RIPA buffer (50 mM Tris-HCl, pH 8.0, 150 mM NaCl, 1 % IGPAL, 0.5 % sodiumdesoxychelate, 0.1 % SDS) containing 4 % cOmplete ULTRA Protease Inhibitor-Cocktail with EDTA (Roche) for 30 minutes at 4 °C and subsequent centrifugation for 15 minutes at 4 °C at 16.400xg. Supernatant was collected and protein content for each sample was measured using a Bradford assay. The samples were stored at -80 °C until further use.

To detect the presence of insoluble mHTT in these samples, we performed a filter trap assay[427] optimized for the detection of mHTT. The method is based on the SDS-insolubility of mHTT aggregates, which are retained when filtered through a nitrocellulose membrane. For this purpose, 20 µg of protein lysate was mixed with SDS (final concentration 2 %) and filtered using a dot blotter (Dot blotter SRC 96 D, S&S Minifold I, Schleicher & Schuell, Germany). The membrane (Protran Nitrocellulose Membrane, Whatman) was afterwards probed with 1C2 anti-polyQ-antibody (MAB1574, Millipore, 1:2000) over night at 4 °C and on the next day incubated for 1 hour at room temperature with the secondary, horse-radish-peroxidase-linked anti-mouse IgG, antibody (NA931, Amersham Biosciences, 1:2500). Chemiluminescence was created using ECL Western Blotting Detection Reagent (Amersham Biosciences) and detected with the Odyssey FC (LI-COR Biosciences), showing SDS-insoluble forms of polyQ-containing protein (mHTT).

Axonal mitochondrial transport

We quantitatively assessed the motility of mitochondria along axonal processes of BACHD and WT rat neurons. For this, primary neurons were seeded at a density of 250,000 cells (striatum) or 200,000 cells (cortex) into coverglass chambers (4-chamber Lab-Tek™ II chambered coverglass, Nunc) and transfected with DsRed2Mito (encoding a fusion of *Discosoma sp*. red fluorescent protein (DsRed2) and a mitochondria-targeting sequence of human cytochrome *c* oxidase subunit VIII (Mito)) and GFP empty vector (Clontech).

E. BACHD rat primary neuronal cultures

We used two different transfection methods to account for the differential characteristics of striatal and cortical neurons. Cortical projection neurons grow long axonal processes, making it difficult to tell which axons belong to which neurons. In order to properly follow mitochondrial transport in these cultures, a low transfection efficiency was favorable. Thereby, axons of single neurons could be identified with certainty. The low transfection efficiency was achieved by calcium phosphate transfection (ProFection® Mammalian Transfection System, Promega) as previously described[428]. Transfection was carried out on DIV 6 according to the manufacturer's instructions using 1 µg/µl DNA in a ratio of 6:4 for DsRed and GFP, respectively. Striatal neurons, which grow much shorter axons that can be distinguished at higher cell densities, were transfected with a lipofection-based method (Lipofectamine®, Lifetechnologies), which yielded higher transfection efficiency (0.2 µg/µl DNA were used in the same ratio). Media were changed in both cases 4 hours after transfection to reduce cytotoxic effects of the transfection process.

On DIV 7, cells were imaged using an inverted Zeiss Axiovert microscope (Zeiss Plan-Apochromat 63x/1.4) with a CO_2- and temperature-controlled incubation chamber at 5 % CO_2 and 37 °C. Time-lapse videos of axonal mitochondrial transport were recorded with a Zeiss AxioCamMRm camera at a time-lapse interval of 3 seconds over 5 minutes. The image sequence was exported and mitochondrial motility in axonal processes was analyzed with ImageJ[429] as previously described[430].

IGF-1 measurements

In order to determine IGF-1 concentrations, primary striatal neurons were cultivated at a density of 250,000 cells per well in 24 well plates. Culture media samples collected at different times were stored at -80 °C until shipment. IGF-1 levels were measured at the University of Vancouver using a commercial ELISA kit (Mouse Quantikine ELISA kit, R&D Systems) as previously applied [197]. Since the standards in this kit are mouse IGF-1, the concentration refers to the equivalent of mouse IGF-1.

Oxidative DNA damage

The oxidation product 8OHdG is produced when reactive oxygen or nitrogen species oxidize DNA, and represents a common marker for oxidative stress[372]. We measured 8OHdG levels in cell culture media from primary striatal neurons using a commercially available ELISA kit (8-hydroxy-2-deoxy Guanosine EIA Kit, StressMarq Biosciences) and following the manufacturer's instructions.

For this, striatal neurons were seeded at a density of 200,000 per well on 24 well plates, culture media were collected on DIV 7 and diluted 1:10 with ELISA buffer. The sample was loaded on an antibody-coated plate competing with 8OHdG-acetylcholine-esterase-tracer for antibody binding. After incubation and washing steps, acetylcholine esterase substrate was added and the OD was measured at 412 nm. The signal is inversely proportional to the amount of sample 8OHdG.

Results

Breeding efficacy

A total of 41 breedings with two females each (i.e. 82 individual breeding events) were set up. Of these, 17 females conceived, giving a breeding success of 20 %. Vaginal smears (Figure 1) were prepared from 68 of the 82 females. Out of these, 24 showed signs of mating activity, while 45 did not. Thus, predicting pregnancy upon a positive result for mating activity had only a success rate of 52 %. In contrast, excluding rats due to the lack of indicators of mating activity was 96 % accurate.

A better predictor of pregnancy was body weight development after breeding (Figure 3). Pregnant females differed significantly from non-pregnant females in body weight gain after 1 week (25 ± 14 g versus 6 ± 11 g at day 6-9, $P = 0.0006$, Welch-corrected *t*-test). The difference increased further about 3-fold until the day of dissection, (66 ± 20 g versus 13 ± 13 g at day 17-18, $P < 0.0001$, Welch-corrected *t*-test). Only one female rat was found to have increased her body weight dramatically after breeding, while not carrying a litter after 18 days. During dissection, we found that this rat had accumulated large amounts of body fat, which might indicate a pregnancy that was aborted at an earlier time.

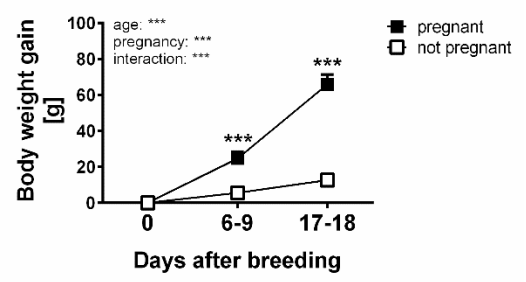

Figure 3. Increased body weight gain in pregnant females after breeding.
The body weight gain of females was measured on the day of breeding (day 0) and at different days after breeding. Mean values from 14 rats that did not conceive after breeding (not pregnant) and 13 rats that did conceive after breeding (pregnant) are shown. Two-way ANOVA, Sidak's post-test, * $P < 0.05$, ** $P < 0.01$, *** $P < 0.001$.

Viability of neuronal cultures

Isolated cells were viable in culture, readily attached to the culture dish surface and formed axonal processes (Figure 4).

When comparing the viability of primary cultures from BACHD rats and their WT littermates at DIV 3, we did not detect any differences regarding their mortality or cell metabolism, as measured by the LDH and MTT assays, respectively (Figure 5).

Mutant huntingtin expression

As published before[358], we detected insoluble forms of mHTT in primary striatal and cortical neurons from BACHD rats at DIV 7 by filter trap assay (Figure 6). This result confirms the expression of mHTT in BACHD rat primary neurons as well as the presence of mHTT aggregates at that age. Cortex revealed more aggregated mHTT, consistent with a higher expression level and higher amount of aggregate formation in BACHD rats *in vivo*[142] as well as in HD patient brains[86]

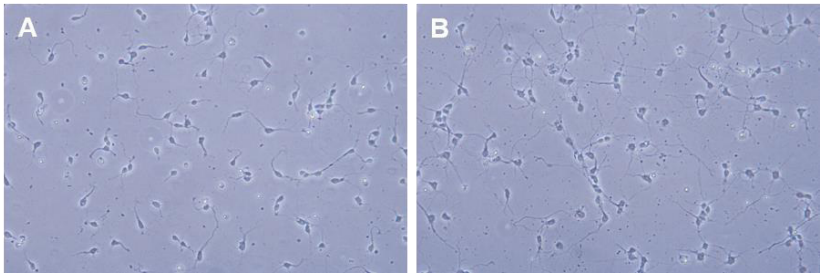

Figure 4. Primary neuronal cultures.
The photographs show primary striatal (**A**) and cortical (**B**) neurons at DIV 3 at a density of 200,000 cells per well in a 24 well plate. Cortical neurons are larger than striatal neurons and grow longer axonal processes. Images were taken with a light microscope at 400x magnification.

E. BACHD rat primary neuronal cultures

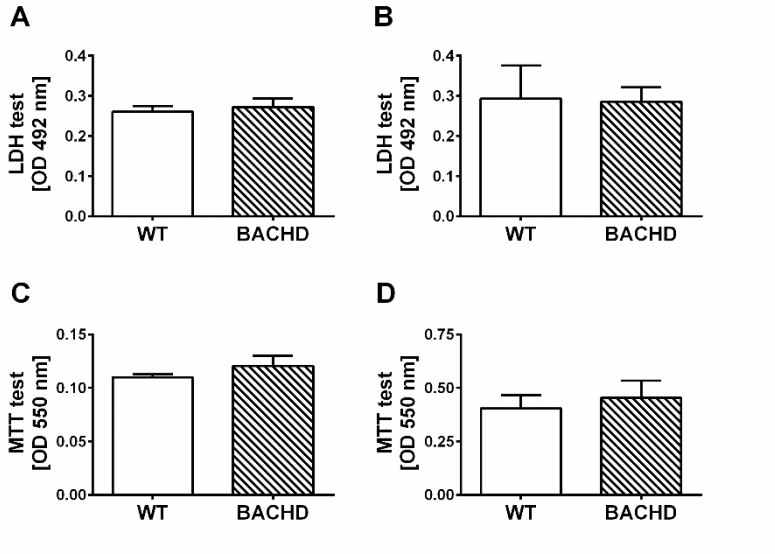

Figure 5. BACHD primary neuronal cultures do not show reduced cell viability.
Cell viability was determined at DIV 7 based on the LDH release of dead cells (**A, B**) and the dehydrogenase-dependent MTT conversion (**C, D**). Neither cell mortality measured in the LDH test, nor cell metabolism measured in the MTT test, differed between WT and BACHD rat striatal (**A, C**) or cortical (**B, D**) primary neuronal cultures. The same individual embryos were used for the cultures for LDH and MTT assay (n = 3 WT and 5 BACHD for striatum, and n = 3 WT and 3 BACHD for cortex). Welch-corrected *t*-tests, * $P < 0.05$, ** $P < 0.01$, *** $P < 0.001$.

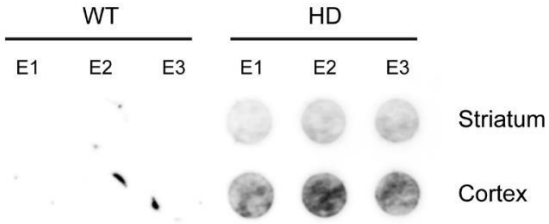

Figure 6. BACHD rat primary neuronal cultures contain insoluble mHTT.
SDS-insoluble proteins were trapped on a nitrocellulose membrane and probed with a polyQ-specific antibody. The presence of insoluble polyQ-containing protein in primary striatal and cortical cultures from BACHD rat embryos but not their WT littermates indicates the expression of aggregated forms of mHTT

in these neurons. Each dot is the extract from a separate neuronal culture prepared from an individual embryo (three embryos per genotype and brain region).

Axonal mitochondrial transport

Several studies report an impairment of axonal trafficking in HD[46,288,431,432]. Compromised mitochondrial transport in particular[288,289,433] might contribute to deficits in cellular energy metabolism observed in HD[398]. Therefore, we tracked axonal transport of mitochondria in our primary cultures by measuring the amount of motile mitochondria within axonal processes. On average, WT cells contained 30–40 % of motile mitochondria, which is common for healthy cells[434]. On the other hand, a significant reduction of the percentage of motile mitochondria was detected in striatal (Figure 7A) and cortical neurons (Figure 7B) from BACHD rats compared to WT littermates, pointing to an HD-related transport defect.

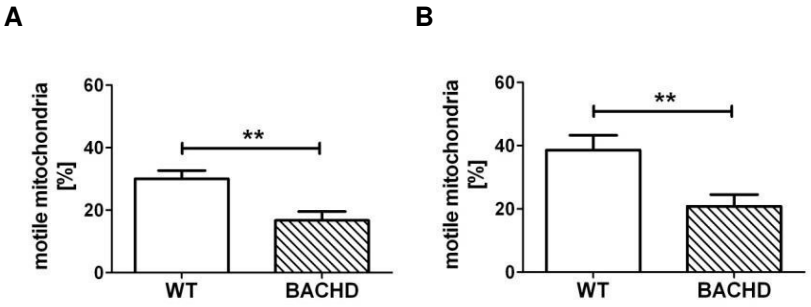

Figure 7. Axonal mitochondrial transport is impaired in BACHD rat neurons.
BACHD rat striatal (left side) and cortical (right side) neurons have a lower percentage of motile mitochondria compared to neurons from their WT littermates. The graph displays mean plus SEM of neurons tracked from three independent measurements (striatum: n = 12 WT and 12 BACHD neurons; cortex: n = 18 WT and 21 BACHD neurons). Welch-corrected *t*-test, * $P < 0.05$, ** $P < 0.01$, *** $P < 0.001$.

IGF-1 levels

It has been shown that the axonal transport defect is restored, if mHTT is phosphorylated at serine 421[400]. In HD, reduced IGF-1 levels[197] lead to decreased Akt signaling[435] and reduced phosphorylation of mHTT at serine 421[400]. Thus, we investigated the levels of IGF-1 in BACHD rat primary striatal cultures. We observed reduced levels of IGF-1 in these neurons (Figure 8). Interestingly, IGF-1 levels seemed to be slightly increased in BACHD rat cultures at DIV 3, while this trend changed into reduced IGF-1 levels at DIV 6 and 9, cumulating in a significant difference at DIV 12.

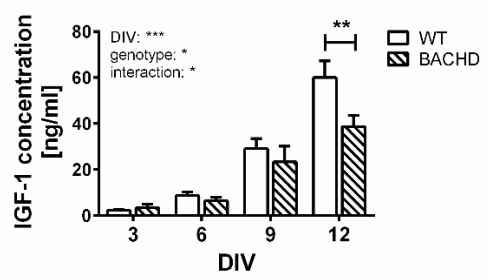

Figure 8. IGF-1 levels are reduced in BACHD rat primary striatal neurons at longer cultivation times.

BACHD rat primary striatal neurons show lower IGF-1 concentration in their culture media at 12 days *in vitro* (DIV). Samples were taken from cultures deriving from six individual embryos per genotype. Two-way ANOVA, Sidak's post-test, * $P < 0.05$, ** $P < 0.01$, *** $P < 0.001$.

Oxidative DNA damage

Oxidative stress, and associated DNA damage have been described as a part of mitochondrial dysfunction in HD[246]. These pathologies are considered to be related to a negative influence of mHTT on mitochondrial function[265,269]. Since we had found that striatal but not cortical neurons from BACHD rats display deficits in energy metabolism at DIV 7[358], we were interested in assessing if oxidative stress as a result of profound mitochondrial damage would be present in these cells after longer cultivation times. However, we found that the levels of 8OHdG released by dead cells did not differ between WT and BACHD rats, neither at DIV 3 nor at the late DIV 12 (Figure 9).

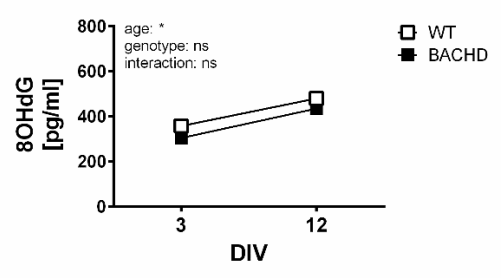

Figure 9. BACHD rat primary striatal neurons do not show enhanced oxidative DNA damage.
Levels of 8OHdG, measured by ELISA were similar in BACHD and WT rat striatal neurons at early and late cultivation times. Data points represent samples from four individual embryos per genotype and day *in vitro* (DIV). Two-way repeated measurements ANOVA, Sidak's post-test. * $P < 0.05$, ** $P < 0.01$, *** $P < 0.001$.

Discussion

We demonstrated that our protocol for isolation and cultivation of primary BACHD rat neurons revealed viable cultures, which were subsequently used for a variety of assays to analyze cell functions. BACHD rat primary neurons show impaired cell functions, which resemble the pathology found in the HD patient. Thus, BACHD rat primary neurons can be regarded a useful tool for the analysis of disease mechanisms, and to test the therapeutic efficacy of drugs or compounds for HD.

The dissection of striatal and cortical tissue followed previous protocols established for mice. The original protocols were combined, adapted for rats and optimized for easier parallel application. Optimization was necessary, as the parallel preparation of primary striatal and cortical cultures would have otherwise been immensely time-consuming, since the original protocols differed on several steps. The combined protocol is sophisticated in the sense that it is more time-efficient and the procedures have higher practicability. In addition, it allows for direct comparison between striatum and cortex from a given embryo.

It should be mentioned that our optimization strategy did not aim at increasing the yield in neuronal tissue. Our focus was to reduce the amount of time needed to perform the laborious procedures. In case that tissue yield is crucial, for instance if the model organisms are mice instead of rats, the dissection and trituration steps can be refined. Also, pooled samples might be chosen instead of keeping samples from individual embryos separate.

Our protocol could in principle be varied or extended for the parallel culture of other brain regions such as for instance hippocampus, as the hippocampus can be easily identified and dissected in the embryonic brain at E 17.5 or E 18.5. Similarly, cerebellar neurons or glia cells from different areas could be cultured using our extraction protocol, simply by adapting the specific culture media required. This way, our approach is not only useful for studying molecular mechanisms of HD but also those of other neurological disorders.

In our isolated neurons, we analyzed four interconnected parameters implicated in the cellular pathology of HD. We found that mHTT is expressed in primary neuronal cultures. Moreover, mHTT had formed aggregates in these cells at DIV 7, similar to primary striatal cultures from mice transfected with mHTT *in vitro*[94]. Aggregates of mHTT are not considered to be *per se* cytotoxic, however, they derive from N-terminal mHTT fragments which are highly toxic to

cells. Thus, the presence of mHTT aggregates in BACHD rat primary neurons indicates that mHTT is cleaved into toxic fragments, resembling the condition found in the HD brain. BACHD rat primary neurons further displayed HD-related pathologies. We found the cells to recapitulate a prominent molecular pathology of HD, an axonal transport defect induced by reduced IGF-1/Akt signaling[197,400,435]. We further analyzed the presence of oxidative DNA damage, to detect if BACHD rat primary neurons showed profound mitochondrial dysfunction. However, this was not the case.

Publications

The last part contains the published manuscripts.

Manuscripts are given in chronological order:

I. Verwaest et al. 2011, *Biochimica et Biophysica Acta*.

II. Yu-Taeger et al. 2012, *Journal of Neuroscience*.

III. Gouarné et al. 2013, *PLoS One*.

IV. Clemens et al. 2014, *Genes, Brain & Behavior*.

V. Eckmann & Clemens et al. 2014, *Molecular Neurobiology*.

VI. Jansson & Clemens et al. 2014, *PLoS One*.

VII. Clemens & Weber et al. 2015, *Brain*.

Biochimica et Biophysica Acta 1812 (2011) 1371–1379

Contents lists available at SciVerse ScienceDirect

Biochimica et Biophysica Acta

journal homepage: www.elsevier.com/locate/bbadis

^{1}H NMR based metabolomics of CSF and blood serum: A metabolic profile for a transgenic rat model of Huntington disease

Kim A. Verwaest [a,e,*], Trung N. Vu [b,e], Kris Laukens [b,e], Laura E. Clemens [c,e], Huu P. Nguyen [c,e], Bjorn Van Gasse [d,e], José C. Martins [d,e], Annemie Van Der Linden [d,e], Roger Dommisse [a,e]

[a] Department of Chemistry, University of Antwerp, Groenenborgerlaan 171, 2020 Antwerp, Belgium
[b] Department of Mathematics & Computer Science, University of Antwerp, Middelheimlaan 1, 2020 Antwerp, Belgium
[c] Department of Medical Genetics, University of Tuebingen, Calwerstrasse 7, 72076 Tuebingen, Germany
[d] Department of Organic Chemistry, University of Ghent, Krijgslaan 281 S4, 9000 Gent, Belgium
[e] Department of Biomedical Science, University of Antwerp, Groenenborgerlaan 171, 2020 Antwerp, Belgium

ARTICLE INFO

Article history:
Received 22 April 2011
Received in revised form 19 July 2011
Accepted 8 August 2011
Available online 16 August 2011

Keywords:
Huntington disease
CSF
Serum
Metabolomics
Transgenic rat
^{1}H NMR spectroscopy

ABSTRACT

Huntington disease (HD) is a hereditary brain disease. Although the causative gene has been found, the exact mechanisms of the pathogenesis are still unknown. Recent investigations point to metabolic and energetic dysfunctions in HD neurons.

Both univariate and multivariate analyses were used to compare proton nuclear magnetic resonance spectra of serum and cerebrospinal fluid (CSF) taken from presymptomatic HD transgenic rats and their wild-type littermates. N-acetylaspartate (NAA), was found to be significantly decreased in the serum of HD rats compared to wild-type littermates. Moreover, in the serum their levels of glutamine, succinic acid, glucose and lactate are significantly increased as well. An increased concentration of lactate and glucose is also found in CSF. There is a 1:1 stoichiometry coupling glucose utilization and glutamate cycling. The observed increase in the glutamine concentration, which indicates a shutdown in the neuronal-glial glutamate-glutamine cycling, results therefore in an increased glucose concentration. The elevated succinic acid concentration might be due to an inhibition of succinate dehydrogenase, an enzyme linked to the mitochondrial respiratory chain and TCA cycle. Moreover, reduced levels of NAA may reflect an impairment of mitochondrial energy production. In addition, the observed difference in lactate supports a deficiency of oxidative energy metabolism in rats transgenic for HD as well.

The observed metabolic alterations seem to be more profound in serum than in CSF in presymptomatic rats. All findings suggest that even in presymptomatic rats, a defect in energy metabolism is already apparent. These results support the hypothesis of mitochondrial energy dysfunction in HD.

1. Introduction

Huntington disease (HD) is an autosomal dominant neurodegenerative disorder, characterized by progressive motor, cognitive and psychiatric dysfunctions. Although the disease can occur at any age, the median age of onset is 40 years. Most patients die one to two decades after disease onset.

HD is caused by a mutation in the gene coding for the protein huntingtin. The exact function of this protein is still unknown. Normal individuals have a CAG-trinucleotide repeat length of less than 37 [1]. People whose CAG repeat length exceeds this number will develop HD. The length of the CAG expansion is proportional to the severity of the disease and inversely proportional to the age of onset [2]. At present, the exact mechanism of the HD pathology is still unknown. However, recent evidence points to metabolic and energetic dysfunction in HD neurons [2–4]. Better knowledge about this mechanism is expected to lead to more appropriate analyses, which in turn should result in a better understanding of the disease. Moreover, this will help to direct the quest for improved treatments in the proper direction.

According to Nicholson et al. [5], metabolomics is defined as 'the quantitative measurement of the dynamic multiparametric metabolic response of living systems to pathophysiological stimuli or genetic modifications'. Since 1999, applications of this technique have emerged in other fields (e.g. environmental sciences) [6]. Metabolites in biofluids are in dynamic equilibrium with those in cells and tissues. A healthy individual attempts to retain the concentration of metabolites in cells and tissues constant by homeostasis. Abnormal

* Corresponding author at: Department of Chemistry, University of Antwerp, Groenenborgerlaan 171, 2020 Antwerp, Belgium. Tel.: +32 32653267.
E-mail addresses: kim.verwaest@ua.ac.be (K.A. Verwaest), TrungNghia.Vu@ua.ac.be (T.N. Vu), kris.laukens@ua.ac.be (K. Laukens), Laura.Clemens@med.uni-tuebingen.de (L.E. Clemens), hoa.nguyen@med.uni-tuebingen.de (H.P. Nguyen), Bjorn.vangasse@UGent.be (B. Van Gasse), jose.martins@UGent.be (J.C. Martins), Annemie.VanDerLinden@ua.ac.be (A. Van Der Linden), roger.dommisse@ua.ac.be (R. Dommisse).

0925-4439/$ – see front matter © 2011 Elsevier B.V. All rights reserved.
doi:10.1016/j.bbadis.2011.08.001

cellular processes due to sickness, toxins, etc. result in altered biofluid compositions. Various analytical techniques are available to detect low molecular weight metabolites. The ones most commonly applied in metabolomic studies are nuclear magnetic resonance spectroscopy (NMR) and mass spectrometry (MS). The latter is frequently used in combination with a chromatographic separation technique (liquid chromatography, gas chromatography, etc.) [7]. Although NMR is less sensitive than MS, this technique offers some important advantages. It is a high-throughput analysis that does not require any preceding chromatographic separation or purification procedure. Additionally, sample preparation is very straightforward. Furthermore, it is a non-destructive method capable of detecting all non-exchangeable protons, provided they are present above a certain threshold concentration (μM concentrations). Moreover, the measurements are very reproducible and inexpensive on a per sample basis [8–10]. All these advantages have contributed to the application of NMR spectroscopy in clinical diagnoses of diseases and in the follow-up of subjects participating in medical treatment studies [11].

The NMR spectrum of a biofluid is generally extremely complex in nature, since each molecule present in the biofluid gives rise to one or several peaks in most cases. Moreover, many peaks show some fine structure and splittings which cause a prominent overlap of signals originating from different molecules [12]. Visual inspection of the spectra will therefore only reveal a small percentage of the available information [13].

Spectral interpretation can be simplified by applying automatic data reduction methods. Subsequently, these reduced datasets can be analyzed with univariate [2,14–22] or multivariate [13,23–27] statistical methods.

In this study we applied ^{1}H NMR spectroscopy in order to disentangle the metabolic profile of serum and cerebrospinal fluid (CSF) from a rat model for HD. Both univariate and multivariate statistical analyses were applied in a search for pathology specific differences. It is anticipated that these investigations lead to a gain in knowledge about the pathogenesis of HD and make it possible to identify some potential biomarkers.

2. Materials and methods

2.1. Animals

Transgenic HD rats carrying a truncated huntingtin cDNA fragment with 51 CAG repeats under the control of the native rat huntingtin promoter, and their wild-type littermates were used [28]. The expressed gene product was 75 kDa, corresponding to 22% of the full-length huntingtin (cDNA positions 324–2321, amino acid positions 1–709/825, corresponding to exons 1–16), which are under the control of 886 bp of the rat huntingtin promoter (positions 900 to 15). Genotyping was carried out as previously described [28]. The number of CAG repeats was analyzed in a subset of transgenic rats using these primers: cggctgaggcagcagcggctgt (forward) and ccttcgagtccct-caagtccttc (reverse). The reverse primer is labelled at the 5′ end with the fluorescent dye Cy5. The PCR amplicon length was then analyzed on the Beckman coulter sequencer (CEQ 8000 Cycle Sequencer, Krefeld, Germany). In more than 15 generations only a small variation of ±1–2 CAGs were observed in transgenic rats of HD. Also for this study, in a subset of animals, the CAG-length was checked and it was found to be 51±2 CAGs. After genotyping, rats were housed in gender- and genotyped matched groups of two, according to FELASA recommendations. All rats were kept under a 12:12 hours light–dark cycle with lights on at 06.00 a.m. and food (Altromin lab chow pallets, Altromin standard diet: 1320; Lage, Germany) and tap water available ad libitum. All research and animal care procedures had been approved by the district government of Tuebingen, Germany, and followed principles described in the European Community's Council Directive of 24th November, 1986 (86/609/EEC).

For this study, we used serum and CSF from female, transgenic HD rats (n = 10 for serum and n = 8 for CSF) at an age of two months and compared these with age-matched wild-type (WT) littermates (n = 12 for serum and respectively 9 for CSF). We are aware of the fact that the number of samples used in this study is rather small. However, this was determined by keeping in mind the well-being of animals and in order to reduce costs. Moreover, in the literature a lot of studies where even less samples per group are investigated, can be found [15,27,29–32].

2.2. Sample collection and preparation

2.2.1. CSF samples

Rats were sacrificed by CO_2 inhalation and immediately exsanguinated. Subsequently, each animal was placed prone onto the stereotaxic instrument. A sagittal incision of the skin was made inferior to the occiput. The subcutaneous tissue and neck muscles through the midline were bluntly separated. Next, the rat was laid down in a way that the body made a 135° angle with the fixed head. In this angle, the dura mater of cisterna magna was exposed sufficiently. The dura was then penetrated with an insulin syringe and CSF was drawn. All samples were transferred into polypropylene tubes, immediately snap frozen in liquid nitrogen and stored at −80 °C until shipped for NMR analysis. Upon arrival, CSF samples were immediately stored at −80 °C until measurement.

All CSF samples (40 μL) were simultaneously lyophilized. In cases where less than 40 μL of CSF was available, the total available volume was lyophilized. The freeze-dried samples were then stored at −20 °C in sealed vials until analysis. In order to keep the time spent at room temperature to a minimum, samples were randomly divided in five batches. Samples gathered in one batch were prepared together. Prior to NMR analysis, each sample was reconstituted in 8 μL sodium phosphate buffer (50 mM dissolved in D_2O, pH = 7.05) containing 0.05 mM sodium azide in order to prevent bacterial contamination. Finally, this volume was transferred to a 1 mm NMR tube.

2.2.2. Serum samples

Samples were taken as done previously [33]. In short: rats were sacrificed with CO_2 and blood was drawn directly from the heart. All rats were tested for diabetes immediately after sample collection. The blood was incubated for 1 h at 37 °C, followed by centrifugation for 30 min at 3000 ×*g*. The serum was collected and immediately stored at −80 °C until shipped for NMR analysis. Upon arrival, serum samples were immediately stored at −80 °C until measurement.

In order to keep the time spent at room temperature to a minimum, samples were randomly divided in three groups. Samples assembled in one group were prepared together. Just before their acquisition, samples were thawed to room temperature. An aliquot of serum (250 μL) from each sample was mixed with 300 μL of an aqueous saline solution. In this way, each sample contains 0.1 M NaCl and 10% D_2O. The addition of an internal standard like DSS is prohibited by its interaction with proteins present in the sample. Subsequently, the total volume was transferred to a 5 mm NMR tube.

2.3. ^{1}H NMR spectroscopy

Prepared samples were analyzed on a Bruker Avance II-700 spectrometer, operating at a proton frequency of 700.13 MHz. The spectrometer is equipped with a BACS-60 automatic sample changer and a 5 mm inverse TXI-Z probe when measuring serum samples. Since the brain volume of rats is rather small, the amount of CSF that can be collected at once from one animal is too small to perform a classical NMR analysis (>100 μL is necessary, prior to dilution to the final 550 μL measuring volume, in order to get a good S/N). Combining CSF taken from different animals within a population is not advisable, since this will remove the possibility to detect individual differences.

Recently, Bach and co-workers [10,34] demonstrated that the use of a 1 mm probe setup provides an alternative to address the measurement of such volume restricted samples. Therefore, CSF samples were measured with a 1 mm inverse TXI-Z probe, requiring only 8 μL of sample volume. The samples were held at room temperature while on the sample changer and at 303 K during acquisition. Carr–Purcell–Meiboom–Gill (CPMG) experiments were executed in order to get 1D ^{1}H NMR spectra of the samples. The individual CPMG spin echo (in total 1 ms) was repeated 20 times, resulting in a total spin-spin relaxation delay of 20 ms. Suppression of the water signal was performed using 2.22 s presaturation during the relaxation delay. For serum 64 scans (32 K data points each) were sampled whereas 1024 scans were needed for CSF. Each scan had an acquisition time of 0.78 s. To keep variation due to sample handling to a minimum, tuning and matching as well as shimming were performed automatically for each sample. Digital filtering was performed using the 'baseopt' option available in Topspin 2.0 (Bruker Biospin Corporation) which results in flat baselines. Prior to Fourier transformation, the Free Induction Decays (FIDs) were zero-filled to 64 K and an exponential window function with a line broadening factor of 0.3 Hz was applied. The acquired NMR spectra were consecutively processed for phase and baseline correction. In the absence of an external reference (vide supra 2.2.2), all serum spectra were referenced to the methyl doublet of lactate at 1.33 ppm. After initial referencing of the CSF spectra using the anomeric glucose ^{1}H signal at 5.225 ppm, the spectra were still shifted one against the other. They were aligned using an in house developed spectral alignment algorithm (Vu T.N. et. al, submitted).

2.4. Data reduction of the NMR spectra

The ^{1}H NMR spectra were automatically reduced into consecutive integrated spectral regions (buckets) of an equal width (0.05 ppm) applying R (version 2.7.2, http://www.r-project.org). In order to eliminate spectral variations due to different quality of water suppression from one spectrum to another, the region containing the water resonance (4.5–5.0 ppm) was not included in the analysis. In order to account for differences in concentration between samples, the subdivided spectra were scaled to their total intensity.

2.4.1. Multivariate analysis

Prior to multivariate analysis, the data were scaled to unit variance. Besides unit variance scaling, also pareto scaling and no scaling were tested on the dataset. However, these did not generate significant differences. Since all the variables possess an equal weight, irrespective of their absolute magnitude in the original data when unit variance scaling is applied, this method was preferred.

Principal component analysis (PCA) is used to project the data in two or three dimension in order to be able to discern outliers. This method transforms the original variables in new, uncorrelated variables or principal components (PC) in such a way that the first PC represents most of the variation present in the original dataset. Higher PC will subsequently contain less amount of the variance [5,7,26].

Partial least squares-discriminant analysis (PLS-DA) is a multivariate classification method based on PLS, a regression extension of PCA. This technique uses a priori knowledge about the data to maximize the separation between samples belonging to different classes [7,35]. Here, it concerns information about the pathological condition (healthy or HD) of each sample. The obtained scores plots are used to visualize the separation between the samples based on their class membership. The corresponding loading plots contain information about the variables responsible for the observed separation. Both PCA and PLS calculations were performed with R (R version 2.7.2, http://www.r-project.org, packages *FactoMineR* version 1.14, *caret* version 4.76). A double cross-validation (2CV) strategy and permutation test [36] were applied to estimate the quality of the developed PLS-DA model. The data points were randomly divided into 5 fractions, of which one was used for testing, whereas the others were used for training and validation. Leave-one-out cross-validation (LOOCV) [36] is used for validation in order to select the optimal model. LOOCV uses all but one data point as the training set. The left-out data point is used for validation. The data were randomly ordered 100 times. The average of area under the ROC curve (AUROC) was used as the criterion. In order to select the optimal number of components for PLS-DA, different numbers were tested (from 1 to the number of samples). Furthermore, the number of misclassifications and the Q^2 value were collected. A distribution was generated for the H0 hypothesis that no difference exists between the two classes. In the permutation test, the class labels of control and disease are permutated by randomly assigning them to different individuals. With 'wrong' class labels, a classification model is again calculated. The data were permutated 1000 times. For each permutated set, the cross-validation was repeated 20 times and the average parameter values were computed.

2.4.2. Univariate analysis

The bucket table created for the multivariate analysis was exported to Excel (Microsoft Office 2003) in order to carry out a Student's *t*-test. P levels smaller than 0.05 were considered to be significant. An advanced classifier, Support Vector Machine (SVM) [37], was applied to classify the samples based on the significantly differential buckets. Each sample contains one out of two possible labels, and is represented by a feature vector based on the values of the significant buckets. The data samples were randomly divided into 5 fractions, of which one was used for testing, whereas the others were used for training and validation. The data were randomly ordered 100 times. The average of area under the ROC curve (AUROC) was used as the criterion. To estimate the quality of the developed SVM model, the double cross-validation (2CV) strategy and permutation test described in [36] used for PLS-DA were applied again. In all experiments, the SVM function in the package e1071 (version 1.5-22) in R (R version 2.7.2, http://www.r-project.org) was used with the default setting parameters, e.g. linear kernel and cost equals 1.

3. Results

3.1. Visual inspection of NMR spectra

There is a lot of information comprised in ^{1}H NMR spectra of serum and CSF samples. Visual inspection of the spectra can already reveal some interesting features in some cases. A representative ^{1}H Carr–Purcell–Meiboom–Gill (CPMG) serum spectrum of both a wild-type and a transgenic HD rat is represented in Additional file A. The projection of all available serum spectra onto each other makes a clear differentiation between wild-type (WT) and HD rats possible. Peaks representing glucose and succinic acid seem to be elevated in spectra from HD rats (Fig. 1). This indicates that both glucose and succinic acid are increased in concentration in the serum of transgenic animals. Visual examination of an overlay of the CSF spectra does not indicate an immediate difference between WT and HD rats.

3.2. PCA to detect outliers

Principal component analysis (PCA) was applied on the data in order to uncover inherent similarities and differences potentially present within the spectral profiles. The scores plot of the first two principal components gives a representative overview of the data (Fig. 2).

3.2.1. Serum samples

The first principal component (PC1) accounts for 76.42% of the total variation present in the dataset. The second principal component

(PC2) accounts for an additional 10.02% of the total variation. Data points lying outside the 95% confidence ellipse (Hotelling T²) can be considered as outliers, i.e. observations that have an aberrant behaviour. As indicated in Fig. 2, two data point are laying outside the Hotelling T² plot. Reconsidering these spectra reveals that the water suppression technique, which has been used while acquiring the spectra, has caused a shift of the baseline in comparison with the other spectra. This slightly different prospect is revealed by this multivariate statistical tool. However, these two spectra are not discarded for further analysis, as their differences are not from a biological nature.

3.2.2. CSF samples

The scores plot of the first two principal components accounts for 45.57% of the total variation present in the CSF dataset. Possible outliers present in the dataset were uncovered by spotting the data points lying outside the 95% confidence ellipse of this scores plot. Consecutive PCA indicate three data points (one WT and two HD samples) with an aberrant behaviour (see Additional file B, Additional file C and Additional file D). Those spectra correspond with low available volume samples (<40 μL lyophilized). For this reason, these spectra were excluded from the dataset before further analysis.

3.3. Discrimination between normal and pathological samples using PLS-DA

A partial least squares-discriminant analysis (PLS-DA) model was developed in order to discriminate samples according to their class membership, i.e. healthy or HD. The results of this analysis are depicted in Fig. 3. The scores plot shows a reasonable separation between both sample groups. The corresponding loading plot reveals the metabolites that are responsible for the observed separation. Annotation of the loadings was confirmed by a comparison with reference spectra of an in house database recorded at 700 MHz. A

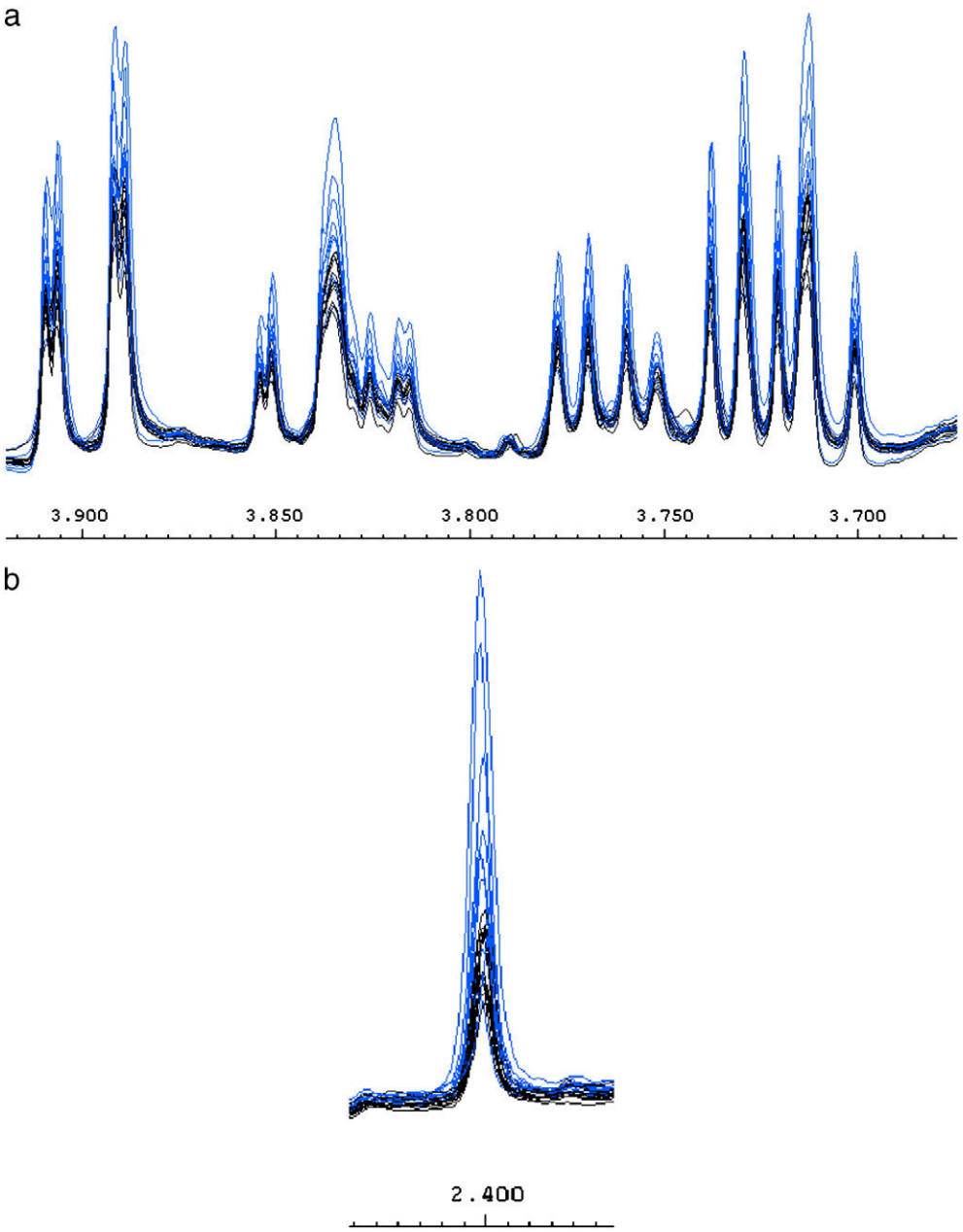

Fig. 1. Visual comparison of serum spectra. An overlay of all acquired ^{1}H NMR 700 MHz serum spectra, a some representative peaks of glucose b signal of succinic acid. Spectra of wild-type rats are coloured black; those of HD rats blue.

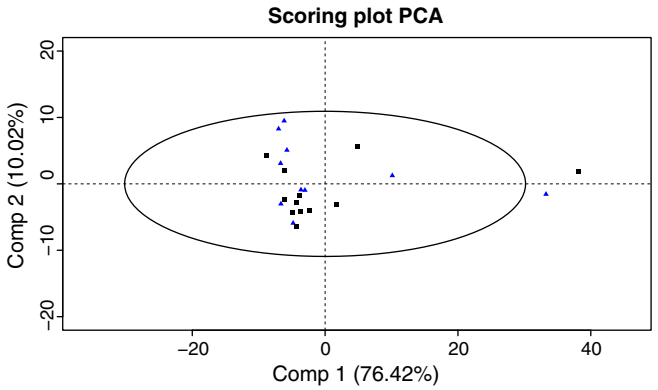

Fig. 2. PCA to detect outliers. PCA scores plot of the first and second principal component mapping the serum spectra of twelve wild-type and ten HD rats (females, 2 months old). The Hotelling T^2 ellipse is used to elucidate outliers. Colour coding: black squares = wild-type rats, blue triangles = HD.

double cross-validation (2CV) strategy and permutation test were applied to estimate the quality of the developed PLS-DA model, as described in [36]. This yielded an area under the ROC curve (AUROC) of 84.90% and 72.73% for serum and CSF respectively. For all assessment parameters (Q^2 value and the number of misclassifications), there is a clear distinction between the permutation distribution and the original classification. This shows that the specific classification is significant (see Additional files E1 for serum and E2 for CSF).

3.3.1. Serum samples

The loading coefficients responsible for the separation of the serum samples according to their pathological condition correspond to the metabolites glucose (δ3.28, δ3.38, δ3.43, δ3.48, δ3.53, δ3.73, δ3.78, δ3.83, δ3.88, δ3.93 and δ5.23), lactate (δ1.33 and δ4.13), lipids (δ0.83, δ0.88, δ1.23, δ1.28, δ1.58, δ2.03, δ2.23, δ2.73, δ2.78, δ5.28 and δ5.33), succinic acid (δ2.43), glutamine (δ2.13 and δ2.43) and NAA (δ2.03). An overview of these results is given in Table 1.

3.3.2. CSF samples

The most relevant loadings in the separation of CSF samples according to their pathological condition are situated around δ3.38, δ3.43, δ3.48, δ3.73, δ3.78, δ3.83 and δ3.88 (glucose) and δ1.33 (lactate).

3.4. Discrimination between normal and pathological samples using a univariate analysis

A Student's *t*-test is used to uncover the metabolites that show a statistically significant concentration difference between the two observed populations. Thus, these metabolites can be used to differentiate HD from healthy samples. The bucket table, which was created for the multivariate analysis, was used as input variable for the univariate analysis. For each bucket, the corresponding p-value was calculated. A p-value smaller than 0.05 was considered as significant.

3.4.1. Serum samples

The bucket comprising both the singlet peak of the methylene groups of succinic acid and the multiplet peak of CH_2CO of glutamine was found to be significantly different between WT and TG rats. In order to assign this statistically significant difference unambiguously to the correct metabolite, both signals were integrated referenced to the methylene singlet of creatine at 3.93 ppm. A visual representation of these results is displayed in Fig. 4. These boxplots reveal that both metabolites contribute to the differentiation of the samples according

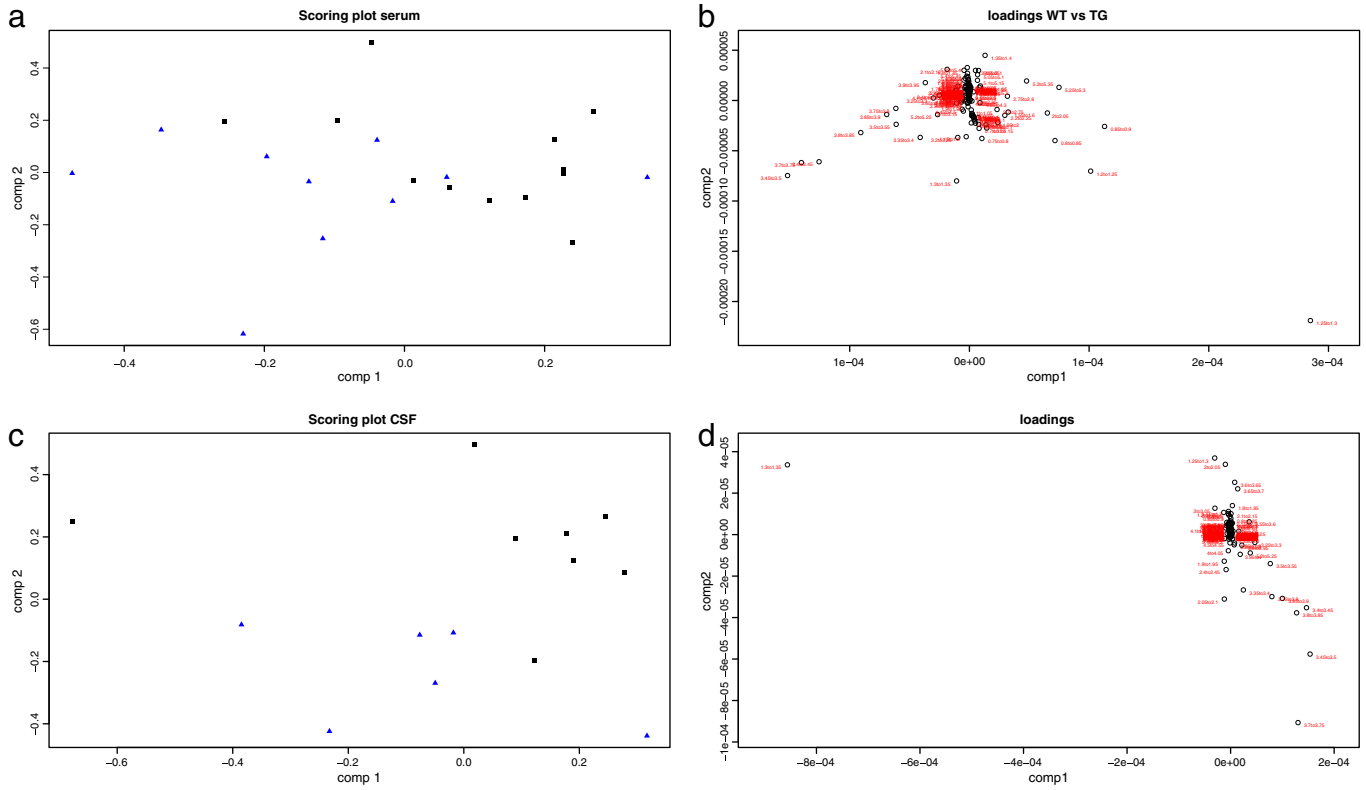

Fig. 3. PLS, clustering of samples according to their pathological condition. a PLS scores plot of ^{1}H NMR serum spectra of twelve wild-type (black squares) and ten HD (blue triangles) rats (females, 2 months old). b The corresponding loading plot represents the variables attributable to the observed class separation. c PLS scores plot of ^{1}H NMR CSF spectra of nine wild-type (black squares) and eight HD (blue triangles) rats (females, two months old). d The loading coefficient plot corresponding to the scores plot (c).

Table 1
Overview of the metabolites responsible for the separation of serum samples according to their pathological condition.

	Metabolites
Higher concentration in TG animals	Glucose Lactate Succinic acid Glutamine
Lower concentration in TG animals	NAA Lipids

to their genotype. Both glutamine ($p<0.05$) and succinic acid ($p<0.005$) were found to be significantly increased in HD rats compared to WT littermates. Glucose was found to be elevated in HD rats as well ($p<0.05$). Furthermore, NAA was decreased in HD rats ($p<0.05$). Moreover, the bucket comprising the area between 4.30 and 4.25 ppm (see Fig. 5) is found to be significantly decreased in HD rats. At present, we have not been able to identify the component(s) present in this bucket. These results are illustrated in Fig. 4. The thirteen most significant buckets for whom the p-value is smaller than 0.05, able in discriminating between healthy and HD samples, were used to build an SVM classifier. An area under the ROC curve (AUROC) of 71.44% could be obtained. For all the assessment parameters, a clear distinction between the permutation distribution and the original classification is obtained. This demonstrates that the specific classification is significant (see Additional file E3).

3.4.2. CSF samples

In CSF, a Student's *t*-test could not reveal any statistically significant metabolite concentration difference between WT and HD rats.

4. Discussion

In this study we have shown that rats transgenic for the HD mutation can be discriminated from healthy, wild-type littermates

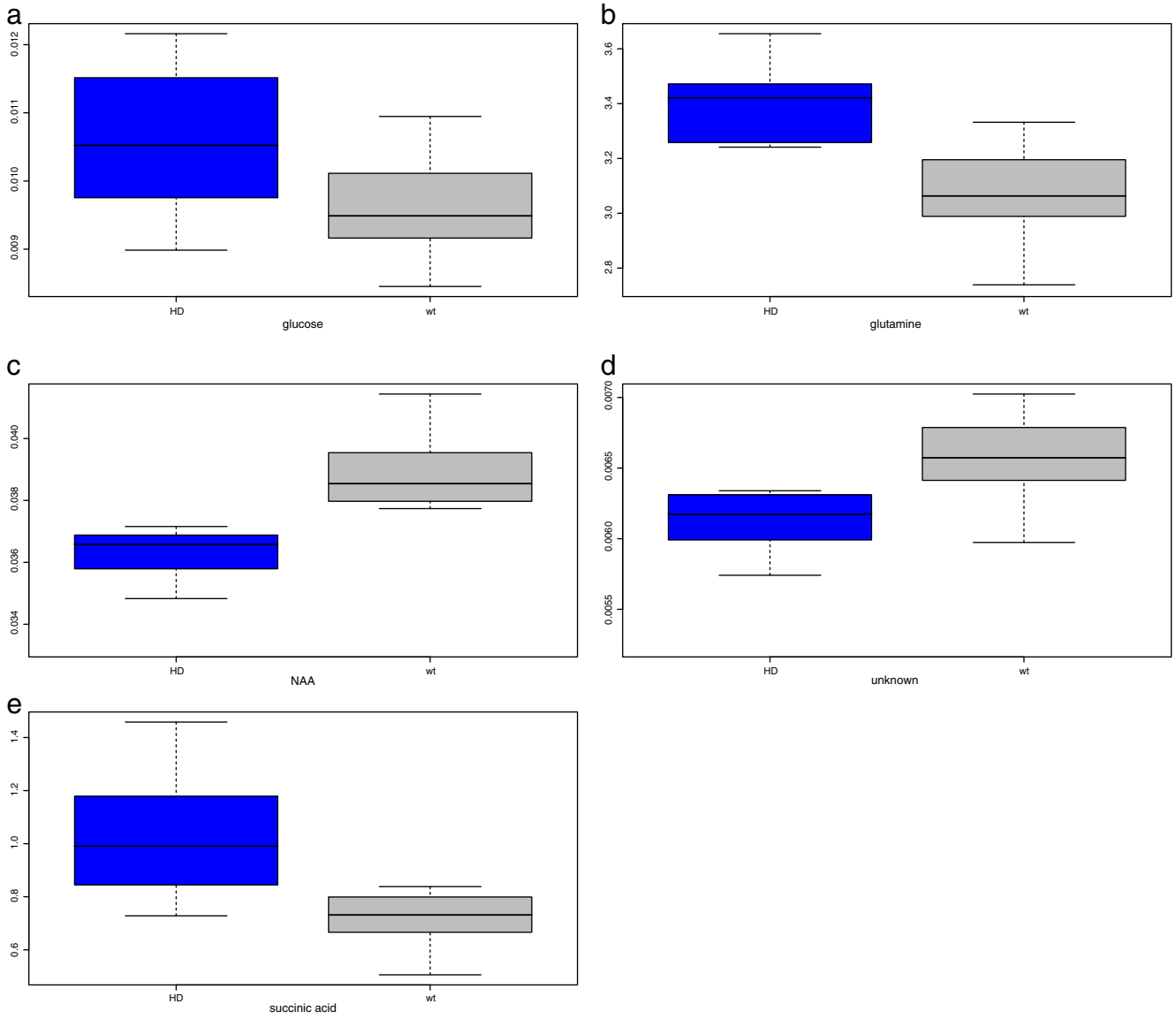

Fig. 4. Visualization of the results obtained by univariate analysis. A boxplot is used to visualize the data of the Student's *t*-test. The boxplot is based on the five-number-summary, i.e. the median (black line), 25% quartile (lower box line), 75% quartile (upper box line), minimum (lower whisker) and maximum (upper whisker). This means that 50% of the data points are situated in the box. The range between the 25% quartile (Q25) and 75% quartile (Q75) is called the interquartile range (IQR). Subsequently, the whiskers are calculated by the formula $f_{lower} = Q25 - 1.5 * IQR$ for the lower whisker and respectively $f_{upper} = Q75 + 1.5 * IQR$ for the upper whisker. a glucose, b glutamine, c NAA, d the unknown component in the bucket comprising the area between 4.30 and 4.25 ppm and e succinic acid. The boxplot of WT samples is coloured grey whereas the boxplot of TG samples has a blue colour.

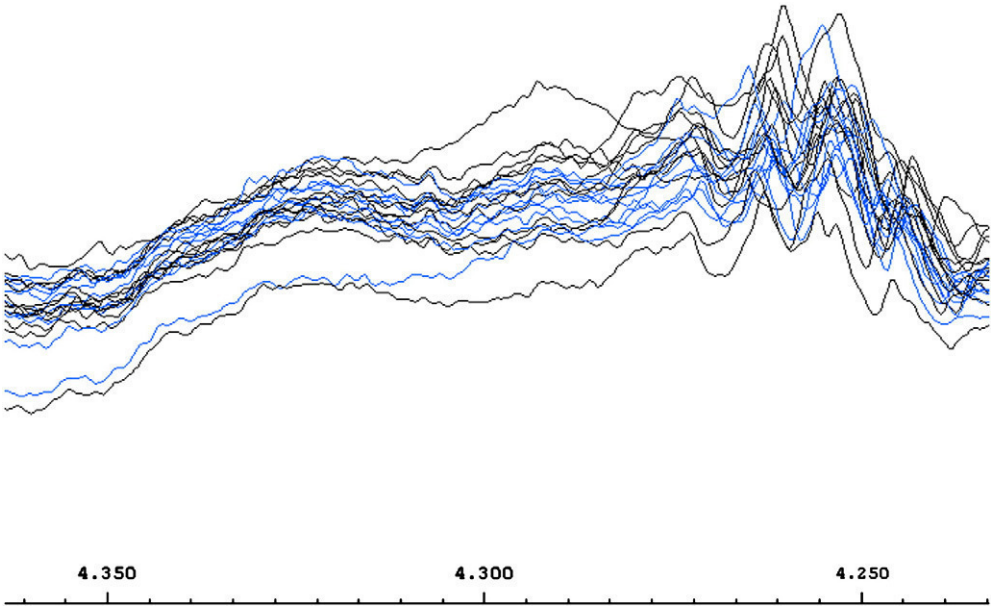

Fig. 5. Spectral region between 4.35 and 4.25 ppm. The univariate analysis indicates the bucket comprising the chemical shift region between 4.30 and 4.25 ppm as significantly different between WT and HD rats. The signals within this bucket are illustrated.

even prior to the onset of motor deficits [38]. A comparable study was already executed by Tsang and co-workers on a different animal model [27]. However, there are some inconsistencies between the figures and text described in their paper. The metabolites they indicated in the loading plot of the serum samples correspond to those mentioned for urine samples in the text and vice versa.

We used three different methods for the analysis. Visual inspection of the serum spectra already suggests that glucose as well as succinic acid levels are elevated in HD rats. These results are statistically confirmed by means of a univariate analysis. Moreover, the Student's *t*-test discloses that glutamine and NAA are able to discriminate between HD and WT rats in serum samples. PLS, a supervised multivariate statistical technique, was performed in order to reveal the discriminative power of different metabolites between the studied groups. For the serum samples, the loadings which are able to separate healthy from pathological samples correspond to the metabolites glucose, glutamine, lipids, lactate, succinic acid and NAA. Regarding CSF spectra, visual inspection and univariate analysis are not able to discriminate WT from HD rats. PLS, on the other hand, distinguishes both glucose and lactate as discriminating metabolites.

In CSF as well as in serum samples, glucose is indicated as a biomarker to detect Huntington disease presymptomatically. Although the literature [2,4,39] exposes some evidence of diabetes in subjects with HD, plasma glucose measurements in the same transgenic rat model at different ages do not reach the threshold for diabetes [28]. Thus, the observed difference in glucose must have been caused by a perturbation in another metabolic pathway. Some evidence of a disturbed glucose metabolism in HD can be found in the literature [4,40,41]. A possible explanation for the observed increased concentrations of glutamine and glucose is also documented: according to Sibson et al. [32], there is a 1:1 stoichiometry between the consumption of glucose and the formation of glutamate. The observed increase in glutamine can reflect a decreased glutaminase activity. Glutaminase is a mitochondrial enzyme found in neurons that takes care of the conversion of glutamine in glutamate. A perturbation of the glutamate–glutamine cycling may indicate an impairment of energy metabolism and mitochondrial respiration [27]. Thus, a decrease in glutaminase activity precludes the conversion of glutamine into glutamate. Owing to this, the neurons will have a lack of glutamate for neurotransmission. Finally, this will result in an elevated concentration of glutamine and glucose (due to decreased glucose utilization) as observed in our experiments [4]. This theory can be affirmed by previous studies which also point to a disruption of energy metabolism in HD [42,43].

In addition, the observed difference in lactate supports the theory of a deficiency of oxidative energy metabolism in rats transgenic for HD. The conversion of glucose to pyruvate during glycolysis involves the concomitant reduction of 2 mol of NAD^+ to NADH. In cells undergoing an aerobic respiration, pyruvate is subsequently oxidized to acetyl-Coenzyme A (Acetyl-CoA), which in turn, enters the citric acid cycle. In this way, the NADH produced during glycolysis is reoxidized through the mitochondrial electron transport chain. However, a perturbation in the Krebs cycle or mitochondrial electron transport chain might prevent pyruvate to enter the oxidative energy metabolism. Since NADH needs to be reoxidized to NAD^+ to maintain a steady state condition, an alternative pathway to transfer electrons is accomplished, i.e. the reduction of pyruvate to lactate by the catalyzed reaction of lactate dehydrogenase. As a result, an increased concentration of lactate, the end product of anaerobic glycolysis, indicates a defect in energy metabolism as well [44].

An elevated concentration of succinic acid is probably due to an inhibition of succinate dehydrogenase. This enzyme has two important functions in the mitochondria. First, it supports the oxidation of succinic acid to fumarate in the tricarboxylic acid (TCA) cycle. Second, it is linked to the respiratory chain, i.e. complex II of the mitochondrial electron transport chain [45,46]. A decrease in mitochondrial complex II activity has already been observed in HD [3,47,48]. Our finding of an elevated succinic acid concentration is therefore in line with these previous results.

A decreased NAA concentration is known to be a marker of neuronal dysfunction [27,49]. Reduced NAA levels have been well documented for several neurological diseases, e.g. Alzheimer disease [50], Huntington disease [4,27,51] and Parkinson disease [17,50]. Moreover, in HD it clearly correlates with the duration of symptoms and the CAG repeat length [16,52]. The enzyme responsible for the synthesis of NAA, L-*N*-acetylaspartyl transferase, is exclusively found in mitochondria [50]. Since inhibitors of the mitochondrial respiratory chain seem to decrease the concentration of NAA [4], reduced NAA levels may reflect an impaired mitochondrial energy production [27].

Obviously, a change in the concentration of each of these metabolites can be linked to a variety of conditions. However, the changes observed for all metabolites combined could allow for a more narrow correlation, i.e. with HD.

5. Conclusions

In conclusion, this study shows that metabolic alterations already emerge in the serum and CSF of these rats before overt symptoms of HD are manifested. In an early stage of the disease, metabolic alterations seem to be more pronounced in serum compared to CSF. All metabolites found being able at discriminating WT from HD rats point to a disruption of the mitochondrial respiratory chain and energy metabolism. These findings suggest that compounds which act on mitochondria might have a positive effect on HD pathology. Moreover, this study shows that ^{1}H NMR spectroscopy is an appropriate tool to investigate the metabolic disturbance occurring in early stages of HD. A more profound knowledge of the disease pathology can be obtained by performing a metabolomic analysis of samples originating from more mature rats. Such an analysis could give more insight into the development of this disease, which in turn may lead to improved therapeutic interventions.

Supplementary materials related to this article can be found online at doi:10.1016/j.bbadis.2011.08.001.

Conflict of interests statement

The authors declare that they have no competing interests.

Acknowledgements

KAV thanks the University of Antwerp (UA) and the FWO-Vlaanderen for funding. AVDL, JCM and RD thank the FWO-Vlaanderen for research funding (G.0064.07). The 700 MHz NMR spectrometer (Ghent, Belgium) of the interuniversity NMR facility was financed by Ghent University, the Free University of Brussels (VUB) and the UA via the 'Zware Apparatuur' FFEU Incentive of the Flemish Government. KL and TNV are supported by an SBO grant (IWT-600450) and a BOF interdisciplinary grant of the University of Antwerp. LC and HN are supported by the European Community 'RATstream STREP project'.

References

[1] The Huntington's Disease Collaborative Research Group, A novel gene containing a trinucleotide repeat that is expanded and unstable on Huntington's disease chromosomes, Cell 72 (1993) 971–983.
[2] O.A. Andreassen, A. Dedeoglu, R.J. Ferrante, B.G. Jenkins, K.L. Ferrante, M. Thomas, A. Friedlich, S.E. Browne, G. Schilling, D.R. Borchelt, S.M. Hersch, C.A. Ross, M.F. Beal, Creatine increases survival and delays motor symptoms in a transgenic animal model of Huntington's disease, Neurobiol. Dis. 8 (2001) 479–491.
[3] S.J. Tabrizi, M.W.J. Cleeter, J. Xuereb, J.-W. Taanman, J.M. Cooper, A.H.V. Schapira, Biochemical abnormalities and excitotoxicity in Huntington's disease brain, Ann. Neurol. 45 (1999) 25–32.
[4] B.G. Jenkins, P. Klivenyi, E. Kustermann, O.A. Andreassen, R.J. Ferrante, B.R. Rosen, M.F. Beal, Nonlinear decrease over time in N-acetyl aspartate levels in the absence of neuronal loss and increases in glutamine and glucose in transgenic Huntington's disease mice, J. Neurochem. 74 (2000) 2108–2119.
[5] J.K. Nicholson, J.C. Lindon, E. Holmes, 'Metabonomics': understanding the metabolic responses of living systems to pathophysiological stimuli via multivariate statistical analysis of biological NMR spectroscopic data, Xenobiotica 29 (1999) 1181–1189.
[6] J.G. Bundy, M.P. Davey, M.R. Viant, Environmental metabolomics: a critical review and future perspectives, Metabolomics 5 (2009) 3–21.
[7] J.C. Lindon, J.K. Nicholson, E. Holmes, The Handbook of Metabonomics and Metabolomics, Elsevier, Amsterdam, 2007.
[8] M.R. Viant, B.G. Lyeth, M.G. Miller, R.F. Berman, An NMR metabolomic investigation of early metabolic disturbances following traumatic brain injury in a mammalian model, NMR Biomed. 18 (2005) 507–516.
[9] O.A.C. Petroff, R.K. Yu, T. Ogino, High-resolution proton magnetic resonance analysis of human cerebrospinal fluid, J. Neurochem. 47 (1986) 1270–1276.
[10] P. Khandelwal, C.E. Beyer, Q. Lin, L.E. Schechter, A.C. Bach, Studying rat brain neurochemistry using nanoprobe NMR spectroscopy: a metabonomics approach, Anal. Chem. 76 (2004) 4123–4127.
[11] J.C. Lindon, J.K. Nicholson, J.R. Everett, NMR spectroscopy of biofluids, Annu. Rep. Spectrosc. 38 (1999) 1–88.
[12] A.D. Maher, D. Crockford, H. Toft, D. Malmodin, J.H. Faber, M.I. McCarthy, A. Barrett, M. Allen, M. Walker, E. Holmes, J.C. Lindon, J.K. Nicholson, Optimization of human plasma ^{1}H NMR spectroscopic data processing for high-throughput metabolic phenotyping studies and detection of insulin resistance related to type 2 diabetes, Anal. Chem. 80 (2008) 7354–7362.
[13] J.C. Lindon, E. Holmes, J.K. Nicholson, Pattern recognition methods and applications in biomedical magnetic resonance, Prog. Nucl. Magn. Reson. Spectrosc. 39 (2001) 1–40.
[14] R. Hewer, J. Vorster, F.E. Steffens, D. Meyer, Applying biofluid ^{1}H NMR-based metabonomic techniques to distinguish between HIV-1 positive/AIDS patients on antiretroviral treatment and HIV-1 negative individuals, J. Pharm. Biomed. Anal. 41 (2006) 1442–1446.
[15] M.A. Constantinou, A. Tsantili-Kakoulidou, I. Andreadou, E.K. Iliodromitis, D.T. Kremastinos, E. Mikros, Application of NMR-based metabonomics in the investigation of myocardial ischemia–reperfusion, ischemic preconditioning and antioxidant intervention in rabbits, Eur. J. Pharm. Sci. 30 (2007) 303–314.
[16] B.G. Jenkins, H.D. Rosas, Y.C.I. Chen, T. Makabe, R. Myers, M. MacDonald, B.R. Rosen, M.F. Beal, W.J. Koroshetz, ^{1}H NMR spectroscopy studies of Huntington's disease — correlations with CAG repeat numbers, Neurology 50 (1998) 1357–1365.
[17] H.M. Baik, B.Y. Choe, H.K. Lee, T.S. Suh, B.C. Son, J.M. Lee, Metabolic alterations in Parkinson's disease after thalamotomy, as revealed by ^{1}H MR spectroscopy, Korean J. Radiol. 3 (2002) 180–188.
[18] A.R. Tate, S.J.P. Damment, J.C. Lindon, Investigation of the metabolite variation in control rat urine using ^{1}H NMR spectroscopy, Anal. Biochem. 291 (2001) 17–26.
[19] A. Bender, D.P. Auer, T. Merl, R. Reilmann, P. Saemann, A. Yassouridis, J. Bender, A. Weindl, M. Dose, T. Gasser, T. Klopstock, Creatine supplementation lowers brain glutamate levels in Huntington's disease, J. Neurol. 252 (2005) 36–41.
[20] S. Kasparová, Z. Sumbalová, P. Bystrický, J. Kucharská, T. Liptaj, V. Mlynárik, A. Gvozdjáková, Effect of coenzyme Q10 and vitamin E on brain energy metabolism in the animal model of Huntington's disease, Neurochem. Int. 48 (2006) 93–99.
[21] P. Verbessem, J. Lemiere, B.O. Eijnde, S. Swinnen, L. Vanhees, M. Van Leemputte, P. Hespel, R. Dom, Creatine supplementation in Huntington's disease — a placebo-controlled pilot trial, Neurology 61 (2003) 925–930.
[22] I. Tkác, C.D. Keene, J. Pfeuffer, W.C. Low, R. Gruetter, Metabolic changes in quinolinic acid-lesioned rat striatum detected non-invasively by in vivo ^{1}H NMR spectroscopy, J. Neurosci. Res. 66 (2001) 891–898.
[23] E. Holmes, H. Antti, Chemometric contributions to the evolution of metabonomics: mathematical solutions to characterising and interpreting complex biological NMR spectra, Analyst 127 (2002) 1549–1557.
[24] T.M. Alam, M.K. Alam, Chemometric analysis of NMR spectroscopy data: a review, Annu. Rep. Spectrosc. 54 (2005) 41–80.
[25] E.M. Lenz, J. Bright, I.D. Wilson, A. Hughes, J. Morrisson, H. Lindberg, A. Lockton, Metabonomics, dietary influences and cultural differences: a ^{1}H NMR-based study of urine samples obtained from healthy British and Swedish subjects, J. Pharm. Biomed. Anal. 36 (2004) 841–849.
[26] W. El-deredy, Pattern recognition approaches in biomedical and clinical magnetic resonance spectroscopy: a review, NMR Biomed. 10 (1997) 99–124.
[27] T.M. Tsang, B. Woodman, G.A. Mcloughlin, J.L. Griffin, S.J. Tabrizi, G.P. Bates, E. Holmes, Metabolic characterization of the R6/2 transgenic mouse model of Huntington's disease by high-resolution MAS ^{1}H NMR spectroscopy, J. Proteome Res. 5 (2006) 483–492.
[28] S. von Hörsten, I. Schmitt, H.P. Nguyen, C. Holzmann, T. Schmidt, T. Walther, M. Bader, R. Pabst, P. Kobbe, J. Krotova, D. Stiller, A. Kask, A. Vaarmann, S. Rathke-Hartlieb, J.B. Schulz, U. Grasshoff, I. Bauer, A.M.M. Vieira-Saecker, M. Paul, L. Jones, K.S. Lindenberg, B. Landwehrmeyer, A. Bauer, X.J. Li, O. Riess, Transgenic rat model of Huntington's disease, Hum. Mol. Genet. 12 (2003) 617–624.
[29] I.F. Duarte, B.J. Goodfellow, A. Barros, J.G. Jones, C. Barosa, L. Diogo, P. Garcia, A.M. Gil, Metabolic characterisation of plasma in juveniles with glycogen storage disease type 1a (GSD1a) by high-resolution ^{1}H NMR spectroscopy, NMR Biomed. 20 (2007) 401–412.
[30] E. Brouillet, P. Hantraye, R.J. Ferrante, R. Dolan, A. Leroy-Willig, N.W. Kowall, M.F. Beal, Chronic mitochondrial energy impairment produces selective striatal degeneration and abnormal choreiform movements in primates, Proc. Natl. Acad. Sci. U.S.A. 92 (1995) 7105–7109.
[31] I. Tkác, J.M. Dubinsky, C.D. Keene, R. Gruetter, W.C. Low, Neurochemical changes in Huntington R6/2 mouse striatum detected by *in vivo* ^{1}H NMR spectroscopy, J. Neurochem. 100 (2009) 1397–1406.
[32] N.R. Sibson, A. Dhankhar, G.F. Mason, D.L. Rothman, K.L. Behar, R.G. Shulman, Stoichiometric coupling of brain glucose metabolism and glutamatergic neuronal activity, Proc. Natl. Acad. Sci. U.S.A. 95 (1998) 316–321.
[33] P. Conforti, C. Ramos, B.L. Apostol, D.A. Simmons, H.P. Nguyen, O. Riess, L.M. Thompson, C. Zuccato, E. Cattaneo, Blood level of brain-derived neurotrophic factor mRNA is progressively reduced in rodent models of Huntington's disease: restoration by the neuroprotective compound CEP-1347, Mol. Cell. Neurosci. 39 (2008) 1–7.
[34] P. Khandelwal, C.E. Beyer, Q. Lin, P. McGonigle, L.E. Schechter, A.C. Bach, Nanoprobe NMR spectroscopy and in vivo microdialysis: new analytical methods to study brain neurochemistry, J. Neurosci. Methods 133 (2004) 181–189.
[35] L. Eriksson, E. Johansson, H. Antti, E. Holmes, Multi-and megavariate data analysis: finding and using regularities in metabonomics data, in: D.G. Robertson, J. Lindon (Eds.), Metabolomics in Toxicity Assessment, Taylor & Francis Group, Boca Raton, 2005, pp. 263–335.
[36] J.A. Westerhuis, H.C.J. Hoefsloot, S. Smit, D.J. Vis, A.K. Smilde, E.J.J. van Velzen, J.P.M. van Duijnhoven, F.A. van Dorsten, Assessment of PLSDA cross validation, Metabolomics 4 (2008) 81–89.
[37] N. Cristianini, J. Shawe-Taylor, An Introduction to Support Vector Machines and Other Kernel-Based Learning Methods, Cambridge University Press, Cambridge, 2000.

[38] H.P. Nguyen, P. Kobbe, H. Rahne, T. Wörpel, B. Jäger, M. Stephan, R. Pabst, C. Holzmann, O. Riess, H. Korr, O. Kántor, E. Petrasch-Parwez, R. Wetzel, A. Osmand, S. von Hörsten, Behavioral abnormalities precede neuropathological markers in rats transgenic for Huntington's disease, Hum. Mol. Genet. 15 (2006) 3177–3194.
[39] M.S. Hurlbert, W. Zhou, C. Wasmeier, F.G. Kaddis, J.C. Hutton, C.R. Freed, Mice transgenic for an expanded CAG repeat in the Huntington's disease gene develop diabetes, Diabetes 48 (1999) 649–651.
[40] S.E. Browne, M.F. Beal, The energetics of Huntington's disease, Neurochem. Res. 29 (2004) 531–546.
[41] A. Ciarmiello, M. Cannella, S. Lastoria, M. Simonelli, L. Frati, D.C. Rubinsztein, F. Squitieri, Brain white-matter volume loss and glucose hypometabolism precede the clinical symptoms of Huntington's disease, J. Nucl. Med. 47 (2006) 215–222.
[42] B.G. Jenkins, W.J. Koroshetz, M.F. Beal, B.R. Rosen, Evidence for impairment of energy metabolism in vivo in Huntington's disease using localized ^{1}H NMR spectroscopy, Neurology 43 (1993) 2689–2695.
[43] M. Gu, M.T. Gash, V.M. Mann, F. Javoy-Agid, J.M. Cooper, A.H.V. Schapira, Mitochondrial defect in Huntington's disease caudate nucleus, Ann. Neurol. 39 (1996) 385–389.
[44] C.K. Mathews, K.E. van Holde, K.G. Ahern, Carbohydrate Metabolism I: Anaerobic Processes in Generating Metabolic Energy, Biochemistry, Addison Wesley Longman, San Francisco, 2000, pp. 446–482.
[45] B.R. Underwood, D. Broadhurst, W.B. Dunn, D.I. Ellis, A.W. Michell, C. Vacher, D.E. Mosedale, D.B. Kell, R.A. Barker, D.J. Grainger, D.C. Rubinsztein, Huntington disease patients and transgenic mice have similar pro-catabolic serum metabolite profiles, Brain 129 (2006) 877–886.
[46] C. Dautry, F. Condé, E. Brouillet, V. Mittoux, M.F. Beal, G. Bloch, P. Hantraye, Serial 1H-NMR spectroscopy study of metabolic impairment in primates chronically treated with succinate dehydrogenase inhibitor 3-nitropropionic acid, Neurobiol. Dis. 6 (2006) 259–268.
[47] S.E. Browne, A.C. Bowling, U. MacGarvey, M.J. Baik, S.C. Berger, M.M.K. Muqit, E.D. Bird, M.F. Beal, Oxidative damage and metabolic dysfunction in Huntington's disease: selective vulnerability of the basal ganglia, Ann. Neurol. 41 (1997) 646–653.
[48] M. Gu, M.T. Gash, V.M. Mann, F. Javoy-Agid, J.M. Cooper, A.H.V. Schapira, Mitochondrial defect in Huntington's disease caudate nucleus, Ann. Neurol. 39 (1996) 385–389.
[49] C. Demougeot, C. Marie, M. Giroud, A. Beley, N-acetylaspartate: a literature review of animal research on brain ischaemia, J. Neurochem. 90 (2004) 776–783.
[50] J.K. Choi, A. Dedeoglu, B.G. Jenkins, Application of MRS to mouse models of neurodegenerative illness, NMR Biomed. 20 (2007) 216–237.
[51] A. van Dellen, J. Welch, R.M. Dixon, P. Cordery, D. York, P. Styles, C. Blakemore, A.J. Hannan, N-acetylaspartate and DARPP-32 levels decrease in the corpus striatum of Huntington's disease mice, Neuroreport 11 (2000) 3751–3757.
[52] J.C.H. van Oostrom, P.E. Sijens, R.A.C. Roos, K.L. Leenders, ^{1}H magnetic resonance spectroscopy in preclinical Huntington disease, Brain Res. 1168 (2007) 67–71.

Neurobiology of Disease

A Novel BACHD Transgenic Rat Exhibits Characteristic Neuropathological Features of Huntington Disease

Libo Yu-Taeger,[1] Elisabeth Petrasch-Parwez,[2] Alexander P. Osmand,[3] Adriana Redensek,[1] Silke Metzger,[1] Laura E. Clemens,[1] Larry Park,[4] David Howland,[5] Carsten Calaminus,[6] Xiaofeng Gu,[7] Bernd Pichler,[6] X. William Yang,[7] Olaf Riess,[1] and Huu Phuc Nguyen[1]

[1]Department of Medical Genetics, University of Tuebingen, 72076 Tuebingen, Germany, [2]Department of Neuroanatomy and Molecular Brain Research, Ruhr-University Bochum, 44801 Bochum, Germany, [3]Department of Medicine, University of Tennessee Graduate School of Medicine, Knoxville, Tennessee 37920, [4]CHDI Management/CHDI Foundation, Los Angeles, California 90045, [5]CHDI Management/CHDI Foundation, Princeton, New Jersey 08540, [6]Laboratory for Preclinical Imaging and Imaging Technology of the Werner Siemens-Foundation, University of Tuebingen, 72076 Tuebingen, Germany, and [7]Department of Psychiatry and Biobehavioral Sciences, David Geffen School of Medicine, University of California at Los Angeles, Los Angeles, California 90095

Huntington disease (HD) is an inherited progressive neurodegenerative disorder, characterized by motor, cognitive, and psychiatric deficits as well as neurodegeneration and brain atrophy beginning in the striatum and the cortex and extending to other subcortical brain regions. The genetic cause is an expansion of the CAG repeat stretch in the *HTT* gene encoding huntingtin protein (htt). Here, we generated an HD transgenic rat model using a human bacterial artificial chromosome (BAC), which contains the full-length *HTT* genomic sequence with 97 CAG/CAA repeats and all regulatory elements. BACHD transgenic rats display a robust, early onset and progressive HD-like phenotype including motor deficits and anxiety-related symptoms. In contrast to BAC and yeast artificial chromosome HD mouse models that express full-length mutant huntingtin, BACHD rats do not exhibit an increased body weight. Neuropathologically, the distribution of neuropil aggregates and nuclear accumulation of N-terminal mutant huntingtin in BACHD rats is similar to the observations in human HD brains. Aggregates occur more frequently in the cortex than in the striatum and neuropil aggregates appear earlier than mutant htt accumulation in the nucleus. Furthermore, we found an imbalance in the striatal striosome and matrix compartments in early stages of the disease. In addition, reduced dopamine receptor binding was detectable by *in vivo* imaging. Our data demonstrate that this transgenic BACHD rat line may be a valuable model for further understanding the disease mechanisms and for preclinical pharmacological studies.

Introduction

Huntington disease (HD) is an autosomal dominant, progressive neurodegenerative disorder commonly manifesting in adulthood (Harper, 1991). Clinical features include motor deficits, cognitive decline, and psychological disturbances (Vonsattel and DiFiglia, 1998). The hallmark of HD neuropathology is initial striatal atrophy, which expands at later stages to the cerebral cortex and other subcortical brain regions (Bruyn, 1979; Vonsattel et al., 1985). Interestingly, neuropil and nuclear huntingtin (htt) aggregates are abundant in the cortex, but are only sparsely observed in the striatum of HD-affected brains (Gutekunst et al., 1999; Kuemmerle et al., 1999).

Expansions of the CAG repeat (>38) in exon 1 of the gene encoding htt were first discovered in 1993 and represent to date the sole genetic cause for the disease (The Huntington's Disease Collaborative Research Group, 1993). A number of mouse models expressing full-length htt or truncated htt fragments were developed for therapeutic studies and to better understand the pathogenesis of disease (Menalled and Chesselet, 2002; Ehrnhoefer et al., 2009; Crook and Housman, 2011; Munoz-Sanjuan and Bates, 2011). However, mouse models are in general limited for studying certain functional and behavioral measurements (Tecott and Nestler, 2004; Rodriguiz and Wetsel, 2006; Herrmann et al., 2012). The limitations of mouse models as well as pharmacogenomic differences between the species (Toutain et al., 2010) necessitate either the laborious development of test designs appropriate for mouse models or the use of additional species to generate HD models in which these test designs are readily available.

Rat models have made substantial contributions to our understanding of biological function and behavior. Numerous rat disease models have successfully proven their utility for modeling

Received March 8, 2012; revised Sept. 1, 2012; accepted Sept. 5, 2012.

Author contributions: L.Y.-T., E.P.-P., L.P., D.H., B.P., X.W.Y., O.R., and H.P.N. designed research; L.Y.-T., E.P.-P., A.R., S.M., L.E.C., C.C., X.G., and H.P.N. performed research; A.P.O. contributed unpublished reagents/analytic tools; L.Y.-T., E.P.-P., and H.P.N. analyzed data; L.Y.-T., E.P.-P., L.E.C., C.C., and H.P.N. wrote the paper.

This work was supported by the CHDI Foundation and this rat model is available to the HD community for HD research. We are grateful to Professor Gillian P. Bates for providing us the sheep polyclonal antibody S830. We thank Esteban Portal for the technical support in data analysis for the PhenoMaster experiments and Joachim Täger for the helpful discussions. The skillful technical assistance of Marlen Löbbecke-Schumacher and Hans-Werner Habbes is also gratefully acknowledged.

Correspondence should be addressed to Dr. Huu Phuc Nguyen, Department of Medical Genetics, University of Tuebingen, Calwerstrasse 7, 72076 Tuebingen, Germany. E-mail: hoa.nguyen@med.uni-tuebingen.de.

DOI:10.1523/JNEUROSCI.1148-12.2012

 0270-6474/12/3215426-13$15.00/0

the human condition (Hammer et al., 1990; von Hörsten et al., 2003; Yamada et al., 2004; Liu et al., 2008). Although learning and memory can be studied with some restrictions in mice, the current scientific knowledge concerning the complexity of learning and memory, as well as the multiplicity of brain systems supporting it, has come largely from behavioral research using rats (Report of the NIH Rat Model Priority Meeting, 1999, http://www.nhlbi.nih.gov/resources/docs/ratmtg.pdf). Compared to mice, rats show excellent learning abilities, a mandatory requirement for the identification of the subtle cognitive deficits that may be present in the early stages of HD. Another practical advantage of rats is their larger brain size, which facilitates direct invasive procedures. In addition, miniaturized physiological *in vivo* approaches, such as structural and functional imaging of small brain structures, are more difficult in mouse models due to size limitation.

We have previously generated an HD transgenic rat line (tgHD rats), which expresses a fragment of mutant htt (von Hörsten et al., 2003). This rat model demonstrated many aspects of HD, but lacking the full-length mutant htt (fl-mhtt) protein certain aspects of the human disease would be imperfectly replicated.

In this study, we generated and characterized a new bacterial artificial chromosome (BAC) HD transgenic rat model expressing fl-mhtt under the control of the human *HTT* promoter and all its regulatory elements to determine its similarity to the human condition across the molecular, behavioral, and anatomical domains.

Materials and Methods

Animals

Generation of transgenic rats. BACs, containing human genomic DNA spanning the full-length *HTT* gene with 97 CAG/CAA repeats and including all regulatory elements (Gray et al., 2008), were microinjected into oocytes of Sprague Dawley rats. Genotyping and determination of BAC transgene integrity were performed via PCR analysis using genomic DNA extracted from ear biopsy tissue (High Pure PCR Template Preparation Kit; Roche). Two primer pairs were designed, one pair binding to exon 1 (FW: 5′-ATGGCGACCCTGGAAAAGC-3′; RV: 5′-AGGTCGGTGCAGAGGCTCCTCTG-3′) of both endogenous *Htt* and exogenous mutant *HTT* with different amplicon lengths, while the second primer pair binds specifically to the last exon of the *HTT* transgene (FW: 5′-TGTGATTAATTTGGTTGTCAAGTTTT-3′;RV:5′-AGCTGGAAACATCACCTACATAGACT-3′).

To estimate relative transgene copy number of the BAC insertion and number of integration sites, probe-based real-time PCR (TaqMan PCR) was performed using genomic DNA. Briefly, primers and probe were designed to bind specifically to intron 29 of the *HTT* transgene (FW: 5′-ACCGACCTTCTGAAGCCTACTTCT-3′;RV:5′-TTCTCCTCCAAAGGATCACAACTC-3′; probe: 5′FAM-CTAAGTGGCGCTGCGTAGTGCGAA-3′Bhq). The Ct values of all samples were normalized to β-actin serving as reference gene (FW: 5′-AGCCATGTACGTAGCCATCCA-3′; RV: 5′-TCTCCGGAGTCCATCACAATG-3′; probe: 5′CY-TGTCCCTGTATGCCTCTGGTCGTACCAC-3′Bhq). The relative copy number of all F1 rats was compared within and between each line.

RNA analysis. Expression levels of mRNA from each line were analyzed via real-time PCR using QuantiTect SYBR Green PCR Kits (Qiagen). Total mRNA was extracted from whole brain using the RNeasy Lipid Tissue Midi Kit (Qiagen) and cDNA was synthesized using a QuantiTect Reverse Transcription Kit (Qiagen) following the manufacturer's instructions. The relative mRNA expression levels were compared with endogenous wild-type (WT) htt. The primers were designed for transgenic *HTT* (FW: 5′-GTGGAGGTTTGCTGAGCTG-3′; RV: 5′-GCAAAATTGCCAAAAGAAGC-3′) and rat *Htt* (FW: 5′-ATCTTGAGCCACAGCTCCAGCCA-3′; RV: 5′-TCTGAAAACGTCTGAGACTTCACCAGA-3′) spanning at least one exon–exon junction.

Measurement of the CAG-CAA repeat length in BACHD rats

To verify the conservation of the polyQ repeat length, we analyzed the PCR fragment length of DNA samples extracted from 100 peripheral tissues and different brain regions. DNA extractions were performed as described before and rat samples were collected considering different rat generations, gender, and ages of the rats. PCRs were performed using a Cy5labeled forward primer and a reverse primer amplifying a fragment of *HTT* exon 1 including the CAG-CAA repeats (forward primer: 5′-GAT GAA GGC CTT CGA GTC CCT CAA GTC CTT CT-3′, reverse primer: 5′-CGG CTG AGG CAG CAG CGG CTG T-3′). The fragment lengths of the amplicons were determined and analyzed using the fluorescence-based capillary electrophoresis Sequencer CEQ8800 and genetic analysis system software in a complete set from Beckman Coulter. CAG-CAA repeat numbers were calculated according to the individual fragment length and the human *HTT* sequence published on the NCBI database.

Identification of alternative HTT splicing variants in BACHD transgenic rats

Splicing variants may possess a considerable effect on protein function with two or more splicing products fulfilling distinct functions in the expressing cells. Therefore, BACHD transgenic rats carrying the genomic sequence with upstream and downstream flanking regions instead of cDNA sequence were generated. Two protein-encoding splicing variants of the human mRNA have been identified and listed in the Ensemble Genome Browser (http://www.ensembl.org/Homo_sapiens/Gene/Summary?g=ENSG00000197386;r=4:3076408-3245676) so far (HTT-001, transcript ID: ENST00000355072 and HTT-011, transcript ID: ENST00000509618). The longer one (HTT-001) includes all 67 exons encoding for the full-length huntingtin; the smaller one (HTT-011) consists only of 3 exons, the last 31 bases of exon 29, exon 30, and 31 as well as the 96 bases of the following intron 31–32. A forward primer was designed to bind to both transcripts in exon 31 of HTT-001 and reverse primers were chosen to bind specifically to each variant. For HTT-001, the reverse primer binds to exon 32 whereas for HTT-011, the primer was directed against a region within the last 96 nucleotides. Brain samples from the striatum, the cortex, and the cerebellum were taken and after purification of the mRNA subjected to real-time PCR using the QuantiTect SYBR Green PCR Kit (Qiagen).

Western blotting. Expression levels of transgenic mhtt in different lines and different brain regions were quantified using Western blot and ImageJ (National Institutes of Health, NIH) analysis. One-month-old rat brains were homogenized with a homogenizer at a speed of 30,000 rpm in modified radioimmunoprecipitation assay buffer (Gray et al., 2008). The lysates were centrifuged at 4°C for 15 min at 16,200 $\times$ *g*, and the supernatant was removed and stored at −80°C for Western blot analysis. Western blot analysis was performed as described previously (Gray et al., 2008). The blots were probed with two monoclonal antibodies: MAB2166 (1:2000; Millipore) recognizing the N-terminal region of both human and rat htt, and 1C2 (1:2000; Millipore) binding to the expanded polyQ sequence of human htt but not to the nonexpanded polyQ sequence of the endogenous rat htt.

Behavioral assessment

Rats were group-housed with mixed genotypes in a constant temperature-humidity room (22 ± 1°C, 55 ± 10% relative humidity) with a 12 h light/dark cycle (lights on/off at 2:00 A.M./P.M.). Food and water were provided *ad libitum*. All behavioral tests were performed only with male rats during the dark phase, which is the physiological activity period of the rats. Controls were an equal mix of WT littermates from both lines and the experimenters were blind to the individual animals' genotype. All animal procedures were approved by the state government of Baden–Württemberg, Germany, and are in accordance with animal protection guidelines.

Rotarod test. Rotarod experiments (Accelerated rotarod for rats 7750, Ugo Basile) were used to measure forelimb and hindlimb motor coordination. BACHD transgenic rats and WT littermates were trained on 3 consecutive days with four trials per day. Directly after training they were tested on 2 consecutive days with two trials per day and an interval of 1 h between individual trials. During the training period, the rats were placed on the rotating rod at a constant speed of 12 rpm for 2 min. Rats were

returned to the rod after falling during the training period up to 10 falls per trial. Individual tests were assessed for a maximum of 5 min with accelerating speed from 4 to 40 rpm over a period of 4 min, and the latencies to fall were recorded. Rats from the same cohort ($n = 12$) were tested every month from 1 to 15 months of age. Three rats were excluded from the analysis because already at younger ages they fell off the rotarod immediately when placed on it, despite extensive training.

Footprint test. We used a footprint test to analyze gait abnormalities in BACHD rats. BACHD transgenics and WT littermates were evaluated in this task at 14 months of age ($n = 11$). The front and hindpaws of the animals were painted with nontoxic paint of different colors. On the day before testing, the rats were trained in three sessions. The best performance out of three tests with each rat was selected for data analysis. The stride width of the hindpaw, the step length (left paw to left paw), and the overlap (distance between front and hindpaw) were measured in three consecutive steps, and the average was taken for further analysis.

Elevated plus maze. An elevated plus maze was used to assess the anxiety of BACHD rats. To eliminate the possibility of habituation effects, different cohorts of rats were tested at 1 ($n = 13$ per genotype), 4 ($n = 13$ per genotype), and 12 (TG5:WT = 8:11) months of age as described previously (Nguyen et al., 2006). Rats were placed at the center of an elevated plus maze (with two open and two closed arms) facing an open arm and were monitored for 5 min. The time spent in the open arms was recorded as a percentage of the total time for analysis.

Locomotor activity and food intake. Rats were monitored using the PhenoMaster system (TSE Systems), which represents a modular setup that screens rats in a home cage-like environment for their ambulatory activity and rearing as well as feeding and drinking behavior. The activity detection is achieved using infrared sensor pairs arranged in horizontal (*x,y* level for ambulatory activity) and vertical (*z* level for rearing) strips. Food and water consumption were recorded by two weighting sensors. The same cohort of animals (TG5:TG9:WT = 16:19:18) was individually screened for 22 h every 3 months until the age of 18 months. Data were automatically collected with 1 min intervals and analyzed either entirely or only for the dark (active) phase. Rats, which did not drink >3 ml of water within 24 h were excluded from the data analysis since this might have confounded feeding behavior and activity.

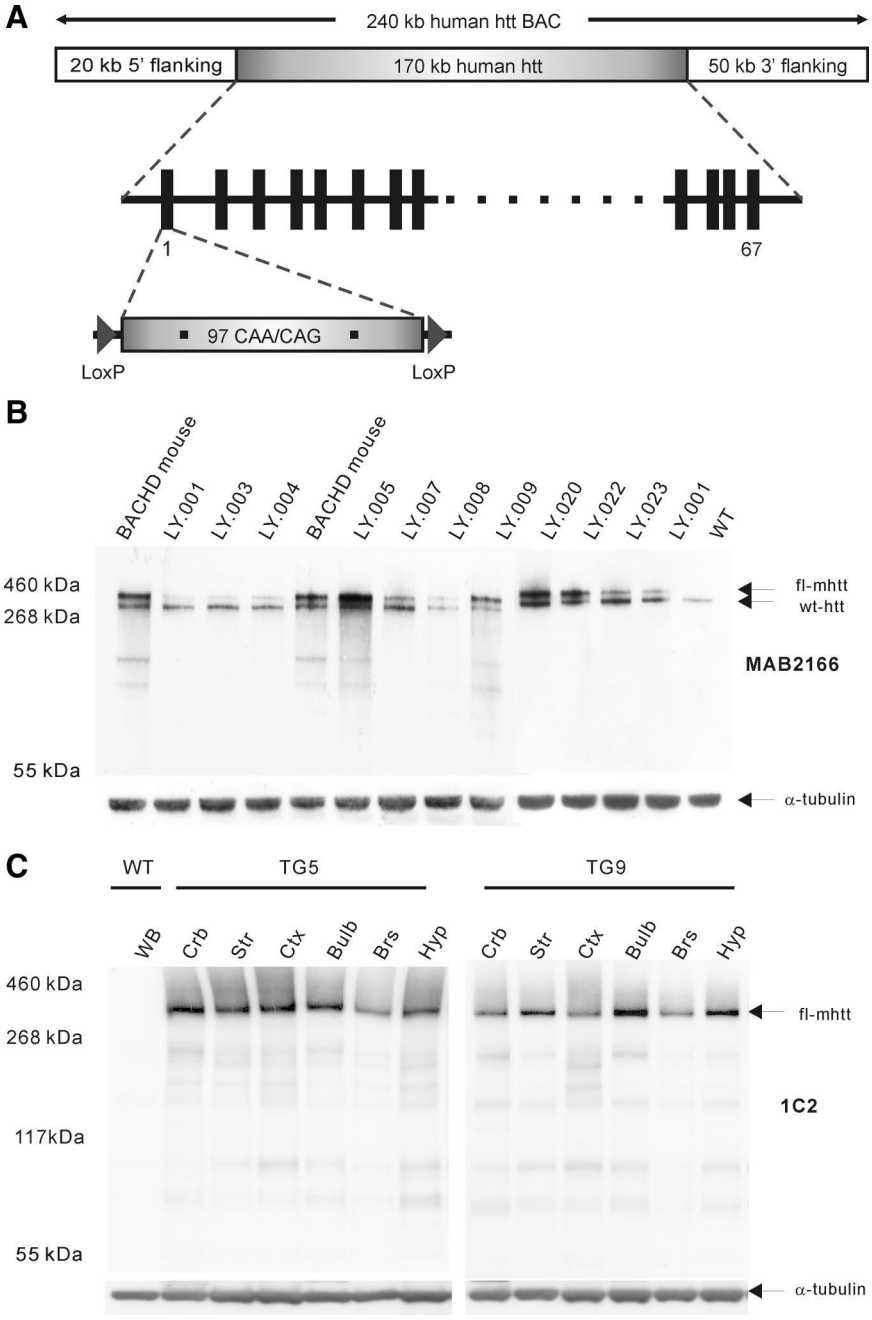

Figure 1. Generation of BACHD transgenic rats. ***A***, BACHD construct was designed using a BAC containing the entire 170 kb of the *HTT* genomic locus with ~20 kb upstream and 50 kb downstream flanking sequences. The mutant *HTT* exon 1 including 97 CAA-CAG trinucleotide repeats in place of endogenous *HTT* exon 1 is flanked by two loxP sites. ***B***, Western blot analysis of mhtt expression in different transgenic rat lines and compared with BACHD mouse expression. Both mhtt and endogenous WT rat htt are recognized by MAB2166 showing bands of ~360 and ~330 kDa, respectively (arrows). Line 5 presents the highest mhtt expression and line 9 shows a comparable mhtt expression level to the BACHD mouse. ***C***, Western blot analysis of mhtt expression in various brain regions in transgenic line 5 (TG5) and transgenic line 9 (TG9) using antibody 1C2. In TG5 rats mhtt is abundantly present in cerebellum (Crb), striatum (Str), and cortex (Ctx), whereas olfactory bulb (Bulb), brainstem (Brs), and hypothalamus (Hyp) show a relatively reduced expression of mhtt. In TG9 rats higher expression levels were found in striatum, olfactory bulb, and hypothalamus compared with cerebellum, cortex, and brainstem. WB, Whole brain.

Light and electron immunohistochemistry

Rats were deeply anesthetized with ketamine/xylazine (100/10 mg/kg, i.p.) and transcardially perfused with 4% paraformaldehyde in 0.1 M sodium cacodylate buffer, pH 7.4, followed by postfixation of the brains in the same fixative overnight. For lightmicroscopical immunohistochemistry 16 rat brains were embedded in one gelatin block; 40 μm coronal sections were freeze-cut and collected into 24 series (NeuroScience Associates). Free-floating staining was performed as previously described (Osmand et al., 2006). Sections were incubated with the polyclonal S830 antibody (1:15,000; ~10 ng/ml, kindly provided by G. Bates), EM48 (1:300, MAB5374; Millipore Bioscience Research Reagents) or the polyclonal anti-calbindin D-28K antibody (1:50,000; Swant Swiss antibodies) followed by the respective secondary antibodies: biotinylated rabbit anti-sheep IgG antibody (1:1000, BA-6000; Vector Laboratories), biotinylated goat anti-mouse IgG antibody (1:1000, BA-9200; Vector Laboratories), or biotinylated goat anti-rabbit IgG antibody

(1:1000, BA-1000; Vector Laboratories). Then sections were treated with an avidin–biotin–peroxidase complex (Vector Laboratories), and exposed to nickel-DAB-H_2O_2 (0.6% nickel sulfate, 0.01% DAB, and 0.001% hydrogen peroxide) until a suitable staining intensity had developed. S830 staining was routinely amplified using a single round of biotinylated tyramine amplification before the final ABC step. Images were taken using an Axioplan 2 Microscope (Zeiss) with a digital camera (AxioCam MRm; Zeiss) and imaging acquisition software (AxioVision-6; Zeiss). Quantification was performed using ImageJ (NIH).

For electron microscopy BACHD and control rat brains (13 and 16.5 months of age) were adjusted in Plexiglas frames according to the coordinates of a rat brain atlas (Paxinos and Franklin, 2006), embedded in 2% agarose, and cut into 3 mm coronal brain blocks. Blocks were cut into series of 50 μm vibratome sections and immunostained with the monoclonal EM48 antibody (1:100, MAB5374; Millipore Bioscience Research Reagents) the specificity of which was controlled in WT rats. Immunostained sections were photodocumented for later detection of the reaction product and flat embedded in Araldite (Serva) as described previously (Petrasch-Parwez et al., 2007). Ultrathin sections (90 nm) were contrasted with 5% aqueous uranyl acetate and lead citrate (pH 12).

Quantitative assessment of morphological changes in the striosome compartment

Calbindin immunostaining of rats at 6 months of age was used (TG5:TG9:WT = 5:4:5) to perform a relative quantification of the striatal striosome compartment. Four striata of each rat were measured in coronal 40-μm-thick brain sections between bregma 1.44 and −0.24 mm (Paxinos and Franklin, 2006). The striatum was outlined medially adjacent to the lateral ventricle, dorsolaterally below the corpus callosum, and ventrally by a line through the ventral tip of the ventricle as the region of interest (ROI) using ImageJ (NIH). The striosomal area was determined within the ROI by outlining the faintly stained calbindin areas. The ratter was blind to the rat's genotype.

[^{11}C]raclopride positron emission tomographic imaging

For longitudinal positron emission tomography (PET) experiments, transgenic BACHD and control rats were imaged at 6, 12, and 18 months of age (n = 6 of each genotype at each time point) using an Inveon dedicated small-animal PET scanner (Siemens Preclinical Solutions), yielding a spatial resolution of ~1.3 mm in the reconstructed image. Conscious animals were lightly restrained and injected with 29.6 MBq [^{11}C]raclopride via one of the lateral tail veins. A 60 min dynamic PET scan was obtained immediately after tracer injection followed by a 15 min attenuation correction. During imaging, the animals were anesthetized with a mixture of 1.5% isoflurane in 100% oxygen. The animals were centered in the field of view of the PET scanner. Anesthesia was monitored by measuring respiratory frequency, and the body temperature was kept at 37°C by a heating pad underneath the animal. PET data were acquired in list mode; graphed in time frames of 4 × 60 s, 3 × 120 s, 7 × 300 s and 2 × 450 s; and reconstructed using a filtered backprojection algorithm with a matrix size of 256 × 256 and a zoom factor of two. Image files were analyzed using PMOD and AsiPro software (Siemens Preclinical Solutions). The PMOD image fusion software allowed for linear transformation and rotation to overlay the PET and magnetic resonance (MR) template images. The fusioned PET/MR images were analyzed to calculate specific ROIs in different brain areas with reference to the stereotactic brain atlas of Paxinos and Franklin (2006). With the PMOD software we also analyzed the [^{11}C]raclopride uptake in two brain areas including cerebellum and striatum. The cerebellum was chosen as a reference region, to correlate the unspecific uptake with the tracer uptake in the striatum.

Statistical analysis

Standard two-way ANOVA (data not matched) and repeated-measures two-way ANOVA (repeated or matched data) were conducted to assess the effects of genotype and age and genotype × age interaction. Bonferroni *post hoc* tests were conducted to compare individual genotype effects at individual ages. For the analysis of the rotarod test results, only data until 10 months were taken into account because most TG5 rats fell immediately from the rotarod during the final 5 months (from age 11 to 15 months) leading to a non-normal distribution of the data in the final 5 months. For data where only one time point was assessed (such as the footprint test and matrix/striosome analysis), one-way ANOVA was conducted to evaluate the effects of genotype, followed by Tukey's *post hoc* test for multiple comparisons. Data are presented as mean ± SEM. Differences were considered significant if $p < 0.05$.

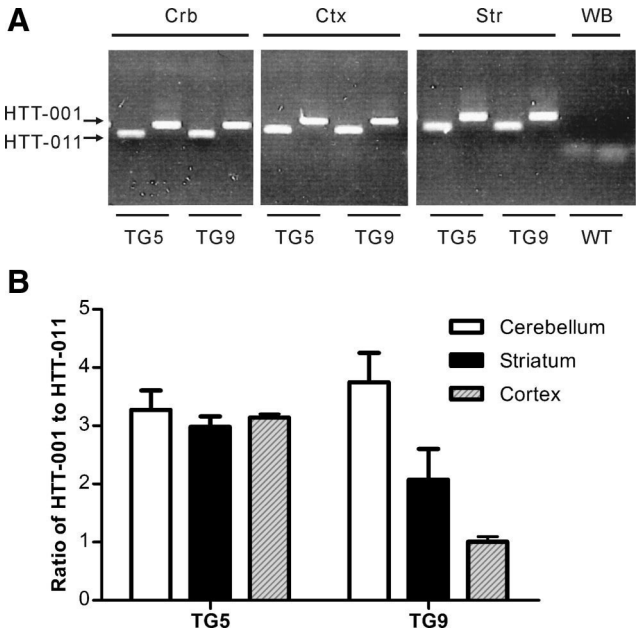

Figure 2. Alternative splicing variants in BACHD transgenic rats. Real-time PCR was performed using one common forward primer binding to both variants of HTT-001 and HTT-011; the reverse primers were chosen specifically to bind to each variant. ***A***, Image of gel electrophoresis. The BACHD rats TG5 and TG9 exhibit both transcription variants HTT-001 and HTT-011 in cerebellum (Crb), cortex (Ctx), and striatum (Str). Whole-brain (WB) mRNA of a WT rat was taken as negative control. ***B***, Quantification of the proportion of HTT-001/HTT-011 in different brain regions of both transgenic lines. The ratios of HTT-001 and HTT-011 vary between 2.49 and 4.40 in all brain regions investigated in both TG5 and TG9, except in the cortex of TG9 rats, where an equal expression of HTT-001 and HTT-011 is present.

Results

Generation and establishment of BACHD rats

BACHD rats expressing full-length mutant human htt, were generated with BACs containing human genomic DNA spanning the full-length *HTT* gene and the flanking genomic sequences of 20 kb upstream and 50 kb downstream, which included all regulatory elements (Yang et al., 1997; Kazantsev et al., 1999; Gray et al., 2008). WT *HTT* exon 1 was replaced by mutant *HTT* exon 1 containing 97 mixed CAA/CAG repeats flanked by two LoxP sites (Fig. 1*A*). Thereby, the BAC construct allows for a conditional and inducible elimination of the mutant *HTT* exon 1 by Cre recombinase activity. Following microinjection, 21 of 24 transgenic founder rats generated F1 progeny, which was used to evaluate the integrity of the transgene. Two different primer pairs were used in the PCR analysis elongating a fragment of the first and last exon of the *HTT* gene. Of 21 founder rats, 18 possessed the full-length *HTT* gene; three founders had to be withdrawn as they were lacking at least the last exon (data not shown). Genomic transgene copy number was analyzed using TaqMan real-time PCR (data not shown). Three lines had multiple insertion sites of the BAC constructs and were therefore excluded from further experimentation. mRNA expression levels were quantified with SYBR Green quantitative PCR, indicating that line LY.005 had the highest mRNA expression of mutant htt (data not shown). Htt protein levels of 1-month-old transgenic rats were

quantified by Western blot analysis with the antibody MAB2166, which recognizes both human and rat htt. Highest protein expression was also found in line LY.005, consistent with the mRNA results (data not shown), whereas line LY.009 displayed a comparable level of mRNA and protein as the well characterized BACHD mice (Fig. 1*B*) (Gray et al., 2008). Consequently, these two lines, which contain a single insertion site and express intact full-length htt were selected for subsequent phenotypic characterization.

The relative fold of transgene expression compared with endogenous rat htt was estimated by semiquantitative analysis of mhtt in each line with respect to the calibration line LY.001, which expressed the same level of mhtt mRNA as endogenous htt mRNA. The estimated expression level of mhtt is ~4.5 times higher than the endogenous in the transgenic line LY.005 (TG5), and 2.5 times higher than endogenous htt in line LY.009 (TG9).

To assess the expression pattern of mhtt in different brain regions of the transgenic BACHD rats, protein extracts of 6 brain subregions (cerebellum, cortex, striatum, olfactory bulbs, brainstem, and hypothalamus) from 1-month-old TG5 and TG9 rats were analyzed using Western blot analysis (Fig. 1*C*). The blots were stained with antibody 1C2 to visualize the signal of mhtt. The results revealed that in TG5 rats mhtt is most expressed in the cerebellum, striatum, cortex, and olfactory bulb, whereas the hypothalamus and brainstem show a lower abundance (Fig. 1*C*). In TG9 rats higher expression levels were found in striatum, olfactory bulb, and hypothalamus compared with cerebellum, cortex, and brainstem.

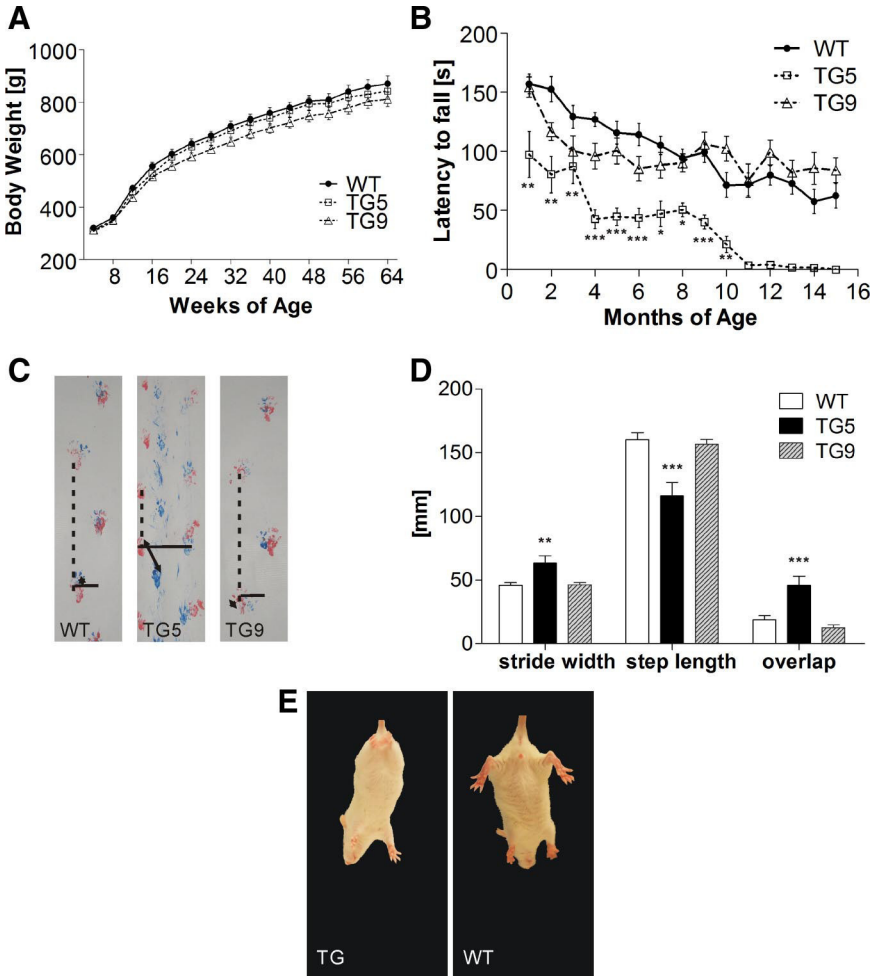

Figure 3. Motor function analysis of BACHD rat lines TG5 and TG9 compared with WT littermates. ***A***, Comparison of body weights of BACHD rats and WT littermates (WT:TG5:TG9, $N = 20:16:22$). The body weight was measured once a week and was not significantly different between genotypes over an observation period of 64 weeks. ***B***, Rats underwent four test sessions each month on an accelerating rod (4–40 rpm in 4 min). Mean latencies to fall (± SEM) were compared among different genotypes over 15 months ($n = 12$). TG5 rats displayed a progressive decrease in performance from 1 month of age, whereas TG9 showed an impaired performance at 3 and 4 months. Starting with the fifth test month, TG9 rats adapted an alternative strategy to remain on the rotating rod, which yielded comparable performances compared with WT rats. ***C***, Footprints at 14 months of age. Stride width: continuous line; step length: dotted line; and overlap between front and hindlimbs: two directional arrows. ***D***, Statistical analysis of footprints examined at 14 months of age. TG5 exhibited a significantly abnormal gait with increased stride width, decreased overlap as indicated by a greater distance between hind and front paw placement, and decreased step length. ***E***, Hindlimb clasping in BACHD transgenic rats at 3 weeks of age. Data are expressed as means ± SEM, $*p < 0.05$; $**p < 0.01$; $***p < 0.0001$.

Stable CAG repeat number and alternative splicing variants of mutant human huntingtin in BACHD rats

The stability of CAG repeat expansions is of critical importance for therapeutic studies, since the age of onset of HD inversely correlates with the number of CAG repeats (Duyao et al., 1993; Stine et al., 1993). In total, 100 samples from different brain regions or peripheral tissue were collected from transgenic rats with ages of up to 18 months of four generations and both genders to verify the stability of the polyglutamine stretch in our transgenic rat model. Our analysis revealed stability of the polyQ encoding sequence in both germlines and in different brain regions at different ages, gender, and rat generations as observed in BACHD mice (data not shown) (Gray et al., 2008).

Real-time PCR was performed to determine alternative splicing variants of the transgene mRNA. Samples of different brain regions of BACHD rats were analyzed for the presence of both mhtt protein-encoding variants, which have been previously identified (transcript HTT-001 and HTT-011 in Ensemble Genome Browser). Both the small (HTT-011) and the 67 exons spanning large transcript (HTT-001) were identified in all analyzed brain samples and the ratio of the transcript variants present in the different brain regions were similar (Fig. 2*A*,*B*).

BACHD rats do not exhibit an increased body weight compared with WT littermates

Since it has been shown that an increased expression of fl-mhtt in mice is associated with a dose-dependent increase in body weight (Van Raamsdonk et al., 2006), we have monitored body weight in both lines of BACHD rats and their WT littermates weekly (Fig. 3*A*). All rats gained body weight until 64 weeks of age with neither significant interaction between genotype and age, nor main effect of genotype (repeated-measures ANOVA, $p > 0.05$).

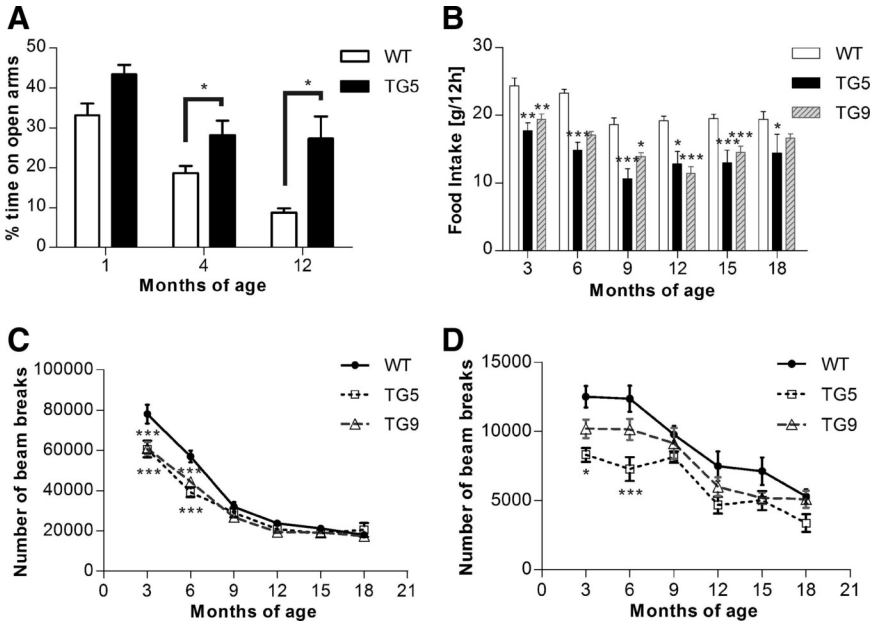

Figure 4. Emotional changes, reduced food intake, and initial hypoactivity in BACHD rats. ***A***, Independent cohorts of TG5 and WT control rats were tested in the elevated plus maze at 1, 4, and 12 months of age. Data are reported as mean ± SEM for the percentage of time spent in the open arms. TG5 rats exhibited significantly increased open-arm exploration compared with WT controls, which was evident at 4 months of age. The time spent in the open arms decreased in both genotypes throughout the study. Over an 18 month period with 3 month intervals, a cohort of TG5 ($n = 16$), TG9 ($n = 19$), and WT rats ($n = 18$) were measured for food intake (***B***), ambulatory activity (***C***), and rearing (***D***) during 12 h of a dark phase. We found significant decreased food consumption in both transgenic lines over a period of 18 months (asterisks), and a highly significant interaction effect between genotype and ambulatory activities. Both ambulatory activity and rearing decreased in all three genotypes over time, whereas significantly lower activity and rearing in both TG5 and TG9 compared with the WT rats were only observed up to 6 months of age. Data are expressed as means ± SEM, $^{*}p < 0.05$; $^{**}p < 0.01$; $^{***}p < 0.0001$.

Early onset and progressive motor deficits in BACHD rats

Motor deficits are an important clinical feature of HD patients including involuntary movements, motor dyscoordination, and gait disturbances. To assess motor dysfunction in our transgenic animals, we performed rotarod tests and footprint analyses and looked for clasping behavior.

Four trials on an accelerated rotarod were conducted with 1-month-old rats and repeated every month until the age of 15 months. The average latency until the animal fell off the rotating rod was measured and analyzed. Repeated-measures ANOVA revealed a highly significant main effect of genotype ($F_{(2,270)} = 22.86$, $p < 0.0001$) and a statistically significant genotype × age interaction ($F_{(18,270)} = 1.67$, $p = 0.0448$), reflecting a significant difference between the performance of BACHD rats and WT rats with increasing age. Subsequent *post hoc* analysis with Bonferroni tests demonstrated a progressive decline in rotarod performance in the TG5 group relative to both WT and TG9 animals (Fig. 3*B*). Significant differences were already evident at 1 month of age ($p < 0.01$). Here, TG5 rats exhibited significant difficulties in maintaining balance on the rod at higher rotation speeds and were unable to remain on the rod longer than 97.31 ± 19.45 s. In comparison, WT rats showed an average latency to fall of 156.88 ± 8.48 s. At 4 months of age, the performance of TG5 rats dropped drastically, but it was maintained over the next 4 months. A similar drastic reduction in performance was observed again between 9 and 11 months of age, when most of the TG5 rats were unable to walk on the rod even at the lowest velocity (4 rpm) (Fig. 3*B*).

Video recordings provided additional insight into the rats' performance on the rotarod. At young ages (<3 months), both transgenic and WT rats displayed similar walking behavior on the rotarod. Starting with 3 and 5 months of age, respectively, TG5 and TG9 transgenic rats adopted an abnormal walking strategy. After being placed on the rod, the transgenic animals turned 180° and instead of performing a coordinated walk, they started to jump backwards. The number of transgenic rats adapting this unusual strategy increased with age, which partly compensated for the decline in rotarod performance. None of the WT littermates displayed this abnormal movement strategy. Together, the results of the rotarod test demonstrated an early onset and progressive motor function deficit in BACHD transgenic rats of line TG5.

To investigate the gait of BACHD transgenic rats, footprints from all genotypes ($n = 11$ each) were analyzed at 14 months of age. The stride width of the hindlimbs as well as the step length and the overlap of hindlimbs and forelimbs of each individual rat were measured. One-way ANOVA revealed that 14-month-old transgenic TG5 rats made significantly shorter steps with forelimbs and hindlimbs ($p < 0.0001$) than TG9 and WT. Furthermore, TG5 rats showed an increased stride width ($p < 0.01$) and a reduced overlap between forelimb and hindlimb placement ($p < 0.0001$) (Fig. 3*C*,*D*) compared with the other groups, indicating that BACHD transgenic rats TG5 have gait abnormalities at older ages compared with WT rats.

Additionally, characteristic hindlimb clasping behavior was observed during tail suspension in both transgenic lines starting at 3 weeks of age (Fig. 3*E*).

Decreased anxiety, initial hypoactivity, and reduced food intake in BACHD rats

Additional clinical features of HD patients involve multiple psychiatric symptoms. To score the anxiety level of the BACHD transgenic rats, we used the elevated plus maze test. Independent cohorts of TG5 rats and WT littermates were used at 1, 4, and 12 months of age. One- and four-month- old BACHD TG5 rats spent significantly more time on the open arms compared with WT (10.30 and 9.55% at 1 and 4 months of age, respectively, $p < 0.05$ at each time point), (Fig. 4*A*). At 12 months of age, the difference between TG5 and WT rats further increased with a mean difference of 13.43% ($p < 0.01$). The significance of these observations was confirmed by two-way ANOVA, which indicated a highly significant main effect of genotype ($F_{(1,65)} = 25.56$, $p < 0.0001$) as well as a main effect of age ($F_{(2,65)} = 37.7$, $p < 0.0001$). However, there was no significant interaction between genotype and age ($F_{(2,65)} = 0.26$, $p = 0.7753$) because the percentage of time spent on the open arms of the maze decreased in both genotypes with increasing age.

Locomotor activity and food consumption of BACHD rats were registered in an automated, home cage-like environment (PhenoMaster; TSE Systems). Measurements were taken from one cohort of each rat line (TG5:TG9:WT = 16:19:18) every 3

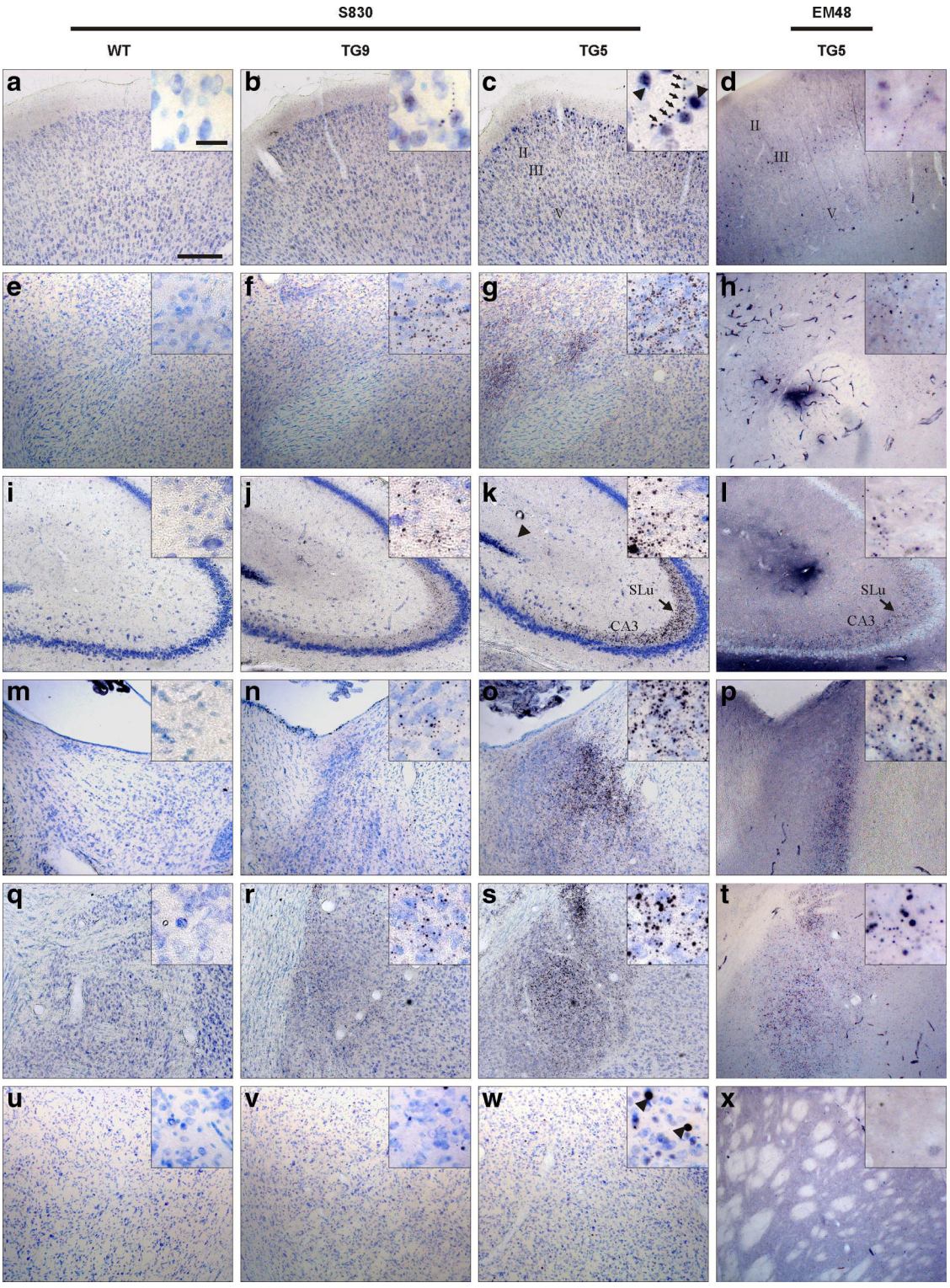

Figure 5. Htt aggregates were investigated using polyclonal sheep antibody S830 and monoclonal mouse antibody EM48 showing similar brain regional distribution pattern. Mutant htt immunoreactivity is widely distributed throughout the cerebrum of BACHD rats by 12 months of age. Nickel-DAB (black) visualizes immuno-activity of mhtt, and the counterstaining with thionin (blue) marks nuclei. In both TG5 and TG9 rats, aggregates varying in size and formation were abundant in the cortex (***a–d***), nucleus accumbens (***e–h***), and hippocampus (***i–l***) and strongly expressed in the stratum lucidum of CA3 area (arrow in ***k*** and ***l***), bed nucleus of stria terminals (***m–p***), and amygdala (***q–t***). Few aggregates were found in caudate–putamen (***u–x***). Most aggregates were localized in the neuropil, some of which arranged in a linear array (arrows in the insert of ***c***). Nuclear htt staining (arrowheads in the insert of ***c***) was only detected in layer II/III of the cortex, a few in caudate–putamen, and in the granule cells of dentate gyrus at 12 months of age. Scale bars: inlay showing high-magnification images, 20 μm; in low-magnification images, 200 μm.

months over a period of 15 months. At each time point, ambulatory activity over 22 h as well as rearing activity during the dark phase were analyzed. Both transgenic and WT rats showed a pronounced dark/light cycle in their behavioral activities with their main activity taking place during the dark phases. The activity pattern did not differ between different genotypes (data not shown).

Highly significant differences in ambulatory activity were found at early time points in both transgenic rat lines compared with WT

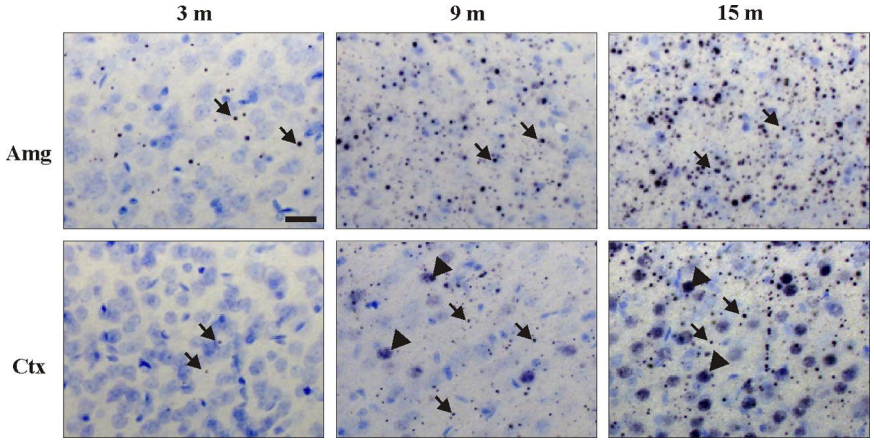

Figure 6. Spatiotemporal accumulation of mhtt in amygdala (Amg) and cortex (Ctx) of TG5 rat brains. An increase in both number and size of neuropil aggregates (arrows) was observed in both regions during aging; nuclear accumulation of mhtt (arrowheads) appeared only in cortex at 9 months of age becoming more abundant at 15 months of age. Scale bar, 20 μm.

(both TG5 and TG9 $p < 0.001$ at 3 and 6 months of age) (Fig. 4*C*,*D*). The reduction in rearing activity was only observed in TG5 compared with WT control rats at early time points ($p < 0.05$ at 3 months of age, $p < 0.0001$ at 6 months of age). The significance of these observations was confirmed by two-way ANOVA, which indicated a highly significant interaction effect (genotype × age: $F_{(10,259)} = 4.22, p < 0.0001$) in ambulatory activity, a main effect of genotype in both ambulatory activity ($F_{(2,259)} = 22.32, p < 0.0001$) and rearing activity ($F_{(2,248)} = 15.11, p < 0.0001$) as well as a main effect of age ($F_{(5,259)} = 217.89, p < 0.0001$ in ambulatory activity; $F_{(5,248)} = 23.23, p < 0.0001$ in rearing activity).

The total food consumption during the dark phase was compared between the three genotypes over 15 months. Analysis with two-way ANOVA revealed a highly significant main effect of genotype ($F_{(2,259)} = 67.80, p < 0.0001$). BACHD rats of both lines showed a reduced food intake throughout the study, which was due to reduction in food intake in both transgenic rat lines compared with WT littermates with a mean value of 8.79 g in TG5 and 4.90 g in TG9 (Fig. 4*B*) compared with 20.71 g in WT. However, there was no significant interaction between genotype and age ($F_{(10,259)} = 1.06$, $p = 0.3965$).

Huntingtin aggregates increase over time and are widely distributed in BACHD rats

To investigate the regional distribution pattern of mhtt-positive aggregates in BACHD transgenic rats, we used the polyclonal sheep antibody S830 and the monoclonal mouse antibody EM48 in serial brain sections at 12 months of age (Fig. 5). Immunohistological staining with both antibodies demonstrated a similar distribution pattern in BACHD transgenic rats. However, mEM48 staining was weaker and may exhibit an unspecific immunoreactivity with blood vessels (Fig. 5*h*). For this reason, the results obtained with the S830 antibody are described in more detail in the following. In TG5 and TG9 brains, the aggregates were found to be widely distributed in all regions with prominent expression in the neocortex and in limbic areas including nucleus accumbens, hippocampus (specifically in the CA3 region), bed nucleus of the stria terminalis, and the amygdala (Fig. 5). A lower expression was observed in the hypothalamus and in most thalamic nuclei (data not shown). In comparison, very few aggregates were detected in the dorsolateral caudate–putamen, the lateral globus pallidus, and the substantia nigra (data not shown). The cerebellar cortex showed a few small aggregates throughout all three layers (data not shown). Both the size and number of aggregates increased with age, showing the largest and most abundant aggregates in amygdala, in the CA3 region of the hippocampus, and in the cerebral cortex, indicating that aggregate formation continued to progress in these regions (Fig. 6). Nuclear accumulation of N-terminal huntingtin was only observed in outer layers of cerebral cortex, in striatum, and in the granule cells of the dentate gyrus in older rats (after 9 months of age) and increased thereafter (Figs. 5, 6). Mhtt aggregates were more prominent in TG5 than in TG9 rats at all ages investigated. No immunoreactivity was observed in WT rats.

Subcellular localization of N-terminal htt aggregates and neurodegeneration

Using light microscopy, aggregates varying in size and form as well as chain-like structures were observed throughout the brain areas with abundant mhtt. These data indicate that mhtt aggregates are primarily located in the neuropil (Figs. 5, 6). Subcellular localization of N-terminal htt aggregates and neurodegeneration were further investigated ultrastructurally in TG5 rat brains at advanced ages by EM48 immunohistochemistry (Fig. 7) when aggregates were abundantly expressed. Electron microscopy confirmed that most aggregates were localized in the neuropil. Htt deposits were predominantly detected in axons (Fig. 7*C*,*K*) and synaptic terminals (Fig. 7*D*,*G*,*L*). Dark degenerating neurons and dark dendrites were also identified in these areas as documented in the nucleus accumbens (Fig. 7*B*), bed nucleus of the stria terminalis (Fig. 7*F*), and the cortex (Fig. 7*J*). Dark neurons with condensed nucleus and cytoplasm were often localized adjacent to normal light neurons (Fig. 7*B*,*F*). Dark degenerating terminals were seen in apposition to large pallidal dendrites (Fig. 7*H*). Some dark cortical neurons displayed a fine granular immunoreaction product (Fig. 7*J*) similar to that seen by light microscopy in the respective area (Fig. 6). The prominent S830 immunoreactivity in the stratum lucidum of the CA3 region of the hippocampus (Fig. 5) corresponded to immunopositive unmyelinated mossy fibers (Fig. 7*K*) and their terminals, some of which were engulfed by lamellated structures as a sign of degeneration (Fig. 7*L*).

Reduced dopamine receptor binding potential in aged BACHD transgenic rats

A specific uptake of the D2-receptor antagonist [^{11}C]raclopride was demonstrated in dynamic PET scans in the striatum of WT and BACHD TG5 rats, while there was no specific tracer uptake in the corresponding cerebella. Longitudinal measurements up to 18 months of age revealed a significant decrease in the striatal uptake of [^{11}C]raclopride in BACHD rats (two-way ANOVA for the main effect of genotype, $F_{(1,24)} = 8.77, p < 0.01$). This reduction of dopamine receptor binding potential was evident at 18 months of age ($p < 0.01$), as confirmed by Bonferroni *post hoc* multiple-comparison test (Fig. 8). However, there was no significant interaction between genotype and age ($F_{(2,24)} = 2.33, p = 0,1185$).

Imbalance of striosome and matrix compartments in early disease stages of BACHD rats

Calbindin immunostaining was performed to determine changes in the striosome and matrix compartments, as calbindin is

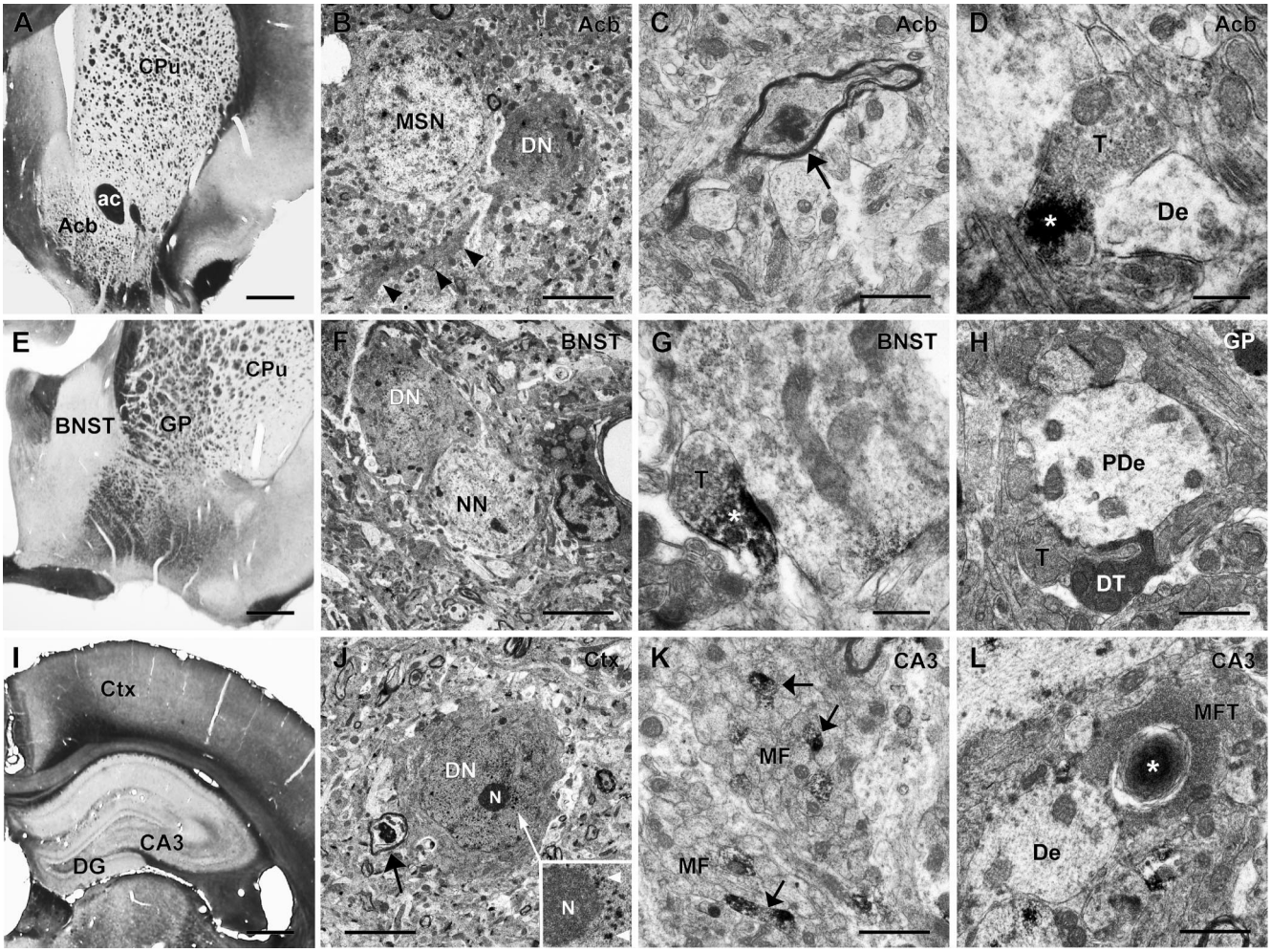

Figure 7. Neurodegeneration and subcellular localization of mhtt aggregates in TG5 brains (***A***, ***E***, ***I***). Vibratome sections (50 μm) show the areas investigated by EM48 immune-electron microscopy (***B***, ***F***, ***J***). Dark degenerated neurons (DN) and dendrites (***B***, arrowheads) were detected in the nucleus accumbens (Acb), bed nucleus of the stria terminalis (BNST), and cortex (Ctx), the latter with punctate nuclear htt reactivity as seen adjacent to the nucleolus (N) at higher enlargement (N, inlay in ***J***). DNs were seen localized near normal neurons, MSN (***B***), or myelinated nerve fibers showing evidence of degeneration (arrow in ***J***). Htt aggregates (*) were observed in axons (arrow in ***C***) and synaptic terminals (T in ***D*** and ***G***) often contacting dendrites (De). Dark terminals (DT in ***H***) were seen in the globus pallidus (GP) apposing pallidal dendrites (PDe). In the hippocampal CA3 region of hippocampus mossy fiber bundles (MF) emerging from the dentate gyrus (DG) exhibited immunoreactive unmyelinated fibers (***K***, arrows); htt reactivity engulfed by lamellated structures was also observed in mossy fiber terminals (MFT in ***L***), adjacent to neuronal dendrites (De). Caudate–putamen (CPu); anterior commissure (ac). Scale bars: (in ***A***, ***E***, ***I***), 0.5 mm; (in ***B***, ***F***, ***J***), 5 μm; (in ***C***, ***H***, ***K***, ***L***), 1 μm; (in ***D***, ***G***), 0.5 μm.

strongly expressed in the matrix surrounding the Calbindin-poor striosomes (Fig. 9*A*). The intensity of the calbindin staining neither in the matrix nor in the irregular-shaped striosomes (Fig. 9*A*) was altered in BACHD rats compared with WT littermates. One-way ANOVA demonstrated that both total matrix area and number of the striosomes in BACHD transgenic animals did not differ from that of their WT littermates (Fig. 9*B*). However, the total striosome area (Fig. 9*C*) and the mean area of the striosomes (Fig. 9*D*) were significantly different among the three genotypes, which subsequent Tukey's multiple-comparison test determined was due to the reduction in total and mean striosomal area in TG5 transgenic rats compared with WT littermates (29% in total area, $p = 0.0359$; 34% in mean area, $p = 0{,}0196$). This imbalance in the striosome-matrix compartments in TG5 rats may affect the equilibrium of inhibitory and excitatory output from the striatum to downstream neurons.

Discussion

BACHD transgenic rats expressing fl-mhtt, exhibit several robust HD-like behavioral phenotypes as well as changes at the molecular and cellular levels (Fig. 10). Importantly, there was no significant difference in body weight between BACHD rats of both lines and WT littermates (Fig. 3*A*). This is in contrast to what has been reported in BACHD mice and YAC128 mice (Menalled et al., 2009), where overexpression of fl-mhtt is associated with a significantly increased body weight. It has been postulated that body weight is modulated by levels of fl-htt with increased levels of fl-wthtt or fl-mhtt leading to an increased body and organ weight in mice, while a decrease of fl-htt is associated with body weight loss (Van Raamsdonk et al., 2006). The increase of body weight in mice resulted from an increase of both total fat mass and fat-free mass and was associated with increased levels of plasma IGF-1 (Pouladi et al., 2010). Interestingly, we also observed an increase in body fat mass in BACHD rats. But in contrast to the published mouse data a decrease in organ weight in BACHD rats of line TG5 was found resulting in a comparable body weight between BACHD rats and WT rats (preliminary results, data not shown). This discrepancy is especially intriguing since the same construct was used to generate BACHD mice and

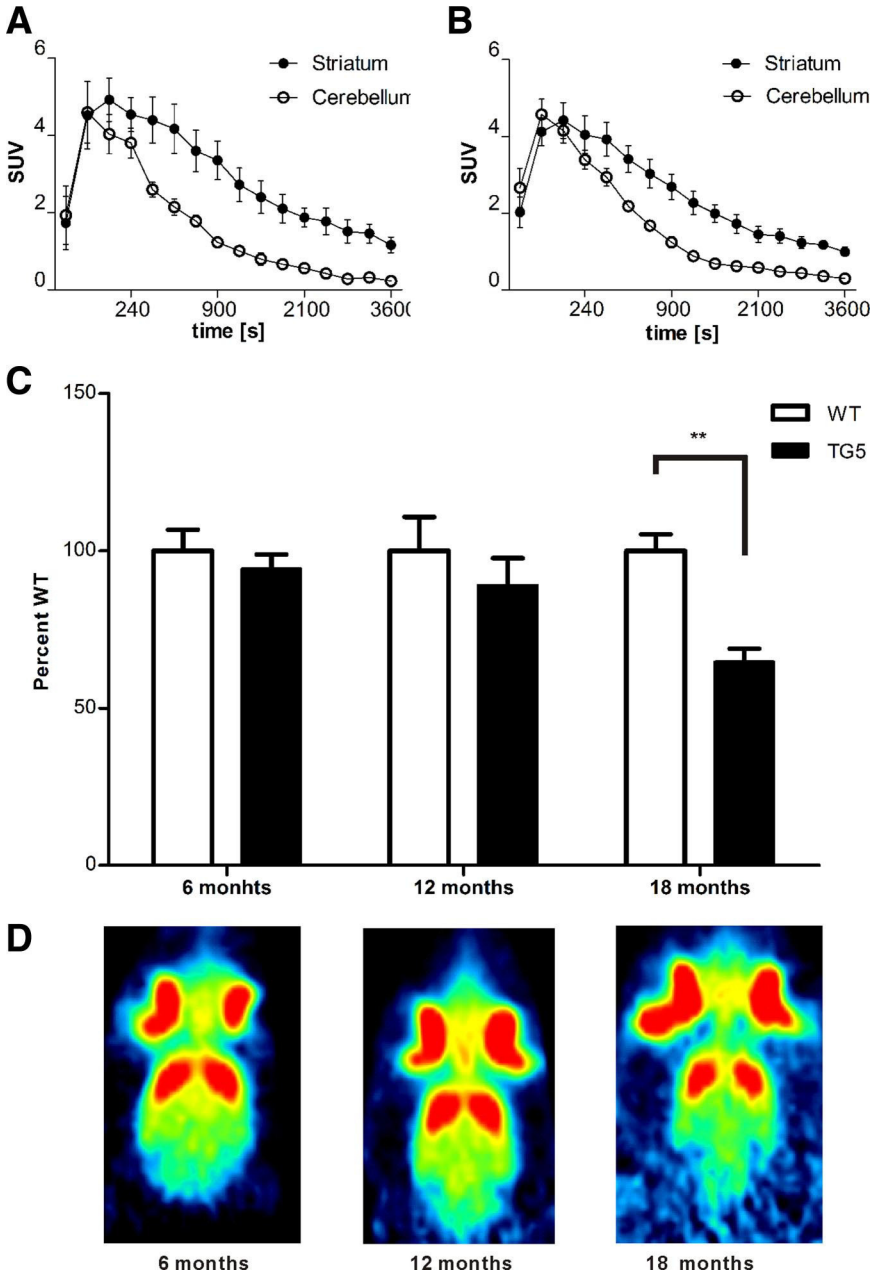

Figure 8. [11C]raclopride PET imaging reveals D2 receptor loss in striatum of BACHD rats TG5. [11C]raclopride uptake was measured as standard uptake volume (SUV) of different brain areas. PET time activity curves of target (striatum) and reference region (cerebellum) are plotted for the control (***A***) and BACHD rats (***B***). ***C***, Corresponding binding potential (BP_{ND}) values are shown in the striatum. There was no significant difference in BP_{ND} between the first two time points in transgenic and control rats. After 18 months the BP_{ND} of BACHD was significantly lower than in control littermates. Representative images of [11C]raclopride uptake at each age is shown in ***D***. Data are expressed as means ± SEM, $^{**}p < 0.01$.

rats. It might be attributed to species-specific differences and is less likely caused by integration site effects as we did not observe an increased body weight in any of the 18 full-length BACHD rat lines. Furthermore, there is a proportional correlation between the severity of the HD phenotype and the protein expression level in the two BACHD lines arguing against an integration site effect. As progressive rotarod deficits are readily apparent in BACHD rats of line TG5 these are very likely motor defects rather than a consequence of increased body weight. Also, we can exclude that differences in body weight confound other behavioral tests in BACHD rats rendering this model valuable for further phenotype studies.

Another advantage of the BACHD rat is its strong phenotype. Compared with the already existing fragment tgHD rats BACHD rats show an earlier onset and a faster progression of motor deficits without the need to breed for homozygosity as heterozygous tgHD rats show only subtle deficits (Nguyen et al., 2006; Brooks et al., 2009). Recently, a milder phenotype in tgHD rats as originally described has been reported (Casteels et al., 2011; Antonsen et al., 2012; Blockx et al., 2012). Also, while striatal atrophy was found in some groups of old tgHD rats (von Hörsten et al., 2003; Kántor et al., 2006; Nguyen et al., 2006), other studies revealed little or no evidence for atrophy (Winkler et al., 2006; Bode et al., 2008; Blockx et al., 2011).

In addition, the expression of fl-mhtt compared with a fragment of mhtt may add important features. For example, transgenic *HTT* in BACHD rats undergoes natural splicing as confirmed by the presence of the two naturally occurring mRNA isoforms. Even though the small splicing variant does not contain a polyQ stretch, it may fulfill additional functions relevant for the disease process. Since both of these isoforms were found in humans (www.ensembl.org/Homo_sapiens/Gene/Summary?g=ENSG00000197386;r=4:3076408-3245676), the BACHD rat model closely resembles the HD patient condition in this respect.

In BACHD rats, we found a significantly decreased D2 receptor binding potential by [11C]raclopride PET, which is in accordance with findings in HD patients and has been proposed as a neuroimaging biomarker for HD (Pavese et al., 2003; van Oostrom et al., 2005). Due to the relatively large size of the rat brain, *in vivo* MRI and PET imaging are more practicable than in mice, thus providing an excellent tool to study disease progression. To our knowledge, this is the first study showing clear longitudinal changes by [11C]raclopride PET in an HD animal model, making the BACHD rats a valuable model for noninvasive neuroimaging studies with novel ligands to be subsequently translated into the clinics.

Remarkably, the BACHD rat model reflects many aspects of the aggregation pattern of mhtt found in HD patients. The aggregates occur more frequently in the cortex than in the striatum and neuropil aggregates appear earlier than mhtt accumulation in the nucleus (DiFiglia et al., 1997; Gutekunst et al., 1999). In contrast, R6/2 mice display mainly diffusible mhtt throughout the nucleus with intensively stained nuclear aggregates (Kosinski et al., 1999; Wang et al., 2008). In the fragment rat model for HD, cortical aggregates are far less expressed than in the limbic striatum (von Hörsten et al., 2003; Nguyen et al., 2006). BACHD mice display a similar mhtt aggregate distribution pattern as our BACHD rats

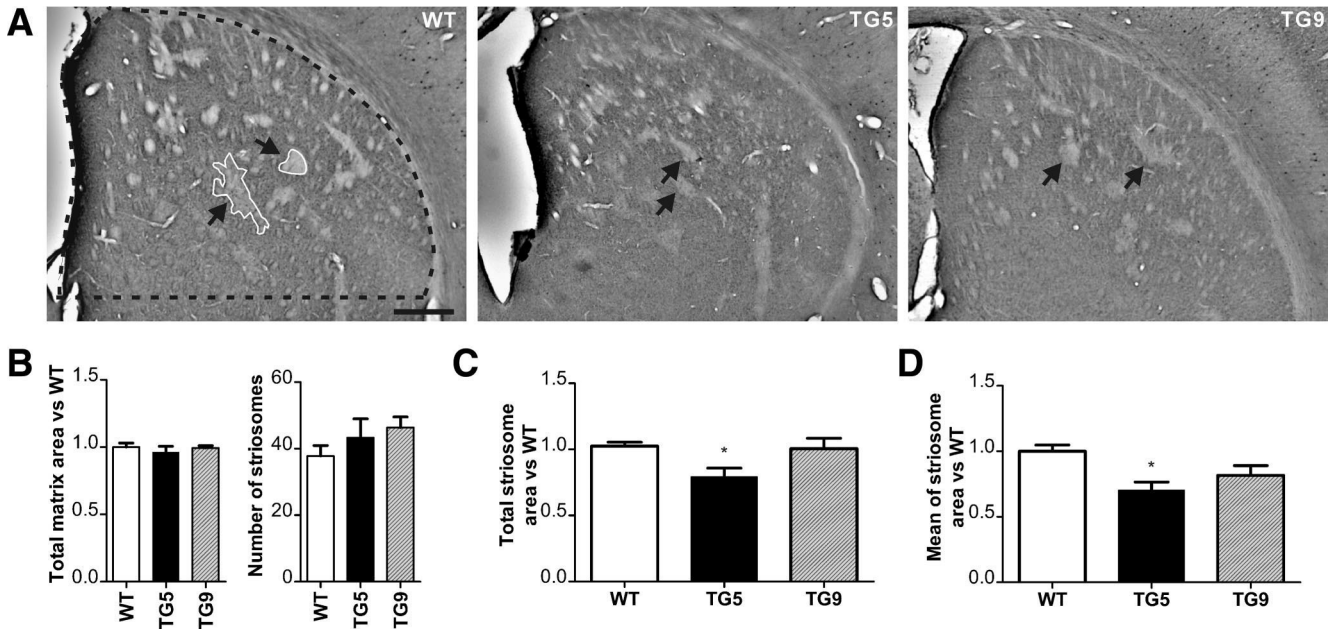

Figure 9. Striosome abnormalities in the striatum of BACHD rats. The ROI is outlined by a dotted black line. ***A***, Calbindin immunostained sections of WT, TG5, and TG9 rats at 6 months of age show striosomes visible by faint calbindin staining (arrows and outlined by a continuous white line), while the intense staining visualizes the matrix surrounding the striosomes. Scale bar, 0.5 cm. ***B***, The total matrix area and number of striosomes was similar in WT, TG5, and TG9 rats. A significant decrease in both total (***C***) and mean striosome areas (***D***) was only observed in TG5 rats compared with WT littermates. Data are expressed as means ± SEM, $*p < 0.05$.

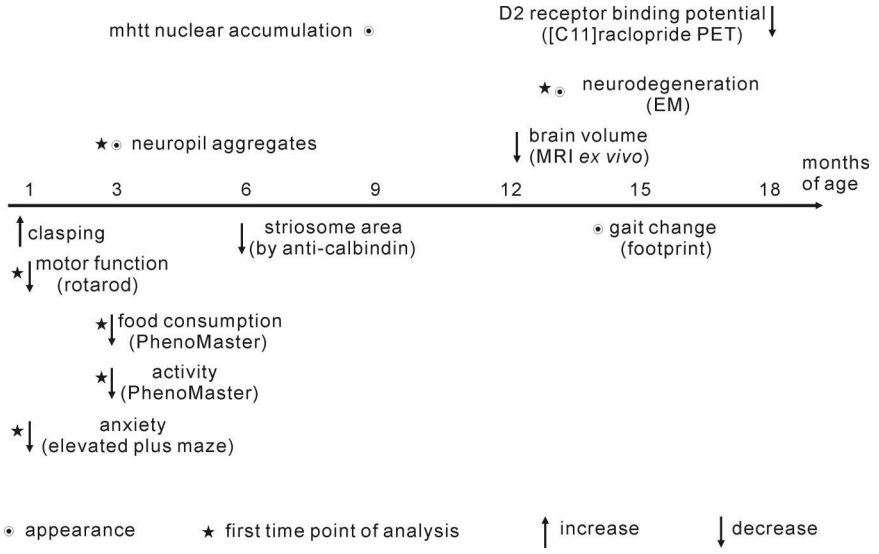

Figure 10. Progression of various phenotypes in BACHD TG5 rats. The findings of this study are summarized according to the earliest onset or appearance of each phenotype.

with prevalence of neuropil aggregates and paucity of intranuclear inclusions, but both are less abundant than in BACHD rats and appear at a later time point; the diffuse nuclear mhtt accumulation was not detected until 18 months of age (Gray et al., 2008). In comparison, YAC128 mice display both neuropil aggregates and intranuclear inclusions, which were present at 15 months of age, particularly in ventral striatum, amygdala, and cortex (Bayram-Weston et al., 2012). Interestingly, neuropil aggregates are much more common in HD patients with an adult onset than in juvenile onset patients, and the number of neuropil aggregates correlates with the extent of disease. While intranuclear aggregates were not detected in the presymptomatic patient, neuropil aggregates were observed in the cortex of the same presymptomatic patient (DiFiglia et al., 1997; Gourfinkel-An et al., 1998; Gutekunst et al., 1999). This difference in the aggregation pattern might be explained by sequence differences in the human mutant *HTT* transgenes harbored by the BACHD models and the YAC128 mice, including single nucleotide polymorphisms as well as differences in the nature of CAA interruptions of the CAG tract (Pouladi et al., 2012).

However, whether the extent of aggregation or numbers of aggregates predict neuronal death remains controversial. The formation of neuropil aggregates can induce axonal degeneration (Li et al., 2001). Additionally, they can influence the mitochondrial transport along both axons and dendrites, thereby impairing energy supply within neuronal processes (Chang et al., 2006). Importantly, BACHD rats show mhtt deposits prominently expressed in axons and synaptic terminals (Fig. 7). In contrast, other studies have suggested that aggregation may exert beneficial effects by protecting against polyglutamine toxicity, since the aggregation of N-terminal htt reduces the amount of monomeric and oligomeric N-terminal htt, which possesses a higher toxicity (Arrasate et al., 2004; Lajoie and Snapp, 2010; Miller et al., 2010). In BACHD rats, numerous dark degenerating neurons and dendrites were found in brain regions, where prominent numbers of aggregates were present. Furthermore, dark neurons and dendrites containing aggregates were frequently observed together suggesting a connection between aggregate formation and neurodegeneration. However, further studies would be needed to investigate this association.

The striatum is composed of two interdependent compartments: the striosome (patch) and the matrix, which can be distinguished by the differential expression of neurotransmitter-related molecules (Goldman-Rakic, 1982; Graybiel et al., 1990; Holt et al., 1997). Discriminative input and output connections suggest that the striosome and matrix compartments participate in limbic-based and sensorimotor/associative forebrain circuits, respectively (Donoghue and Herkenham, 1986; Gerfen, 1992). In HD patients, an imbalanced loss of neurons in the striosome and matrix compartments has been described leading to a reduced total matrix area whereas the volume of the striosome is not affected (Ferrante et al., 1987; Seto-Ohshima et al., 1988; Hersch and Ferrante, 1997). Conversely, it has also been reported that this imbalance in neuron loss is initially found in the striosomes but affects both compartments equally in later stages of the disease (Reiner et al., 1988; Hedreen and Folstein, 1995; Lawhorn et al., 2008). Striosomes exchange information with the surrounding matrix, the integrated signal will be subsequently sent through D1 (excitatory) and D2 (inhibitory) medium spiny neurons (MSNs) via direct and indirect pathways to the thalamocortical circuits. However, the striosome and matrix compartments contain disproportionate amounts of D1 and D2 neurons and the imbalance of those two compartments influence the proportion of excitatory and inhibitory signaling in limbic-based and sensorimotor/associative forebrain circuits. Thus, a change in the established equilibrium, as is the case in HD, causes a disorder of the basal ganglia. In BACHD rats, we observed early changes in the pattern of striosome and matrix compartments, as well as a decrease in the total and mean striosome area. This could cause alterations in the basal ganglia and lead to neuronal dysfunction and clinical signs of HD. However, the exact mechanism behind this is unknown and how this is linked to the neuropil aggregates within the sensorimotor circuit and the limbic-based circuits still needs to be answered.

In summary, we have developed a novel transgenic rat model for Huntington disease, which expresses fl-mhtt with 97 polyQ repeats under the control of the human htt promoter and regulatory elements. These BACHD rats display a robust, early onset and progressive HD-like phenotype combined with characteristic neuropathological features of Huntington disease making them a valuable model for further understanding the disease mechanisms and for preclinical pharmacological studies.

References

Antonsen BT, Jiang Y, Veraart J, Qu H, Nguyen HP, Sijbers J, von Hörsten S, Johnson GA, Leergaard TB (2012) Altered diffusion tensor imaging measurements in aged transgenic Huntington disease rats. Brain Struct Funct. Advance online publication. Retrieved July 30, 2012. doi:10.1007/s00429-012-0427-0. CrossRef Medline

Arrasate M, Mitra S, Schweitzer ES, Segal MR, Finkbeiner S (2004) Inclusion body formation reduces levels of mutant huntingtin and the risk of neuronal death. Nature 431:805–810. CrossRef Medline

Bayram-Weston Z, Jones L, Dunnett SB, Brooks SP (2012) Light and electron microscopic characterization of the evolution of cellular pathology in YAC128 Huntington's disease transgenic mice. Brain Res Bull 88:137–147. CrossRef Medline

Blockx I, Van Camp N, Verhoye M, Boisgard R, Dubois A, Jego B, Jonckers E, Raber K, Siquier K, Kuhnast B, Dollé F, Nguyen HP, Von Hörsten S, Tavitian B, Van der Linden A (2011) Genotype specific age related changes in a transgenic rat model of Huntington's disease. Neuroimage 58:1006–1016. CrossRef Medline

Blockx I, De Groof G, Verhoye M, Van Audekerke J, Raber K, Poot D, Sijbers J, Osmand AP, Von Hörsten S, Van der Linden A (2012) Microstructural changes observed with DKI in a transgenic Huntington rat model: evidence for abnormal neurodevelopment. Neuroimage 59:957–967. CrossRef Medline

Bode FJ, Stephan M, Suhling H, Pabst R, Straub RH, Raber KA, Bonin M, Nguyen HP, Riess O, Bauer A, Sjoberg C, Petersén A, von Hörsten S (2008) Sex differences in a transgenic rat model of Huntington's disease: decreased 17beta-estradiol levels correlate with reduced numbers of DARPP32+ neurons in males. Hum Mol Genet 17:2595–2609. CrossRef Medline

Brooks S, Fielding S, Döbrössy M, von Hörsten S, Dunnett S (2009) Subtle but progressive cognitive deficits in the female tgHD hemizygote rat as demonstrated by operant SILT performance. Brain Res Bull 79:310–315. CrossRef Medline

Bruyn GW (1979) Huntington's chorea. Tijdschr Ziekenverpl 32:101–105. Medline

Casteels C, Vandeputte C, Rangarajan JR, Dresselaers T, Riess O, Bormans G, Maes F, Himmelreich U, Nguyen H, Van Laere K (2011) Metabolic and type 1 cannabinoid receptor imaging of a transgenic rat model in the early phase of Huntington disease. Exp Neurol 229:440–449. CrossRef Medline

Chang DT, Rintoul GL, Pandipati S, Reynolds IJ (2006) Mutant huntingtin aggregates impair mitochondrial movement and trafficking in cortical neurons. Neurobiol Dis 22:388–400. CrossRef Medline

Crook ZR, Housman D (2011) Huntington's disease: can mice lead the way to treatment? Neuron 69:423–435. CrossRef Medline

DiFiglia M, Sapp E, Chase KO, Davies SW, Bates GP, Vonsattel JP, Aronin N (1997) Aggregation of huntingtin in neuronal intranuclear inclusions and dystrophic neurites in brain. Science 277:1990–1993. CrossRef Medline

Donoghue JP, Herkenham M (1986) Neostriatal projections from individual cortical fields conform to histochemically distinct striatal compartments in the rat. Brain Res 365:397–403. Medline

Duyao M, Ambrose C, Myers R, Novelletto A, Persichetti F, Frontali M, Folstein S, Ross C, Franz M, Abbott M (1993) Trinucleotide repeat length instability and age of onset in Huntington's disease. Nat Genet 4:387–392. Medline

Ehrnhoefer DE, Butland SL, Pouladi MA, Hayden MR (2009) Mouse models of Huntington disease: variations on a theme. Dis Model Mech 2:123–129. CrossRef Medline

Ferrante RJ, Kowall NW, Beal MF, Martin JB, Bird ED, Richardson EP Jr (1987) Morphologic and histochemical characteristics of a spared subset of striatal neurons in Huntington's disease. J Neuropathol Exp Neurol 46:12–27. Medline

Gerfen CR (1992) The neostriatal mosaic: multiple levels of compartmental organization. Trends Neurosci 15:133–139. Medline

Goldman-Rakic PS (1982) Cytoarchitectonic heterogeneity of the primate neostriatum: subdivision into Island and Matrix cellular compartments. J Comp Neurol 205:398–413. Medline

Gourfinkel-An I, Cancel G, Duyckaerts C, Faucheux B, Hauw JJ, Trottier Y, Brice A, Agid Y, Hirsch EC (1998) Neuronal distribution of intranuclear inclusions in Huntington's disease with adult onset. Neuroreport 9:1823–1826. CrossRef Medline

Gray M, Shirasaki DI, Cepeda C, André VM, Wilburn B, Lu XH, Tao J, Yamazaki I, Li SH, Sun YE, Li XJ, Levine MS, Yang XW (2008) Full-length human mutant huntingtin with a stable polyglutamine repeat can elicit progressive and selective neuropathogenesis in BACHD mice. J Neurosci 28:6182–6195. CrossRef Medline

Graybiel AM, Ohta K, Roffler-Tarlov S (1990) Patterns of cell and fiber vulnerability in the mesostriatal system of the mutant mouse weaver. I. Gradients and compartments. J Neurosci 10:720–733. Medline

Gutekunst CA, Li SH, Yi H, Mulroy JS, Kuemmerle S, Jones R, Rye D, Ferrante RJ, Hersch SM, Li XJ (1999) Nuclear and neuropil aggregates in Huntington's disease: relationship to neuropathology. J Neurosci 19:2522–2534. Medline

Hammer RE, Maika SD, Richardson JA, Tang JP, Taurog JD (1990) Spontaneous inflammatory disease in transgenic rats expressing HLA-B27 and human beta 2m: an animal model of HLA-B27-associated human disorders. Cell 63:1099–1112. CrossRef Medline

Harper P (1991) Huntington's disease. London: Saunders.

Hedreen JC, Folstein SE (1995) Early loss of neostriatal striosome neurons in Huntington's disease. J Neuropathol Exp Neurol 54:105–120. Medline

Herrmann KH, Schmidt S, Kretz A, Haenold R, Krumbein I, Metzler M, Gaser C, Witte OW, Reichenbach JR (2012) Possibilities and limitations for high resolution small animal MRI on a clinical whole-body 3T scanner. MAGMA 25:233–244. CrossRef Medline

Hersch S, Ferrante R (1997) Neuropathology and pathophysiology of Huntington's disease (Watts RL, Koller WC, eds). New York: McGraw-Hill.
Holt DJ, Graybiel AM, Saper CB (1997) Neurochemical architecture of the human striatum. J Comp Neurol 384:1–25. Medline
Kántor O, Temel Y, Holzmann C, Raber K, Nguyen HP, Cao C, Türkoglu HO, Rutten BP, Visser-Vandewalle V, Steinbusch HW, Blokland A, Korr H, Riess O, von Hörsten S, Schmitz C (2006) Selective striatal neuron loss and alterations in behavior correlate with impaired striatal function in Huntington's disease transgenic rats. Neurobiol Dis 22:538–547. CrossRef Medline
Kazantsev A, Preisinger E, Dranovsky A, Goldgaber D, Housman D (1999) Insoluble detergent-resistant aggregates form between pathological and nonpathological lengths of polyglutamine in mammalian cells. Proc Natl Acad Sci U S A 96:11404–11409. Medline
Kosinski CM, Cha JH, Young AB, Mangiarini L, Bates G, Schiefer J, Schwarz M (1999) Intranuclear inclusions in subtypes of striatal neurons in Huntington's disease transgenic mice. Neuroreport 10:3891–3896. CrossRef Medline
Kuemmerle S, Gutekunst CA, Klein AM, Li XJ, Li SH, Beal MF, Hersch SM, Ferrante RJ (1999) Huntington aggregates may not predict neuronal death in Huntington's disease. Ann Neurol 46:842–849. Medline
Lajoie P, Snapp EL (2010) Formation and toxicity of soluble polyglutamine oligomers in living cells. PLoS One 5:e15245. CrossRef Medline
Lawhorn C, Smith DM, Brown LL (2008) Striosome-matrix pathology and motor deficits in the YAC128 mouse model of Huntington's disease. Neurobiol Dis 32:471–478. CrossRef Medline
Li H, Li SH, Yu ZX, Shelbourne P, Li XJ (2001) Huntingtin aggregate-associated axonal degeneration is an early pathological event in Huntington's disease mice. J Neurosci 21:8473–8481. Medline
Liu L, Orozco IJ, Planel E, Wen Y, Bretteville A, Krishnamurthy P, Wang L, Herman M, Figueroa H, Yu WH, Arancio O, Duff K (2008) A transgenic rat that develops Alzheimer's disease-like amyloid pathology, deficits in synaptic plasticity and cognitive impairment. Neurobiol Dis 31:46–57. CrossRef Medline
Menalled LB, Chesselet MF (2002) Mouse models of Huntington's disease. Trends Pharmacol Sci 23:32–39. CrossRef Medline
Menalled L, El-Khodor BF, Patry M, Suárez-Fariñas M, Orenstein SJ, Zahasky B, Leahy C, Wheeler V, Yang XW, MacDonald M, Morton AJ, Bates G, Leeds J, Park L, Howland D, Signer E, Tobin A, Brunner D (2009) Systematic behavioral evaluation of Huntington's disease transgenic and knock-in mouse models. Neurobiol Dis 35:319–336. CrossRef Medline
Miller J, Arrasate M, Shaby BA, Mitra S, Masliah E, Finkbeiner S (2010) Quantitative relationships between huntingtin levels, polyglutamine length, inclusion body formation, and neuronal death provide novel insight into huntington's disease molecular pathogenesis. J Neurosci 30:10541–10550. CrossRef Medline
Munoz-Sanjuan I, Bates GP (2011) The importance of integrating basic and clinical research toward the development of new therapies for Huntington disease. J Clin Invest 121:476–483. CrossRef Medline
Nguyen HP, Kobbe P, Rahne H, Wörpel T, Jäger B, Stephan M, Pabst R, Holzmann C, Riess O, Korr H, Kántor O, Petrasch-Parwez E, Wetzel R, Osmand A, von Hörsten S (2006) Behavioral abnormalities precede neuropathological markers in rats transgenic for Huntington's disease. Hum Mol Genet 15:3177–3194. CrossRef Medline
Osmand AP, Berthelier V, Wetzel R (2006) Imaging polyglutamine deposits in brain tissue. Methods Enzymol 412:106–122. CrossRef Medline
Pavese N, Andrews TC, Brooks DJ, Ho AK, Rosser AE, Barker RA, Robbins TW, Sahakian BJ, Dunnett SB, Piccini P (2003) Progressive striatal and cortical dopamine receptor dysfunction in Huntington's disease: a PET study. Brain 126:1127–1135. CrossRef Medline
Paxinos G, Franklin K (2006) The rat brain in stereotaxic coordinate, Ed 6. San Diego: Academic.
Petrasch-Parwez E, Nguyen HP, Löbbecke-Schumacher M, Habbes HW, Wieczorek S, Riess O, Andres KH, Dermietzel R, Von Hörsten S (2007) Cellular and subcellular localization of Huntingtin [corrected] aggregates in the brain of a rat transgenic for Huntington disease. J Comp Neurol 501:716–730. CrossRef Medline
Pouladi MA, Xie Y, Skotte NH, Ehrnhoefer DE, Graham RK, Kim JE, Bissada N, Yang XW, Paganetti P, Friedlander RM, Leavitt BR, Hayden MR (2010) Full-length huntingtin levels modulate body weight by influencing insulin-like growth factor 1 expression. Hum Mol Genet 19:1528–1538. CrossRef Medline
Pouladi MA, Stanek LM, Xie Y, Franciosi S, Southwell AL, Deng Y, Butland S, Zhang W, Cheng SH, Shihabuddin LS, Hayden MR (2012) Marked differences in neurochemistry and aggregates despite similar behavioural and neuropathological features of Huntington disease in the full-length BACHD and YAC128 mice. Hum Mol Genet 21:2219–2232. CrossRef Medline
Reiner A, Albin RL, Anderson KD, D'Amato CJ, Penney JB, Young AB (1988) Differential loss of striatal projection neurons in Huntington disease. Proc Natl Acad Sci U S A 85:5733–5737. Medline
Rodriguiz RM, Wetsel WC (2006) Assessments of cognitive deficits in mutant mice, Chap 5 (Levin ED, Buccafusco JJ, eds). Boca Raton, FL: CRC.
Seto-Ohshima A, Emson PC, Lawson E, Mountjoy CQ, Carrasco LH (1988) Loss of matrix calcium-binding protein-containing neurons in Huntington's disease. Lancet 1:1252–1255. CrossRef Medline
Stine OC, Pleasant N, Franz ML, Abbott MH, Folstein SE, Ross CA (1993) Correlation between the onset age of Huntington's disease and length of the trinucleotide repeat in IT-15. Hum Mol Genet 2:1547–1549. Medline
Tecott LH, Nestler EJ (2004) Neurobehavioral assessment in the information age. Nat Neurosci 7:462–466. CrossRef Medline
The Huntington's Disease Collaborative Research Group (1993) A novel gene containing a trinucleotide repeat that is expanded and unstable on Huntington's disease chromosomes. Cell 72:971–983. CrossRef Medline
Toutain PL, Ferran A, Bousquet-Melou A (2010) Species differences in pharmacokinetics and pharmacodynamics. Handb Exp Pharmacol 19–48. CrossRef Medline
van Oostrom JC, Maguire RP, Verschuuren-Bemelmans CC, Veenma-van der Duin L, Pruim J, Roos RA, Leenders KL (2005) Striatal dopamine D2 receptors, metabolism, and volume in preclinical Huntington disease. Neurology 65:941–943. CrossRef Medline
Van Raamsdonk JM, Gibson WT, Pearson J, Murphy Z, Lu G, Leavitt BR, Hayden MR (2006) Body weight is modulated by levels of full-length huntingtin. Hum Mol Genet 15:1513–1523. CrossRef Medline
von Hörsten S, Schmitt I, Nguyen HP, Holzmann C, Schmidt T, Walther T, Bader M, Pabst R, Kobbe P, Krotova J, Stiller D, Kask A, Vaarmann A, Rothke-Hartlieb S, Schulz JB, Grasshoff U, Bauer I, Vieira-Saecker AM, Paul M, Jones L, et al (2003) Transgenic rat model of Huntington's disease. Hum Mol Genet 12:617–624. CrossRef Medline
Vonsattel JP, DiFiglia M (1998) Huntington disease. J Neuropathol Exp Neurol 57:369–384. Medline
Vonsattel JP, Myers RH, Stevens TJ, Ferrante RJ, Bird ED, Richardson EP Jr (1985) Neuropathological classification of Huntington's disease. J Neuropathol Exp Neurol 44:559–577. Medline
Wang CE, Tydlacka S, Orr AL, Yang SH, Graham RK, Hayden MR, Li S, Chan AW, Li XJ (2008) Accumulation of N-terminal mutant huntingtin in mouse and monkey models implicated as a pathogenic mechanism in Huntington's disease. Hum Mol Genet 17:2738–2751. CrossRef Medline
Winkler C, Gil JM, Araújo IM, Riess O, Skripuletz T, von Hörsten S, Petersén A (2006) Normal sensitivity to excitotoxicity in a transgenic Huntington's disease rat. Brain Res Bull 69:306–310. CrossRef Medline
Yamada M, Iwatsubo T, Mizuno Y, Mochizuki H (2004) Overexpression of alpha-synuclein in rat substantia nigra results in loss of dopaminergic neurons, phosphorylation of alpha-synuclein and activation of caspase-9: resemblance to pathogenetic changes in Parkinson's disease. J Neurochem 91:451–461. CrossRef Medline
Yang XW, Model P, Heintz N (1997) Homologous recombination based modification in Escherichia coli and germline transmission in transgenic mice of a bacterial artificial chromosome. Nat Biotechnol 15:859–865. CrossRef Medline

Genes, Brain and Behavior
Official publication of the International Behavioural and Neural Genetics Society

Genes, Brain and Behavior (2014) ***13:*** *305–321* doi: 10.1111/gbb.12093

A behavioral comparison of the common laboratory rat strains Lister Hooded, Lewis, Fischer 344 and Wistar in an automated homecage system

L. E. Clemens[†,‡], E. K. H. Jansson[†,‡], E. Portal[†,‡], O. Riess[†,‡] and H. P. Nguyen[†,‡,*]

[†] *Institute of Medical Genetics and Applied Genomics, and*
[‡] *Centre for Rare Diseases, University of Tuebingen, Tuebingen, Germany*
**Corresponding author: H. P. Nguyen, Institute of Medical Genetics and Applied Genomics, Centre for Rare Diseases, University of Tuebingen, Tuebingen 72076, Germany. E-mail: hoa.nguyen@med.uni-tuebingen.de*

Behavioral characterization is an important part of establishing novel animal models, but classical behavioral tests struggle to reveal conclusive results due to problems with both reproducibility and validity. On the contrary, automated homecage observations are believed to produce robust outcomes that relate more to natural animal behavior. However, information on the behavior of background strains from such observations, which could provide important reference material, is rare. For this reason, we compared the behavior of the commonly used Lister Hooded, Lewis, Fischer 344 and Wistar rats during 70 h of exposure to an automated homecage system at 2, 4 and 6 months of age. We found considerable strain differences in metabolic parameters, novelty-induced and baseline activity-related behavior as well as differences in the development of these parameters with age. The results are discussed in terms of advantages and disadvantages of the system compared to classical behavioral tests, as well as the system's ability to recreate common findings in literature.

Keywords: Activity, animal welfare, automated homecage system, exploratory behavior, fischer 344, lewis, lister hooded, metabolism, PhenoMaster, rat strains, social isolation, standardization, strain differences, wistar

Received 4 July 2013, revised 18 September 2013 and 7 October 2013, accepted for publication 7 October 2013

Detailed behavioral characterization is an important part of establishing novel animal models in a variety of research fields. For this purpose, the animals' behavior is often assessed in a range of classical behavioral tests such as the open field, elevated plus maze or the Morris water maze. Although this enables the comparison with previously published results, there are known problems with classical tests of this kind. Many classical tests are based on running brief trials in non-homecage setups. This enables the researcher to control many aspects of the test, but it has also been suggested that the results mainly reflect the confrontation with an unfamiliar situation and environment rather than a baseline behavior (Tecott & Nestler 2004). Furthermore, many classical tests rely on non-standardized equipment and protocols. This low level of standardization can lead to difficulties in replication and generalization of study outcomes (Chesler *et al.* 2002; Izídio *et al.* 2005; Mandillo *et al.* 2008; Tucci *et al.* 2006; van der Staay & Steckler 2002; Vyssotski *et al.* 2002; Wahlsten *et al.* 2003a,b). Finally, classical tests involve direct handling of the animals by the experimenter prior to the test session. The experimenter has been shown to influence the outcome of some tests (Chesler *et al.* 2002) and might be considered a source of variation, even if equipment and procedures are carefully standardized (Crabbe *et al.* 1999).

Automated homecage observation has been promoted to provide a good solution to the problems stated above (Kas & van Ree 2004) and a series of systems for computer-based acquisition of homecage activities of rats and mice as well as analysis software are in use (e.g. de Visser *et al.* 2006; Goulding *et al.* 2008; Hübener *et al.* 2011; Jhuang *et al.* 2010; Voikar *et al.* 2010; Zarringhalam *et al.* 2012). Such systems offer a standardized testing environment, while also allowing standardized customization to run specific protocols. As the animals are housed in a homecage-like environment, their behavior is thought to better reflect a natural state (de Visser *et al.* 2006; Tecott & Nestler 2004). In addition, as the measurements are highly computerized, behavioral data is gathered objectively. The systems are further able to measure a broad spectrum of behaviors including activity, food and water intake as well as cognitive aspects. Thus, a well-functioning automated homecage system could in theory be used for the complete behavioral characterization of an animal model. But there is currently a lack of literature on automated homecage behavior of background strains, in contrast to classical behavioral tests (e.g. Berton *et al.* 1997; Brooks *et al.* 2004, 2005; Richards *et al.* 2013; Wilhelm & Mitchell 2009). Studies that focus on the behavior of background strains constitute important reference material and can aid researchers in their choice of both background strain and behavioral test setup. Due to this, we conducted a study aimed at evaluating the practicality and sensitivity of an automated behavioral testing system in differentiating the four commonly used rat strains Lister Hooded, Lewis, Fischer 344 and Wistar.

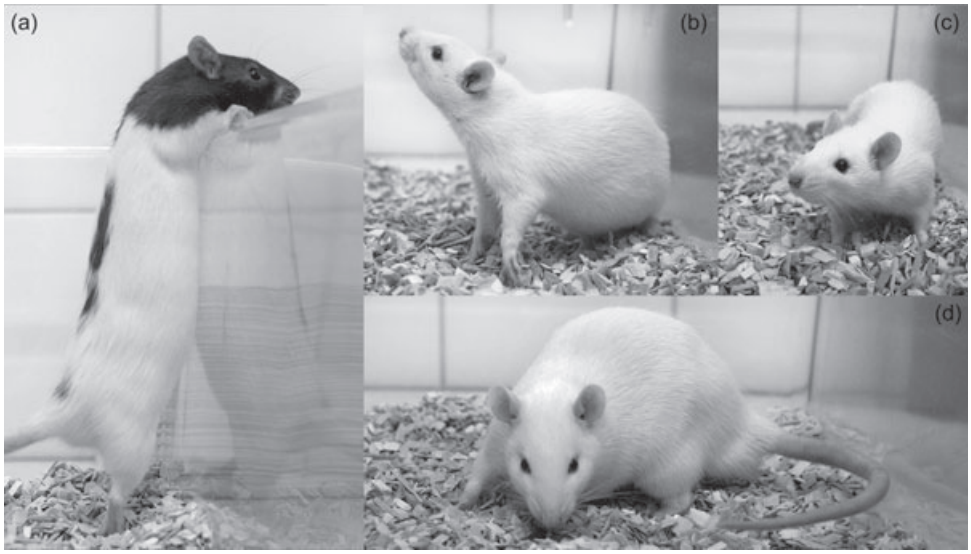

Figure 1: Rat strains. For our study, the common laboratory rat strains Lister Hooded (a), Lewis (b), Fischer 344 (c) and Wistar (d) were obtained from Charles River Laboratories, Germany.

Animals and methods

Rats

We used 12 male rats from each of the four strains Lister Hooded (Crl:LIS), Lewis (Crl:LEW), Fischer 344 (F344/DuCrl) and Wistar (Crl:WI) (Fig. 1). The animals were obtained from Charles River (Charles River Laboratories, Research Models and Services, Germany GmbH, Sulzfeld, Germany) at the age of 4 weeks.

All experiments were approved by the commission for animal experiments at the *Regierungspräsidium Tübingen* in accordance with the guidelines of the German animal welfare act. The behavioral experiments were all carried out by the same experimenter, trained and experienced in laboratory animal research.

Housing conditions followed the recommendations of the European Union (ETS 123 A). The environmental conditions in the housing room were kept at 21–23°C ambient temperature, 55 ± 10% humidity and a 12/12 h light/dark cycle with lights off at 1400 h and lights on at 0200 h. Animals were kept in groups of four animals of the same genotype in type IV autoclavable plastic cages with high lid (38 × 55 cm wide, 24.5 cm high) (Fig. 2b). Cages contained 1000 g of autoclaved wooden bedding and were cleaned twice a week. Food (ssniff V1534-000 standard rat chow) and tap water were delivered *ad libitum*.

The animals were weighed and inspected weekly in order to assess their general health status and accustom them to human handling. The rats were given 2 weeks of acclimatization in our animal facility prior to the start of the experiments.

Measurements

Body weight

The animals were weighed weekly using a kitchen balance (accuracy was ±1 g) in order to record body weight development.

Body weight and body length at 10 weeks of age

At 10 weeks of age, we measured the body length and body weight of the animals in order to assess differences in body size. For the measurement of body length, the animals were briefly anesthetized with isoflurane and the length from the tip of the nose to the base of the tail (head-trunk length) was measured, using a ruler (accuracy was ±0.1 cm).

Automated homecage observations

Measurements were carried out at the age of 2, 4 and 6 months. For this purpose, the animals were transferred to the testing cages, where they were housed individually. The measurements started 40 ± 5 min before the onset of the dark phase. Data were collected in 20-min sample intervals during a total of 70 h of recording. The animals were assigned to one of the 12 cages in a pseudo-randomized manner. Each run of 12 animals contained four animals from three strains, respectively, so that each time point comprised four runs and lasted 12 days in total.

During testing, the animals were inspected daily for proper food and water intake and the system for accurate functioning.

In between runs, the system was cleaned thoroughly and new bedding as well as fresh water and food pellets was supplied.

Automated homecage system

For the behavioral analysis, we used the automated homecage system PHENOMASTER (PM) (TSE Systems, Bad Homburg, Germany) (Fig. 2a) with the software version 1.3.7 (2010). Our customized setup included a set of 12 homecage-like autoclavable plastic cages (37.5 × 48 cm wide, 20 cm high) plus a reference cage. All cages were equipped with a frame with infrared light beams for activity detection (Actimot2, 302020 series). Our setup further included metabolic units for measurement of water and food consumption (Drink/Feed, 259980 series) and the analysis of respiratory gases (CaloSys, 994600 series). For this purpose, the cages contained a drinking bottle and a food basket suspended from high-precision sensors. The cages were further sealed with an airtight plastic lid containing an input tube for air supply and an output tube for gas sampling.

Activity

Infrared light beams were installed at two different height levels around the cage and spaced1.5 cm apart from each other. The lower set was located at a height of 3 cm (2-month-old animals) or 4 cm (4- and 6-month-old animals) to measure activity in the *x*- and *y*-axis (*locomotion*). A higher set of beams at 8 cm (2-month-old animals) or 12 cm (4- and 6-month-old animals) detected activity in the *z*-axis (*rearing*). The height of the beams was initially evaluated using Sprague Dawley rats. We decided on having fixed setups for all rat strains, but differing between the ages, since the biggest difference

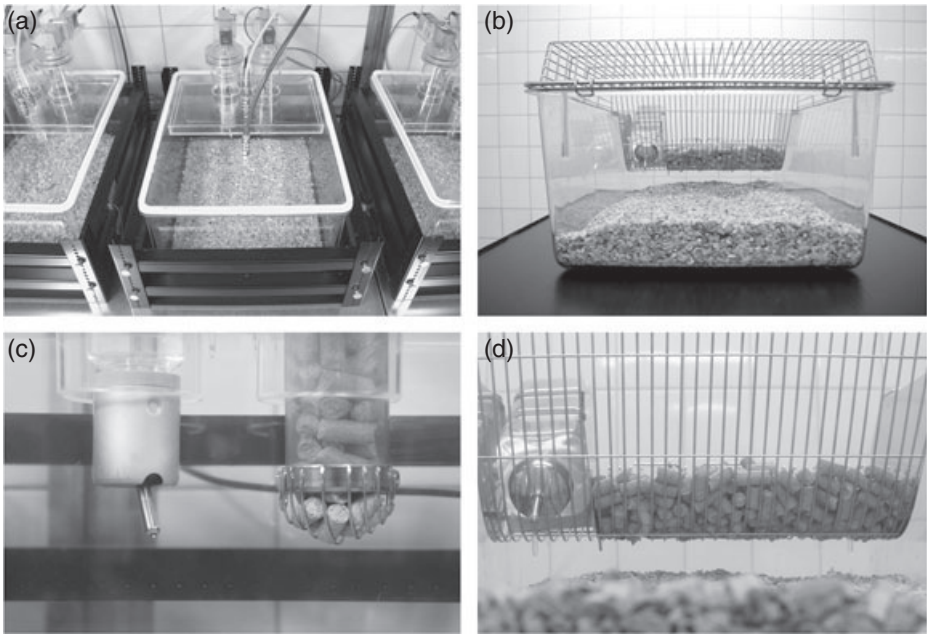

Figure 2: PHENOMASTER metabolic cage and homecage. The homecage-like PM cages (a, c) differ from standard housing cages for rats (b, d). Differences concern cage dimensions, constitution of the lid and presentation of water and food. The PM cages have a moderately smaller floor area and a considerably lower height due to their flat lids. The airtight lids of the metabolic cages further isolate the inner of the cage to a larger degree from the surroundings. Water and food bins are hanging lower than in the homecage and the food baskets offer a substantially smaller surface for feeding.

in size did not occur between strains but between the youngsters at 2 months of age and the adult animals at 4 and 6 months of age. For more accurate measurements, the amount of bedding placed in the cages during the measurements was set to 250 g.

Locomotion was further subdivided into overall ambulatory activity (*ambulation*), *fine movements* and ambulatory activity in the periphery and the center of the cage. The system recorded a movement as ambulatory activity, when three or more different light beams were disrupted consecutively, whereas it was recorded as fine movement, when adjacent light beams were disrupted alternately. In order to analyze activity in specific parts of the cage, a peripheral and central area was defined with the software. The center accounted for the inner 16.5×12 cm ($198\,cm^2$) of the total 48×37.5 cm ($1800\,cm^2$). From this, we calculated the ratio of periphery to center activity (*per/cen*). The sensors were scanning activity with a rate of 100 Hz and were programmed to a refractory period of 0.8 seconds. The activity measurement relied on the number of beam breaks (*counts*) made by the animal. It is important to note that as each animal was always breaking several light beams at a given time, the number of beam breaks was much higher than the number of events underlying the recorded counts. The software also provided the option to count all beam breaks detected at a time as one single event. However, having it counted as only one event would disregard the quality (i.e. duration, intensity) of the event. For this reason, we decided to have all beam breaks counted separately.

Novelty-induced behavior

Analysis of activity levels during the first hour served as a measure for the behavioral response to a novel environment. Ambulatory and rearing activity were regarded as exploratory-related behaviors, whereas *per/cen* was considered to be anxiety-related.

Water and food intake

Water and food intake was measured with high-precision sensors. The water bottle contained 150 ml of fresh tap water and the food basket was loaded with 150 g of ssniff V1534-000 standard rat chow. Water and food intake are given in ml per hour (ml/h) and g per hour (g/h) or in ml per hour per kg of body weight (ml/h/kg) and g per hour per kg of body weight (g/h/kg), respectively in order to account for body weight differences between the individuals and the groups. Containers were filled before the start of the measurement and the amount of food and water was sufficient for the 70-h measurement. A minimum consumption of 0.01 ml of water and 0.01 g of food as well as a maximum consumption of 0.1 ml of water and 0.1 g of food were set in order to exclude values caused through spillage or leaky bottles.

Indirect calorimetry

In order to obtain data on respiratory gases, the PM cages were fed with room air via an in-bound tube with a constant air flow of 1.8 l per min. Every 20 min, an out-bound tube conducted 0.25 l of sample air first to a cooling unit, where the sample was dried, and further to the measuring unit containing O_2- and CO_2-electrodes. Subtraction of the respective gas pressure from that of a reference cage revealed the VO_2 and VCO_2 (carbon dioxide production). From these values, the software further calculated the respiratory quotient ($RQ = VCO_2/VO_2$). VO_2 and RQ are only presented for the age of 2 and 4 months, since a problem with the gas calibration occurred at the last age.

Data analysis

Processing of raw data with R statistics

The PM software itself includes an analysis and graphing function. However, in order to conduct a detailed statistical analysis, we decided to export the data table and use additional software.

By means of R statistics (R: A Language and Environment for Statistical Computing, R Development Core Team, R Foundation for Statistical Computing, Vienna, Austria, 2011, ISBN 3-900051-07-0,

http://www.R-project.org), we developed a script that sorted the data from all recordings according to animal number (1–12), study groups (strains) and time point of measurement (age 2, 4 or 6 months). From this, it created either an hourly sum of the respective parameter (ambulation, fine movements, rearing, per/cen) or an hourly mean (VO_2, RQ). The data were separated into a habituation period (first hour of measurement) and a long-term measurement of additional 69 h. For this 3-day observation period, the script further calculated mean values for light and dark phase separately.

Graphs

Graphs were created using GraphPad Prism 6.00. Illustrations on the basis of photographic images were arranged with Adobe Photoshop CS3.

Statistical analysis

For statistical evaluation of the development of the four strains over time, we performed analyses of variance (ANOVA). Body size at 10 weeks of age was compared with a one-way ANOVA (ANOVA1) and Tukey's multiple comparison test (Tukey post-test), while all the parameters obtained at more than one age were analyzed with a repeated measurements two-way ANOVA (rmANOVA2). Differences between strains in these parameters were investigated using Tukey post-test. Age effects were analyzed with Dunnett's multiple comparisons test (Dunnett post-test), comparing the second and third measurement to the first one. Body weight gain before and during the PM were compared using Sidak's multiple comparisons test (Sidak's post-test).

Statistics were performed with GRAPHPAD PRISM version 6.00 for Windows (GRAPHPAD Software, San Diego, CA, USA, http://www.graphpad.com). Values given in the text refer to group mean and standard deviation. The α-level was set to 0.05. Respective *P*-values are given in the text or in the figures down to a level of 0.0001 as reported by GRAPHPAD PRISM.

We excluded a total of 88 of 1968 data sets from the two-way analysis of variance (ambulation (7/384), rearing (9/384), per/cen activity (20/96), fine movements (2/144), drinking (16/144), feeding (10/144)), because 88 out of the 5904 individual values in these data sets were most likely erroneous due to hardware problems. For activity, we found the system to register very high counts for some animals. This might have been due to bedding that was shifted around by the animal. We only excluded values that were more than three times higher than the group mean and did not occur repeated times for the same animal. Measuring per/cen activity revealed a special problem: After the initial exploration of the test cages, we found some of the rats to lie down and sleep, usually in a corner of the cage, leading to low ambulatory activity counts in general and even lower or zero activity counts for the central area. Thus, such an animal displayed either a very high per/cen value or no value at all in case of zero center activity. For food and water intake, it was detected that drinking bottles were leaking from time to time (leading to unreasonably high values for water intake) and the food got stuck in the food basket, so that the animal was not able to reach it (leading to unreasonably low values for food intake). For activity, drinking and feeding, the values that were excluded are spread equally among groups and testing cages, suggesting that they are not the result of a systematic error or having a biological meaning. In contrary, the number of values that had to be taken out of the analysis of per/cen activity differ between rat strains and are clearly related to a difference in behavior.

Results

Because of the large amount of data obtained, values for group means and standard deviation as well as most of the statistics obtained from post hoc analysis are listed in separate tables. Only the statistical results from the ANOVAs are given in the text, together with the description of the results.

Part I: morphology

The four rat strains showed morphological differences. Lister rats were the only pigmented rats, while the others were albinos (Fig. 1).

Furthermore, there were differences in body weight and size (Fig. 3). At 10 weeks of age, body weight was highest in Wistar followed by Lister and Lewis rats and Fischer rats weighed least ($F_{3,44} = 106.3$, $P < 0.0001$, Fig. 3a).

Similarly, body length at 10 weeks of age was highest in Wistar rats, Lister and Lewis rats were medium sized and Fischer rats were smallest ($F_{3,44} = 57.12$, $P < 0.0001$, Fig. 3b).

Further investigation showed that significant differences between strains remained after relating body weight to body length ($F_{3,44} = 79.93$, $P < 0.0001$, Fig. 3c).

The weekly measurements of body weight revealed significant differences between the strains ($F_{3,44} = 178.6$, $P < 0.0001$) as well as a significant development of body weight with age ($F_{72,1056} = 70.68$, $P < 0.0001$, Fig. 3d,e). Wistar rats weighed significantly more than the other strains at any time throughout the study, while the three other strains did not differ at young ages. From 8 weeks on, Fischer rats showed a significantly lower body weight than all other strains. At the age of 25 weeks, Lister rats separated from Lewis rats, with Lister being the heavier ones. The exact level of significance for these comparisons varied with age (Fig. 3e).

Part II: behavioral observations in the automated homecages

As described above, we used an automatic homecage system to monitor activity and metabolism in Lister, Wistar, Lewis and Fischer rats. The rats' behavior was assessed during a 70-h experiment. The first hour of observation was used to investigate the response to the novel environment, while activity-related and metabolic parameters were followed for another 69 h. Group means and standard deviation are given in Table 1 for activity-related parameters and in Table 2 for metabolic parameters; *P*-values from post-testing are displayed in Tables 3 (activity) and 4 (metabolism).

Novelty-induced behavior

The first hour of measurement

Ambulatory and rearing activity as well as the activity in the periphery relative to the activity in the center of the cage (per/cen) were analyzed during the first hour in the PM. Rats showed a similar change in behavior during the first hour at all ages (Fig. S1). For convenience, only the results from 2-month-old rats are displayed and discussed here (Fig. 4, Table 1).

Ambulation decreased significantly from the first to the second 20-min interval and remained at a low level during the third 20-min interval in most animals ($F_{2,88} = 47.95$, $P < 0.0001$, Fig. 4).

Rearing activity also decreased within the first hour of observation ($F_{2,88} = 15.14$, $P < 0.0001$). However, this only reached statistical significance for Lewis and Fischer rats, although Lister and Wistar rats also showed a gradual decline

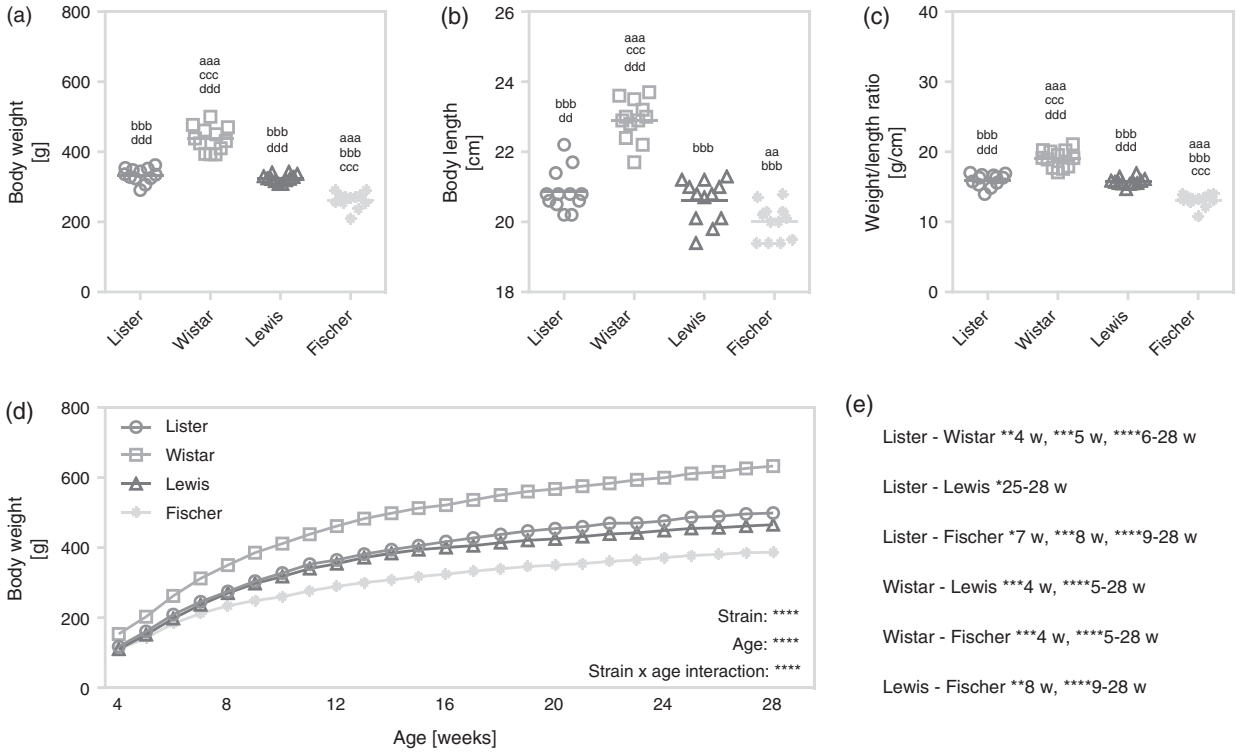

Figure 3: Body size. Body length (a), body weight (b) and weight/length ratio at 10 weeks of age (c) as well as body weight development from 4 to 28 weeks of age (d) are shown for the four rat strains Lister, Wistar, Lewis and Fischer. The (a)–(c) show values for individual animals with the group mean being indicated by a horizontal line. (d) Displays weekly mean and standard deviation for the four rat strains. Statistics: ANOVA1 (a–c), *P*-values for group comparison are given as lowercase letters with one letter = $P < 0.05$, two letters = $P < 0.01$, three letters = $P < 0.001$, four letters = $P < 0.0001$ and meaning a = significantly different from Lister rats, b = significantly different from Wistar rats, c = significantly different from Lewis rats and d = significantly different from Fischer rats. rmANOVA2 (d–e), *P*-values for strain, time and strain*time differences (d) and *P*-values for the Bonferroni post-test (e) are given as asterisks with $*P < 0.05$, $**P < 0.01$, $***P < 0.001$ and $****P < 0.0001$. For the group comparison (e), the additional information on the time point, the *P*-value was observed for is added (w = weeks).

in rearing (Fig. 4). Per/cen activity did not significantly change during the first hour (Fig. 4).

It appeared that some animals decreased their ambulatory and rearing activity to a very low level or even to zero within the first hour. Observations by the experimenter revealed that a part of the animals went to sleep after an initial exploration of the cage. While no animals were found with a particularly low activity during the first 20 min, the number of animals with a low level of activity differed between strains during the following 40 min. The frequency was highest for Lewis rats (9/12), followed by Fischer (6/12) and Wistar rats (4/12 animals), and did not occur at all in Lister rats.

Strain differences during the first 20 min of testing

Because of the decrease in activity, which can be regarded as habituation effect, only the behavior during the initial 20 min was used to assess differences in novelty-induced behavior between the different rat strains.

Novelty-induced ambulation and rearing decreased with age (ambulation: $F_{2,88} = 35.72$, $P < 0.0001$; rearing: $F_{2,88} = 39.60$, $P < 0.0001$, Fig. 5). Age also influenced per/cen activity, with older rats showing a lower per/cen ratio ($F_{2,86} = 25.59$, $P < 0.0001$, Fig. 5). Significant strain differences were observed in all three parameters (ambulation: $F_{3,44} = 4.571$, $P = 0.0072$; rearing: $F_{3,44} = 5.407$, $P = 0.0030$; per/cen: $F_{3,43} = 7.224$, $P = 0.0005$). Post hoc analysis indicated that these were mainly based on Lister rats differing from the other strains in ambulatory and rearing activity, while Lewis rats differed in per/cen activity. Lister rats showed higher mean values for ambulatory activity compared to the other strains at all ages. Significant differences were found between Lister and Wistar rats at 2 months ($P < 0.05$) and between Lister and Fischer rats at 6 months of age ($P < 0.01$, Fig. 5). Lister rats also appeared to rear more than the other strains at 4 and 6 months of age, reaching statistical significance compared to Fischer rats at 4 months ($P < 0.01$) and compared to Lewis ($P < 0.05$) and Fischer rats ($P < 0.05$) at 6 months of age (Fig. 5). Significant differences in per/cen activity occurred between Lister and Lewis rats at 2 months ($P < 0.05$) and 4 months of age ($P < 0.05$), whereat Lewis rats showed highest mean values

Table 1: Activity-related parameters

	Ambulation (counts)	Rearing (counts)	Per/cen (ratio)	Ambulation (counts)			Fine movements (counts)			Rearing (counts)		
	Adaptation	Adaptation	Adaptation	Light phase	Dark phase	Total	Light phase	Dark phase	Total	Light phase	Dark phase	Total
2 months												
Lister	6067 ± 1848	1505 ± 664	2.6 ± 1.1	74250 ± 20949	104312 ± 25916	178562 ± 16940	29255 ± 6879	37499 ± 5775	66754 ± 5063	23909 ± 8329	36585 ± 22287	60493 ± 27512
Wistar	4405 ± 1655	1436 ± 606	2.9 ± 1.7	41526 ± 8306	163442 ± 21241	204968 ± 23441	17985 ± 2838	49467 ± 4163	67452 ± 5746	16567 ± 6733	69395 ± 16341	85962 ± 22151
Lewis	5274 ± 1769	1275 ± 576	3.8 ± 1.5	49421 ± 9078	135590 ± 12322	185011 ± 16064	20256 ± 3945	44544 ± 3364	64800 ± 5066	15400 ± 4958	45015 ± 9688	59268 ± 12931
Fischer	5222 ± 2513	1281 ± 576	2.8 ± 1.0	45449 ± 6853	155415 ± 27776	201017 ± 25892	19897 ± 2003	47076 ± 5385	67158 ± 5206	11377 ± 3970	43666 ± 7447	55552 ± 8310
4 months												
Lister	5434 ± 1051	1296 ± 168	1.7 ± 0.4	38307 ± 6078	105400 ± 12112	143707 ± 10181	17703 ± 2310	37133 ± 3131	54836 ± 3468	6117 ± 2150	20052 ± 4263	26170 ± 5872
Wistar	4366 ± 1659	905 ± 342	1.9 ± 0.4	26447 ± 3910	113585 ± 22812	140032 ± 24979	15803 ± 3214	38652 ± 4407	54455 ± 6515	3375 ± 1769	18324 ± 5894	21699 ± 7476
Lewis	3504 ± 808	918 ± 486	2.7 ± 0.8	27868 ± 4817	104299 ± 8356	132167 ± 9227	15118 ± 3157	37295 ± 2126	52413 ± 3572	4233 ± 3628	21436 ± 12323	22444 ± 8932
Fischer	4311 ± 1064	688 ± 218	2.0 ± 0.5	30310 ± 4152	115154 ± 27025	145270 ± 26648	16215 ± 3301	38533 ± 4653	54936 ± 5612	3266 ± 1376	17110 ± 6476	20375 ± 7383
6 months												
Lister	3612 ± 801	904 ± 180	1.6 ± 0.3	28095 ± 3604	78098 ± 7063	106193 ± 7138	15058 ± 2224	30271 ± 2469	45598 ± 3498	5416 ± 2829	18174 ± 7026	23589 ± 9477
Wistar	2796 ± 1433	740 ± 625	1.7 ± 0.5	18927 ± 2709	87040 ± 16662	105966 ± 17113	13821 ± 2248	32923 ± 3648	46328 ± 4575	3916 ± 3639	17944 ± 10232	21860 ± 13697
Lewis	2285 ± 904	473 ± 239	2.4 ± 0.9	24960 ± 3478	78695 ± 6529	103655 ± 6852	13685 ± 1649	30987 ± 2214	44996 ± 3457	4057 ± 2459	15352 ± 5386	19698 ± 7186
Fischer	3248 ± 799	410 ± 150	1.6 ± 0.3	28792 ± 6976	98357 ± 20191	126640 ± 22923	17422 ± 3847	34863 ± 3646	51288 ± 6647	3595 ± 2337	15122 ± 4731	18717 ± 6891

Group mean and standard deviation for rat strains in novelty-induced behavior as well as activity-related parameters during the three-day observation period are given for 2, 4 and 6 months of age.

for per/cen activity of all strains. However, we detected a very high individual variability in this parameter (Fig. 5).

3-Day observation of activity-related and metabolic parameters

Following the first hour of observation, the animals were monitored for an additional 69-h period. Ambulation, fine movements, rearing, water intake, food intake, VO_2 and RQ were assessed and analyzed for the overall three-day observation as well as for light and dark phase separately.

Circadian rhythm

Time series analysis indicated that all rats showed a circadian rhythm entrained by the 12/12 h dark/light cycle. In line with this, all four rat strains showed higher levels of ambulation, rearing, drinking, feeding, VO_2 and RQ during the dark phase compared to the light phase. Since the results were similar for all parameters at all ages, only the data for ambulation are displayed as an example (Figs. 6,S2).

Ambulatory activity

Total values for ambulation revealed moderate differences between the rat strains ($F_{3,43} = 3.680$, $P = 0.0191$), but showed a clear age effect, with older animals having a lower ambulatory activity ($F_{2,86} = 352.6$, $P < 0.0001$) as well as a significant strain difference in the influence of age on ambulation ($F_{6,86} = 3.226$, $P = 0.0066$, Fig. 7). Total ambulatory activity was highest in Wistar and Fischer rats at 2 months of age. No significant differences between strains were detected at 4 months of age, while Fischer rats were again most active at 6 months of age.

Separate analysis of light and dark phases revealed similar significant age effects as seen for the total observation period ($F_{2,88} = 172.1$, light phase: $P < 0.0001$; dark phase: $F_{2,86} = 147.5$, $P < 0.0001$) but showed highly significant strain effects (light phase: $F_{3,44} = 24.37$, $P < 0.0001$; dark phase: $F_{3,43} = 9.793$, $P < 0.0001$) as well as strain*age interactions (light phase: $F_{6,88} = 9.486$, $P < 0.0001$; dark phase: $F_{6,86} = 8.032$, $P < 0.0001$, Fig. 7). Strain differences were based to a large degree on Lister rats, being significantly more active during the light phase and in turn less active during the dark phase at 2 months and 4 months of age. Wistar rats on the other hand were least active during the light phase, becoming significantly different from Lister and Fischer rats at 6 months of age.

Fine movements

Analysis of the total amount of fine movements revealed minor differences between strains ($F_{3,43} = 3.401$, $P = 0.0260$, Fig. 7). Fine movements were also found to decrease with age in all strains ($F_{2,86} = 180.5$, $P < 0.0001$). The development over time did not differ between strains. Strain differences in fine movements resulted from an increased amount in Fischer rats at 6 months of age.

Analysis of the distribution of fine movements during the light and dark phase revealed more pronounced strain differences (light phase: $F_{3,44} = 13.89$, $P < 0.0001$;

Table 2: Metabolic parameters

	Body weight (g)		Water intake (ml)			Relative water intake (ml/kg)			Relative VO_2 (ml O_2/kg/h)		
	Before test	After test	Light phase	Dark phase	Total	Light phase	Dark phase	Total	Light phase	Dark phase	Total
2 months											
Lister	224 ± 15	231 ± 20	27.2 ± 7.8	34.1 ± 10.6	61.5 ± 6.4	42.9 ± 15.2	52.9 ± 14.7	95.7 ± 11.4	2058 ± 138	2136 ± 197	2097 ± 106
Wistar	293 ± 20	311 ± 18	12.4 ± 4.0	82.1 ± 12.8	93.9 ± 11.1	13.9 ± 4.7	93.8 ± 17.4	107.3 ± 16.2	1723 ± 114	2133 ± 154	1928 ± 130
Lewis	210 ± 28	226 ± 31	14.7 ± 7.3	54.6 ± 12.0	69.6 ± 11.2	24.7 ± 13.4	87.6 ± 13.3	113.1 ± 19.2	2108 ± 230	2339 ± 137	2224 ± 179
Fischer	195 ± 20	206 ± 18	7.0 ± 3.3	45.0 ± 7.2	52.1 ± 5.6	12.6 ± 7	77.3 ± 10.1	90.2 ± 11.9	1848 ± 189	2101 ± 124	1974 ± 150
4 months											
Lister	420 ± 11	413 ± 18	13.6 ± 3.0	57.6 ± 8.5	70.7 ± 7.0	11.0 ± 2.8	46.2 ± 6.3	57.0 ± 5.3	1165 ± 38	1442 ± 62	1304 ± 35
Wistar	520 ± 35	521 ± 34	12.7 ± 4.9	80.7 ± 15.8	92.0 ± 16.3	8.1 ± 2.9	51.8 ± 11.9	58.9 ± 12.1	1064 ± 55	1394 ± 72	1229 ± 60
Lewis	398 ± 21	402 ± 22	5.9 ± 3.2	61.8 ± 5.8	67.1 ± 6.5	4.9 ± 2.6	51.9 ± 4.8	56.5 ± 5	1203 ± 62	1525 ± 38	1364 ± 40
Fischer	324 ± 15	322 ± 12	5.6 ± 2.4	38.7 ± 6.8	44.5 ± 7.8	5.8 ± 2.6	40.3 ± 8	46.4 ± 9.2	1193 ± 67	1393 ± 66	1293 ± 59
6 months											
Lister	516 ± 12	505 ± 24	12.7 ± 3.7	49.8 ± 14.6	59.2 ± 9.2	8.4 ± 2.7	32.5 ± 8.7	39.0 ± 6.0	NA	NA	NA
Wistar	646 ± 50	637 ± 48	6.7 ± 4.7	65.1 ± 15.8	71.5 ± 15.2	3.3 ± 2.2	34.2 ± 10	37.5 ± 9.5	NA	NA	NA
Lewis	474 ± 25	475 ± 24	4.3 ± 2.3	53.4 ± 5.9	57.6 ± 5.3	3 ± 1.6	37.8 ± 4.7	40.7 ± 4.2	NA	NA	NA
Fischer	396 ± 15	387 ± 14	6.0 ± 2.8	32.3 ± 5.9	38.2 ± 5.2	5.1 ± 2.4	27.4 ± 5.3	32.4 ± 4.9	NA	NA	NA

	Weight gain (g/3d)		Food intake (g)			Relative food intake (g/kg)			RQ (ml O_2/kg/h)		
	Before test	During test	Light phase	Dark phase	Total	Light phase	Dark phase	Total	Light phase	Dark phase	Total
2 months											
Lister	19 ± 2	17 ± 3	30.5 ± 5.1	38.3 ± 7.5	68.7 ± 4.4	33.2 ± 8	81.5 ± 7.7	114.7 ± 11.5	0.85 ± 0.01	0.86 ± 0.01	0.86 ± 0.01
Wistar	21 ± 3	17 ± 7	18.8 ± 5.4	60.4 ± 9.8	79.2 ± 11.0	25.5 ± 5.7	67.2 ± 8.9	92.7 ± 9.8	0.80 ± 0.02	0.84 ± 0.01	0.82 ± 0.01
Lewis	18 ± 1	16 ± 3	21.9 ± 5.3	45.9 ± 8.3	67.8 ± 4.7	27.1 ± 7.2	89.4 ± 15.1	116.5 ± 13.8	0.83 ± 0.03	0.85 ± 0.04	0.84 ± 0.03
Fischer	14 ± 1	10 ± 4	12.8 ± 2.0	37.6 ± 4.0	50.8 ± 2.3	21.3 ± 4.3	56.7 ± 9	77.5 ± 8.8	0.83 ± 0.01	0.86 ± 0.01	0.84 ± 0.01
4 months											
Lister	10 ± 1	3 ± 4	20.7 ± 4.1	51.3 ± 4.6	72.0 ± 4.6	16.7 ± 3.6	41.3 ± 3.4	58 ± 4.1	0.81 ± 0.01	0.83 ± 0.01	0.82 ± 0.01
Wistar	11 ± 2	1 ± 6	22.5 ± 5.2	59.0 ± 5.8	81.4 ± 6.5	14.2 ± 2.7	37.7 ± 4.6	51.9 ± 3.6	0.74 ± 0.02	0.79 ± 0.02	0.77 ± 0.02
Lewis	9 ± 1	4 ± 4	16.8 ± 4.7	54.5 ± 5.0	71.4 ± 3.7	14.1 ± 3.8	46 ± 4.6	60.1 ± 2.8	0.80 ± 0.02	0.83 ± 0.02	0.81 ± 0.02
Fischer	5 ± 1	−2 ± 4	12.5 ± 3.1	32.8 ± 3.1	44.8 ± 3.2	12.8 ± 3.1	33.8 ± 3.6	46.2 ± 3.7	0.80 ± 0.02	0.83 ± 0.02	0.82 ± 0.01
6 months											
Lister	0 ± 1	−1 ± 3	19.3 ± 3.0	51.9 ± 5.2	71.1 ± 5.1	12.7 ± 2.1	34.1 ± 3.3	46.7 ± 3.5	NA	NA	NA
Wistar	3 ± 2	−10 ± 6	19.1 ± 6.5	53.1 ± 7.2	72.2 ± 8.5	9.8 ± 3	27.7 ± 4.9	37.5 ± 5.1	NA	NA	NA
Lewis	2 ± 1	2 ± 6	18.4 ± 4.2	53.6 ± 5.6	71.9 ± 5.8	13 ± 3	38.1 ± 5.5	51.1 ± 6.2	NA	NA	NA
Fischer	2 ± 1	−9 ± 4	11.5 ± 1.3	27.8 ± 2.4	39.5 ± 2.6	9.7 ± 1	23.4 ± 2.1	33.2 ± 2.2	NA	NA	NA

Group mean and standard deviation for rat strains in body weight before and after testing, body weight gain over 3 days before and after testing as well as metabolic parameters during the three-day observation period are given for 2, 4 and 6 months of age.

Table 3: Post-test results for activity-related parameters

	Ambulation (counts)	Rearing (counts)	Per/cen (ratio)	Ambulation (counts)			Fine movements (counts)			Rearing (counts)		
	2 months	4 months	6 months	2 months	4 months	6 months	2 months	4 months	6 months	2 months	4 months	6 months
Light												
Lister–Wistar	*	ns	ns	****	**	*	****	ns	ns	***	ns	ns
Lister–Lewis	ns	**	ns	****	*	ns	****	ns	ns	****	ns	ns
Lister–Fischer	ns	ns	ns	****	ns	ns	****	ns	ns	****	ns	ns
Wistar–Lewis	ns	ns	ns	ns	ns	ns	ns	ns	ns	ns	ns	ns
Wistar–Fischer	ns	ns	ns	ns	ns	*	ns	ns	ns	*	ns	ns
Lewis–Fischer	ns	ns	ns	ns	ns	ns	ns	ns	*	ns	ns	ns
Dark												
Lister–Wistar	ns	ns	ns	****	ns	ns	****	ns	ns	****	ns	ns
Lister–Lewis	ns	*	ns	***	ns	ns	***	ns	ns	ns	ns	ns
Lister–Fischer	**	*	ns	****	ns	ns	****	ns	*	ns	ns	ns
Wistar–Lewis	ns	ns	ns	**	ns	ns	*	ns	ns	****	ns	ns
Wistar–Fischer	ns	ns	ns	ns	ns	ns	ns	ns	ns	****	ns	ns
Lewis–Fischer	ns	ns	ns	ns	ns	ns	ns	ns	ns	ns	ns	ns
Total												
Lister–Wistar	ns	ns	ns	**	ns	ns	ns	ns	ns	****	ns	ns
Lister–Lewis	ns	ns	ns	ns	ns	ns	ns	ns	ns	ns	ns	ns
Lister–Fischer	ns	ns	ns	*	ns	*	ns	ns	*	ns	ns	ns
Wistar–Lewis	ns	ns	ns	*	ns	ns	ns	ns	ns	****	ns	ns
Wistar–Fischer	ns	ns	ns	ns	ns	*	ns	ns	ns	****	ns	ns
Lewis–Fischer	ns	ns	ns	ns	ns	*	ns	ns	*	ns	ns	ns

Significance levels from group comparisons for rat strains in novelty-induced behavior as well as activity-related parameters during the three-day observation period are given for 2, 4 and 6 months of age (*$P < .05$, **$P < .01$, ***$P < .001$, ***$P < .0001$).

Table 4: Post-test results for metabolic parameters

	Water intake (ml)			Relative water intake (ml/kg)			Relative VO_2 (ml O_2/kg/h)		Food intake (g)			Relative food intake (g/kg)			RQ (ml O_2/kg/h)	
	2 months	4 months	6 months	2 months	4 months	6 months	2 months	4 months	2 months	4 months	6 months	2 months	4 months	6 months	2 months	4 months
Light																
Lister–Wistar	****	ns	*	****	ns	ns	****	ns	****	ns	ns	***	ns	ns	****	****
Lister–Lewis	****	***	****	****	ns	ns	ns	ns	****	ns	ns	**	ns	ns	*	ns
Lister–Fischer	****	***	**	****	ns	ns	***	ns	****	***	***	****	ns	ns	*	ns
Wistar–Lewis	ns	**	ns	**	ns	ns	****	*	ns	*	ns	ns	ns	ns	**	****
Wistar–Fischer	*	**	ns	ns	ns	ns	ns	ns	**	****	***	ns	ns	ns	**	****
Lewis–Fischer	***	ns	ns	***	ns	ns	****	ns	****	ns	**	*	ns	ns	ns	ns
Dark																
Lister–Wistar	****	****	**	****	ns	ns	ns	ns	****	*	ns	****	ns	ns	ns	****
Lister–Lewis	****	ns	ns	****	ns	ns	****	ns	*	ns	ns	*	ns	ns	ns	ns
Lister–Fischer	ns	***	***	****	ns	ns	ns	ns	ns	****	****	****	ns	**	ns	ns
Wistar–Lewis	****	***	ns	ns	ns	ns	****	*	****	ns	ns	****	*	**	ns	***
Wistar–Fischer	****	****	****	**	ns	ns	ns	ns	****	****	****	**	ns	ns	*	****
Lewis–Fischer	ns	****	****	ns	*	ns	****	*	**	****	****	****	***	****	ns	ns
Total																
Lister–Wistar	****	****	*	ns	ns	ns	**	ns	***	**	ns	****	ns	*	****	****
Lister–Lewis	ns	ns	ns	***	ns	ns	*	ns	ns	ns	ns	ns	ns	ns	ns	ns
Lister–Fischer	ns	****	****	ns	ns	ns	*	ns	****	****	****	****	**	***	ns	ns
Wistar–Lewis	****	****	**	ns	ns	ns	****	*	****	***	ns	****	*	***	*	****
Wistar–Fischer	****	****	****	**	ns	ns	ns	ns	****	****	****	****	ns	ns	**	****
Lewis–Fischer	***	****	****	****	ns	ns	****	ns	****	****	****	****	****	****	ns	ns

Significance levels from group comparisons for rat strains in metabolic parameters during the three-day observation period are given for 2, 4 and 6 months of age (*$P < .05$, **$P < .01$, ***$P < .001$, ***$P < .0001$).

RQ, respiratory quotient.

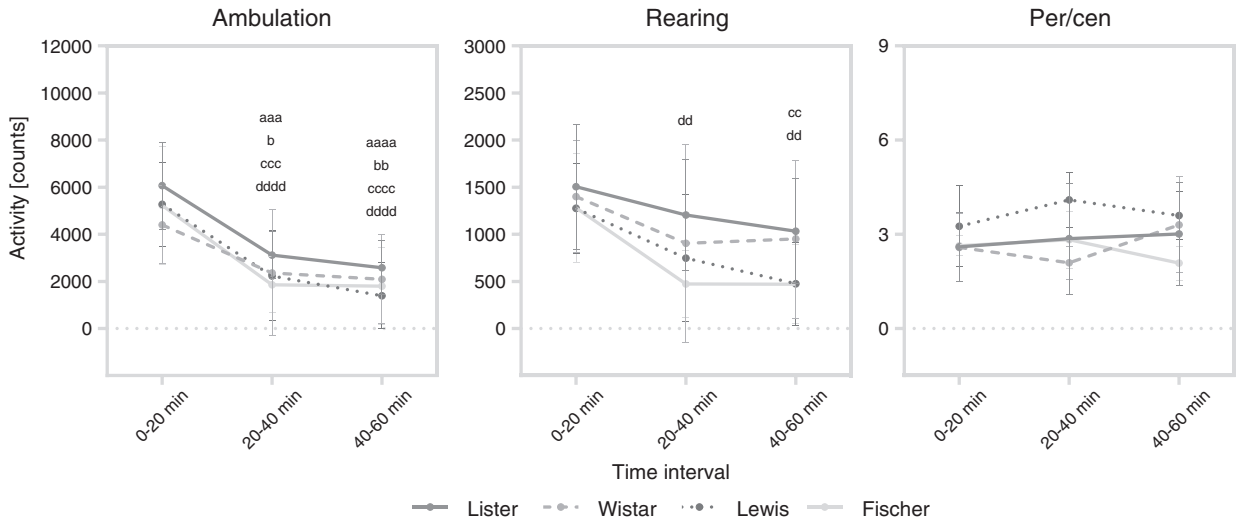

Figure 4: Habituation to the PHENOMASTER cages. Ambulation, rearing and per/cen activity are shown for Listar, Wistar, Lewis and Fischer rats during the first, second and third 20 min time interval in the PHENOMASTER. Values are group mean and standard deviation of the sum of beam break counts over 20 min. Statistics: rmANOVA2, Dunnett's post-test, *P*-values for the comparison of the second and third 20-min time interval with the first 20-min time interval are given as lowercase letters (a = Lister rats, b = Wistar rats, c = Lewis rats and d = Fischer rats) with one letter = $P < 0.05$, two letters = $P < 0.01$, three letters = $P < 0.001$ and four letters = $P < 0.0001$.

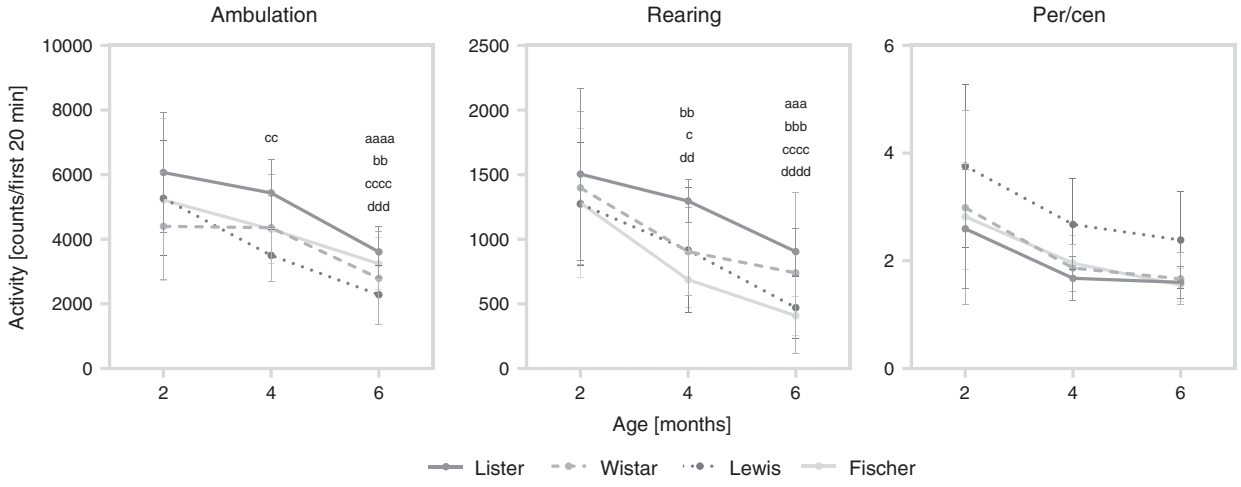

Figure 5: Novelty-induced behavior. Ambulation, rearing and per/cen activity are shown for Listar, Wistar, Lewis and Fischer rats at the age of 2, 4 and 6 months. Values are group mean and standard deviation of the sum of beam break counts over 20 min. Statistics: rmANOVA2, Dunnett's post-test, *P*-values for the comparison of activity at 4 and 6 months with the activity at 2 months of age are given as lowercase letters (a = Lister rats, b = Wistar rats, c = Lewis rats and d = Fischer rats) with one letter = $P < 0.05$, two letters = $P < 0.01$, three letters = $P < 0.001$ and four letters = $P < 0.0001$.

dark phase: $F_{3,43} = 10.85$, $P < 0.0001$) and a significant age effect (light phase: $F_{2,88} = 56.68$, $P < 0.0001$; dark phase: $F_{2,86} = 146.4$, $P < 0.0001$) as well as strain*age interaction (light phase: $F_{6,88} = 8.242$, $P < 0.0001$; dark phase: $F_{6,86} = 6.015$, $P < 0.0001$, Fig. 7). Lister rats showed significantly more fine movements during the light phase and less fine movements during the dark phase at 2 months of age. The increased total amount of fine movements found for Fischer rats at 6 months of age was based on a moderately higher number of counts during the dark phase and a more prominently higher number of counts during the light phase.

Rearing activity

Total rearing activity decreased with age ($F_{2,84} = 178.7$, $P < 0.0001$) and the strains developed differently over time ($F_{6,84} = 4.780$, $P < 0.0001$) (Fig. 7). Strain differences were present ($F_{3,42} = 4.239$, $P = 0.0028$), but appeared only at 2 months of age according to post-test results. At that

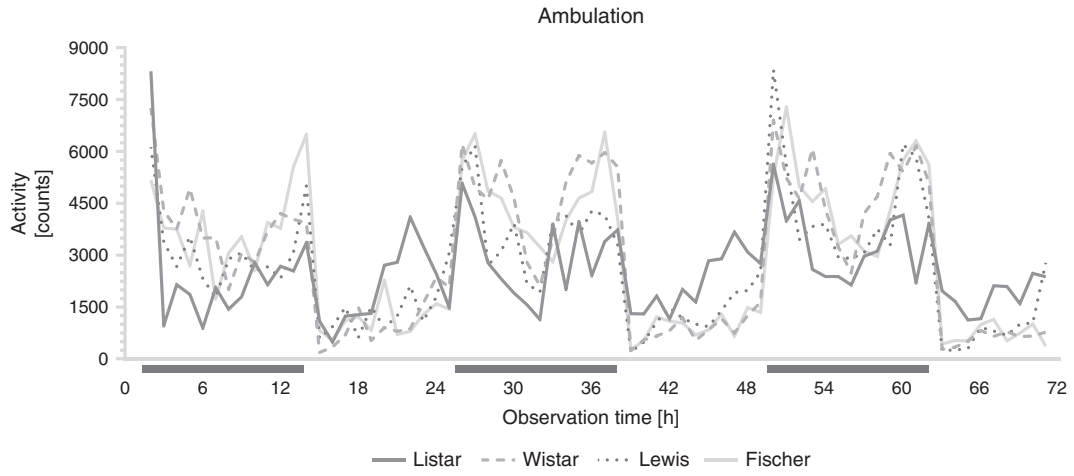

Figure 6: Ambulatory activity over the three observation days. Ambulatory activity is displayed as sum of counts per hour over the 70-h observation period at 2 months of age. Each point represents the group mean of Lister, Wistar, Lewis and Fischer rats. Error bars are not shown in order to enable a better visual comparison. The dark phase is indicated by the black bars below the *x*-axis.

age, Wistar rats reared in total significantly more than the other rats.

Looking at light and dark phase also revealed significant differences between strains at 2 months of age (light phase: $F_{3,42} = 12.09$, $P < 0.0001$; dark phase: $F_{3,43} = 5.626$, $P = 0.0002$) as well as a significant age effect (light phase: $F_{2,84} = 131.7$, $P < 0.0001$; dark phase: $F_{2,86} = 148.2$, $P < 0.0001$) as well as strain*age interaction (light phase: $F_{6,84} = 3.848$, $P = 0.0019$; dark phase: $F_{6,86} = 8.497$, $P < 0.0001$, Fig. 7). The higher total amount of rearing found for Wistar rats at 2 months of age, was based on a significantly higher rearing activity during the dark phase. Similar as it was found for ambulation and fine movements, Lister rats reared more than the other strains during the light phase at 2 months of age. Fischer rats reared least during the light phase.

Water intake

Total water intake differed significantly between strains at each age ($F_{3,37} = 48.83$, $P < 0.0001$) (Fig. 8). It further developed differently over time in the three rat strains ($F_{6,74} = 5.626$, $P < 0.0001$) with Wistar, Lewis and Fischer rats showing a decrease in water consumption from 2 to 6 months of age (mean difference in water intake between 2 and 6 months Wistar: 22.4 ml, $P < 0.0001$; Lewis: 11.9 ml, $P > 0.001$; Fischer 13.9 ml, $P < 0.0001$), while Lister rats increased their water consumption from 2 to 4 months of age (mean difference in water intake between 2 and 4 months: −9.1 ml, $P < 0.01$). Strain differences in the overall amount of water consumed during the 3-day experiment reflected the differences in body size of the animals. In total, Wistar rats drank significantly more than the other strains at all ages. Lister and Lewis rats did not differ in their overall water intake and Fischer rats drank least at any time.

The amount of water consumed during the light and dark phase was also found to differ significantly between strains (light phase: $F_{3,37} = 33.10$, $P < 0.0001$; dark phase: $F_{3,37} = 33.86$, $P < 0.0001$) with a significant effect of age (light phase: $F_{2,74} = 45.78$, $P < 0.0001$; dark phase: $F_{2,74} = 15.46$, $P < 0.0001$) and a significant strain*age interaction (light phase: $F_{6,74} = 9.520$, $P < 0.0001$; dark phase: $F_{6,74} = 11.94$, $P < 0.0001$, Fig. 8). The strain differences in total water intake were mostly recapitulated in the results for dark phase water intake. During the light phase, Lister rats had the highest water intake at all ages and Wistar rats drank more than Lewis and Fischer rats at 4 months of age.

Total water intake relative to body weight [ml/kg] decreased with age in all strains ($F_{2,74} = 653.4$, $P < 0.0001$), but also showed differences in the exact development over time between the strains ($F_{6,74} = 3.475$, $P = 0.0044$, Fig. 8). Strain differences in relative water intake resulted from differences at 2 months of age ($F_{3,37} = 6.165$, $P = 0.0017$). At that age, Lewis and Wistar rats consumed most, while Fischer rats consumed least.

Relative water intake during light and dark phase both decreased with age in all strains (light phase: $F_{2,82} = 111.5$, $P < 0.0001$; dark phase: $F_{2,76} = 363.8$, $P < 0.0001$), but not in a similar manner (light phase: $F_{6,82} = 13.78$, $P < 0.0001$; dark phase: $F_{6,76} = 16.91$, $P < 0.0001$, Fig. 8). Strain differences were found at 2 months only (light phase: $F_{3,41} = 22.48$, $P < 0.0001$; dark phase: $F_{3,38} = 10.66$, $P < 0.0001$) with Lister and Lewis rats consuming significantly more water relative to body weight than Wistar rats, which in turn consumed more than Fischer rats during the light phase. During the dark phase, Lister rats drank the least amount of water per kg body weight compared to the other strains.

Food intake

The three rat strains differed significantly in their total food consumption ($F_{3,40} = 194.6$, $P < 0.0001$, Fig. 8). The strains further developed differently with age ($F_{6,80} = 5.396$, $P < 0.0001$), with Wistar and Fischer rats decreasing their food consumption from 2 to 6 months of age (mean

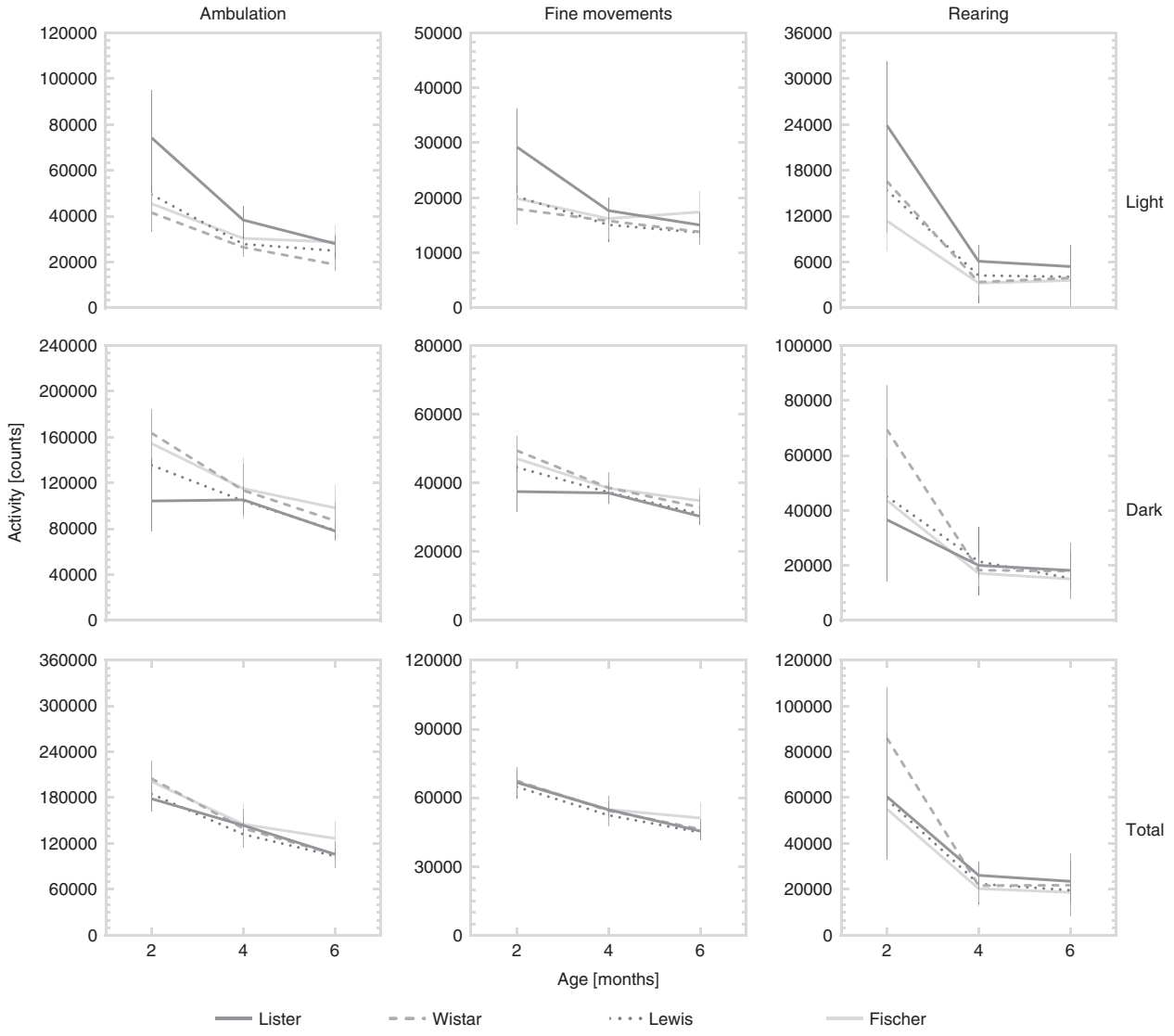

Figure 7: Light phase, dark phase and total amount of activity-related parameters. Ambulatory activity, fine movements and rearing activity are given per light phase, dark phase and total 70-h observation period for Lister, Wistar, Lewis and Fischer rats. Each data point represents group mean and standard deviation at 2 months, 4 months and 6 months of age.

difference in food intake between 2 and 6 months Wistar: 7.1 g, $P < 0.01$; Fischer 12.0 g, $P < 0.0001$), while Lister and Lewis rats kept a constant consumption level (age effect: $F_{2,80} = 5.502$, $P = 0.0036$). Strain differences in food intake resembled body weight to a lesser degree than water intake: At 2 months of age, the results for food intake were in accordance with body weight, with Wistar rats eating most, Fischer rats eating least and Lister and Lewis rats eating the same amount of food during the 3-day observation period. At 4 and 6 months of age though, the difference between Wistar, Lister and Lewis rats disappeared due to the drop in food intake in Wistar rats.

Significant strain differences appeared as well when looking at light and dark phases separately (light phase: $F_{3,40} = 33.73$, $P < 0.0001$; dark phase: $F_{3,41} = 77.85$, $P < 0.0001$) with a significant effect of age on food intake (light phase: $F_{2,80} = 10.05$, $P = 0.0001$; dark phase: $F_{2,82} = 6.121$, $P = 0.0033$) and a significantly different development of the strains with age (light phase: $F_{6,80} = 6.431$, $P < 0.0001$; dark phase: $F_{6,82} = 13.85$, $P < 0.0001$, Fig. 8). As it was found for water intake, food intake during the dark phase was reflecting differences in total food consumption, while during the light phase differences between groups were smaller and were based on Lister rats eating most at 2 months of age and Fischer rats eating least at all ages.

Food intake relative to body weight (g/kg) decreased with age in all strains ($F_{2,80} = 1077$, $P < 0.0001$) showing a significant strain*age interaction ($F_{6,80} = 13.20$, $P < 0.0001$,

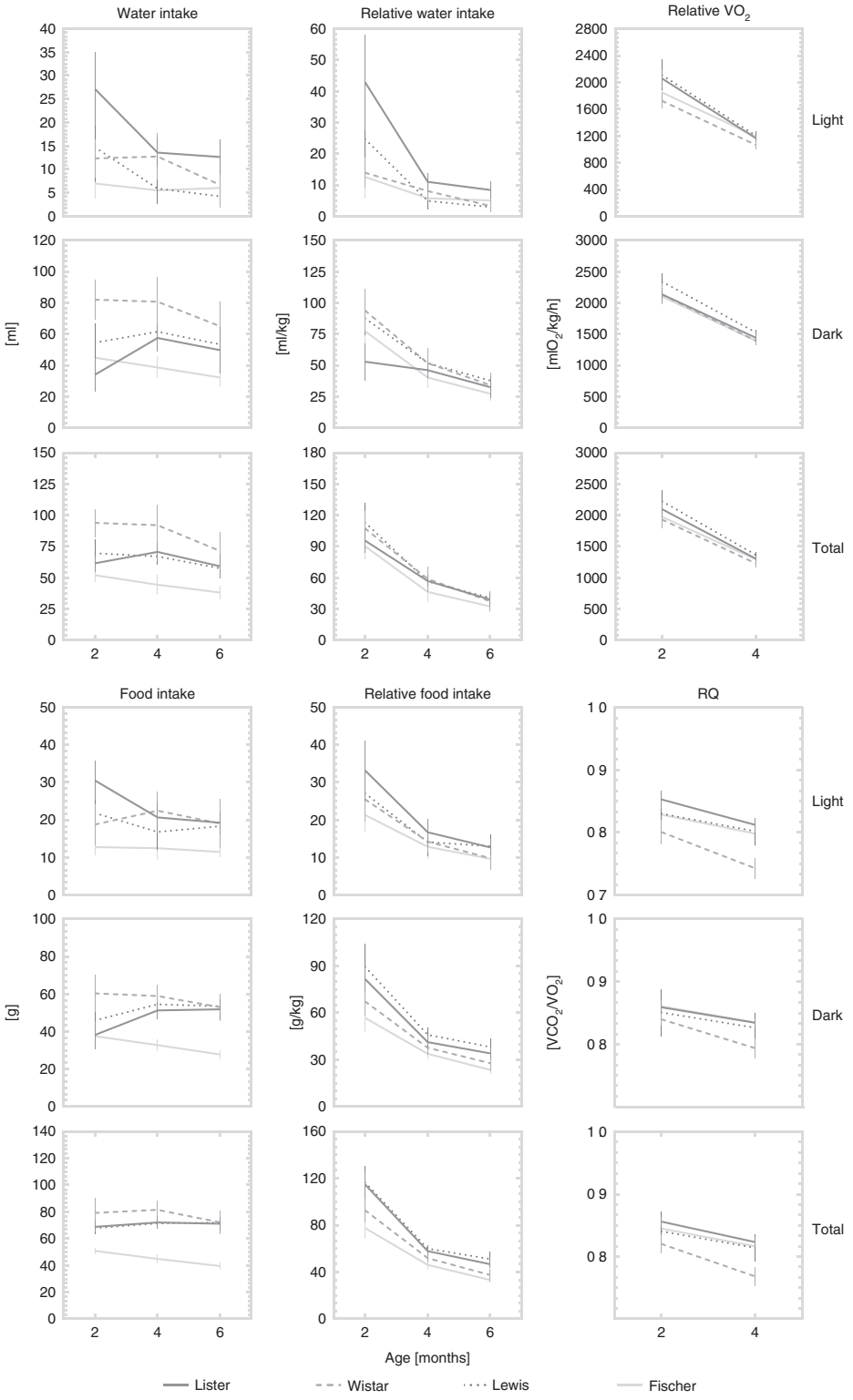

Figure 8: Light phase, dark phase and total amount of metabolic parameters. Absolute water intake in ml, relative water intake in ml per kg of body weight, absolute food intake in g, relative food intake in g per kg of body weight, relative oxygen consumption in ml per kg of body weight per hour and respiratory quotient are given per light phase, dark phase and total 70-h observation period for Lister, Wistar, Lewis and Fischer rats. Each data point represents group mean and standard deviation at 2 months, 4 months and 6 months of age.

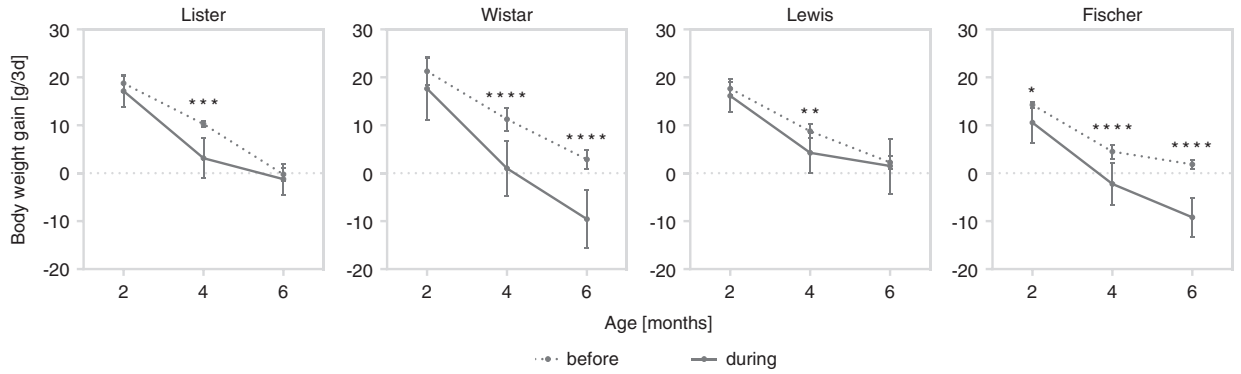

Figure 9: Body weight development over 3 days measured before and during the experiment. We calculated the average weight gain over 3 days measured one week before the experiment and compared it to the weight gain during the 3 days while exposed to the automated homecage system in Lister, Wistar, Lewis and Fischer rats. Values represent group mean and standard deviation. Statistics: rmANOVA2, Sidak's multiple comparison test, *P*-values are given as asterisks with $*P < 0.05$, $**P < 0.01$, $***P < 0.001$ and $****P < 0.0001$.

Fig. 8). Lister and Lewis rats had a higher food intake relative to body weight compared to Wistar rats at all ages ($F_{3,40} = 49.98$, $P < 0.0001$) and Wistar rats ate more than Fischer rats at 2 months of age.

The decrease in the relative amount of food intake (light phase: $F_{2,80} = 259.2$, $P < 0.0001$; dark phase: $F_{2,82} = 812.5$, $P < 0.0001$) as well as the difference in strain*age interaction was also found for both light and dark phase (light phase: $F_{6,80} = 4.425$, $P = 0.0007$, dark phase: $F_{2,82} = 10.63$, $P < 0.0001$, Fig. 8). At 2 months of age, Lister rats showed the highest relative food consumption during the light phase, in accordance with their absolute amount of food intake; at the same age, Lewis rats consumed more food than all other strains, followed by Lister rats, while Fischer rats ate least. Differences were less pronounced at older ages, but mean values of Lister and particularly Lewis rats remained above Wistar and Fischer rats.

VO_2

The relative hourly consumption of oxygen (ml O_2/kg/h) showed significant strain differences ($F_{3,44} = 16.72$, $P < 0.0001$; Fig. 8), a significant decrease of VO_2 relative to body weight with age ($F_{1,44} = 1277$, $P < 0.0001$) and a significant strain* age interaction ($F_{3,44} = 3.876$, $P < 0.0152$). Strain differences comprised a higher metabolic rate of Lewis over Lister rats and in turn Lister over Wistar and Fischer rats at 2 months of age. At 4 months of age, metabolic rates converged, leaving only Lewis rats at a slightly higher level.

Strain differences (light phase: $F_{3,44} = 20.16$, $P < 0.0001$; dark phase: $F_{3,44} = 12.68$, $P < 0.0001$), age effect (light phase: $F_{1,44} = 831.9$, $P < 0.0001$; dark phase: $F_{1,44} = 1752$, $P < 0.0001$) and strain*age interaction (light phase: $F_{3,44} = 6.73$, $P < 0.0008$; dark phase: $F_{3,44} = 2.304$, $P = 0.0900$) were also found for light and dark phase separately and were mainly based on differences at 2 months of age (Fig. 8). The higher VO_2 of Lister rats resulted from an increase during the light phase, while Lewis rats showed high VO_2 levels during both light and dark phase.

Respiratory quotient

Strains differed significantly in their mean RQ during the experiment ($F_{3,44} = 23.82$, $P < 0.0001$), based on Wistar rats having a significantly lower RQ compared to all other strains (Fig. 8). Respiratory quotient further decreased with age in all strains ($F_{1,44} = 172.1$, $P < 0.0001$), but in a moderately different manner ($F_{3,44} = 4.8914$, $P < 0.0051$).

Strain differences in RQ were also found during the light ($F_{3,44} = 34.13$, $P < 0.0001$) and dark phase ($F_{3,44} = 10.46$, $P < 0.0001$) and were consistent with the differences observed for food intake (Fig. 8). Lister rats had a significantly higher RQ during the light phase, while the RQ was significantly reduced in Wistar rats during both light and dark phase compared to the other strains. The decrease of RQ with age was also present for light ($F_{1,44} = 144.3$, $P < 0.0001$) and dark phase ($F_{1,44} = 98.61$, $P < 0.0001$) with a moderate difference in strain*age interaction (light phase: $F_{3,44} = 4.214$, $P < 0.0105$; dark phase $F_{3,44} = 2.984$, $P < 0.0413$).

Weight gain before and during the experiment

A comparison of the average weight gain one week prior to the experiment with the weight gain during the experiment revealed a significant drop in body weight gain during the experiment in Wistar and Fischer rats (Wistar: $F_{1,22} = 32.76$; $P < 0.0001$; Fischer: $F_{1,22} = 41.74$; $P < 0.0001$; Fig. 9). Lister and Lewis rats seemed to be less affected in their weight gain during the experiment, but showed a significantly decreased weight gain at least at 4 months of age (Lister: $F_{1,18} = 17.25$; $P = 0.0006$; Lewis: $F_{1,22} = 8.671$; $P < 0.0075$).

Discussion

The PhenoMaster system

Automated homecage systems are of particular interest for the behavioral phenotyping of laboratory animals, as these systems are believed to provide more robust and valid

measurements of behavior compared to classical tests. Our study provides basic data on the behavior of four commonly used rat strains in an automated homecage system and reveals some important aspects to consider when using such a system.

The PHENOMASTER system as replacement for other tests

The PM software offers the measurement of activity in specific parts of the cage. In order to investigate, if these measurements could provide a valid replacement for an open field (OF) test, we measured ambulatory, rearing and per/cen activity during the first 60 min of testing. The drop in ambulation and rearing after the first 20 min indicates that the animals initially explored and later habituated to the test cage in a similar fashion as it would be expected in an OF (Daenen *et al.* 2001; Hoy *et al.* 1999; Simon *et al.* 1994; Thiel *et al.* 1999). Habituation behavior was also found in a characterization study of a mouse model using both OF and PM (Painsipp *et al.* 2008). In contrast to ambulation and rearing, per/cen activity remained constant throughout the first hour of measurement. Although there are indications of habituation effects on similar parameters in the OF (Fonio *et al.* 2012; Ossenkopp *et al.* 1994; Simon *et al.* 1994; Thiel *et al.* 1999), it is at the moment unclear how the PM results would relate to those, as the smaller size of the cages and the presence of food and water baskets could affect the rats' tendency for thigmotaxis (Eilam 2003; Russell & Williams 1973).

The PHENOMASTER as a homecage

A large part of the promotion of automated behavioral testing systems such as the PM focuses on their homecage-like aspects. It is believed that testing animals in a known environment reduces stress and offers results that better represent natural behavior (de Visser *et al.* 2006; Lipp *et al.* 2005; Tecott & Nestler 2004). However, the PM system differs notably from the typical homecage environment in our animal facilities. The most profound difference is the demand of single housing. Housing the animals individually is usually avoided because of ethical considerations, but also because it is known to influence performance in behavioral tests (reviewed in Hall 1998; Lukkes *et al.* 2009). Other aspects concern the cage setup itself. The airtight lids used in our setup are lower than the lids of the actual homecages and might therefore restrain rearing in old or big rats. Further, the lids likely create different acoustic and olfactory conditions compared to the homecages. Finally, food and water is not provided in the same way as in a typical homecage. It might be tempting to neglect these differences and consider the conditions close enough to the normal homecage. However, our measurements suggest that the rats experience some form of stress during testing as indicated by the drop in weight gain. Since this is a general phenomenon we observe with both mouse and rat PM systems using different setups in different animal facilities, it is an important issue for further evaluation. Indeed, it is known from metabolic cages, where the animals are also transferred to a different cage setup and isolated for the duration of the test, that these conditions are stressful to mice and rats (Gil *et al.* 1999; Kalliokoski *et al.* 2013). From the current study, it cannot be concluded whether the stress experienced during the PM experiment is a result of the testing conditions per se or rather due to the change in housing conditions. Thus it is possible that keeping the rats in the PM system constantly, or adapting the homecages to better approximate the PM setup, might avoid a stress response. However, as either option would include long-term social isolation, obtained data would most likely not reflect the natural behavior of a social animal. In this regard, it might be better to work with other automated homecage systems like the commercially available PhenoTyper (Noldus Information Technology, Wageningen, The Netherlands) or IntelliCage (NewBehavior AG, Zurich, Switzerland), which allow the assessment of group-housed animals.

Comparison of four common background rat strains

Novelty-induced behavior

The first 20 min of exposure to the PM cages could constitute a replacement at least for the activity parameter of an OF. Our results indicate that Lister rats are generally more active in terms of total ambulation and rearing counts. These findings might reflect a general trait among pigmented rats, suggesting that they are exploratory rather than anxious when exposed to a new environment (Broersen & Uylings 1999; Onaivi *et al.* 1992; Ramos *et al.* 1997; Rex *et al.* 1996; van der Staay *et al.* 1996, 2009; Weiss *et al.* 2000). Although post hoc analysis did not reveal significant strain differences, per/cen ratio indicated that Lewis rats had a stronger preference for sticking to the periphery of the PM cages. However, Lewis rats also showed the steepest decline in ambulatory activity and the highest number of animals with almost no ambulatory and rearing activity after the initial 20 min. Thus, we conclude that the high per/cen ratio might have resulted rather from a reduced exploratory activity than from increased anxiety, again pointing to difficulties in using the PM for the assessment of anxiety parameters. Accordingly, Lewis rats have previously been found to be less explorative (Rex *et al.* 1996) and either more or equally anxious compared to Fischer rats (Chaouloff *et al.* 1995; van der Staay *et al.* 2009). However, it is important to note that different anxiety tests are known to reveal different phenotypes and comparisons to classical anxiety tests might at this time be premature. A more thorough investigation of the per/cen measurement and potential anxiogenic factors of the PM system must be made to provide better understanding of which studies it can be expected to replicate.

3-Day observation period

The data obtained from each 3-day test period were divided into light phase, dark phase and total activity. The total values for ambulation, fine movement and rearing did not reveal any consistent differences between the rat strains. However, when analyzing light and dark phase separately, it became apparent that Lister rats were more active in all three parameters during the day. Furthermore, they showed the least amount of activity during the night. This finding is in line with a comparative study on behavioral pharmacology, revealing a higher diurnal and lower nocturnal homecage

locomotor activity during a 24-h observation in Lister Hooded compared to Sprague Dawley and Wistar rats (McDermott & Kelly 2008). As the total level of activity was largely similar between Lister rats and the other strains, this indicates that Lister rats have a different circadian rhythm of activity.

Drinking and feeding differed significantly between the rat strains, and absolute values seemed to recapitulate differences in body size. However, looking at food and water intake relative to body weight revealed that Wistar and Fischer rats ate less than the others. Comparing weight gain before and during testing further showed that Wistar and Fischer rats did not grow properly during PM exposure. Accordingly, oxygen consumption, and even more meaningful respiratory quotient, was lower in Wistar rats compared to the other strains, pointing to inappropriate food supply. Lewis rats had the highest metabolic rate and showed the least effect on body weight gain during the test, indicating them to be least affected by the testing conditions. This idea is supported by literature on Lewis rats being less susceptible to stress due to physiological alterations (Chaouloff *et al.* 1995; Dhabhar *et al.* 1993). Lister rats once again showed higher diurnal activity in food and water intake and consistently in oxygen consumption and RQ, which further reinforces the differences seen in their activity pattern.

Summary notes

Automated homecage observation has been promoted as a powerful tool to study animal behavior. The essential advantage lies in the possibility to assess behavioral parameters over long periods of time, which in turn enables analysis across circadian phases as well as separate analysis of both novelty-induced and baseline homecage behavior.

In this study, data on the behavior of wild type rat strains was collected with the commercially available automated homecage system PHENOMASTER. The first hour of observation revealed strain differences in novelty-induced behavior, which recreate common findings in literature. In a following 3-day observation period, further differences in circadian activities were identified, which offer new results that can be a useful reference for further studies.

It has to be noted that although the system allowed for minimal animal handling, a range of other stressors appeared to be present. Thus, further investigation is needed in order to establish optimal protocols for behavioral assessment, and to better judge the potential of the PM system.

References

Berton, O., De, P.M., Chaouloff, F., Ramos, A. & Mormède, P. (1997) A multiple-test study of anxiety-related behaviours in six inbred rat strains. *Behav Brain Res* **85**, 57–69.

Broersen, L.M. & Uylings, H.B.M. (1999) Visual attention task performance in Wistar and Lister Hooded rats: response inhibition deficits after medial prefrontal cortex lesions. *Neuroscience* **94**, 47–57.

Brooks, S.P., Pask, T., Jones, L. & Dunnett, S.B. (2004) Behavioural profiles of inbred mouse strains used as transgenic backgrounds. I: motor tests. *Genes. Brain Behav* **3**, 206–215.

Brooks, S.P., Pask, T., Jones, L. & Dunnett, S.B. (2005) Behavioural profiles of inbred mouse strains used as transgenic backgrounds. II: cognitive tests. Genes. *Brain Behav* **4**, 307–317.

Chaouloff, F., Kulikov, A., Sarrieau, A., Castanon, N., Mormède, P. & De, P.M. (1995) Male Fischer 344 and Lewis rats display differences in locomotor reactivity, but not in anxiety-related behaviours: relationship with the hippocampal serotonergic system. *Brain Res* **693**, 169–178.

Chesler, E.J., Wilson, S.G., Lariviere, W.R., Rodriguez-Zas, S.L. & Mogil, J.S. (2002) Identification and ranking of genetic and laboratory environment factors influencing a behavioral trait, thermal nociception, via computational analysis of a large data archive. *Neurosci Biobehav Rev* **26**, 907–923.

Crabbe, J.C., Wahlsten, D. & Dudek, B.C. (1999) Genetics of mouse behavior: interactions with laboratory environment. *Science* **284**, 1670–1672.

Daenen, E.W., Van der Heyden, J.A., Kruse, C.G., Wolterink, G. & Van Ree, J.M. (2001) Adaptation and habituation to an open field and responses to various stressful events in animals with neonatal lesions in the amygdala or ventral hippocampus. *Brain Res* **918**, 153–165.

De Visser, L., Van den Bos, R., Kuurman, W.W., Kas, M.J.H. & Spruijt, B.M. (2006) Novel approach to the behavioural characterization of inbred mice: automated home cage observations. *Genes Brain Behav* **5**, 458–466.

Dhabhar, F.S., Mcewen, B.S. & Spencer, R.L. (1993) Stress response, adrenal steroid receptor levels and corticosteroid-binding globulin levels--a comparison between Sprague–Dawley, Fischer 344 and Lewis rats. *Brain Res* **616**, 89–98.

Eilam, D. (2003) Open-field behavior withstands drastic changes in arena size. *Behav Brain Res* **142**, 53–62.

Fonio, E., Benjamini, Y. & Golani, I. (2012) Short and long term measures of anxiety exhibit opposite results. *PLoS One* **7**, e48414.

Gil, M.C., Aguirre, J.A., Lemoine, A.P., Segura, E.T., Barontini, M. & Armando, I. (1999) Influence of age on stress responses to metabolic cage housing in rats. *Cell Mol Neurobiol* **19**, 625–633.

Goulding, E.H., Schenk, A.K., Juneja, P., MacKay, A.W., Wade, J.M. & Tecott, L.H. (2008) A robust automated system elucidates mouse home cage behavioral structure. *Proc Natl Acad Sci USA* **30**, 20575–20582.

Hall, F.S. (1998) Social deprivation of neonatal, adolescent, and adult rats has distinct neurochemical and behavioral consequences. *Crit Rev Neurobiol* **12**, 129–162.

Hoy, J.B., Cody, B.A., Karlix, J.L., Schmidt, C.J., Tebbett, I.R., Toffollo, S., Van Haaren, F. & Wielbo, D. (1999) Pyridostigmine bromide alters locomotion and thigmotaxis of rats: gender effects. *Pharmacol Biochem Behav* **63**, 401–406.

Hübener, J., Vauti, F., Funke, C., Wolburg, H., Ye, Y., Schmidt, T., Wolburg-Buchholz, K., Schmitt, I., Gardyan, A., Driessen, S., Arnold, H.H., Nguyen, H.P. & Riess, O. (2011) N-terminal ataxin-3 causes neurological symptoms with inclusions, endoplasmic reticulum stress and ribosomal dislocation. *Brain* **134**, 1925–1942.

Izídio, G.S., Lopes, D.M., Spricigo, L. & Ramos, A. (2005) Common variations in the pretest environment influence genotypic comparisons in models of anxiety. *Genes Brain Behav* **4**, 412–419.

Jhuang, H., Garrote, E., Mutch, J., Yu, X., Khilnani, V., Poggio, T., Steele, A.D. & Serre, T. (2010) Automated home-cage behavioural phenotyping of mice. *Nat Commun* **7**, 1–68.

Kalliokoski, O., Jacobsen, K.R., Darusman, H.S., Henriksen, T., Weimann, A., Poulsen, H.E., Hau, J. & Abelson, K.S.P. (2013) Mice do not habituate to metabolism cage housing – a three week study of male BALB/c mice. *PLoS One* **8**, e58460.

Kas, M.J. & van Ree, J.M. (2004) Dissecting complex behaviours in the post-genomic era. *Trends Neurosci* **27**, 366–369.

Lipp, H., Litvin, O., Galsworthy, M., Vyssotski, D.L., Vyssotski, A.L., Zinn, P. & Rau, A.E. (2005) Automated behavioral analysis of mice using INTELLICAGE: inter-laboratory comparisons and validation with exploratory behavior and spatial learning. In Noldus, L.P.J.J., Grieco, F., Loijens, L.W.S. & Zimmerman, H.P. (eds), *Proceedings of Measuring Behavior 2005. Fifth International Conference on Methods and Techniques in Behavioral Research*. Noldus Information Technology, Wageningen, Netherlands, pp. 66–69.

Lukkes, J.L., Watt, M.J., Lowry, C.A. & Forster, G.L. (2009) Consequences of post-weaning social isolation on anxiety behavior and related neural circuits in rodents. *Front Behav Neurosci* **3**, 18.
Mandillo, S., Tucci, V., Hölter, S.M. *et al.* (2008) Reliability, robustness, and reproducibility in mouse behavioral phenotyping: a cross-laboratory study. *Physiol Genomics* **34**, 243–255.
McDermott, C. & Kelly, J.P. (2008) Comparison of the behavioural pharmacology of the Lister-Hooded with 2 commonly utilised albino rat strains. *Prog Neuropsychopharmacol Biol Psychiatry* **32**, 1816–1823.
Onaivi, E.S., Maguire, P.A., Tsai, N.F., Davies, M.F. & Loew, G.H. (1992) Comparison of behavioral and central BDZ binding profile in three rat lines. *Pharmacol Biochem Behav* **43**, 825–831.
Ossenkopp, K.-P., Sorenson, L. & Mazmanian, D.S. (1994) Factor analysis of open-field behavior in the rat (Rattus norvegicus): application of the three-way PARAFAC model to a longitudinal data set. *Behav Process* **31**, 129–144.
Painsipp, E., Wultsch, T., Edelsbrunner, M.E., Tasan, R.O., Singewald, N., Herzog, H. & Holzer, P. (2008) Reduced anxiety-like and depression-related behavior in neuropeptide Y Y4 receptor knockout mice. *Genes Brain Behav* **7**, 532–542.
Ramos, A., Berton, O., Mormède, P. & Chaouloff, F. (1997) A multiple-test study of anxiety-related behaviours in six inbred rat strains. *Behav Brain Res* **85**, 57–69.
Rex, A., Sondern, U., Voigt, J.P., Franck, S. & Fink, H. (1996) Strain differences in fear-motivated behavior of rats. *Pharmacol Biochem Behav* **54**, 107–111.
Richards, J.B., Lloyd, D.R., Kuehlewind, B., Militello, L., Paredez, M., Solberg Woods, L. & Palmer, A.A. (2013) Strong genetic influence on measures of behavioral-regulation among inbred rat strains. *Genes Brain Behav* **12**, 490–502.
Russell, P.A. & Williams, D.I. (1973) Effects of repeated testing on rats' locomotor activity in the open-field. *Anim Behav* **21**, 109–111.
Simon, P., Dupuis, R. & Costentin, J. (1994) Thigmotaxis as an index of anxiety in mice. Influence of dopaminergic transmissions. *Behav Brain Res* **61**, 59–64.
Tecott, L.H. & Nestler, E.J. (2004) Neurobehavioral assessment in the information age. *Nat Neurosci* **7**, 462–466.
Thiel, C.M., Müller, C.P., Huston, J.P. & Schwarting, R.K. (1999) High versus low reactivity to a novel environment: behavioural, pharmacological and neurochemical assessments. *Neuroscience* **93**, 243–251.
Tucci, V., Lad, H.V., Parker, A., Polley, S., Brown, S.D.M. & Nolan, P.M. (2006) Gene-environment interactions differentially affect mouse strain behavioral parameters. *Mamm Genome* **17**, 1113–1120.
Van der Staay, F.J. & Steckler, T. (2002) The fallacy of behavioral phenotyping without standardisation. *Genes Brain Behav* **1**, 9–13.
Van der Staay, F.J., Blokland, A. & Ring, N. (1996) Behavioral differences between outbred Wistar, inbred Fischer 344, brown Norway, and hybrid Fischer 344 x brown Norway rats. *Physiol Behav* **60**, 97–109.
Van der Staay, F.J., Schuurman, T., Van Reenen, C.G. & Korte, S.M. (2009) Emotional reactivity and cognitive performance in aversively motivated tasks: a comparison between four rat strains. *Behav Brain Funct* **5**, 50.
Voikar, V., Colacicco, G., Gruber, O., Vannoni, E., Lipp, H.-P. & Wolfer, D.P. (2010) Conditioned response suppression in the IntelliCage: assessment of mouse strain differences and effects of hippocampal and striatal lesions on acquisition and retention of memory. *Behav Brain Res* **213**, 304–312.
Vyssotski, Alexei L., Omo, G.D., Poletaeva, I.I., Vyssotski, Dmitri L., Minichiello, L., Wolfer, D.P., Lipp, H.-P., Dell'Omo, G., Vyssotski, D.L. & Klein, R. (2002) Long-term monitoring of hippocampus-dependent behavior in naturalistic settings: mutant mice lacking neurotrophin receptor TrkB in the forebrain show spatial learning but impaired behavioral flexibility. *Hippocampus* **12**, 27–38.
Wahlsten, D., Metten, P., Phillips, T.J. *et al.* (2003a) Different data from different labs: lessons from studies of gene-environment interaction. *J Neurobiol* **54**, 283–311.
Wahlsten, D., Rustay, N.R., Metten, P. & Crabbe, John C. (2003b) In search of a better mouse test. *Trends Neurosci* **26**, 132–136.
Weiss, I.C., Di Iorio, L., Feldon, J., Domeney, A.M., Di, L. & Annette, M. (2000) Strain differences in the isolation-induced effects on prepulse inhibition of the acoustic startle response and on locomotor activity. *Behav Neurosci* **114**, 364–373.
Wilhelm, C.J. & Mitchell, S.H. (2009) Strain differences in delay discounting using inbred rats. *Genes Brain Behav* **8**, 426–434.
Zarringhalam, K., Ka, M., Kook, Y.-H., Terranova, J.I., Suh, Y., King, O.D. & Um, M. (2012) An open system for automatic home-cage behavioral analysis and its application to male and female mouse models of Huntington's disease. *Behav Brain Res* **229**, 216–225.

Acknowledgments

The study was supported through institutional funds of the Institute of Medical Genetics and Applied Genomics. None of the authors have a conflict of interest. The PHENOMASTER system was obtained from TSE as part of the RATstream project (EU-FP6-37846). However, the company was not involved in design or execution of the study and did not participate in data interpretation.

Supporting Information

Additional supporting information may be found in the online version of this article at the publisher's web-site:

Figure S1: Habituation to the PHENOMASTER cages. Ambulation, rearing and per/cen activity are shown for Lister, Wistar, Lewis and Fischer rats during the first, second and third 20-min time interval at 2, 4 and 6 months of age in the PHENOMASTER. Values are group mean and standard deviation of the sum of beam break counts over 20 min. Statistics: rmANOVA2, Dunnett's post-test, *P*-values for the comparison of the second and third 20 min time interval with the first 20 min time interval are given as lowercase letters with one letter = $P < 0.05$, two letters = $P < 0.01$, three letters = $P < 0.001$, four letters = $P < 0.0001$, and meaning a = significantly different from Lister rats, b = significantly different from Wistar rats, c = significantly different from Lewis rats and d = significantly different from Fischer rats.

Figure S2: Ambulatory activity over the 3 observation days. Ambulatory activity is displayed as sum of beam breaks per hour over the 70-h observation period at 2 months, 4 months and 6 months of age. Each point represents the group mean ± SEM of Lister, Wistar, Lewis and Fischer rats. The dark phase is indicated by the black bars below the *x*-axis.

Supporting Information

Figure S1

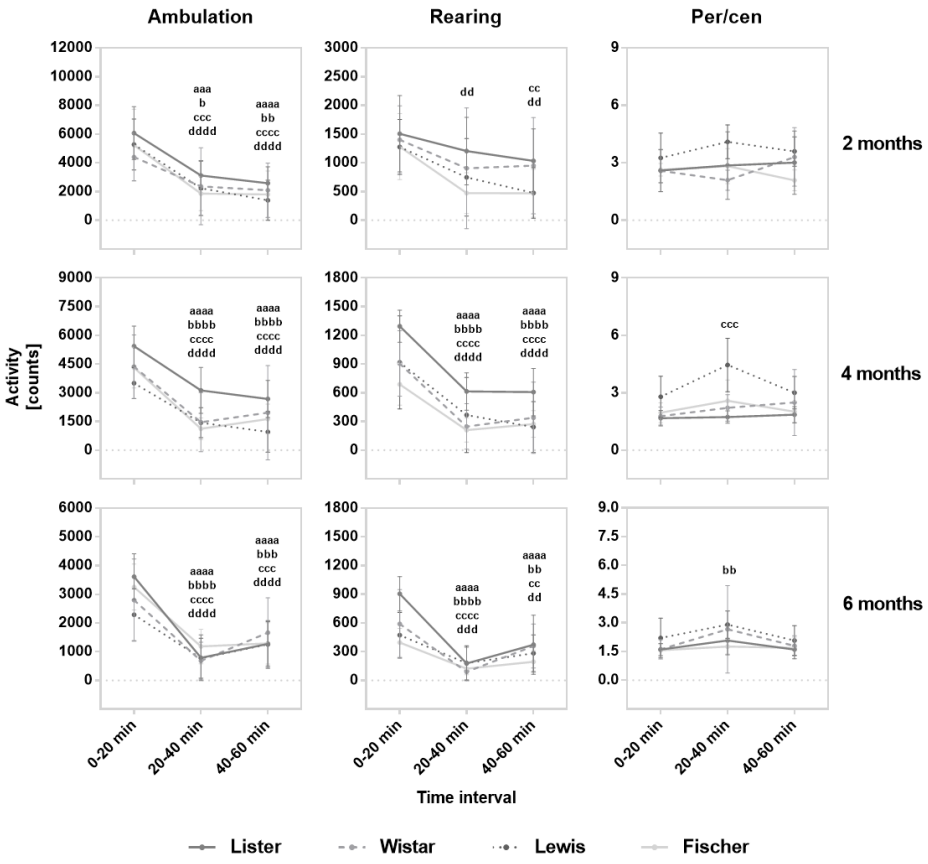

Figure S2

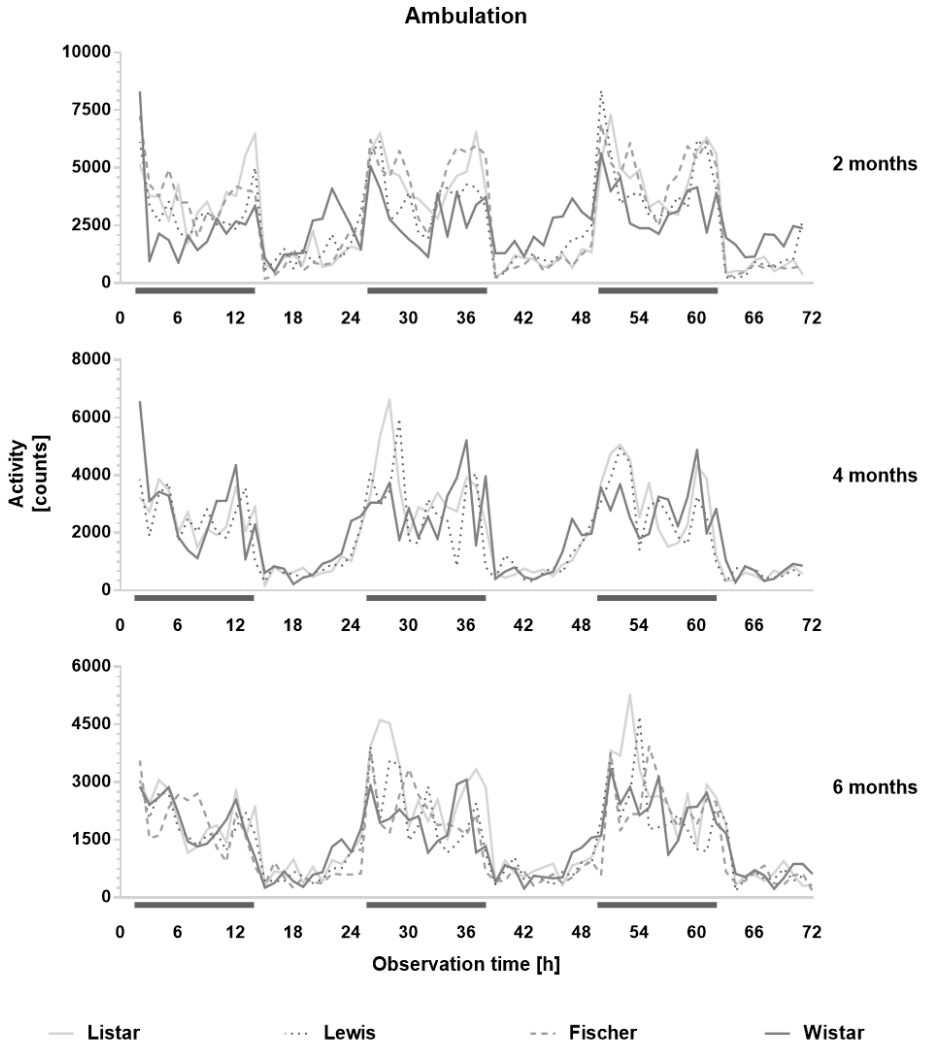
Ambulation
10000
7500
5000
2500
0
2 months
8000
6000
4000
2000
0
4 months
6000
4500
3000
1500
0
6 months
Activity [counts]
0 6 12 18 24 30 36 42 48 54 60 66 72
Observation time [h]
Listar
Lewis
Fischer
Wistar

OPEN ACCESS Freely available online

PLOS ONE

Early Deficits in Glycolysis Are Specific to Striatal Neurons from a Rat Model of Huntington Disease

Caroline Gouarné[1], Gwenaëlle Tardif[1], Jennifer Tracz[1], Virginie Latyszenok[1], Magali Michaud[1], Laura Emily Clemens[2,3], Libo Yu-Taeger[2,3], Huu Phuc Nguyen[2,3], Thierry Bordet[1], Rebecca M. Pruss[1*]

1 Trophos, Parc Scientifique de Luminy, Luminy Biotech Entreprises, Marseille, France, **2** Institute of Medical Genetics and Applied Genomics, University of Tuebingen, Tuebingen, Germany, **3** Center for Rare Diseases, University of Tuebingen, Tuebingen, Germany

Abstract

In Huntington disease (HD), there is increasing evidence for a link between mutant huntingtin expression, mitochondrial dysfunction, energetic deficits and neurodegeneration but the precise nature, causes and order of these events remain to be determined. In this work, our objective was to evaluate mitochondrial respiratory function in intact, non-permeabilized, neurons derived from a transgenic rat model for HD compared to their wild type littermates by measuring oxygen consumption rates and extracellular acidification rates. Although HD striatal neurons had similar respiratory capacity as those from their wild-type littermates when they were incubated in rich medium containing a supra-physiological glucose concentration (25 mM), pyruvate and amino acids, respiratory defects emerged when cells were incubated in media containing only a physiological cerebral level of glucose (2.5 mM). According to the concept that glucose is not the sole substrate used by the brain for neuronal energy production, we provide evidence that primary neurons can use lactate as well as pyruvate to fuel the mitochondrial respiratory chain. In contrast to glucose, we found no major deficits in HD striatal neurons' capacity to use pyruvate as a respiratory substrate compared to wild type littermates. Additionally, we used extracellular acidification rates to confirm a reduction in anaerobic glycolysis in the same cells. Interestingly, the metabolic disturbances observed in striatal neurons were not seen in primary cortical neurons, a brain region affected in later stages of HD. In conclusion, our results argue for a dysfunction in glycolysis, which might precede any defects in the respiratory chain itself, and these are early events in the onset of disease.

Citation: Gouarné C, Tardif G, Tracz J, Latyszenok V, Michaud M, et al. (2013) Early Deficits in Glycolysis Are Specific to Striatal Neurons from a Rat Model of Huntington Disease. PLoS ONE 8(11): e81528. doi:10.1371/journal.pone.0081528

Editor: Hemachandra Reddy, Oregon Health & Science University, United States of America

Received May 22, 2013; **Accepted** October 14, 2013; **Published** November 26, 2013

Funding: Funding was provided by Trophos and by the European Union under the 7th Framework Program for RTD - Project MitoTarget - Grant Agreement HEALTH-F2-2008-223388. The funders had no role in study design, data collection and analysis, decision to publish, or preparation of the manuscript.

Competing interests: The authors have the following interests. This study was partly funded by Trophos, the employer of CG, GT, JT, VL, MM, TB and RMP and who hold Trophos shares or stock options. There are no patents, products in development or marketed products to declare. This does not alter the authors' adherence to all the PLOS ONE policies on sharing data and materials, as detailed online in the guide for authors.

* E-mail: rpruss@trophos.com

Introduction

Huntington disease (HD) is a hereditary neurodegenerative disorder caused by a CAG repeat extension in the coding region of the huntingtin gene, leading to striatal atrophy which later expands to the cerebral cortex and other subcortical brain regions [1,2]. Clinically, the disease is characterized by psychiatric symptoms, movement disorders, progressive dementia and also by pronounced weight loss despite sustained caloric intake [3] supporting to the hypothesis of impaired ATP synthesis in HD [4,5]. This was further confirmed by the detection of significant alterations in the glucose concentration by brain imaging [6-8] and in the concentration of energetic metabolites (mainly N-acetylaspartate, glutamine/glutamate, and lactate) in brain or in the cerebrospinal fluid of HD patients [9-15]. Whether this results from reduced mitochondrial ATP synthesis and/or reduced glycolytic ATP levels is not known. The observation of a severe reduction in the activity of the mitochondrial respiratory chain complexes II/III and a milder reduction in the activity of complex IV in the caudate/putamen from post-mortem brain samples suggested that mitochondrial abnormalities may underlie HD pathogenesis [16-18]. However, whether respiratory chain impairment is the cause or the consequence of neuronal loss in HD remains unclear, since such defects were not observed in pre-symptomatic patients [19,20].

To further address the precise nature and the role of metabolic and mitochondrial dysfunction in HD, studies were performed in genetic models of HD, particularly in mice expressing full-length mutant huntingtin (fl-mHtt). As observed

in pre-symptomatic and early HD patients, no major impairment in the enzymatic activity of the mitochondrial respiratory chain complexes I–IV was evidenced in either the striatum or the sensorimotor cortex of these mice [19]. By contrast, deficits in respiration rate and ATP production reported in ST*Hdh* Q111 striatal cell lines derived from knock-in mice with 111 CAG repeats introduced into the mouse HTT homologue *Hdh* [21-23]. However, the impairment could not be assigned to defects in individual respiratory complexes in these cells. Moreover, differences in mitochondrial respiratory rates were no longer present when using isolated mitochondria from the same cell lines [24], suggesting that detection of some mitochondria deficits may only be detected in intact cells. In that sense, Oliveira and colleagues measured mitochondrial respiratory rates in intact, non-permeabilized, primary striatal neurons from *Hdh*150 knock-in mice and did not find any deficit under resting condition when compared to wild type controls [25]. However, when challenged with an energy-demanding stimulus (NMDA-receptor activation) and incubated in pyruvate-based media to accentuate mitochondrial metabolism, *Hdh*150 neurons were more vulnerable to calcium overload than neurons from their wild-type littermates [26]. These results highlight the importance of assessing mitochondrial function in the cellular environment including both neuronal cell bodies and neurites. It is also important to survey the use of various glycolytic and oxidative substrates to better understand how cells cope with metabolic demands *in situ*.

To pursue these questions, we investigated mitochondrial respiration in specific primary neuronal subpopulations cultured from a new HD transgenic rat model expressing fl-mHtt and all regulatory elements integrated from a bacterial artificial chromosome (BACHD rats). These rats display a robust, earlier onset and faster progressive HD-like phenotype even in heterozygous transgenic rats compared to previously described HD rats expressing a mHtt fragment [27]. Oxygen consumption rates and anaerobic glycolysis were measured using a variety of substrates *in situ*, directly in the culture well, preserving the neuronal network integrity.

Materials and Methods

Ethics statement

All experiments were approved and performed in accordance with internal institutional guidelines; Trophos is an accredited institution for animal experimentation in France (French ministry of Agriculture, Agreements No. B-13-055-15) and in strict accordance with national and European regulations (Directive 86/609/EEC of the European Economic Community regarding the protection of animals used for experimental and other scientific purposes). All efforts were made to avoid or minimize animal suffering and to reduce and refine the experimentation.

Animals

Male heterozygous transgenic BACHD rats (HD) expressing high levels of fl-mHtt protein containing 97 CAG/CAA repeats (line LY.005) [27] were bred with female wild type (WT) rats obtained from Elevage Janvier (Le Genest Saint Isle, France). The rats were housed in a controlled environment (room temperature 22°C ± 2; reverse 12h light dark cycle, 50% ± 5 humidity) with food and water available ad libitum. Pregnant female rats were euthanized at embryonic day 17 (E17) by gradual fill CO_2 overdose. Rats were placed in a hermetic box then exposed to a mixture of O_2/CO_2 (40-60% respectively) until sleep was induced. The % CO_2 was then progressively increased up to 100% while O_2 was decreased (0.5L/min every 30 sec. for 3 min up to 5L/min) and then maintained for 4-5 min.

Genotype identification

Rat embryos from a single pregnant female rat were used for each independent experiment. All embryos were genotyped to identify WT and HD animals. During genotyping, brains were maintained in Hibernate® conservation medium (BrainBits) at 4°C. The embryos were genotyped with a PCR-based assay using DNA from tail tissue. The mHTT gene product was detected using the primers 5'-ATGGCGACCCTGGAAAAGCTG-3' and 5'-AGGTCGGTGCAGAGGCTCCTC-3' (Eurofins). PCR conditions were: 30 cycles at 94°C (30 s), 60°C (30 s), 72°C (1 min).

Primary neuronal cultures

E17 primary striatal neurons were prepared by an adapted method previously described [28]. Briefly, striata were thoroughly minced into 1 mm sections, washed in HBSS medium (Invitrogen) complemented with 7 mM HEPES (Invitrogen) and 0.45% glucose (w/v) (Sigma) and incubated for 15 min at 37°C with 0.25% of trypsin (Invitrogen). The tissues were mechanically dissociated by several pipetting and centrifugation steps (5 min at 250 x g). Primary striatal neurons were seeded onto poly-ornithine (Invitrogen) and laminin (BD) coated Seahorse 24-well plates at a density of 150,000 cells/well in Neurobasal™ media (Invitrogen), complemented with 2% B-27 supplement (Gibco) and 1 mM pyruvate (Invitrogen). The two cell populations (WT and HD) were seeded in different wells of the same plate with 4 to 8 replicates per plate depending on the protocol. The cells were incubated for 7 days at 37°C in a humidified incubator in an atmosphere of 95% O_2, 5% CO_2. E17 primary cortical neurons were prepared using a similar protocol and seeded at a density of 110,000 cells/well. Striatal and cortical neuronal culture purity was controlled by immunofluorescence using NeuN antibody (Millipore) to identify neurons, GFAP (Millipore) for astrocytes and F4/80 (Santa Cruz) for microglial cells. Both striatal and cortical neuronal cultures were 98% pure. The presence of mHtt, already in the form of aggregates, was confirmed in primary striatal and cortical neuronal cultures derived from HD rats (see in Protocol S1 and Figure S1).

Oxygen consumption rate and extracellular acidification rate measurements-

Cellular oxygen consumption and extracellular acidification rate (ECAR) reflecting lactate release were concomitantly measured using a XF24 extracellular flux analyzer (Seahorse Bioscience) as previously described [29].

Respiration experiments in substrate-rich medium

Experiments in substrate-rich media were performed using Dulbecco's Modified Eagle's Medium (DMEM) containing 25 mM glucose without bicarbonate (Invitrogen) and complemented with 1 mM fresh pyruvate (assay medium). One hour before the start of the respiration measurements, the original culture medium was replaced by assay medium and plates were placed into the XF analyzer calibrated at 37°C. After 10 min of equilibration, OCR was measured for 1.5 min to establish a baseline rate. The medium was then gently mixed for 2 min followed by a 3 min pause to restore normal oxygen tension in the microenvironment surrounding the cells. After baseline measurements, oligomycin (final concentration 0.5 µg/ml) (Sigma) was injected into each well in order to inhibit mitochondrial ATP synthase to determine proton leak-dependent OCR (State 4o). After this, the uncoupling agent carbonilcyanide *p*-triflouromethoxyphenylhydrazone (FCCP; final concentration 2 µM) (Sigma) was injected to determine maximal OCR (state 3u). Finally, rotenone (final concentration 75 nM) (Sigma) and antimycin A (final concentration 150 ng/ml) (Sigma) were injected to inhibit complex 1 and complex 3 respectively and to completely abolish mitochondrial respiration. After each injection step, two measurement cycles (measurement + mix + pause) were performed (Figure 1) and after rotenone and antimycin A injection, 4 measurement cycles were performed. Preliminary experiments determined the optimal concentration of these agents to optimally inhibit or stimulate respiration without inducing toxicity.

Substrate-dependent respiration experiments

To assay the ability of different substrates to support respiration, experiments were designed using a simple substrate-free modified Krebs Henseleit Buffer (KHB) (NaCl 111 mM, KCl 4.7 mM, $MgSO_4$ 2 mM, Na_2HPO_4 1.2 mM, pH 7.4), complemented with 2 mM GlutaMAX™ (Invitrogen). One hour before the start of the assay, the original culture medium was replaced by KHB and the plates were placed in an incubator at 37°C without CO_2 and then in the XF analyzer. After 10 min of equilibration in the instrument, OCR was measured for 1.5 min to establish a substrate free basal rate. Medium was then gently mixed for 2 min followed by a 3 min pause to restore normal oxygen tension in the microenvironment surrounding the cells. After baseline measurements, the substrates D-glucose (Sigma), pyruvate (Sigma) or lactate (Sigma) were injected and OCR was measured for 1.5 min followed by injections of oligomycin, FCCP and rotenone plus antimycin A as described above. After each injection, two or three measurement cycles (measurement + mix + pause) were performed.

Respiration parameters calculation

When oxygen consumption rate measurements ended, cells were incubated for 20 minutes with 2 µg/ml calcein-AM to measure the relative neuronal cell density and viability in each well. Only experiments with a similar cell density based on calcein fluorescence between WT and HD (Student's t test $p > 0.05$) were validated and analyzed. Respiration parameters were calculated from data obtained during the steps of OCR measurement. For basal respiration and oligomycin respiration, the last OCR measurement of the cycle was selected for calculation. For FCCP the first OCR measurement of the cycle was selected to avoid the effect of substrates depletion on maximal OCR. For further details please refer to the legend of the respective figures. Because non-mitochondrial oxygen consumption rate (measured after antimycin A injection) was overestimated due to the fact that FCCP injection activated non-mitochondrial oxidase and because the rate was negligible (according to preliminary assays), we decided to not remove non-mitochondrial OCR from all measurements. Cell respiratory control ratio (RCR) was calculated by dividing the maximal rate (uncoupled) by the oligomycin rate (proton leak). Spare respiratory capacity was calculated by subtracting the basal rate from the maximal (uncoupled) rate. Coupling efficiency was calculated by dividing the fraction of basal mitochondrial oxygen consumption used for ATP synthesis (basal rate minus oligomycin rate) by the basal rate. The substrate response was determined by dividing the OCR obtained after substrate addition (glucose, pyruvate, lactate, or combinations) by the substrate-free basal rate in KHB.

Statistical analysis

Data are expressed as means ± SEM. Comparisons between two groups were performed using an unpaired Student's t test. Comparisons of several groups or differences between treatments and experimental groups were conducted using a one way or two way analysis of variance (ANOVA) followed by Dunnett's post test. A p-value of less than 0.05 was considered statistically significant.

Results

Characterization of WT and HD striatal neuron respiration in substrate-rich medium

E17 primary striatal neurons from HD and WT rat embryos were cultured for 7 days in Neurobasal™ medium and then placed in DMEM with similar concentrations of amino acids, vitamins and glucose (25 mM) to measure OCR. Their response to the respiration analysis paradigm in substrate rich medium is shown in Figure 1A. Basal OCR is strongly controlled by ATP turnover and to a lesser extent by substrate oxidation and proton leak [30]. Addition of oligomycin induced a decrease in OCR and under this condition (state 4o), respiration is strongly controlled by proton leak kinetics and partially by substrate oxidation [30]. In contrast, OCR sensitive to oligomycin is strongly driven by the proton flux accompanying ATP synthesis. Addition of the uncoupler (FCCP) caused an increase in OCR until the maximum respiration rate was reached (state3u). This respiratory rate reflects the maximal respiratory chain activity as well as the maximal substrate oxidation rate that is achievable [30]. Finally, addition of rotenone (complex 1 inhibitor) and antimycin A (complex 3 inhibitor) totally blocked the respiratory chain and the residual OCR represented non-mitochondrial respiration, probably driven by NADPH oxidase activity [30]. In these experiments performed in substrate rich DMEM, no differences in OCR or respiratory parameters were detectable between WT

Figure 1

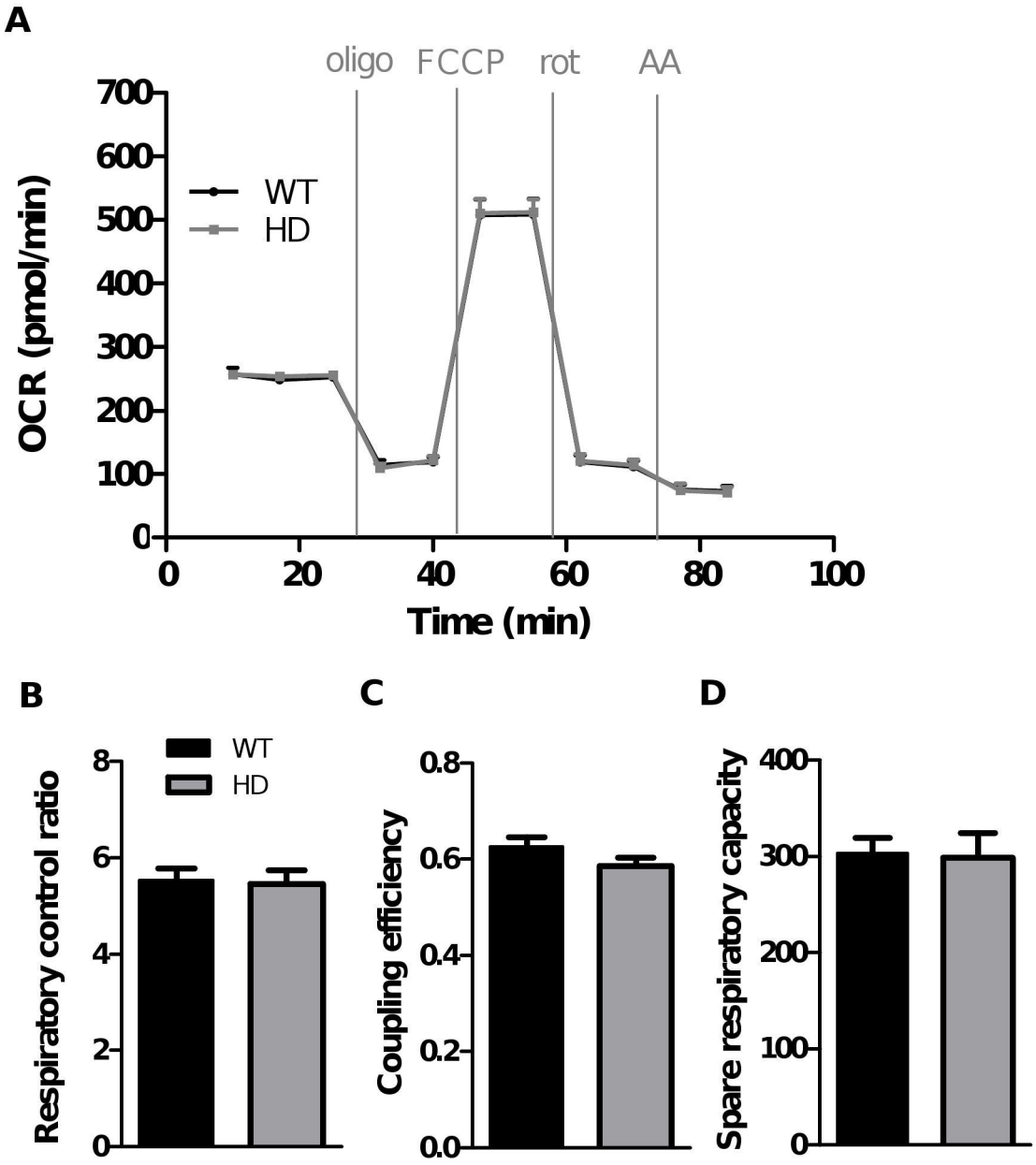

Figure 1. No differences in respiratory parameters are detected between HD and WT striatal neurons incubated in substrate-rich medium. OCR measurements were performed in bicarbonate- and HEPES-free DMEM containing 25 mM glucose complemented with pyruvate (1 mM) and began 10 min after cell plate installation in the Seahorse analyser. A) OCR was measured sequentially in basal conditions (time points 1-3), after injections of oligomycin (oligo; time points 4 and 5), FCCP (time points 6 and 7), rotenone (time points 8 and 9) and then antimycin A (AA; time points 10 and 11) at the indicated times. Data shown are mean ± SEM from a representative experiment (eight replicates). Respiratory parameters were derived from OCR measured during each phase of the experiment as shown in A: B) respiratory control ratio = [FCCP rate (time point 6) / oligo rate (time point 5)]; C) coupling efficiency = [basal rate (time point 3) – oligo rate (time point 5)] / basal rate (time point 3); D) spare respiratory capacity = [FCCP rate (time point 6) – basal rate (time point 3)]. Respiratory parameters shown in panels B-D are mean ± SEM calculated from all replicates (eight replicates in each of three independent experiments).

doi: 10.1371/journal.pone.0081528.g001

and HD striatal neurons (Figure 1). Similarly, HD striatal neurons showed no deficits in RCR, which detects substrate oxidation efficiency and respiration due to proton leak, but not driven by ATP synthesis (Figure 1B), coupling efficiency, which is strongly controlled by ATP turnover and proton leak (Figure 1C) or spare respiratory capacity, which reflects the capacity of the respiratory chain to respond to an increase in energy demand and the ability of substrates to provide fuel (Figure 1D).

Glucose supported respiration in striatal neurons

In first experiments, the medium used to measure respiration contained 25 mM glucose to mimic their original culture conditions. This is a high, supra-physiological concentration compared to the glucose concentrations found in brain that are estimated to be around 2.5 mM in rats [31]. To check whether there was any difference in the ability of HD striatal neurons to use more physiological levels of glucose as well as various other substrates to support oxidative phosphorylation, we performed a series of experiments adding specific substrates to cells incubated in KHB. Different concentrations of glucose were injected (final concentrations of 2.5 - 25 mM) followed by oligomycin, FCCP, and rotenone + antimycin A injections (Figure 2A). In the absence of glucose, neurons were able to maintain basal respiration but they were not able to respond to FCCP stimulation (Figure 2A). All concentrations of glucose between 2.5 and 25 mM induced a similar increase in basal OCR (Figure 2B) but even though basal respiration was similar in the presence of physiological and supra-physiological glucose concentrations (Figure 2B), FCCP-stimulated respiration and RCR were glucose-concentration dependent (Figure 2C). These results suggest that the physiological glucose concentration found in brain, although sufficient to support respiration under basal conditions (low energy demand) may be limiting under conditions of high respiratory demand.

Neurons can use lactate and pyruvate to support respiration

Increasing evidence supports the idea that glucose is not the sole energy substrate for neurons in the brain. Oxidative substrates such as pyruvate or even lactate provided by glial cells could be supplementary fuel for neurons [32]. Results presented in Figure 3 reinforced this hypothesis. WT neurons were incubated for 1 hour in KHB medium lacking metabolic substrates then provided with various concentrations of pyruvate (Figure 3A) or lactate (Figure 3B). Then respiratory parameters were derived following injection of oligomycin, FCCP, and rotenone + antimycin A. As observed in the previous study assaying the response to glucose, in the absence of substrates, neurons were able to maintain basal respiration but were not able to respond to FCCP stimulation (Figure 3A; 3B). Addition of either pyruvate or lactate increased basal respiration as previously seen with glucose and restored the neurons' capacity to respond to FCCP stimulation (Figure 3A, 3B). In the case of pyruvate, a similar basal respiration rate was detected over the concentration range tested (1-30 mM) but maximal respiration and RCR reached a plateau between 1 and 10 mM (Figure 3A, 3C, 3E). Addition of 1 or 10 mM lactate resulted in a similar basal respiration rate, which was significantly increased in the presence of 30 mM lactate (Figure 3B-F). FCCP stimulated respiration was also supported by lactate but to a lesser extent than pyruvate. This can be explained by the observation that 30 mM lactate induced a significant increase in proton leak respiration in addition to ATP synthesis-driven respiration (Figure 3G). This was not the case for 30 mM pyruvate (Figure 3D). Because 30 mM lactate increased mitochondrial proton leak, potentially disturbing mitochondrial function, this concentration was not considered in further analysis of RCR as a function of pyruvate and lactate concentrations (Figure 3I). We observed a concentration-dependent increase in RCR for both lactate and pyruvate, plateauing at 10 mM for pyruvate. Comparing the RCR between 10 mM pyruvate and lactate shows that pyruvate is clearly a better substrate, most likely due to the fact that lactate must first be converted to pyruvate.

Comparison of respiratory parameters in WT and HD striatal neurons in the presence of a physiological glucose concentration

To see whether there is any difference in the capacity of WT and HD striatal neurons to use physiological glucose concentrations, OCR was measured in KHB as shown in Figure 2. First, OCR was measured after one hour of substrate deprivation. Although there were some differences noted during the equilibration period seen in some experiments, overall, there were little or no significant differences detected between the two genotypes following more than one hour in this challenging condition, suggesting that intracellular substrates and neurons' capacity to mobilize them were similar between WT and HD striatal neurons (Figure 4A). Furthermore, as observed in Figure 2, addition of 2.5 mM glucose increased OCR to a similar basal level in both WT and HD striatal neurons (Figure 4A) and oligomycin injection induced a similar reduction in OCR and in proton leak respiration in the two genotypes (Figure 4A). These results show that there is no underlying mitochondrial dysfunction in HD striatal neurons or their ability to use glucose to support basal respiration and ATP synthesis. By contrast, when respiration was stimulated with FCCP, OCR deficits associated with lower RCR and spare respiratory capacity were detected in HD striatal neurons compared to WT (Figure 4B, 4C), suggesting mitochondrial respiratory chain dysfunction and/or a defect in glucose metabolism that generates pyruvate (glycolysis) under stimulated conditions.

Respiration in WT and HD striatal neurons supported by pyruvate or lactate

We also evaluated HD and WT striatal neurons' capacity to use alternative substrates, pyruvate and lactate according the protocol set up in Figure 3. The concentration chosen for this exploration was 10 mM for each substrate, which was the concentration inducing the maximal OCR response under stimulated conditions without causing proton leak. As previously shown in Figure 4, after more than one hour of substrate deprivation, OCR was similar between WT and HD

Figure 2

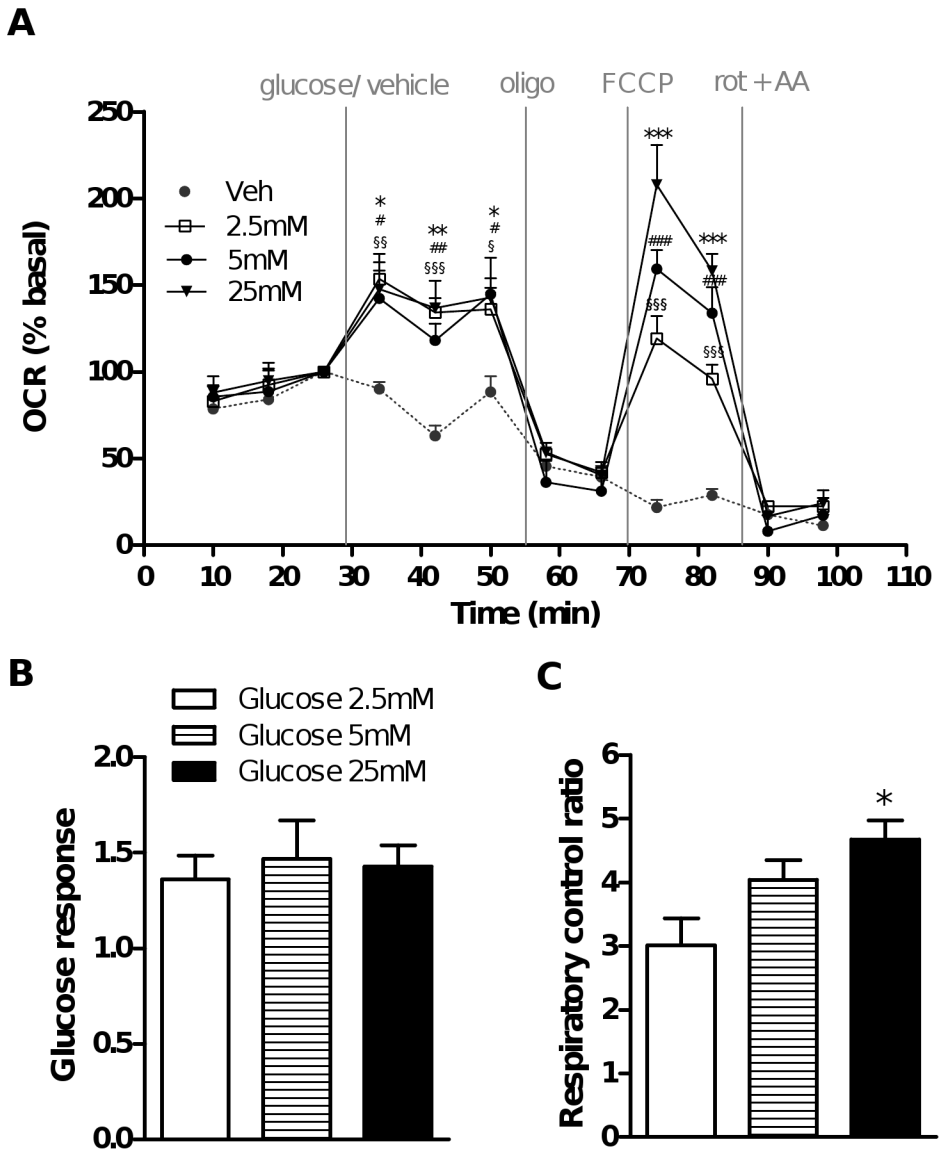

Figure 2. Respiration parameters measured in WT striatal neurons as a function of glucose concentration. On the day of the respiration experiments, medium was replaced with substrate-free KHB and cells were incubated for 1 h at 37°C. OCR measurements began 10 min after cell plate installation in the Seahorse analyser. A) After measuring the initial OCR in the absence of substrates, various concentrations of glucose in KHB (vehicle; Veh) were injected (final concentrations: 0, 2.5, 5 or 25 mM). OCR was then measured in the presence of substrate and following successive injections of oligomycin (oligo), FCCP, then rotenone and antimycin A (rot + AA) at the indicated times. Data are expressed as the percentage of the basal value measured at the time point 3 (four replicates). § $p < 0.05$, §§ $p < 0.01$, §§§ $p < 0.001$ (0 mM vs. 2.5 mM glucose); # $p < 0.05$, ## $p < 0.01$, ### $p < 0.001$ (0 mM vs. 5 mM glucose); * $p < 0.05$, ** $p < 0.01$, ***$p < 0.001$ (0 mM vs. 25 mM glucose). Respiratory parameters were derived from OCR measured during each of these phases; B) glucose response = [basal glucose rate (time point 6) / basal free substrate rate (time point 3)]; C) respiratory control ratio = [FCCP rate (time point 9) / oligomycin rate (time point 8)]. * $p < 0.05$ compared to 2.5 mM glucose.

doi: 10.1371/journal.pone.0081528.g002

Figure 3

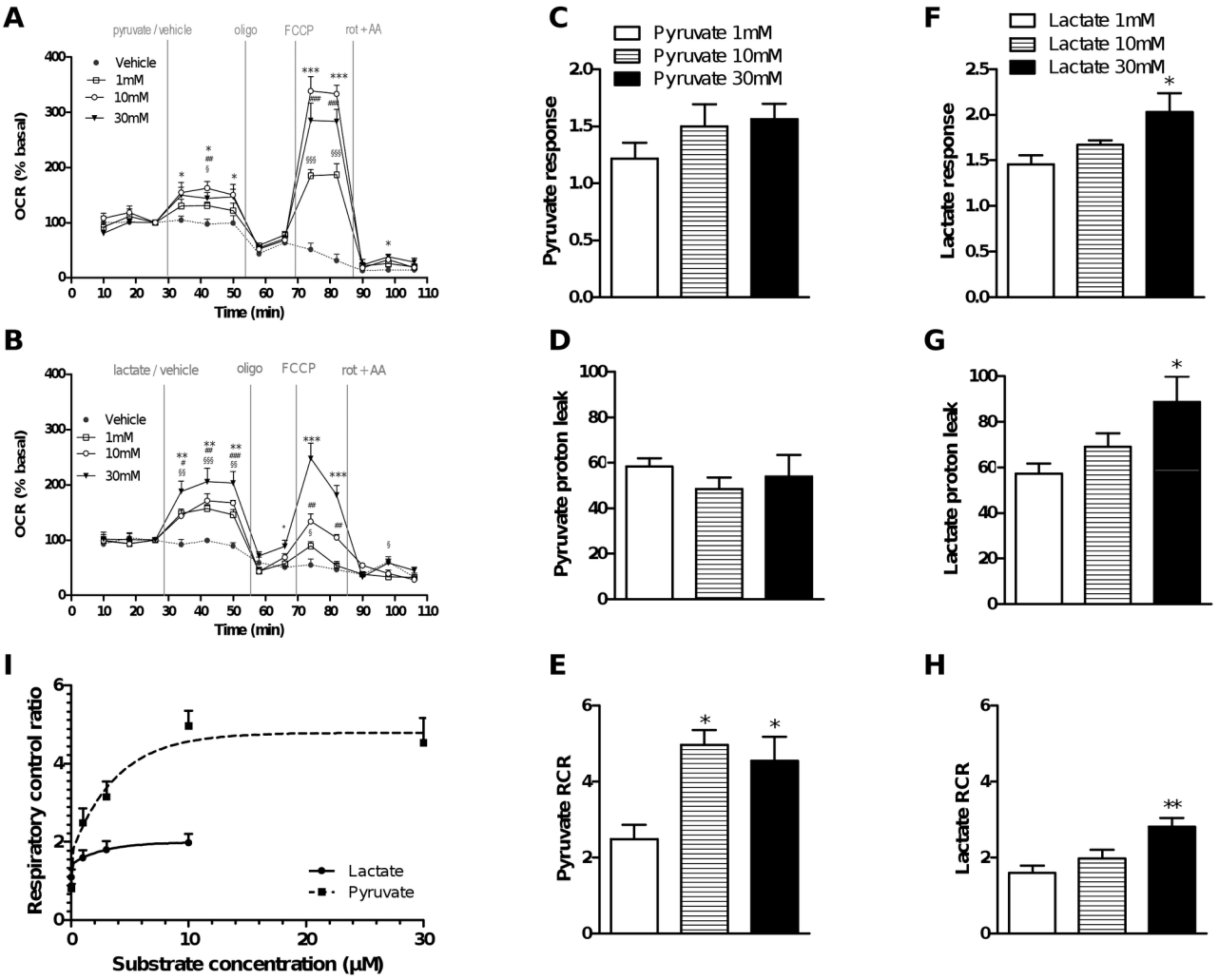

Figure 3. Striatal neurons can use alternative substrates to glucose to support respiration. On the day of the respiration experiments, medium was replaced with substrate-free KHB and cells were incubated as described in Figure 2. After measuring the initial OCR in the absence of substrates, various concentrations of pyruvate (A) or lactate (B) in KHB (vehicle; Veh) were injected (final concentrations: 0, 1, 10 or 30 mM). OCR was then measured in the presence of substrate and following successive injections of oligomycin (oligo), FCCP, then rotenone and antimycin A (rot + AA) at the indicated times. Data are expressed as the percentage of the basal value measured at time point 3 (four replicates). § $p < 0.05$, §§ $p < 0.01$, §§§ $p < 0.001$ (0 mM vs. 1 mM pyruvate or lactate); # $p < 0.05$, ## $p < 0.01$, ### $p < 0.001$ (0 mM vs. 10 mM pyruvate or lactate); * $p < 0.05$, ** $p < 0.01$, ***$p < 0.001$ (0 mM vs. 30 mM pyruvate or lactate). Respiratory parameters were derived from the various phases following pyruvate (C-E) or lactate (F-H) injection: substrate response = [basal pyruvate or lactate rate (time point 6) / basal substrate free rate (time point 3)]; proton leak rate (time point 7); respiratory control ratio = [FCCP rate (time point 9) / oligomycin rate (time point 8)]. * $p < 0.05$, ** $p < 0.01$ compared to 1 mM pyruvate (C-E) or lactate (F-H). I). Respiratory control ratio expressed as a function of pyruvate (1, 3, 10 or 30 mM) or lactate (1, 3 or 10 mM) concentration.

doi: 10.1371/journal.pone.0081528.g003

neurons (Figure 5A, 5D). Pyruvate addition induced a significant increase in basal OCR and restored neurons' capacity to respond to FCCP (Figure 5A). No significant differences were detected in HD striatal neurons compared to WT (Figure 5A-C). Lactate addition induced a similar increase in basal OCR as pyruvate, which was again not different between WT and HD neurons (Figure 5D). Even though respiration in the presence of 10 mM lactate was similar or only slightly lower in HD neurons, the resulting RCR and spare respiratory capacity appeared to be significantly lower in FCCP-stimulated HD neurons compare to WT (Figure 5E-F).

Figure 4

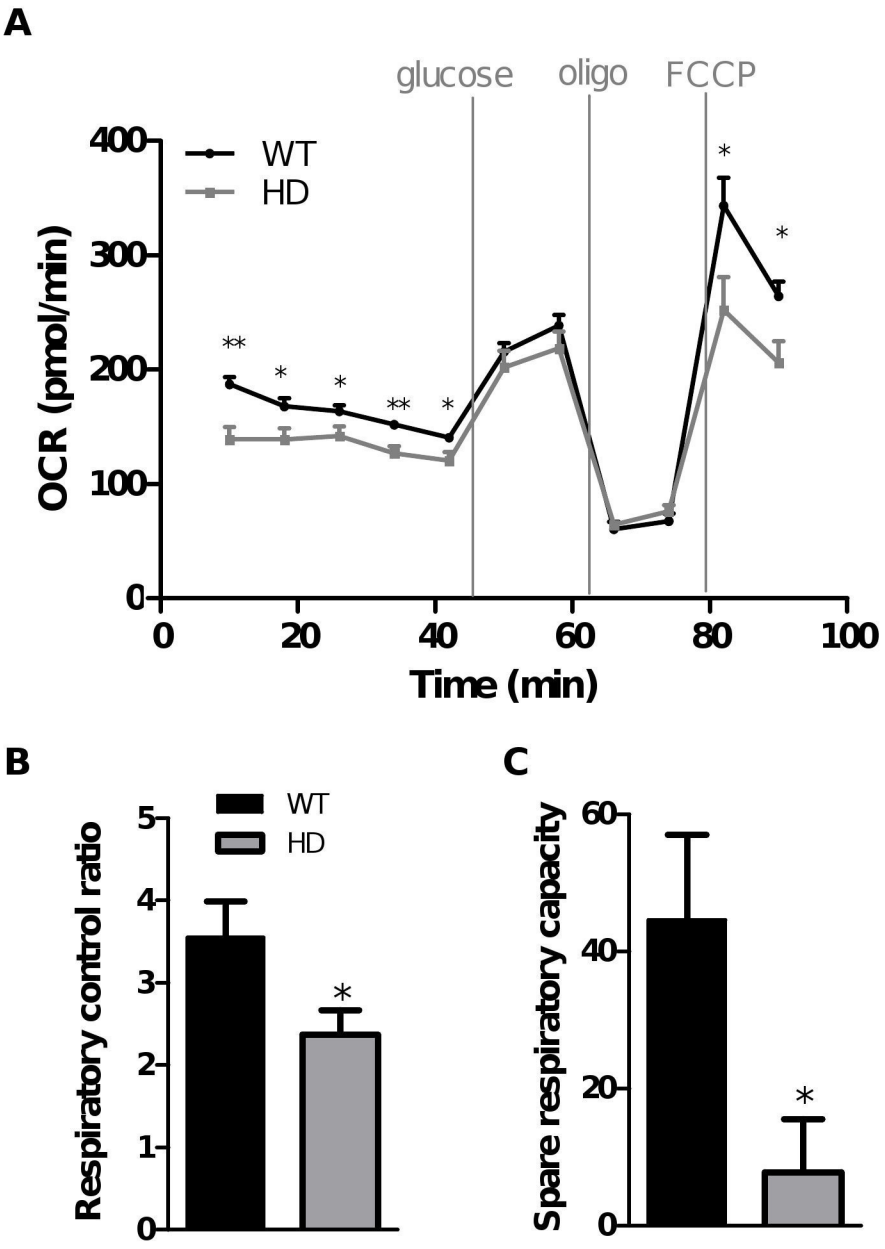

Figure 4. OCR measurements performed using a physiological glucose concentration revealed respiratory deficits in HD striatal neurons. OCR measurements were performed as described in Figures 2. A) OCR measurements were taken following injection of glucose (final concentration, 2.5 mM), oligomycin (oligo) then FCCP at the indicated times. Data shown are mean ± SEM from a representative experiment. Respiratory parameters were derived from the various phases following glucose injection (B-C): respiratory control ratio = [FCCP rate (time point 10) / oligo rate (time point 9)]; glucose spare respiratory capacity = [FCCP rate (time point 10) – glucose rate (time point 7)]. Data shown are mean ± SEM from all replicates (six replicates in each of three independent experiments). * $p < 0.05$, ** $p < 0.01$ comparing HD vs. WT.

doi: 10.1371/journal.pone.0081528.g004

To see how neurons respond to a mixture of metabolic substrates, OCR was measured in WT and HD striatal neurons in the presence of 2.5 mM glucose followed by addition of 10 mM lactate or pyruvate (Figure 6). Neither pyruvate nor lactate

Figure 5

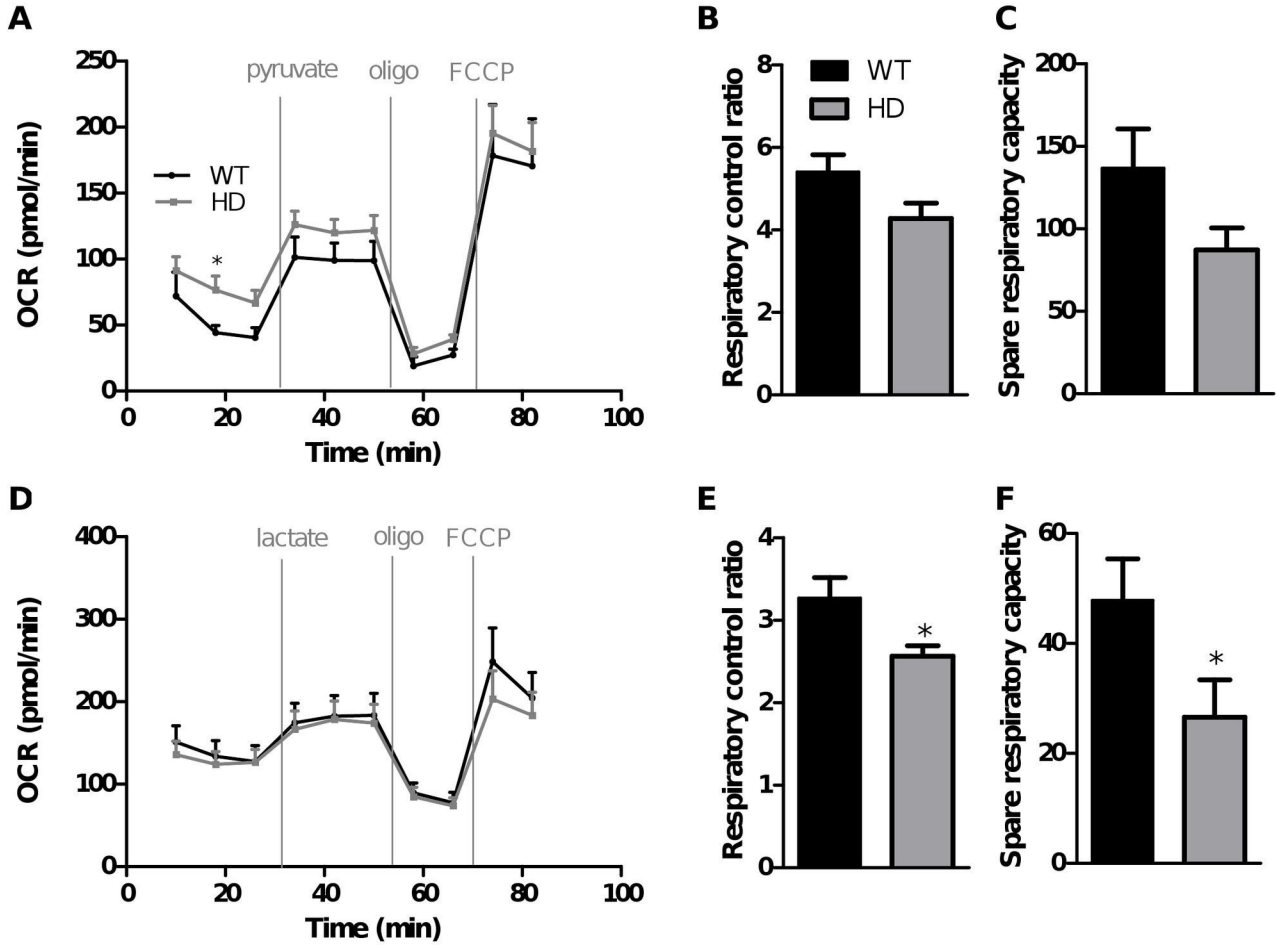

Figure 5. Comparison of HD and WT striatal neurons' ability to use pyruvate and lactate in the absence of glucose. OCR measurements were performed as described in Figure 3. OCR measurements were taken following injection of 10 mM pyruvate (A) or lactate (D), oligomycin (oligo) and FCCP (2 μM) at the indicated times. Data shown are mean ± SEM from a representative experiment (six or ten replicates for pyruvate or lactate, respectively). Respiratory parameters were derived from the various phases following pyruvate (B-C) or lactate (E-F) injection: respiratory control ratio = [FCCP rate (time point 9) / oligo rate (time point 8)]; spare respiratory capacity = [FCCP rate (time point 9) – pyruvate or lactate rate (time point 6)]. Data for respiratory parameters are mean ± SEM calculated from all replicates (three independent experiments). * $p < 0.05$ comparing HD vs. WT.

doi: 10.1371/journal.pone.0081528.g005

increased basal OCR further when neurons were already supplied with a physiological glucose concentration (Figure 6A-D), suggesting that glucose alone was sufficient to support basic neuron energy requirements. Moreover, this result confirmed that under basal conditions, respiration is probably strongly controlled by the rate of mitochondrial ATP turnover or proton leak and is not limited by the rate of substrate oxidation. FCCP injection induced a large increase in OCR in the two conditions tested. In the presence of glucose and pyruvate, RCR was higher compared to glucose or pyruvate alone (9.2 ± 0.8, 5.4 ± 0.4, 3.5 ± 0.4; glucose + pyruvate RCR, pyruvate RCR, glucose RCR, respectively; mean ± SEM). Similar results were obtained with lactate, with higher RCR in the presence of glucose and lactate compared to glucose or lactate alone (6.2 ± 0.5, 3.3 ± 0.2, 3.5 ± 0.4; glucose + lactate RCR, lactate RCR, glucose RCR, respectively; mean ± SEM). These results suggest that in the presence of a physiological glucose concentration, maximal respiration can be improved when alternative substrates such as pyruvate or lactate are available. However, it can be seen that FCCP-stimulated OCR was significantly lower in HD compared to WT striatal neurons when supplied with either pyruvate or lactate in addition to a physiological glucose concentration (Figure 6A-D). This shows that the respiratory defects observed under stress conditions in

Figure 6

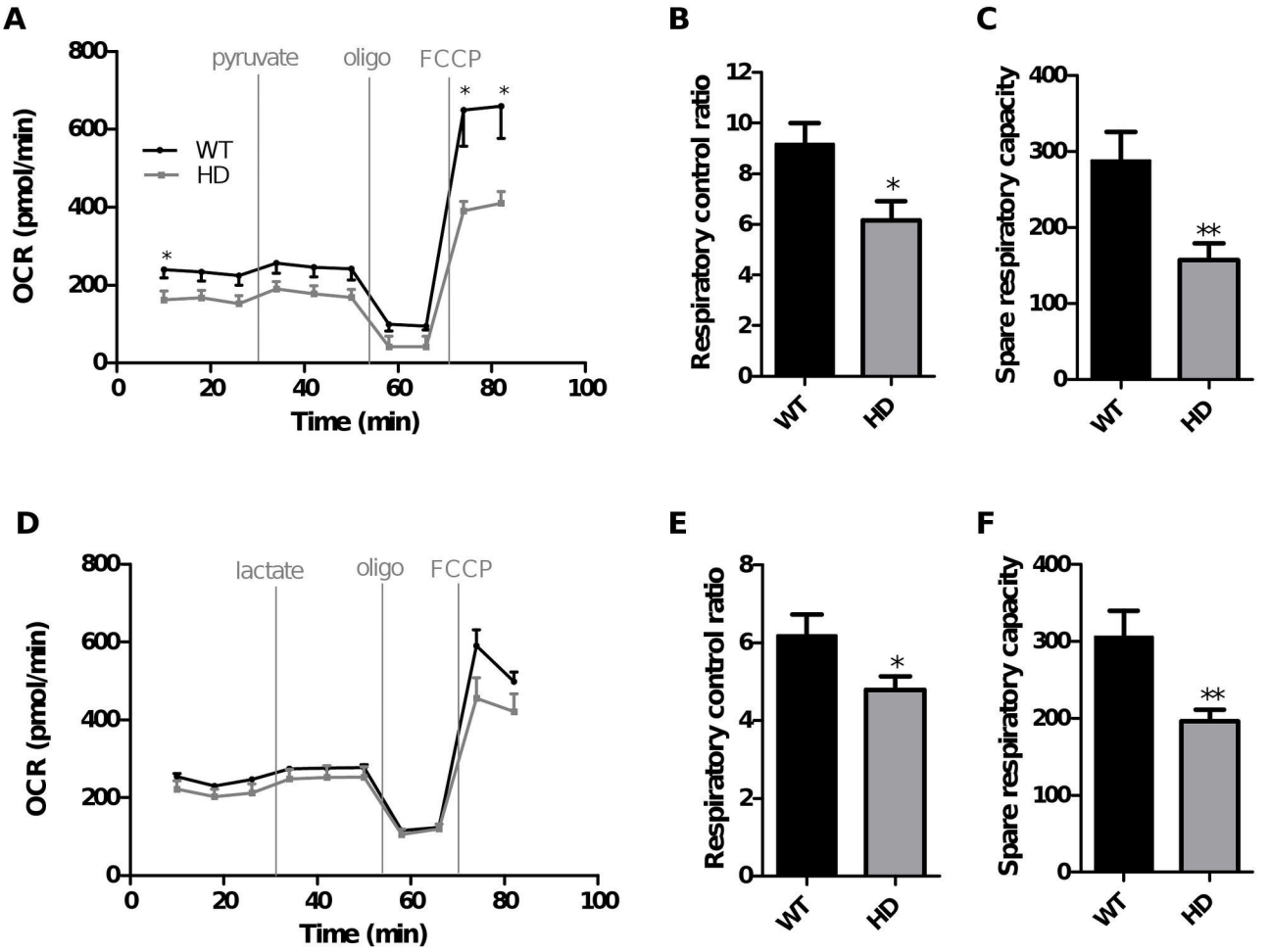

Figure 6. HD striatal neurons have a lower capacity to use glucose under high respiratory demands, even when supplemented with pyruvate or lactate. Striatal neurons were cultivated for 7 days as described in Figure 1. One hour before the start of the respiration experiments, medium was replaced with substrate-free KHB complemented with 2.5 mM glucose. OCR measurements were performed as described in Figure 3. OCR measurements following injection of 10 mM pyruvate (A) or lactate (D), oligomycin (oligo) and FCCP (2 μM) at the indicated times. Data shown are mean ± SEM from a representative experiment (five or four replicates for pyruvate or lactate, respectively). Respiratory parameters were derived from the various phases following pyruvate (B-C) or lactate (E-F) injection: respiratory control ratio = [FCCP rate (time point 9) / oligo rate (time point 8)]; spare respiratory capacity = [FCCP rate (time point 9) - pyruvate or lactate rate (time point 6)]. Data for respiratory parameters are mean ± SEM calculated from all replicates (three independent experiments). * $p < 0.05$, ** $p < 0.01$ comparing HD vs. WT.

doi: 10.1371/journal.pone.0081528.g006

the presence of physiological concentration of glucose (Figure 4) were not completely compensated by the presence of alternative substrates, such as pyruvate or lactate.

Comparison of ECAR in WT and HD primary striatal neurons

To investigate if OCR deficits observed in the presence of 2.5 mM glucose in HD primary striatal neurons were associated with a defect in anaerobic glycolysis, we measured ECAR in HD and WT striatal neurons. First, we observed under basal conditions that ECAR in WT striatal neurons remained stable regardless of the glucose concentration used (Figure 7A). After oligomycin injection, the inhibition of ATP synthesis by the respiratory chain resulted in ECAR activation as previously described [29]. Interestingly, this activation was glucose concentration dependent (Figure 7A). Because FCCP increases H^+ extrusion, ECAR could not be used as a measure of glycolysis under uncoupling conditions; therefore, data

obtained after FCCP injection was not analyzed. Then, ECAR was measured in WT and HD primary striatal neurons incubated either in rich substrate DMEM or in KHB containing 2.5 mM glucose (Figure 7B). Under basal conditions, no significant difference was observed between WT and HD neurons. In contrast, oligomycin-stimulated ECAR as an indicator of glycolysis was significantly lower in HD neurons both in rich and low glucose medium, suggesting a specific defect in their maximal anaerobic glycolysis capacity. At the same time, intracellular pH measured using 2',7'-Bis-(2-Carboxyethyl)-5-(and-6)-Carboxyfluorescein (BCECF Invitrogen, 0.3μM) was similar in WT and HD neurons suggesting no difference in lactate release between the two genotypes (data not shown).

Comparison of respiration parameters in WT and HD cortical neurons

To investigate if the deficits seen in HD striatal neurons were common to all types of neurons, we performed similar experiments using primary cortical neurons, a brain region affected later in Huntington disease [33]. In contrast to striatal neurons, no respiratory deficits were detected in the presence of 2.5 mM glucose alone under basal or uncoupling conditions (Figure 8A) and RCR was similar between HD and WT cortical neurons. Additionally, in the presence of glucose (2.5 mM) and pyruvate (10 mM) or lactate (10 mM), no defect was detected in HD cortical neurons in any of the respiratory parameters (Figure 8B-C). ECAR measurements were also performed in presence of 2.5 mM glucose in primary cortical neurons and results did not show any defects in HD compared to WT (Figure 8D).

Discussion

In this study, we measured the ability of various substrates to support mitochondrial respiration in intact primary striatal and cortical neurons obtained from WT and HD rat embryos. These studies were designed to detect potential metabolic differences in HD neurons that could contribute to the pattern of neurodegeneration found in HD. We detected no specific mitochondrial respiratory chain defects in either cortical or striatal neurons from HD rats. By contrast, we found defects in glycolysis that are present even in cells prepared from embryos, but only in primary striatal and not cortical neurons derived from this rat HD model even though mHtt aggregates are present in both types of neurons (see Figure S1).

As previously mentioned, most of the studies exploring mitochondrial defects in HD models were done using brain extracts containing heterogeneous mixtures of neuronal and glial mitochondria, which may have precluded clear conclusions. In this study, we monitored metabolic rates in specific primary neuronal subpopulations (cortical or striatal) attached to the culture plates after 7 days in culture using extracellular flux measurement technology [29]. This allowed us to measure OCR in intact cells including all mitochondria populations located in neuronal cell bodies as well as neurites. Indeed, mitochondria localized in dendrites, axon shafts and presynaptic terminals play a key role in neuronal metabolism and in neuroplasticity [34] and these structures are largely left behind when neurons are detached from their culture surface for respiration measurements; this mitochondrial fraction is important especially when considering that axonal transport is disturbed in HD [35]. In addition, these studies highlighted the importance of alternate substrates to support neuronal respiration along with physiological glucose concentrations found in brain, particularly when respiration demand is high. The normal plasma glucose concentration is around 4.5 mM; however, the glucose concentration in the CNS is only about 2.5 mM [31,36]. Neurobasal™ medium, commonly used to culture primary neurons contains 25 mM glucose, a supra-physiological concentration. We found that glucose dose-dependently increased neuronal spare respiratory capacity and RCR and that 2.5 mM glucose was clearly suboptimal to support neurons under high respiratory demand. We then found that both lactate and pyruvate were individually able to support mitochondrial respiration in intact neurons and that these alternative substrates could provide additional respiratory capacity beyond that provided by CNS levels of glucose when neurons were challenged with an uncoupling agent. These results highlight the importance of neuronal glial coupling whereby glucose utilization by astrocytes results in the release of lactate that can then be taken up and used by neurons to support respiration [37-39]. Lactate conversion to pyruvate may take place preferentially in nerve terminals depending on differential distribution of LDH isoforms found in neuron cell bodies and terminals [40]. Furthermore, MCT1 transporters have recently been implicated in lactate exchange between oligodendrocytes and neuronal axons [41]. Interestingly, we observed an additive effect of glucose and pyruvate on maximal, FCCP-stimulated OCR (refer to maximal OCR in Figures 4, 5, 6). These results support the existence of a glucose dependent but pyruvate independent system transferring electrons to the respiratory chain in neurons. Indeed, the glycerol 3-phosphate shuttle directly transfers electrons to coenzyme Q in the mitochondrial inner membrane. This shuttle, active in neurons, is regulated by NADH/NAD+ and calcium and depends on the first step of glycolysis [42-44].

When HD striatal neurons were incubated in substrate-rich media containing a supra-physiological glucose concentration, no respiratory deficits were detected. These results are consistent with previous results obtained in HD knock-in mouse primary striatal neurons [25] where mitochondrial respiration was monitored in medium containing 15 mM glucose. In addition to these results, we now show that when the respiration demand is high, HD striatal neurons exhibit respiratory deficits when supplied with 2.5 mM glucose either alone or when supplemented with lactate or pyruvate. When pyruvate was the sole substrate present in the assay media, no significant respiratory deficits were observed in HD striatal neurons. These results argue for an alteration in glucose uptake and/or in glycolysis in HD rather than any defects in the respiratory chain itself. This hypothesis is further supported by the fact that deficits were only detected in the presence of physiological glucose concentrations but not when glucose was abundant. Moreover, because glucose defects in OCR were not compensated by pyruvate addition, it appears that a

Figure 7

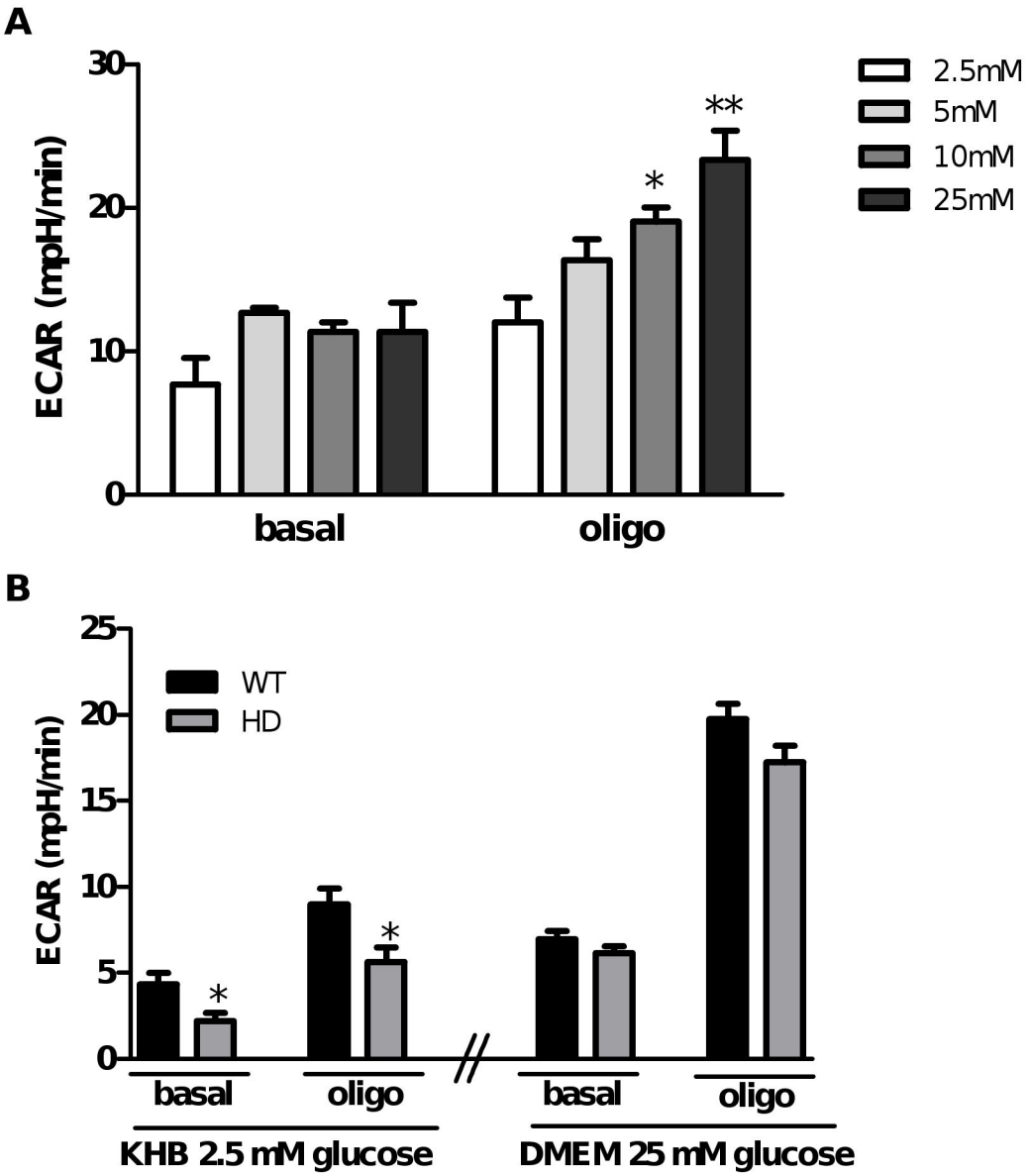

Figure 7. HD striatal neurons have a lower capacity to use anaerobic glycolysis in the presence of high and low glucose concentrations. Striatal neurons were cultivated for 7 days in Neurobasal™ medium containing 25 mM glucose and complemented with B27 and pyruvate (1 mM). A) On the day of the respiration experiments, medium was replaced with substrate-free KHB and WT cells were incubated for 1 h at 37°C. ECAR was measured after injection of different concentrations of glucose then oligomycin. Data are mean ± SEM and derived from the same experiment presented in Figure 2. * $p < 0.05$, ** $p < 0.01$ vs. 2.5 mM glucose. B) On the day of the respiration experiments, cells were incubated in 2.5 mM glucose in KHB medium or bicarbonate- and HEPES-free DMEM containing 25 mM glucose complemented with pyruvate (1 mM) for 1 h at 37°C. ECAR was measured under basal conditions and after oligomycin stimulation. Data are mean ± SEM from all independent experiments (2.5 mM glucose: five replicates in each of five experiments, n=25; 25 mM glucose: eleven replicates in each of seven experiments, n=77). . * $p<0.05$, ** $p < 0.01$ comparing WT vs. HD.

doi: 10.1371/journal.pone.0081528.g007

Figure 8

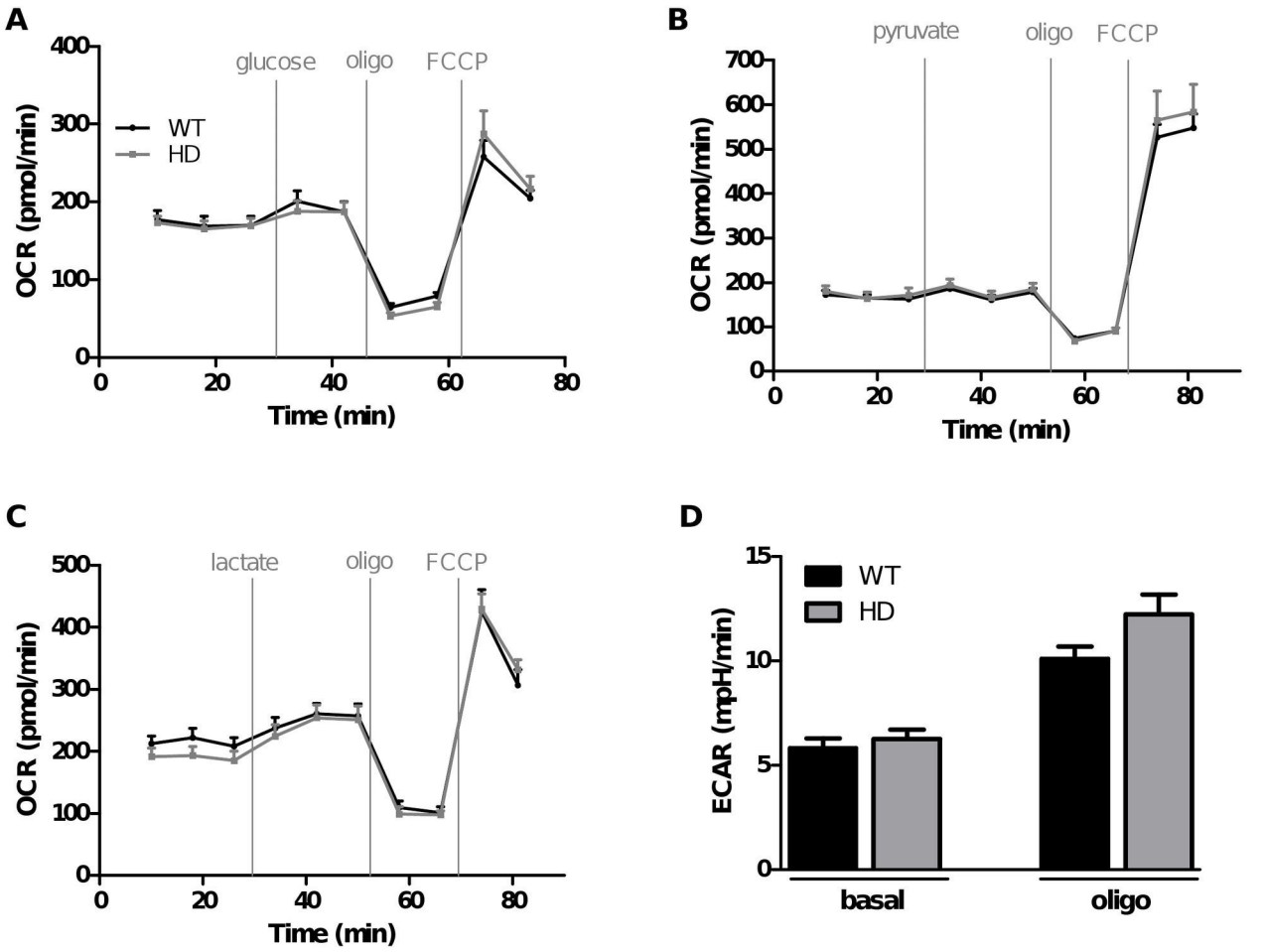

Figure 8. HD cortical neurons had no metabolic deficits regardless of the substrate supplied. HD and WT cortical neurons were cultivated for 7 days in Neurobasal™ medium complemented with B27 and pyruvate (1 mM). One hour before the start of respiration experiments, medium was replaced with substrate-free KHB and incubated at 37°C before being placed in the Seahorse analyser. OCR measurements were performed as described in Figures 2 and 3. OCR measurements following injection of (A) 2.5 mM glucose, (B) 10 mM pyruvate or (C) 10 mM lactate followed by oligomycin (oligo) and FCCP (2 µM) at the indicated times. D) ECAR was measured in the presence of 2.5 mM glucose under basal conditions and after oligomycin stimulation. Data shown in panels A-C are from representative experiments while data in panel D is the mean ± SEM calculated from all replicates (eight replicates for each substrate in each of two independent experiments)..

doi: 10.1371/journal.pone.0081528.g008

glucose-dependent but pyruvate independent electron transfer pathway is down regulated in HD primary striatal neurons. Extracellular acidification is a valid indicator of the anaerobic glycolysis rate (metabolic pathway converting glucose into lactate) and a valuable tool for analysing cellular bioenergetics [29,45]. Here, we observed that ECAR deficits were detected in HD striatal neurons both when incubated in culture medium containing a supra-physiological glucose concentration but also in KHB containing 2.5 mM glucose. Taken together, the OCR and ECAR data strongly support the hypothesis that striatal glycolysis deficits occur early in HD pathogenesis. Dysregulation in glycolysis has been reported in several studies in animal and cellular HD models or in patients [20,46-48]. Additionally, Powers and colleagues reported a preserved mitochondrial oxidative metabolism in early HD patients with striatal atrophy, indicating that defects in respiratory chain enzymes observed in post mortem brain are either not sufficient to explain oxidative phosphorylation impairments or are not present early in the time course of the disease [20]. They also reported in the same early HD patients

a decrease in cerebral glucose metabolism indicating a selective impairment of striatal glycolytic metabolism [20]. Very recently, Zala et al. showed that the glycolytic enzyme, GAPDH, is located on neuron vesicles and that local glycolysis powers vesicular fast axonal transport. Additionally, the authors demonstrated that huntingtin is a scaffold that joins GAPDH to these vesicles, suggesting that mutations in huntingtin could perturb glycolysis-generated ATP necessary for vesicle motility [49].

Interestingly, in our study, even though mHtt aggregates are present in both cell types, metabolic defects were only detected in embryonic striatal neurons and not in cortical neurons, a brain region affected later in Huntington disease progression. Indeed, cortical neurons showed neither OCR deficits nor ECAR alterations in the presence of a physiological concentration of glucose. These results provide additional insight into the mechanisms of selective striatal neurodegeneration and into the relative metabolic vulnerability of different cellular populations to mHtt toxicity. In the light of the present study, it might be argued that striatal neurons seem to have different metabolic requirements compared to cortex and may have a reduced capacity to manage substrate deprivation. Indeed, we can observe in Figures 4A and 8A that glucose injection did not have the same impact on basal OCR in striatal and cortical neurons. In striatal neurons a significant increase of 31.5 ± 5.8% was observed in response to glucose injection; for cortical neurons, which had a higher basal OCR in the absence of glucose, the response was only 9 ± 2.9%.

In summary, early glycolysis defects are found specifically in HD striatal neurons. These subtle defects, observed only with levels of glucose found in brain, may only have adverse consequences after prolonged stress or in combination with other age-related declines in metabolism, explaining why neurodegeneration only becomes evident in HD gene carriers in middle age. These results can be related to new insights in pre-symptomatic carriers of apolipoprotein E4, who show reduced cerebral glucose metabolism even before Aβ aggregation and decades before the onset of AD pathology [50,51]. These brain functional abnormalities in neurodegenerative disease gene carriers argue for early prevention therapies, decades before the onset of cognitive or motor symptoms.

Supporting Information

Protocol S1. Methods for assessing mhtt expression in primary neuronal cultures.
(DOC)

Figure S1. Confirmation of mhtt expression in primary neuronal cultures. Primary striatal and cortical neurons from HD rats express mhtt. SDS-insoluble and thus aggregated proteins were trapped on a nitrocellulose membrane and probed with a polyQ-specific antibody. The presence of aggregated polyQ-containing protein in primary striatal and cortical cultures from HD rat embryos but not their WT littermates indicates the expression of aggregated forms of mhtt in these neurons. Each dot is the extract from a separate neuronal culture, prepared from an individual WT or HD embryo.
(TIF)

Acknowledgements

We are grateful to all the members of the Mitotarget consortium for their helpful comments throughout the project. We also thank colleagues at Trophos for their assistance and comments during the course of this work.

Author Contributions

Conceived and designed the experiments: CG LEC HPN TB RMP. Performed the experiments: CG GT JT VL LEC MM. Analyzed the data: CG LEC HPN TB RMP. Contributed reagents/materials/analysis tools: LEC LY-T HPN. Wrote the manuscript: CG LEC HPN TB RMP.

References

1. Bruyn GW (1979) Huntington's chorea. Tijdschr Ziekenverpl 32: 101-105. PubMed: 154197.
2. Vonsattel JP, Myers RH, Stevens TJ, Ferrante RJ, Bird ED et al. (1985) Neuropathological classification of Huntington's disease. J Neuropathol Exp Neurol 44: 559-577. doi:10.1097/00005072-198511000-00003. PubMed: 2932539.
3. Djoussé L, Knowlton B, Cupples LA, Marder K, Shoulson I et al. (2002) Weight loss in early stage of Huntington's disease. Neurology 59: 1325-1330. Available online at: doi:10.1212/01.WNL.0000031791.10922.CF. PubMed: 12427878.
4. Browne SE (2008) Mitochondria and Huntington's disease pathogenesis: insight from genetic and chemical models. Ann N Y Acad Sci 1147: 358-382. doi:10.1196/annals.1427.018. PubMed: 19076457.
5. van der Burg JM, Bacos K, Wood NI, Lindqvist A, Wierup N et al. (2008) Increased metabolism in the R6/2 mouse model of Huntington's disease. Neurobiol Dis 29: 41-51. doi:10.1016/j.nbd.2007.07.029. PubMed: 17920283.
6. Hayden MR, Martin WR, Stoessl AJ, Clark C, Hollenberg S et al. (1986) Positron emission tomography in the early diagnosis of Huntington's disease. Neurology 36: 888-894. doi:10.1212/WNL.36.7.888. PubMed: 2940474.
7. Kuhl DE, Phelps ME, Markham CH, Metter EJ, Riege WH et al. (1982) Cerebral metabolism and atrophy in Huntington's disease determined by 18FDG and computed tomographic scan. Ann Neurol 12: 425-434. doi:10.1002/ana.410120504. PubMed: 6217782.
8. Kuwert T, Lange HW, Langen KJ, Herzog H, Aulich A et al. (1990) Cortical and subcortical glucose consumption measured by PET in patients with Huntington's disease. Brain 113 (5): 1405-1423. doi: 10.1093/brain/113.5.1405. PubMed: 2147116.
9. Jenkins BG, Koroshetz WJ, Beal MF, Rosen BR (1993) Evidence for impairment of energy metabolism in vivo in Huntington's disease using localized 1H NMR spectroscopy. Neurology 43: 2689-2695. doi: 10.1212/WNL.43.12.2689. PubMed: 8255479.
10. Koroshetz WJ, Jenkins BG, Rosen BR, Beal MF (1997) Energy metabolism defects in Huntington's disease and effects of coenzyme Q10. Ann Neurol 41: 160-165. doi:10.1002/ana.410410206. PubMed: 9029064.
11. Martin WR, Wieler M, Hanstock CC (2007) Is brain lactate increased in Huntington's disease? J Neurol Sci 263: 70-74. doi:10.1016/j.jns.2007.05.035. PubMed: 17655868.
12. Reynolds NC Jr., Prost RW, Mark LP (2005) Heterogeneity in 1H-MRS profiles of presymptomatic and early manifest Huntington's disease.

Brain Res 1031: 82-89. doi:10.1016/j.brainres.2004.10.030. PubMed: 15621015.
13. Sánchez-Pernaute R, García-Segura JM, del Barrio Alba A, Viaño J, de Yébenes JG (1999) Clinical correlation of striatal 1H MRS changes in Huntington's disease. Neurology 53: 806-812. doi:10.1212/WNL.53.4.806. PubMed: 10489045.
14. Unschuld PG, Edden RA, Carass A, Liu X, Shanahan M et al. (2012) Brain metabolite alterations and cognitive dysfunction in early Huntington's disease. Mov Disord 27: 895-902. doi:10.1002/mds.25010. PubMed: 22649062.
15. van den Bogaard SJ, Dumas EM, Teeuwisse WM, Kan HE, Webb A et al. (2011) Exploratory 7-Tesla magnetic resonance spectroscopy in Huntington's disease provides in vivo evidence for impaired energy metabolism. J Neurol 258: 2230-2239. doi:10.1007/s00415-011-6099-5. PubMed: 21614431.
16. Gu M, Gash MT, Mann VM, Javoy-Agid F, Cooper JM et al. (1996) Mitochondrial defect in Huntington's disease caudate nucleus. Ann Neurol 39: 385-389. doi:10.1002/ana.410390317. PubMed: 8602759.
17. Browne SE, Bowling AC, MacGarvey U, Baik MJ, Berger SC et al. (1997) Oxidative damage and metabolic dysfunction in Huntington's disease: selective vulnerability of the basal ganglia. Ann Neurol 41: 646-653. doi:10.1002/ana.410410514. PubMed: 9153527.
18. Damiano M, Galvan L, Déglon N, Brouillet E (2010) Mitochondria in Huntington's disease. Biochim Biophys Acta 1802: 52-61. doi:10.1016/j.bbadis.2009.07.012. PubMed: 19682570.
19. Guidetti P, Charles V Chen EY, Reddy PH, Kordower JH et al. (2001) Early degenerative changes in transgenic mice expressing mutant huntingtin involve dendritic abnormalities but no impairment of mitochondrial energy production. Exp Neurol 169: 340-350. doi:10.1006/exnr.2000.7626. PubMed: 11358447.
20. Powers WJ, Videen TO, Markham J, McGee-Minnich L, Antenor-Dorsey JV et al. (2007) Selective defect of in vivo glycolysis in early Huntington's disease striatum. Proc Natl Acad Sci U S A 104: 2945-2949. doi:10.1073/pnas.0609833104. PubMed: 17299049.
21. Milakovic T, Johnson GV (2005) Mitochondrial respiration and ATP production are significantly impaired in striatal cells expressing mutant huntingtin. J Biol Chem 280: 30773-30782. doi:10.1074/jbc.M504749200. PubMed: 15983033.
22. Seong IS, Ivanova E, Lee JM, Choo YS, Fossale E et al. (2005) HD CAG repeat implicates a dominant property of huntingtin in mitochondrial energy metabolism. Hum Mol Genet 14: 2871-2880. doi:10.1093/hmg/ddi319. PubMed: 16115812.
23. Siddiqui A, Rivera-Sánchez S, Castro MD, Acevedo-Torres K, Rane A et al. (2012) Mitochondrial DNA damage Is associated with reduced mitochondrial bioenergetics in Huntington's disease. Free Radic Biol Med, 53: 1478–88. PubMed: 22709585.
24. Milakovic T, Quintanilla RA, Johnson GV (2006) Mutant huntingtin expression induces mitochondrial calcium handling defects in clonal striatal cells: functional consequences. J Biol Chem 281: 34785-34795. doi:10.1074/jbc.M603845200. PubMed: 16973623.
25. Oliveira JM, Jekabsons MB, Chen S, Lin A, Rego AC et al. (2007) Mitochondrial dysfunction in Huntington's disease: the bioenergetics of isolated and in situ mitochondria from transgenic mice. J Neurochem 101: 241-249. doi:10.1111/j.1471-4159.2006.04361.x. PubMed: 17394466.
26. Oliveira JM, Chen S, Almeida S, Riley R, Gonçalves J et al. (2006) Mitochondrial-dependent Ca2+ handling in Huntington's disease striatal cells: effect of histone deacetylase inhibitors. J Neurosci 26: 11174-11186. doi:10.1523/JNEUROSCI.3004-06.2006. PubMed: 17065457.
27. Yu-Taeger L, Petrasch-Parwez E, Osmand AP, Redensek A, Metzger S et al. (2012) A Novel BACHD Transgenic Rat Exhibits Characteristic Neuropathological Features of Huntington Disease. J Neurosci 32: 15426-15438. doi:10.1523/JNEUROSCI.1148-12.2012. PubMed: 23115180.
28. Friedman WJ, Ibáñez CF, Hallböök F, Persson H, Cain LD et al. (1993) Differential actions of neurotrophins in the locus coeruleus and basal forebrain. Exp Neurol 119: 72-78. doi:10.1006/exnr.1993.1007. PubMed: 8432352.
29. Wu M, Neilson A, Swift AL, Moran R, Tamagnine J et al. (2007) Multiparameter metabolic analysis reveals a close link between attenuated mitochondrial bioenergetic function and enhanced glycolysis dependency in human tumor cells. Am J Physiol Cell Physiol 292: C125-C136. PubMed: 16971499.
30. Brand MD, Nicholls DG (2011) Assessing mitochondrial dysfunction in cells. Biochem J 435: 297-312. doi:10.1042/BJ20110162. PubMed: 21726199.
31. Silver IA, Erecińska M (1994) Extracellular glucose concentration in mammalian brain: continuous monitoring of changes during increased neuronal activity and upon limitation in oxygen supply in normo-, hypo-, and hyperglycemic animals. J Neurosci 14: 5068-5076. PubMed: 8046468.
32. Magistretti PJ, Pellerin L (1999) Cellular mechanisms of brain energy metabolism and their relevance to functional brain imaging. Philos Trans R Soc Lond B Biol Sci 354: 1155-1163. doi:10.1098/rstb.1999.0471. PubMed: 10466143.
33. Han I, You Y, Kordower JH, Brady ST, Morfini GA (2010) Differential vulnerability of neurons in Huntington's disease: the role of cell type-specific features. J Neurochem 113: 1073-1091. PubMed: 20236390.
34. Cheng A, Hou Y, Mattson MP (2010) Mitochondria and neuroplasticity. ASN. New_Eur 2: e00045. PubMed: 20957078.
35. Li XJ, Orr AL, Li S (2010) Impaired mitochondrial trafficking in Huntington's disease. Biochim Biophys Acta 1802: 62-65. doi:10.1016/j.bbadis.2009.06.008. PubMed: 19591925.
36. Routh VH (2002) Glucose-sensing neurons: are they physiologically relevant? Physiol Behav 76: 403-413. doi:10.1016/S0031-9384(02)00761-8. PubMed: 12117577.
37. Magistretti PJ, Sorg O, Naichen Y, Pellerin L, de Rham S et al. (1994) Regulation of astrocyte energy metabolism by neurotransmitters. Ren Physiol Biochem 17: 168-171. PubMed: 7518950.
38. Pellerin L, Bouzier-Sore AK, Aubert A, Serres S, Merle M et al. (2007) Activity-dependent regulation of energy metabolism by astrocytes: an update. Glia 55: 1251-1262. doi:10.1002/glia.20528. PubMed: 17659524.
39. Pellerin L, Magistretti PJ (1994) Glutamate uptake into astrocytes stimulates aerobic glycolysis: a mechanism coupling neuronal activity to glucose utilization. Proc Natl Acad Sci U S A 91: 10625-10629. doi:10.1073/pnas.91.22.10625. PubMed: 7938003.
40. O'Brien J, Kla KM, Hopkins IB, Malecki EA, McKenna MC (2007) Kinetic parameters and lactate dehydrogenase isozyme activities support possible lactate utilization by neurons. Neurochem Res 32: 597-607. doi:10.1007/s11064-006-9132-9. PubMed: 17006762.
41. Fünfschilling U, Supplie LM, Mahad D, Boretius S, Saab AS et al. (2012) Glycolytic oligodendrocytes maintain myelin and long-term axonal integrity. Nature 485: 517-521. PubMed: 22622581.
42. McKenna MC, Waagepetersen HS, Schousboe A, Sonnewald U (2006) Neuronal and astrocytic shuttle mechanisms for cytosolic-mitochondrial transfer of reducing equivalents: current evidence and pharmacological tools. Biochem Pharmacol 71: 399-407. doi:10.1016/j.bcp.2005.10.011. PubMed: 16368075.
43. Nguyen NH, Bråthe A, Hassel B (2003) Neuronal uptake and metabolism of glycerol and the neuronal expression of mitochondrial glycerol-3-phosphate dehydrogenase. J Neurochem 85: 831-842. doi:10.1046/j.1471-4159.2003.01762.x. PubMed: 12716415.
44. Ramos M, del Arco A, Pardo B, Martinez-Serrano A, Martinez-Morales JR et al. (2003) Developmental changes in the Ca2+-regulated mitochondrial aspartate-glutamate carrier aralar1 in brain and prominent expression in the spinal cord. Brain Res. Dev Brain Res 143: 33-46. doi:10.1016/S0165-3806(03)00097-X.
45. Gohil VM, Sheth SA, Nilsson R, Wojtovich AP, Lee JH et al. (2010) Nutrient-sensitized screening for drugs that shift energy metabolism from mitochondrial respiration to glycolysis. Nat Biotechnol 28: 249-255. PubMed: 20160716.
46. Ferreira IL, Cunha-Oliveira T, Nascimento MV, Ribeiro M, Proença MT et al. (2011) Bioenergetic dysfunction in Huntington's disease human cybrids. Exp Neurol 231: 127-134. doi:10.1016/j.expneurol.2011.05.024. PubMed: 21684277.
47. Oláh J, Klivényi P, Gardián G, Vécsei L, Orosz F et al. (2008) Increased glucose metabolism and ATP level in brain tissue of Huntington's disease transgenic mice. FEBS J 275: 4740-4755. doi:10.1111/j.1742-4658.2008.06612.x. PubMed: 18721135.
48. Jin YN, Hwang WY, Jo C, Johnson GV (2012) Metabolic state determines sensitivity to cellular stress in Huntington disease: normalization by activation of PPARgamma. PLOS ONE 7: e30406. doi:10.1371/journal.pone.0030406. PubMed: 22276192.
49. Zala D, Hinckelmann MV, Yu H, Lyra da Cunha MM, Liot G et al. (2013) Vesicular glycolysis provides on-board energy for fast axonal transport. Cell 152: 479-491. doi:10.1016/j.cell.2012.12.029. PubMed: 23374344.
50. Jagust WJ, Landau SM (2012) Apolipoprotein E, Not Fibrillar beta-Amyloid, Reduces Cerebral Glucose Metabolism in Normal. Aging - J Neuroscience 32: 18227-18233. doi:10.1523/JNEUROSCI.3266-12.2012.
51. Reiman EM, Chen K, Alexander GE, Caselli RJ, Bandy D et al. (2004) Functional brain abnormalities in young adults at genetic risk for late-onset. Alzheimer'S Dementia - Proc Natl Acad Sci U S A 101: 284-289. doi:10.1073/pnas.2635903100.

Supporting Information

Protocol S1

Striatal and cortical neurons prepared from individual HD and WT embryos were cultured in 6-well plates at a density of 1,000,000 cells/well for cortex and 2,000,000 cells/well for striatum. After 7 days in vitro, cells were harvested by trypsinization (1 ml of 0.25 % trypsin with EDTA (Gibco) per well) and centrifugation (10 min at 400xg). Proteins were extracted from cell pellets by incubation in 100 µl RIPA buffer (50 mM Tris-HCl, pH 8.0, 150 mM NaCl, 1 % IGPAL (NP-40 substitute), 0.5 % sodiumdesoxychelate, 0.1 % SDS) containing 4 % cOmplete ULTRA Protease Inhibitor-Cocktail with EDTA (Roche) for 30 min at 4 °C and subsequent centrifugation for 15 min at 4 °C at 16.400xg. Supernatant was collected and protein content for each sample was measured using a Bradford assay. The samples were stored at -80 °C until further use. For the analysis of mhtt expression in these samples, we performed a filter trap assay [1] optimized for the detection of mhtt. The method is based on the SDS-insolubility of mhtt aggregates, which are retained when filtered through a nitrocellulose membrane. For this purpose, 20 µg of lysate protein was mixed with SDS (final concentration 2 %) and filtered using a dot blotter (Dot blotter SRC 96 D, S&S Minifold I, Schleicher & Schuell, Germany). The membrane (Protran Nitrocellulose Membrane, Whatman) was afterwards probed with 1C2 anti-polyQ-antibody (MAB1574, Millipore, 1:2000) overnight at 4 °C and on the next day incubated for 1 hour at room temperature with the secondary, horse-radish-peroxidase-linked anti-mouse IgG antibody (NA931, Amersham Biosiences, 1:2500). Chemiluminescence was created using ECL Western Blotting Detection Reagent (Amersham Biosciences) and detected with the Odyssey FC (LI-COR Biosciences), showing aggregated forms of polyQ-containing protein (mhtt) (Fig S1).

1. Wanker EE, Scherzinger E, Heiser V, Sittler A, Eickhoff H, et al. (1999) Membrane filter assay for detection of amyloid-like polyglutamine-containing protein aggregates. Methods Enzymol 309: 375-386.

Figure S1

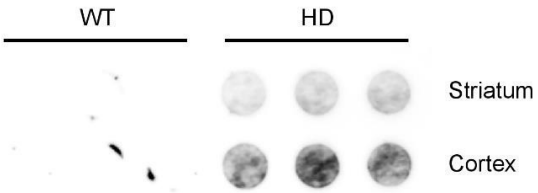

Mol Neurobiol
DOI 10.1007/s12035-014-8663-3

Mitochondrial Membrane Fluidity is Consistently Increased in Different Models of Huntington Disease: Restorative Effects of Olesoxime

Janett Eckmann · Laura E. Clemens · Schamim H. Eckert · Stephanie Hagl · Libo Yu-Taeger · Thierry Bordet · Rebecca M. Pruss · Walter E. Muller · Kristina Leuner · Huu P. Nguyen · Gunter P. Eckert

Received: 18 October 2013 / Accepted: 18 February 2014

Abstract Huntington disease (HD) is a fatal neurodegenerative disorder caused by a CAG repeat expansion in exon 1 of the huntingtin gene (*HTT*). One prominent target of the mutant huntingtin protein (mhtt) is the mitochondrion, affecting its morphology, distribution, and function. Thus, mitochondria have been suggested as potential therapeutic targets for the treatment of HD. Olesoxime, a cholesterol-like compound, promotes motor neuron survival and neurite outgrowth in vitro, and its effects are presumed to occur via a direct interaction with mitochondrial membranes (MMs). We examined the properties of MMs isolated from cell and animal models of HD as well as the effects of olesoxime on MM fluidity and cholesterol levels. MMs isolated from brains of aged *Hdh* Q111/Q111 knock-in mice showed a significant decrease in 1,6-diphenyl-hexatriene (DPH) anisotropy, which is inversely correlated with membrane fluidity. Similar increases in MM fluidity were observed in striatal ST*Hdh* Q111/Q111 cells as well as in MMs isolated from brains of BACHD transgenic rats. Treatment of ST*Hdh* cells with olesoxime decreased the fluidity of isolated MMs. Decreased membrane fluidity was also measured in olesoxime-treated MMs isolated from brains of HD knock-in mice. In both models, treatment with olesoxime restored HD-specific changes in MMs. Accordingly, olesoxime significantly counteracted the mhtt-induced increase in MM fluidity of MMs isolated from brains of BACHD rats after 12 months of treatment in vivo, possibly by enhancing MM cholesterol levels. Thus, olesoxime may represent a novel pharmacological tool to treat mitochondrial dysfunction in HD.

Keywords BACHD rat · Huntington disease · Membrane cholesterol · Membrane fluidity · Mitochondrial membrane

Abbreviations

AD	Alzheimer disease
α-FGF	Acidic fibroblast growth factor
CHOD-PAP	Cholesteroloxidase-peroxidase-aminophenazon-phenol
DMEM	Dulbecco's modified Eagle's medium
DMSO	Dimethylsulfoxide
DPH	1,6-Diphenyl-hexatriene
EDTA	Ethylenediamine tetra acetic acid
ETC.	Electron transfer chain

Janett Eckmann, Laura E. Clemens, Huu P. Nguyen, and Gunter P. Eckert contributed equally to this work.

J. Eckmann · S. H. Eckert · S. Hagl · W. E. Muller · K. Leuner · G. P. Eckert (✉)
Department of Pharmacology, Biocenter, Goethe-University Campus Riedberg, Biocentre Geb. N260, R.1.09, Max-von-Laue Str. 9, 60438 Frankfurt, Germany
e-mail: G.P.Eckert@em.uni-frankfurt.de
URL: www.nutritional-neuroscience.com

L. E. Clemens · L. Yu-Taeger · H. P. Nguyen
Institute of Medical Genetics and Applied Genomics, and Centre for Rare Diseases, University of Tuebingen, Calwerstr. 7, 72076 Tuebingen, Germany

H. P. Nguyen
e-mail: hoa.nguyen@med.uni-tuebingen.de

T. Bordet · R. M. Pruss
Discovery Research, Trophos SA, Parc Scientifique de Luminy - Case 931, 13288 Marseille, France

T. Bordet
e-mail: tbordet@gmail.com

R. M. Pruss
e-mail: rpruss@trophos.com

K. Leuner
Molecular and Clinical Pharmacy, University of Erlangen-Nuremberg, Erlangen, Germany

Published online: 18 March 2014

FCS	Fetal calf serum
HCl	Hydrochloride
HD	Huntington disease
HMG-CoA	3-Hydroxy-3-methyl-glutaryl-CoA
htt	Huntingtin gene
htt	Huntingtin protein
HTT	Human huntingtin gene
HEPES	4-2-Hydroxyethyl-1-piperazineethanesulfonic acid
IBMX	3-Isobutyl-1-methylxanthine
MβCD	Methyl-β-cyclodextrine
mhtt	Mutant huntingtin protein
mPT	Mitochondrial permeability transition
PBS	Phosphate-buffered saline
SPM	Synaptosomal plasma membrane
TPA	Phorbol 12-myristate 13-acetate
Tris	Trishydroxymethylaminomethan
TUDCA	Tauroursodeoxycholic acid
VDAC	Voltage-dependent anion channel

Introduction

Huntington disease (HD) is a fatal neurodegenerative disorder caused by a single genetic mutation—a CAG repeat expansion in exon 1 of the gene coding for the huntingtin protein (Htt) [1]. The disease is manifested mostly around the age of 40–50 [2] with symptoms including involuntary movements, psychiatric abnormalities, cognitive decline and metabolic disturbances, inevitably leading to the death of the patient [3]. To date, there is no effective treatment available to ameliorate the symptoms or prevent disease progression.

HD research has recently been focused on mitochondrial dysfunction. Mitochondria are complex organelles composed of two phospholipid bilayer membranes: the inner mitochondrial membrane (IMM) and outer mitochondrial membrane (OMM) [4]. Like other membranes, MMs are dynamic two-dimensional fluids consisting mainly of proteins and lipids [5]. The fluidity of the phospholipid bilayer modulates numerous essential cell functions, including the interaction and regulation of membrane-associated enzymes, receptors, and ion channels [6–9]. Membrane fluidity is mainly dependent on the protein and lipid composition, which in turn is determined by the types of unsaturated fatty acids and phospholipids as well as the cholesterol content [10]. Mitochondria generally contain only small amounts of cholesterol, concentrated in the OMM [11]. There is evidence that mitochondrial membrane fluidity regulates or modulates the function of essential proteins within the mitochondrial membrane and vice versa. The IMM harbors the proteins of the electron transfer chain (ETC.), and its integrity is critical for the activity of the ETC. complexes, which drive ATP production. Accordingly, a correlation between membrane fluidity and the mobility and function of single complexes of the ETC. has been established [12–15]. Recent studies also revealed that changes in mitochondrial membrane fluidity might have a direct impact on membrane-based processes such as fission-associated morphological changes, recruitment of pro-apoptotic factors, and mitochondrial permeability transition (mPT) [16, 17].

In HD, mitochondria are strongly affected by the presence of mutant htt (mhtt). Early mitochondrial impairments seem to concern defects in glycolysis [18, 19], while during disease progression, the functioning of the whole mitochondrial network is compromised (for review, please refer to [20–24]). N-terminal mhtt fragments have been shown to bind to the OMM [25–28], altering the activity of the fission and fusion proteins Drp1 and Mfn2 and leading to a fragmentation of the mitochondrial network [28–32] as well as an impairment of axonal mitochondrial transport [27, 31–33]. In the presence of mhtt, mitochondria further seem to be more susceptible to oxidative stress and have a lower Ca^{2+} uptake capacity, lower respiratory capacity, and decreased ATP production rates [26, 34, 35].

Based on the strong evidence for mitochondrial impairments in HD, mitochondria-targeting molecules as coenzyme Q10, *N*-acetyl-L-cysteine, carnitine, or bezafibrate have been evaluated in therapeutic approaches with beneficial effects [36–41]. Another promising compound has been identified in a phenotypic screening approach to promote the survival of primary motor neurons [42]. Olesoxime (cholest-4-en-3-one, oxime) is a cholesterol-like molecule that was found to interact with the voltage-dependent anion channel (VDAC) and the translocator protein (TSPO) [42]. VDAC and TSPO are two proteins of the outer mitochondrial membrane that are involved in Ca^{2+} homeostasis [43], metabolite exchange [44], and cholesterol transport [45]. Both proteins are further involved in mPT. Consistent with this, olesoxime was able to rescue cortical neurons from apoptotic cell death induced by camptothecin [18]. Furthermore, olesoxime has shown beneficial effects in disease models of amyotrophic lateral sclerosis [42, 46] and peripheral neuropathies [47, 48]. Furthermore, olesoxime is readily taken up by cells and accumulates in mitochondria [49].

Based on the initial finding of changed fluidity parameters in membranes isolated from *Hdh* Q111/Q111 knock-in mice [50], this study was carried out in order to evaluate membrane fluidity as a common feature for mitochondrial dysfunction in HD and to test the efficacy of olesoxime in targeting changes in membrane properties of mitochondria using in vitro and in vivo models of HD.

Materials and Methods

Chemicals

Chemicals were purchased from Sigma-Aldrich, Hamburg, Germany, cell culture media were purchased from Invitrogen

GmbH, Karlsruhe, Germany, and olesoxime (TRO19622) was kindly provided by Trophos SA, Marseille, France.

Animal and Cell Models of HD

All experiments were carried out by individuals with appropriate training and experience according to the requirements of the Federation of European Laboratory Animal Science Associations and the European Communities Council Directive (Directive 2010/63/EU). The commission for animal experiments at the "Regierungspräsidium Tübingen" in accordance with the guidelines of the German Animal Welfare Act approved all experiments.

STHdh Cells In our experiments, we used a striatal cell line derived from *Hdh* Q111/111 knock-in mice (detailed description below) containing homozygous huntingtin gene (*htt*) loci with a humanized exon 1 with 111 CAG repeats (ST*Hdh* Q111/Q111) and a striatal cell line derived from wild-type mice containing endogenous *htt* with 7 CAG repeats (ST*Hdh* Q7/Q7). ST*Hdh* cell lines were purchased from Coriell Cell Repositories and originate from the laboratory of Dr. Marcy MacDonald (Harvard Medical School, Boston, USA).

Cell Culture

Both cell lines were cultured in Dulbecco's modified Eagle's medium (DMEM), supplemented with 10 % heat-inactivated fetal calf serum (FCS), 100 units/ml penicillin, 100 μg/ml streptomycin, and 0.4 mg/ml G418. The cells were cultured at 37 °C in a humidified incubator containing 5 % CO_2.

Differentiation of ST*Hdh* Cells and Olesoxime Treatment

Cells were grown in T175 flasks with a complete medium until they reached 70 % confluence. Cells were treated with fresh media including 1.0, 3.0, or 10.0 μM olesoxime (in dimethylsulfoxide (DMSO)) or fresh media including 0.05 % DMSO only for control. After 18 h of olesoxime treatment, differentiation was initiated by adding 7 ml of dopamine cocktail (Forskolin 50 μmol/l, 3-isobutyl-1-methylxanthine (IBMX) 250 μmol/l, TPA 0.2 μmol/l, dopamine 10 μmol/l, and α-FGF 10 ng/ml in DMEM). Morphological changes were visible as early as 30 min after induction of differentiation. After 6 h, cells were harvested in ice-cold phosphate-buffered saline (PBS; pH 7.4) at 4 °C. The cell suspension was centrifuged for 10 min at 600×*g*. The supernatant was discarded, and the cell pellets were stored at −20 °C until membrane isolation was performed.

HD Knock-in Mice Hdh Q111/111 knock-in mice (C57BL/6 J-*Hdh*(111Q)KI-MacD) were obtained from Dr. Marcy MacDonald (Harvard Medical School, Boston, USA) and bred for more than ten generations in our facility before the study. They were kept at 21–23 °C ambient temperature, 55± 10 % humidity, and a 12:12-h light/dark cycle with lights on from 3:00 a.m. to 3:00 p.m. According to the ETS 123, Appendix A, animals were kept in groups of two to five animals of the same sex and mixed genotype in type IV, autoclavable plastic cages with high lid, containing autoclaved wooden bedding and nesting material. Cages were cleaned once a week. Food and water were delivered ad libitum. The mice were weaned at 21 days of age and kept without any behavioral testing until they were sacrificed at the age of 3–9 months (adult) or 18–20 months (aged).

BACHD Rats The SPRD-BACHDflhtt97Q-TG5 rat [51] was generated with a BAC construct, previously implemented to generate the BACHD mouse [52]. BACHD rats express the full-length human mutant huntingtin gene (m*HTT*) with 97 mixed CAA-CAG repeats. BACHD rat line TG5, which was used in this study, is characterized by a high copy number of m*HTT* as well as a high RNA and protein expression. BACHD rats display behavioral abnormalities and neuropathology similar to HD patients [51].

Housing conditions followed the recommendations of the European Union (ETS 123, Appendix A). The environmental conditions in the housing room amounted to 21–23 °C ambient temperature, 55±10 % humidity, and a 12:12-h light/dark cycle with lights off at 2:00 p.m. and lights on at 2:00 a.m. Animals were kept in groups of four animals of mixed genotype (two wt to two mut) in type IV, autoclavable plastic cages with high lid, containing autoclaved wooden bedding. Cages were cleaned twice a week. Food and water were delivered ad libitum.

Animals were weaned at 21 days of age. At 5 weeks of age, the food was changed from a standard rat housing chow (ssniff V1534-000, SSNIFF Germany) to either a control diet (Altromin C1000, Altromin Germany) or the same diet loaded with 600 mg/kg olesoxime. At 13 months of age, after 12 months of olesoxime treatment, the rats were sacrificed, and mitochondrial parameters were measured.

Membrane Isolation from Cells

For the isolation of cellular mitochondrial and plasma membranes, harvested cell pellets were homogenized in 5 mmol/l trishydroxymethylaminomethan-hydrochloride (Tris–HCl) (pH 8.5) applying 15 strokes with a Teflon® pestle at 1,100 rpm. The homogenate was lysed on ice for 1 h and 15 min and vortexed vigorously every 15 min. After lysis, the homogenate was centrifuged at 20,000 rpm, and the pellet was resuspended in ice-cold deionized water and homogenized once more as described above (15 strokes, 1,100 rpm). The homogenate was under-layered with a sucrose solution

(1.5 mol/l sucrose, 10 mmol/l 4-2-hydroxyethyl-1-piperazineethanesulfonic acid (HEPES), 0.25 mmol/l ethylenediamine tetra acetic acid (EDTA)) and centrifuged at 68,000×*g*. The resulting pellet containing mitochondrial membranes was resuspended in 5 mmol/l Tris–HCl (pH 7.4) and stored at −20 °C. The interface was collected, washed with ice-cold deionized water, and centrifuged at 20,000×*g*. The pellet containing the plasma membranes was resuspended in 5 mmol/l Tris–HCl (pH 7.4) and stored at −20 °C.

Membrane Isolation from Brain Tissue

The isolation of mitochondrial and synaptosomal plasma membranes (SPMs) was performed according to Eckert et al. [53]. Two mouse brains or one rat hemisphere (without brain stem and cerebellum) were homogenized in buffer I (0.32 M sucrose, 10 mM HEPES; 1 mM EDTA, pH 7.4) and centrifuged at 585×*g* at 4 °C. The supernatant was centrifuged twice at 17,400×*g* at 4 °C. Pellets contained synaptosomes and mitochondria. The pellets were resuspended in buffer I and layered over a density gradient of 7.5 and 13 % Ficoll solution (wt/vol). The gradients were centrifuged for 60 min at 87,300×*g*. The pellet containing enriched brain mitochondrial membranes was resuspended in 5 mmol/l Tris–HCl and stored at −20 °C. After centrifugation, the lower interface of the gradient was collected, suspended in buffer I, centrifuged first at 17,400×*g*, and after resuspension in buffer I, centrifuged again at 14,600×*g* for washing. The resulting synaptosomal pellet was resuspended in buffer II (5 mmol/l Tris–HCl; pH 8.5). For lysis, the synaptosomes were kept on ice for 1 h while vortexing every 10 min. After this, the suspension was centrifuged for 20 min at 43,000×*g*. The pellet was resuspended in ice-cold deionized water, under-layered with a sucrose solution (1.5 M sucrose, 10 mM HEPES, 0.25 mM EDTA), and centrifuged for 45 min at 41,000×*g*. The synaptosomal plasma membranes at the interface were carefully removed, suspended in 50 mM Tris–HCl buffer, and stored at −20 °C.

Membrane Fluidity Measurement

Membrane fluidity was assessed using the lipophilic probe 1,6-diphenyl-hexatriene (DPH) and fluorescence polarization spectrometry [10]. Hereby, fluorescence anisotropy is inversely correlated with membrane fluidity. DPH mainly localizes in the hydrocarbon core and intercalates preferentially axial, between the acyl chains of the phospholipid bilayer. Thus, steady state polarization of DPH provides an overall measure of the structural order of the membrane interior. For DPH measurements, 30 μl of membrane suspension (in 5 mM Tris–HCl, pH 7.4) with a protein concentration of 30 μg/100 μl (protein concentration was determined according to the Lowry method [54]) was incubated with 250 μl Tris–HCl (5 mM, pH 7.4). Then, 350 μl of a 1:150 diluted DPH stock solution (5 mM in tetrahydrofuran) and either 70 μl of Tris–HCl (5 mM, pH 7.4) as a control or 70 μl of olesoxime suspension (in case of mouse brains) were added and incubated at 37 °C for 45 min. Steady state anisotropy was directly measured at 37 °C in a quartz cuvette (Hellma analytics, Müllheim Germany) in a SLM Luminescence Spectrometer Aminco-Bowman® Series 2 (SLM Aminco, Urbana, USA) using excitation and emission wave lengths of 360 and 450 nm (slits 4 nm), respectively. The detector signal was adjusted to a maximum photomultiplier voltage of 80 %. Steady state fluorescence polarization (P_S) was expressed as the anisotropy r_S of the probe according to the equation: $r_S = 2P_S / 3 - P_S$.

Cholesterol Determination

Cholesterol was determined according to the cholesteroloxidase-peroxidase-aminophenazon-phenol (CHOD-PAP) method with slight modifications according to Kirsch et al. [55]. In brief, 0.5 % (*w*/*v*) methyl-β-cyclodextrine (MβCD) in combination with Brij 35 as a 15 % (*w*/*v*) aqueous solution was used to improve cholesterol extraction from the membrane. After 2 h of incubation, cholesterol was measured in triplicates at 490 nm in a micro-plate reader (DigiScan, ASYS Hitech GmbH).

Solubilization of Olesoxime

For in vitro application, olesoxime was freshly solubilized before each experiment in low amounts of MβCD. Briefly, 10 μl of olesoxime stock solution (20 mM in DMSO) was mixed with 990 μl of 0.5 mM MβCD in Tris–HCl, vortexed vigorously, and mixed on a thermomixer for 24 h at 1,400 rpm and 37 °C in order to reveal a homogenous, stabilized suspension. MβCD is known to extract cholesterol from biological membranes [56]. Thus, we carefully assessed the effects of MβCD on the parameters determined in the study and approved that the maximum concentration applied did not exert any effects per se.

Statistical Analysis

The data are given as the mean ± standard error of the mean (SEM). For statistical comparison, unpaired and two-sided *t*-tests and two-way ANOVA followed by Bonferroni post hoc test for multiple comparisons were used (GraphPad Software for Mac 5.0, San Diego, USA), since all data proved to be normally distributed. p values <0.05 were considered to be statistically significant.

Results

Mitochondrial dysfunction is a prominent pathological feature observed in HD disease models as well as HD patients. However, the properties of the mitochondrial membrane have not been addressed yet. For this reason, we measured membrane fluidity and cholesterol levels as its main determinant in mitochondrial membranes (MMs) and plasma membranes (PMs) or synaptosomal plasma membranes (SPMs) isolated from ST*Hdh* cells as well as 18–20-month-old HD knock-in mice and 13-month-old BACHD rats and their wild-type littermates. Membrane fluidity was assessed spectrophotometrically using the fluorescent probe DPH, which correlates inversely with the acyl-chain flexibility of fatty acids in the hydrocarbon core of lipid bilayers.

Mitochondrial Membrane Fluidity Is Altered in HD

Isolated MMs from differentiated ST*Hdh* cells showed a significant increase in mitochondrial membrane fluidity in the mutant ST*Hdh* Q111/Q111 cells compared to ST*Hdh* Q7/Q7 control cells (Fig. 1(a)).

We had reported before that mitochondrial membranes but not synaptosomal plasma membranes isolated from brains of adult (3–9-month-old) HD knock-in mice showed a similar increase in membrane fluidity, as we have now shown for ST*Hdh* cells, the cell line originating from these mice [50]. In order to investigate a potential progressive nature of mitochondrial membrane fluidity changes, we here analyzed membrane fluidity in aged (18–20-month-old) HD knock-in mice (Fig. 1(b)). A comparison between the previously obtained data of adult mice with the new data of aged mice (Fig. 2) showed that age had a significant impact on membrane fluidity but influenced the two genotypes in a different manner. Wild-type mice showed a significant increase in both mitochondrial membrane fluidity (Fig. 2(a)) and synaptosomal membrane fluidity (Fig. 2(b)), which is typically observed with aging [50, 53, 57]. On the contrary, no change in synaptosomal plasma membrane fluidity was observed in HD knock-in mice with aging (Fig. 2(a)), which leads to a significant genotype difference in synaptosomal plasma membrane fluidity in aged mice. Moreover, mitochondrial membrane fluidity further increased in aged HD knock-in mice (Fig. 2(b)). Overall, these findings point towards a disease-specific, progressive impairment in mutant mice.

In accordance with the results obtained from HD knock-in mice and ST*Hdh* cells, MMs isolated from BACHD rats also exhibited a disease-specific increase in membrane fluidity (Fig. 1(c)).

In contrast to MMs, the fluidity of PMs and SPMs was unchanged in HD cell and animal models (Fig. 1(a–c)).

HD-Related Alterations in Mitochondrial Membrane Fluidity Are Not Reflected by Changes in Cholesterol Content

Cholesterol represents a major modulator of membrane fluidity [58]. In line with our previous data, showing that plasma and mitochondrial membranes noticeably differ in cholesterol levels [50], MMs contained only a small amount of cholesterol compared to plasma membranes (Fig. 1(d–f)). Higher cholesterol levels in SPMs may account for their lower fluidity compared to MMs (Fig. 1(a–c)). In the HD models studied, a significant reduction of MM cholesterol was found only in BACHD rats (Fig. 1(f)). Cholesterol levels were unchanged in ST*Hdh* cells and HD knock-in mice (Fig. 1(d, e)). Thus, cholesterol levels might not be the major determinant of membrane fluidity changes found in MMs or SPMs isolated from different HD models.

Olesoxime Restores Membrane Fluidity and Cholesterol Levels Affected in HD Models

Olesoxime has cholesterol-like structure, enters the cell, and concentrates in mitochondria [42, 49], thus representing a possible modulator of mitochondrial membrane fluidity.

Treatment of differentiated HD cells with olesoxime for 24 h led to a disease-unspecific and dose-dependent decrease in mitochondrial membrane fluidity (Fig. 3). In both cell lines, 10 μM olesoxime decreased the fluidity of isolated MMs (Fig. 3(a, b)). In addition, olesoxime significantly enhanced the cholesterol content in MMs isolated from HD mutant and control cells (Fig. 3(c, d)). In contrast, olesoxime significantly reduced the cholesterol content in PMs isolated from HD mutant (1, 3, and 10 μM) and control cells (10 μM) (Fig. 3(e, f)).

Incubation of MMs isolated from brains of aged HD knock-in mice with olesoxime in vitro led to a dose-dependent increase in anisotropy, indicative of a decrease in membrane fluidity. As it was found for ST*Hdh* cells, a concentration of 10 μM olesoxime restored MM fluidity to control levels (Fig. 4a). Incubation of SPM isolated from brains of adult and aged HD mice with 30 μM olesoxime in vitro led to an increase in anisotropy, indicative of a decrease in membrane fluidity (Fig. 4b). Incubation of MMs and SPMs with olesoxime had no effect on cholesterol levels (data not shown).

In order to investigate if the effect of olesoxime on membrane fluidity found in vitro for MMs isolated from cells or mouse brains could also be demonstrated in vivo, membrane fluidity and cholesterol content were measured in MM and SPM fractions prepared from BACHD rats pretreated with olesoxime for 12 months. We found olesoxime restored brain MM fluidity as well as cholesterol content (Fig. 5), without affecting the fluidity or cholesterol content of SPM (Fig. 5b, d).

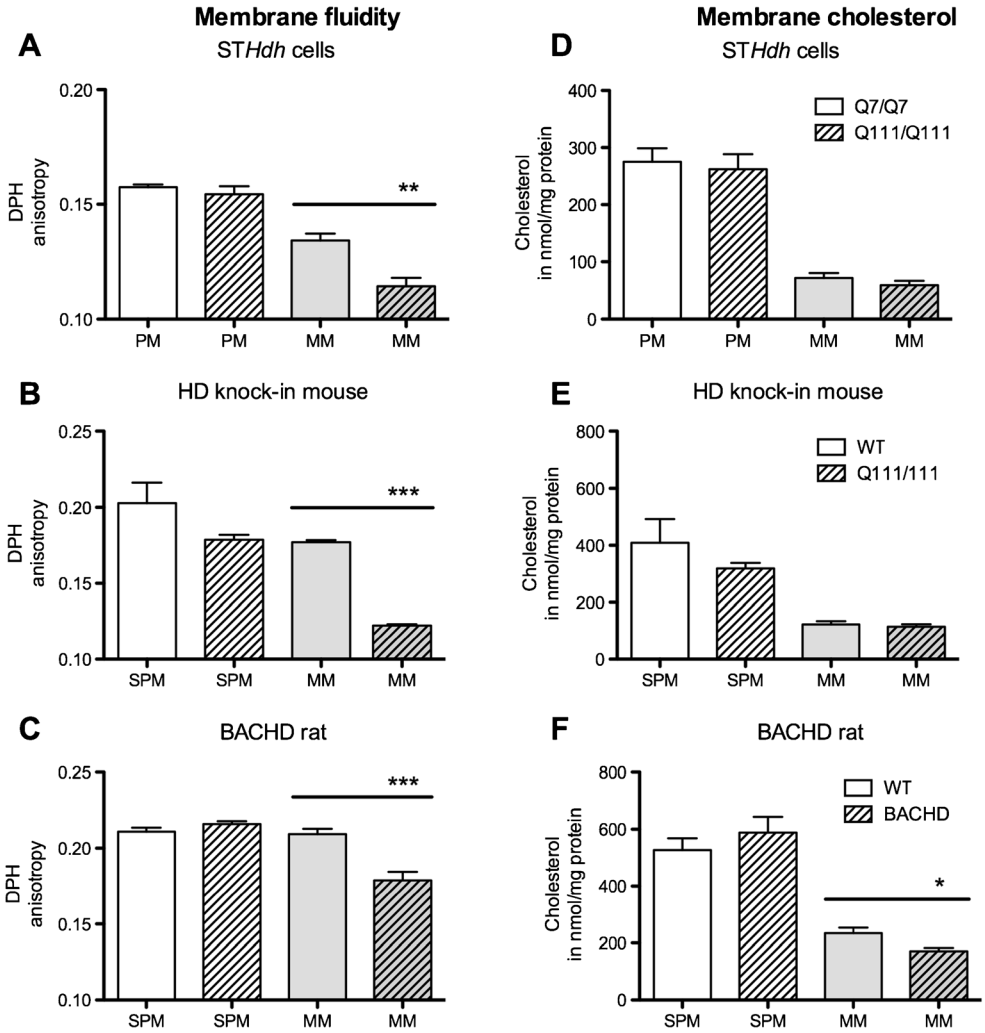

Fig. 1 Membrane properties of cell and animal models of HD. Mitochondrial membranes (*MM*) and plasma membranes (*PM*) from cell samples or synaptosomal plasma membranes (*SPM*) from brain samples were isolated by gradient centrifugation. **a**–**c** Membrane anisotropy of DPH was measured, which correlates inversely with membrane fluidity. *Graphs* show the DPH anisotropy of isolated membranes from ST*Hdh* Q7/Q7 and Q111/Q111 cells after 6 h of differentiation (**a**), DPH anisotropy of isolated membranes from the brains of *Hdh* Q111/111 knock-in mice and their wild-type (WT) litter mates at 18–20 months of age (**b**), as well as BACHD rats and their WT litter mates at 13 months of age (**c**). **d**, **e** Membrane cholesterol content was assessed by the CHOD-PAP method. *Graphs* display the cholesterol content of isolated membranes from ST*Hdh* Q7/Q7 and Q111/Q111 cells after 6 h of differentiation (**d**), cholesterol content of isolated membranes from the brains of *Hdh* Q111/111 knock-in mice and their WT litter mates at 18–20 months of age (**e**), as well as BACHD rats and their WT litter mates at 13 months of age (**f**). *Bars* show mean ± SEM, n=4–7/group. *$p<0.05$; **$p\leq0.01$

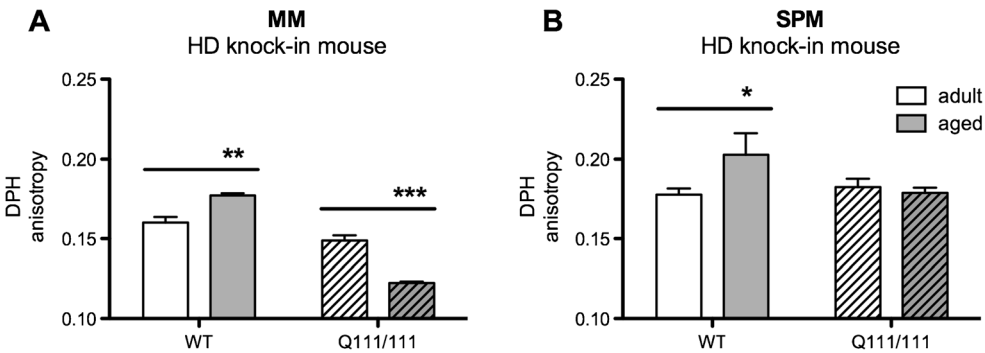

Fig. 2 Membrane fluidity in adult and aged mice. DPH anisotropy, which correlates inversely with membrane fluidity, was measured in mitochondrial membranes (*MM*) (**a**) and synaptosomal plasma membranes (*SPM*) (**b**) from *Hdh* Q111/111 knock-in mice and their wild-type littermates (control) (**b**) at younger (adult, 3–9 months) and older (aged, 18–20 months) age. *Bars* show mean ± SEM, n=6/group, *$p<0.05$; **$p\leq0.01$; ***$p\leq0.0001$,two-way ANOVA and Bonferroni post hoc analysis

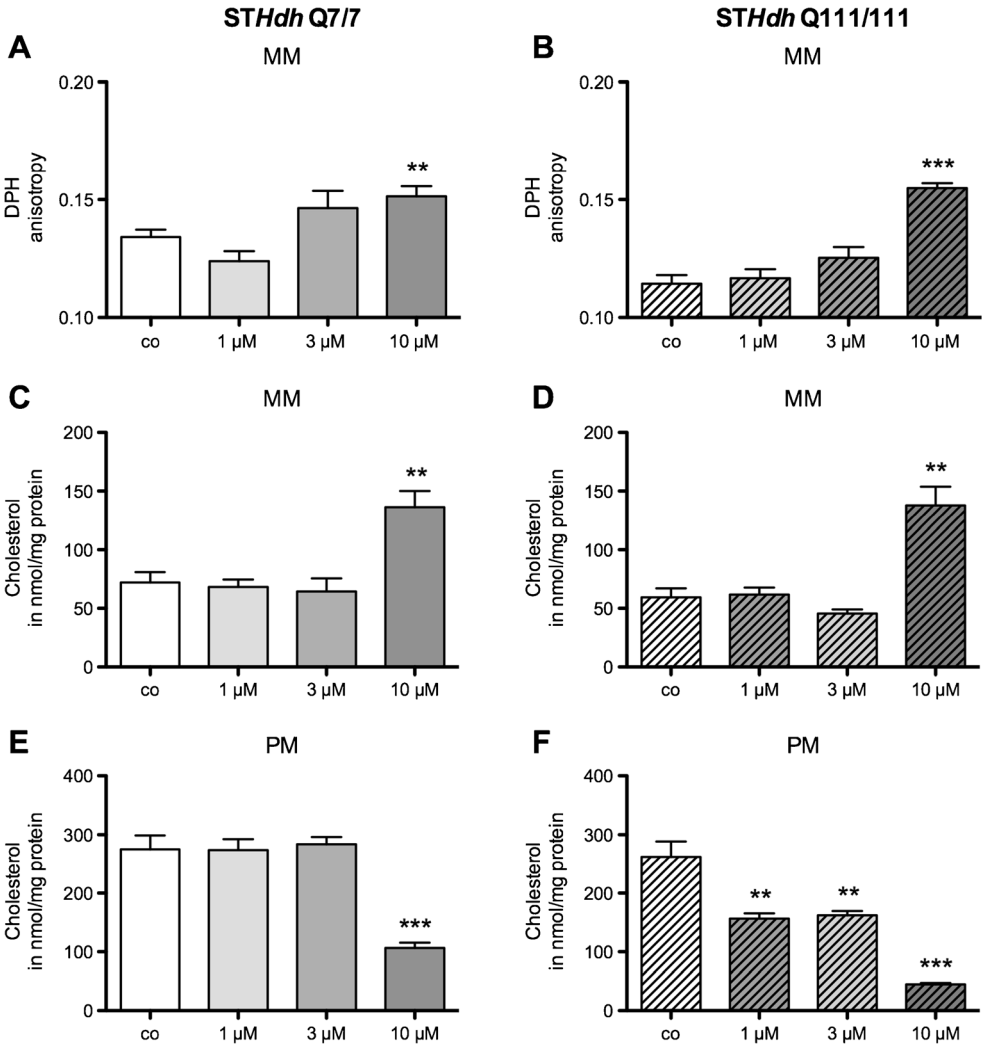

Fig. 3 In vitro effects of olesoxime on membranes from ST*Hdh* cells. Mitochondrial membranes (*MM*) and plasma membranes (*PM*) were isolated from control ST*Hdh* Q7/Q7 (*plain bars*) or mutant ST*Hdh* Q111/Q111 cells (*striped bars*) after 6 h of differentiation and 24 h of treatment with olesoxime (1–10 µM). Controls were treated with DMSO only. *a*, *b* The graphs display the influence of olesoxime on DPH anisotropy of MM from STHdh Q7/7 (**a**) and Q111/111 cells (**b**) as well as its influence on cholesterol content of MM from STHdh Q7/7 (**c**) and Q111/111 cells (**d**) and plasma membranes from STHdh Q7/7 (**e**) and Q111/111 cells (**f**).Bars represent mean ± SEM, n=5/group, *$p \leq 0.05$; **$p \leq 0.01$; ***$p \leq 0.0001$, *t*-test

Unexpectedly, we found olesoxime decreased SPM fluidity in wild-type control rats (Fig. 5a, c), while no change in cholesterol content was observed in these animals (Fig. 5c, d).

Discussion

Mitochondrial dysfunction has been studied intensely during the last decade in HD research [20–24]. The impact of mhtt on

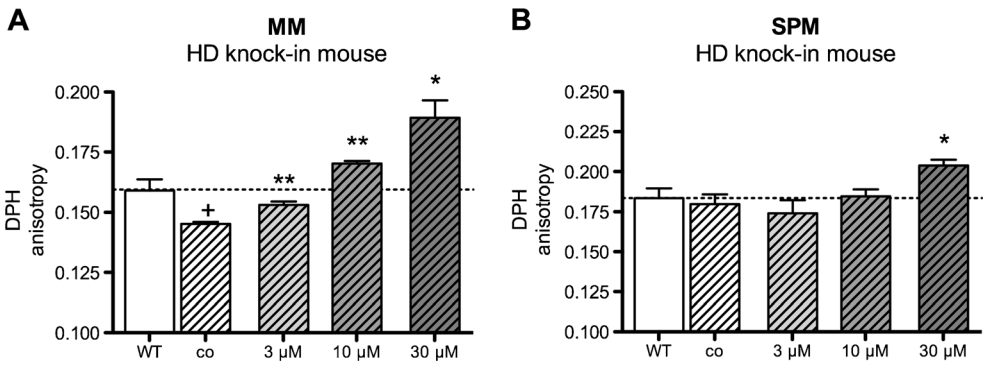

Fig. 4 In vitro effects of olesoxime on brain membranes from HD knock-in mice. Isolated mitochondrial membranes (*MM*) (**a**) and synaptosomal plasma membranes (*SPM*) (**b**) from the brains of aged (18–20 months old) *Hdh* Q111/111 knock-in mice were incubated with 3, 10, or 3 µM olesoxime. DPH anisotropy, which correlates inversely with membrane fluidity, was measured. *Bars* show mean ± SEM; n=6/group, *plus sign* = compared to untreated wild-type litter mates, *asterisk* = compared to untreated knock-in mouse samples (co). *,$^{+}p<0.05$; **,$^{++}p \leq 0.01$; ***,$^{+++}p<0.0001$, *t* test

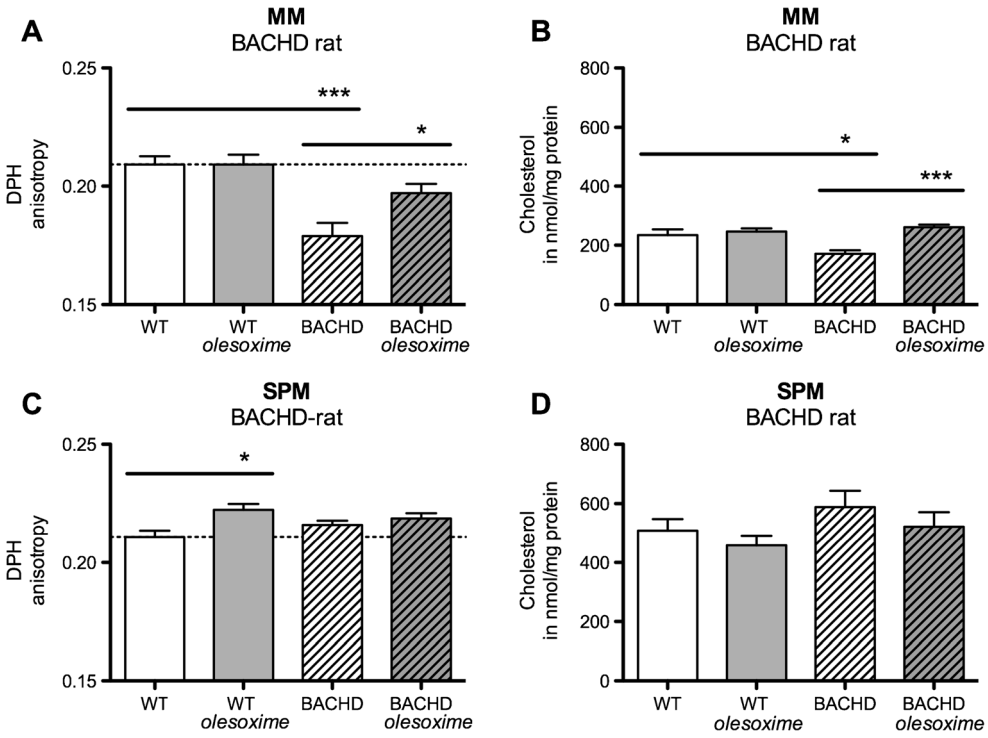

Fig. 5 In vivo effects of olesoxime on brain membranes from BACHD rats. Mitochondrial membranes (*MM*) and synaptosomal plasma membranes (*SPM*) were isolated from 13-month-old BACHD rats and their wild-type (WT) litter mates treated with either control diet or 600 mg/kg olesoxime for 12 months. DPH anisotropy, which correlates inversely with membrane fluidity, was measured in MM (**a**) and SPM (**c**). Membrane cholesterol levels were determined by the CHOD-PAP method in MM (**b**) SPM (**d**). *Bars* represent mean ± SEM, n=4–7/group. *p<0.05; **p<0.01; ***p<0.0001, *t* test

mitochondrial integrity is manifold, affecting mitochondrial shape [28–32, 59, 60], intracellular distribution [27, 31–33], and functioning [61]. mhtt thereby acts either directly [25–28] or indirectly through transcriptional dysregulation of genes involved in mitochondrial function. Mitochondrial network dysfunction has been considered a key player in HD pathogenesis, since mitochondria orchestrate energy supply and Ca^{2+} homeostasis in healthy cells but also trigger apoptosis when their buffering capacity becomes insufficient. However, it could not yet be clarified whether mitochondrial damage is the primary cause for the neuronal cell degeneration observed in HD or whether it is secondary to other events. Furthermore, mitochondria have been suggested as potential therapeutic targets, and various HD animal and cellular models have been used to identify treatments that improve specific mitochondrial defects implicated in HD [36–41].

Mitochondrial Membrane Fluidity as a Common Pathological Feature in HD

Inner and outer mitochondrial membranes constitute an important interface of phospholipid bilayers, containing proteins and lipid rafts that control signal transduction, energy production, and apoptosis initiation [50]. Decreased membrane fluidity has been observed previously in synaptosomal and mitochondrial membranes isolated from the brains of aged or Alzheimer disease (AD) mouse models and is considered to play a key role in the pathogenic events in AD and aging [50, 53]. We had also provided the first results on changes in mitochondrial membrane fluidity in HD [50]. In contrast to aging and AD, we found membrane fluidity to be significantly increased in mitochondrial membranes isolated from HD knock-in mice of relatively young age (3–9 months).

Consistent with this finding, aged HD knock-in mice showed a significant increase in membrane fluidity of brain mitochondria compared to their wild-type littermates. This effect was even more pronounced compared to our initial finding of increased fluidity in the younger mice. Importantly, while wild-type mice display a decrease in membrane fluidity in both plasma and mitochondrial membranes common to aging [50, 53, 57], HD knock-in mice show a further increase in mitochondrial membrane fluidity and do not follow the decrease in plasma membrane fluidity observed in wild types. This suggests a progressive impairment of mitochondrial membrane properties in these animals.

Importantly, the specific increase in mitochondrial membrane fluidity was also identified in ST*Hdh* Q111/111 cells as well as BACHD rats. Thus, the change in mitochondrial membrane fluidity is robustly observed across different species, strongly suggesting a direct or indirect involvement of mhtt in mitochondrial membrane perturbation. Recent results argue for a direct interaction of mhtt with proteins of the mitochondrial membrane [25, 34, 62, 63] and mitochondrial raft-like micro-domains [64]. In particular, it has been shown that the first 17 amino acids (N17) of htt control its mitochondrial localization. It appears that N17 has lipid-binding properties and also enhances aggregate formation, and together with the expanded polyQ repeat, it acutely disrupts calcium

homeostasis, leading to mitochondrial dysfunction [65]. Furthermore, cells overexpressing htt with 74 or 138 polyglutamine repeats were more sensitized to oxidative stress-induced mitochondrial fragmentation, had reduced ATP levels, and showed altered mitochondrial dynamics [28].

It was shown previously that synaptosomal plasma membranes isolated from the brains of rats pretreated with 3-nitropropionic acid (3-NP, rat model of HD) displayed decreased membrane fluidity selectively in striatal membranes [66]. In our study, we did not observe significant differences in the fluidity of synaptosomal plasma membranes. Since 3-NP is a mitochondrial toxin, 3-NP treatment severely damages mitochondria, leading to cell death and specific striatal lesions [67]. Therefore, it is likely that the mitochondrial phenotype in a 3-NP model exceeds the one in most of our genetic disease models. In accordance with this idea, membrane fluidity data obtained from patient fibroblasts also did not reveal changes in plasma membrane fluidity [68].

The Role of Cholesterol for Determining Membrane Fluidity in HD

Changes in membrane fluidity also affect membrane lipid micro-domains [69, 70], which have recently been identified to play a role in mitochondrial impairments in HD [64]. The fluidity of biological membranes is determined by the membrane lipid composition and individual phospholipids, including their interaction with cholesterol and their level of saturation [10]. Cholesterol is one of the major regulators of membrane fluidity [71], and changes in cellular cholesterol metabolism have been associated with HD (summarized in [72–75]). Valenza et al. [76] have demonstrated decreased levels of specific sterols in HD model systems including one of our HD rat models. Reduced mitochondrial cholesterol levels in HD were presumed to be linked to inhibitory effects of mhtt on the expression of 3-hydroxy-3-methyl-glutaryl-CoA (HMG-CoA) reductase in astrocytes and neurons and/or on ABCA1 transporters in astrocytes. Here, we report a reduction in cholesterol levels in brain mitochondrial membranes isolated from BACHD rats, but not HD knock-in mice or ST*Hdh* cells. However, Marullo et al. [77] pointed out that outcomes on cholesterol levels might crucially depend on the method used for detection. A more detailed follow-up study on the concentration and distribution of cholesterol in HD would be required in order to draw final conclusions.

Olesoxime as a Therapeutic Drug for Mitochondrial Dysfunction in HD

Based on the strong evidence for mitochondrial impairments in HD [78, 79], mitochondria have been identified as targets for therapeutic approaches [80, 81]. Herein, we tested the effect of olesoxime on mitochondrial membrane properties in vitro and in vivo. We found olesoxime to specifically decrease mitochondrial membrane fluidity when applied in either condition. In vitro treatment of ST*Hdh* Q111/111 and Q7/7 cells revealed a genotype-nonspecific effect of the drug. However, the decrease in membrane fluidity changed the membrane properties in the direction of untreated controls. Intriguingly, olesoxime specifically affected mitochondrial membrane fluidity when administered per os (via the food) in BACHD rats. Mitochondrial membrane fluidity was decreased almost down to normal levels in olesoxime-treated transgenic rats and did not affect mitochondrial membranes of wild-type littermates.

That olesoxime specifically affects the mitochondrial and not the plasma membranes is consistent with the observation of its entering the cell and concentrating at mitochondria in primary cortical neurons [49]. Furthermore, previous observations revealed that olesoxime interacts with TSPO and VDAC in the outer mitochondrial membrane [42]. Both proteins are involved in multiple key cellular processes [82]. TSPO is primarily localized in the outer mitochondrial membrane. One of its main functions is the transport of cholesterol into mitochondria [83] and its delivery to the inner mitochondrial membrane [45]. The TSPO ligand PK11195 induces changes in the distribution of intracellular cholesterol, which is removed from membranes and accumulates into lipid droplets [84]. The same TSPO ligand increases mitochondrial membrane fluidity [85]. However, whether or not the effects of olesoxime on cholesterol distribution and mitochondrial membrane fluidity are linked to TSPO needs further investigation. TSPO is, together with VDAC, also involved in mitochondrial homeostasis, such as energy production or calcium signalling. VDAC acts as a gatekeeper for the entry and exit of mitochondrial metabolites and thus plays a crucial role in the regulation of metabolic and energetic functions of mitochondria [44]. It is also recognized to function in mitochondria-mediated apoptosis by the release of pro-apoptotic factors, such as cytochrome *c* [82]. Interestingly, mPT was found to be associated with increased membrane fluidity [86]. Thus, VDAC appears to be a convergence point for a variety of cell survival and cell death signals. Even though there are still multiple models and viewpoints regarding mitochondrial permeability transition and mPT pore components, the prevention of mPT has been shown to provide neuroprotection in different paradigms [87] and might be relevant for the olesoxime mechanism of action. This pharmacological characteristic of olesoxime could be of relevance for HD, as inhibitors of cytochrome *c* release have been proposed to have therapeutic potential in HD [88–90]. Olesoxime had demonstrated therapeutic efficacy for the treatment of mitochondrial dysfunction and mitochondria-related disease pathology in cell and animal models of amyotrophic lateral sclerosis [42, 46], multiple sclerosis [91], and peripheral neuropathy [47]. Chemically, olesoxime is a cholesterol oxime that shares

structural analogy with tauroursodeoxycholic acid (TUDCA), a cholesterol derivative with anti-apoptotic function [92] that was found to be beneficial in 3-NP models of HD [93, 94]. Thus, steroids may represent potent molecules for the development of disease-specific drugs targeting mitochondrial dysfunction in HD.

Summary Notes

Our study reveals alterations in mitochondrial membrane fluidity to be a common pathological feature related to mitochondrial dysfunction in HD. Mitochondrial membrane fluidity is consistently increased in cell and animal models of HD, a condition which has been linked to the initiation of apoptosis. A detailed investigation of the connection between mitochondrial membrane fluidity changes and other mitochondrial impairments, which are abundant in HD, is required in order to understand when the changes occur and what the underlying mechanisms are. Evaluation of the modulatory effect of the mitochondria-targeting drug olesoxime, which inhibits apoptosis, further revealed a decrease in membrane fluidity, consistent with a rescue of mitochondrial membrane fluidity changes in HD. Further studies need to be conducted in order to uncover the mechanism of action and potential benefits for the behavioral and neuropathological disease phenotype.

Acknowledgements The data presented herein were assessed in the framework of the seventh framework program for RTD of the European Union—Project MitoTarget—(Grant Agreement HEALTH-F2-2008-223388). We are grateful to all MitoTarget members for their helpful discussions. We further thank Martina Piekorz and Therese Stanek for their excellent support in animal care.

References

1. The Huntington's Disease Collaborative Research Group (1993) A novel gene containing a trinucleotide repeat that is expanded and unstable on Huntington's disease chromosomes. Cell 72(6):971–983
2. Stine OC, Pleasant N, Franz ML, Abbott MH, Folstein SE, Ross CA (1993) Correlation between the onset age of Huntington's disease and length of the trinucleotide repeat in IT-15. Hum Mol Genet 2(10): 1547–1549
3. Vonsattel JP, DiFiglia M (1998) Huntington disease. J Neuropathol Exp Neurol 57(5):369–384
4. Nijtmans LGJ, Ugallde C, van den Heuvel LP, Smeitink JAM (2004) Function and dysfunction of the oxidative phospharylation system. In: Koehler C, Bauer MF (eds) Mitochondrial function and biogenetics. Springer Inc., Heidelberg, pp 149–167
5. Wisniewska A, Draus J, Subczynski WK (2003) Is a fluid-mosaic model of biological membranes fully relevant? Studies on lipid organization in model and biological membranes. Cell Mol Biol Lett 8(1):147–159
6. Helmreich EJ (2003) Environmental influences on signal transduction through membranes: a retrospective mini-review. Biophys Chem 100(1–3):519–534
7. Los DA, Murata N (2004) Membrane fluidity and its roles in the perception of environmental signals. Biochim Biophys Acta 1666(1–2):142–157
8. Maxfield FR, Tabas I (2005) Role of cholesterol and lipid organization in disease. Nature 438(7068):612–621
9. Peters I, Igbavboa U, Schutt T, Haidari S, Hartig U, Rosello X, Bottner S, Copanaki E, Deller T, Kogel D, Wood WG, Muller WE, Eckert GP (2009) The interaction of beta-amyloid protein with cellular membranes stimulates its own production. Biochim Biophys Acta 1788(5):964–972
10. Fajardo VA, McMeekin L, LeBlanc PJ (2011) Influence of phospholipid species on membrane fluidity: a meta-analysis for a novel phospholipid fluidity index. J Membr Biol 244(2):97–103
11. Comte J, Maisterrena B, Gautheron DC (1976) Lipid composition and protein profiles of outer and inner membranes from pig heart mitochondria. Comparison with microsomes. Biochim Biophys Acta 419(2):271–284
12. Montecucco C, Smith GA, Dabbeni-sala F, Johannsson A, Galante YM, Bisson R (1982) Bilayer thickness and enzymatic activity in the mitochondrial cytochrome *c* oxidase and ATPase complex. FEBS Lett 144(1):145–148
13. Madden TD, Hope MJ, Cullis PR (1983) Lipid requirements for coupled cytochrome oxidase vesicles. Biochemistry 22(8):1970–1974
14. Ricchelli F, Gobbo S, Moreno G, Salet C (1999) Changes of the fluidity of mitochondrial membranes induced by the permeability transition. Biochemistry 38(29):9295–9300
15. Aleardi AM, Benard G, Augereau O, Malgat M, Talbot JC, Mazat JP, Letellier T, Dachary-Prigent J, Solaini GC, Rossignol R (2005) Gradual alteration of mitochondrial structure and function by beta-amyloids: importance of membrane viscosity changes, energy deprivation, reactive oxygen species production, and cytochrome c release. J Bioenerg Biomembr 37(4):207–225
16. Colell A (2003) Cholesterol impairs the adenine nucleotide translocator-mediated mitochondrial permeability transition through altered membrane fluidity. J Biol Chem 278(36):33928–33935
17. Garofalo T, Tinari A, Matarrese P, Giammarioli AM, Manganelli V, Ciarlo L, Misasi R, Sorice M, Malorni W (2007) Do mitochondria act as "cargo boats" in the journey of GD3 to the nucleus during apoptosis? FEBS Lett 581(21):3899–3903
18. Gouarné C, Tardif G, Tracz J, Latyszenok V, Michaud M, Clemens LE, Yu-Taeger L, Nguyen HP, Bordet T, Pruss RM (2013) Early deficits in glycolysis are specific to striatal neurons from a rat model of huntington disease. PLoS One 8(11):e81528
19. Jin YN, Yu YV, Gundemir S, Jo C, Cui M, Tieu K, Johnson GV (2013) Impaired mitochondrial dynamics and Nrf2 signaling contribute to compromised responses to oxidative stress in striatal cells expressing full-length mutant huntingtin. PLoS One 8(3):e57932
20. Lin MT, Beal MF (2006) Mitochondrial dysfunction and oxidative stress in neurodegenerative diseases. Nature 443(7113):787–795
21. Browne SE (2008) Mitochondria and Huntington's disease pathogenesis: insight from genetic and chemical models. Ann N Y Acad Sci 1147:358–382
22. Reddy PH, Mao P, Manczak M (2009) Mitochondrial structural and functional dynamics in Huntington's disease. Brain Res Rev 61(1): 33–48
23. Oliveira JM (2010) Mitochondrial bioenergetics and dynamics in Huntington's disease: tripartite synapses and selective striatal degeneration. J Bioenerg Biomembr 42(3):227–234
24. Rosenstock TR, Duarte AI, Rego AC (2010) Mitochondrial-associated metabolic changes and neurodegeneration in Huntington's disease—from clinical features to the bench. Curr Drug Targets 11(10):1218–1236
25. Choo YS, Johnson GVW, MacDonald M, Detloff PJ, Lesort M (2004) Mutant huntingtin directly increases susceptibility of mitochondria to the calcium-induced permeability transition and cytochrome *c* release. Hum Mol Genet 13(14):1407–1420

26. Gellerich FN, Gizatullina Z, Nguyen HP, Trumbeckaite S, Vielhaber S, Seppet E, Zierz S, Landwehrmeyer B, Riess O, von Horsten S, Striggow F (2008) Impaired regulation of brain mitochondria by extramitochondrial Ca^{2+} in transgenic Huntington disease rats. J Biol Chem 283(45):30715–30724
27. Orr AL, Li S, Wang CE, Li H, Wang J, Rong J, Xu X, Mastroberardino PG, Greenamyre JT, Li XJ (2008) N-terminal mutant huntingtin associates with mitochondria and impairs mitochondrial trafficking. J Neurosci 28(11):2783–2792
28. Wang H, Lim PJ, Karbowski M, Monteiro MJ (2009) Effects of overexpression of huntingtin proteins on mitochondrial integrity. Hum Mol Genet 18(4):737–752
29. Costa V, Giacomello M, Hudec R, Lopreiato R, Ermak G, Lim D, Malorni W, Davies KJ, Carafoli E, Scorrano L (2010) Mitochondrial fission and cristae disruption increase the response of cell models of Huntington's disease to apoptotic stimuli. EMBO Mol Med 2(12): 490–503
30. Kim J, Moody JP, Edgerly CK, Bordiuk OL, Cormier K, Smith K, Beal MF, Ferrante RJ (2010) Mitochondrial loss, dysfunction and altered dynamics in Huntington's disease. Hum Mol Genet 19(20): 3919–3935
31. Shirendeb U, Reddy AP, Manczak M, Calkins MJ, Mao P, Tagle DA, Reddy PH (2011) Abnormal mitochondrial dynamics, mitochondrial loss and mutant huntingtin oligomers in Huntington's disease: implications for selective neuronal damage. Hum Mol Genet 20(7):1438–1455
32. Song W, Chen J, Petrilli A, Liot G, Klinglmayr E, Zhou Y, Poquiz P, Tjong J, Pouladi MA, Hayden MR, Masliah E, Ellisman M, Rouiller I, Schwarzenbacher R, Bossy B, Perkins G, Bossy-Wetzel E (2011) Mutant huntingtin binds the mitochondrial fission GTPase dynamin-related protein-1 and increases its enzymatic activity. Nat Med 17(3): 377–382
33. Trushina E, Dyer RB, Badger JD 2nd, Ure D, Eide L, Tran DD, Vrieze BT, Legendre-Guillemin V, McPherson PS, Mandavilli BS, Van Houten B, Zeitlin S, McNiven M, Aebersold R, Hayden M, Parisi JE, Seeberg E, Dragatsis I, Doyle K, Bender A, Chacko C, McMurray CT (2004) Mutant huntingtin impairs axonal trafficking in mammalian neurons in vivo and in vitro. Mol Cell Biol 24(18): 8195–8209
34. Panov AV, Gutekunst C-A, Leavitt BR, Hayden MR, Burke JR, Strittmatter WJ, Greenamyre JT (2002) Early mitochondrial calcium defects in Huntington's disease are a direct effect of polyglutamines. Nat Neurosci 5(8):731–736
35. Milakovic T, Johnson GV (2005) Mitochondrial respiration and ATP production are significantly impaired in striatal cells expressing mutant huntingtin. J Biol Chem 280(35):30773–30782
36. Goety CG, Tanner CM, Cohen JA, Thelen JA, Carroll VS, Klawans HL, Fariello RG (1990) L-Acetyl-carnitine in Huntington's disease: double-blind placebo controlled crossover study of drug effects on movement disorder and dementia. Mov Disord 5(3):263–265
37. Ferrante RJ, Andreassen OA, Dedeoglu A, Ferrante KL, Jenkins BG, Hersch SM, Beal MF (2002) Therapeutic effects of coenzyme Q10 and remacemide in transgenic mouse models of Huntington's disease. J Neurosci 22(5):1592–1599
38. Vamos E, Voros K, Vecsei L, Klivenyi P (2010) Neuroprotective effects of L-carnitine in a transgenic animal model of Huntington's disease. Biomed Pharmacother 64(4):282–286
39. Hickey MA, Zhu C, Medvedeva V, Franich NR, Levine MS, Chesselet MF (2012) Evidence for behavioral benefits of early dietary supplementation with CoEnzymeQ10 in a slowly progressing mouse model of Huntington's disease. Mol Cell Neurosci 49(2):149–157
40. Johri A, Calingasan NY, Hennessey TM, Sharma A, Yang L, Wille E, Chandra A, Beal MF (2012) Pharmacologic activation of mitochondrial biogenesis exerts widespread beneficial effects in a transgenic mouse model of Huntington's disease. Hum Mol Genet 21(5): 1124–1137
41. Sandhir R, Sood A, Mehrotra A, Kamboj SS (2012) *N*-Acetylcysteine reverses mitochondrial dysfunctions and behavioral abnormalities in 3-nitropropionic acid-induced Huntington's disease. Neurodegener Dis 9(3):145–157
42. Bordet T, Buisson B, Michaud M, Drouot C, Galea P, Delaage P, Akentieva NP, Evers AS, Covey DF, Ostuni MA, Lacapere JJ, Massaad C, Schumacher M, Steidl EM, Maux D, Delaage M, Henderson CE, Pruss RM (2007) Identification and characterization of cholest-4-en-3-one, oxime (TRO19622), a novel drug candidate for amyotrophic lateral sclerosis. J Pharmacol Exp Ther 322(2):709–720
43. Gincel D, Zaid H, Shoshan-Barmatz V (2001) Calcium binding and translocation by the voltage-dependent anion channel: a possible regulatory mechanism in mitochondrial function. Biochem J 358(Pt 1):147–155
44. Shoshan-Barmatz V, De Pinto V, Zweckstetter M, Raviv Z, Keinan N, Arbel N (2010) VDAC, a multi-functional mitochondrial protein regulating cell life and death. Mol Aspects Med 31(3):227–285
45. Hu J, Zhang Z, Shen WJ, Azhar S (2010) Cellular cholesterol delivery, intracellular processing and utilization for biosynthesis of steroid hormones. Nutr Metab (Lond) 7:47
46. Sunyach C, Michaud M, Arnoux T, Bernard-Marissal N, Aebischer J, Latyszenok V, Gouarné C, Raoul C, Pruss RM, Bordet T, Pettmann B (2012) Olesoxime delays muscle denervation, astrogliosis, microglial activation and motoneuron death in an ALS mouse model. Neuropharmacology 62(7):2346–2352
47. Xiao WH, Zheng FY, Bennett GJ, Bordet T, Pruss RM (2009) Olesoxime (cholest-4-en-3-one, oxime): analgesic and neuroprotective effects in a rat model of painful peripheral neuropathy produced by the chemotherapeutic agent, paclitaxel. Pain 147(1–3):202–209
48. Xiao WH, Zheng H, Bennett GJ (2012) Characterization of oxaliplatin-induced chronic painful peripheral neuropathy in the rat and comparison with the neuropathy induced by paclitaxel. Neuroscience 203:194–206
49. Bordet T, Berna P, Abitbol JL, Pruss R (2010) Olesoxime (TRO19622): a novel mitochondrial-targeted neuroprotective compound. Pharmaceuticals (Basel) 3:345–368
50. Eckmann J, Eckert SH, Leuner K, Muller WE, Eckert GP (2013) Mitochondria: mitochondrial membranes in brain ageing and neurodegeneration. Int J Biochem Cell Biol 45:76–80
51. Yu-Taeger L, Petrasch-Parwez E, Osmand AP, Redensek A, Metzger S, Clemens LE, Park L, Howland D, Calaminus C, Gu X, Pichler B, Yang XW, Riess O, Nguyen HP (2012) A novel BACHD transgenic rat exhibits characteristic neuropathological features of Huntington disease. J Neurosci 32(44):15426–15438
52. Gray M, Shirasaki DI, Cepeda C, Andre VM, Wilburn B, Lu XH, Tao J, Yamazaki I, Li SH, Sun YE, Li XJ, Levine MS, Yang XW (2008) Full-length human mutant huntingtin with a stable polyglutamine repeat can elicit progressive and selective neuropathogenesis in BACHD mice. J Neurosci 28(24):6182–6195
53. Eckert GP, Wood WG, Muller WE (2001) Effects of aging and beta-amyloid on the properties of brain synaptic and mitochondrial membranes. J Neural Transm 108(8–9):1051–1064
54. Lowry OH, Rosebrough NJ, Farr AL, Randall RJ (1951) Protein measurement with the Folin phenol reagent. J Biol Chem 193:265–275
55. Kirsch C, Eckert GP, Muller WE (2003) Statins affect cholesterol micro-domains in brain plasma membranes. Biochem Pharmacol 65(5):843–856
56. Kirsch C, Eckert GP, Mueller WE (2002) Cholesterol attenuates the membrane perturbing properties of beta-amyloid peptides. Amyloid 9(3):149–159
57. Choe M, Jackson C, Yu BP (1995) Lipid peroxidation contributes to age-related membrane rigidity. Free Radic Biol Med 18(6):977–984
58. Lentz BR (1988) Membrane fluidity from anisotropy measurements. In: Loew LM (ed) Spectroscopic membrane probes, vol 1. CRC, Boca Raton, pp 13–42

59. Tellez-Nagel I, Johnson AB, Terry RD (1974) Studies on brain biopsies of patients with Huntington's chorea. J Neuropathol Exp Neurol 33(2):308–332
60. Goebel HH, Heipertz R, Scholz W, Iqbal K, Tellez-Nagel I (1978) Juvenile Huntington chorea: clinical, ultrastructural, and biochemical studies. Neurology 28(1):23–31
61. Gines S, Seong IS, Fossale E, Ivanova E, Trettel F, Gusella JF, Wheeler VC, Persichetti F, MacDonald ME (2003) Specific progressive cAMP reduction implicates energy deficit in presymptomatic Huntington's disease knock-in mice. Hum Mol Genet 12(5):497–508
62. Petrasch-Parwez E, Nguyen HP, Lobbecke-Schumacher M, Habbes HW, Wieczorek S, Riess O, Andres KH, Dermietzel R, Von Horsten S (2007) Cellular and subcellular localization of Huntingtin [corrected] aggregates in the brain of a rat transgenic for Huntington disease. J Comp Neurol 501(5):716–730
63. Turner C, Schapira AH (2010) Mitochondrial matters of the brain: the role in Huntington's disease. J Bioenerg Biomembr 42(3):193–198
64. Ciarlo L, Manganelli V, Matarrese P, Garofalo T, Tinari A, Gambardella L, Marconi M, Grasso M, Misasi R, Sorice M, Malorni W (2012) Raft-like microdomains play a key role in mitochondrial impairment in lymphoid cells from patients with Huntington's disease. J Lipid Res 53(10):2057–2068
65. Rockabrand E, Slepko N, Pantalone A, Nukala VN, Kazantsev A, Marsh JL, Sullivan PG, Steffan JS, Sensi SL, Thompson LM (2007) The first 17 amino acids of Huntingtin modulate its sub-cellular localization, aggregation and effects on calcium homeostasis. Hum Mol Genet 16(1):61–77
66. LaFontaine MA, Geddes JW, Butterfield DA (2002) 3-nitropropionic acid-induced changes in bilayer fluidity in synaptosomal membranes: implications for Huntington's disease 1. Neurochem Res 27(6):507–511
67. Brouillet E, Conde F, Beal MF, Hantraye P (1999) Replicating Huntington's disease phenotype in experimental animals. Prog Neurobiol 59(5):427–468
68. Schroeder F, Goetz IE, Roberts E (1984) Membrane anomalies in Huntington's disease fibroblasts. J Neurochem 43(2):526–539
69. Eckert GP, Igbavboa U, Muller WE, Wood WG (2003) Lipid rafts of purified mouse brain synaptosomes prepared with or without detergent reveal different lipid and protein domains. Brain Res 962(1–2): 144–150
70. Eckert GP, Muller WE (2009) Presenilin 1 modifies lipid raft composition of neuronal membranes. Biochem Biophys Res Commun 382(4):673–677
71. Wood WG, Igbavboa U, Muller WE, Eckert GP (2011) Cholesterol asymmetry in synaptic plasma membranes. J Neurosci 116(5):684–689
72. Block RC, Dorsey ER, Beck CA, Brenna JT, Shoulson I (2010) Altered cholesterol and fatty acid metabolism in Huntington disease. J Clin Lipidol 4(1):17–23
73. Karasinska JM, Hayden MR (2011) Cholesterol metabolism in Huntington disease. Nat Rev Neurol 7(10):561–572
74. Valenza M, Cattaneo E (2011) Emerging roles for cholesterol in Huntington's disease. Trends Neurosci 34(9):474–486
75. Leoni V, Caccia C (2013) 24S-hydroxycholesterol in plasma: a marker of cholesterol turnover in neurodegenerative diseases. Biochimie 95(3):595–612
76. Valenza M, Leoni V, Karasinska JM, Petricca L, Fan J, Carroll J, Pouladi MA, Fossale E, Nguyen HP, Riess O, MacDonald M, Wellington C, DiDonato S, Hayden M, Cattaneo E (2010) Cholesterol defect is marked across multiple rodent models of Huntington's disease and is manifest in astrocytes. J Neurosci 30(32):10844–10850
77. Marullo M, Valenza M, Leoni V, Caccia C, Scarlatti C, De Mario A, Zuccato C, Di Donato S, Carafoli E, Cattaneo E (2012) Pitfalls in the detection of cholesterol in Huntington's disease models. PLoS Curr 4:e505886e9a1968
78. Brouillet E, Hantraye P, Ferrante RJ, Dolan R, Leroy-Willig A, Kowall NW, Beal MF (1995) Chronic mitochondrial energy impairment produces selective striatal degeneration and abnormal choreiform movements in primates. Proc Natl Acad Sci U S A 92(15):7105–7109
79. Damiano M, Galvan L, Deglon N, Brouillet E (2010) Mitochondria in Huntington's disease. Biochim Biophys Acta 1802(1):52–61
80. Burchell VS, Gandhi S, Deas E, Wood NW, Abramov AY, Plun-Favreau H (2010) Targeting mitochondrial dysfunction in neurodegenerative disease: part II. Expert Opin Ther Targets 14(5):497–511
81. Moreira PI, Zhu X, Wang X, Lee HG, Nunomura A, Petersen RB, Perry G, Smith MA (2010) Mitochondria: a therapeutic target in neurodegeneration. Biochim Biophys Acta 1802(1):212–220
82. Shoshan-Barmatz V, Ben-Hail D (2012) VDAC, a multi-functional mitochondrial protein as a pharmacological target. Mitochondrion 12(1):24–34
83. Rupprecht R, Papadopoulos V, Rammes G, Baghai TC, Fan J, Akula N, Groyer G, Adams D, Schumacher M (2010) Translocator protein (18 kDa) (TSPO) as a therapeutic target for neurological and psychiatric disorders. Nat Rev Drug Discov 9(12):971–988
84. Falchi AM, Battetta B, Sanna F, Piludu M, Sogos V, Serra M, Melis M, Putzolu M, Diaz G (2007) Intracellular cholesterol changes induced by translocator protein (18 kDa) TSPO/PBR ligands. Neuropharmacology 53(2):318–329
85. Miccoli L, Oudard S, Beurdeley-Thomas A, Dutrillaux B, Poupon MF (1999) Effect of 1-(2-chlorophenyl)-*N*-methyl-*N*-(1-methylpropyl)-3-isoquinoline carboxamide (PK11195), a specific ligand of the peripheral benzodiazepine receptor, on the lipid fluidity of mitochondria in human glioma cells. Biochem Pharmacol 58(4):715–721
86. Rolo AP, Oliveira PJ, Moreno AJ, Palmeira CM (2003) Chenodeoxycholate induction of mitochondrial permeability transition pore is associated with increased membrane fluidity and cytochrome c release: protective role of carvedilol. Mitochondrion 2(4):305–311
87. Mattson MP, Liu D (2003) Mitochondrial potassium channels and uncoupling proteins in synaptic plasticity and neuronal cell death. Biochem Biophys Res Commun 304(3):539–549
88. Jana NR, Zemskov EA, Wang G, Nukina N (2001) Altered proteasomal function due to the expression of polyglutamine-expanded truncated N-terminal huntingtin induces apoptosis by caspase activation through mitochondrial cytochrome c release. Hum Mol Genet 10(10):1049–1059
89. Lim D, Fedrizzi L, Tartari M, Zuccato C, Cattaneo E, Brini M, Carafoli E (2008) Calcium homeostasis and mitochondrial dysfunction in striatal neurons of Huntington disease. J Biol Chem 283(9): 5780–5789
90. Wang X, Zhu S, Pei Z, Drozda M, Stavrovskaya IG, Del Signore SJ, Cormier K, Shimony EM, Wang H, Ferrante RJ, Kristal BS, Friedlander RM (2008) Inhibitors of cytochrome *c* release with therapeutic potential for Huntington's disease. J Neurosci 28(38): 9473–9485
91. Magalon K, Zimmer C, Cayre M, Khaldi J, Bourbon C, Robles I, Tardif G, Viola A, Pruss RM, Bordet T, Durbec P (2012) Olesoxime accelerates myelination and promotes repair in models of demyelination. Ann Neurol 71(2):213–226
92. Rivard AL, Steer CJ, Kren BT, Rodrigues CM, Castro RE, Bianco RW, Low WC (2007) Administration of tauroursodeoxycholic acid (TUDCA) reduces apoptosis following myocardial infarction in rat. Am J Chin Med 35(2):279–295
93. Rodrigues CM, Stieers CL, Keene CD, Ma X, Kren BT, Low WC, Steer CJ (2000) Tauroursodeoxycholic acid partially prevents apoptosis induced by 3-nitropropionic acid: evidence for a mitochondrial pathway independent of the permeability transition. J Neurochem 75(6):2368–2379
94. Keene CD, Rodrigues CM, Eich T, Linehan-Stieers C, Abt A, Kren BT, Steer CJ, Low WC (2001) A bile acid protects against motor and cognitive deficits and reduces striatal degeneration in the 3-nitropropionic acid model of Huntington's disease. Exp Neurol 171(2):351–360

OPEN ACCESS Freely available online

PLOS ONE

Reduced Motivation in the BACHD Rat Model of Huntington Disease Is Dependent on the Choice of Food Deprivation Strategy

Erik Karl Håkan Jansson[◔], **Laura Emily Clemens**[◔], **Olaf Riess, Huu Phuc Nguyen***

Institute of Medical Genetics and Applied Genomics, University of Tuebingen, Tuebingen, Germany; and Centre for Rare Diseases, University of Tuebingen, Tuebingen, Germany

Abstract

Huntington disease (HD) is an inherited neurodegenerative disease characterized by motor, cognitive, psychiatric and metabolic symptoms. Animal models of HD show phenotypes that can be divided into similar categories, with the metabolic phenotype of certain models being characterized by obesity. Although interesting in terms of modeling metabolic symptoms of HD, the obesity phenotype can be problematic as it might confound the results of certain behavioral tests. This concerns the assessment of cognitive function in particular, as tests for such phenotypes are often based on food depriving the animals and having them perform tasks for food rewards. The BACHD rat is a recently established animal model of HD, and in order to ensure that behavioral characterization of these rats is done in a reliable way, a basic understanding of their physiology is needed. Here, we show that BACHD rats are obese and suffer from discrete developmental deficits. When assessing the motivation to lever push for a food reward, BACHD rats were found to be less motivated than wild type rats, although this phenotype was dependent on the food deprivation strategy. Specifically, the phenotype was present when rats of both genotypes were deprived to 85% of their respective free-feeding body weight, but not when deprivation levels were adjusted in order to match the rats' apparent hunger levels. The study emphasizes the importance of considering metabolic abnormalities as a confounding factor when performing behavioral characterization of HD animal models.

Citation: Jansson EKH, Clemens LE, Riess O, Nguyen HP (2014) Reduced Motivation in the BACHD Rat Model of Huntington Disease Is Dependent on the Choice of Food Deprivation Strategy. PLoS ONE 9(8): e105662. doi:10.1371/journal.pone.0105662

Editor: Xiao-Jiang Li, Emory University, United States of America

Received June 16, 2014; **Accepted** July 25, 2014; **Published** August 21, 2014

Data Availability: The authors confirm that all data underlying the findings are fully available without restriction. All relevant data are within the paper and its Supporting Information files.

Funding: The study was funded by yearly funds allocated to the Institute of Medical Genetics and Applied Genomics by the Medical Faculty of the University of Tuebingen, to maintain animals. Erik Jansson received a stipend from the German Academic Exchange Program (DAAD: https://www.daad.de/en/) under the Procope program, project number: 54366469. The authors also acknowledge support by Deutsche Forschungsgemeinschaft and Open Access Publishing Fund of Tuebingen University for publication costs. The funders had no role in study design, data collection and analysis, decision to publish, or preparation of the manuscript.

Competing Interests: The authors have declared that no competing interests exist.

* Email: hoa.nguyen@med.uni-tuebingen.de

◔ These authors contributed equally to this work.

Introduction

Huntington disease (HD) is an autosomal dominantly inherited neurodegenerative disease with a prevalence of 6 per 100,000 in Europe and North America [1]. Development of HD is dependent on a single mutation that results in the extension of the CAG repeat sequence present in the gene for the Huntingtin protein [2]. HD patients display a range of symptoms that can be grouped into motor, psychiatric, cognitive and metabolic symptoms. Symptoms gradually worsen as the disease progresses, and due to the lack of disease modifying treatments HD is invariably fatal.

There are numerous transgenic animal models of HD [3], and as with any disease model, a major focus of working with these is to assess how well their phenotypes mirror symptoms found in HD patients. This is complicated due to the multitude of phenotypes that are often present, and the potential risk of some phenotypes confounding the assessment of others. The metabolic phenotypes are especially interesting in this regard. While HD patients typically lose weight [4,5,6,7,8,9], the body weight and body composition phenotypes of transgenic animal models of HD vary [3]. Animals that express the full-length mutant huntingtin gene typically show an increased body weight, due to increased fat mass [10,11]. Although this is interesting in terms of modeling the metabolic symptoms of HD, an increase in body weight has been suggested to result in reduced performance on the rotarod [12,13], a common test of motor capacity and limb coordination.

Metabolic phenotypes are also of interest when considering tests of cognitive function, as these are often based on having food deprived animals perform certain tasks to retrieve food rewards [14]. Ideally, animals should be equally hungry and interested in food rewards when performing such tests, as studies where motivational differences are present can give misleading results [15]. Changes in body composition, such as the ones seen in HD models, are likely to either be caused by or lead to a change in *ad libitum* food consumption. Unless careful adjustments are made, such phenotypes might persist even after food deprivation. One

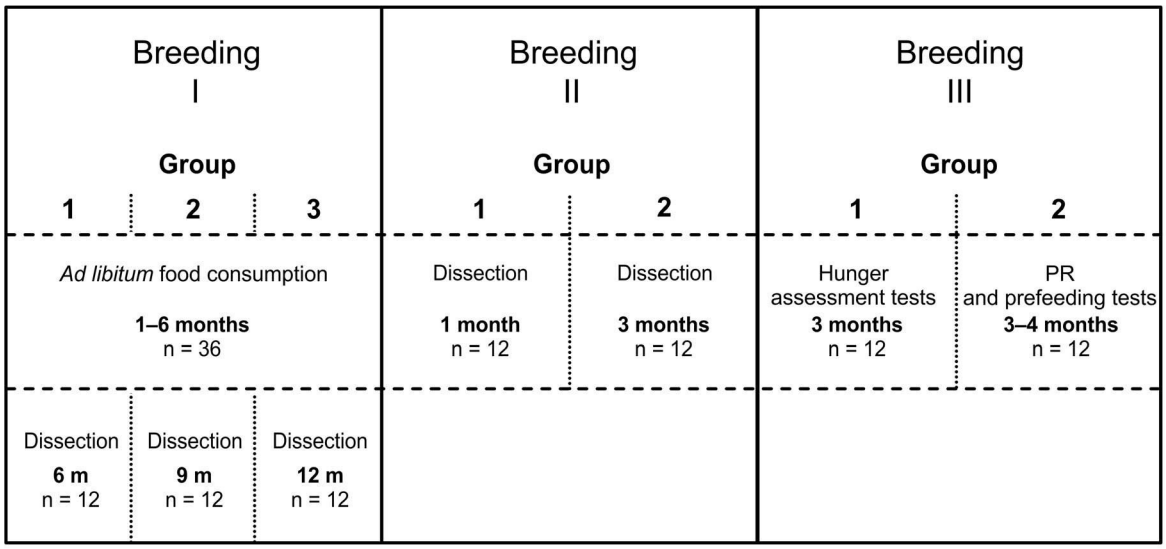

Figure 1. Overview of study groups. A total of seven groups of rats were used in the current study. These were derived from different breeding events and used in different tests, as shown in the figure. The "n" indicates the number of animals used from each genotype. Note that a total of two animals were excluded during analysis, as explained in detail under "Statistical analysis".
doi:10.1371/journal.pone.0105662.g001

proposed method to avoid this when working with HD models is to adjust food deprivation levels until animals show similar consumption rates in tests where they are given brief access to food [16,17]. Similar tests are occasionally used to assess hunger and food interest, [18,19,20,21] although in HD research one should also consider that a slowed consumption rate could be caused by motor impairments. Thus, detailed knowledge about body composition and feeding behavior of an animal model, both when deprived and *ad libitum* fed, is important for planning and interpreting a variety of behavioral tests.

The BACHD rat is a recently established animal model for HD. These rats carry a large construct containing the full-length gene for human mutant Huntingtin, with its endogenous regulatory sequences [22]. Previous studies have shown that BACHD rats have motor impairments and neuropathological phenotypes reminiscent of symptoms seen among HD patients [22]. In addition, BACHD rats appear to be impaired in some cognitive tests [23]. Previous studies have indicated that BACHD rats eat less than WT rats [22], although the setup used for that particular study demanded social isolation, and its validity for assessing natural behavior has been questioned [24]. Further, although it has been pointed out that BACHD rats appear obese [22], there has not been any study on their body composition. Therefore, we performed a longitudinal study where food intake was measured in a social homecage setup, and body composition was assessed through detailed dissections. As further behavioral characterization of the BACHD rats will be dependent on tests that require food deprivation, we also sought to evaluate an optimal food deprivation strategy for BACHD rats. For this, consumption rate of reward pellets and regular food, as well as performance in a progressive ratio test with prefeedings was assessed at different levels of food deprivation.

Materials and Methods

Animals

A total of 168 male rats were used for the study. These were acquired from three separate in-house breeding events, with heterozygous BACHD males from the TG5 line [22] paired with WT females. All animals were on Sprague Dawley background. Animals were genotyped according to previously published protocols [22] and housed in type IV cages (38×55 cm), with high lids (24.5 cm from cage floor), and free access to water. Food availability and social conditions differed between the experimental groups. Rats used for *ad libitum* food intake and body composition measurements were housed in genotype-matched pairs, and had free access to food (SNIFF V1534-000 standard chow) during the entire length of their respective test. Importantly, food was provided on the cage floor and not on the cage top. Body weight was measured weekly to assess general health, and cages were changed twice per week. Rats used for hunger assessment and PR tests were housed in genotype-matched groups of three rats per cage. They had free access to food from the cage top until the age of ten weeks. At that point, the rats were food deprived as described below. Body weight was measured daily in order to assess food deprivation levels, and cages were changed weekly. The animal facility kept 21–23°C, 55–10% humidity, and was set to a partially inverted light/dark cycle with lights on/off at 02:00/14:00 during summer, and 01:00/13:00 during winter.

The seven groups of animals were used in different tests, as described below. An overview of the animal groups, and the tests, is shown in Figure 1. All experiments were approved by the local ethics committee (Regierungspraesidium Tuebingen) and carried out in accordance with the German Animal Welfare Act and the guidelines of the Federation of European Laboratory Animal Science Associations, based on European Union legislation (Directive 2010/63/EU).

Ad libitum food consumption in a social homecage environment

Ad libitum food consumption was measured using a total of 72 rats, acquired from one breeding event. At the age of five weeks, all rats were arranged into genotype-matched pairs, and housed as described above. This gave a total of 36 cages, 18 cages per genotype. Cages with WT and BACHD rats were evenly distributed over two racks, which were placed next to each other in the same housing room. Food and water intake was assessed

twice weekly, when cages were changed. Cages were changed on Mondays and Thursdays during the last two hours of the light phase. At each cage-changing event, a known amount of food was placed inside each new cage, and the fresh water bottles were weighed. The weights of the old water bottles as well as the weight of the food left in each old cage were then measured to assess the amount of food and water consumed since the last cage change. The food was manually collected from the bedding of the old cages. After removing large food pieces, the bedding was sifted in a homemade sieve with a 1 mm mesh in order to collect small food pieces generated by food grinding. The animals' food and water consumption was followed in this way until the age of 26 weeks. Sifting of bedding materials started when animals were 15 weeks old.

Dissection for body composition assessment

A detailed dissection was performed in order to study the body composition of BACHD rats. Five different rat groups were sacrificed at 1, 3, 6, 9, and 12 months of age respectively, with each group being composed of 12 WT and 12 BACHD rats. The rat groups used for dissection at 6, 9, and 12 months of age were the same rats that were followed during the *ad libitum* food consumption test. The rat groups used for dissection at 1 and 3 months of age were acquired from a separate breeding. Housing conditions were identical for all animals, and according to the description above. Aside from the weekly food and water consumption assessment made during the *ad libitum* food intake test, food and water consumption were measured monthly as animals aged. When rats reached an age of interest, a dissection group was arranged based on the animals' food consumption, water intake, and body weights, so that the dissected group well represented the full group.

Rats were sacrificed in a carbon dioxide chamber two to four hours before dark-phase onset. Blood samples were collected after sacrifice, through retro-orbital bleeding. Body lengths and body weights were measured on the intact animals, with body length measured from nose tip to tail tip. Additional measurements of head, trunk, and tail lengths were measured from nose tip to back of the head, back of the head to anus, and anus to tail tip, respectively. After these external measurements, skin and subcutaneous adipose tissue deposits were removed and weighed. Then, internal organs and adipose deposits located in the abdomen and chest cavities were removed and weighed. The remaining carcass was weighed before removal of the brain. By later subtracting the brain weight, a measurement of bone and muscle weight (denoted bone/muscle) was acquired for each rat. Dissection of a given age group was carried out during four to six days, with rats of both genotypes being assessed on each day.

Hunger assessment tests

Two tests were used to assess hunger levels in WT and BACHD rats at three different food deprivation levels. A group of 24 animals with equal numbers of WT and BACHD rats was used for both tests. This group was acquired from a breeding separate from the ones used for the *ad libitum* food consumption and body composition measurements. As mentioned above, food deprivation started when the rats were ten weeks old. Body weights were compared to control data from age- and genotype-matched free-feeding animals, on a weekly basis, in order to acquire measurements of food deprivation levels (relative body weight). It should be noted that the control data was not gathered in the current study, but in previous tests. Rats were given small daily amounts of food inside their social homecages, approximately four hours after dark phase onset, to maintain food deprivation. During the first week of food deprivation, animals were habituated to the reward pellets (Bio-Serv, Dustless Precision Pellets® F0021, purchased through Bilaney Consultants, Duesseldorf, Germany) by daily giving each cage a spoon-full of reward pellets together with the daily amount of food. Behavior assessment started one hour after dark phase onset, and was performed in the animals' housing room, using soft red light. Rats were 13 weeks old when behavioral assessment started.

Rats were assessed in both tests on each given testing occasion. The first test assessed the rats' interest in consuming 100 reward pellets. The test used a glass cage (28.5×29×29.5 cm) with mirrors, which allowed a good view of the feeding animals. At the start of each trial, a rat was placed inside the cage, and was allowed two explore it freely during two minutes. Afterwards, a glass Petri dish containing 100 reward pellets was placed inside the cage, in one of the corners that faced the experimenter. The rats were then given a total of five minutes to consume the reward pellets, while the experimenter scored their behavior. The experimenter used two timers to separately record the total time taken to consume the reward pellets, and the time each rat actually spent eating. Thus, one timer was started when the rat first discovered the pellets, and stopped either when all pellets were consumed or when five minutes had passed. The second timer was also started when the rat first discovered the pellets, but was stopped whenever the rat stopped eating, and explored the test arena. Roughly three hours were needed to assess all 24 rats. The test schedule was arranged so that entire cages of BACHD and WT rats were assessed in an alternating manner. Thus, three rats of a given genotype were assessed in sequence, followed by three rats of the other genotype. The experimenter was blinded to the animals' genotypes.

The second test assessed the rats' interest in regular food. In this test, rats were given free access to a large amount of food in their homecages. Food was made available to the rats when four hours remained of the dark phase. Identical amounts of food were placed in the cage tops, with one-minute spacing between cages, alternating between BACHD and WT cages. The remaining food was then measured each half hour, until the end of the dark phase. A final measurement was made at the end of the subsequent light phase. At each measurement, the cages were briefly inspected for larger pieces of food, as they occasionally dropped between the bars of the cage lids.

The rats were assessed in these two tests on three separate occasions. On the first, both WT and BACHD rats were deprived to 85% of their respective free-feeding body weights. In an attempt to reverse the phenotypes that were found, the food deprivation levels were then adjusted so WT and BACHD rats were at 95 and 80% of their respective free-feeding body weights. On the final trial, the previous deprivation levels were switched, so that WT and BACHD rats were at 80 and 95% of their respective free-feeding body weights. Each test occasion was separated by a week of food deprivation, to allow gradual adjustment of deprivation levels.

Progressive ratio test

A progressive ratio (PR) test was run to assess the rats' motivation to work for a food reward at two different food deprivation settings. A group of 24 animals with equal numbers of WT and BACHD rats was used for the test. This group was acquired from the same breeding as the group used for the hunger tests described above. Food deprivation was initiated and maintained as described above. Behavioral assessment started 30 minutes after dark phase onset, in a room separate from the

animals' housing room, using soft red light. Rats were 11 weeks old when behavioral assessment started.

A bank of six operant conditioning chambers (Coulbourn Instruments, H10-11R-TC with H10-24 isolation boxes, purchased through Bilaney Consultants, Duesseldorf, Germany) was used to run the test. Each chamber was equipped with two retractable levers, placed 6 cm above the chamber floor, protruding 2 cm from the wall. The levers were placed on either side of a central pellet receptacle trough, which was placed 2 cm above the chamber floor. The pellet receptacle trough contained a yellow light, which was used to signal the delivery of a reward pellet in all protocols described below. The chambers also contained a red house light, on the wall opposite from the levers and pellet receptacle trough, which shined during the full duration of the training sessions. A water bottle was also available on this wall, to ensure *ad libitum* access to water during testing. All protocols were designed and run with Graphic State 4.1.04. Rats were given single daily sessions, meaning that a total of four daily runs with all six operant chambers were needed to assess the whole group. Each run assessed three WT and three BACHD rats in a determined order, so that a given rat was trained on the same time of day through the entire test. Each rat was assigned to a specific operant chamber, although this was arranged so that each operant chamber was used to assess equal numbers of WT and BACHD rats. Rats received their daily regimen of regular food four hours after the completion of the last run of the day.

During initial training, rats of both genotypes were deprived to 85% of their respective free-feeding body weights. Afterwards, all rats received two habituation sessions in the conditioning chambers. During these, both levers were retracted and a single reward pellet was delivered to the pellet trough at 10, 15, 20, 25, or 30-second intervals. The pellet delivery interval varied in a pseudo-randomized fashion so that each set of five deliveries used each given interval once. Pellet retrieval, or failure to retrieve the pellet within five seconds after delivery, lead to the start of the next pellet delivery interval. After the habituation sessions, rats were trained to lever push for a pellet reward. During these sessions, both levers were extended into the chamber, but only one was reinforced. Rats were either trained to push the right or the left lever, with the reinforced lever position being counter-balanced within the genotype groups. During training, the experimenter would reward rats for approaching, sniffing and touching the reinforced lever, until rats started to reliably push the lever on their own. During this, each lever push was rewarded with one pellet. Training continued until rats completed 100 lever pushes within a 30-minute session, without any help from the experimenter. The rats were then trained on an FR3 protocol, where they had to push the reinforced lever three times before being rewarded with a pellet. When a rat completed 100 ratios within a 30-minute session, it progressed to an FR5 protocol. Rats now had to push the reinforced lever five times before being rewarded with a pellet. Training on the FR5 protocol continued until rats completed 100 ratios within a 30-minute session, on three consecutive sessions. Afterwards, rats were trained on a PR protocol adapted from [16]. In the current protocol, the ten first ratios were of FR5 type. Afterwards, the required number of lever pushes increased after each completed ratio. During this progression, the required number of lever pushes increased in an arithmetic fashion within each block of ten ratios, but also changed between the blocks, to give an overall exponential progression. Thus, during the first, second and third block of ten ratios, the ratio requirement increased with one, three and five pushes per completed ratio, respectively. The PR sessions lasted 80 minutes. The main behavioral parameter of interest was a set of break points, defined as the first ratio where a rat made no responses on the reinforced lever during 10, 25, 50, 100, 300 or 600 seconds. Rats were trained until both genotype groups reached a stable performance, which in this case required 18 sessions. Performance during the six last sessions was defined as baseline performance.

Once stable PR performance had been reached, the rats were challenged in a set of four prefeeding tests. During these tests, the rats were fed specific amounts of reward pellets or regular food, just prior to their daily PR session. Rats were prefed by placing them in individual cages that contained the specified amount of food. Each prefeeding condition was assessed once, in the following order: 100 reward pellets, 250 reward pellets, 4.5 g of regular food, 11.25 g of regular food. Each prefeeding test was separated by two regular PR sessions to ensure that rats returned to their baseline performance.

After completion of the first round of prefeeding tests, the food deprivation level of WT rats was adjusted until they consumed food at the same rate as BACHD rats. Consumption rate was assessed daily by measuring the amount of food consumed during 15 minutes of free access to regular food, placed in the cage tops of the rats' homecages. The rats were still given daily PR sessions during food deprivation adjustments. The food consumption tests were run four hours after completion of the last PR run, i.e. at the time when the rats were usually given their daily food ration. When WT rats had reached a consumption rate equal to that of BACHD rats, six additional PR sessions were run to establish a new baseline. The prefeeding tests were then repeated in the same manner as described above. Rats were 20 weeks old at the end of the test.

Statistical analyses

All statistical analyses were conducted using GraphPad Prism v.6.01 (GraphPad Software, San Diego California USA, http://www.graphpad.com).

Food consumption in the *ad libitum* food consumption test was analyzed both in terms of the absolute amount of food consumed and the amount of food consumed relative to the animals' body weight. The main analysis of food consumption was based on the weight of large food pieces, as the food debris gathered through sifting of the bedding material also contained hair and bedding pieces. A separate analysis where food consumption was corrected for the amount of food debris was still performed. For this, the mean amount of food debris was calculated for each cage, based on their longitudinal data. This was then added to the weight of the large food pieces measured at each cage changing. For the relative food consumption, rats in a given cage were assumed to eat equal amounts of food. The approximate amount of food consumed by one of the rats was subsequently related to the mean body weight of the two rats. Two-way repeated measures ANVOAs were used to analyze body weight as well as absolute and relative food consumption. Age was used as within-subject factor, and genotype as between-subject factor.

For data gathered in the dissection study, body weight, absolute weight of adipose and bone/muscle tissues, as well as bone/muscle weight relative to body length were analyzed using regular two-way ANOVAs. The factors of interest were still age and genotype. The weights of adipose tissue, bone/muscle tissue and internal organs relative to body weight were analyzed in individual t-tests, or Mann-Whitney tests, between genotypes, within each age group. As the observed phenotypes did not vary between different adipose tissue deposits, only the combined weight of all deposits will be addressed here. One BACHD rat meant for the dissection of six months old animals died before the dissection, making that particular age group 12 WT and 11 BACHD rats.

Results from the two hunger tests were analyzed both within and between each testing occasion. For each test occasion of the reward pellet consumption test, the time needed to consume the pellets was analyzed with t-tests to compare the two genotypes. The time spent exploring the test arena was only analyzed on the first test occasion, using t-test, as rats showed essentially no interest in exploring the arena on later trials. One BACHD rat was excluded from the analysis of the last trial, as he failed to consume all reward pellets within the maximum trial time. The amount of food consumed during the food consumption test was on each test occasion analyzed with two-way repeated measures ANOVA, using time as within-subject factor, and genotype as between-subject factor. To better understand the effect of repeated testing and food deprivation levels, the time needed to consume 100 reward pellets, and the amount of food consumed during the first 30 minutes of the food consumption test were analyzed in additional detail. Thus, data from all three test-occasions were analyzed in two-way repeated measures ANOVAs, using genotype as between-subject factor, and either session number or food deprivation level as within-subject factor. Analysis of baseline performance during the PR test was also made with repeated measures two-way ANOVAs, with break point as within-subject factor, and genotype as between-subject factor. Drops in motivation during prefeeding sessions were analyzed for the 600-seconds break point, as a percentage of the ratio reached during the two preceding PR sessions. Once again, repeated two-way ANOVAs were used to analyze the results, using prefeeding condition as within-subject factor, and genotype as between-subject factor. Separate analyses were performed for prefeeding with reward pellets, and regular food. Bonferroni *post-hoc* test was used to follow up any significant effects of genotype, or interaction effects found in the two-way ANOVAs. Alpha for all analyses was set to 0.05.

Results

Ad libitum food consumption

To assess BACHD rats' growth and food consumption in a low-stress and social environment, we housed genotype-matched rats in pairs (Figure 2A), and measured their weekly body weight and food consumption. Rats of both genotypes grew steadily during the test, as indicated by the significant effect of age on body weight ($p<0.0001$, $F_{(21,1449)} = 2766$) (Figure 2B). BACHD and WT rats grew at a similar rate, and showed similar body weights through the entire test, with no significant genotype effect or age x genotype interaction. The rats' food consumption also changed with age ($p<0.0001$, $F_{(20,680)} = 110.5$) (Figure 2C). In general, food consumption increased gradually until the age of nine weeks, and then slowly dropped. Importantly, WT and BACHD rats consumed equal amounts of food between six and eight weeks of age, but there were a number of differences seen at older ages. At nine and ten weeks of age, BACHD rats appeared to consume more food that WT rats, although this did not reach statistical significance. Directly following this, food consumption dropped steadily among BACHD rats, while WT rats remained arguably stable until the age of 16 weeks. Due to this, BACHD rats eventually ate less than WT rats, as indicated by the significant results from the *post-hoc* analysis at 17 weeks of age and onwards ($p<0.05$–0.01). The difference in how food consumption changed with age among BACHD and WT rats was also evident in a significant age x genotype interaction ($p<0.0001$, $F_{(20,680)} = 19.06$). Relating food consumption to the rats' body weight gave largely the same results, with a significant age effect ($p<0.0001$, $F_{(60,680)} = 1930$) and age x genotype interaction ($p<0.0001$, $F_{(20,680)} = 12.99$) (Figure 2D). However, this analysis made the increased food intake among young BACHD rats more apparent, with the *post-hoc* test indicating significant differences between BACHD and WT at seven to ten weeks of age ($p<0.01$–0.0001). In contrast, the decreased food consumption among old BACHD rats was less apparent, with the *post-hoc* test only indicating a few significant data points at 18 to 21 weeks of age ($p<0.05$–0.01). It should be noted that BACHD rats produced less food debris compared to WT rats (Figure S1A and B). Correcting for this did not dramatically affect the food consumption phenotype, although the genotype differences became less apparent (Figure S1C). Finally, BACHD rats consumed dramatically less water compared to WT rats (Figure S1D).

Body composition of BACHD rats

In order to assess BACHD rats' body composition, we dissected BACHD and WT rats at five different ages. As expected, older rats weighed more, leading to a significant age effect on body weight ($p<0.0001$, $F_{(4,109)} = 444.1$) (Figure 3A). In line with previous data, there were no differences in body weight between the genotypes in any age group, and also no significant difference in apparent growth. The body composition of BACHD rats was however different from that of WT rats. BACHD rats had significantly lower percentage of bone and muscle ($p<0.001$, all ages), and higher percentage of adipose tissue ($p<0.05$–0.001) in all age groups (Figure 3B). These differences were also apparent when analyzing the absolute weights of the respective tissues. Both WT and BACHD rats gained adipose tissue with age, as indicated by a significant age effect on the weight of total adipose tissue ($p<0.0001$, $F_{(4,109)} = 142$) (Figure 3C). However, BACHD rats carried an excess amount of adipose tissue, as indicated by both a significant genotype effect ($p<0.0001$, $F_{(1,109)} = 81.25$), and significant results from the *post-hoc* analysis of all groups, except the one-month old rats ($p<0.05$–0.0001). There was also a significant age x genotype interaction ($p<0.0001$, $F_{(4,109)} = 7.686$) that was dependent on data from the one and three months old groups. The bone/muscle weight also increased with age for both genotypes ($p<0.0001$, $F_{(4,109)} = 555.4$) (Figure 3D). However, BACHD rats were found to have significantly less bone/muscle tissue compared to WT rats in all but the one-month old age groups. This was indicated both by a significant genotype effect ($p<0.0001$, $F_{(1,109)} = 70.69$), and significant results from the *post-hoc* analysis ($p<0.01$–0.0001). A significant age x genotype interaction ($p<0.001$, $F_{(4,109)} = 4.18$) also indicated that there was a difference in the rats' growth. Importantly, this effect was dependent on the data of the one–month old group.

The rats' body length also increased with age for both genotypes ($p<0.0001$, $F_{(4,109)} = 1517$), although a significant genotype effect ($p<0.0001$, $F_{(1,109)} = 86.46$) and *post-hoc* tests ($p<0.01$–0.0001) revealed that BACHD rats were smaller than WT (Figure 3E). This was apparent in all age groups except the one-month old animals. It should, however, be noted that one-month old BACHD rats were shorter than WT rats when analyzing litter-matched groups (data not shown). The reduced body length among BACHD rats was mainly due to them having shorter tails and heads compared to WT rats (Figure S2).

BACHD rats also showed a lower amount of bone/muscle tissues in relation to their body length (Figure 3F). Rats of both genotypes gained relative amounts of bone and muscle with age ($p<0.0001$, $F_{(4,109)} = 570.6$). However, BACHD rats had lower relative amounts of bone and muscle from three months of age, as evident from a significant genotype effect ($p<0.0001$, $F_{(1,109)} = 47.32$) and *post-hoc* analysis ($p<0.05$–0.0001).

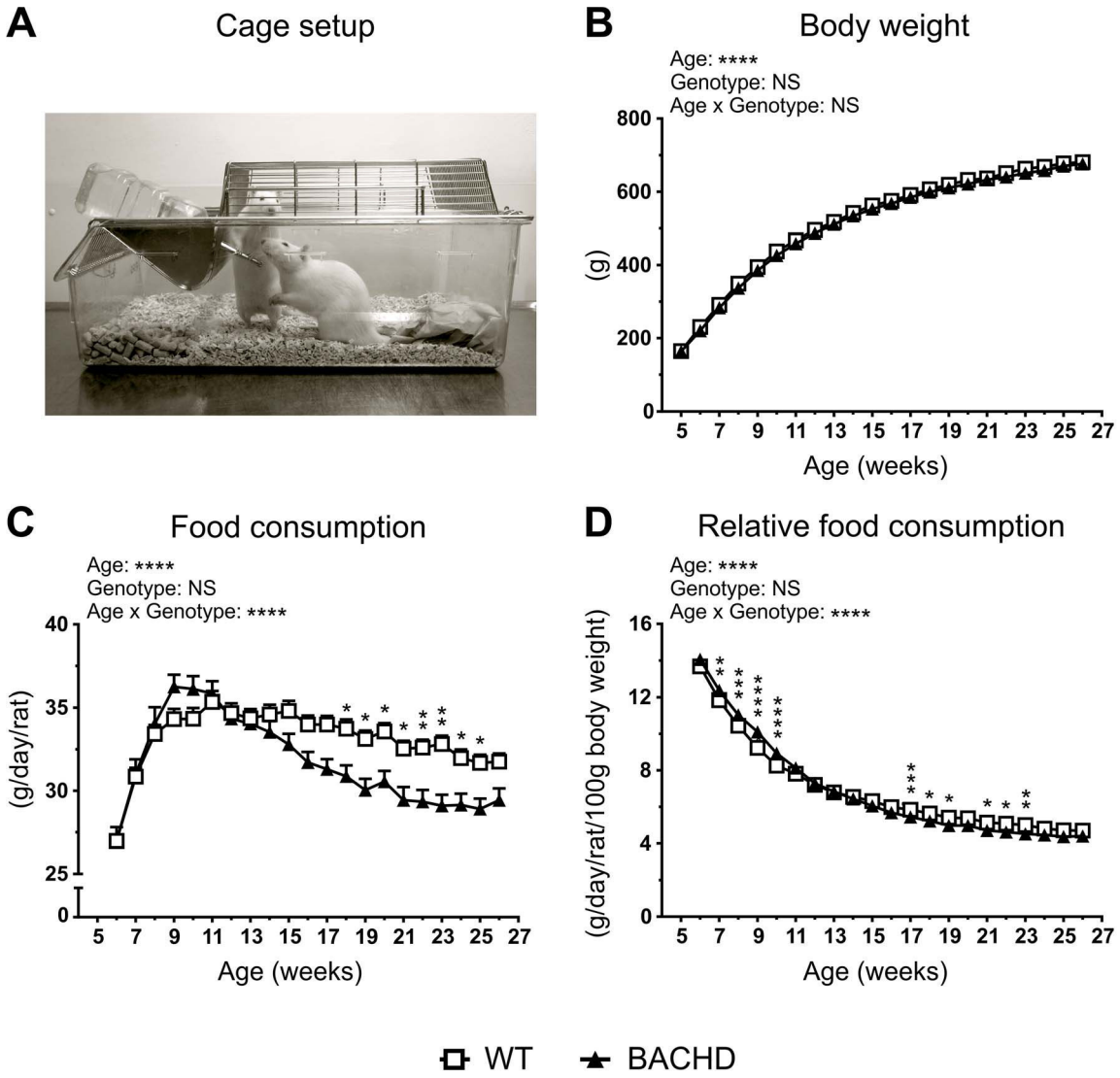

Figure 2. Body weight and food consumption. (**A**) Housing conditions during the *ad libitum* food consumption test. (**B**) Body weight of rats plotted against their age. (**C**) Approximate daily food consumption per rat (calculated from weekly food consumption per cage), plotted against the age of the animals. (**D**) Relative daily food consumption per rat (calculated from weekly food consumption and average body weight per cage), plotted against the age of the animals. The graphs show group mean plus standard error of the mean. Two-way ANOVA results are displayed above each graph, and significant results from *post-hoc* analysis are displayed for individual data points. Genotype differences are indicated by ($p<0.05$) *, ($p<0.01$) **, ($p<0.001$) *** and ($p<0.0001$) ****.
doi:10.1371/journal.pone.0105662.g002

Assessment of hunger during food deprivation of BACHD rats

Two tests based on voluntary consumption of reward pellets and regular food, were run to assess BACHD rats' hunger level at different levels of food deprivation (Figure 4A). When both WT and BACHD rats were deprived to 85% of their respective free-feeding body weights, BACHD rats were found to consume both reward pellets and regular food at a slower rate than WT rats (Figure 4B). In the pellet consumption test, BACHD rats needed longer time to eat the reward pellets ($p<0.01$), but did not spend more time exploring the arena, compared to WT rats. The slower feeding speed led to a significant increase in trial time for BACHD rats (data not shown). In the food consumption test, BACHD rats were found to have eaten less than WT rats at almost all investigated intervals, as evident from the significant genotype effect ($p<0.01$, $F_{(1,6)} = 14.62$), and the significant results from the *post-hoc* analysis ($p<0.05$–0.01). It should be noted that a difference in actual consumption rate was only seen during the first 30 minutes, resulting in an initial difference in the amount of food consumed, which then persisted through the remaining part of the test. This difference in behavior gave a significant time x genotype interaction ($p<0.01$, $F_{(9,54)} = 2.840$) in the amount of food consumed by the rats.

In an attempt to reverse the phenotypes described above, the food deprivation levels were adjusted so that BACHD and WT rats were at 80 and 95% of their respective free-feeding body weights (Figure 4C). In the pellet consumption tests, BACHD rats now needed a similar amount of time to consume the reward pellets, although there was a borderline significant trend towards BACHD rats needing more time ($p = 0.0535$). With the exception of one WT rat, all rats spent the entire trial eating, and showed minimal interest in exploring the test arena. In the food

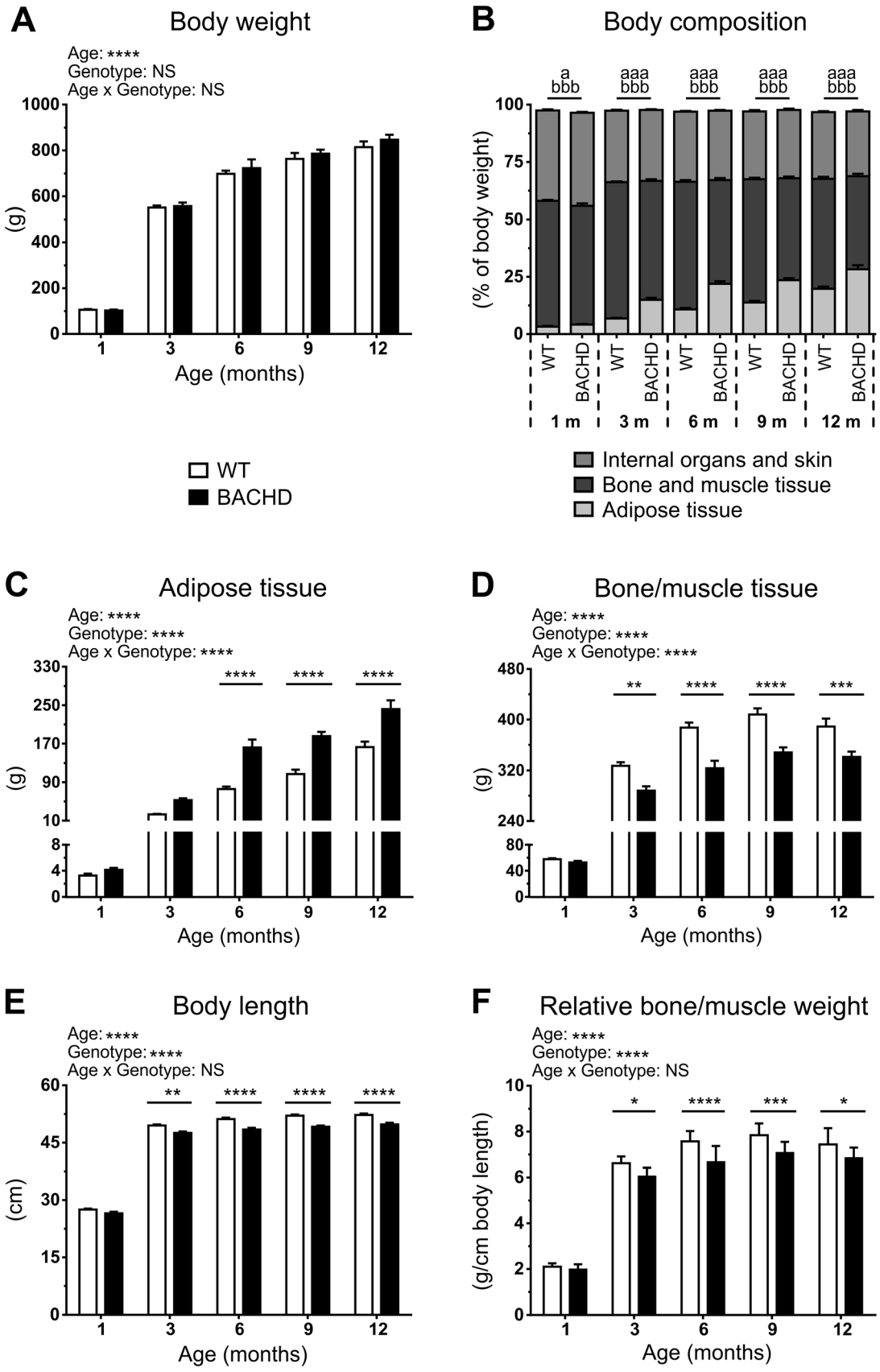
A
Body weight
Age: ****
Genotype: NS
Age x Genotype: NS
(g)
Age (months)
WT
BACHD
B
Body composition
a
bbb
aaa
bbb
(% of body weight)
WT
BACHD
1 m
3 m
6 m
9 m
12 m
Internal organs and skin
Bone and muscle tissue
Adipose tissue
C
Adipose tissue
Age: ****
Genotype: ****
Age x Genotype: ****
D
Bone/muscle tissue
Age: ****
Genotype: ****
Age x Genotype: ****
E
Body length
Age: ****
Genotype: ****
Age x Genotype: NS
(cm)
F
Relative bone/muscle weight
Age: ****
Genotype: ****
Age x Genotype: NS
(g/cm body length)

Figure 3. Body composition assessed through dissection. (**A–F**) Data from the dissection groups as stated in the graph titles. The graphs show group mean plus standard error of the mean. Two-way ANOVA results are displayed above each graph, and significant results from *post-hoc* analysis are displayed inside each graph. Significant genotype differences are indicated by ($p<0.05$) *, ($p<0.01$) **, ($p<0.001$) *** and ($p<0.0001$) ****. For (**B**), ANOVA was not performed, and the indicated differences concern single comparisons between WT and BACHD rats within the age groups. Significant differences are indicated with "a" and "b" for differences in the relative amount of adipose and bone/muscle tissue respectively, written according to the same grading as above.
doi:10.1371/journal.pone.0105662.g003

consumption tests, BACHD and WT rats consumed food at the same rate during the first 150 minutes. During the remaining part of the test, WT rats ate more, eventually leading to a significant difference in the total amount of food consumed during the test ($p<0.01$). The behavioral differences led to a significant time x genotype interaction effect ($p<0.0001$, $F_{(9,54)} = 8.642$).

In a final test, the food deprivation levels were adjusted so that BACHD and WT rats were at 95 and 80% of their respective free-feeding body weights (Figure 4D). At this point, BACHD rats consumed the reward pellets at the same rate as WT rats, as the aforementioned trend was no longer present. With the exception of two BACHD rats, all rats spent the entire trial eating, and showed minimal interest in exploring the test arena. One BACHD rat did not consume all reward pellets within five minutes. In the food consumption test, BACHD rats were once again found to have consumed less food than WT at all investigated intervals, resulting in a significant genotype effect ($p<0.001$, $F_{(1,6)} = 42.52$), and significant results from the *post-hoc* analysis ($p<0.05$–0.0001). BACHD rats ate at a slower rate during the first hour. The consumption rate gradually declined among WT rats, while it gradually increased among BACHD rats, ending up at similar levels after 150 minutes. This difference in behavior gave a significant time x genotype interaction ($p<0.0001$, $F_{(9,54)} = 8.47$) in the amount of food consumed by the rats.

A more detailed analysis of the results was performed with the aim of better assessing the impact of food deprivation levels on the consumption rate in the two tests. Separate two-way ANOVA analysis of the time needed to consume 100 reward pellets, using genotype as between-subject factor, and either food deprivation level or the number of test sessions as within-subject factor, revealed similar statistical results (Figure 5A). In either case, there was a significant genotype effect ($p<0.05$, $F_{(1,21)} = 5.476$), and performance on the first session, where both genotypes were deprived to 85%, differed significantly between genotype groups ($p<0.05$). Both analyses also revealed a significant effect of their respective within-subject parameter ($p<0.01$, $F_{(2,42)} = 7.861$ and 6.6333 for session and deprivation level, respectively). However, inspection of the graphed data indicated that the time needed to consume the reward pellets did not clearly decrease with increasing food deprivation levels, but did so with increased numbers of test sessions. Performing the same analyses on the amount of food consumed during the first 30 minutes of the food consumption test revealed different results (Figure 5B). Both analyses once again revealed a significant genotype effect ($p<0.01$, $F_{(1,6)} = 15.59$), and significant effects of their respective within-subject parameters ($p<0.01$, $F_{(2,12)} = 8.220$ and 17.04 for session and deprivation level, respectively). *Post-hoc* analysis of data analyzed in terms of food deprivation level revealed a significant difference in consumption rate when rats of both genotypes were deprived to 85% of their free-feeding body weight. This was also found when analyzing the data in terms of the number of test sessions given to the rats, although that analysis also revealed a significant difference in consumption rate during the third session. In contrast to the results from the pellet consumption test, the consumption rate in the food consumption test appeared to gradually increase with an increased food deprivation level, while not showing any gradual change during repeated testing.

Progressive ratio performance during different levels of food deprivation

To better assess differences in the motivational state among the rats, a progressive ratio test was run with two different food deprivation settings. All rats learned to push the lever in order to obtain a reward pellet, although there were some discrete behavioral differences between WT and BACHD rats during the initial training steps. During habituation, BACHD rats made fewer entries into the pellet receptacle (Figure S3A, B) and were initially slower at retrieving the pellets (Figure S3C). During CRF, FR3 and FR5 training, BACHD rats were generally slower at both retrieving the pellets, and returning to the reinforced lever (Figure S4 and S5).

During the fixed ratio part of the PR protocol, BACHD rats were still slower at retrieving the reward pellets, but they no longer showed an increase in lever return latencies (Figure S6). These results were largely unaffected when food deprivation levels were adjusted. WT rats tended to take longer time to complete the FR5 ratios, although this became significant only after adjustment of their deprivation level (Figure S6). Importantly, there were no overt differences between genotypes in the overall response frequency on the rewarded lever during the fixed ratios (Figure S6). The same was true for the mean number of lever pushes made on the non-reinforced lever during the entire PR session (Figure S7).

Analysis of how the rats reached a series of break points, when all were deprived to 85% of their free-feeding body weight, revealed both a significant genotype effect ($p<0.01$, $F_{(1,22)} = 10.66$) and differences in the three highest break points ($p<0.01$), with BACHD rats reaching lower ratios (Figure 6A). These differences were not present when the food deprivation level of WT rats had been adjusted so that their food consumption rate matched that of BACHD rats. Similarly, when all rats were deprived to 85% of their free-feeding body weight, BACHD rats responded with more pronounced drops in motivation during prefeeding of both reward pellets and regular food, as indicated by significant genotype effects ($p<0.01$, $F_{(1,22)} = 9.461$ and $p<0.01$, $F_{(1,21)} = 8.343$ for reward pellet and regular food prefeeding, respectively) and prefeeding x genotype interactions ($p<0.001$, $F_{(2,44)} = 11.19$ and $p<0.05$, $F_{(1,21)} = 8.341$ for reward pellet and regular food prefeeding, respectively) (Figure 6B). Once again, these phenotypes were not present when the food deprivation level of WT rats had been adjusted, leading to identical responses in the prefeeding tests. It should be noted that only the last break point, break point 600, was suitable for prefeeding analysis. Prefeeding induced a strong interest in water among WT rats, which dramatically affected their early break points (data not shown). It should also be noted that there was a significant difference in body weight once the food deprivation levels had been adjusted, with WT rats being significantly heavier than BACHD rats (data not shown). The WT rats weighed roughly 50 g more than BACHD rats, resulting in them being at 95% of their free-feeding body weight.

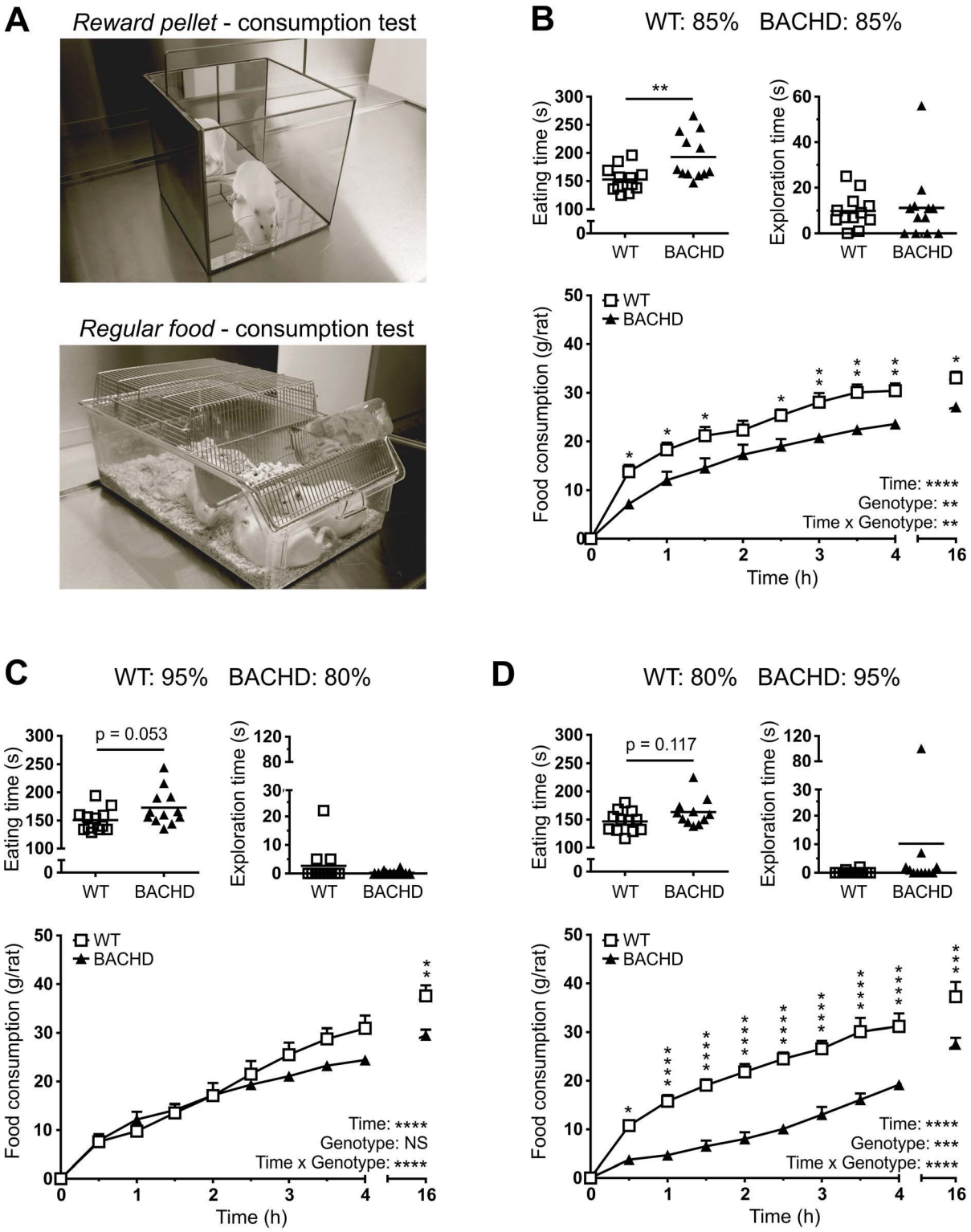

Figure 4. Hunger and food interest assessment. Setups (**A**) and performance in the two consumption tests during the first (**B**), second (**C**) and third test session (**D**), with the different food deprivation levels stated in the title of each figure panel. The time needed to eat 100 reward pellets and the time spent exploring in the reward pellet consumption setup, are displayed in the top left and right graphs of each panel, respectively. The bottom graph of each panel shows the cumulative food consumed per rat during the regular food consumption test. Scatter plots for reward pellet consumption test results indicate individual values and group mean. Line graphs for regular food consumption indicate group mean plus standard error of the mean. Statistical test results are given inside the graphs. For the regular food consumption test, two-way ANOVA results are displayed in the bottom right corner, and results from *post-hoc* analysis are shown for individual data points. Significant genotype differences are indicated by ($p<0.05$) *, ($p<0.01$) **, ($p<0.001$) *** and ($p<0.0001$) ****.
doi:10.1371/journal.pone.0105662.g004

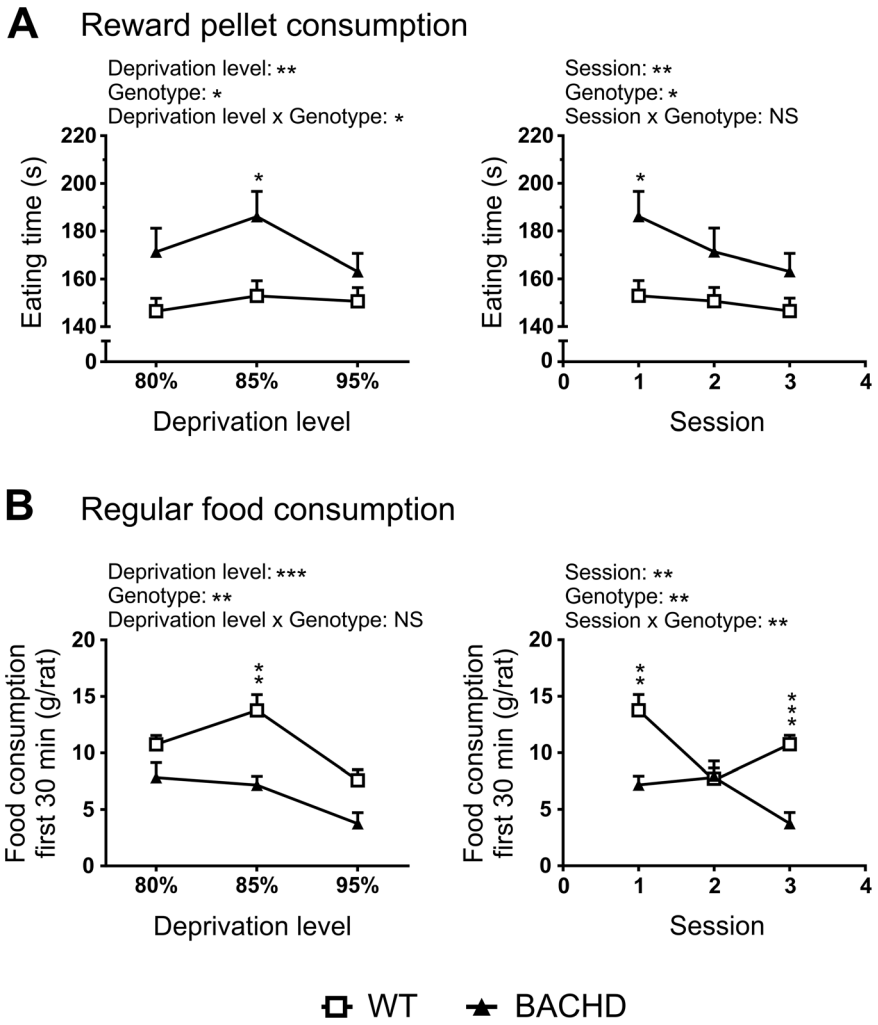

Figure 5. Impact of repeated testing and food deprivation on consumption tests. (**A**) The time needed to consume 100 reward pellets is plotted against the deprivation level (left graph) and session number (right graph). (**B**) The food consumed during the first 30 minutes of the regular food consumption test is plotted against the deprivation level (left graph) and session number (right graph). The graphs show mean plus standard error of the mean. Two-way ANOVA results are displayed above each graph, and results from *post-hoc* analysis are shown for individual data points. Significant genotype differences are indicated by ($p<0.05$) *, ($p<0.01$) **, ($p<0.001$) *** and ($p<0.0001$) ****.
doi:10.1371/journal.pone.0105662.g005

Discussion

Body composition and food intake of BACHD rats

Many transgenic animal models of HD show an altered body weight compared to their WT littermates. Animals that express a fragment of the disease-causing gene typically have a reduced body weight [25,26,27], while the ones that express the full-length gene typically have an increased body weight [10,11]. We show here, that although BACHD rats did not differ from WT rats in terms of body weight, they displayed several changes in body composition. Strikingly, BACHD rats carried an excess amount of adipose tissue. This is in line with phenotypes of other full-length models of HD, as the increased body weight of BACHD and YAC128 mice has been shown to at least in part be due to an increase in adipose tissue mass [28,29]. It should be pointed out that R6/2 and N171-82Q mice, which only express a fragment of the disease-causing gene, also carry excess amounts of adipose tissue [25,30]. R6/2 mice have further been shown to maintain this increased fat mass even when they start to lose weight [25]. Thus, the increase in adipose tissue seems to be a common phenotype of transgenic HD models, although it does not always result in obesity.

Increased amounts of adipose tissue could theoretically be the result of increased food intake, decreased home cage activity, metabolic disturbances, or a combination of the three. While BACHD mice have been shown to eat more than their WT littermates [28], R6/2 and YAC128 mice have been found to have unchanged food intake [25,29]. A previous study on BACHD rats, in which food intake was followed from three to eighteen months of age, indicated that the transgenic rats ate less than their WT littermates [22]. These results were well reproduced here, despite the different housing conditions. The current study also assessed food intake at ages younger than three months, where BACHD rats appeared to consume more food compared to WT rats. It should be noted, however, that the appearance of the food consumption phenotypes was to some degree dependent on whether or not the weight of the consumed food was normalized to the animals' body weight. The aim of this normalization was to relate the rats' food intake to a measurement of their body size, and through this investigate if the reduced food intake among

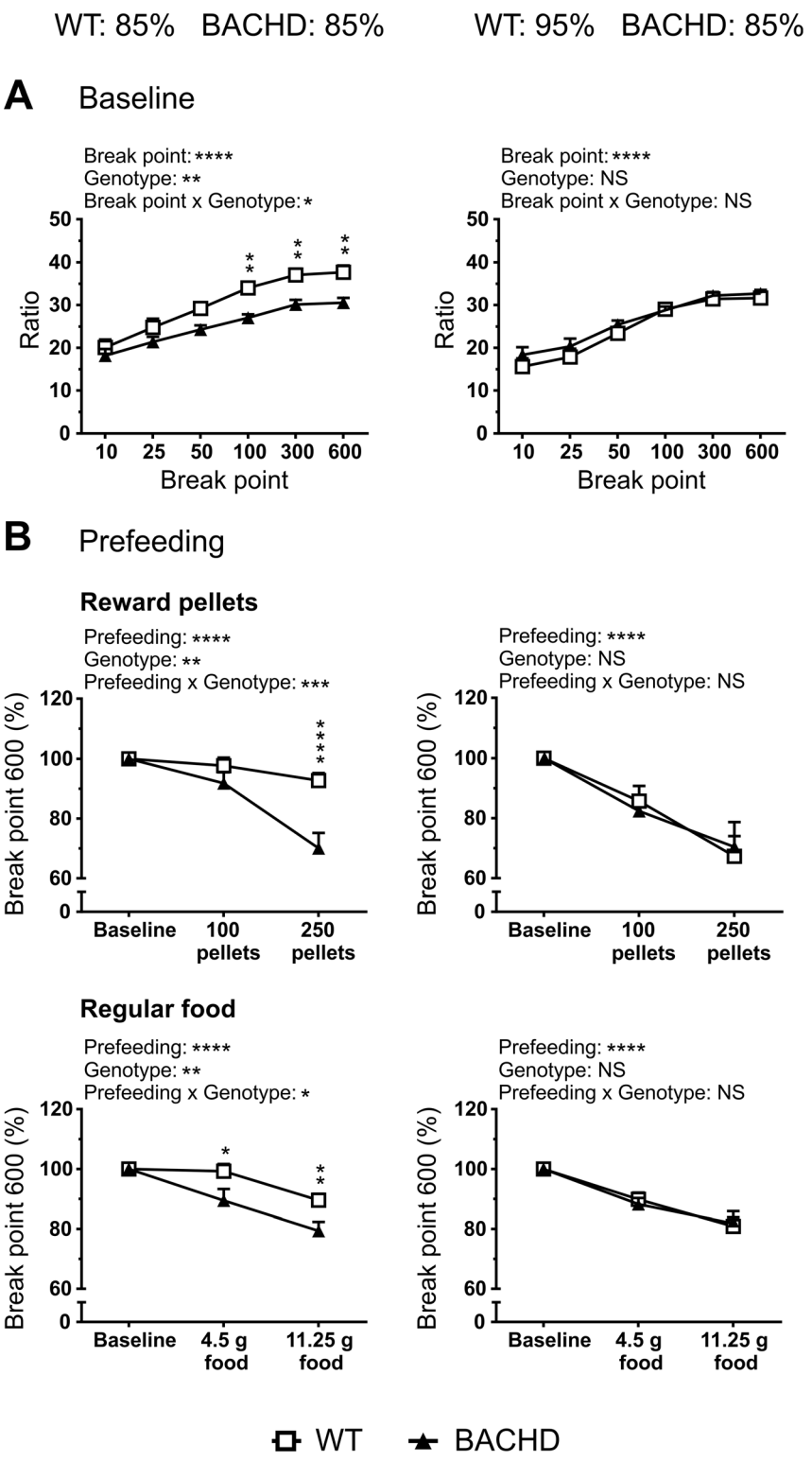

Figure 6. Progressive ratio test performance. Performance in the PR test is shown for when animals of both genotypes were deprived to 85% of their free-feeding body weight (graphs to the left in each figure panel) and when the deprivation level of WT rats had been adjusted to achieve equal food consumption rates between genotypes (graphs on the right of each figure panel). (**A**) Baseline performance during six consecutive PR sessions preceding the prefeeding tests. The ratio, where a given break point was reached, is indicated. (**B**) Performance during prefeeding with reward pellets (top panel) and regular food (bottom panel). The drop in motivation is displayed as percentage of baseline performance for break point 600. The graphs show group mean plus standard error of the mean. Two-way ANOVA results are displayed above each graph, and results from *post-hoc* analysis are shown for individual data points. Significant genotype differences are indicated by ($p<0.05$) *, ($p<0.01$) **, ($p<0.001$) *** and ($p<0.0001$) ****.

doi:10.1371/journal.pone.0105662.g006

BACHD rats could be due to them being smaller than WT rats. Using body weight as an approximation of body size is, however, probably only suitable at young ages, as the body weight of older BACHD rats is distorted due to obesity. Thus, further studies are needed to reach conclusions on this matter. In addition, as food intake phenotypes are unlikely to explain the increase in adipose tissue, metabolic parameters of BACHD rats need to be further characterized. In this regard, it is important to note that the obesity phenotype of BACHD mice was abolished when the expression of mutant Huntingtin was silenced in the hypothalamus [28]. Interestingly, hypothalamic lesions can induce obesity that is not always associated with increased food intake, but can persist despite unchanged or even reduced food intake [31,32,33,34,35]. The differential effects appear to depend on which specific neuronal population is damaged [35,36], which might relate to the common phenotype of increased fat mass, but varied food intake seen across HD animal models.

In the current study, BACHD rats were shown to have a smaller body size and disproportionately lower amount of bone/muscle tissue compared to WT rats. Information about similar parameters is scarce for other HD models, although YAC128 mice have been shown to have unchanged lean body mass [29], while R6/2 mice show a progressive reduction in lean body mass as they age [25]. These are both in contrast to the bone/muscle phenotype seen in BACHD rats, as the lower amount of bone/muscle tissue seen in the current study did not seem to progress with age. Instead, the body size and bone/muscle phenotypes seen in the BACHD rats appeared to be caused by discrete developmental deficits and stunted growth. It is unlikely that these phenotypes were the result of malnutrition during testing, as food was available *ad libitum* on the cage floor. It is possible, however, that BACHD pups might have had difficulties when competing for mothers' milk, leading to malnutrition at early ages. Such factors have been shown to affect the growth of animals from large litters [37]. Alternatively, the growth of BACHD rats might be disturbed on a molecular level, as Huntingtin has been shown to be important during fetal development [38]. The fact that BACHD rats had smaller heads compared to WT rats is particularly interesting, as similar symptoms have been seen in HD gene-carriers [39]. Thus, the discrete developmental deficits found in the BACHD rats might be closely connected to developmental deficits of human patients.

Food deprivation and motivation of BACHD rats

Behavioral assessment of HD animal models through the use of operant conditioning tests is of interest, as cognitive symptoms are common in HD patients and might become valuable to clinically track disease progression and treatment effects [40,41,42]. Many conditioning protocols require food deprivation in order to both efficiently train the animals to perform a given task and to maintain high performance. However, food deprivation of HD models requires extra care as they can be expected to have changes in body composition. To better understand how to optimally food deprive BACHD rats, we assessed their interest in food in a total of three different tests.

Free intake of reward pellets and regular food is sometimes used to assess an animal's hunger level and interest in food [18,19,20,21]. In the current study, WT and BACHD rats deprived to 85% of their free-feeding body weight did not seem to differ in their interest in consuming 100 reward pellets, although BACHD rats needed more time to eat all pellets. Food deprivation levels were then adjusted in an attempt to reverse the phenotypes, however, this did not seem to affect the rats' behavior. Instead, both the time spent exploring the arena and the time needed to consume all pellets decreased with repeated testing. The training effect on the consumption rate eventually led to BACHD rats consuming the reward pellets at an equal rate compared to WT rats. There were indications that rats deprived to 95% of their free-feeding body weight spent more time exploring the arena compared to rats deprived to 80%, but this generally concerned one or two rats of an entire group of twelve. As the current protocol did not appear to be sensitive even to large changes in food deprivation levels, it is unlikely to be a suitable test for assessing discrete differences in food interest. It is also clear that the apparent training effect could be misinterpreted as a food deprivation effect, if one assessed a given group of animals repeatedly with the aim of gradually adjusting their food deprivation level. The slowed consumption speed seen among BACHD rats in the pellet consumption test is, however, an interesting phenotype on its own. While eating, rats typically stood on all four paws and used their tongue to pick up the pellets. Thus, the slower feeding rate among BACHD rats is likely due to impairments in quite basic processes that are needed for eating. These could include impaired chewing, swallowing or tongue movements as well as reduced saliva production. It is tempting to hypothesize that the slower feeding speed among BACHD rats could be due to phenotypes similar to the tongue protrusion symptoms that are often seen among HD patients [43,44]. Interestingly, there are protocols for measuring tongue protrusion [45] in rats, although these tests must be performed carefully, as the smaller head size of BACHD rats likely means that they have shorter tongues as well.

In the regular food consumption test, BACHD rats consumed less food than WT rats when both groups were deprived to 85% of their respective free-feeding body weight. Consumption rate during the first 30 minutes of the test changed in a predictable way when deprivation levels were adjusted, with more deprived rats eating at a faster rate. This suggests that the protocol was well suited for the assessment of food interest and hunger levels. Our results further showed that when BACHD and WT rats were deprived to 80 and 95% of their respective free-feeding body weights, they consumed food at an identical rate for the initial 150 minutes, indicating that the rats were equally hungry. As the test session continued, BACHD rats once again ate less than WT rats, which likely reflected differences in the rats' satiety levels. It should be noted that the feeding behavior of either genotype did not significantly differ when comparing their 80 and 85% food deprivation test sessions. Thus, although the test seems suitable to assess food interest, it does not appear to be very sensitive. Assessing food consumption in single animals, rather than in groups, would most likely improve the test's sensitivity. It would further allow separate scoring of the time spent eating and the time spent not eating, as it was done in the reward pellet consumption test. However, despite extensive habituation, we have found it difficult to get our rats to efficiently consume regular food in any other setup than their home cages. As the test did not allow separate scoring of the time the rats spent feeding and doing other activities, it was not possible to conclude if the difference in consumption rate was strictly due to a difference in hunger and food interest. This idea is especially difficult to support when considering the results of the pellet consumption test. In an attempt to reach a conclusion on the matter, we ran a PR test with prefeedings.

When both WT and BACHD rats were deprived to 85% of their respective free-feeding body weight, BACHD rats were clearly less motivated to work for food rewards in the PR test. Similar phenotypes have been found in other HD models [16,46] and they are typically discussed in terms of apathy, which is a common symptom among HD patients [47,48]. However,

BACHD rats also responded with more pronounced drops in motivation during the prefeeding tests, which would typically be interpreted as BACHD rats being less hungry compared to WT rats [49,50,51]. This would also support the idea that the BACHD rats' lower consumption rate in the first session of the food consumption test was to some degree caused by lower hunger and food interest. When the food deprivation level of WT rats was adjusted to achieve equal food consumption rates to those of the BACHD rats, all genotype differences that were previously seen in the PR test disappeared. As WT and BACHD rats did not differ during prefeeding tests, it is reasonable to assume that they were equally hungry and that the food consumption test was suitable for establishing food deprivation levels that ensured this. As they also no longer differed in baseline performance, the motivational deficit seen in the first PR test was likely dependent on a difference in hunger levels, rather than an apathy-related phenotype. It is interesting to note that after the food deprivation levels had been adjusted, BACHD rats weighed approximately 50 g less than WT rats. This difference was similar to the one found in bone/muscle tissue, suggesting that WT and BACHD rats carried a similar amount of adipose tissue. Secretion of leptin, which affects satiety and food intake [52,53], is proportional to adipose tissue mass [54], and it is possible that the food deprivation adjustment led to equal hunger and food interest due to equal levels of leptin. Importantly, higher leptin levels have been shown to reduce motivation in PR tests [55], which gives a possible explanation for the initial motivational difference.

Most of the conclusions above are based on the idea that prefeeding responses depend exclusively on hunger levels and not on other aspects of motivation. One could argue that animals that suffer from motivational deficits not related to hunger, might also respond stronger on the prefeeding tests. Thus, seeking a situation where animals respond equally to prefeeding could in itself lead to the lack of differences in PR performance. It is therefore important to note that other studies have found motivational differences despite identical responses on prefeeding tests [51], and that motivational deficits have been found in BACHD mice after adjusting deprivation levels until animals consumed food at the same rate [16]. It should also be noted that the true nature of the motivational phenotype seen here is mainly of importance when such phenotypes are being characterized. If one simply wishes to minimize motivational differences when working with BACHD rats, regardless if these are due to hunger levels or other aspects of motivation, adjusting deprivation levels so that WT and BACHD rats consume regular food at a comparable rate should suffice. Still, the current study only considered quite young animals. It is possible that older BACHD rats suffer from motor impairments that could affect the validity of the food consumption test. Also, motivational phenotypes not related to hunger might become apparent among older BACHD rats. We aim at addressing these ideas in a longitudinal study of PR performance.

Summary

In the current study, BACHD rats were found to have metabolic disturbances, which is in line with other animal models of HD. We further found that unless these phenotypes were taken into consideration during food deprivation, BACHD rats were less motivated than WT rats in a progressive ratio test. Thus, metabolic phenotypes are important to consider as possible confounding factors when assessing apathy-related phenotypes of BACHD rats. The same is likely true for other HD animal models with metabolic abnormalities.

Our results further indicated that basing the animals' food deprivation levels on their consumption rates of regular food was a convenient way to avoid motivational differences between BACHD and WT rats. Thus, previous studies that applied this method when studying apathy in HD animal models [16] likely avoided hunger-based motivational differences, and our results support the future use of this method. It is also important to consider its use in behavioral tests where the main readout is not directly related to apathy or motivation, such as [17], as motivational differences have been shown to affect animals' behavior in such tests too [15].

Supporting Information

Figure S1 Food debris and water consumption during the *ad libitum* food consumption test. (**A**) The approximate daily amount of food debris produced per cage (calculated from a three- to four-day average), plotted against the age of the rats. (**B**) The approximate amount of food debris per cage relative to the average food consumption per cage, plotted against the age of the rats. (**C**) The approximate daily food consumption per rat (calculated from the weekly food consumption per cage) after accounting for food debris left in the cages, plotted against the age of the rats. (**D**) The approximate daily water consumption per rat (calculated from the weekly water consumption per cage), plotted against the age of the rats. The graphs indicate group mean plus standard error of the mean. Two-way ANOVA results are displayed above each graph, and results from *post-hoc* analysis are shown for individual data points. Significant genotype differences are indicated by ($p<0.05$) *, ($p<0.01$) **, ($p<0.001$) *** and ($p<0.0001$) ****. For (**D**), WT and BACHD rats differed highly significant (****) for all data points between 11 and 26 weeks of age.
(TIF)

Figure S2 Body length measurements. (**A–D**) Data from length measurement as stated in the graph titles. The graphs show group mean plus standard error of the mean. Two-way ANOVA results are displayed above each graph, and significant results from *post-hoc* analysis are displayed inside each graph. Significant genotype differences are indicated by ($p<0.05$) *, ($p<0.01$) **, ($p<0.001$) *** and ($p<0.0001$) ****.
(TIF)

Figure S3 Habituation to the operant conditioning boxes. (**A**) The total number of head entries made into the pellet receptacle during habituation sessions. (**B**) The total time spent with the head inside of the pellet receptacle during habituation sessions as a measurement of the duration of receptacle visits. (**C**) The mean latency to enter the pellet receptacle after the delivery of a reward pellet. The graphs indicate group mean plus standard error of the mean. Two-way ANOVA results are displayed above each graph, and results from *post-hoc* analysis are shown for individual data points. Significant genotype differences are indicated by ($p<0.05$) *, ($p<0.01$) **, ($p<0.001$) *** and ($p<0.0001$) ****.
(TIF)

Figure S4 Performance on the CRF protocol. Results from the final session of CRF training are shown as indicated by graph titles. Session duration measured the time the rats needed to complete 100 ratios. Retrieval latency measured the time between the release of the reinforced lever and the entry into the pellet receptacle. Lever return latency was defined as the interval between the first receptacle entry following reward delivery and the lever push that followed. Graphs indicate the performance of individual rats and group mean. Results from t-tests or Mann-Whitney tests are indicated in the graphs. Significant genotype

differences are indicated by ($p<0.05$) *, ($p<0.01$) **, ($p<0.001$) *** and ($p<0.0001$) ****.
(TIF)

Figure S5 Performance on fixed ratio protocols. Results for several basic parameters of FR3 and FR5 protocols are shown as indicated by the graph titles. Session duration measured the time the rats needed to complete 100 ratios. Ratio duration measured the time between the first and last lever push of each ratio. Ratio interval was defined as the time between the last lever push of one ratio and the first lever push of the ratio that followed. Retrieval latency measured the time between the release of the reinforced lever and the entry into the pellet receptacle. Lever return was defined as the interval between the first receptacle entry following reward delivery and the first lever push of the ratio that followed. Scatter plots of FR3 results indicate the performance of individual rats and group mean. Results from t-tests or Mann-Whitney tests are indicated in the graphs. Only results from the final session, where rats performed at criterion, are displayed. Line graphs of FR5 results indicate group mean plus standard error of the mean, plotted against the training session. Only the three final sessions, where rats performed at criterion, are included. Two-way ANOVA results are displayed at the top right corner of each FR5 graph, and significant results from *post-hoc* analysis are shown for individual data points. Significant genotype differences are indicated by ($p<0.05$) *, ($p<0.01$) **, ($p<0.001$) *** and ($p<0.0001$) ****.
(TIF)

Figure S6 Performance on the fixed ratio part of the progressive ratio protocol. Results for the basic parameters of the ten FR5 ratios run at the start of each PR session. (**A**) Data from sessions where BACHD and WT rats were both deprived to 85% of their respective free-feeding body weights. (**B**) Data from sessions where food deprivation was adjusted to match the food consumption rate of BACHD and WT rats. Details for each parameter are described in the figure legend of Figure S4 and S5. Lever push frequency was calculated based on the pushes made on the reinforced lever during the full length of a ratio, i.e. the ratio duration plus interval to subsequent ratio. Results displayed were obtained from the sessions used for baseline curves in Figure 6A. The graphs indicate group mean plus standard error of the mean. Two-way ANOVA results are displayed at the top right corner of each graph, and results from *post-hoc* analysis are shown for individual data points. Significant genotype differences are indicated by ($p<0.05$) *, ($p<0.01$) **, ($p<0.001$) *** and ($p<0.0001$) ****.
(TIF)

Figure S7 Mean number of errors for the fixed ratio part of the progressive ratio protocol. Errors made by the rats during the ten FR5 ratios run at the start of each PR session. (**A**) Data from sessions where BACHD and WT rats were both deprived to 85% of their respective free-feeding body weights. (**B**) Data from sessions where food deprivation was adjusted to match the food consumption rate of BACHD and WT rats. Results were obtained from the sessions used for baseline curves in Figure 6A. Graphs indicate the performance of individual rats and group mean. Results from t-tests or Mann-Whitney tests are indicated in the graphs. Significant genotype differences are indicated by ($p<0.05$) *, ($p<0.01$) **, ($p<0.001$) *** and ($p<0.0001$) ****.
(TIF)

Acknowledgments

The authors wish to thank Celina Tomczak for support with breeding, genotyping, animal care and data gathering.

Author Contributions

Conceived and designed the experiments: EKHJ LEC OR HPN. Performed the experiments: EKHJ LEC. Analyzed the data: EKHJ LEC. Contributed to the writing of the manuscript: EKHJ LEC HPN.

References

1. Pringsheim T, Wiltshire K, Day L, Dykesman J, Steeves T, et al. (2012) The incidence and prevalence of huntington's disease: a systematic review and meta-analysis. Mov Disord 9: 1083–1091.
2. The Huntington's disease collaborative research group (1993) A novel gene containing a trinucleotide repeat that is expanded and unstable on huntington's disease chromosomes. Cell 72: 971–983.
3. Zuccato C, Valenza M, Cattaneo E (2010) Molecular mechanism and potential therapeutocal targets in huntington's disease. Physiol Rev 90: 905–981.
4. Djoussé L, Knowlton B, Cupples LA, Marder K, Shoulson I, et al. (2002) Weight loss in early stage of huntington's disease. Neurology 59: 1325–1330.
5. Kirkwood SC, Su JL, Conneally M, Foround T (2001) Progression of symptoms in the early and middle stages of huntington disease. Arch Neurol 58: 273–278.
6. Aziz NA, van der Burg JMM, Landwehrmeyer GB, Brundin P, Stinjen T, et al. (2008) Weight loss in huntington disease increases with higher CAG repeat number. Neurology 71: 1506–1513.
7. Robbins AO, Ho AK, Barker RA (2006) Weight changes in huntington's disease. Eur J Neurol 13: e7.
8. van der Burg JMM, Björkqvist M, Brundin P (2009) Beyond the brain: widespread pathology in huntington's disease. Lancet Neurol 8: 765–774.
9. Aziz NA, van der Marck MA, Pijl H, Olde Rikkert MGM, Bloem BR, et al. (2008) Weight loss in neurodegenerative disorders. J Neurol 255: 1872–1880.
10. Gray M, Shirasaki DI, Cepeda C, André VM, Wilburn B, et al. (2008) Full-length human mutant huntingtin with a stable polyglutamine repeat can elicit progressive and selective neuropathogenesis in BACHD mice. J Neurosci 28: 6182–6195.
11. van Raamsdonk JM, Metzler M, Slow E, Pearson J, Schwab C, et al. (2007) Pheontypic abnormalities in the YAC128 mouse model of huntington disease are penetrant on multiple genetic backgrounds and modulated by strain. Neurobiol Dis 26: 189–200.
12. Kudwa AE, Menalled LB, Oakeshott S, Murphy C, Mushlin R, et al. (2013) Increased body weight of the BAC HD transgenic mouse model of huntington's disease accounts for some but not all of the observed HD-like motor deficits. PLoS Curr 30: 5. Available: http://currents.plos.org/hd/article/increased-body-weight-of-the-bac-hd-transgenic-mouse-model-of-huntingtons-disease-accounts-for-some-but-not-all-of-the-observed-hd-like-motor-deficits/. Accessed 12 January 2014.
13. McFadyen MP, Kusek G, Bolivar VJ, Flaherty L (2003) Differences among eight inbred strains of mice in motor ability and motor learning on a rotorod. Genes Brain Behav 2: 214–219.
14. Trueman RC, Dunnett SB, Brooks SP (2012) Operant-based instrumental learning for analysis of genetically modified models of huntington's disease. Brain Res Bull 88: 261–275.
15. Youn J, Ellenbroek BA, van Eck I, Roubos S, Verhage M, et al. (2011) Finding the right motivation: Genotype-dependent differences in effective reinforcements for spatial learning. Behav Brain Res226: 397–403.
16. Oakeshott S, Port R, Cummins-Sutphen J, Berger J, Watson-Johnson J, et al. (2012) A mixed fixed ratio/progressive ratio procedure reveals an apathy phenotype in the BAC HD and the z_Q175 KI mouse models of Huntington's disease. PLoS Curr 25: 4. Available: http://currents.plos.org/hd/article/a-mixed-fixed-ratioprogressive-ratio-procedure-reveals-an-apathy-phenotype-in-the-bac-hd-and-the-z_q175-ki-mouse-models-of-huntingtons-disease/. Accessed 13 June 2012.
17. Oakeshott S, Farrar A, Port R, Cummins-Sutphen J, Berger J, et al. (2013) Deficits in a simple visual Go/No-go discrimination task in two mouse models of huntington's disease. PLoS Curr 7: 5. Available: http://currents.plos.org/hd/article/deficits-in-a-simple-visual-gono-go-discrimination-task-in-two-mouse-models-of-huntingtons-disease/. Accessed 12 January 2014.
18. Enkel T, Berger SM, Schönig K, Tews B, Bartsch D (2014) Reduced expression of Nogo-A leads to motivational deficits in rats. Front Behav Neurosci 8: 10. Available: http://journal.frontiersin.org/Journal/10.3389/fnbeh.2014.00010/full. Accessed 7 March 2014.
19. Bradbury MJ, Campbell U, Giracello D, Chapman D, King C, et al. (2005) Metabotropic glutamate receptor mGlu5 is a mediator of appetite and energy balance in rats and mice. J Pharmacol Exp Ther 313: 395–402.

20. Roth JD, D'Souza L, Griffin PS, Athanacio J, Trevaskis JL, et al. (2012) Interactions of amylinergic and melanocortinergic systems in the control of food intake and body weight in rodents. Diabetes Obes Metab 14: 608–615.
21. Fielding SA, Brooks SP, Klein A, Bayram-Weston Z, Jones J, et al. (2012) Profiles of motor and cognitive impairment in the transgenic rat model of huntingtin's disease. Brain Res Bull 88: 223–236.
22. Yu-Taeger L, Petrasch-Parwez E, Osmand AP, Redensek A, Metzger S, et al. (2012) A novel BACHD transgenic rat exhibits characteristic neuropathological features of huntington disease. J Neurosci 32: 15426–15438.
23. Abada YK, Nguyen HP, Ellenbroek B, Schreiber R (2013) Reversal learning and associative memory impairments in a BACHD rat model for huntington disease. PLoS One 8: 10. Available: http://www.plosone.org/article/info%3Adoi%2F10.1371%2Fjournal.pone.0071633. Accessed 24 November 2013.
24. Clemens LE, Jansson EKH, Portal E, Riess O, Nguyen HP (2014) A behavioral comparison of the common laboratory rat strains lister hooded, lewis, fischer 344 and wistar in an automated homecage system. Genes Brain Behav 13: 305–21.
25. She P, Zhang Z, Marchionini D, Diaz WC, Jetton T, et al. (2011) Molecular characterization of skeletal muscle atrophy in the R6/2 mouse model of huntington's disease. Am J Physiol Endocrinol Metab 301: E49–E61.
26. Schilling G, Becher MW, Sharp AH, Jinnah HA, Duan K, et al. (1999) Intranuclear inclusions and neuritic aggregates in transgenic mice expressing a mutant N-terminal fragment of huntingtin. Hum Mol Genet 8: 397–407.
27. von Hörsten S, Schmitt I, Nguyen HP, Holzmann C, Schmidt T, et al. (2003) Transgenic rat model of huntington's disease. Hum Mol Genet 12: 617–624.
28. Hult S, Soylu R, Björklund T, Belgardt BF, Mauer J, et al. (2011) Mutant huntingtin causes metabolic imbalance by disruption of hypothalamic neurocircuits. Cell Metab 13: 428–439.
29. van Raamsdonk JM, Gibson WT, Pearson J, Murphy Z, Lu G, et al. (2006) Body weight is modulated by levels of full-length huntingtin. Hum Mol Genet 15: 1513–1523.
30. Weydt P, Pineda W, Torrence AE, Libby RT, Satterfield TF, et al. (2006) Thermoregulatory and metabolic dfects in Huntington's disease transgenic mice implicate PGC-1alpha in Huntington's disease neurodegeneration. Cell Metab 4: 349–362.
31. Hollopeter G, Erickson JC, Palmiter RD (1998) Role of neuropeptide Y in diet-, chemical and genetic-induced obesity of mice. Int J Obes Relat Metab Disord 22: 506–512.
32. Tanaka K, Shimada M, Nakao K, Kusunoki T (1978) Hypothalamic lesion induced by injection of monosodium glutamate in suckling period and subsequent development of obesity. Exp Neurol 62: 191–199.
33. Morris MJ, Tortelli CF, Filippis A, Proietto J (1998) Reduced BAT as a mechanism for obesity in the hypophagic, neuropeptide Y deficient monosodium glutamate-treated rat. Regul Pept 25: 441–447.
34. Chen W, Chen Z, Xue N, Zheng Z, Li S, et al. (2013) Effect of CB1 receptor blockade on monosodium glutamate induced hypometabolic and hypothalamic obesity in rats. Naunyn Schmiedebergs Arch Pharmacol 8: 721–732.
35. Scallet AC and Olney JW (1986) Components of hypothalamic obesity: bipiperidyl-mustard lesions add hyperphagia to monosodium glutamate-induced hyperinsulinemia. Brain Res (2): 380–384.
36. Bergen HT, Mizuno TM, Taylor J, Mobbs CV (1998) Hyperphagia and weight gain after gold-thioglucose: relation to hypothalamic neuropeptide Y and proopiomelanocortin. Endocrinology 139: 4483–4488.
37. Remmers F, Fodor M, Delemarre-van de Waal H (2008) Neonatal food restriction permanently alters rat body dimensions and energy intake. Physiol Behav 95: 208–215.
38. Nguyen GD, Molero AE, Gokhan S, Mehler MF (2013) Functions of huntingtin in germ layer specification and organogenesis. PLoS One 8: 8. Available: http://www.plosone.org/article/info%3Adoi%2F10.1371%2Fjournal.pone.0072698. Accessed 11 March 2014.
39. Lee JK, Mathews K, Schlaggar B, Perlmutter J, Paulsen JS, et al. (2012) Measures of growth in children at risk for Huntington disease. Neurology 79: 668–674.
40. Lawrence AD, Sahakian BJ, Hodges JR, Rosser AE, Lange KW, et al. (1996) Executive and mnemotic functions in early huntington's disease. Brain 119: 1633–1645.
41. Lemiere J, Decruyenaere M, Evers-Kiebooms G, Vandenbussche E, Dom R (2004) Cognitive changes in patients with huntington's disease (HD) and asymptomatic carriers of the HD mutation a longitudinal follow-up study. J Neurol 251: 935–942.
42. Harrington DL, Smith MM, Zhang Y, Carlozzi NE, Paulsen JS, et al. (2012) Cognitive domains that predict time to diagnosis in prodromal huntington disease. J Neurosurg Psychiatry 83: 612–619.
43. Meyer C, Landwehrmeyer B, Schwenke C, Doble A, Orth M, et al. (2012) Rate of change in early huntington's disease: a clinicometric analysis. Mov Disord 27: 118–124.
44. Vaccarino AL, Anderson K, Borowsky B, Duff K, Giuliano J, et al. (2011) An item response analysis of the motor and behavioral subscales of the unified huntington's disease rating scale in huntington disease gene expansion carriers. Mov Disord 26: 877–884.
45. Whisaw IQ, Tompkins GJ (1988) An optic-fiber photocell detector for measuring tongue protrusion in the rat: evaluation of recovery from localized cortical lesions. Psychol Behav 43: 397–401.
46. Trueman RC, Brooks SP, Jones L, Dunnett SB (2009) Rule learning, visuospatial function and motor performance in the HdhQ92 knock-in mouse model of Huntington's disease. Behav Brain Res 203: 215–222.
47. Paulsen JS, Ready RE, Hamilton JM, Mega MS, Cummings JL (2001) Neuropsychiatric aspects of huntington's disease. J Neurol Neurosurg Psychiatry 71: 310–314.
48. Naarding P, Janzing JGE, Eling P, van der Werf S, Kremer B (2009) Apathy is not depression in huntington's disease. J Neuropsuchiatry Clin Neurosci 21: 266–270.
49. Skjoldager P, Pierre PJ, Mittleman G (1993) Reinforcer magnitude and progressive ratio responding in the rat: effect of increased effort, prefeeding, and extinction. Learning Motivation 24: 303–343.
50. Eagle DM, Humby T, Dunnett SB, Robbins TW (1999) Effects of regional striatal lesions on motor, motivational, and executive aspects of progressive-ratio performance in rats. Behav Neurosci 133: 718–731.
51. Schmelzeis MC, Mittleman G (1996) The hippocampus and reward: effects of hippocampal lesions on progressive-ratio responding. Behav Neurosci 110: 1049–1066.
52. Halaas JL, Gajiwala KS, Maffei M, Cohen SL, Chait BT, et al. (1995) Weight-reducing effects of the plasma protein encoded by the obese gene. Science 269: 543–546.
53. Halaas JL, Boozer C, Blair-West J, Fidahusein N, Denton DA, et al. (1997) Physiological response to long-term peripheral and central leptin infusion in lean and obese mice. Proc Natl Acad Sci 94: 8878–8883.
54. Maffei M, Halaas J, Ravussin E, Pratley RE, Lee GH, et al. (1995) Leptin levels in human and rodent: Measurement of plasma leptin and ob RNA in obese and weight-reduced subjects. Nat Med 1: 1155–1161.
55. Kanoski SE, Alhadeff AL, Fortin SM, Gilbert JR, Grill HJ (2014) Leptin signaling in the medial nucleus tractus solitarius reduced food seeking and willingness to work for food. Neuropsychopharmacology 39: 605–613.

Supporting Information

Figure S1

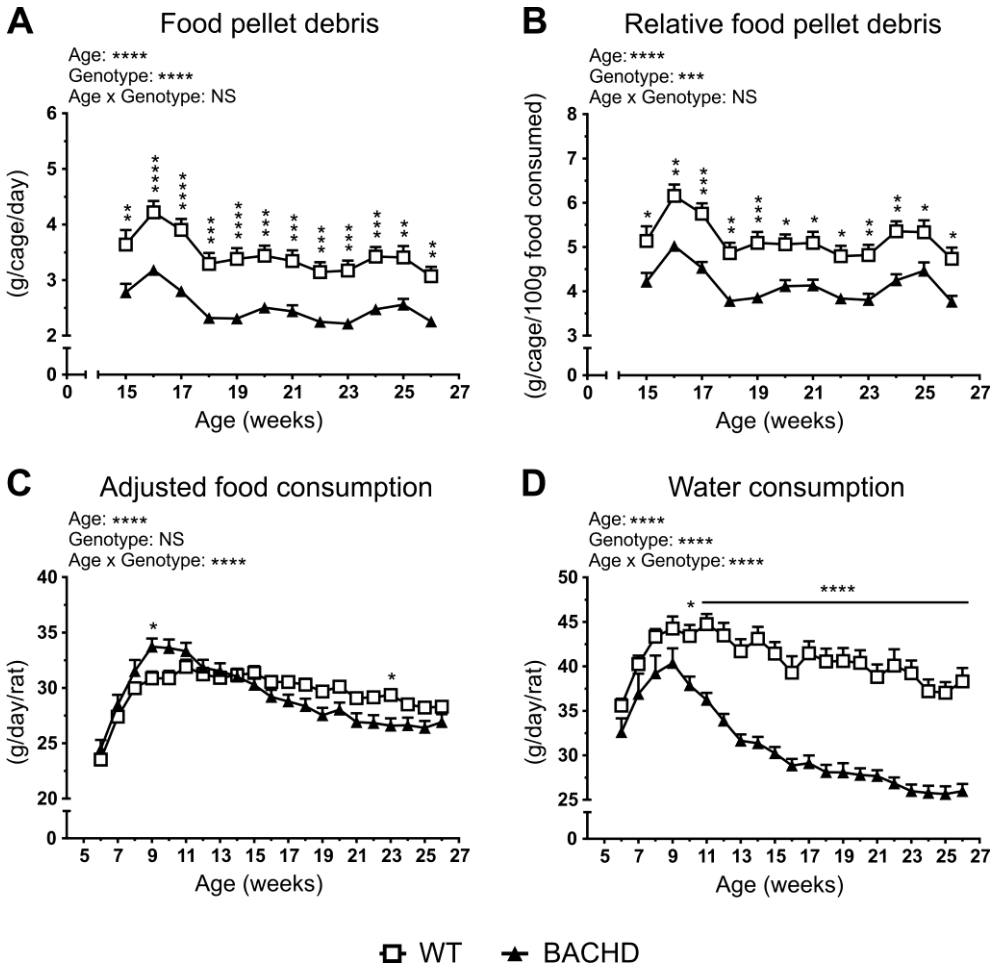

Figure S2

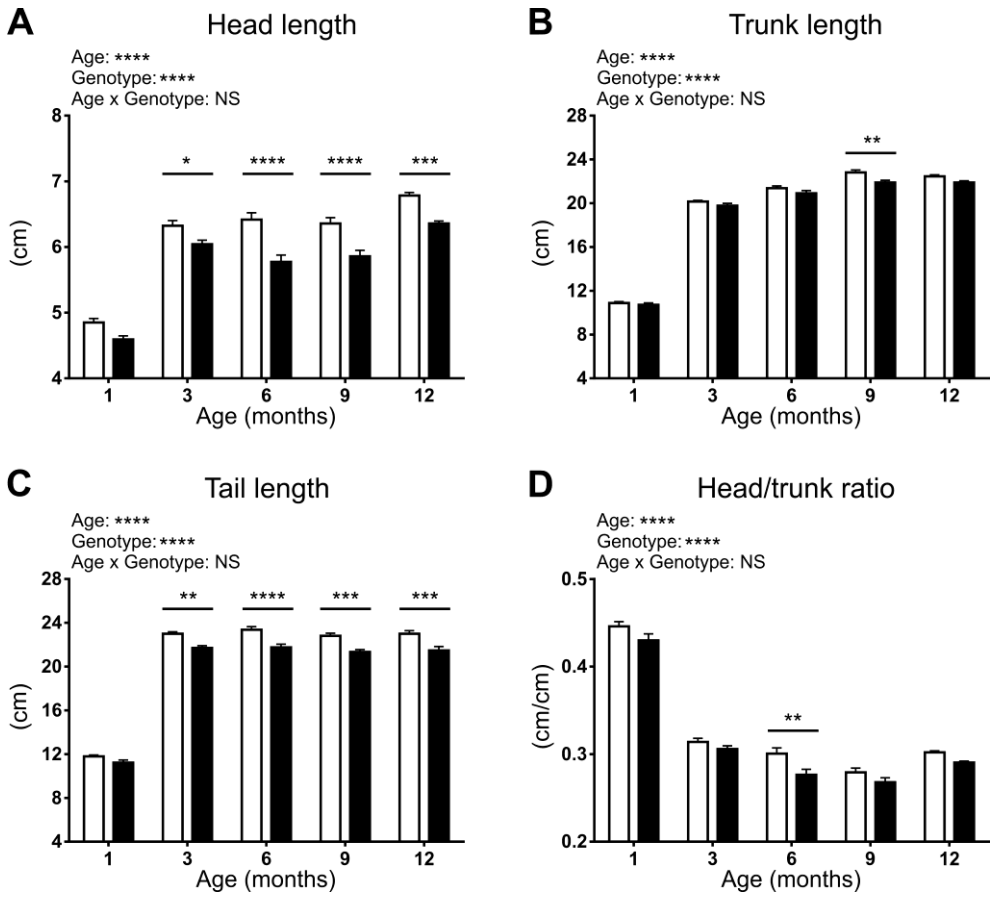
A
Head length
Age: ****
Genotype: ****
Age x Genotype: NS
(cm)
Age (months)
B
Trunk length
Age: ****
Genotype: ****
Age x Genotype: NS
(cm)
Age (months)
C
Tail length
Age: ****
Genotype: ****
Age x Genotype: NS
(cm)
Age (months)
D
Head/trunk ratio
Age: ****
Genotype: ****
Age x Genotype: NS
(cm/cm)
Age (months)

Figure S3

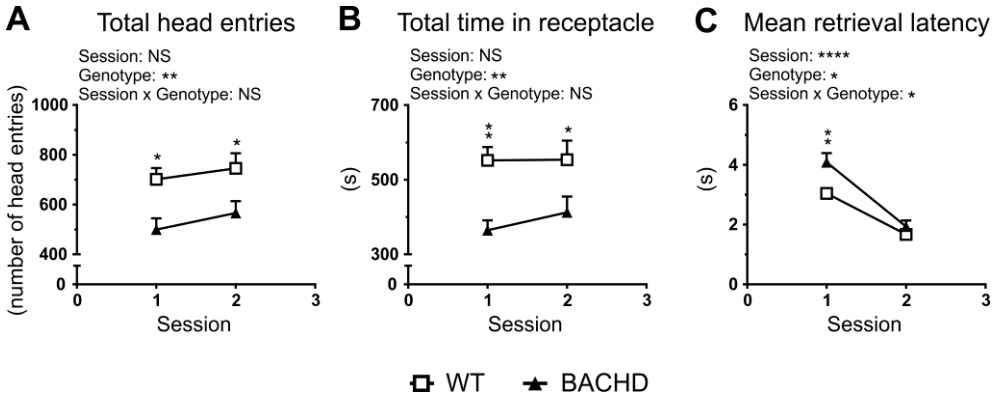
A
Total head entries
Session: NS
Genotype: **
Session x Genotype: NS
(number of head entries)
1000
800
600
400
0
0
1
2
3
Session
B
Total time in receptacle
Session: NS
Genotype: **
Session x Genotype: NS
(s)
700
500
300
0
0
1
2
3
Session
C
Mean retrieval latency
Session: ****
Genotype: *
Session x Genotype: *
(s)
6
4
2
0
0
1
2
3
Session
WT
BACHD

Figure S4

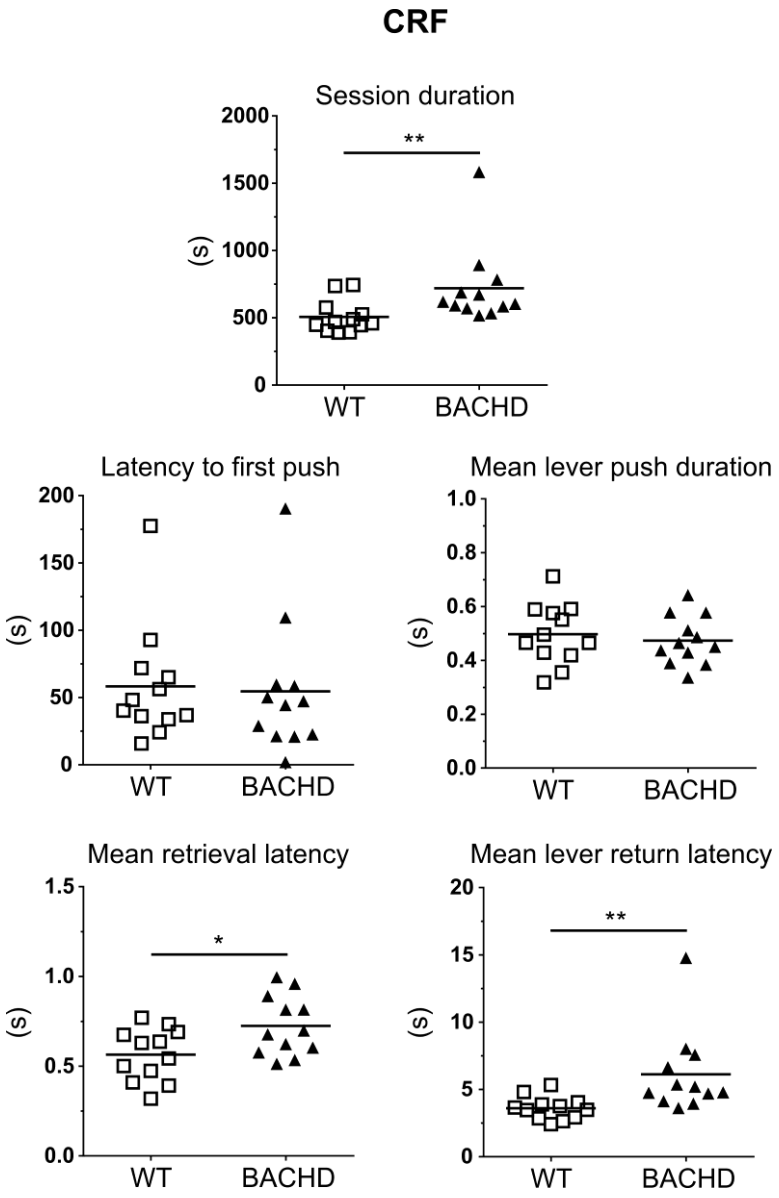
CRF
Session duration
2000
1500
1000
500
0
(s)
**
WT
BACHD
Latency to first push
200
150
100
50
0
(s)
WT
BACHD
Mean lever push duration
1.0
0.8
0.6
0.4
0.2
0.0
(s)
WT
BACHD
Mean retrieval latency
1.5
1.0
0.5
0.0
(s)
*
WT
BACHD
Mean lever return latency
20
15
10
5
0
(s)
**
WT
BACHD

Figure S5

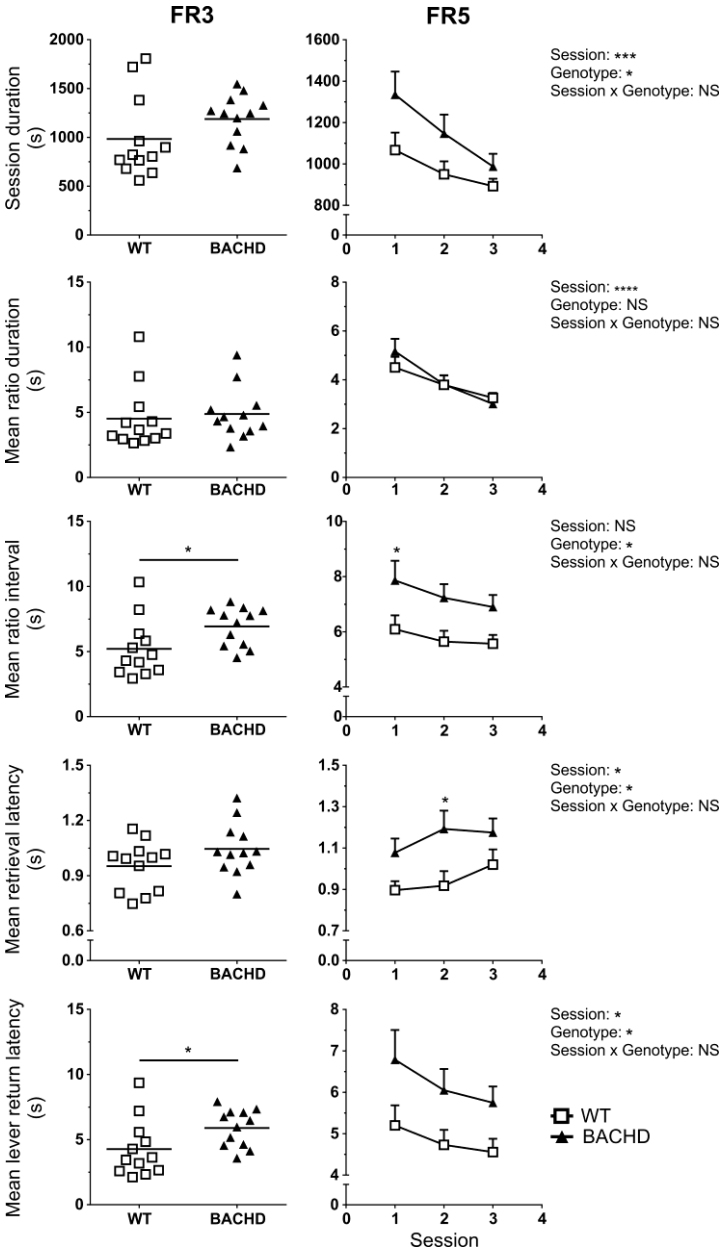
FR3
FR5
Session duration (s)
Mean ratio duration (s)
Mean ratio interval (s)
Mean retrieval latency (s)
Mean lever return latency (s)
WT
BACHD
Session
Session: ***
Genotype: *
Session x Genotype: NS
Session: ****
Genotype: NS
Session x Genotype: NS
Session: NS
Genotype: *
Session x Genotype: NS
Session: *
Genotype: *
Session x Genotype: NS
Session: *
Genotype: *
Session x Genotype: NS

Figure S6

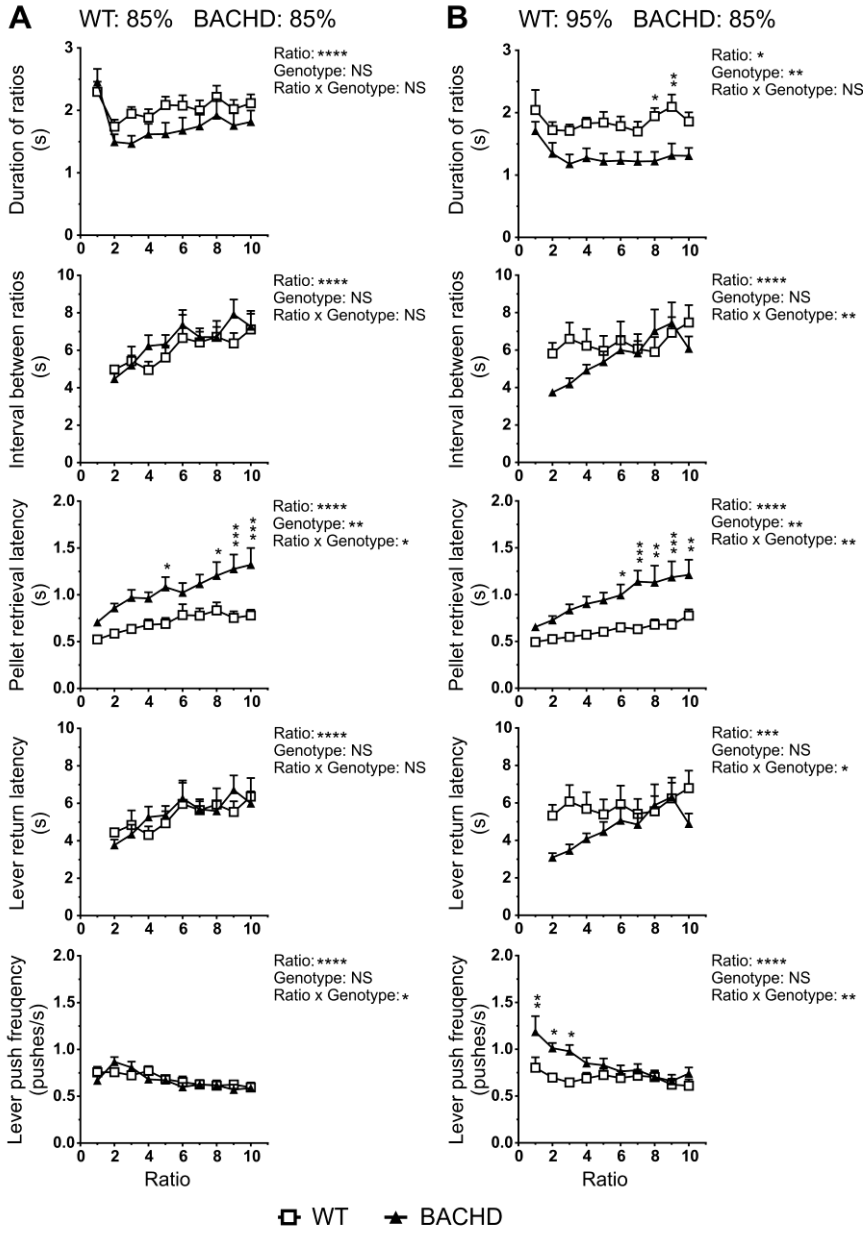
A
WT: 85% BACHD: 85%
B
WT: 95% BACHD: 85%
Duration of ratios (s)
Interval between ratios (s)
Pellet retrieval latency (s)
Lever return latency (s)
Lever push freuqency (pushes/s)
Ratio
WT
BACHD

Figure S7

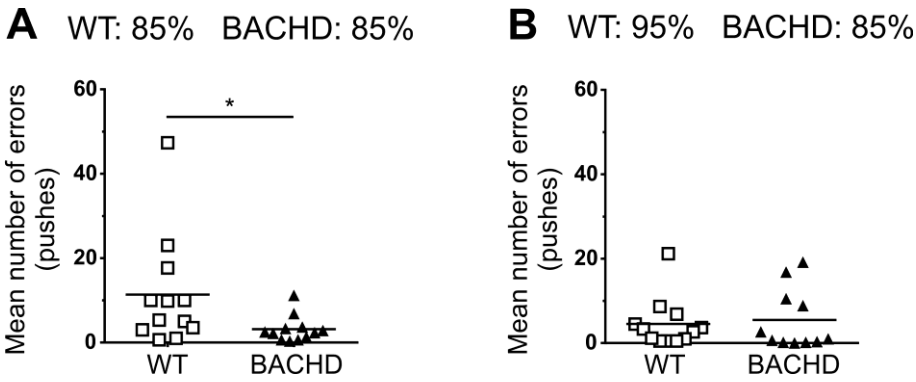
A
WT: 85%
BACHD: 85%
Mean number of errors (pushes)
60
40
20
0
*
WT
BACHD
B
WT: 95%
BACHD: 85%
Mean number of errors (pushes)
60
40
20
0
WT
BACHD

doi:10.1093/brain/awv290 BRAIN 2015: 138; 3632–3653 | 3632

BRAIN
A JOURNAL OF NEUROLOGY

Olesoxime suppresses calpain activation and mutant huntingtin fragmentation in the BACHD rat

Laura E. Clemens,[1,2,#,*] Jonasz J. Weber,[1,2,*] Tanja T. Wlodkowski,[1,2,Φ] Libo Yu-Taeger,[1,2] Magali Michaud,[3] Carsten Calaminus,[4] Schamim H. Eckert,[5] Janett Gaca,[5,Ψ] Andreas Weiss,[6,†] Janine C. D. Magg,[1,2] Erik K. H. Jansson,[1,2] Gunter P. Eckert,[5] Bernd J. Pichler,[4] Thierry Bordet,[3,‡] Rebecca M. Pruss,[3] Olaf Riess[1,2] and Huu P. Nguyen[1,2]

*These authors contributed equally to this work.

Huntington's disease is a fatal human neurodegenerative disorder caused by a CAG repeat expansion in the *HTT* gene, which translates into a mutant huntingtin protein. A key event in the molecular pathogenesis of Huntington's disease is the proteolytic cleavage of mutant huntingtin, leading to the accumulation of toxic protein fragments. Mutant huntingtin cleavage has been linked to the overactivation of proteases due to mitochondrial dysfunction and calcium derangements. Here, we investigated the therapeutic potential of olesoxime, a mitochondria-targeting, neuroprotective compound, in the BACHD rat model of Huntington's disease. BACHD rats were treated with olesoxime via the food for 12 months. *In vivo* analysis covered motor impairments, cognitive deficits, mood disturbances and brain atrophy. *Ex vivo* analyses addressed olesoxime's effect on mutant huntingtin aggregation and cleavage, as well as brain mitochondria function. Olesoxime improved cognitive and psychiatric phenotypes, and ameliorated cortical thinning in the BACHD rat. The treatment reduced cerebral mutant huntingtin aggregates and nuclear accumulation. Further analysis revealed a cortex-specific overactivation of calpain in untreated BACHD rats. Treated BACHD rats instead showed significantly reduced levels of mutant huntingtin fragments due to the suppression of calpain-mediated cleavage. In addition, olesoxime reduced the amount of mutant huntingtin fragments associated with mitochondria, restored a respiration deficit, and enhanced the expression of fusion and outer-membrane transport proteins. In conclusion, we discovered the calpain proteolytic system, a key player in Huntington's disease and other neurodegenerative disorders, as a target of olesoxime. Our findings suggest that olesoxime exerts its beneficial effects by improving mitochondrial function, which results in reduced calpain activation. The observed alleviation of behavioural and neuropathological phenotypes encourages further investigations on the use of olesoxime as a therapeutic for Huntington's disease.

1 Institute of Medical Genetics and Applied Genomics, University of Tuebingen, Calwerstrasse 7, 72076 Tuebingen, Germany
2 Centre for Rare Diseases, University of Tuebingen, Calwerstrasse 7, 72076 Tuebingen, Germany
3 Trophos SA., Parc Scientifique de Luminy Case 931, 13288 Marseille Cedex 9, France
4 Werner Siemens Imaging Center, Department of Preclinical Imaging and Radiopharmacy, University of Tuebingen, Roentgenweg 13, 72076 Tuebingen, Germany
5 Department of Pharmacology, Goethe University Frankfurt am Main, Max-von-Laue Str. 9, 60438 Frankfurt, Germany
6 Novartis Institutes for BioMedical Research, Klybeckstrasse 141, 4057 Basel, Switzerland

[#]Present address: QPS Austria, Research and Development, Parkring 12, 8074 Grambach, Austria
[Φ]Present address: Paediatric Nephrology Division, Heidelberg University Hospital, Im Neuenheimer Feld 430, 69120 Heidelberg, Germany

Received April 24, 2015. Revised July 21, 2015. Accepted August 11, 2015. Advance Access publication October 21, 2015

ΨPresent address: Merz Pharmaceuticals, Eckenheimer Landstraße 100, 60318 Frankfurt am Main, Germany
†Present address: Evotec AG, Manfred Eigen Campus, Essener Bogen 7, 22419 Hamburg, Germany
‡Present address: AFM Téléthon, Biotherapies Institute for Rare Diseases, 1 Rue de l'Internationale, Evry 91002, France

Correspondence to: Dr Huu Phuc Nguyen,
Institute of Medical Genetics and Applied Genomics,
Centre for Rare Diseases,
University of Tuebingen,
Calwerstrasse 7,
Tuebingen,
Germany
E-mail: hoa.nguyen@med.uni-tuebingen.de

Keywords: Huntington's disease; olesoxime; calpain; mitochondrial dysfunction; mutant huntingtin aggregates

Abbreviation: BACHD rat = Huntington's disease rat model expressing full-length mutant huntingtin from a bacterial artificial chromosome

Introduction

Huntington's disease, a fatal human neurodegenerative disorder, results from a CAG repeat expansion in exon 1 of *HTT* (The Huntington's Disease Collaborative Research Group, 1993). The mutation translates into an elongated polyglutamine tract close to the N-terminus of the mutant huntingtin protein (HTT) (Persichetti *et al.*, 1995). Patients with Huntington's disease suffer from a broad range of symptoms including motor, psychiatric, cognitive and metabolic disturbances (Vonsattel and DiFiglia, 1998), which are associated with neuronal dysfunction, and the selective degeneration of cortical and striatal projection neurons (Tabrizi *et al.*, 2011; Poudel *et al.*, 2014).

The intrinsic toxicity of mutant HTT has been linked to the formation of N-terminal protein fragments (Rigamonti *et al.*, 2000; Nagai *et al.*, 2007; Wang *et al.*, 2008). These fragments interfere with important intracellular pathways (Zuccato *et al.*, 2010), accumulate in the nucleus (Landles *et al.*, 2010), and form protein aggregates in nucleus and cytoplasm (Cooper *et al.*, 1998; Li and Li, 1998), which is a hallmark of Huntington's disease (Gutekunst *et al.*, 1999). Mutant HTT fragments derive from proteolytic cleavage of the full-length protein. Several classes of proteolytic enzymes have been identified to mediate this process, including calpains (Gafni and Ellerby, 2002), caspases (Goldberg *et al.*, 1996), cathepsins (Kim *et al.*, 2006) and matrix metalloproteinases (Miller *et al.*, 2010). Calpains, which play a general role in neurodegenerative processes (Yang *et al.*, 2013), are overactivated in Huntington's disease (Gafni and Ellerby, 2002), and inhibition of the calpain-mediated cleavage of mutant HTT has been found to ameliorate Huntington's disease-related pathologies (Gafni *et al.*, 2004).

Calpains are activated in response to cytosolic Ca^{2+} currents (Goll *et al.*, 2003), and Ca^{2+} homeostasis is disrupted at several levels in Huntington's disease (Miller and Bezprozvanny, 2010). Moreover, Ca^{2+} derangements have been considered to be causal for the neuronal damage in Huntington's disease, as the selective demise of vulnerable neurons is thought to result from their particular sensitivity to excitotoxicity, which is characterized by intracellular Ca^{2+} overload and subsequent cell death (Fan and Raymond, 2007). Mitochondria are particularly involved in this process, as they are crucial for maintaining low intracellular Ca^{2+} levels, and pivotal for triggering cell death programs when their buffering capacity is exhausted (Calì *et al.*, 2012). Mutant HTT affects mitochondrial function by directly binding to the outer mitochondrial membrane (Panov *et al.*, 2002; Choo *et al.*, 2004; Rockabrand *et al.*, 2007; Gellerich *et al.*, 2008; Wang *et al.*, 2009) and by disturbing the transcription of nuclear-encoded mitochondrial effector genes (Bae *et al.*, 2005; Cui *et al.*, 2006). As a consequence, mitochondrial Ca^{2+} handling ability is impaired, making cells more susceptible to excitotoxic insults (Panov *et al.*, 2003; Tang *et al.*, 2005).

The current study was designed to evaluate the therapeutic potential of the orphan drug candidate, olesoxime (Bordet *et al.*, 2007), on disease-related phenotypes of the BACHD rat model of Huntington's disease (Yu-Taeger *et al.*, 2012). Olesoxime is a small cholesterol-like molecule that accumulates at the site of mitochondria (Bordet *et al.*, 2010). Olesoxime's mechanism of action is not fully understood, although it has been shown to inhibit mitochondrial permeability transition (Bordet *et al.*, 2010; Gouarné *et al.*, 2013, 2015), which is a Ca^{2+}-sensitive process that can trigger cell death (Lemasters *et al.*, 2009). Olesoxime has demonstrated therapeutic efficacy in several neurodegenerative diseases (Bordet *et al.*, 2007; Sunyach *et al.*, 2012; Eckmann *et al.*, 2013; Richter *et al.*, 2014) and peripheral neuropathies (Bordet *et al.*, 2008; Xiao *et al.*, 2009, 2012; Rovini *et al.*, 2010), and just recently yielded impressive beneficial effects on motor function in a phase II clinical trial in patients with spinal muscular atrophy (Dessaud *et al.*, 2014).

Here, we found that olesoxime treatment ameliorated psychiatric and cognitive abnormalities in the BACHD rat. The treatment further increased their frontal cortex thickness and improved mitochondrial function. Prominently, it appeared that the main effect of olesoxime was to reduce Huntington's disease-related calpain overactivation. Thereby, the formation of mutant HTT fragments was drastically decreased. This yet undiscovered function opens a new view on

olesoxime's mechanism of action, and highlights it as a novel tool for reducing calpain activation and the accumulation of toxic mutant HTT fragments.

Materials and methods

Ethical statement

Behavioural experiments were performed at the University of Tuebingen, by individuals with appropriate training and experience. Experiments were approved by the local ethics committee at Regierungspraesidium Tuebingen, and carried out in accordance with the German Animal Welfare Act and the guidelines of the Federation of European Laboratory Animal Science Associations, based on European Union legislation (Directive 2010/63/EU).

The BACHD rat

The BACHD rat of line TG5 [Crl:CD(SD)-Tg(HTT*97Q)21.2Hpn/Hpn], hereafter referred to as the BACHD rat, overexpresses full-length *HTT* with 97 CAA/CAG repeats on a BAC (bacterial artificial chromosome) (Yu-Taeger *et al.*, 2012). The construct has previously been used to generate the BACHD mouse (Gray *et al.*, 2008).

General husbandry and genotyping

All rats were bred at the University of Tuebingen and study groups derived from a total of 24 different breedings to reduce possible litter bias. Male BACHD rats, hemizygous for mutant HTT, and male wild-type littermates from respective breedings were spread across study groups. The rats were weaned and genotyped at 21 days of age. Genotyping was confirmed at the end of the study when the animals were sacrificed, and followed established protocols (Yu-Taeger *et al.*, 2012). From weaning onwards, the animals were kept in autoclavable plastic cages with high lids (38 cm × 55 cm wide × 24.5 cm high). Cages contained 3 l of autoclaved wooden bedding and were cleaned twice a week. Food (initially standard rat chow: Ssniff V1534-000, SSNIFF Germany, later changed to: Altromin C1000, Altromin; details in the next section) and tap water were delivered *ad libitum*. Housing conditions followed the European Convention for the Protection of Vertebrate Animals used for Experimental and other Scientific Purposes (ETS 123, Appendix A: Guidelines for accommodation and care of animals). The environmental conditions in the housing room were kept at 21–23°C ambient temperature, 55 ± 10% humidity and a 12/12 h light/dark cycle with lights off at 1:00 p.m. and lights on at 1:00 a.m. during winter, or with lights off at 2:00 p.m. and lights on at 2:00 a.m. during summer.

Olesoxime treatment and experimental groups

The study included two cohorts of rats. Cohort I served a longitudinal study to assess the treatment effect on relevant behavioural, neuropathological and molecular phenotypes (Supplementary Fig. 1). This cohort was composed of 30 wild-type (15 treated, 15 non-treated) and 30 BACHD rats (15 treated, 15 non-treated), kept in groups of four of mixed genotype (two wild-type rats and two BACHD rats per cage). Two weeks after weaning (5 weeks of age), food was changed from regular rodent chow (as stated above) to either control diet or the same diet loaded with 0.6 mg/g olesoxime (provided by Trophos SA). Behavioural characterization was carried out until the age of 13 months and was followed by MRI and post-mortem analyses.

Cohort II was used for the measurement of olesoxime concentration in plasma and brain as well as its distribution in different brain areas (nine olesoxime-treated and three non-treated control animals per genotype). These rats were kept in groups of three of the same genotype. Olesoxime-containing or control diet was administered for 2 weeks starting at the age of 4 months.

Body weight and food intake were measured as safety parameters for the olesoxime treatment. Body weight was measured weekly. For food intake measurements, the rats were housed individually for 70 h in an automated behavioural test system (PhenoMaster, TSE Systems) at 2, 4, 6, 8 and 12 months of age. Test protocol, system specifications and data analysis were the same as described in detail in Clemens *et al.* (2014).

Clasping behaviour

Clasping behaviour was investigated as a measure of a striatum-based motor dysfunction (Soll *et al.*, 2013). To detect hind limb clasping, each animal was lifted on its tail for ~2 s. The test was performed weekly from 5 weeks until the age of 10 months (33 observations). The clasping frequency in per cent of all observations was analysed.

Rotarod test

The animals were trained to walk on an accelerating rod (Rat Rotarod 7750, Ugo Basile) to assess fore limb/hind limb coordination at 2, 4 and 8 months of age as a measure of striatum-based motor dysfunction (Bergeron *et al.*, 2014). Rats were given four daily trials at 2 months of age, or three daily trials at older ages, during a total of five consecutive days. Trials were separated by 1-h intervals. The experiments were run during the dark phase. During the first 3 days, the rats were trained to a stable performance. At this stage, the maximum rotation speed of the rod was set to 12 rpm (increasing from 2 to 12 rpm over 30 s), and trials lasted either 120 s, or until the rat had fallen off the rod a total of five times. The number of falls served as the performance readout. On the last 2 days, the rats' maximum motor capacity was tested. For this, the rotation speed of the rod increased from 4 to 40 rpm over 240 s and the trials lasted either 300 s or until the rat had fallen off the rod for a total of five times. The total amount of time the animals spent on the rod (excluding the time spent not running during falls) was measured and analysed as the animals' running capacity. The number of rats included in the analysis decreased, as an increasing number of particularly BACHD rats refused to stay on the rod at older ages (as discussed previously in Yu-Taeger *et al.*, 2012; Abada *et al.*, 2013*b*).

Simple swim test

At the age of 7 months, cognitive abilities were investigated using a simple swim test. The animals were trained to swim to a hidden platform placed at one end of a rectangular water tank of 150 × 25 × 40 cm (adapted from Van Raamsdonk *et al.*, 2005). Training was carried out in dimmed red light during the dark phase, alternating between cages with placebo- and olesoxime-treated rats. During an initial training phase, the animals were placed into the middle of the tank facing away from the platform, forcing them to turn around to reach it. The training was carried out on two consecutive days in 3 × 3 trials on the first and three trials on the following day. On the third day, the platform was repositioned to the opposite side ('reversal') and the rats' performance was measured again on two consecutive days. In this reversal training, the rats needed to swim straight ahead in order to reach the platform. The rats were trained in 3 × 3 trials on the first day and three trials on the second day. Individual blocks of trials were separated by 1 h. The water was kept at room temperature, and coloured with non-toxic black paint (Marabu Fingerfarbe). The water tank was virtually divided into four areas: the starting area, the area opposite to the platform, the area towards the platform, and the platform. The trials were videotaped and tracked using TSE VideoMot 2 equipment (TSE Systems). Raw data on time and distance covered before reaching the platform as well as swim speed were exported from the software, sorted according to genotype and treatment, and analysed as average values for each block of three trials, using a script for R statistics developed at the University of Tuebingen.

Elevated plus maze

The rats' preference for exploring the closed rather than the open arms of an elevated plus maze was assessed as a measurement of anxiety-like behaviour at 13 months of age. The setup comprised four arms (12-cm wide and 42-cm long), connected by a 12 × 12 cm central area. Two of the arms were enclosed by 42-cm high walls (closed arms), while the other two arms had no walls (open arms). The arena was positioned 52 cm above ground. The experimental room was lit with white light, leaving the open arms exposed to light, while the closed arms remained substantially darker. The test was carried out for all rats on one day during the early dark phase, and cages with placebo- and olesoxime-treated rats were tested in an alternating order. At the start of each trial, a rat was placed inside the central area of the maze, facing one of the open arms, and allowed to freely explore the maze for a total of 5 min. The time spent in the open arms of the elevated plus maze was measured and subsequently analysed as per cent of the total trial duration.

Magnetic resonance imaging

MRI was performed at the Werner Siemens Imaging Center (Tuebingen, Germany). For this purpose, the rats were anaesthetized with 2% isoflurane and maintained at 1.2% vaporized in 100% O_2 at a flow rate of 1.5 l/min. Body temperature and ventilation rate were monitored throughout the MRI acquisition, with body temperature kept in the stable range of 37 ± 0.5°C. Anatomical T_2-weighted images were acquired with a rat brain surface coil using a 3D-spoiled turbo spin echo sequence (256 × 160 matrix, 25 × 25 mm^2 field of view, repetition time = 3000 ms, echo time = 205 ms, slice thickness = 0.22 mm). For MRI data evaluation, image analysis was performed using Inveon Research Workplace software (Siemens Healthcare) and referring to the rat brain atlas (*The Rat Brain in Stereotaxic coordinates*, 6th edition, 2006). Size differences in whole brain, cerebellum and striatum were determined with high accuracy by measuring the respective volume, as these brain regions have a clear delimitation in MRI. By contrast, differences in the size of the cerebral cortex were evaluated more accurately by measuring the thickness of the frontal part at −1.56 mm relative to bregma at the most dorsal point of the corpus callosum.

Measurement of olesoxime concentration

The concentration of olesoxime in plasma and brain samples was measured via HPLC-MS at Trophos SA using the Alliance® HPLC System (Waters S.A.S.). Samples were collected as explained below and thawed at room temperature. Plasma was mixed with 150 µl of acetonitrile, vortexed for 10 s and centrifuged for 10 min at 13 200*g*. Brain tissue was first homogenized at a concentration of 1 g/ml in Hank's balanced salt solution (10 mM HEPES, 141 mM NaCl, 4 mM KCl, 28 mM $CaCl_2$, 1 mM $MgSO_4$, 1 mM NaH_2PO_4). Homogenates were then mixed with 300 µl dichloromethane, vortexed for 10 s and centrifuged for 10 min at 13 200*g*. The organic phase was collected, evaporated at low pressure and 40°C and resolubilized in 110 µl acetonitrile. Assays were run once. Calculations were performed against a calibration curve prepared from olesoxime-spiked, normal rat plasma or brain homogenate, respectively.

Blood sampling

Blood was collected from rats of Cohort I during the longitudinal study at 3, 6, 9 and 13 months of age, and from rats of Cohort II after 2 weeks of olesoxime treatment at 4 months of age. For Cohort I, blood was collected by puncturing the animals' tail veins (the procedure did not require anaesthesia), while for Cohort II, blood was sampled retro-orbitally post-mortem. In either case, sampling was carried out within 2 h during the late light phase to minimize variation based on circadian rhythms. Blood was collected into EDTA-coated tubes on ice. Samples were centrifuged at 1500*g* for 10 min, plasma was removed, transferred into cryotubes and stored at −80°C.

Brain tissue sampling

For immunohistochemical techniques, the rats were deeply anaesthetized with an intraperitoneal injection of ketamin/xylazin (100 mg/kg or 5–8 mg/kg, respectively) and perfused transcardially with 4% paraformaldehyde in phosphate-buffered saline (pH 7.4). Brains were removed and stored at 4°C in 0.5% paraformaldehyde in phosphate-buffered saline (pH 7.4).

For all other analyses, the animals were sacrificed by CO_2 inhalation. Brains were immediately dissected on ice and whole

brain, or brain regions, were sampled. Tissue was shock-frozen in liquid nitrogen and either stored at −80°C or immediately processed to obtain live mitochondria for high-resolution respirometry. Tissue sampling was performed within 2 h during the late light phase to minimize variation based on any circadian phase-related changes.

Isolation of mitochondria and high resolution respirometry

Mitochondria were isolated from the frontal brain and respiration was measured at the Department of Pharmacology, Goethe University Frankfurt, Germany. For this purpose, tissue samples were homogenized in respiration media (20 mM HEPES, 110 mM sucrose, 0.5 mM EGTA, 3 mM magnesium dichloride, 60 mM lactobionic acid, 20 mM taurine, 10 mM potassium dihydrogenphosphate and 1 g/l essentially fatty acid-free bovine serum albumin, pH 7.4) containing 4% protease inhibitors (Complete® Protease Inhibitor, Roche). Homogenates were centrifuged at 1400*g* for 7 min, supernatant was collected and centrifuged at 1400*g* for 3 min and finally recollected and centrifuged at 10 000*g* for 5 min to pellet the mitochondria-containing fraction. Pellets were gently resuspended in respiration media, aliquots for the determination of protein concentration and citrate synthase activity (procedure described below) were collected, frozen in liquid nitrogen and stored at −80°C, while respiration was recorded immediately.

Respiration was measured with the Oxygraph (Oroboros), which allows the measurement of mitochondrial respiration in two samples simultaneously. Analysis was made using sample pairs of different genotypes (wild-type and BACHD) but identical treatment (placebo or olesoxime). Data were acquired with DatLab software, version 4.3.2.7. The rate of mitochondrial respiration was monitored at 37°C according to a protocol by Prof. Dr Erich Gnaiger (University of Innsbruck, Austria) (Kuznetsov *et al.*, 2002). A series of substrates and inhibitors were added to the samples in sequence to assess the function of different components of the mitochondrial respiratory chain. The capacity for OXPHOS (oxidative phosphorylation) was measured after addition of the complex I substrates (CI_{OXPHOS}) glutamate (5 mM), malate (2 mM) and ADP (2 mM), followed by the addition of succinate, the substrate for complex II (CI + II_{OXPHOS}). Blocking the ATP synthase by addition of oligomycin, further allowed for the measurement of respiration driven by the mitochondrial proton leak only. Subsequent titration of the artificial uncoupler FCCP (trifluorocarbonylcyanide phenylhydrazone), injected in steps of 1 µM up to 4 µM until saturation occurred revealed the maximum capacity of the electron transport system (ETS). Afterwards, addition of the complex I inhibitor rotenone revealed uncoupled CII activity (CII_{ETS}). Residual oxygen consumption (oxygen consumption caused by enzymes not belonging to the ETS) was measured after inhibition of complex III with 2.5 µM antimycin A, and subtracted from all measurements. Cytochrome C oxidase (complex IV) activity was determined after addition of 0.5 mM TMPD (tetramethylphenylenediamine), an artificial substrate and 2 mM ascorbate, which keeps TMPD in the reduced state. Complex IV respiration was corrected for the auto-oxidation rate of TMPD, determined by addition of azide (≥100 mM).

Respiration data were normalized to citrate synthase activity, a marker for mitochondrial mass (Kuznetsov *et al.*, 2002). Citrate synthase activity was assessed spectrophotometrically. For this purpose, samples were thawed and diluted 1:2 in deionized water. Reaction media [0.1 M Tris-HCl, 0.1 mM DTNB (5,5-dithiobis-2-nitrobenzoic acid), 0.5 mM oxaloacetate, 50 µM EDTA, 0.31 mM acetyl coenzyme A, 5 mM triethanolamine hydrochloride] were warmed for 5 min at 30°C, samples were added, and the formation of TNB (5-thio-2-nitrobenzoic acid) was measured immediately via absorbance at 412 nm.

Immunohistochemistry

Paraformaldehyde-fixed brains were embedded in gelatin blocks (16 brains per block) and cut serially into 40-µm thick coronal sections (performed by NeuroScience Associates). Sections were stored in antigen-preserve solution (Fisher Scientific) at −20°C. Free-floating staining was performed at room temperature, as described previously (Osmand *et al.*, 2006). Briefly, a series of 24 sections were warmed up at room temperature for 2 h and incubated for 30 min in 0.5% $NaBH_4$ for blocking purpose. After washing, the sections were probed overnight with sheep polyclonal S830 antibody (1:20 000, kindly provided by Prof. Dr Gillian Bates, King's College London, UK) for the detection of N-terminal mutant HTT. On the next day, the sections were incubated with biotinylated rabbit anti-sheep IgG secondary antibody (1:1000, BA-6000, Vector Laboratories) for 2 h and subsequently with avidin-enzyme complex (Vectastain® Elite ABC Kit Rabbit IgG, Linaris) for 1 h. To further enhance the signal, biotinylated thyramine plus 0.001% H_2O_2 was added for 10 min and the sections were once more incubated with avidin-biotin complex. Colour development was achieved with nickel-DAB-H_2O_2 (0.6% nickel, 0.01% DAB and 0.001% H_2O_2) dissolved in TI buffer (0.05 M Tris, 0.05 M imidazole). Nissl staining was performed using 1% thionine acetate to visualize nuclei. Sections were mounted and stored at room temperature.

Images were acquired using a Zeiss Axioplan microscope (Pl × 10 ocular, Plan-NEOFLUAR × 40/0.75 objective, AxioCam MRc) and Axiovision 4.8 software (Zeiss). Images were exported from Axiovision in tiff format, and imported into Corel Draw X5, where they were cropped to display the region of interest, and moderately adjusted in brightness, contrast and saturation to better visualize the structures of interest. The aforementioned adjustments did in no way change the information that was subject to analysis, namely the total number of S830-positive nuclei and cytoplasmic aggregates. The quantification, i.e. counting the number of cytoplasmic aggregates and the number of nuclei positive for mutant HTT staining, was performed manually.

Immunoblotting

Immunoblotting was performed with striatal and cortical tissue as well as mitochondrial membranes isolated from cerebral hemispheres.

Striata and cortices were thawed and homogenized on ice in TES buffer (50 mM Tris, 2 mM EDTA, 100 mM NaCl, pH 7.5) containing protease inhibitors (4% Complete® Protease Inhibitor, Roche). Homogenates were diluted 1:10 in TNES

buffer (90% TES buffer, 10% Igepal CA630), incubated for 1 h at 4°C and centrifuged 2 × 30 min at 16 100*g*. Supernatant (cell lysates) were collected and stored at −80°C in 10% glycerin.

Mitochondria-enriched heavy membrane fractions were isolated from cerebral hemispheres (brain stem, cerebellum and olfactory bulbs had been removed). Tissue was homogenized on ice in HEPES buffer (10 mM HEPES, 0.32 M sucrose, 1 mM EDTA, pH 7.4) and centrifuged at 585*g* for 10 min. Supernatant was collected and further centrifuged twice at 17 400*g* for 20 min. Pellets were resuspended and layered over a Ficoll density gradient (7.5% and 13%, w/v). After 60 min of ultracentrifugation at 87 300*g*, the pellet, which at this point contained the mitochondrial fraction, was sampled, resuspended in 5 mM Tris-HCl and stored at −20°C.

At the time of immunoblotting, all samples were thawed on ice, and the protein concentration was measured spectrophotometrically using Bradford reagent. Western blot analysis was performed according to standard procedures. Briefly, 15 µg of mitochondrial protein or 30 µg of protein from tissue lysates were assayed using sodium dodecyl sulphate (SDS) polyacrylamide gel electrophoresis on Tris-glycine or purchased Tris-acetate gels (Life Technologies). Proteins were transferred on nitrocellulose or polyvinyl difluoride membranes, and probed overnight at 4°C with the primary antibody (Supplementary Table 1). One hour of incubation with a horseradish peroxidase-conjugated secondary or IRDye® antibody (Supplementary Table 1) at room temperature followed. Chemiluminescence and fluorescence signals were detected with the LI-COR ODYSSEY FC Imaging system (LI-COR Biosciences). Protein levels were quantified by densitometry using ImageJ (Abràmoff *et al.*, 2004).

Filter retardation assay

For the detection of SDS-insoluble HTT species, 30 µg of cortical or striatal proteins were diluted in 100 µl DPBS (Life Technologies) with 2% SDS and incubated for 5 min at room temperature. A nitrocellulose membrane (0.45 µm; Bio-Rad) was equilibrated in 0.1% SDS in DPBS and samples were filtered through this membrane using a Minifold® II Slot Blot System (Schleicher & Schuell). The membrane was then washed twice with DPBS and blocked with 5% SlimFast (Unilever) in Tris-buffered saline for 1 h at room temperature. Retained SDS-insoluble HTT was detected using anti-HTT primary antibody (1:1000; clone 1HU-4C8, MAB2166, EMD Millipore) and the respective anti-mouse horseradish peroxidase-conjugated secondary antibody. Chemiluminescence signals were detected with the LI-COR ODYSSEY FC Imaging system and quantified using the ODYSSEY® Server software version 4.1 (both LI-COR Biosciences).

Calpain activation assays

In vitro calpain activation assays of brain lysates were performed as previously described (Hübener *et al.*, 2013). Briefly, 30 µg of protein from TNES lysates were diluted in 40 µl calpain reaction buffer (20 mM HEPES/KOH pH 7.6, 10 mM KCl, 1.5 mM $MgCl_2$, 1 mM dithiothreitol). The positive control was incubated with 20 ng of recombinant calpain-1 (EMD Millipore), and 2 mM $CaCl_2$ for indicated times at room temperature, while the negative control was pretreated with 100 µM of the calpain inhibitor CI-III (carbobenzoxy-valinyl-phenylalaninal) (EMD Millipore) prior to calpain-1 addition. Calpain activity of all samples was quenched by addition of 4× NuPAGE LDS sample buffer (Life Technologies) and heat denaturation for 10 min at 70°C. Samples were subsequently assayed by immunoblotting, as described above.

Time-resolved fluorescence energy transfer for soluble mutant HTT detection

Time-resolved fluorescence energy transfer (TR-FRET) was performed with cortical and striatal lysates (sampled as described in the 'Immunoblotting' section), and conducted according to Baldo *et al.* (2012) at Novartis. Briefly, samples were ultracentrifuged at 80 000*g* for 90 min. Supernatant was transferred to 384-microtitre plates, diluted 1:5 in detection buffer (50 mM NaH_2PO_4, 400 mM NaF, 0.1% bovine serum albumin, and 0.05% Tween) and probed with fluorophore-labelled antibodies 2B7-Tb and MW1-d2 in a ratio of 1:10. TR-FRET was read with an EnVision Reader (PerkinElmer). After the excitation of the donor fluorophore Tb at 320 nm and a time delay of 100 ms, the resulting Tb and d2 emission signals were read at 620 nm and 665 nm, respectively.

Experimental design

Sample size estimation was based on behavioural data previously obtained for the BACHD rat. Fifteen animals per genotype and treatment group were assigned to the Rotarod test, 12 to the simple swim test, five to the elevated plus maze and 10 to MRI analysis. *Ex vivo* analyses were planned with five rats per group. The final assignment differed slightly from this, as one cage of placebo-treated rats originally intended for the elevated plus maze and mitochondrial respiration analysis was used in addition for MRI measurements. Furthermore, three animals died during the study (without any bias regarding genotype or treatment groups). For *ex vivo* analyses, a final number of three to five rats per group were used, as sample material was limited.

During behavioural studies, the experimenter was blind to the animals' genotype, but not treatment, as the cages had to be labelled to ensure that the right kind of food, either placebo or olesoxime-loaded pellets, was provided at all times. Aggregate count was performed by one observer, who was blind to genotype and treatment group.

The *n* analysed, refers to the biological replicate of individual animals of a given genotype and treatment group, except for drug concentration analysis in brain regions, where samples from two to three individuals were pooled in order to reach a proper amount of sample material.

Statistical analysis

Data were analysed and graphed using GraphPad Prism 6.00 for Windows (GraphPad Software, San Diego California USA, http://www.graphpad.com). Values refer to group mean and standard error of the mean (SEM) for all figures, and group mean and standard deviation (SD) for Table 1. The α-level was set to 0.05. Complete data sets proved to be normally

distributed. Longitudinal data were analysed using repeated measurements two-way ANOVA, with time (e.g. age or trial) as a within-group factor and group (e.g. genotype and treatment) as between-group factor. Single data sets were analysed using regular two-way ANOVAs to identify genotype and treatment effects. For both, two-way repeated measures ANOVA and two-way ANOVA, the results are implemented in each graph and specify the respective between-group factors. Fisher's least significant difference (LSD) was performed as ANOVA post-test, and did not account for multiple comparisons, favouring false positive over false negative results in this first evaluation of olesoxime effects on Huntington's disease-related phenotypes. There was one two-group comparison (treatment effects specific to BACHD rats), which was analysed using a Student's *t*-test. Results from two-way ANOVAs and Fisher's LSD post-test, and post-test as well as *t*-test results for the comparisons *wild-type versus BACHD rats; #untreated versus treated wild-type rats; and +untreated versus treated BACHD rats are indicated in respective figures, with ns = not significant, $^{*/\#/+}P < 0.05$; $^{**/\#\#/++}P \leqslant 0.01$; and $^{***/\#\#\#/+++}P \leqslant 0.001$.

Some behavioural data were excluded from the analysis based on predefined criteria or technical problems. Concerning technical problems, the data could either not be properly acquired or the acquired data were inconclusive (as explained in detail below). We did not predefine exclusion criteria for outliers, or exclude data in order to reach a normal distribution. Moreover, the values we excluded were spread equally among groups, suggesting that it did not have a biological meaning or exclusion was skewing the results. Food intake measurements: nine of the 60 animals were excluded from the analysis because in at least one of the five measurements (at 2, 4, 6, 8 or 12 months of age), the food became stuck in the food basket leaving the animal unable to reach it and resulting in unreasonably low values for food intake during the respective night. Rotarod test: no data were excluded, but the number of rats available for analysis decreased with age, as an increasing number of mainly BACHD rats refused to stay on the rod at older ages (as discussed previously in Yu-Taeger *et al.*, 2012; Abada *et al.*, 2013*b*). Simple swim test: the tracking software produced a variety of errors, which made it necessary to exclude animals with individual erroneous runs. Elevated plus maze: one of the 20 animals was excluded from the analysis, as it did not move at all during the test. MRI: two of the 40 animals were excluded from the analysis, as they moved their heads during measurements and no sharp images could be acquired. Drug concentration analysis: two of the 16 samples were excluded as they had far higher drug concentrations than the rest of the rats. The high drug load in the two animals is considered to be due to food intake just prior to blood sampling, as we did not food deprive the animals. *Ex vivo* analyses: no data were excluded. Numbers of animals analysed in each experiment are listed in Supplementary Table 2.

Results

A timeline and overview of the parameters assessed in this study are given in Supplementary Fig. 1.

Olesoxime ameliorates cognitive and psychiatric phenotypes of BACHD rats

We previously reported that BACHD rats show a broad range of behavioural abnormalities reminiscent of the symptoms found in patients with Huntington's disease (Yu-Taeger *et al.*, 2012; Abada *et al.*, 2013*a*, *b*). The cognitive phenotype of the BACHD rat is characterized by difficulties in strategy shifting (Abada *et al.*, 2013*a*). Accordingly, we found that 7-month-old BACHD rats displayed reversal learning deficits in a simple swim test. Untreated, but not olesoxime-treated BACHD rats, needed longer to find a hidden platform after the platform had been relocated (Fig. 1A). Swim speed did not differ between groups (data not shown), suggesting that BACHD rats' general ability to swim was not impaired.

Anxiety-related changes were assessed by measuring the time spent on the open arms of an elevated plus maze at 13 months of age. In line with our previous findings (Yu-Taeger *et al.*, 2012), BACHD rats spent a significantly longer amount of time on the open arms than wild-type rats. Olesoxime treatment clearly ameliorated this phenotype (Fig. 1B).

Longitudinal assessment of clasping behaviour and rotarod performance were carried out as common tests of striatum-based motor dysfunction (Soll *et al.*, 2013; Bergeron *et al.*, 2014). BACHD rats showed hind limb clasping, similar to previous cohorts (Yu-Taeger *et al.*, 2012) (Fig. 1C). Furthermore, rotarod performance, which is among the earliest pathological phenotypes detected in the BACHD rat (Yu-Taeger *et al.*, 2012), was found to be impaired at 2, 4 and 8 months of age (Fig. 1D). Olesoxime treatment, which started when the motor abnormalities were already manifest, did not reverse the pathology (Fig. 1C and D).

Olesoxime increases frontal cortex thickness

Olesoxime has been ascribed with neuroprotective properties, as it was found to increase the survival of neurons expressing disease proteins (Bordet *et al.*, 2010; Gouarné *et al.*, 2013, 2015). We performed MRI scans in 13-month-old rats to evaluate if olesoxime was able to ameliorate brain atrophy observed in BACHD rats (Yu-Taeger *et al.*, 2012). BACHD rats had significantly smaller cerebra (Fig. 1E), striata (Fig. 1F) and prefrontal cortices (Fig. 1G) compared to their wild-type littermates. While olesoxime treatment did not significantly affect cerebral or striatal volume (Fig. 1E and F), frontal cortex thickness was significantly increased, pointing to a region-specific neuroprotective effect of olesoxime (Fig. 1G).

Olesoxime is enriched in prefrontal and frontal cortex

After finding significant beneficial, but apparently region-specific effects of olesoxime, we analysed the drug

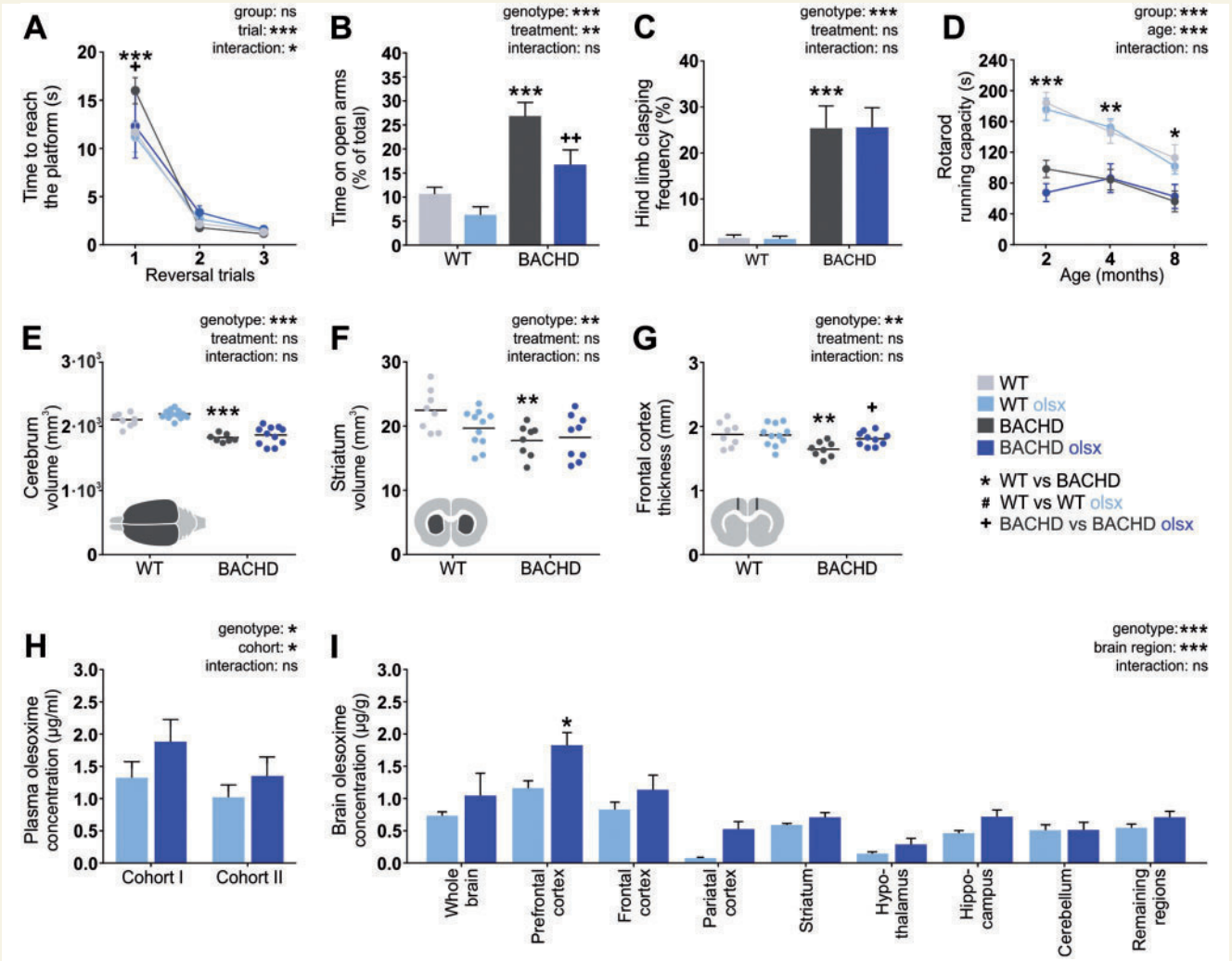

Figure 1 Olesoxime accumulates in the frontal cortex and exerts specific beneficial effects on behavioural and neuropathological phenotypes of the BACHD rat. (**A**) A simple swim test was used to assess cognitive flexibility at 7 months of age. The graph shows the time the animals needed to find a hidden platform after the position of the platform had been changed (reversal training). (**B**) Anxiety-related behaviour was assessed in an elevated plus maze at 13 months of age. The graph shows the time the animals spent on the open arms of the maze relative to trial duration. (**C**) Clasping behaviour was assessed weekly as an indicator for motor dysfunction. The graph displays the clasping frequency between the age of 1 and 10 months. (**D**) Motor abnormalities were further investigated longitudinally using a Rotarod test. The graph displays the mean running capacity during tests. (**E–G**) MRI was performed at 13 months of age. Images in the lower left corner illustrate the site of measurement. (**H** and **I**) Plasma olesoxime levels were measured in the main cohort of rats used for all *in vivo* and *ex vivo* analyses (Cohort I) at 3 months of age, after 7 weeks of treatment. In addition, plasma and brain olesoxime levels were determined in a second cohort of rats (Cohort II) at 4 months of age, after 2 weeks of treatment. Olsx = olesoxime, EPM = elevated plus maze; WT = wild-type; ns = not significant. $^{*/\#/+}P < 0.05$; $^{**/\#\#/++}P \leqslant 0.01$ and $^{***/\#\#\#/+++}P \leqslant 0.001$.

concentration in plasma and brain regions in a separate cohort of rats after 2 weeks of olesoxime treatment at 4 months of age (Cohort II). Analysis revealed similar plasma levels as found for the main cohort at 3 months of age (Cohort I) (Fig. 1H), which were presumed to lie in the pharmacologically active range of olesoxime based on the results of previous studies (Bordet *et al.*, 2007, 2010; Richter *et al.*, 2014). Furthermore, BACHD rats tended to have higher plasma (Fig. 1H) and brain (Fig. 1I) olesoxime levels than wild-type rats. In addition, we detected significant differences in the olesoxime concentration among brain regions, with highest concentrations measured in prefrontal and frontal cortex (Fig. 1I). The general trend to higher olesoxime concentrations in BACHD rats was not the result of increased food intake (data not shown) and there was no difference in body weight between genotype or treatment groups, thus the results might point to altered pharmacokinetics of olesoxime in the BACHD rat.

Olesoxime reduces mutant HTT aggregates and nuclear accumulation

Aggregation and nuclear accumulation of mutant HTT are prominent neuropathological features of Huntington's

disease (Gutekunst *et al.*, 1999). Consistent with our previous results (Yu-Taeger *et al.*, 2012), 13-month-old BACHD rats show mutant HTT aggregates (reflected by distinct S830-positive punctae) and nuclear accumulation (reflected by S830-positive nuclei) in variable magnitude throughout the brain (Figs 2, 3A and B). Aggregates were found predominantly in cortex, hypothalamus and amygdala. Mutant HTT nuclear accumulation prevailed in the cortex, lateral striatum and hippocampus. Similar to patients with Huntington's disease (Gutekunst *et al.*, 1999), cerebral cortex hosted a high amount of mutant HTT aggregates and nuclear accumulation of mutant HTT, while neither form was abundant in the central caudate putamen, the major part of the striatum. Olesoxime-treated BACHD rats showed a significant reduction in both aggregate load and nuclear mutant HTT accumulation (Figs 2, 3A and B). Moreover, not only the number of aggregates and mutant HTT-positive nuclei was reduced due to olesoxime treatment, but also aggregate size and the density of mutant HTT in the nuclei of olesoxime-treated BACHD rats seemed to be lowered.

The results from immunohistochemical staining were validated using a filter retardation assay to detect the amount of non-soluble, and thus aggregated, mutant HTT in cortical and striatal lysates from untreated and olesoxime-treated BACHD rats. In both cortical and striatal samples, aggregated mutant HTT was significantly reduced due to olesoxime treatment (Fig. 3C).

Olesoxime decreases mutant HTT fragments and increases full-length mutant HTT by reducing calpain-mediated cleavage

To further investigate the cause and consequences of reduced mutant HTT aggregate formation and nuclear accumulation, we analysed the levels of soluble full-length and truncated forms of mutant HTT in cortical and striatal lysates from 13-month-old BACHD and wild-type rats.

Total levels of soluble mutant HTT were measured by TR-FRET analysis as described previously (Baldo *et al.*, 2012). Consistent with the reduction of aggregated mutant HTT throughout the cortex, soluble mutant HTT levels were highly increased in the cortices but not striata from olesoxime-treated BACHD rats (Fig. 3D).

As mutant HTT fragments are particularly prone to aggregate formation (Cooper *et al.*, 1998; Li and Li, 1998; Martindale *et al.*, 1998) and nuclear accumulation (Davies *et al.*, 1997; DiFiglia *et al.*, 1997; Zhou *et al.*, 2003), we further quantified the levels of truncated mutant HTT by western blot analysis (Fig. 3E–G). By using the HTT-specific D7F7 antibody (epitope around proline 1220 of human HTT) to detect mutant HTT, as well as endogenous rat HTT, and the polyglutamine-specific 1C2 antibody to detect mutant HTT only, we obtained a variety of protein fragments in cortex and striatum of both wild-type and BACHD rats (Fig. 3E). Untreated BACHD rats showed clearly enhanced fragmentation of mutant HTT in cortex (Fig. 3E and F) but not striatum (Fig. 3E and G). In addition, the cortex samples from untreated BACHD rats contained a variety of shorter HTT fragments that were not detectable in cortical samples from wild-type rats, or striatal samples of either genotype (Fig. 3E). Olesoxime treatment reduced HTT fragmentation in BACHD rats below wild-type level in both cortex and striatum (Fig. 3E–G). Similar to the TR-FRET analysis, olesoxime-treated BACHD rats showed a significant increase in full-length mutant HTT, specifically in cortex (Fig. 3E and F).

Based on the apparent influence of olesoxime on mutant HTT proteolysis, we then investigated the origin of mutant HTT fragments by analysing the activity of calpains and caspases, the main contributors to proteolytic cleavage of mutant HTT (Goldberg *et al.*, 1996; Gafni and Ellerby, 2002). We did not find marked differences between genotype or treatment groups in the expression levels of caspase-3, or the activation status of caspase-6 in either cortex or striatum (data not shown). On the other hand, strong activation of the calpain system was detected specifically in cortex (Fig. 4A) but not striatum (Fig. 4B) of untreated BACHD rats. While the expression levels of full-length calpain-1, calpain-2 and calpain-10 were unchanged (data not shown), overactivation of the calpain system was evidenced by a distinct increase in processed calpain-1, elevated levels of the cleaved form of the calpain substrate α-spectrin, and decreased levels of the endogenous calpain inhibitor calpastatin (Fig. 4A). Olesoxime treatment reversed the dysregulation by decreasing active calpain-1, increasing calpastatin levels, and reducing α-spectrin cleavage (Fig. 4A). Even though calpain activity was not increased in the striata of untreated BACHD compared to wild-type rats, olesoxime reduced calpain-1 activation and spectrin cleavage also in this brain region, while no significant effects on calpastatin levels were detected (Fig. 4B).

To validate that the cortical mutant HTT fragments reduced by olesoxime treatment were calpain-derived, we performed *in vitro* calpain cleavage assays on cortical lysates (Fig. 4C and D). Incubation with recombinant calpain-1 resulted in increased fragmentation accompanied by a decrease in the levels of both full-length HTT and mutant HTT (Fig. 4C). The accumulation of calpain-derived wild-type and mutant HTT fragments was time-dependent, and concerned a variety of N-terminal and C-terminal fragments as detected by double-immunostaining with D7F7 and the N-terminal 4C8 antibody (epitope between amino acids 181 and 810) (Fig. 4D). Calpain dependency was further confirmed by addition of the specific calpain inhibitor CI-III, which abolished the fragmentation. *In vitro* calpain activation resulted in a clear fragmentation of HTT in wild-type rats, resembling the fragmentation pattern found in BACHD rats. Fragmentation was also enhanced in BACHD rats, although the effect was less strong due to high basal fragmentation of mutant HTT.

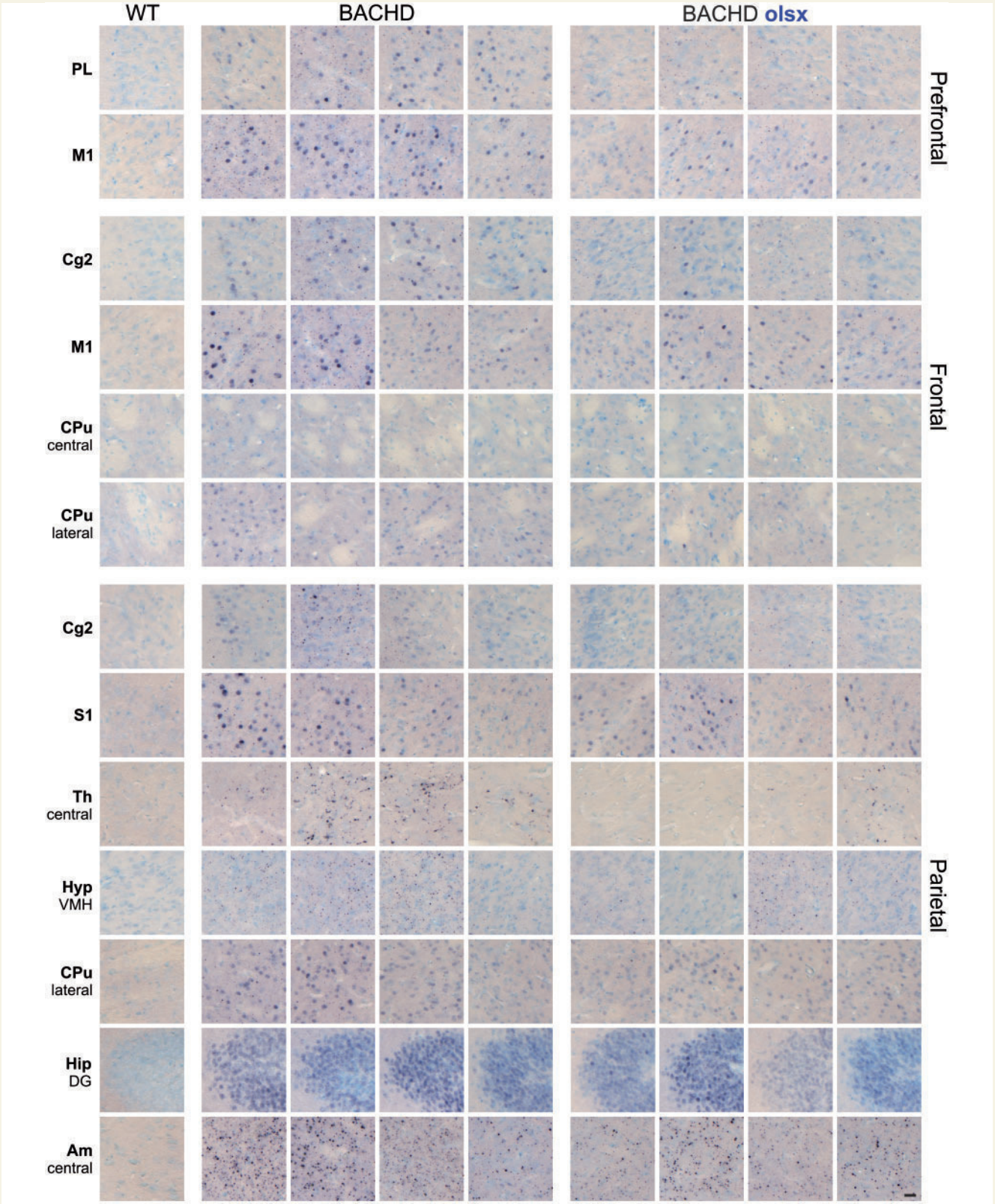

Figure 2 Effects of olesoxime on mutant huntingtin aggregates and nuclear accumulation in different brain regions. Aggregation and nuclear accumulation of mutant HTT were investigated in coronal brain sections from 13-month-old rats, stained with S830 N-terminal mutant HTT antibody. Images were taken from prefrontal, frontal and parietal brain areas. Columns display series of images from individual rats [wild-type (WT) $n = 1$, BACHD, $n = 4$]. Distinct punctae represent mutant HTT cytoplasmic aggregates and large circular staining represents mutant HTT nuclear accumulation. Black–purple staining = S830 huntingtin signal; blue staining = thionine nuclear signal. Magnification: $\times 400$; Scale bar = 10 μM. Olsx = olesoxime; PL = prelimbic cortex; M1 = motor cortex 1; Cg = cingulate cortex; CPu = caudate putamen; S = somatosensory cortex; Th = thalamus; Hyp = hypothalamus; VMH = ventro-medial hypothalamus; Hip = hippocampus; DG = dentate gyrus; Am = amygdala.

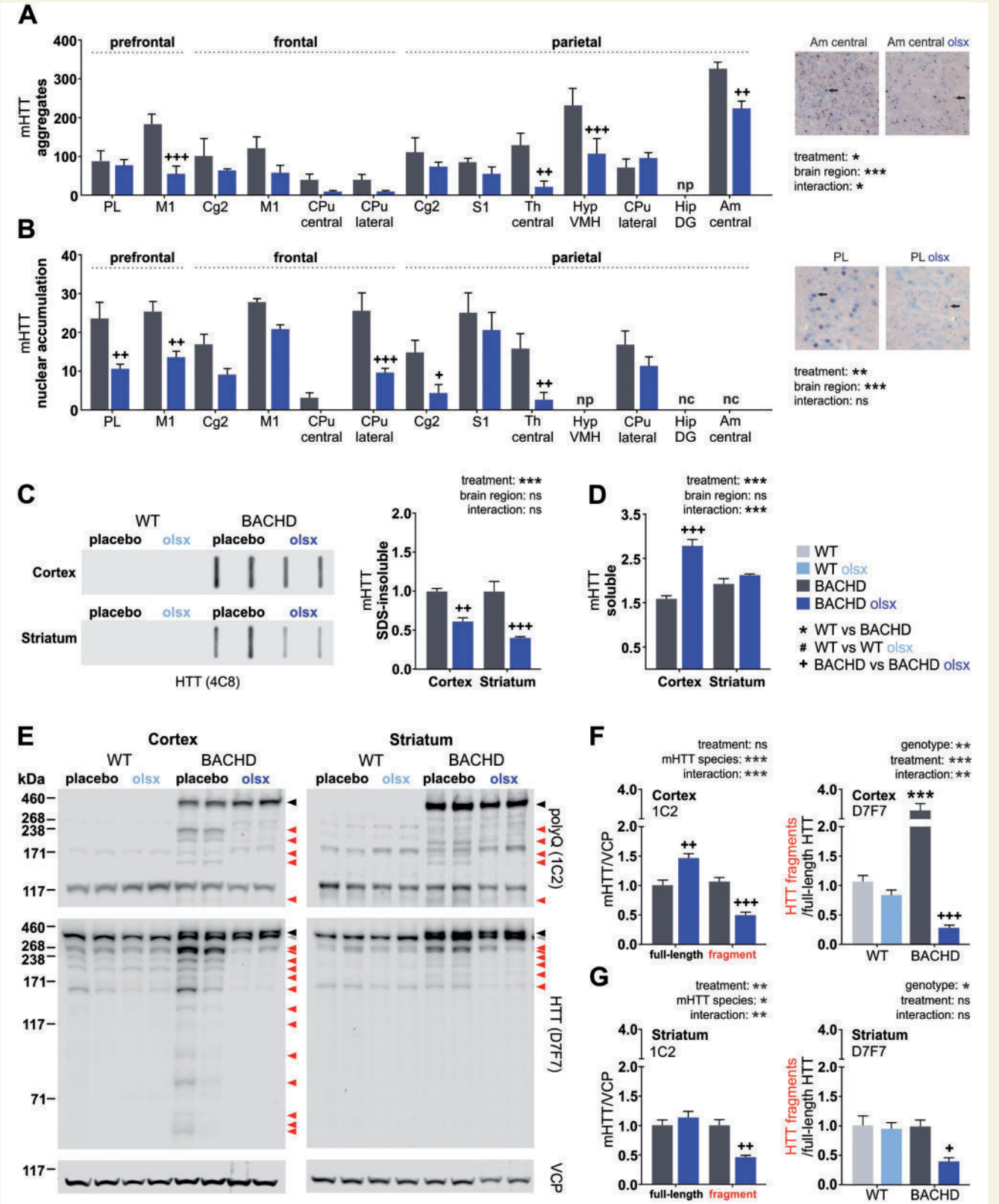

Figure 3 Olesoxime reduces mutant HTT aggregation, nuclear accumulation and fragmentation, and increases soluble full-length forms of mutant HTT. (**A** and **B**) Total numbers of S830-positive punctae [mutant HTT (mHTT) aggregates] and nuclei (nuclear accumulation of mutant HTT) were counted manually from the brain regions displayed in Fig. 2. Images on the *right* illustrate the structures counted, with arrows pointing to mutant HTT aggregates or mutant HTT-positive nuclei, respectively. Nc = not counted; np = not present; PL = prelimbic cortex; M1 = motor cortex 1; Cg = cingulate cortex; CPu = caudate putamen; S = somatosensory cortex; Th = thalamus; Hyp = hypothalamus; VMH = ventro-medial hypothalamus; Hip = hippocampus; DG = dentate gyrus; Am = amygdala. (**C**) SDS-insoluble proteins

(continued)

These results suggest that calpain cleavage constituted the major contributor to proteolytic cleavage in the BACHD rat and that the additional small fragments found in BACHD rat cortex, which were cleared by olesoxime treatment, derived from enhanced calpain-mediated cleavage.

Olesoxime reduces mitochondria-associated HTT fragments and improves mitochondrial function

Given that olesoxime accumulates at the site of mitochondria (Bordet *et al.*, 2010), we investigated the impact of olesoxime on mitochondrial properties.

First, we analysed the activation status of the calpain system in mitochondria-enriched heavy membrane fractions isolated from the cerebra of 13-month-old, placebo- and olesoxime-treated, wild-type and BACHD rats (Fig. 5A), as calpains are also located in mitochondria (Arrington *et al.*, 2006; Badugu *et al.*, 2008; Smith and Schnellmann, 2012). Enrichment in mitochondrial protein in the mitochondrial fractions is demonstrated by higher citrate synthase levels compared to whole cell lysate (Fig. 5A and B). Calpain activation was not increased in the mitochondrial fractions of untreated BACHD rats (Fig. 5A). However, olesoxime treatment repressed mitochondrial calpain activity in both BACHD and wild-type rat samples, as indicated by a reduced amount of active calpain-1 and cleaved α-spectrin, as well as increased amounts of calpastatin (Fig. 5A).

As HTT and mutant HTT are known to associate with mitochondria (Choo *et al.*, 2004; Gellerich *et al.*, 2008; Orr *et al.*, 2008), we further investigated their presence and cleavage in the mitochondrial fractions from wild-type and BACHD rats (Fig. 5B). Full-length protein as well as truncated forms of endogenous rat HTT and mutant HTT were detected. More mitochondria-associated fragments of HTT were found in untreated BACHD compared to wild-type rats. Olesoxime treatment reduced the amount of HTT fragments associated with mitochondria, in both wild-type and BACHD rats. In the BACHD rat, olesoxime additionally increased mitochondria-associated full-length endogenous rat HTT and mutant HTT. Together with the results on whole cell lysate, these findings indicate that olesoxime mediates a genotype-independent reduction in mitochondrial calpain activation, and reduces tissue-specific, whole cell calpain overactivation in the Huntington's disease context of the BACHD rat.

To test if olesoxime affected mitochondrial function, we further investigated mitochondrial respiratory chain activity (Fig. 5C) and the expression of mitochondrial proteins (Table 1). Mitochondrial function has not been assessed in the BACHD rat previously. Mitochondria isolated from 13-month-old untreated BACHD rat cerebra showed an overall lower oxygen consumption rate compared to wild-type rats, and olesoxime treatment reduced this respiration deficit (Fig. 5C). Expression levels of mitochondrial proteins were not strikingly altered in 13-month-old untreated BACHD compared to wild-type rats, but olesoxime strongly affected the protein expression in BACHD and wild-type rats in a differential manner (Table 1). While we observed a general increase in the expression of many mitochondrial proteins in cortex and striatum of olesoxime-treated wild-type rats, indicative of an overall increase in mitochondrial mass, we detected more specific effects in BACHD rats with olesoxime treatment. In cortex, olesoxime increased the expression of ATP synthase and the fusion-promoting proteins MFN1, MFN2 and OPA1, while the expression of fission-promoting proteins was either unaffected (FIS1) or decreased (DRP1), suggesting a higher capacity for respiration and fusion processes in this tissue due to olesoxime treatment. Olesoxime further dramatically increased the expression of the outer mitochondrial membrane transporter TOMM20, in both cortex and striatum of the BACHD rat. This finding led us to consider a general effect of olesoxime on transport across the mitochondrial membrane, and particularly the exchange of Ca^{2+}, as the overactivation of calpain found in BACHD rat cortex might be due to a mitochondrial Ca^{2+} buffering deficit.

Olesoxime affects the expression of proteins involved in Ca^{2+} homeostasis

It had been demonstrated that calpain-derived fragments of mutant HTT are formed in response to Ca^{2+} stress (Gafni *et al.*, 2004). Olesoxime might influence Ca^{2+} homeostasis, as it interacts with voltage-dependent anion channels (VDACs) (Bordet *et al.*, 2007), which are involved in intracellular Ca^{2+} translocation (Gincel *et al.*, 2001; Szabadkai *et al.*, 2006; Min *et al.*, 2012). Western blot analysis revealed no alteration in VDAC1/VDAC2 expression in 13-month-old untreated BACHD rats compared to wild-type rats, but a dramatic increase in the expression of both isoforms in cortex (Fig. 6A) and striatum (Fig. 6B) from olesoxime-treated BACHD rats. The strong effect on VDAC expression was also seen in the cortex of wild-type rats (Fig. 6A).

Figure 3 Continued

from cortical and striatal lysates were trapped on a nitrocellulose membrane and probed with the HTT-specific 4C8 antibody to quantify the amount of aggregated mutant HTT. (**D**) Levels of soluble mutant HTT were measured in cortical and striatal lysates from untreated and olesoxime-treated BACHD rats via TR-FRET analysis. (**E–G**) Full-length and fragment forms of mutant HTT were assessed in cortical and striatal lysates using the HTT-specific D7F7 and the polyglutamine-specific 1C2 antibodies. Black arrowheads = full-length mutant HTT; grey arrowhead = full-length endogenous rat HTT; red arrowheads = HTT fragments (1C2-positive bands in wild-type rats label polyglutamine-containing proteins other than mutant HTT); VCP/p97 = loading control; Olsx = olesoxime; ns = not significant. $^{*/\#/+}P < 0.05$; $^{**/\#\#/++}P \leqslant 0.01$ and $^{***/\#\#\#/+++}P \leqslant 0.001$.

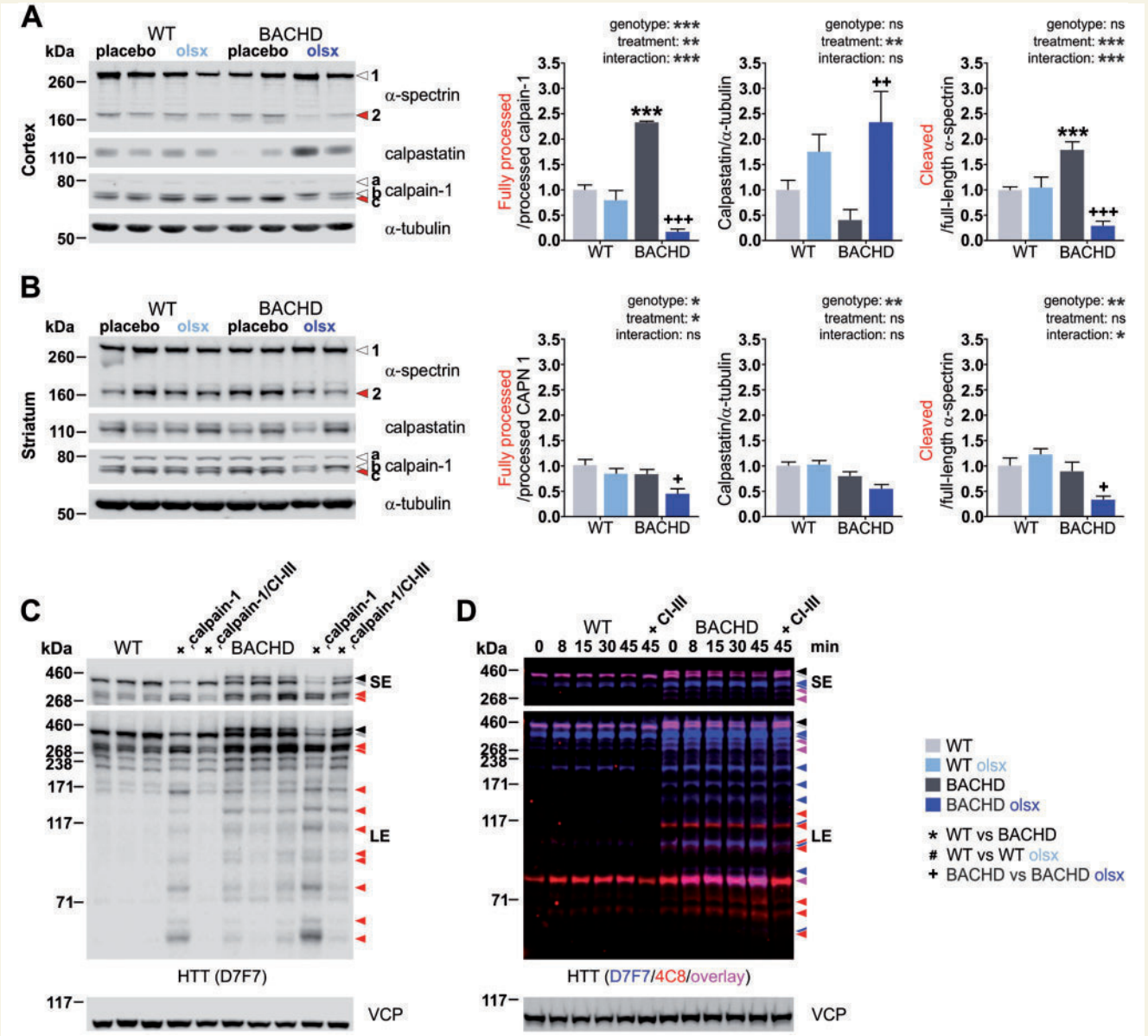

Figure 4 Olesoxime reduces the calpain-mediated cleavage of HTT, the major source of HTT fragments in the BACHD rat. (**A** and **B**) Calpain activation was investigated by western blot analysis of the protease calpain-1, its endogenous inhibitor calpastatin and cleavage substrate α-spectrin, in cortical and striatal lysates from 13-month-old rats. Arrowhead 1 = full-length α-spectrin; arrowhead 2 = α-spectrin fragment; arrowhead a = full-length calpain-1; arrowhead b = processed calpain-1; arrowhead c = further processed calpain-1 (active calpain1 refers to the ratio c/b); α-tubulin = loading control. (**C**) The dependency of HTT cleavage on calpain activity was assessed qualitatively in a calpain activation assay performed with cortical lysates from untreated, 13-month-old wild-type (WT) and BACHD rats. Samples were treated with recombinant calpain-1 and $CaCl_2$ (rcalpain-1) for 15 min, or additionally pretreated with calpain inhibitor III (CI-III) to demonstrate calpain-1 specificity. HTT fragments were detected with the HTT-specific D7F7 antibody. Black arrowhead = full-length mutant HTT; grey arrowhead = full-length endogenous rat HTT; red arrowheads = HTT fragments. Shorter exposure of the membrane was used to distinguish high molecular weight bands, while longer exposure revealed low molecular weight HTT fragments. (**D**) Another calpain activation assay was performed with cortical lysates from one untreated, 13-month-old wild-type and one BACHD rat, respectively, to illustrate the variety of N-terminal and more C-terminal HTT fragments. For this, the samples were first treated with recombinant calpain-1 and $CaCl_2$ (rcalpain-1) for an increasing amount of time or pretreated with calpain inhibitor III (CI-III) to demonstrate calpain-1 specificity. Samples were then probed with the HTT-specific D7F7 antibody as well as the HTT-specific 4C8 antibody, labelling central and N-terminal mutant HTT, respectively. The figure shows the overlay of the two detections with exclusive staining of HTT with D7F7 in blue, exclusive staining of HTT with 4C8 in red and double-staining of HTT with both antibodies in pink. Black arrowhead = full-length mutant HTT; grey arrowhead = full-length endogenous rat HTT; blue, red and pink arrowheads = HTT fragments; ns = not significant. Shorter exposure of the membrane was used to distinguish high molecular weight bands, while longer exposure revealed low molecular weight HTT fragments. $^{*/\#/+}P < 0.05$; $^{**/\#\#/++}P \leqslant 0.01$ and $^{***/\#\#\#/+++}P \leqslant 0.001$.

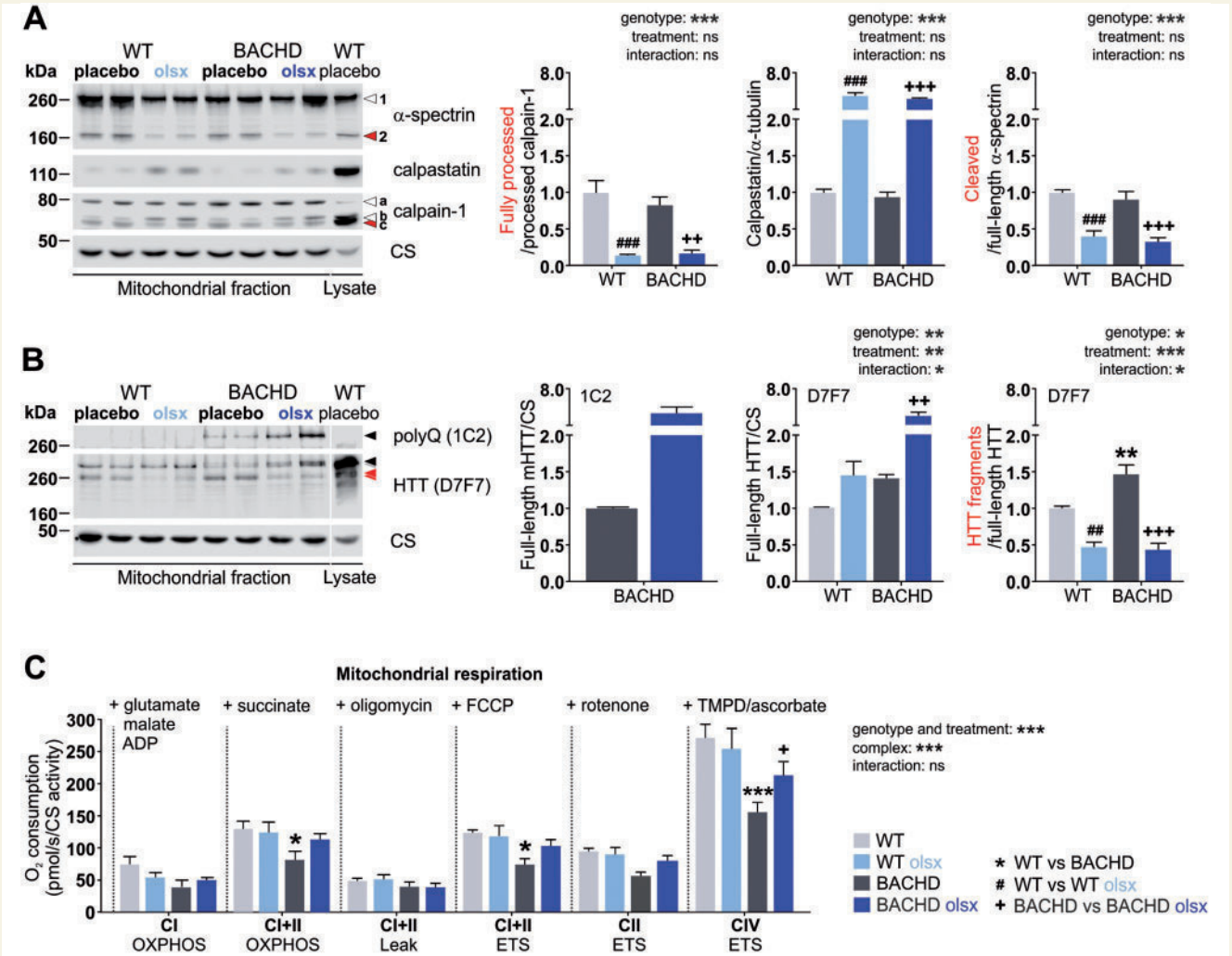

Figure 5 Olesoxime reduces the activation of mitochondrial calpains and mitochondria-associated HTT fragments and restores mild respiratory deficits in BACHD rats. (**A**) Calpain activation was investigated in cerebral mitochondria-enriched heavy membranes (mitochondrial fraction) from 13-month-old rats by western blot analysis of the protease calpain-1, its endogenous inhibitor calpastatin and cleavage substrate α-spectrin, in cortical and striatal lysates. Arrowhead 1 = full-length α-spectrin; arrowhead 2 = α-spectrin fragment; arrowhead a = full-length calpain-1; arrowhead b = processed calpain-1; arrowhead c = further processed calpain-1 (active calpain-1 refers to the ratio c/b); citrate synthase (CS) = loading control. (**B**) Full-length and fragment forms of mutant HTT were assessed in cortical and striatal lysates from 13-month-old rats using the HTT-specific D7F7 and the polyglutamine-specific 1C2 antibodies. Black arrowheads = full-length mutant HTT; grey arrowhead = full-length endogenous rat HTT; red arrowheads = HTT fragments. One sample of wild-type cortex lysate was loaded to demonstrate the enrichment of the mitochondrial marker citrate synthase in the mitochondrial fraction. (**C**) Mitochondrial respiratory chain activity was assessed by measuring oxygen consumption of isolated cerebral mitochondria from 13-month-old rats. Addition of substrates and inhibitors was performed as indicated in the figure and described in detail in the 'Materials and methods' section. CI_{OXPHOS} = complex I-fueled respiration; $CI + II_{OXPHOS}$ = complex I- and II-fueled respiration; $CI + II_{LEAK}$ = membrane leakage; $CI + II_{ETS}$ = maximum respiratory capacity; CII_{ETS} = maximum capacity dependent on complex II; CIV_{ETS} = maximum capacity dependent on complex IV; ns = not significant. Oxygen consumption rates were normalized to citrate synthase activity. $^{*/\#/+}P < 0.05$; $^{**/\#\#/++}P \leqslant 0.01$ and $^{***/\#\#\#/+++}P \leqslant 0.001$.

We further analysed the levels of the endoplasmic reticulum-associated Ca^{2+}-transporter IP3R1, as it is implicated in neurodegenerative diseases (Stutzmann and Mattson, 2011). Specifically, IP3R1 (encoded by *ITPR1*) protein expression is upregulated in response to elevated Ca^{2+} levels (Genazzani *et al.*, 1999), and excessive IP3R1-mediated Ca^{2+}-release into the cytosol primes apoptosis (Stutzmann and Mattson, 2011). Furthermore, both interaction with mutant HTT and calpain cleavage have been shown to facilitate IP3R1 activity upon stimulation, and render neurons more vulnerable to excitotoxic stimuli (Tang *et al.*, 2003; Kopil *et al.*, 2012). We found the levels of IP3R1 to be increased in cortex (Fig. 6A) of untreated BACHD compared to wild-type rats. While no significant effect of

Table 1 Expression levels of mitochondrial proteins

		Cortex				Striatum			
		WT		BACHD		WT		BACHD	
		Placebo	Olsx	Placebo	Olsx	Placebo	Olsx	Placebo	Olsx
MFN1	Mean	1.00	**1.33$^{\#\#}$**	**0.77***	**1.18^{++}**	1.00	1.66	1.10	0.96
	SD	0.18	0.11	0.16	0.14	0.32	0.36	0.57	0.71
	n	4	4	4	4	3	4	4	3
MFN2	Mean	1.00	1.17	0.93	**1.87^{++}**	1.00	2.41	1.63	1.63
	SD	0.16	0.29	0.38	0.39	0.11	0.37	0.90	1.63
	n	4	4	4	4	3	4	4	3
OPA1	Mean	1.00	**1.84$^{\#\#}$**	0.96	**2.33^{+++}**	1.00	1.90	1.39	1.37
	SD	0.40	0.30	0.29	0.52	0.49	0.55	0.60	0.88
	n	4	4	4	4	3	4	4	3
DRP1	Mean	1.00	0.92	0.84	**0.52^{++}**	1.00	1.36	0.98	1.04
	SD	0.06	0.14	0.14	0.05	0.04	0.52	0.15	0.27
	n	4	4	4	4	3	4	4	4
FIS1	Mean	1.00	**1.40$^{\#}$**	1.23	1.17	1.00	**2.16$^{\#}$**	2.08	1.31
	SD	0.13	0.33	0.15	0.31	0.29	0.70	0.93	0.34
	n	4	4	4	4	3	4	4	3
CS	Mean	1.00	**1.95$^{\#}$**	1.23	1.86	1.00	**1.64$^{\#}$**	1.11	0.94
	SD	0.56	0.94	0.33	0.22	0.11	0.36	0.33	0.22
	n	4	4	4	4	3	4	4	3
ATP5A	Mean	1.00	1.85	0.78	**3.20^{++}**	1.00	1.51	1.68	1.68
	SD	0.10	0.66	0.09	1.53	0.19	0.47	1.01	0.39
	n	4	4	4	4	3	4	4	3
TOM20	Mean	1.00	2.05	1.36	**3.19^{+}**	1.00	1.36	1.34	**8.24^{++}**
	SD	0.30	0.99	0.51	1.42	0.78	1.26	0.88	4.68
	n	4	4	4	4	4	4	4	4

The table contains group means, standard deviation (SD) and the number of animals analysed (*n*). Individual values were related to β-actin levels and normalized to the mean expression of placebo-treated wild-type (WT) rats. Significant differences from two-way ANOVA and Fisher LSD post-test are indicated in bold for the comparisons.
*wild-type versus BACHD rats.
#untreated versus treated wild-type.
+untreated versus treated BACHD rats with $^{*/\#/+}P < 0.05$; $^{**/\#\#/++}P \leqslant 0.01$ and $^{***/\#\#\#/+++}P \leqslant 0.001$. Fusion: MFN1, MFN2, OPA1; Fission: DRP1, FIS1; Matrix: citrate synthase (CS); Inner membrane: ATP synthase (ATP 5A); Outer membrane: translocase of the outer mitochondrial membrane (TOM20 encoded by *TOMM20*).

olesoxime treatment on IP3R1 was found in wild-type rats, olesoxime normalized IP3R1 expression in the cortex from BACHD rats (Fig. 6A and B).

Discussion

Olesoxime is a mitochondria-targeting neuroprotective compound (Bordet *et al.*, 2007, 2010) that has shown potential as a treatment for several neurodegenerative diseases (Bordet *et al.*, 2008; Xiao *et al.*, 2009, 2012; Rovini *et al.*, 2010; Sunyach *et al.*, 2012; Eckmann *et al.*, 2013; Richter *et al.*, 2014). We show here that olesoxime exhibited highly beneficial effects on disease-related phenotypes in a Huntington's disease animal model. Importantly, the treatment effects appeared to be conveyed through a previously unknown function of olesoxime, to reduce proteolysis. In Huntington's disease, proteolytic cleavage of mutant HTT results in the generation and accumulation of toxic mutant HTT fragments (Goldberg *et al.*, 1996; Gafni and Ellerby, 2002; Kim *et al.*, 2006; Miller *et al.*, 2010), which are thought to be crucial for disease pathogenesis (Rigamonti *et al.*, 2000; Nagai *et al.*, 2007; Wang *et al.*, 2008). Consistent with this, olesoxime-treated BACHD rats showed reduced activation of the calpain system, reduced amounts of mutant HTT fragments, aggregates and nuclear mutant HTT accumulation, as well as behavioural and neuropathological improvements. Inhibition of mutant HTT cleavage has previously been targeted in Huntington's disease models by genetic manipulations (Gafni *et al.*, 2004; Graham *et al.*, 2006; Miller *et al.*, 2010), or the use of protease inhibitor (Bizat *et al.*, 2003), revealing beneficial effects (Bizat *et al.*, 2003; Gafni *et al.*, 2004; Graham *et al.*, 2006; Miller *et al.*, 2010). However, olesoxime is the first small molecule identified to reduce the level of mutant HTT fragments in a safe and simple approach: the compound can be administered orally, has been shown to be safe and well-tolerated clinically (Lenglet *et al.*, 2014), and its neuroprotective activity has recently been demonstrated in a pivotal clinical trial in patients with spinal muscular atrophy (Dessaud *et al.*, 2014). Thus, our findings highly encourage further investigations of olesoxime for use as a therapeutic for Huntington's disease. Still, some questions arose from the present study, which need to be addressed further.

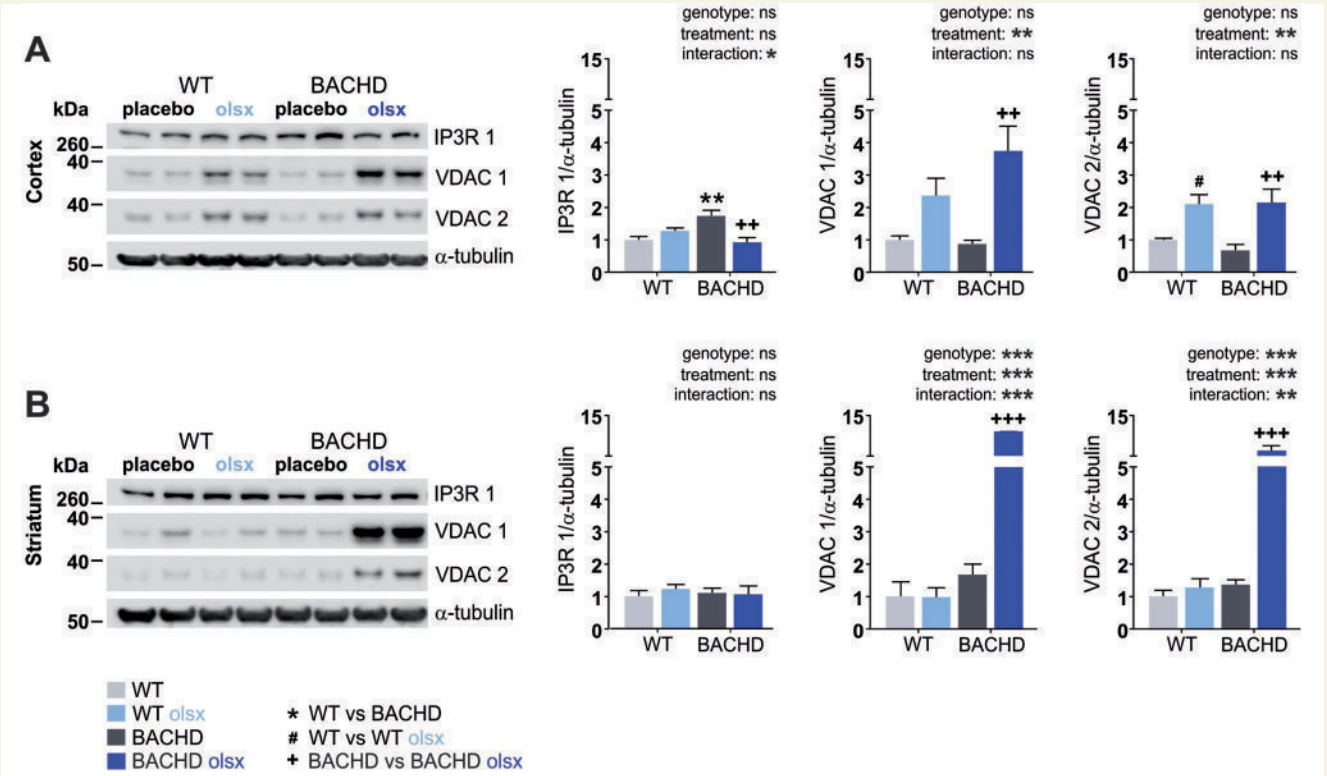

Figure 6 Olesoxime affects the expression of proteins involved in Ca^{2+} homeostasis. (**A** and **B**) Expression levels of the endoplasmic reticulum Ca^{2+} transporter IP3R1, and the outer mitochondrial membrane channels VDAC 1 and VDAC 2, which are also involved in Ca^{2+} transport, were assayed in cortical and striatal lysates from 13-month-old rats. α-tubulin = loading control; ns = not significant. $^{*/\#/+}P < 0.05$; $^{**/\#\#/++}P \leqslant 0.01$ and $^{***/\#\#\#/+++}P \leqslant 0.001$.

Are the beneficial effects of olesoxime restricted to specific brain regions?

The current results indicate that olesoxime reaches higher concentrations in the frontal and prefrontal cortex compared to other brain regions, when given orally. In line with this, both *in vivo* and *ex vivo* analyses indicated a predominant cortical effect of olesoxime treatment. MRI results revealed increased frontal cortex thickness, while atrophy of other brain areas such as the striatum was not alleviated. Further, olesoxime-treated BACHD rats showed a selective improvement of reversal learning and anxiety deficits, while motor phenotypes remained. Important in this regard is that lesion studies have tied attentional set shifting difficulties and reduced anxiety in the elevated plus maze to the prefrontal and frontal cortex (Birrell and Brown, 2000; Shah and Treit, 2003), while motor performance crucially involves the striatum (Soll *et al.*, 2013; Bergeron *et al.*, 2014). Thus, it is possible that the apparent selective effect on behaviour was a result of the uneven distribution of olesoxime. However, it is important to note that olesoxime still exerted strong effects on mutant HTT fragmentation and nuclear accumulation in striatum, despite its lower concentration. The reason for olesoxime not mitigating more striatum-based phenotypes could thus be that neuronal pathologies differ among brain regions. Most notably, the overactivation of the calpain system seemed to be a cortex-specific phenotype in the BACHD rat, and appeared to play a major role in olesoxime's beneficial effects. It is possible that striatal neurons suffer more from other mutant HTT-mediated deficits, and that neuronal dysfunction thus persisted, despite sufficient olesoxime concentrations.

An alternative hypothesis on the selective effects of olesoxime might be that some deficits, such as the rotarod phenotype, were already manifest prior to the start of olesoxime treatment in the current study. Similar results have been obtained in a recent study on the effect of cholesterol oximes on the pathological phenotypes of Parkinson's disease mice. The compounds ameliorated non-motor phenotypes and gene expression changes in mitochondrial genes, but were not able to reverse motor dysfunction with onset prior to the start of treatment (Richter *et al.*, 2014). The fact that olesoxime treatment did not generally ameliorate brain atrophy in BACHD rats could have the same cause, as we recently reported that smaller body and brain sizes among BACHD rats derive from growth impairment rather than progressive degeneration (Jansson *et al.*, 2014).

What is the primary target of olesoxime?

It has previously been proposed that the presence of mutant HTT might initiate a vicious cycle, in which mitochondrial

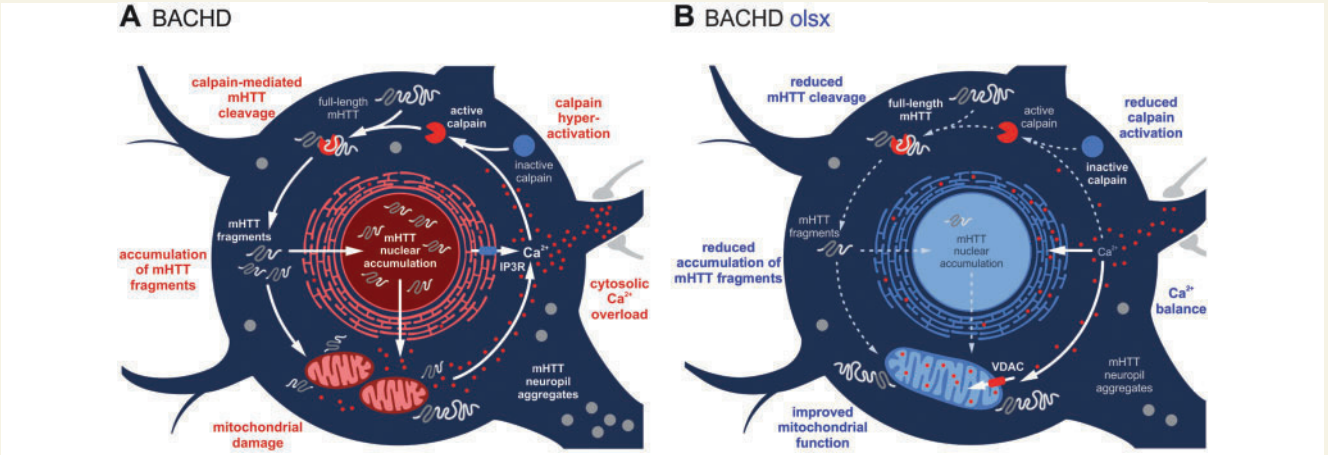

Figure 7 Schematic of the hypothetical Huntington's disease-related pathology and beneficial effects of olesoxime, in a BACHD rat cortical neuron. (**A**) The presence of mutant HTT (mHTT) provokes an increase in cytosolic Ca^{2+}, leading to the overactivation of calpain, a major executer of mutant HTT cleavage in the BACHD rat. Enhanced calpain-mediated cleavage generates large amounts of mutant HTT fragments, which accumulate in cytosol and nucleus, and are recruited to form cytosolic and neuropil aggregates. Mutant HTT fragments impair mitochondrial function by transcriptional dysregulation and direct interaction, thereby reducing mitochondrial Ca^{2+}-buffering capacity, further elevating cytosolic Ca^{2+}-levels and fuelling the vicious cycle. (**B**) Olesoxime interrupts this by improving mitochondrial function, reflected in increased respiratory activity, fusion protein and outer membrane transporter expression. This can in turn improve Ca^{2+} buffering, explaining the reduced calpain activation, mutant HTT cleavage and accumulation of mutant HTT fragments, as well as the decrease in cytosolic and neuropil aggregates seen in the current study.

dysfunction leads to reduced Ca^{2+} buffering, subsequent protease activation and generation of mutant HTT fragments that further enhance the cytotoxic events (Petersén *et al.*, 1999; Bizat *et al.*, 2003). Accordingly, we observed a respiratory chain deficit, along with increased calpain activation and mutant HTT fragmentation in BACHD rats, pathologies which were all alleviated by olesoxime (Fig. 7). Thus, we suggest that olesoxime interfered with the vicious cycle by stabilizing mitochondria.

It is conceivable that mitochondria were the primary effectors of olesoxime treatment, as olesoxime concentrates at this site (Bordet *et al.*, 2010), and cholesterol-oximes have been shown to affect the expression of genes important for mitochondrial function (Richter *et al.*, 2014). Such gene expression changes include the upregulation of *MFN1* and downregulation of *DRP1*, consistent with our findings on a protein level. Importantly, abnormally increased fission activity has recently been shown to contribute to the cellular pathology in Huntington's disease (Costa and Scorrano, 2012). Counteracting this by inhibiting fission or enhancing fusion, further, has been found to ameliorate Huntington's disease-related phenotypes (Wang *et al.*, 2009; Costa *et al.*, 2010; Song *et al.*, 2011). This is possibly due to improved mitochondrial Ca^{2+} handling, as suppressing fission or enhancing fusion generally renders neurons less susceptible to excitotoxic stress (Jahani-Asl *et al.*, 2011; Nguyen *et al.*, 2011; Grohm *et al.*, 2012; Kushnareva *et al.*, 2013).

Another interesting effect of olesoxime is a modulation of mitochondrial membrane fluidity. We reported earlier that olesoxime was able to reverse an increase in mitochondrial membrane fluidity observed in the BACHD rat and two other Huntington's disease models (Eckmann *et al.*, 2014). We further showed that olesoxime-treated BACHD rats had significantly higher mitochondrial membrane cholesterol levels than untreated BACHD rats, which might be causal for the reduction in membrane fluidity (Eckmann *et al.*, 2014). Here, we demonstrate that olesoxime dramatically increased the levels of the outer mitochondrial membrane transporter VDAC, which is involved in mitochondrial cholesterol import (Rone *et al.*, 2009). The additional increase in the levels of the outer mitochondrial membrane import component TOMM20 suggests that olesoxime exerted a general beneficial effect on transport processes across the mitochondrial membrane. It had been argued before that energetic deficits and impaired Ca^{2+} homeostasis might be the result of impaired communication between mitochondria and cytoplasm due to the accumulation of mutant HTT on the outer mitochondrial membrane (Gellerich *et al.*, 2008, 2010). A recent study specifically demonstrated that mutant HTT impairs mitochondrial protein import by interaction with the inner membrane transport complex TIMM23, and that overexpression of TIMM23 leads to restoration of protein import and prevention of cell death (Yano *et al.*, 2014). Thus, there are several indications that the mitochondrial membrane environment is modulated by olesoxime, which might connect to its beneficial effects.

We hypothesized that the compound had exerted its beneficial effects by improving mitochondrial function, thereby stabilizing Ca^{2+} homeostasis, decreasing Ca^{2+}-related calpain-1 activation and aborting the generation

of toxic HTT fragments as well as their exaggerated negative influence on mitochondria (Fig. 7). As Ca^{2+} levels, Ca^{2+} handling or the effects of olesoxime on Ca^{2+} balance could not be directly evaluated in this study, the proposed mechanism remains hypothetical. However, the finding of overactive calpain-1 itself and the increased protein levels of IP3R1 in untreated BACHD rats, as well as the restorative effects of olesoxime on these parameters, strongly support the idea of improved Ca^{2+} homeostasis, if not as primary effect then at least as part of olesoxime's mechanism of action.

Nonetheless, lacking a clear mechanism of action, it will be difficult to develop pharmacodynamic biomarkers, which will be crucial for conducting successful clinical efficacy trials. This has for instance been proven true for well-tolerated antioxidant molecules such as cysteamine (CYTE-I-HD study), creatine (CREST-E study), ethyl-EPA (TREND-HD study), and coenzyme Q10 (2CARE study). While these small molecules targeting mitochondrial function showed efficacy in some rodent models (Ferrante *et al.*, 2000; Yang *et al.*, 2009; Hickey *et al.*, 2012) (although there is also conflicting data: Menalled *et al.*, 2010), they mainly yielded negative findings in the clinics, emphasizing the urgent need for pharmacodynamic biomarkers. However, olesoxime is the first small molecule to modulate soluble levels of mutant HTT, which can be quantified in CSF, plasma and other tissues from animal models and patients with Huntington's disease using a TR-FRET (Baldo *et al.*, 2012; Weiss *et al.*, 2012) or mutant HTT immunoassay (Wild *et al.*, 2015), and could therefore potentially serve as a biomarker.

Can it be beneficial to reduce mutant HTT aggregation?

We observed a reduction in mutant HTT aggregation in olesoxime-treated BACHD rats. It is widely accepted that aggregates are not the most toxic species of mutant HTT, and reducing aggregation has even been found to enhance Huntington's disease-related pathologies (Arrasate and Finkbeiner, 2012). However, it is likely that in these cases, reduced aggregation was accompanied by an increase in mutant HTT fragments, as truncated mutant HTT, not its full-length form, is thought to mediate mutant HTT toxicity (Arrasate *et al.*, 2004). This is different from our study, as olesoxime specifically reduced mutant HTT fragments, but led to an increase in soluble full-length mutant HTT and endogenous rat HTT. There is evidence that not only mutant HTT but also wild-type HTT fragments have cytotoxic properties (Nasir *et al.*, 1995; Hackam *et al.*, 1998; Kim *et al.*, 1999), while the full-length form of wild-type HTT exerts protective effects (Leavitt *et al.*, 2001; Tanaka *et al.*, 2006). Our results further support the idea that soluble full-length mutant HTT is non-toxic, as we did not detect any adverse effects of olesoxime treatment *in vivo*. Suppression of mutant HTT cleavage and aggregation might also exert secondary beneficial effects by increasing wild-type HTT levels.

It should be noted that the reduction of mutant HTT aggregates in olesoxime-treated BACHD rats might not only derive from reduced cleavage, but could be an effect of increased protein degradation. Calpain activation has been shown to interfere with autophagic degradation processes (Yousefi *et al.*, 2006; Xia *et al.*, 2010), and inhibiting calpain activity enhances autophagy (Kuro *et al.*, 2011; Kim *et al.*, 2013; Menzies *et al.*, 2014). The increase in soluble mutant HTT that paralleled the decline in aggregation in the BACHD rat might, however, argue against a strong increase in mutant HTT degradation.

Is it relevant and safe to suppress calpain activity in neurodegenerative diseases?

The calpain proteolytic system has been recognized as an important player in neurodegenerative diseases (Haacke *et al.*, 2007; Samantaray *et al.*, 2008; Getz, 2012; Stifanese *et al.*, 2014), including Huntington's disease (Gafni and Ellerby, 2002). The pivotal role is underpinned by current studies addressing the mechanistic link between calpains and Ca^{2+} dysbalance (Gladding *et al.*, 2012), mitochondrial dysfunction (Wang *et al.*, 2014), axonal degeneration (Yang *et al.*, 2013), inflammation (Zhang *et al.*, 2014), and apoptosis (Sobhan *et al.*, 2013). A variety of calpain inhibitors have been developed to counteract the detrimental effects of calpain activation, but unspecific inhibitors and strong inhibition might exert off-target and side effects (Donkor, 2014). Such effects are less likely to arise from olesoxime treatment, as this probably affects calpains indirectly, and only lowers their activation. In this regard, we recently demonstrated that decreasing calpain activity in a mouse model of Parkinson's disease by cross-breeding with calpastatin-overexpressing mice, ameliorates Parkinson's disease-related pathologies (Diepenbroek *et al.*, 2014). These, as well as other data (Menzies *et al.*, 2014), suggest that long-term reduction of calpain activity does not have deleterious effects in mice *in vivo*.

Conclusion

Our study reveals behavioural and neuropathological improvements in olesoxime-treated BACHD rats due to improved mitochondrial function, which halts a vicious cycle of mitochondrial defects and calpain-mediated cleavage of mutant HTT. The current findings once more emphasize the connection between mitochondrial dysfunction and the generation of calpain-derived mutant HTT fragments, which underlies the molecular pathogenesis of Huntington's disease, and constitutes a pivotal therapeutic target. As safety, tolerance and neuroprotective properties of olesoxime have been demonstrated, both clinically and in several

neurodegenerative disease models, the compound represents a promising candidate for the treatment of Huntington's disease.

Acknowledgements

We are grateful to all MitoTarget members for helpful discussions and further want to thank Therese Stanek and Celina Tomczak for support in animal caretaking, Jean Axfanatidis for analytical chemistry, Adriana Rathore for assisting immunohistochemical staining and microscopy, Dr Nicolas Casadei for advice on aggregate quantification, and Julian Clemens for illustration support.

Funding

L.E.C., M.M., S.H.E., J.G., G.P.E., T.B., R.M.P., O.R. and H.P.N. received grants by the European Union 7th Framework Program for RTD, Project MitoTarget, Grant Agreement HEALTH-F2-2008-223388, and J.J.W. was funded by the Baden-Wuerttemberg Foundation, Research Grant Number P-BWS-SPII/3-08.

Conflict of interest

R.M.P. is employed by, and holds stock and stock options on Trophos; R.M.P. and T.B. are named as an inventor on patents covering the use of olesoxime assigned to Trophos; M.M. is currently employed by Trophos; T.B. has been, at the time the study was conducted, employed by Trophos, and is currently employed by AFM Téléthon; L.E.C. is currently employed by QPS Austria, J.G. is currently employed by Merz Pharmaceuticals; A.W. has been, at the time the study was conducted, employed by Novartis, and is currently employed by Evotec.

Supplementary material

Supplementary material is available at *Brain* online.

References

Abada Y-SK, Nguyen HP, Ellenbroek B, Schreiber R. Reversal learning and associative memory impairments in a BACHD rat model for Huntington's disease. PLoS One 2013a; 8: e71633.

Abada Y-SK, Nguyen HP, Schreiber R, Ellenbroek B. Assessment of motor function, sensory motor gating and recognition memory in a novel BACHD transgenic rat model for huntington disease. PLoS One 2013b; 8: e68584.

Abràmoff MD, Magalhães PJ, Sunanda J. Image processing with image. J Biophotonics Int 2004; 11: 36–42.

Arrasate M, Finkbeiner S. Protein aggregates in Huntington's disease. Exp Neurol 2012; 238: 1–11.

Arrasate M, Mitra S, Schweitzer ES, Segal MR, Finkbeiner S. Inclusion body formation reduces levels of mutant huntingtin and the risk of neuronal death. Nature 2004; 431: 805–10.

Arrington DD, Van Vleet TR, Schnellmann RG. Calpain 10: a mitochondrial calpain and its role in calcium-induced mitochondrial dysfunction. Am J Physiol Cell Physiol 2006; 291: C1159–71.

Badugu R, Garcia M, Bondada V, Joshi A, Geddes JW. N terminus of calpain 1 is a mitochondrial targeting sequence. J Biol Chem 2008; 283: 3409–17.

Bae B-I, Xu H, Igarashi S, Fujimuro M, Agrawal N, Taya Y, et al. p53 mediates cellular dysfunction and behavioral abnormalities in Huntington's disease. Neuron 2005; 47: 29–41.

Baldo B, Paganetti P, Grueninger S, Marcellin D, Kaltenbach LS, Lo DC, et al. TR-FRET-based duplex immunoassay reveals an inverse correlation of soluble and aggregated mutant huntingtin in huntington's disease. Chem Biol 2012; 19: 264–75.

Bergeron Y, Chagniel L, Bureau G, Massicotte G, Cyr M. mTOR signaling contributes to motor skill learning in mice. Front Mol Neurosci 2014; 7: 26.

Birrell JM, Brown VJ. Medial frontal cortex mediates perceptual attentional set shifting in the rat. J Neurosci 2000; 20: 4320–4.

Bizat N, Hermel J-M, Boyer F, Jacquard C, Créminon C, Ouary S, et al. Calpain is a major cell death effector in selective striatal degeneration induced *in vivo* by 3-nitropropionate: implications for Huntington's disease. J Neurosci 2003; 23: 5020–30.

Bordet T, Berna P, Abitbol J-L, Pruss RM. Olesoxime (TRO19622): a novel mitochondrial-targeted neuroprotective compound. Pharmaceuticals 2010; 3: 345–68.

Bordet T, Buisson B, Michaud M, Abitbol J-L, Marchand F, Grist J, et al. Specific antinociceptive activity of cholest-4-en-3-one, oxime (TRO19622) in experimental models of painful diabetic and chemotherapy-induced neuropathy. J Pharmacol Exp Ther 2008; 326: 623–32.

Bordet T, Buisson B, Michaud M, Drouot C, Galéa P, Delaage P, et al. Identification and characterization of cholest-4-en-3-one, oxime (TRO19622), a novel drug candidate for amyotrophic lateral sclerosis. J Pharmacol Exp Ther 2007; 322: 709–20.

Calì T, Ottolini D, Brini M. Mitochondrial Ca(2+) and neurodegeneration. Cell Calcium 2012; 52: 73–85.

Choo YS, Johnson GVW, MacDonald M, Detloff PJ, Lesort M. Mutant huntingtin directly increases susceptibility of mitochondria to the calcium-induced permeability transition and cytochrome c release. Hum Mol Genet 2004; 13: 1407–20.

Clemens LE, Jansson EKH, Portal E, Riess O, Nguyen HP. A behavioral comparison of the common laboratory rat strains Lister Hooded, Lewis, Fischer 344 and Wistar in an automated homecage system. Genes Brain Behav 2014; 13: 305–21.

Cooper JK, Schilling G, Peters MF, Herring WJ, Sharp AH, Kaminsky Z, et al. Truncated N-terminal fragments of huntingtin with expanded glutamine repeats form nuclear and cytoplasmic aggregates in cell culture. Hum Mol Genet 1998; 7: 783–90.

Costa V, Giacomello M, Hudec R, Lopreiato R, Ermak G, Lim D, et al. Mitochondrial fission and cristae disruption increase the response of cell models of Huntington's disease to apoptotic stimuli. EMBO Mol Med 2010; 2: 490–503.

Costa V, Scorrano L. Shaping the role of mitochondria in the pathogenesis of Huntington's disease. EMBO J 2012; 31: 1853–64.

Cui L, Jeong H, Borovecki F, Parkhurst CN, Tanese N, Krainc D. Transcriptional repression of PGC-1alpha by mutant huntingtin leads to mitochondrial dysfunction and neurodegeneration. Cell 2006; 127: 59–69.

Davies SW, Turmaine M, Cozens BA, DiFiglia M, Sharp AH, Ross CA, et al. Formation of neuronal intranuclear inclusions underlies the neurological dysfunction in mice transgenic for the HD mutation. Cell 1997; 90: 537–48.

Dessaud E, Carole A, Bruno S, Patrick B, Rebecca P, Cuvier V, et al. 2014 emerging science abstracts. Neurology 2014; 83: e34–40.

Diepenbroek M, Casadei N, Esmer H, Saido TC, Takano J, Kahle PJ, et al. Overexpression of the calpain-specific inhibitor calpastatin reduces human alpha-Synuclein processing, aggregation and synaptic impairment in [A30P]αSyn transgenic mice. Hum Mol Genet 2014; 23: 3975–89.

DiFiglia M, Sapp E, Chase KO, Davies SW, Bates GP, Vonsattel JP, et al. Aggregation of huntingtin in neuronal intranuclear inclusions and dystrophic neurites in brain. Science 1997; 277: 1990–3.

Donkor IO. An updated patent review of calpain inhibitors (2012–2014). Expert Opin Ther Pat 2014: 1–15.

Eckmann J, Clemens LE, Eckert SH, Hagl S, Yu-Taeger L, Bordet T, et al. Mitochondrial membrane fluidity is consistently increased in different models of huntington disease: restorative effects of olesoxime. Mol Neurobiol 2014; 50; 107–18

Eckmann J, Eckert SH, Leuner K, Muller WE, Eckert GP. Mitochondria: mitochondrial membranes in brain ageing and neurodegeneration. Int J Biochem Cell Biol 2013; 45: 76–80.

Fan MMY, Raymond LA. N-methyl-D-aspartate (NMDA) receptor function and excitotoxicity in Huntington's disease. Prog Neurobiol 2007; 81: 272–93.

Ferrante RJ, Andreassen OA, Jenkins BG, Dedeoglu A, Kuemmerle S, Kubilus JK, et al. Neuroprotective effects of creatine in a transgenic mouse model of Huntington's disease. J Neurosci 2000; 20: 4389–97.

Gafni J, Ellerby LM. Calpain activation in Huntington's disease. J Neurosci 2002; 22: 4842–9.

Gafni J, Hermel E, Young JE, Wellington CL, Hayden MR, Ellerby LM. Inhibition of calpain cleavage of huntingtin reduces toxicity: accumulation of calpain/caspase fragments in the nucleus. J Biol Chem 2004; 279: 20211–20.

Gellerich FN, Gizatullina Z, Nguyen HP, Trumbeckaite S, Vielhaber S, Seppet E, et al. Impaired regulation of brain mitochondria by extramitochondrial Ca2 + in transgenic Huntington disease rats. J Biol Chem 2008; 283: 30715–24.

Gellerich FN, Gizatullina Z, Trumbeckaite S, Nguyen HP, Pallas T, Arandarcikaite O, et al. The regulation of OXPHOS by extramitochondrial calcium. Biochim Biophys Acta 2010; 1797: 1018–27.

Genazzani AA, Carafoli E, Guerini D. Calcineurin controls inositol 1,4,5-trisphosphate type 1 receptor expression in neurons. Proc Natl Acad Sci USA 1999; 96: 5797–801.

Getz GS. Calpain inhibition as a potential treatment of Alzheimer's disease. Am J Pathol 2012; 181: 388–91.

Gincel D, Zaid H, Shoshan-Barmatz V. Calcium binding and translocation by the voltage-dependent anion channel: a possible regulatory mechanism in mitochondrial function. Biochem J 2001; 358: 147–55.

Gladding CM, Sepers MD, Xu J, Zhang LYJ, Milnerwood AJ, Lombroso PJ, et al. Calpain and STriatal-Enriched protein tyrosine phosphatase (STEP) activation contribute to extrasynaptic NMDA receptor localization in a Huntington's disease mouse model. Hum Mol Genet 2012; 21: 3739–52.

Goldberg YP, Nicholson DW, Rasper DM, Kalchman MA, Koide HB, Graham RK, et al. Cleavage of huntingtin by apopain, a proapoptotic cysteine protease, is modulated by the polyglutamine tract. Nat Genet 1996; 13: 442–9.

Goll DE, Thompson VF, Li H, Wei W, Cong J. The calpain system. Physiol Rev 2003; 83: 731–801.

Gouarné C, Giraudon-Paoli M, Seimandi M, Biscarrat C, Tardif G, Pruss RM, et al. Olesoxime protects embryonic cortical neurons from camptothecin intoxication by a mechanism distinct from BDNF. Br J Pharmacol 2013; 168: 1975–88.

Gouarné C, Tracz J, Paoli MG, Deluca V, Seimandi M, Tardif G, et al. Protective role of olesoxime against wild-type α-synuclein-induced toxicity in human neuronally differentiated SHSY-5Y cells. Br J Pharmacol 2015; 172: 235–45.

Graham RK, Deng Y, Slow EJ, Haigh B, Bissada N, Lu G, et al. Cleavage at the caspase-6 site is required for neuronal dysfunction and degeneration due to mutant huntingtin. Cell 2006; 125: 1179–91.

Gray M, Shirasaki DI, Cepeda C, André VM, Wilburn B, Lu X-H, et al. Full-length human mutant huntingtin with a stable polyglutamine repeat can elicit progressive and selective neuropathogenesis in BACHD mice. J Neurosci 2008; 28: 6182–95.

Grohm J, Kim S-W, Mamrak U, Tobaben S, Cassidy-Stone A, Nunnari J, et al. Inhibition of Drp1 provides neuroprotection *in vitro* and *in vivo*. Cell Death Differ 2012; 19: 1446–58.

Gutekunst CA, Li SH, Yi H, Mulroy JS, Kuemmerle S, Jones R, et al. Nuclear and neuropil aggregates in Huntington's disease: relationship to neuropathology. J Neurosci 1999; 19: 2522–34.

Haacke A, Hartl FU, Breuer P. Calpain inhibition is sufficient to suppress aggregation of polyglutamine-expanded ataxin-3. J Biol Chem 2007; 282: 18851–6.

Hackam AS, Singaraja R, Wellington CL, Metzler M, McCutcheon K, Zhang T, et al. The influence of huntingtin protein size on nuclear localization and cellular toxicity. J Cell Biol 1998; 141: 1097–105.

Hickey MA, Zhu C, Medvedeva V, Franich NR, Levine MS, Chesselet M-F. Evidence for behavioral benefits of early dietary supplementation with CoEnzymeQ10 in a slowly progressing mouse model of Huntington's disease. Mol Cell Neurosci 2012; 49: 149–57.

Hübener J, Weber JJ, Richter C, Honold L, Weiss A, Murad F, et al. Calpain-mediated ataxin-3 cleavage in the molecular pathogenesis of spinocerebellar ataxia type 3 (SCA3). Hum Mol Genet 2013; 22: 508–18.

Jahani-Asl A, Pilon-Larose K, Xu W, MacLaurin JG, Park DS, McBride HM, et al. The mitochondrial inner membrane GTPase, optic atrophy 1 (Opa1), restores mitochondrial morphology and promotes neuronal survival following excitotoxicity. J Biol Chem 2011; 286: 4772–82.

Jansson EKH, Clemens LE, Riess O, Nguyen HP. Reduced motivation in the BACHD rat model of Huntington disease is dependent on the choice of food deprivation strategy. PLoS One 2014; 9: e105662.

Kim J-S, Wang J-H, Biel TG, Kim D-S, Flores-Toro JA, Vijayvargiya R, et al. Carbamazepine suppresses calpain-mediated autophagy impairment after ischemia/reperfusion in mouse livers. Toxicol Appl Pharmacol 2013; 273: 600–10.

Kim M, Lee HS, LaForet G, McIntyre C, Martin EJ, Chang P, et al. Mutant huntingtin expression in clonal striatal cells: dissociation of inclusion formation and neuronal survival by caspase inhibition. J Neurosci 1999; 19: 964–73.

Kim YJ, Sapp E, Cuiffo BG, Sobin L, Yoder J, Kegel KB, et al. Lysosomal proteases are involved in generation of N-terminal huntingtin fragments. Neurobiol Dis 2006; 22: 346–56.

Kopil CM, Siebert AP, Foskett JK, Neumar RW. Calpain-cleaved type 1 inositol 1,4,5-trisphosphate receptor impairs ER Ca(2 +) buffering and causes neurodegeneration in primary cortical neurons. J Neurochem 2012; 123: 147–58.

Kuro M, Yoshizawa K, Uehara N, Miki H, Takahashi K, Tsubura A. Calpain inhibition restores basal autophagy and suppresses MNU-induced photoreceptor cell death in mice. In Vivo (Brooklyn) 2011; 25: 617–23.

Kushnareva YE, Gerencser AA, Bossy B, Ju W-K, White AD, Waggoner J, et al. Loss of OPA1 disturbs cellular calcium homeostasis and sensitizes for excitotoxicity. Cell Death Differ 2013; 20: 353–65.

Kuznetsov A V, Strobl D, Ruttmann E, Königsrainer A, Margreiter R, Gnaiger E. Evaluation of mitochondrial respiratory function in small biopsies of liver. Anal Biochem 2002; 305: 186–94.

Landles C, Sathasivam K, Weiss A, Woodman B, Moffitt H, Finkbeiner S, et al. Proteolysis of mutant huntingtin produces an exon 1 fragment that accumulates as an aggregated protein in neuronal nuclei in Huntington disease. J Biol Chem 2010; 285: 8808–23.

Leavitt BR, Guttman JA, Hodgson JG, Kimel GH, Singaraja R, Vogl AW, et al. Wild-type huntingtin reduces the cellular toxicity of mutant huntingtin *in vivo*. Am J Hum Genet 2001; 68: 313–24.

Lemasters JJ, Theruvath TP, Zhong Z, Nieminen A-L. Mitochondrial calcium and the permeability transition in cell death. Biochim Biophys Acta 2009; 1787: 1395–401.

Lenglet T, Lacomblez L, Abitbol JL, Ludolph A, Mora JS, Robberecht W, et al. A phase II-III trial of olesoxime in subjects with amyotrophic lateral sclerosis. Eur J Neurol 2014; 21: 529–36.

Li SH, Li XJ. Aggregation of N-terminal huntingtin is dependent on the length of its glutamine repeats. Hum Mol Genet 1998; 7: 777–82.

Martindale D, Hackam A, Wieczorek A, Ellerby L, Wellington C, McCutcheon K, et al. Length of huntingtin and its polyglutamine tract influences localization and frequency of intracellular aggregates. Nat Genet 1998; 18: 150–4.

Menalled LB, Patry M, Ragland N, Lowden PAS, Goodman J, Minnich J, et al. Comprehensive behavioral testing in the R6/2 mouse model of Huntington's disease shows no benefit from CoQ10 or minocycline. PLoS One 2010; 5: e9793.

Menzies FM, Garcia-Arencibia M, Imarisio S, O'Sullivan NC, Ricketts T, Kent BA, et al. Calpain inhibition mediates autophagy-dependent protection against polyglutamine toxicity. Cell Death Differ 2014; 22: 433–44.

Miller BR, Bezprozvanny I. Corticostriatal circuit dysfunction in Huntington's disease: intersection of glutamate, dopamine and calcium. Future Neurol 2010; 5: 735–56.

Miller JP, Holcomb J, Al-Ramahi I, de Haro M, Gafni J, Zhang N, et al. Matrix metalloproteinases are modifiers of huntingtin proteolysis and toxicity in Huntington's disease. Neuron 2010; 67: 199–212.

Min CK, Yeom DR, Lee K-E, Kwon H-K, Kang M, Kim Y-S, et al. Coupling of ryanodine receptor 2 and voltage-dependent anion channel 2 is essential for $Ca^{2}+$ transfer from the sarcoplasmic reticulum to the mitochondria in the heart. Biochem J 2012; 447: 371–9.

Nagai Y, Inui T, Popiel HA, Fujikake N, Hasegawa K, Urade Y, et al. A toxic monomeric conformer of the polyglutamine protein. Nat Struct Mol Biol 2007; 14: 332–40.

Nasir J, Floresco SB, O'Kusky JR, Diewert VM, Richman JM, Zeisler J, et al. Targeted disruption of the Huntington's disease gene results in embryonic lethality and behavioral and morphological changes in heterozygotes. Cell 1995; 81: 811–23.

Nguyen D, Alavi M V, Kim K-Y, Kang T, Scott RT, Noh YH, et al. A new vicious cycle involving glutamate excitotoxicity, oxidative stress and mitochondrial dynamics. Cell Death Dis 2011; 2: e240.

Orr AL, Li S, Wang C-E, Li H, Wang J, Rong J, et al. N-terminal mutant huntingtin associates with mitochondria and impairs mitochondrial trafficking. J Neurosci 2008; 28: 2783–92.

Osmand AP, Berthelier V, Wetzel R. Imaging polyglutamine deposits in brain tissue. Methods Enzymol 2006; 412: 106–22.

Panov A V, Burke JR, Strittmatter WJ, Greenamyre JT. *In vitro* effects of polyglutamine tracts on Ca2 + -dependent depolarization of rat and human mitochondria: relevance to Huntington's disease. Arch Biochem Biophys 2003; 410: 1–6.

Panov A V, Gutekunst C-A, Leavitt BR, Hayden MR, Burke JR, Strittmatter WJ, et al. Early mitochondrial calcium defects in Huntington's disease are a direct effect of polyglutamines. Nat Neurosci 2002; 5: 731–6.

Persichetti F, Ambrose CM, Ge P, McNeil SM, Srinidhi J, Anderson MA, et al. Normal and expanded Huntington's disease gene alleles produce distinguishable proteins due to translation across the CAG repeat. Mol Med 1995; 1: 374–83.

Petersén A, Mani K, Brundin P. Recent advances on the pathogenesis of Huntington's disease. Exp Neurol 1999; 157: 1–18.

Poudel GR, Egan GF, Churchyard A, Chua P, Stout JC, Georgiou-Karistianis N. Abnormal synchrony of resting state networks in premanifest and symptomatic Huntington disease: the IMAGE-HD study. J Psychiatry Neurosci 2014; 39: 87–96.

Richter F, Gao F, Medvedeva V, Lee P, Bove N, Fleming SM, et al. Chronic administration of cholesterol oximes in mice increases transcription of cytoprotective genes and improves transcriptome alterations induced by alpha-synuclein overexpression in nigrostriatal dopaminergic neurons. Neurobiol Dis 2014; 69: 263–75.

Rigamonti D, Bauer JH, De-Fraja C, Conti L, Sipione S, Sciorati C, et al. Wild-type huntingtin protects from apoptosis upstream of caspase-3. J Neurosci 2000; 20: 3705–13.

Rockabrand E, Slepko N, Pantalone A, Nukala VN, Kazantsev A, Marsh JL, et al. The first 17 amino acids of Huntingtin modulate its sub-cellular localization, aggregation and effects on calcium homeostasis. Hum Mol Genet 2007; 16: 61–77.

Rone MB, Fan J, Papadopoulos V. Cholesterol transport in steroid biosynthesis: role of protein-protein interactions and implications in disease states. Biochim Biophys Acta 2009; 1791: 646–58.

Rovini A, Carré M, Bordet T, Pruss RM, Braguer D. Olesoxime prevents microtubule-targeting drug neurotoxicity: selective preservation of EB comets in differentiated neuronal cells. Biochem Pharmacol 2010; 80: 884–94.

Samantaray S, Ray SK, Banik NL. Calpain as a potential therapeutic target in Parkinson's disease. CNS Neurol. Disord. Drug Targets 2008; 7: 305–12.

Shah AA, Treit D. Excitotoxic lesions of the medial prefrontal cortex attenuate fear responses in the elevated-plus maze, social interaction and shock probe burying tests. Brain Res 2003; 969: 183–94.

Smith MA, Schnellmann RG. Calpains, mitochondria, and apoptosis. Cardiovasc Res 2012; 96: 32–7.

Sobhan PK, Seervi M, Deb L, Varghese S, Soman A, Joseph J, et al. Calpain and reactive oxygen species targets Bax for mitochondrial permeabilisation and caspase activation in zerumbone induced apoptosis. PLoS One 2013; 8: e59350.

Soll LG, Grady SR, Salminen O, Marks MJ, Tapper AR. A role for $\alpha4$(non-$\alpha6$)* nicotinic acetylcholine receptors in motor behavior. Neuropharmacology 2013; 73: 19–30.

Song W, Chen J, Petrilli A, Liot G, Klinglmayr E, Zhou Y, et al. Mutant huntingtin binds the mitochondrial fission GTPase dynamin-related protein-1 and increases its enzymatic activity. Nat Med 2011; 17: 377–82.

Stifanese R, Averna M, De Tullio R, Pedrazzi M, Milanese M, Bonifacino T, et al. Role of calpain-1 in the early phase of experimental ALS. Arch Biochem Biophys 2014; 562: 1–8.

Stutzmann GE, Mattson MP. Endoplasmic reticulum Ca(2 +) handling in excitable cells in health and disease. Pharmacol Rev 2011; 63: 700–27.

Sunyach C, Michaud M, Arnoux T, Bernard-Marissal N, Aebischer J, Latyszenok V, et al. Olesoxime delays muscle denervation, astrogliosis, microglial activation and motoneuron death in an ALS mouse model. Neuropharmacology 2012; 62: 2346–52.

Szabadkai G, Bianchi K, Várnai P, De Stefani D, Wieckowski MR, Cavagna D, et al. Chaperone-mediated coupling of endoplasmic reticulum and mitochondrial Ca2 + channels. J Cell Biol 2006; 175: 901–11.

Tabrizi SJ, Scahill RI, Durr A, Roos RA, Leavitt BR, Jones R, et al. Biological and clinical changes in premanifest and early stage Huntington's disease in the TRACK-HD study: the 12-month longitudinal analysis. Lancet Neurol 2011; 10: 31–42.

Tanaka Y, Igarashi S, Nakamura M, Gafni J, Torcassi C, Schilling G, et al. Progressive phenotype and nuclear accumulation of an amino-terminal cleavage fragment in a transgenic mouse model with inducible expression of full-length mutant huntingtin. Neurobiol Dis 2006; 21: 381–91.

Tang T-S, Slow E, Lupu V, Stavrovskaya IG, Sugimori M, Llinás R, et al. Disturbed Ca2 + signaling and apoptosis of medium spiny neurons in Huntington's disease. Proc Natl Acad Sci USA 2005; 102: 2602–7.

Tang T-S, Tu H, Chan EYW, Maximov A, Wang Z, Wellington CL, et al. Huntingtin and huntingtin-associated protein 1 influence neuronal calcium signaling mediated by inositol-(1,4,5) triphosphate receptor type 1. Neuron 2003; 39: 227–39.

The Huntington's Disease Collaborative Research Group. A novel gene containing a trinucleotide repeat that is expanded and unstable on Huntington's disease chromosomes. The Huntington's Disease Collaborative Research Group. Cell 1993; 72: 971–83.

Van Raamsdonk JM, Pearson J, Slow EJ, Hossain SM, Leavitt BR, Hayden MR. Cognitive dysfunction precedes neuropathology and motor abnormalities in the YAC128 mouse model of Huntington's disease. J Neurosci 2005; 25: 4169–80.

Vonsattel JP, DiFiglia M. Huntington disease. J Neuropathol Exp Neurol 1998; 57: 369–84.

Wang C-E, Tydlacka S, Orr AL, Yang S-H, Graham RK, Hayden MR, et al. Accumulation of N-terminal mutant huntingtin in mouse and monkey models implicated as a pathogenic mechanism in Huntington's disease. Hum Mol Genet 2008; 17: 2738–51.

Wang H, Lim PJ, Karbowski M, Monteiro MJ. Effects of overexpression of huntingtin proteins on mitochondrial integrity. Hum Mol Genet 2009; 18: 737–52.

Wang W, Zhang F, Li L, Tang F, Siedlak SL, Fujioka H, et al. Mfn2 couples glutamate excitotoxicity and mitochondrial dysfunction in motor neurons. J Biol Chem 2014; 290: 168–82.

Weiss A, Träger U, Wild EJ, Grueninger S, Farmer R, Landles C, et al. Mutant huntingtin fragmentation in immune cells tracks Huntington's disease progression. J Clin Invest 2012; 122: 3731–6.

Wild EJ, Boggio R, Langbehn D, Robertson N, Haider S, Miller JRC, et al. Quantification of mutant huntingtin protein in cerebrospinal fluid from Huntington's disease patients. J Clin Invest 2015; 125: 1979–86.

Xia H-G, Zhang L, Chen G, Zhang T, Liu J, Jin M, et al. Control of basal autophagy by calpain1 mediated cleavage of ATG5. Autophagy 2010; 6: 61–6.

Xiao WH, Zheng FY, Bennett GJ, Bordet T, Pruss RM. Olesoxime (cholest-4-en-3-one, oxime): analgesic and neuroprotective effects in a rat model of painful peripheral neuropathy produced by the chemotherapeutic agent, paclitaxel. Pain 2009; 147: 202–9.

Xiao WH, Zheng H, Bennett GJ. Characterization of oxaliplatin-induced chronic painful peripheral neuropathy in the rat and comparison with the neuropathy induced by paclitaxel. Neuroscience 2012; 203: 194–206.

Yang J, Weimer RM, Kallop D, Olsen O, Wu Z, Renier N, et al. Regulation of axon degeneration after injury and in development by the endogenous calpain inhibitor calpastatin. Neuron 2013; 80: 1175–89.

Yang L, Calingasan NY, Wille EJ, Cormier K, Smith K, Ferrante RJ, et al. Combination therapy with coenzyme Q10 and creatine produces additive neuroprotective effects in models of Parkinson's and Huntington's diseases. J Neurochem 2009; 109: 1427–39.

Yano H, Baranov S V, Baranova O V, Kim J, Pan Y, Yablonska S, et al. Inhibition of mitochondrial protein import by mutant huntingtin. Nat Neurosci 2014; 17; 822–31

Yousefi S, Perozzo R, Schmid I, Ziemiecki A, Schaffner T, Scapozza L, et al. Calpain-mediated cleavage of Atg5 switches autophagy to apoptosis. Nat Cell Biol 2006; 8: 1124–32.

Yu-Taeger L, Petrasch-Parwez E, Osmand AP, Redensek A, Metzger S, Clemens LE, et al. A novel BACHD Transgenic rat exhibits characteristic neuropathological features of huntington disease. J Neurosci 2012; 32: 15426–38.

Zhang J, Mao X, Zhou T, Cheng X, Lin Y. IL-17A contributes to brain ischemia reperfusion injury through calpain-TRPC6 pathway in mice. Neuroscience 2014; 274: 419–28.

Zhou H, Cao F, Wang Z, Yu Z-X, Nguyen H-P, Evans J, et al. Huntingtin forms toxic NH2-terminal fragment complexes that are promoted by the age-dependent decrease in proteasome activity. J Cell Biol 2003; 163: 109–18.

Zuccato C, Valenza M, Cattaneo E. Molecular mechanisms and potential therapeutical targets in Huntington's disease. Physiol Rev 2010; 90: 905–81.